IMPROVING FLUX IN FLAT PLATE MODULES FOR MEMBRANE DISTILLATION

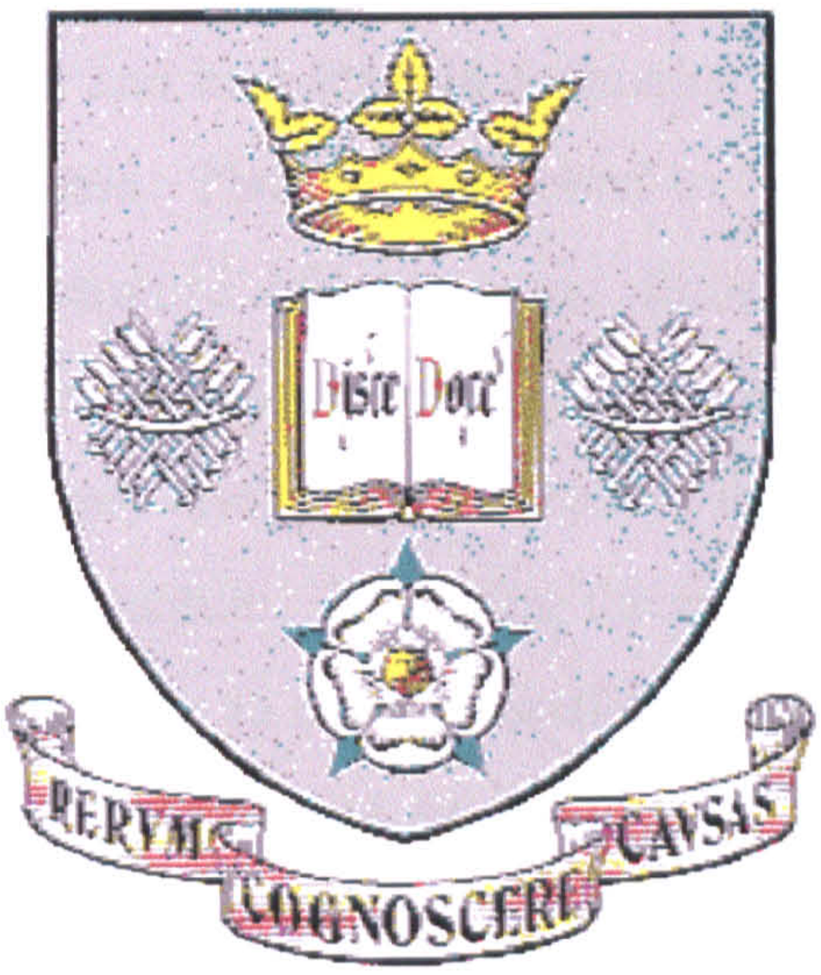

Submission for the degree of

Doctor of Philosophy
by
Andrea Burgoyne

Department of Chemical and Process Engineering, University of Sheffield
August 1998

SUMMARY

This work is concerned with a study of membrane distillation, through modelling and experimental work, in order to determine factors which enhance the permeate flux in this process. The driving force in membrane distillation is a temperature induced vapour pressure difference caused by having a hot feed and a cold permeate.

Three theoretical models were developed in order to analyse the process of membrane distillation in a flat plate module. The first was a flow distribution model utilising the relationship between flow rate and pressure drop in rectangular channels. It was found that increasing the flow rate increased the pressure drop over the module.

The second model used mass and heat transfer to predict the permeate flux for PTFE, PVDF and Versapor membranes. The flux was found to increase with increasing mean membrane temperature, temperature difference, and decreasing channel height. It was concluded that the Versapor membrane was unsuitable for membrane distillation.

The final model utilised boundary layer theory to predict the development of the thermal boundary layers in a flat plate module. Increasing the region where the boundary layer was still growing, reduced the drop in the temperature difference driving force over the module. For a specific velocity, there was an optimum channel height which produced the maximum possible flux.

An experimental program was carried out in order to investigate membrane distillation, to characterise the performance of the flat plate module used and to provide corroborating data for the theoretical models described.

A new module design was developed incorporating boiling and condensing heat transfer to overcome the decline in temperature driving force along a module channel. The heat transfer through the channel walls was found to stop the decline in driving force and introduce equilibrium.

ACKNOWLEDGEMENTS

I could never have got where I am today without the support of my parents, whose initial reaction to my decision of graduate study was,

"She'll be a perpetual student - she's enjoying it too much!!"

Well, mum and dad, you weren't far wrong! To the rest of my family - you may all be far away, but all your visits to Sheffield were enjoyed and I appreciated them all.

I would like to thank Maria Vahdati for her time and patience over the past 4 years, even with the arrival of baby Katrina. Her faith in me has always held strong, and she opened up the field of membranes to me.

To my two best friends, Lydia Hall and Julian Wilkes, you have both helped and enjoyed many of my predicaments!! Thankyou for everything, I know we'll always be there for each other.

My thanks also to Ian Shackley and Moji Moatamedi whose chats in the office kept me sane - although people can't decide whether I was ever sane!!

I'd like to thank everyone in the department, for all the help over the years. I'm sorry you are too numerous for me to thank you personnally.

One last thankyou, and that is to Peter Foster. He has known me the longest and has given help and advice over the past 7 years. He has aided in the development of the boundary layer analysis which required the patience to check pages (and pages!) of equations. Thankyou for making it go so smoothly.

Andrea Burgoyne

June 1998

PUBLICATIONS

Investigation of flux in flat plate modules for membrane distillation

A. Burgoyne, M.M. Vahdati, G.H. Priestman,

Developments in Chemical Engineering & Mineral Processing, 3(3/4), 1995, 161-176

Modelling of membrane distillation in flat plate modules.

Foster P.J; Burgoyne, A.; Vahdati, M.M.,

Proceedings of IMSTEC'96, Sydney Australia, 1996, 200 - 202

Membrane distillation in flat plate modules

Foster, P.J., Burgoyne, A., Vahdati, M.M.

Proceedings of Euromembrane'97, University of Twente, The Netherlands, 1997 , 343

Integrated boundary layer analysis and flux prediction for membrane distillation

Burgoyne, A., Foster, P.J., Vahdati, M.M., Priestman, G.H.

Proceedings of IChemE Research Event, Newcastle, 1998, Cd-Rom

Permeate flux modelling of membrane distillation

Burgoyne, A., Vahdati, M.M.

Suttle Award, Filtration and Separation Society, 1998 (Submitted)

CONTENTS

CHAPTER 1

INTRODUCTION

Membrane processes are utilised for a wide variety of applications. The majority of the processes in industry are for particle separation from a liquid stream, e.g. microfiltration ultrafiltration and reverse osmosis. Processes utilising various other driving forces include gas permeation, electrodialysis, pervaporation and membrane distillation. In membrane processes, the membrane separates two fluid streams, with components permeating through the membrane in liquid or gaseous form, in the direction of the driving force. The membrane can be gaseous, liquid or solid and usually acts as a selective barrier. This work is concerned with the process of membrane distillation.

Membrane distillation has been in use for around thirty years and is currently used mostly at the laboratory scale, with relatively few pilot plants in use around the world. Separations that are possible using this process include cases where,

i) the permeate is the product (desalination, water reclamation)

ii) the concentrated feed is the product (liquid food stuffs)

iii) both feed and permeate are products (azeotropic separation).

Membrane distillation has mostly been used for desalination, and so most of the research carried out concerns salt solution feeds. In the early years of research, the main focus was on discovering the basic trends in permeate flux caused by temperature,

concentration and velocity. Work was also carried out in order to find suitable membranes for the process. The main developments in the process were made in the early 1980's when newer, more suitable membranes became available, for instance hydrophobic PTFE. Recent research [11,12,48] has been mainly concerned with the use of hollow fibre modules to try and avoid large temperature losses in the feed. Such a unit would have application in desalination, and concentration of liquid foods and acid solutions.

The driving force for membrane distillation is a temperature induced vapour pressure difference across the membrane. The membrane itself is hydrophobic containing only vapour in the pores and is used purely as a support for the feed and permeate vapour-liquid interfaces. The mechanism of transport for membrane distillation can be split into three steps. The first is evaporation of the more volatile component, usually water, at the hot membrane surface. The second is the transport of the vapour through the pores of the membrane. The final stage is condensation of the vapour at the cold membrane interface into the permeate stream.

There are problems inherent with membrane distillation. As with all membrane processes, membrane distillation suffers from membrane fouling and the associated flux decay. Another problem is membrane wetting where the hydrophobic pores of the membrane are slowly filled with liquid and hinder the mass transfer of the permeate. Membrane wetting is particularly a problem when the feed contains an organic compound. Temperature and concentration polarisation, which reduce the vapour pressure difference driving force also need to be understood and their effects reduced. This may be accomplished by designing better modules. Currently, microfiltration and ultrafiltration modules are used for research into membrane distillation [9, ,12,14,15,28,45]. These modules do not represent the best choice as microfiltration and ultrafiltration are pressure driven processes, and membrane distillation is a temperature driven process. This means that the fundamental requirements for the module design are different.

The modelling of membrane distillation carried out so far has only been concerned with the actual physical process. In addition, research on the module configurations and its

effect on the flux has been confined to experimental work. Only one paper has been found to cover the modelling of membrane distillation in a module theoretically for membrane distillation [24], but the authors related the temperature and concentration boundary layers to the velocity boundary layer in fixed ratios, which may be inaccurate.

This work is concerned with a study of membrane distillation through modelling and experimental work in order to develop techniques for enhancing the permeate flux in flat plate modules. The work was split into four sections. The first part utilised a flat plate module to experimentally determine the basic characteristics of membrane distillation. The second determined the relationship between pressure and flow through the module. This was then modelled theoretically.

The third part used an expansion of an existing model [86] to model membrane distillation. This model determined the permeate flux which could be achieved given the feed and permeate temperatures and the flat channel height. Experimental work was then carried out to confirm the theoretical results.

The fourth part utilised boundary layer theory to predict the temperature profiles located in a flat plate module. This again was confirmed experimentally. The models associated with the third and fourth parts were then linked to provide accurate permeate flux data for a specific module configuration.

Finally, a new flat plate module design was developed to overcome the temperature polarisation effects of membrane distillation, and to therefore enhance the permeate flux of the process.

CHAPTER 2

LITERATURE REVIEW

2.1 Introduction

Membrane processes are becoming increasingly important in industry, since they give a more compact way to achieve the separation required than traditional methods.

All membrane processes use the same basic system for separation as shown in Figure 2.1. The membrane separates two streams, with components permeating through the membrane in the direction of the driving force. The processes used most frequently are microfiltration, ultrafiltration, reverse osmosis, dialysis and electrodialysis. Membranes used in these processes can be gaseous, liquid or solid, or even a combination, usually acting as a selective barrier. The driving force for these processes varies. Microfiltration, ultrafiltration and reverse osmosis are pressure driven processes, and gas permeation, dialysis and pervaporation are concentration driven processes. Electrodialysis is driven by an electromotive force and membrane distillation is driven by a difference in vapour pressure.

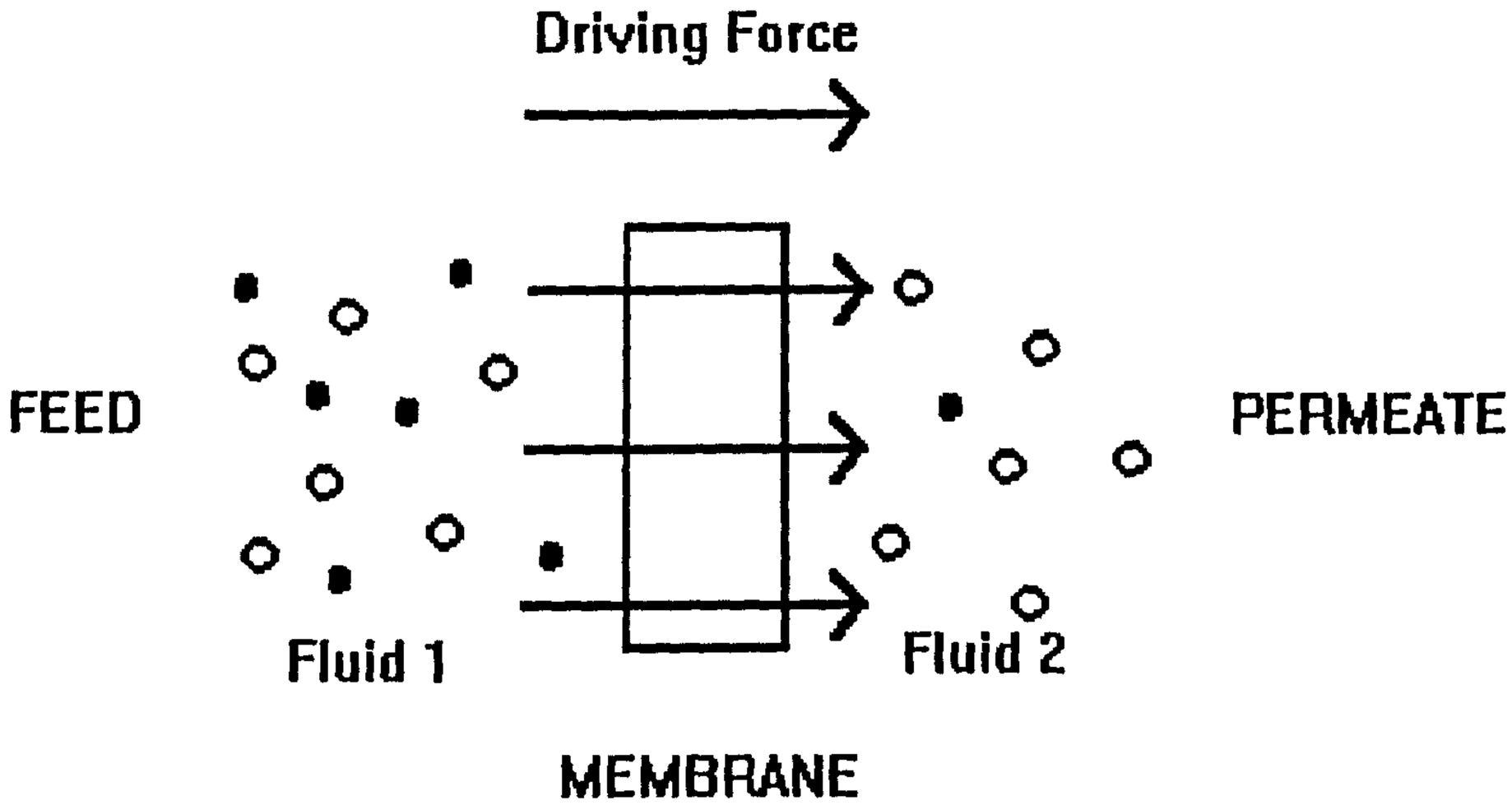

Figure 2.1: System for two phases separated by a membrane
Driving force = ΔC, ΔP, ΔT or ΔE

Low concentration feeds are best suited for membrane processes as the energy requirement is low. As the feed concentration increases, the energy consumption also increases and more traditional separation methods are preferred.

Comparison between the different membrane processes is difficult because of the different driving forces and mechanisms of mass transfer, but some of the benefits of membrane separation are that, i) the separation can be carried out continuously, ii) energy consumption is generally low, iii) membrane processes are easily combined with other separation processes, iv) separation can be carried out under mild conditions, v) membrane properties are variable and can be adjusted, vi) scaling up is easy, and vii) no additives are required.

There are some drawbacks to using a membrane process, namely, i) polarisation effects, ii) membrane fouling, iii) low membrane lifetime, and iv) generally low selectivity.

This work concerns membrane distillation, which is currently found almost exclusively in laboratories. Membrane distillation uses a porous, hydrophobic membrane with liquids in direct contact with both surfaces of the membrane. The driving force is a temperature induced vapour pressure difference caused by having a hot feed and a cold permeate. The mass transfer is accompanied by the transfer of the corresponding latent heat plus the conductive heat leak through the membrane.

The mechanism of transport from the feed to the permeate can be split into three steps. The first is evaporation of the more volatile component at the hot membrane interface. The second is the transport of vapour through the microporous system of the membrane. The final stage is condensation of the vapour at the cold membrane interface [1].

This literature review considers various aspects of membrane distillation. The review covers initial theoretical modelling, temperature polarisation - but not concentration polarisation, the different types of membrane and modules used, applications of the process, experimental work carried out and the process trends found. Sections on the phenomenon of membrane wetting, and energy considerations are also included, along with a section on the closely related process of osmotic distillation. There is also a section on modelling of boundary layers relating to membrane processes.

2.2 Theoretical Modelling

Much work has been carried out on the modelling of membrane distillation. The modelling falls into two distinct areas. Membrane modelling, which looks at the mechanism of transport of permeate through the membrane, and overall modelling which deals with predicting the permeate flux produced at specific operating conditions. Membrane distillation uses porous membranes and so the modelling covered in this chapter only concerns transport through porous membranes.

2.2.1 Membrane Modelling

Resistance to mass transfer through the membrane comes from the presence of air trapped in the membrane and the membrane structure, i.e. pore size, porosity and tortuosity [2]. The resistance to the flow of vapour from the membrane structure can be described by Knudsen diffusion or Poiseuille flow [3]. Poiseuille flow is only dominant when the pore size is larger than the mean free molecular path.

In most applications of membrane distillation, water is the component transported through the membrane. The molecular mean free path for water vapour at 60°C is approximately 0.3μm [3], which is around the pore size distribution of the membranes used for membrane distillation. This means that both Knudsen and Poiseuille flow have to be considered for describing the flow of vapour through the membrane.

Knudsen diffusion is a gas transport mechanism whereby gas molecules under a pressure gradient pass across a porous structure by a series of molecule/wall collisions and is described by,

$$N_K = \frac{D_K \varepsilon (c_1 - c_0)}{\chi \delta} \qquad (2.1)$$

which can be expressed as,

$$N_K = 1.064 \frac{r\varepsilon}{\chi\delta}\left(\frac{M}{RT}\right)^{0.5}(P_1 - P_0) \qquad (2.2)$$

Poiseuille flow is the viscous flow of a gas through a porous structure and is described by,

$$N_P = \frac{(q_{pore} n_{pore} MP_m)}{RT} \tag{2.3}$$

where,

$$q_{pore} = \frac{\pi r^4 \Delta P}{8\mu_g \delta \chi} \tag{2.4}$$

$$n_{pore} = \frac{\varepsilon}{\pi r^2} \tag{2.5}$$

and can also be expressed as,

$$N_P = 0.125 \frac{r^2 \varepsilon}{\chi \delta} \left(\frac{MP_m}{\mu_g RT} \right) (P_1 - P_0) \tag{2.6}$$

A third type of model to describe the transport of vapour through the membrane is Fick diffusion for flow through stagnant air, which is described by [2-4],

$$N_F = \frac{1}{Y_{lm}} \frac{D\varepsilon}{\chi \delta} \frac{M}{RT} (P_1 - P_0) \tag{2.7}$$

Equations (2.2), (2.6) and (2.7) suggest a relationship of,

$$N = C(P_1 - P_0) \tag{2.8}$$

for the mass transfer through the membrane, where C is the membrane mass transfer coefficient.

Schofield *et al* [3] produced a model that is a combination of Knudsen and Poiseuille flow, which shows that the membrane mass transfer coefficient, C, is slightly temperature dependent, decreasing 3% with a 10°C increase in mean temperature. The membrane mass transfer coefficient can also be affected by pressure, but for most cases the membrane mass transfer coefficient is mainly constant [5].

A similar equation to equation (2.8) describing the transport of mass flux through the membrane, by Zotolarev *et al* [6] is,

$$N = \frac{D_m M}{RT_m \delta \left(1 + D/D_K \right)} (P_1 - P_0) \tag{2.9}$$

though this equation requires knowledge of the Knudsen flux and membrane diffusion coefficients.

Equations (2.2), (2.6) and (2.7) describe the transport of vapour through a microporous membrane and they require the morphology of the membrane to be known. The morphology can be difficult to measure, which leads to inaccuracy [7].

Predicted values of the morphology term, $r\varepsilon/\chi\delta$, are low [3] when compared to actual values and may lead to serious error, so the morphology term must be estimated experimentally. Experimental values can be obtained by measuring the evaporation rate of water at varying temperatures and pressures [2].

Assumptions of tortuosity are more common. Tortuosity is a measure of the straightness of a pore from one side of the membrane to the other (1.0 means a straight pore with the actual length of the pore equal to the membrane thickness). Calabro *et al* [8] showed that assuming a tortuosity value of 1.2 for calculating the theoretical flux leads to a good correlation with experimental results of around 99.6%.

Other equations used by researchers to explain the process of mass transfer through the membrane initially seem different, but on closer examination they all correspond to the equations given in this section. The main point arising from this consideration of membrane modelling is that the transport of vapour through the membrane is controlled by both Knudsen and Poiseuille flow. Most studies accept the equations detailing these vapour flow processes as they accurately model the mass transfer through the membrane in membrane distillation.

2.2.2 Overall Modelling

Mass Transfer

In membrane distillation only water and volatile solutes can cross the membrane in the vapour phase [9]. Because the entrainment of dissolved particles is avoided, a permeate with high purity is obtained [10].

Mass transfer occurs by convective and diffusive transport of water vapour, and the membrane modelling discussed in Chapter 2.2.1 results in a relationship given by

equation (2.8). The vapour pressure difference term can be replaced by a temperature difference term to give, for dilute solutions,

$$N = C\frac{dP}{dT}\Big|_{T_m}(T_1 - T_0) \tag{2.10}$$

where the Clausius-Clapeyron equation gives,

$$\frac{dP}{dT}\Big|_{T_m} = \frac{P\lambda M}{RT^2}\Big|_{T_m} \tag{2.11}$$

and, for concentrated solutions,

$$N = C\frac{dP}{dT}\left[(T_1 - T_0) - \Delta T_{th}\right](1 - x_m) \tag{2.12}$$

where,

$$\Delta T_{th} = \frac{RT^2}{M\lambda}\frac{x_1 - x_0}{1 - x_m} \tag{2.13}$$

If $(T_1\text{-}T_0)$ is less than ΔT_{th} a negative flux is produced [3,11], which inhibits the membrane distillation process.

A non-volatile solute in the feed reduces the vapour pressure according to Raoult's Law [12],

$$p = p_0(1 - x) \tag{2.14}$$

It also alters the fluid dynamics through effects on density and viscosity, and influences heat transfer through thermal conductivity and specific heat [13].

The membrane mass transfer coefficient, C, has been found both theoretically, by equation (2.15), and experimentally for various membranes [11].

$$C = \left(\frac{P}{RT}\right)_{av,m}\frac{M\varepsilon d_p}{32\mu\delta\chi} \tag{2.15}$$

Equation (2.15) assumes Knudsen diffusion through the membrane pores. C may also be found from a plot of $(T_H\text{-}T_C)/N\lambda$ against $1/(dP/dT\times\lambda)$. This will give a slope of $1/C\times(1+(k_m/\delta))$ [4]. An example plot is shown in Figure 2.2. The relationship is given by,

$$\frac{T_H - T_C}{N\lambda} = \left[C\lambda\left(\frac{dP}{dT}\right)\right]^{-1}\left(1 + \frac{k_m}{\delta h}\right) + \frac{1}{h} \tag{2.16}$$

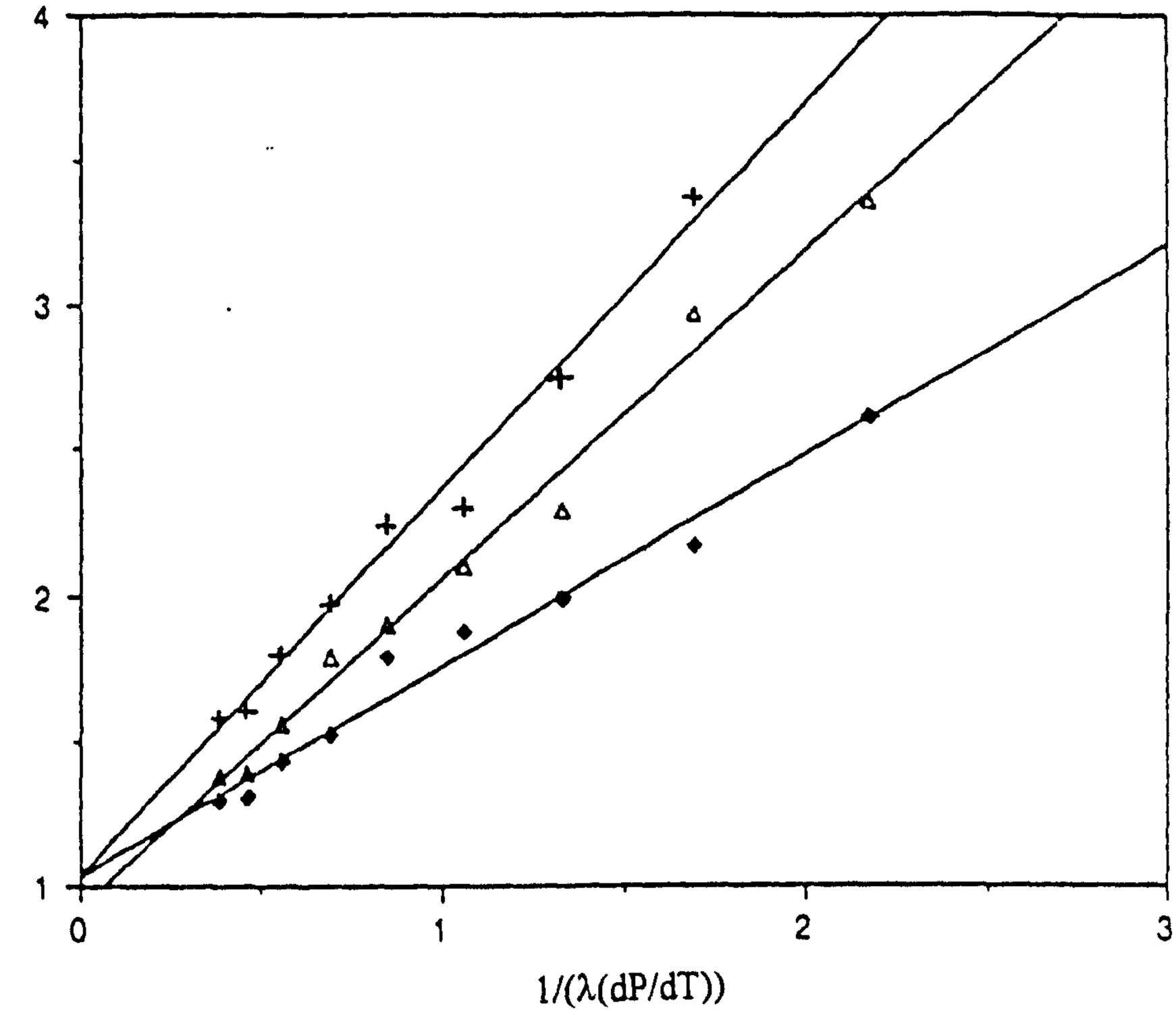

Figure 2.2: Plot of results using equation (2.16) for various membranes (Lida + 0.2μm, Δ 0.5μm, ♦ 1.0μm) stirring rate = 250 rpm [4]

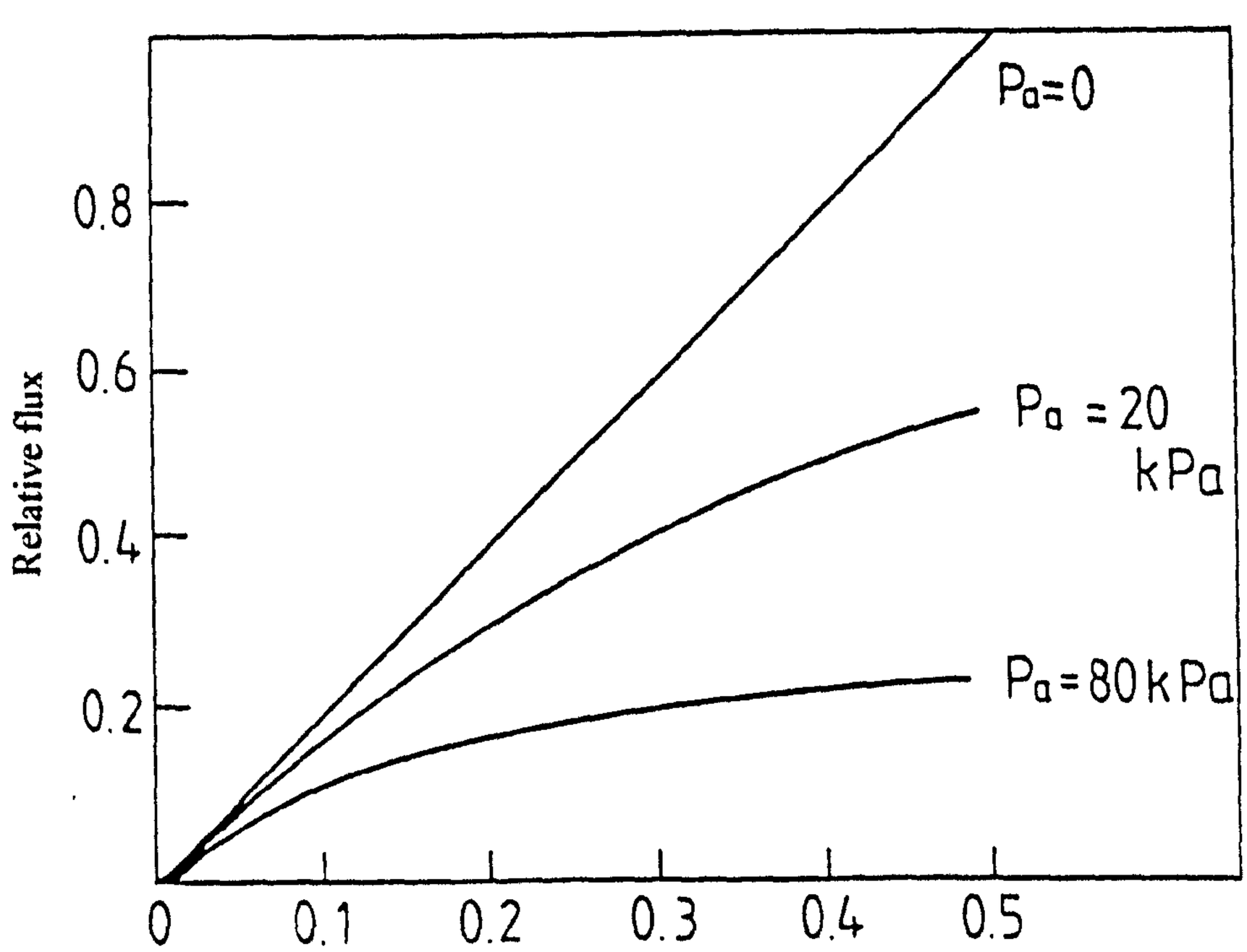

Figure 2.3: Effect of partial pressure of air (Pa) on MD flux for various pore sizes [16]

The graph also enables h, the heat transfer coefficient, to be found.

The theoretical values of the membrane mass transfer coefficient, C, are larger than those found experimentally. Until more accurate theoretical methods are developed, with greater understanding of the controlling model of vapour flow through the membrane, experimental values have to be used [3,11].

Schofield *et al* [3] state that C is slightly temperature dependant, with a 3% decrease in value for a 10°C rise in temperature. Drioli *et al* [14], do not agree and state that C is independant of temperature, but is related to solution chemistry and solute concentration because their experiments show that as concentration increases, the membrane mass transfer coefficient decreases.

Another way of analysing membrane distillation, uses net and global non-isothermal coefficients, B and B′. These are defined by [15],

$$N = B\Delta T = B'\Delta T_b \qquad (2.17)$$

and allow direct correlation of the effect of temperature and temperature polarisation (Section 2.3) on the mass flux.

Aerated systems are often mass transfer limited. Figure 2.3 shows the effect of partial pressure on flux for various pore sizes. It can be seen that decreasing the partial pressure of air increases the flux [16]. A number of studies have looked at deaerating the feed solutions and have been able to produce flux improvements [17]. Deaerating the membrane decreases the molecular diffusion resistance which makes Knudsen flow dominant [49]. This means that an improvement will not be evident when Knudsen flow is already dominant [16]. One way to dearate the membrane is to decrease the pressure of both feed and permeate [17].

When membrane distillation is run under very high concentration conditions, the behaviour is very different to that for a dilute solution. For solutions with a low initial feed concentration, the concentration increase during membrane distillation causes a lowering of the vapour pressure and an increase in the thermal capacity, which counteract each other. The viscosity is also not high enough to affect flow through the module, so the flux remains constant. At high initial concentrations, an increase in viscosity and a decrease in vapour pressure and osmotic pressure can affect the process.

With concentrated solutions, dialysis is present, acting opposite to the required flux and only when the vapour pressure difference across the membrane is big enough to counteract the interference from dialysis, does the membrane distillation process dominate. Solutions with low concentrations only affect the minimum temperature difference which must be overcome in order to obtain pure water as the permeate [18].
Mass transfer decreases as the concentration of the feed increases, and this can lead to membrane distillation crystallisation. If the solute is not easy to crystallise, the viscosity will increase until the flux decreases to zero. If the solute is easy to crystallise, then the flux will continue until supersaturation concentrations are reached, and crystals will then start to precipitate. These crystals can then be collected outside the module, and the membrane distillation continued [18].

Heat Transfer

In direct contact membrane distillation, the evaporation and condensation surfaces are close to each other. As a consequence of this, a high conductive heat flux parallels the mass flux, and the effective temperature difference across the membrane is greatly reduced with respect to the bulk temperature difference [19].
Overall, as membrane distillation utilises a temperature difference to induce the driving force, the process is heat transfer limited and therefore, the film heat transfer coefficients are the most important parameters in governing the mass transport.
Heat transfer occurs by heat conduction, Q_c, and latent heat, Q_v, across the membrane, according to,

$$Q_c = \frac{k_m}{\delta}(T_1 - T_0) \tag{2.18}$$

and,

$$Q_v = N\lambda = C\frac{dP}{dT}\lambda(T_1 - T_0) \tag{2.19}$$

where, k_m is the membrane thermal conductivity given by,

$$k_m = \varepsilon k_g + (1-\varepsilon)k_s \tag{2.20}$$

The membrane thermal conductivity is required in order to describe heat and mass transfer through the membrane as the membrane contains both polymer and vapour. The values of membrane thermal conductivity found by equation (2.20) agree with measured values within 10% [17].

Q_c is the heat conducted through the membrane from the hot to the cold side and has the effect of reducing the driving temperature difference. Q_c should be minimised as it impedes the process of membrane distillation. The heat lost by conduction through the membrane can be considerable. Schofield *et al* [17] state that between 30 and 50 % of the possible temperature driving force is lost through conduction. This is a larger percentage than that predicted by Jonsson *et al* [20] who state that using PTFE membranes with high porosity reduces the membrane thermal conductivity, and as a consequence the heat lost by conduction constitutes only a relatively small part of the total rate of heat transfer. To reduce the heat lost, an air gap on the permeate side can be introduced. This increases the boundary layer thickness and decreases the membrane thermal conductivity leading to a slightly different process called gas-gap membrane distillation [3]. A problem with gas-gap membrane distillation is that it is difficult to control temperature polarisation [16]. This is because the air gap reduces the permeate side heat transfer coefficient. One way to minimise Q_c is to increase the overall temperature. This is because the pressure gradient increases exponentially with respect to temperature. Another way is to increase the membrane pore size, which increases porosity and so reduces the membrane thermal conductivity.

Q_c and Q_v can be combined to obtain an effective heat transfer coefficient, H, to enable the heat transfer membrane distillation to be defined,

$$Q = \left[C\frac{dP}{dT}\lambda + \frac{k_m}{\delta} \right](T_1 - T_0) = H(T_1 - T_0) \qquad (2.21)$$

As the mean temperature of the module increases, the effective heat transfer coefficient also increases [3,12] due to dP and λ increasing with temperature.

The heat transfer in the hot boundary layer can also be found by relating dimensionless groups [6], which for laminar flow in a tube is given by,

$$\frac{h_1 d_h}{\lambda_1} = 1.62\left[\frac{C_p \rho v d_h^2}{\lambda_1 l_m}\right]^{0.3} \tag{2.22}$$

and for turbulent flow in a tube is given by,

$$\frac{h_1 d_h}{\lambda_1} = 0.023\left(\frac{\rho v d_h}{\mu_1}\right)^{0.8}\left(\frac{\mu_1 C_p}{\lambda_1}\right)^{0.25} \tag{2.23}$$

The same equations can be used for the permeate side, using the relevant physical properties. Another correlation for predicting values of film coefficients was suggested from experimental results by Hanbury and Hodgkiss [21], which is,

$$h(T) = 0.0049 T^{1.17} \tag{2.24}$$

with T in °C, and h in kW/m^{2}K. It was found that the heat transfer coefficients of membrane distillation were much lower than obtained with conventional distillation.

Schofield *et al* [17] have used equations (2.21) and (2.22) together with their combined Knudsen and Poiseuille mass flux flow model (Section 2.2.1), to form a combined membrane distillation model. They utilised an iterative procedure to solve mass and energy balances in the direction of the feed, to calculate the permeate flux. This was found to accurately predict the fluxes obtained with direct contact membrane distillation. Ugrozov *et al* [22] also combined heat and mass transfer to develop equations that could accurately model a membrane distillation module. The main conclusion from their work was that the mean temperature across the membrane decreased with increasing distance along the module. This means that the production rate of membrane distillation will not increase directly with module length, as shown in Figure 2.4.

Influence of Stirring

Some modules for membrane distillation incorporate stirring (Chapter 2.5). The stirring rate can have a large effect on concentration and temperature. This is because membrane distillation is affected by polarisation layers, and the thickness of these layers is decreased by stirring.

The effect of stirring rate on flux was studied by Velazquez *et al* [13,23] and is given by,

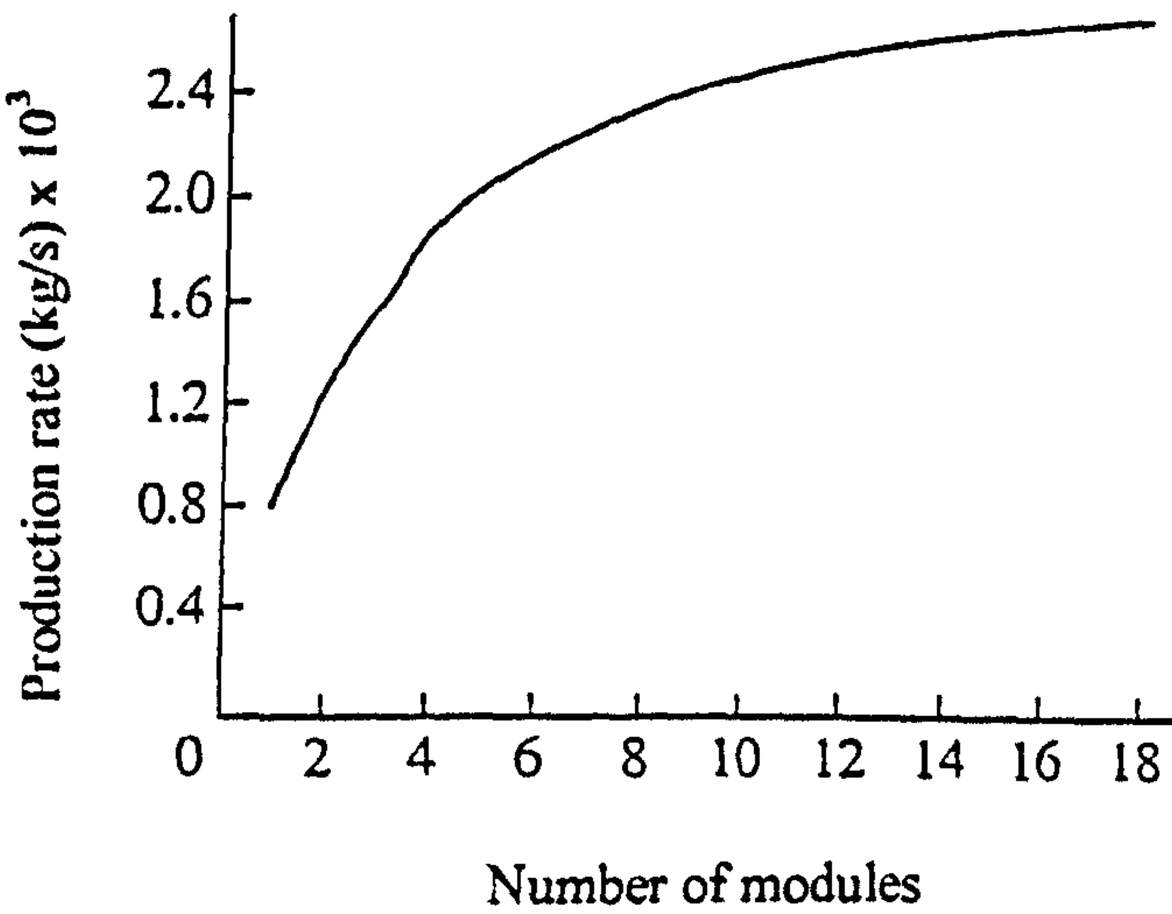

Figure 2.4: Number of modules related to production rate [22]

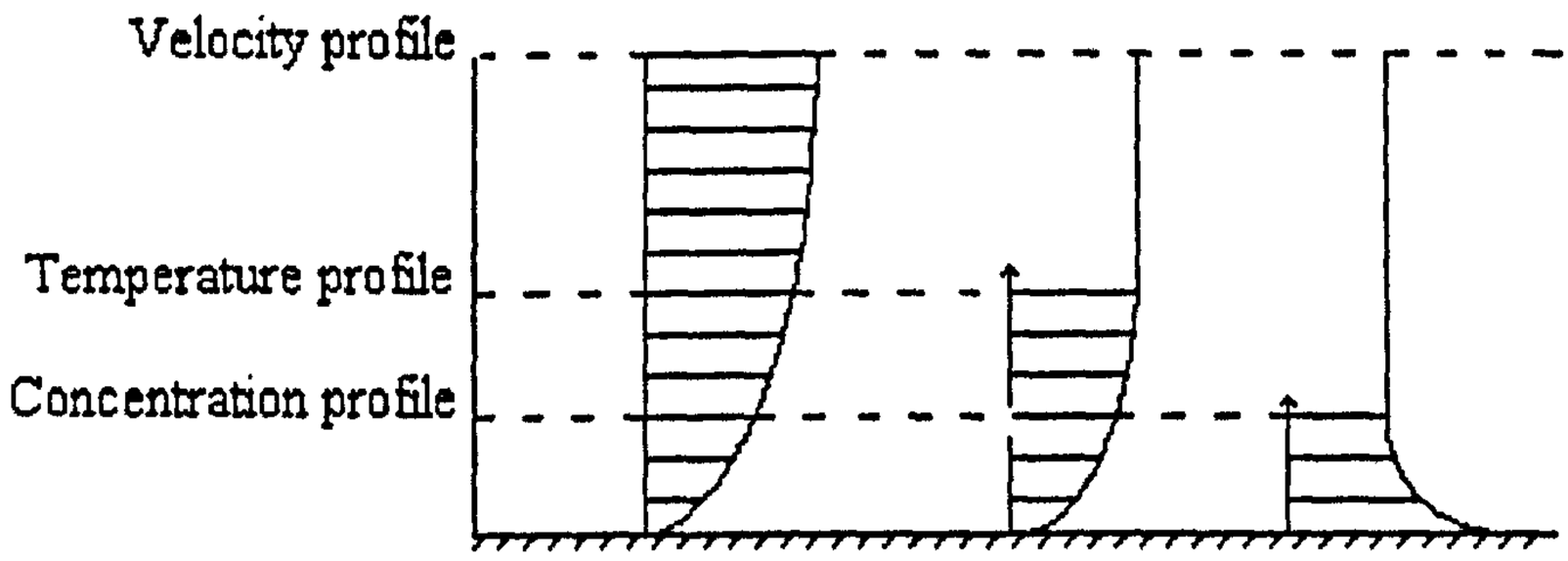

Figure 2.5: Relation of velocity, temperature, and concentration boundary layer profiles [24]

$$\frac{1}{N_{(\varpi)} - N} = X + \frac{W}{\varpi^{\gamma}} \tag{2.25}$$

where X and Y are adjustment factors, and γ is approximately 1.0.

Equation (2.25) only takes into account temperature polarisation, but the work carried out concerned low concentration solutions, and any effect caused by concentration was taken into account in the adjustment factors [23].

Influence of Boundary Layers

A final area of modelling of membrane distillation is consideration of the influence of boundary layers on the permeate flux in modules. This has been studied by Agashichev and Sivakov [24] who used mass and energy balances to define the hydrodynamic, temperature and concentration boundary layers. All the boundary layers were related by fixed ratios to the velocity boundary layer, assuming a flat membrane, and incompressible, continuous laminar flow. The velocity profile used was,

$$v_{\eta} = \frac{v_z}{v} = sin\left(\frac{\pi}{2}\eta\right) \tag{2.26}$$

in which η is a dimensionless co-ordinate (y/Y). The corresponding temperature and concentration boundary layers were then,

$$\frac{t_{\theta} - t_{1m}}{t_1 - t_{1m}} = sin\left(\frac{\pi}{2}\theta\right) \tag{2.27}$$

where,

$$\theta = \eta\left(\frac{C_p\mu}{\lambda}\right)^{1/2} \tag{2.28}$$

and,

$$\frac{x_{\beta} - x_1}{x_{1m} - x_1} = e^{\alpha\beta} \tag{2.29}$$

where, a = -5.0 and,

$$\beta = \left(\frac{\mu}{\rho D}\right)^{1/3}\left(\frac{C_p\mu}{\lambda}\right)^{-1/2} \tag{2.30}$$

This may be inaccurate as they have shown no reason to confirm the validity of the assumed relations between the temperature and concentration boundary layers to the velocity boundary layer. The model formed determines the physical properties of the fluid and the temperature and concentration in both the feed and permeate channels.
They state that the velocity boundary layer is larger than the temperature boundary layer, which is in turn larger than the concentration boundary layer, as shown in Figure 2.5.

Summary

The overall modelling of membrane distillation can be split into four areas. These are mass transfer, heat transfer, the influence of stirring in test cells and the influence of boundary layers in modules.

The main factors affecting membrane distillation are the initial feed concentration, the membrane temperature, temperature difference, stirring rate, thickness of boundary layers, and mass and heat transfer. The mass transfer is given by

$$N = C(P_1 - P_0) \tag{2.8}$$

where C, the membrane mass transfer coefficient is found from a combination of Knudsen and Poiseuille flow. Equation (2.8) can be expressed in terms of the driving force temperature difference as,

$$N = C\left.\frac{dP}{dT}\right|_{T_m}(T_1 - T_0) \tag{2.10}$$

Only water and volatile solutes can cross the membrane in the vapour phase and dearating the system can increase the permeate flux. Concentrated feed solutions behave differently from dilute feed solutions, and if the solute is easy to crystallise, then membrane distillation crystallisation can occur, and a solid product is obtained from the feed.

The heat transfer term consists of two components, the heat conducted through the membrane, Q_c , and the heat carried through the membrane by the vapour, Q_v . Q_c hinders membrane distillation by reducing the temperature driving force. The two components are combined to express the heat transfer in membrane distillation as,

$$Q_e + Q_v = \frac{k_m}{\delta}(T_1 - T_0) + N\lambda \qquad (2.31)$$

The permeate flux in test cells can be improved by stirring as this reduces polarisation layers. One study [24] tried to model these boundary layers in modules to predict the behaviour of membrane distillation in practical equipment. The model developed enabled the simulation of a plate and frame module. It included the determination of the temperature and concentration in the module.

2.3 Temperature Polarisation

Temperature polarisation is a loss of driving force brought about by thermal gradients in the fluids bounding the membrane [3] and is a major problem for membrane distillation. Figure 2.6 shows the effect of temperature polarisation on the bulk temperatures. Temperature polarisation becomes more significant at higher temperatures [16]. It is possible to characterise temperature polarisation by a heat transfer analysis.

The membrane distillation system can be characterised as a system of heat resistances as shown in Figure 2.7, so that the overall heat transfer can be expressed as,

$$Q = h_1(T_H - T_1) = h_o(T_o - T_c) = H(T_1 - T_o) \qquad (2.32)$$

As the driving force is the temperature difference between the interfacial temperatures, T_1 and T_0, rearranging equation (2.31), and defining the Temperature Polarisation Coefficient (TPC) as,

$$TPC = \frac{1}{1 + \frac{H}{h_1} + \frac{H}{h_o}} \qquad (2.33)$$

gives [3,12],

$$(T_1 - T_0) = TPC(T_H - T_C) \qquad (2.34)$$

Ideally TPC should equal 1, but usually it is closer to 0. If the TPC is less than 0.2 then the process is heat transfer limited, i.e. bad module design, and if TPC is greater than 0.6 the process is mass transfer limited, i.e. poor membrane permeability [17]. Chmielewski

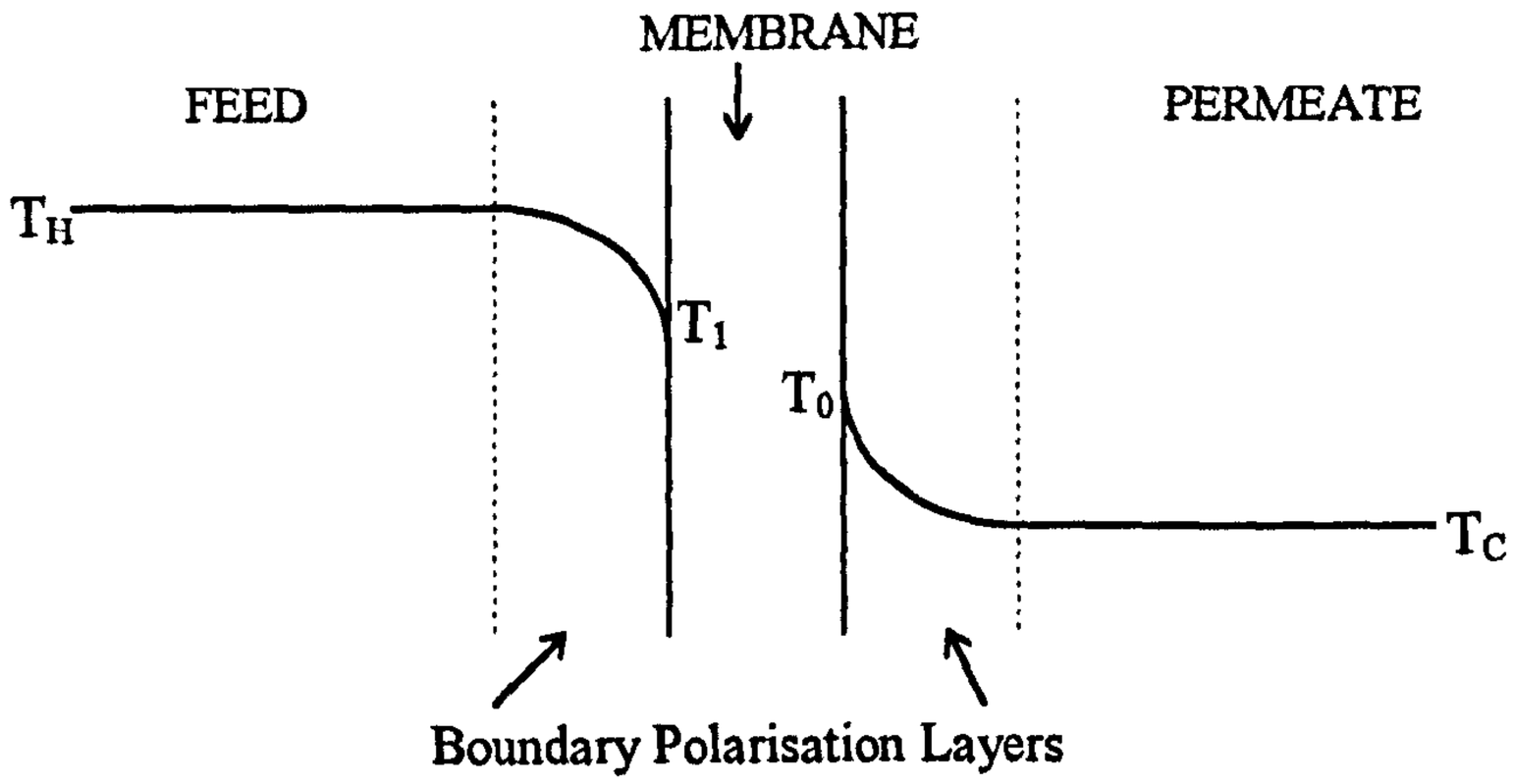

Figure 2.6: Effect of temperature polarisation on bulk temperatures

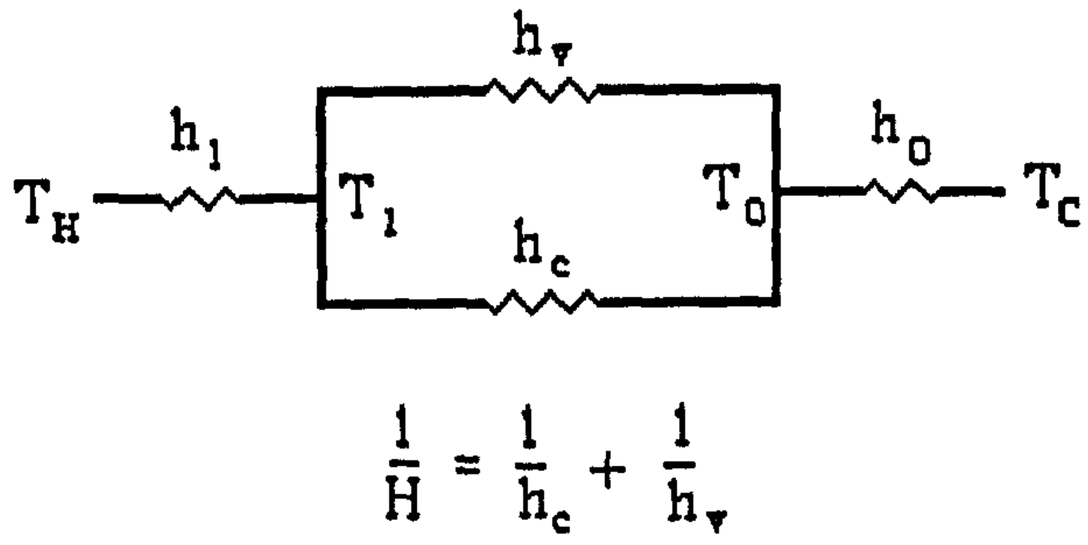

Figure 2.7: Membrane distillation heat resistances

and Zakrzewska-Trznadel [25] used this method to compare experimental values of TPC with theoretical values and found them to agree quite well. They stated that as the temperature increases, the TPC falls. For example, with their flat sheet module, increasing the temperature from 298 K to 323 K decreased the TPC from 0.75 to 0.59. Another equation for TPC is,

$$TPC = \frac{\Delta T}{\Delta T_b} = \frac{B'}{B} \qquad (2.36)$$

using the net, and apparent non-isothermal coefficients, shown in Section 2.2.2 [13]. The TPC is the fraction of external applied thermal driving force that contributes to the mass transfer. A similar equation to equation (2.35) was used to lead to a term concerning flux decline, N/N_i ,which is the current flux over the initial flux [8]. Equation (2.36) uses the fact that as the feed concentration increases, the decrease in vapour pressure is negligible compared to the increase of kinematic viscosity and allows estimation of the flux decay.

$$\frac{N}{N_i} = \frac{\Delta P_B{}^0 v_i}{\Delta P_{Bi}{}^0 v}\bigg|_{T_{F,B}} \qquad (2.36)$$

Equation (2.36) is for a concentration factor of c_F/c_{Fi} when all other parameters are constant.

Schofield *et al* [3] have used the TPC as a tool in designing membrane distillation systems. They looked at various module configurations and calculated the TPC. The closer the TPC was to 1.0, the better the heat transfer in the module, and therefore more suitable for membrane distillation (Table 2.1). They found that the three best module configurations were,

i) 1 mm tube, Re~5000 in the tube,

ii) 0.3 mm tube, Re~300 in the tube,

iii) 0.1 mm film with laminar flow.

They also discovered that temperature polarisation becomes more important as the heat transfer coefficient of the membrane increases. Temperature polarisation can be reduced by, increasing the velocities of the liquids, using turbulence promoters, and decreasing the height of liquid channels [17].

Membrane geometry	Flow characteristics	Nu	d (mm)	h (W/m^2K)	TPC
1 mm i.d. tube	Re=5000	29	1.0	19000	0.9
	Re=3000	20	1.0	13000	0.85
	Re=1000	4.4	1.0	2900	0.54
0.3 mm i.d. tube	Re=300	4.4	0.3	9700	0.8
0.6 o.d. tube bundle	close packed laminar	≈5	0.9	3700	0.6
channel 0.5 m long	v = 2 m/s	970	500	1300	0.51
conducting film					
2 mm thick	laminar	5.4	8	450	0.15
0.5 mm thick	laminar	5.4	2	1800	0.4
0.1 mm thick	laminar	5.4	0.4	8900	0.7
stirred cell	Re=8000	54	50	710	0.2
	Re=32000	120	50	1600	0.4

Table 2.1: Temperature Polarisation Coefficient (TPC) for various module configurations [3]

Usually there is no variation of TPC with temperature difference, it only strongly depends on membrane characteristics, fluid dynamics and feed concentration [11].

Ortiz de Zarate *et al* [15] found no real dependence of TPC on the concentration but did find TPC, and flux, increased with stirring rate. Stirring the fluids either side of the membrane in test cells has been shown to increase flux due to the effect of fluid shear on the temperature polarisation layer. Stirring increases the film heat transfer coefficient, which therefore decreases temperature polarisation.

The interfacial temperatures cannot be measured directly, but they can be found from a knowledge of the heat transfer coefficients throughout the membrane distillation module and bulk fluid temperatures [5].

$$T_1 = T_H - (T_H - T_C)\left(\frac{\frac{1}{h_H}}{\frac{1}{(h_v + h_c)} + \frac{1}{h_H} + \frac{1}{h_C}}\right) \tag{2.37}$$

and,

$$T_0 = T_C - (T_C - T_H)\left(\frac{\frac{1}{h_C}}{\frac{1}{(h_v + h_c)} + \frac{1}{h_H} + \frac{1}{h_C}}\right) \tag{2.38}$$

The film heat transfer coefficients can be estimated from experiments, equations (2.22), (2.23) and (2.24), or from correlations i.e.,

$$h_c = \left(\varepsilon k_g + (1-\varepsilon)k_s\right)/\delta \tag{2.39}$$

and,

$$h_v = \frac{N\Delta H_v}{\Delta T_m} \tag{2.40}$$

Vasquez-Gonzalez and Martinez [26] state that Schofield does not consider the effect of heat transferred by the mass flux through the membrane and only included the heat carried by latent heat transfer accompanying mass flux from one phase to the other. They suggest the following relationship which allows the membrane interfacial temperatures to be determined from easily obtained experimental parameters,

$$\Delta T_b = \Delta T_m \left[1 + \frac{2k}{\delta h} \right] + \frac{2NMQ}{Ah} \qquad (2.41)$$

In summary, temperature polarisation is a major problem for membrane distillation as it is a thermally driven process, and can severely reduce the fluid temperatures. More work has to be carried out to fully understand this phenomenon, and reduce its influence on the process. Any model for membrane distillation must always include the effect of temperature polarisastion.

2.4 Membrane Types

Various membranes are used for membrane distillation, but the most popular include, PTFE (poly tetrafluoroethylene), PVDF (poly vinyldifluoride), and PP (poly propylene). The membrane is used only as a physical barrier between the feed and permeate streams and is not directly involved in the separation. The hydrophobic nature of these membranes prevent the bulk liquid transport of the liquid phase across the membrane [1]. Details of membranes used in studies of membrane distillation can be found in Table 2.2. According to the definition of the process [27], membrane distillation is only possible with hydrophobic membranes, but Ohta *et al* [28,29] have looked at using hydrophilic membranes for membrane distillation. The dense, hydrophilic membranes used were silicone, and a fluoro-carbon composite. Both were applied to seawater desalination. As the membranes are dense, and there are no pores, membrane wetting (Chapter 2.8) is avoided. Their work was only experimental and they did not develop any theory to explain their results. The theory given in Chapter 2.2 cannot be used as that is for porous membranes. For dense, hydrophilic membranes, the transport would probably be controlled by diffusion and absorption. Fluxes of a similar magnitude to those obtained with hydrophobic membranes were achieved. Figure 2.8 shows an example of the flux obtained using the fluoro-carbon membrane.

Membrane type	Origin	Polymer	Pore size (μm)	Thickness (μm)	Porosity (%)	Reference
flat	Enka	PP	0.1	100	75	3
flat	Enka	PP	0.2	140	75	3,17
flat	Gelman	PTFE	1.0	170	80	12,13,34,35
flat	Gelman	PTFE	0.45	178	80	34
flat	Gelman	PTFE	0.2	178	80	13,36
flat	Gelman	PTFE	0.2	60	60	19,35,37
flat	Taflen	PTFE	0.8	60	50	12,38
flat	Vladipor		0.25	120	70	6
flat	Millipore	PVDF	0.45	110	75	3,5,17
flat	Millipore	PVDF	0.11	140	75	8
flat	Millipore	PTFE	0.2	130	70	9,25
flat	Millipore	PTFE		60		39
flat	Millipore	PTFE	0.5	175	85	36
flat	Teknokroma	PTFE	0.2		80	4
flat	Teknokrama	PTFE	0.5		80	4
flat	Teknokrama	PTFE	1.0		80	4
flat		PTFE	0.1	178	80	9,15,23
flat		PTFE	0.2	178	80	9,15,23
flat		PTFE	0.45	178	80	9,15,23
flat		PTFE	0.2	178	70	9,23
flat		PVDF	0.22	80	75	15
flat		PTFE	0.3	80		40
flat		PTFE	0.2			41
flat		PTFE	0.45			41
flat		PTFE		450		42
flat		Silicone	dense	250	non-porous	28
flat		Fluoro-carbon	dense	130	non-porous	29
capillary	Enka	PP	0.43	150	70	14,18
capillary	Enka	PP	0.2		70	1
capillary	Accurel	PP	0.5	150	66	12
capillary	Accurel	PP	0.6	400	74	12
capillary	Accurel	PP		155	75	43
capillary		PP	0.2	150		16
capillary		PVDF	0.03	100	81	44
capillary		PP	0.45	100	70	11

Table 2.2: Membranes used for research of membrane distillation

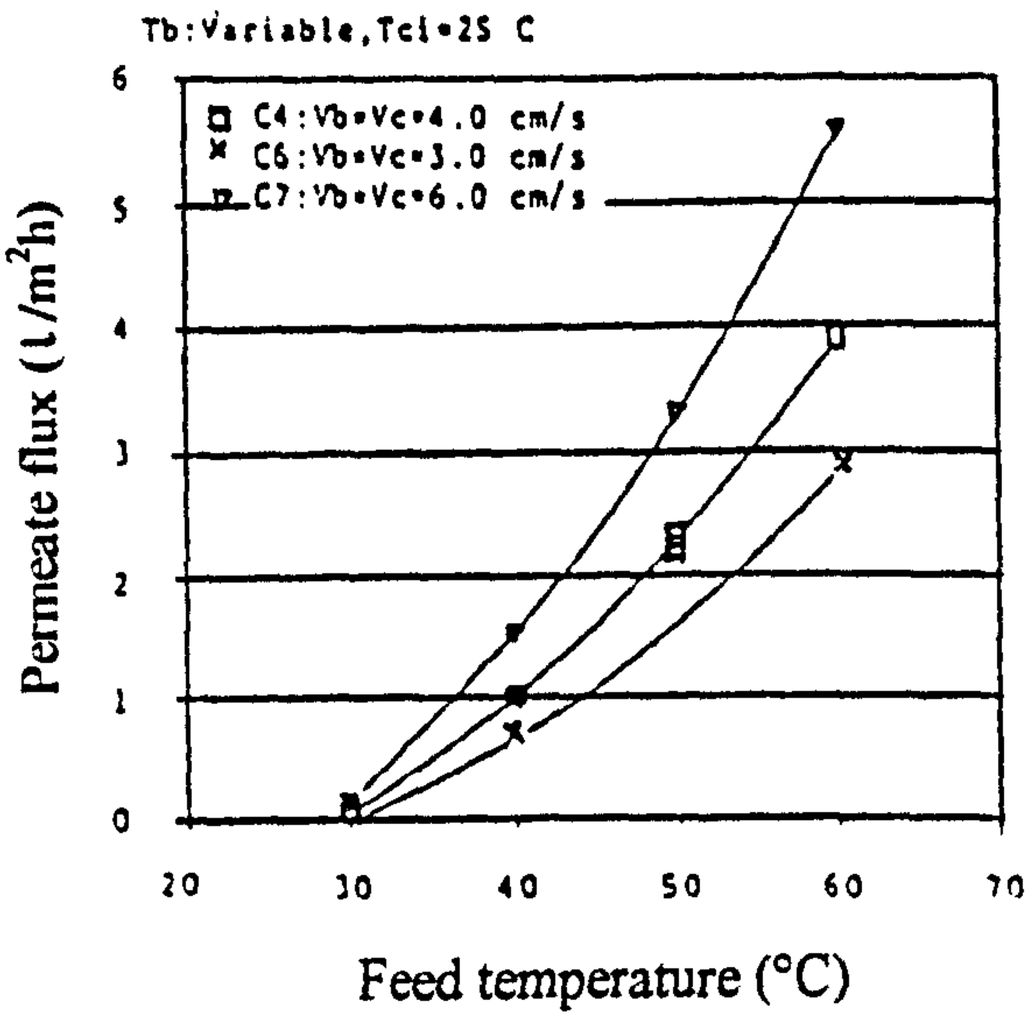

Figure 2.8: Flux obtained with a hydrophillic fluoro-carbon membrane [29]

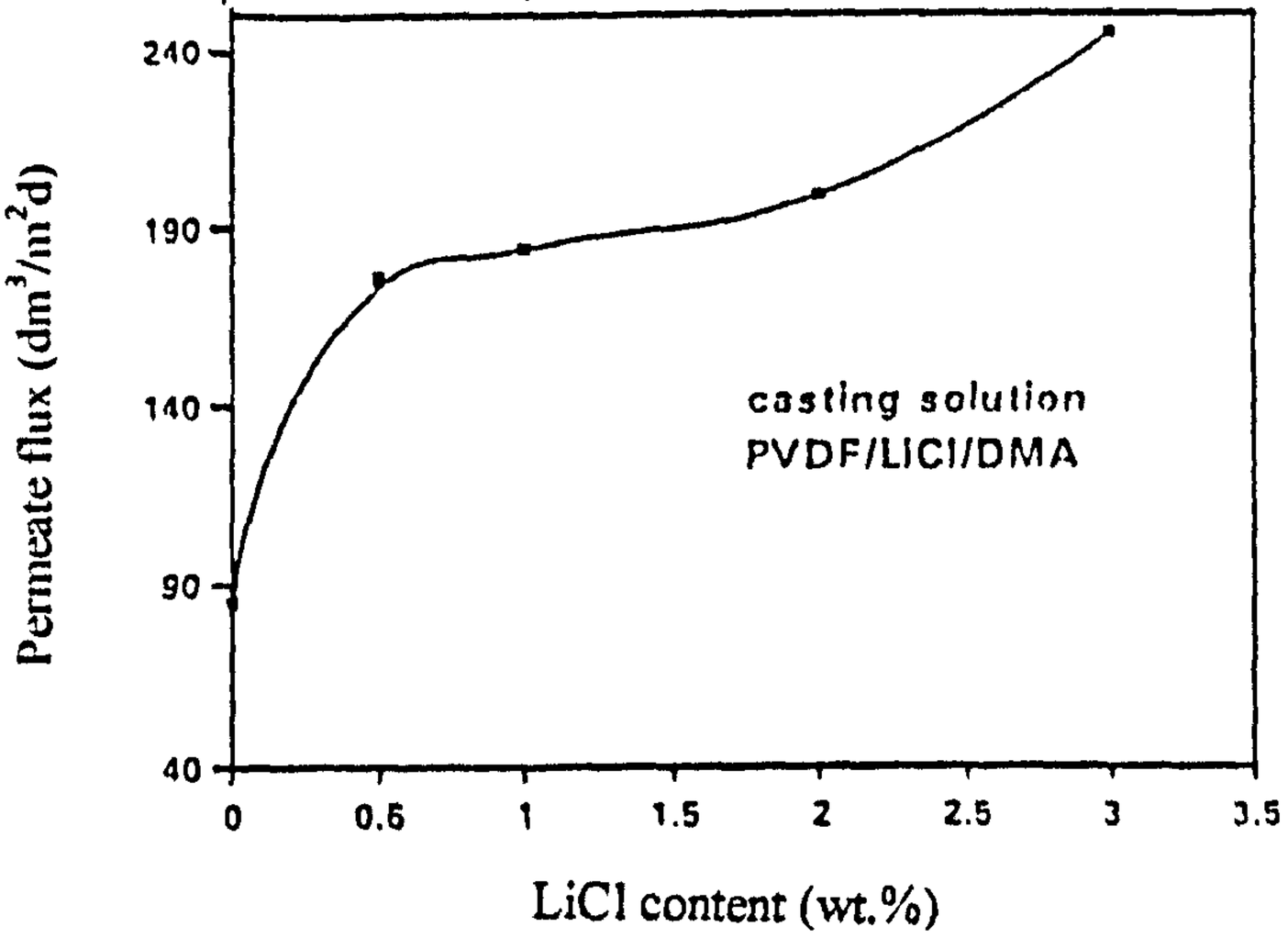

Figure 2.9: Effect of lithium chloride in the membrane casting solution on permeate flux [31]

Membranes with a narrow pore size distribution and high porosity (>50% [3]) are best for membrane distillation [1]. Porosity can be induced by mechanical stretching and/or thermal phase separation techniques. Also, due to temperature polarisation, the thermal conductivity of the polymer is a controlling parameter of the process. Thermal conductivities of commercial membranes lie between 0.04 and 0.06 W/m K, increasing with decreasing porosity [3].

Membrane distillation is usually carried out with commercial microfiltration membranes, but a number of studies have produced their own membranes, to try and design a membrane that is purely for membrane distillation in order to improve the flux and separation. Ortiz de Zarate *et al* [30] looked at using phase polymerisation with PVDF as the polymer and dimethylacetamide (DMA) and dimethylformamide (DMF) as the solvents. They observed that pore diameters and porosity increased as the PVDF content fell. In addition, the flux was not affected by the membrane asymmetry i.e. one side of the membrane having larger holes. In summary, the work did not produce any improvement in flux as compared to those obtained with commercial membranes. Another study by Tomaszewska [31], also used PVDF polymer and DMA and DMF solvents, but also introduced a lithium chloride additive to the casting solution. This had the effect of increasing porosity and pore size. In the membrane distillation of a 1-2% sodium chloride solution, as the lithium chloride content was increased, the permeate flux also increased, as shown in Figure 2.9. The conclusion made was that the characteristics and properties of the membrane were affected by the composition of the casting solution and by the temperature of the coagulation bath used in the phase polymerisation. Wu *et al* [32] used plasma polymerisation to modify the surface of hydrophilic membranes so that they would be suitable for use in membrane distillation. Plasma polymerisation occurs when organic monomers are split and decomposed into various active vapour particles and are then recombined to deposit polymer on the surface of the substrate. This process of membrane preparation produced some membranes suitable for membrane distillation. Figure 2.10 shows the flux and rejection obtained for membrane distillation of a 0.5 M sodium chloride solution. The behaviour is similar to that obtained with hydrophobic membranes.

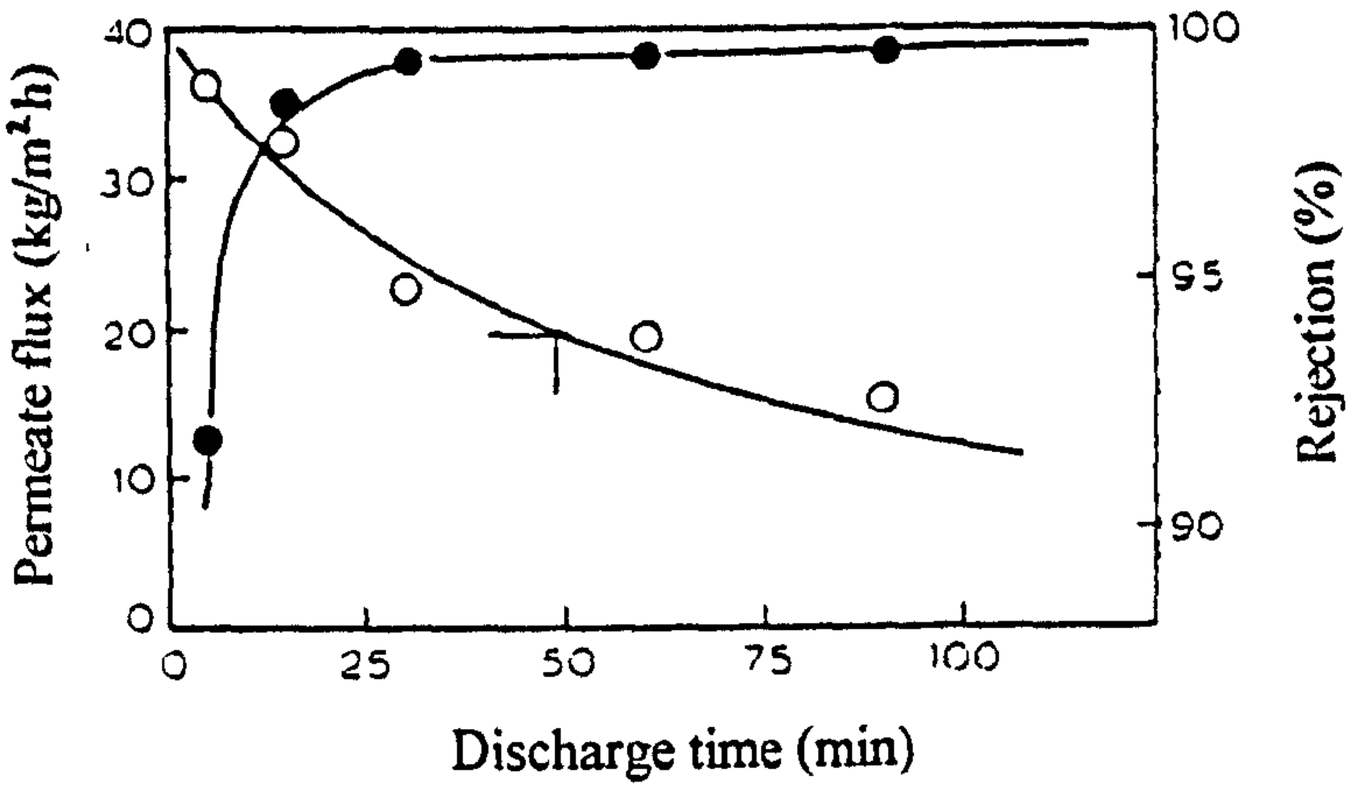

Figure 2.10: Flux and rejection behaviour of a 0.5 M sodium chloride solution [32]

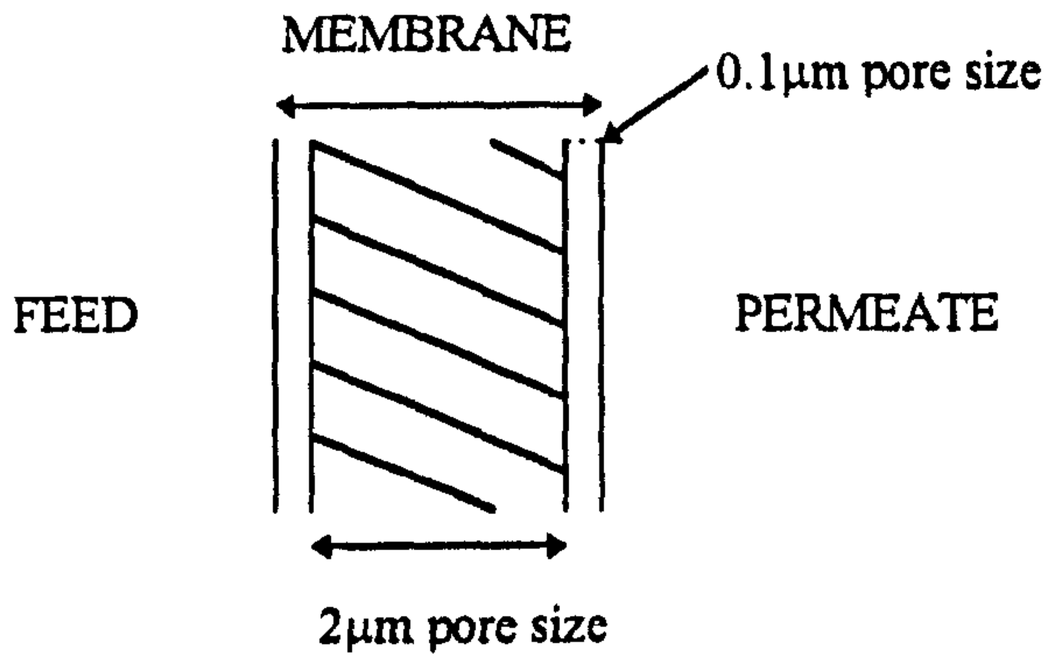

Figure 2.11: Possible membrane design for membrane distillation [16]

Elkina *et al* [33] have modified normal hydrophobic membranes, by forming a hydrophilic film on the surface. This introduces a diffusion step to the process, and enhances selectivity with volatile compounds, whilst maintaining dry pores in the hydrophobic part of the membrane.

Schofield *et al* [16] suggest a possible configuration for a membrane suitable for membrane distillation as shown in Figure 2.11. The membrane would be structured like a sandwich with a thick middle section between two thin layers. The middle section would have large pores of 2 μm, and the thin layers would have small pores of 0.1 μm. The thin layers are to satisfy the need for a high liquid entry pressure of water to maintain the hydrophobicity of the membrane. The whole membrane thickness would be around 500 μm to minimise the heat loss by conduction.

The choice of membrane is a compromise between high flux (thin membrane), and low thermal conductivity (thick membrane) [34].

2.5 Module Configurations

It is understood that the module orientation is important with membrane distillation. It is accepted that having the warm feed on the bottom of the module is best, as free convection of heat enhances the heat transfer rate [38]. Most studies have used flat plate membranes in their experiments, but some have also used hollow fibre membranes. A problem with hollow fibre modules is that as the feed solution travels along the module, the process of membrane distillation will cool the feed thereby reducing the temperature driving force. Work has been carried out in order to overcome this by using counter current flow [46], and Schneider *et al* [43] found that in turbulent flow, a single capillary in a tube suffered less than a 3°C drop in temperature from inlet to outlet.

Direct contact modules are best for membrane distillation as they allow better control of film heat transfer [5], although tubular and hollow fibre systems can show the least temperature polarisation [3]. The TPC can be maximised by arranging tubes in turbulent

flow, arranging fibres in laminar flow, reducing shell side voidage, or having a close packed bundle [47].

It is generally accepted that any membrane distillation system should incorporate a separate heat exchanger [48]. As membrane distillation utilises evaporation and condensation, it is very energy intensive and the heat exchanger would be used to recover and reuse energy. Another suggestion is that a heat exchanger is actually incorporated into the membrane distillation module [46]. For example, this can be achieved by using a spiral wound module that would be like a heat exchanger with the feed being heated through a metal wall by a hot stream and the permeate being cooled by a cold stream. This situation is shown in Figure 2.12. This configuration has the problem of not allowing the distillate to be pumped and so results in a decrease in the heat transfer [46].

The majority of the work carried out on direct contact membrane distillation using flat plate modules, has involved the use of a Lewis test cell (Figure 2.13) [4,23,35,37,39,44] which has stirring capabilities. Schofield *et al* used a thin channel device shown in Figure 2.14. Other flat modules, of the type shown in Figure 2.15 were used by Ortiz de Zarate *et al* [9,15], Ohta *et al* [28,29], and Sarti *et al* [36]. The other type of modules used were of the hollow fibre type [1,11,12,14,18,43,45,48], shown in Figure 2.16. In Figure 2.16, the feed is shown to pass through the shell, but the arrangement could be switched and have the feed flowing through the fibres. Having the fibres twisted or braided, instead of straight, produces more uniform flow in the module and allows for any thermal expansion of the membranes [43].

Overall, the Lewis cell is only suitable for laboratory scale work, but the principles involved can be used in developing larger modules by taking account of variations along the length of a module by boundary layer analysis. The other module types, at the current time, all have similar capabilities of performing membrane distillation.

2.6 Applications

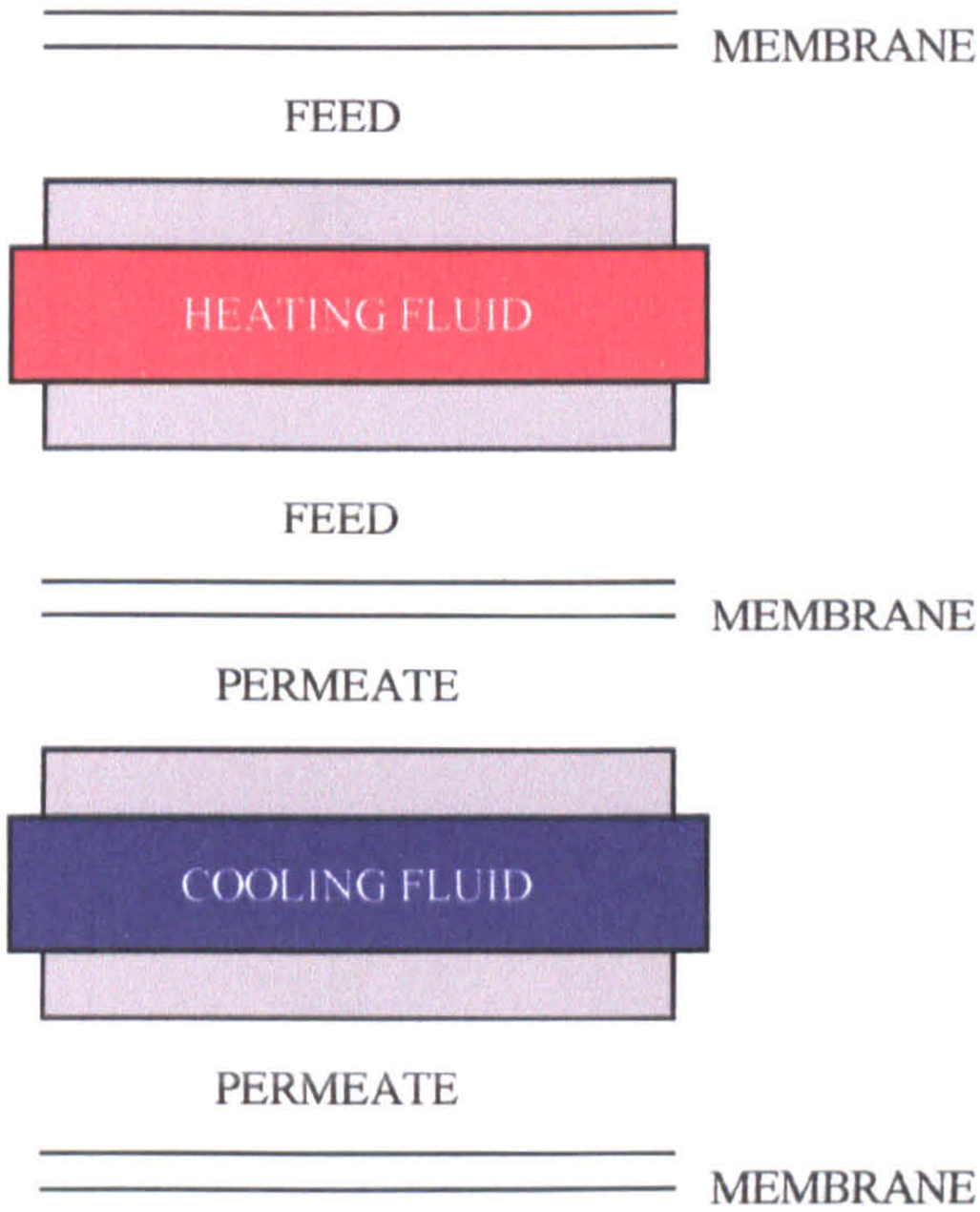

Figure 2.12: Spiral wound membrane distillation module

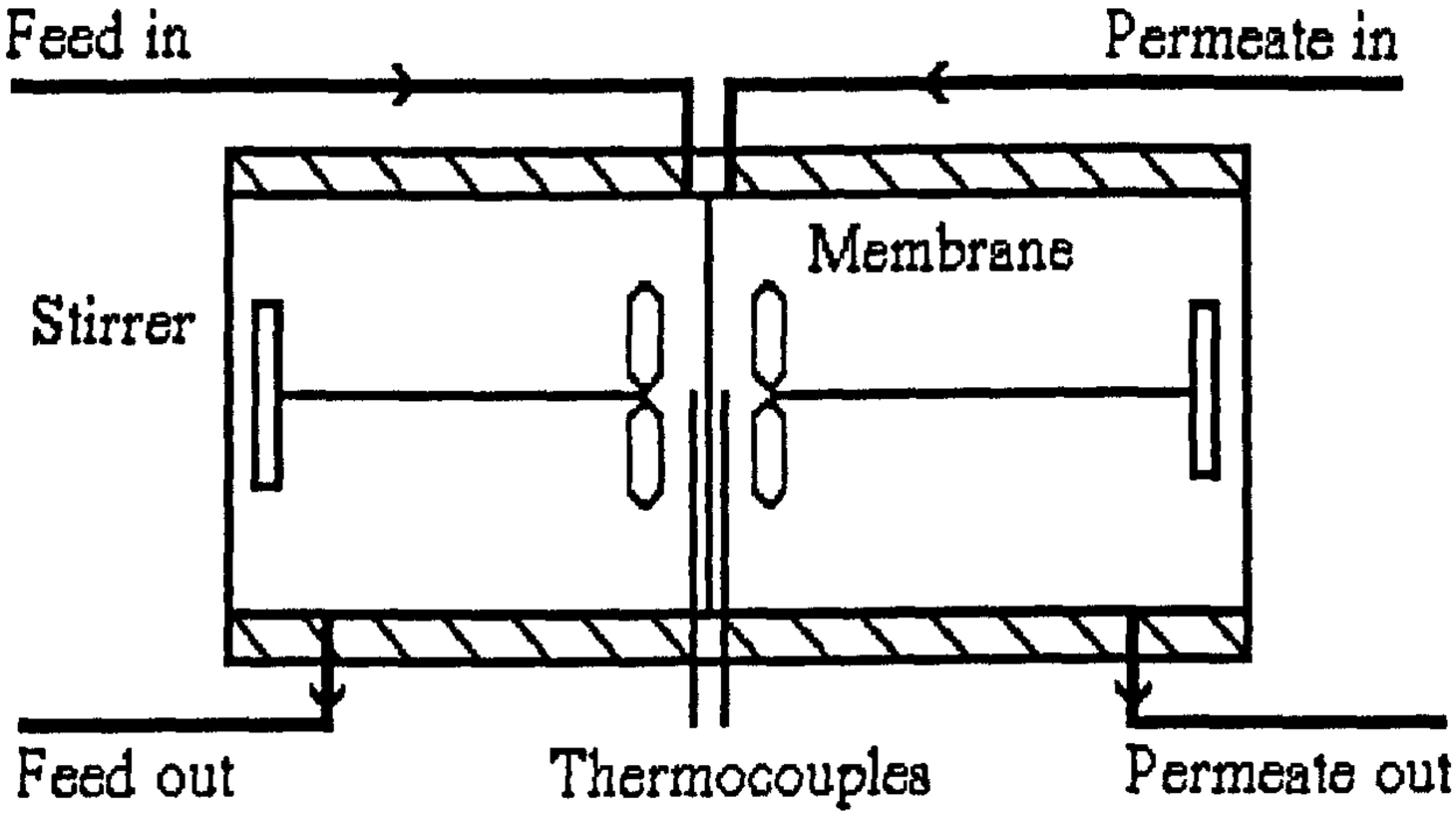

Figure 2.13: A Lewis Cell

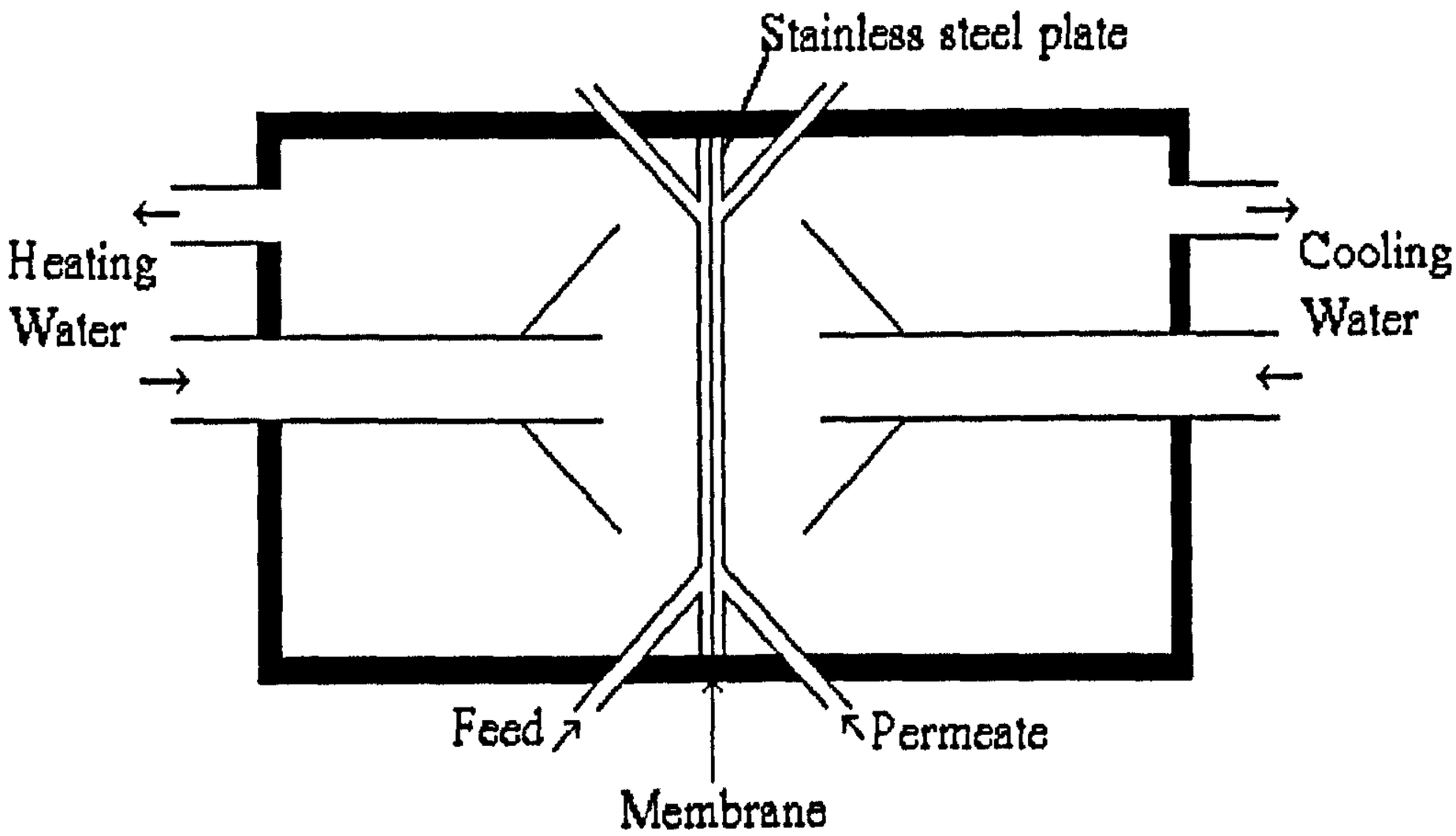

Figure 2.14: A Thin channel module

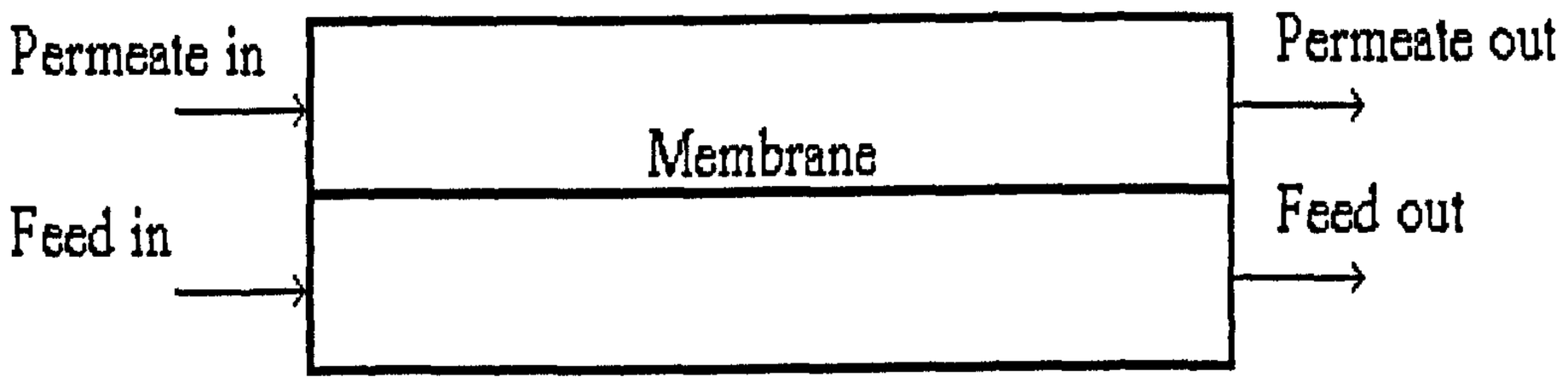

Figure 2.15: Basic flat plate direct contact module

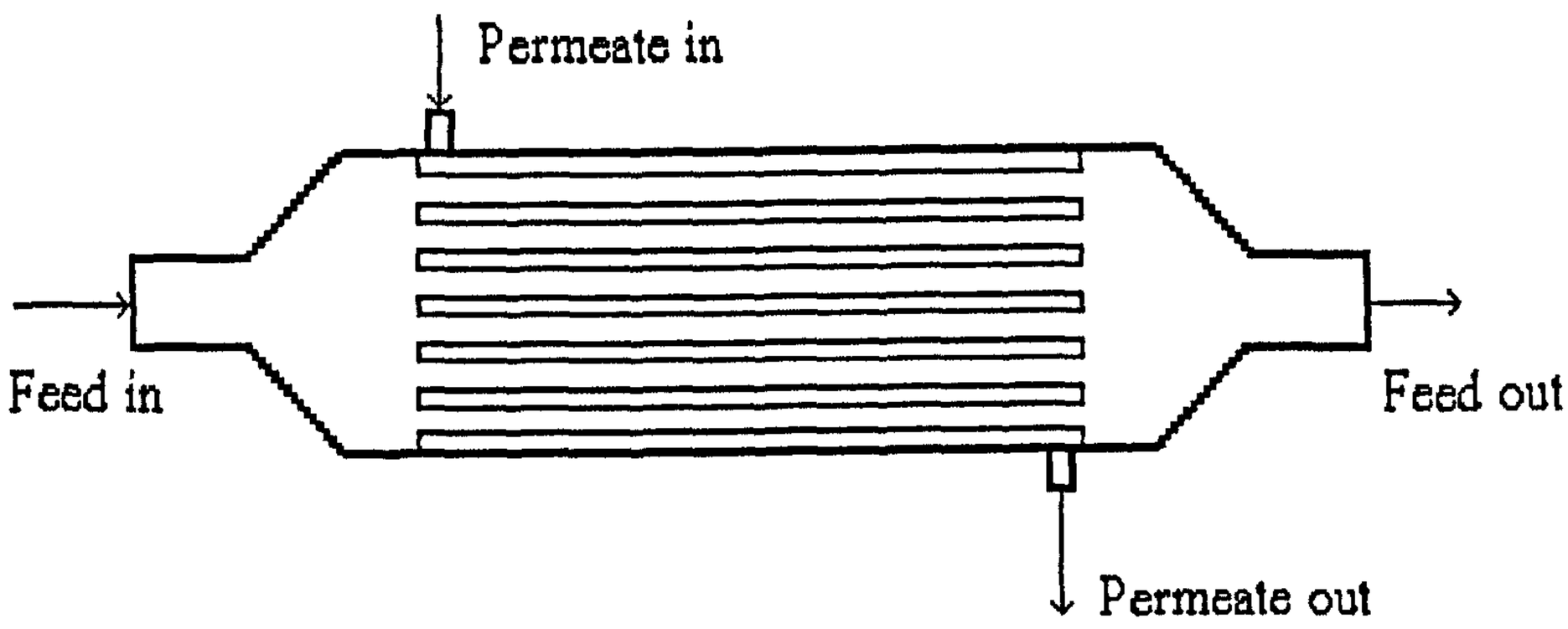

Figure 2.16: A hollow fibre module

There are a number of applications for membrane distillation, but the main ones are for the purification and reclamation of water.

Desalination has been the main application with various studies looking at the effectiveness of membrane distillation both at the laboratory and pilot scale [5,28,29,36,41]. Hogan *et al* [48] built a pilot plant for desalination by membrane distillation, and incorporated energy savings by collecting power from solar panels for use in heating the feed. As salt water usually contains small particles that could foul the module and membrane, the water has to go through some form of pretreatment before entering the membrane module. One type of pretreatment involves sand filters which remove the small particles by passing the water through beds of packed sand, and therefore control fouling [28]. Schneider *et al* [43] state that at the moment, membrane distillation will not be able to compete with the current large scale multi effect evaporation units used for desalination. The evaporators are just large containers in which the solution is heated a number of times by increasing temperature and/or decreasing pressure, and the resulting vapour being removed. Membrane distillation would be competitive if waste heat generated on a plant is used [43]. Lawson [49] states that well designed membrane distillation systems achieve fluxes of up to 75 kg/m^2h which are comparable to those of reverse osmosis.

Production of ultrapure water is an extension of desalination [3,14] as the permeate product is very pure and is suitable for use in the medical and pharmaceutical sectors.

Utilising membrane distillation to effectively manage effluent streams from processes is another viable option. The process has been used to separate and recover chemicals, such as non-volatile salts [14,41], taurine [45], sodium chloride [45], dyes [11], and volatile solutes such as acids [50,51,53].

Fujii *et al* [53] looked at the removal of low concentration organics from water. These types of separations are possible, but only at low concentrations because of membrane wetting (Section 2.8). For example, a 5% ethanol/water solution was separated by membrane distillation with the flux obtained having been 0.7 kg/m^2h.

Tomasewska [50,51] studied a range of acid separations/concentrations, of which the latest are fluosilicic acid, and hydrochloric acid. Membrane distillation has been been

shown to achieve the required separation between both acids and water. A sharper separation can be achieved if an iron salt is added to volatile feed solutions [50].

A new application for membrane distillation is for removing water from azeotropes. Azeotropes occur when the vapour liquid equilibrium crosses and no further separation by normal distillation is possible. Membrane distillation, like pervaporation, would remove the need for an entrainer which is required in conventional azeotropic distillation. Udriot *et al* [42] looked at using membrane distillation for separating the propanoic acid/water azeotrope. This is possible as membrane distillation, although controlled mainly by the vapour/liquid equilibrium, can be influenced by differences in relative rates of diffusion through the gas filled pores. The low diffusivity of the heavy propanoic acid molecules, relative to water, reduces its apparent volatility compared to what it really is according to vapour liquid equilibrium. The effect of diffusion on the vapour/liquid equilibrium is shown in Figure 2.17. Complete azeotropic distillation is not possible using membrane distillation, but mixtures containing large amounts of water can be separated to above and below the azeotropic point.

Another application of membrane distillation is for concentration of the feed. The majority of concentration applications are for the food industry, where membrane distillation has been used to concentrate, orange juice, milk, sugar, and gelatine [42]. Currently, multistage vacuum evaporation is the most widely used technology for these separation processes, but the product loses flavour and colour, and the concentrate can acquire a cooked taste [8]. Membrane distillation is good for concentrating the above mentioned food products as they are susceptible to temperature, and by using a low temperature process such as membrane distillation, it is possible to maintain their flavour and structure.

A specialist application is for the nuclear industry. Chmielewski and Zakrewska-Trznadel [25] successfully enriched deuterium and $oxygen_{18}$ from water and achieved higher separations than obtained with normal fractionation.

Membrane distillation becomes more viable when linked with another membrane process, for example a reverse osmosis pre-concentrator [11]. An ultrafiltration unit also could be used for heavy fouling feeds to remove the larger particles that could increase the

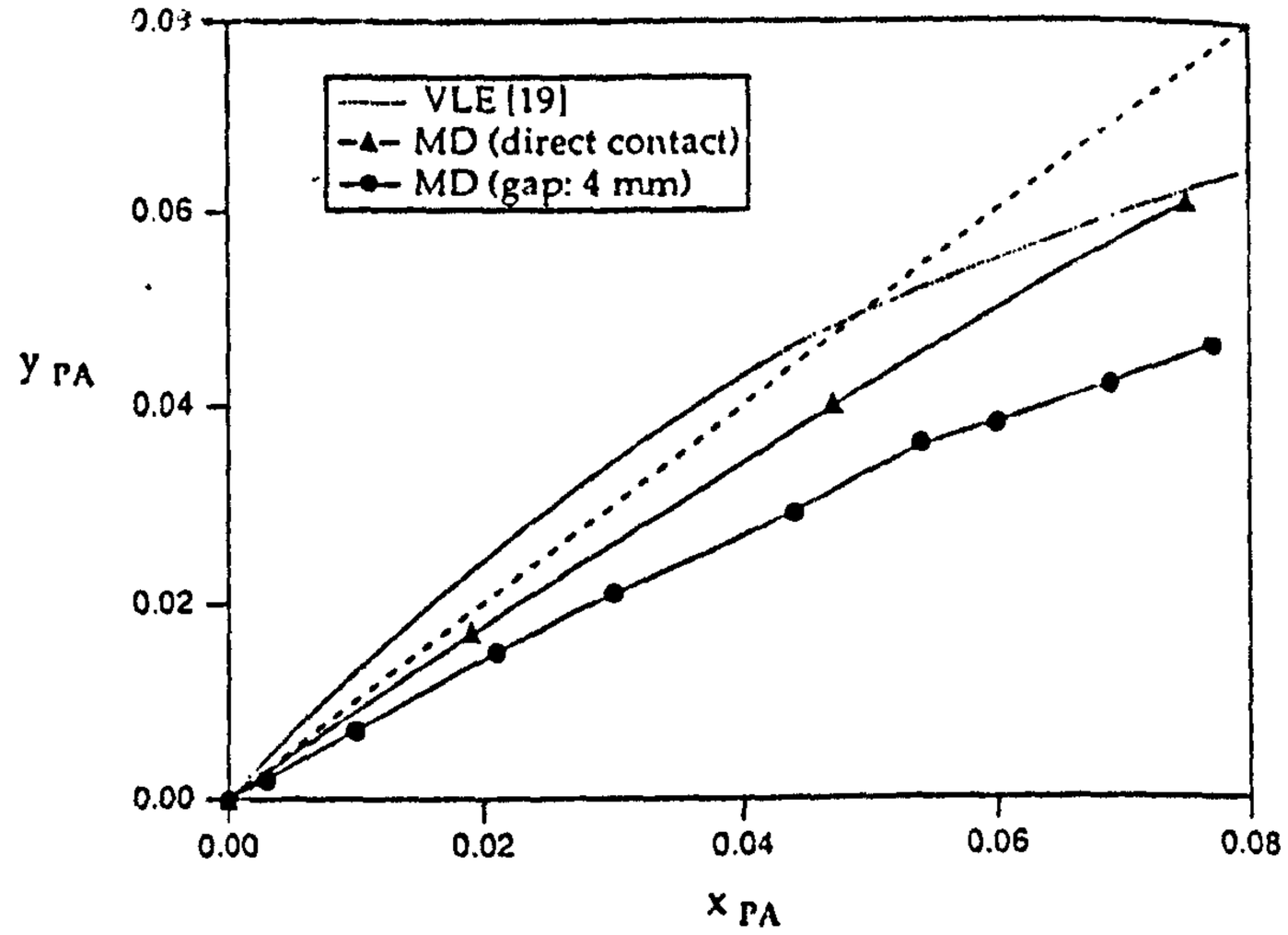

Figure 2.17: Vapour-liquid equilibrium diagram for membrane distillation of propanoic acid/water mixtures [42]

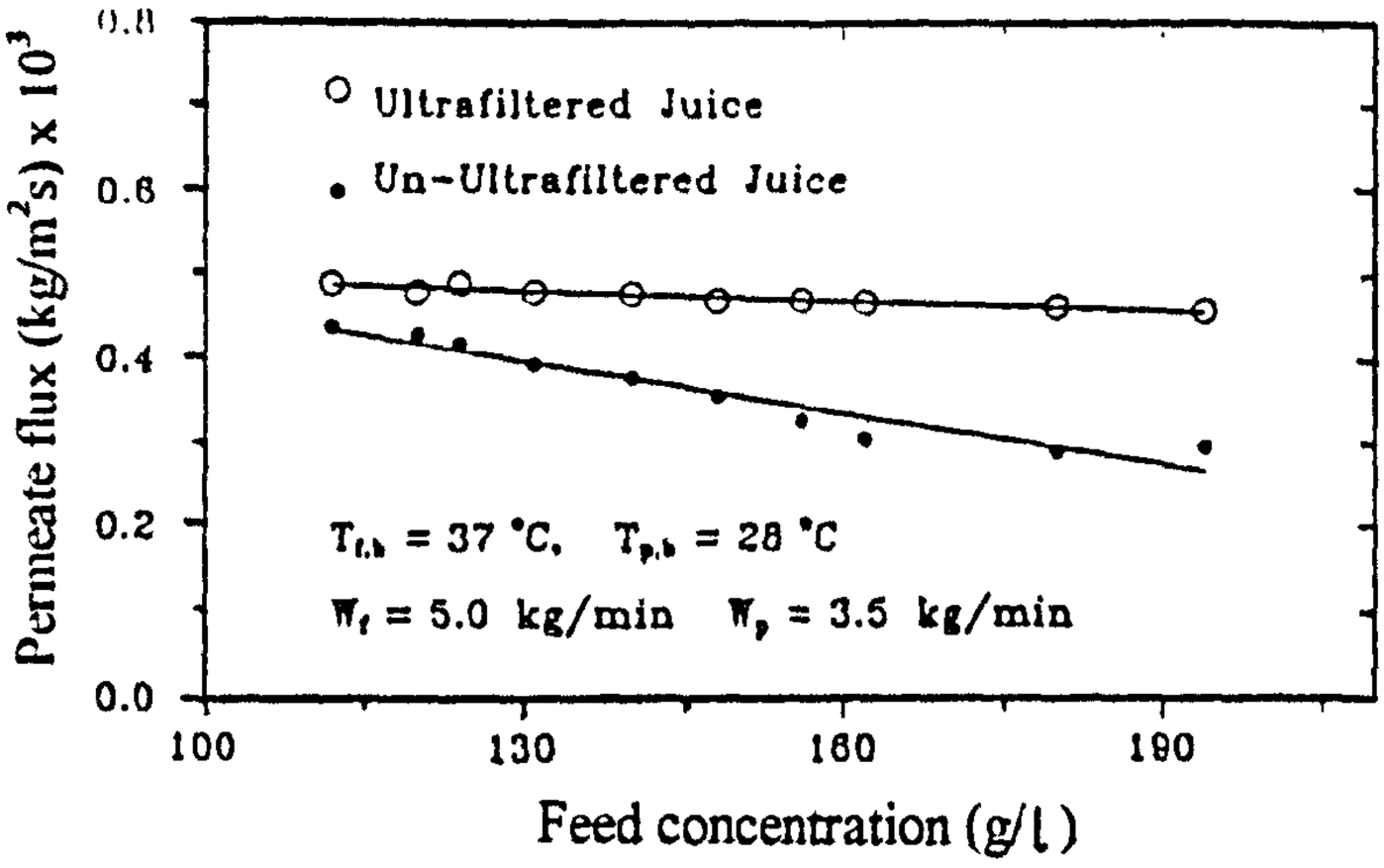

Figure 2.18: Permeate mass flux vs feed concentration, with and without ultrafiltration pretreatment [8]

viscosity of the stream through the membrane distillation unit [8]. An example of the effectiveness of using ultrafiltration pretreatment is given in Figure 2.18 for orange juice, and shows that the ultrafiltration results in the flux remaining almost constant in the membrane distillation unit. Membrane fouling can be a severe problem with food concentrations. Calabro *et al* [8] studied the concentration of orange juice using membrane distillation and managed to restore the initial flux after cleaning the membrane with either sodium hydroxide or hydrochloric acid.

In summary, there are a wide range of applications for which membrane distillation is suitable. They can be split into three groups. The first is where the permeate is the product, for example desalination and water reclamation. The second is where the concentrated feed is the product, for instance food stuffs like orange juice. The final group involves separations when, both feed and permeate are useful products, for example, azeotropic separation.

2.7 Experimental Work

Various experiments have been carried out in order to investigate the effectiveness of membrane distillation. These can be split into two groups. The first uses either pure water or a sodium chloride solution as the feed, and are concerned with the basic process trends of membrane distillation. The second group uses different types of feeds and are concerned with specific applications for the process.

Group one type experiments are the most extensive, and have been investigated by Schofield *et al* [5,17,48], Drioli *et al* [14,18], Ortiz de Zarate *et al* [9,15,23,35,54], as well as many others [28,29,36,41]. A review of the experimental conditions used for these experiments can be found in Table 2.3.

These experiments have allowed the investigation of the effect of the operating conditions on membrane distillation, and a number of trends have been found to exist. The trends are shown in Figures 2.19, 2.20, 2.21 and 2.22, and can be summarised in the following way,

Feed	Initial conc. (M)	Feed Temp. (°C)	Permeate Temp. (°C)	Stirring rate (rpm)	Temp. diff.	Max. flux (kg/m^2h)	Ref.
Water	n/a	25-90		n/a	10-55	40	17
Water	n/a	45-50	40-45	0-360	5		15
Water	n/a	40-50	10-20	0-350	30	72	23
Water	n/a			200	5-20	45	34
Water	n/a	65-75	25-35	n/a	0-30	7.2	37
Water	n/a	30-70	20-60	150-350	10	14.4	4
Water	n/a	50	20	n/a	30	6.2	25
Water	0-5			50-350	0,6	7.2	36
NaCl	0-2.5	61,71,81	21	n/a	41,51,61	60	5
NaCl	0-5.3	30			10-15	5	48
NaCl	0.05-0.5	50		n/a	5,9.5	1.7	14,18
NaCl	0.1-0.3	40-50	10-20	0-350	30	16mol/s	9,23
NaCl	0-4			0-300	5-30	11.8	13
NaCl		40-60	20-40	n/a		4	28,29
NaCl	0-0.9	40-70	20-50	n/a	0-20	0.72	35
NaCl	0-5			50-350	0,6	6.5	36
NaCl	1-2 wt %	50,60	20	n/a	30,40		38
NaCl		35	25	n/a	10	4.5	39
NaCl	0.5	65-75	25-35	n/a	0-30	5.5	37
NaCl	0-30 wt%	100	42	n/a	30-60	9	43

Table 2.3: Experimental conditions used for basic research of membrane distillation

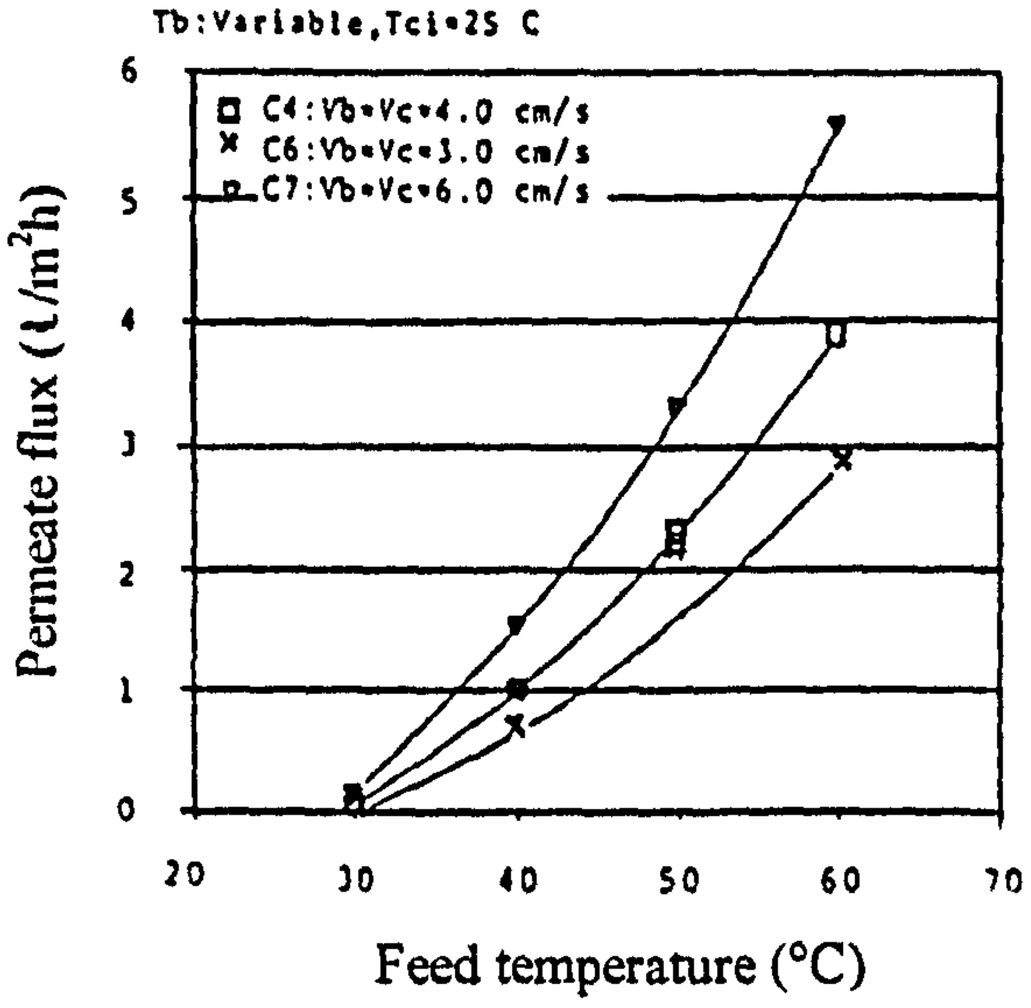

Figure 2.19: Variation of flux with feed temperature [28]

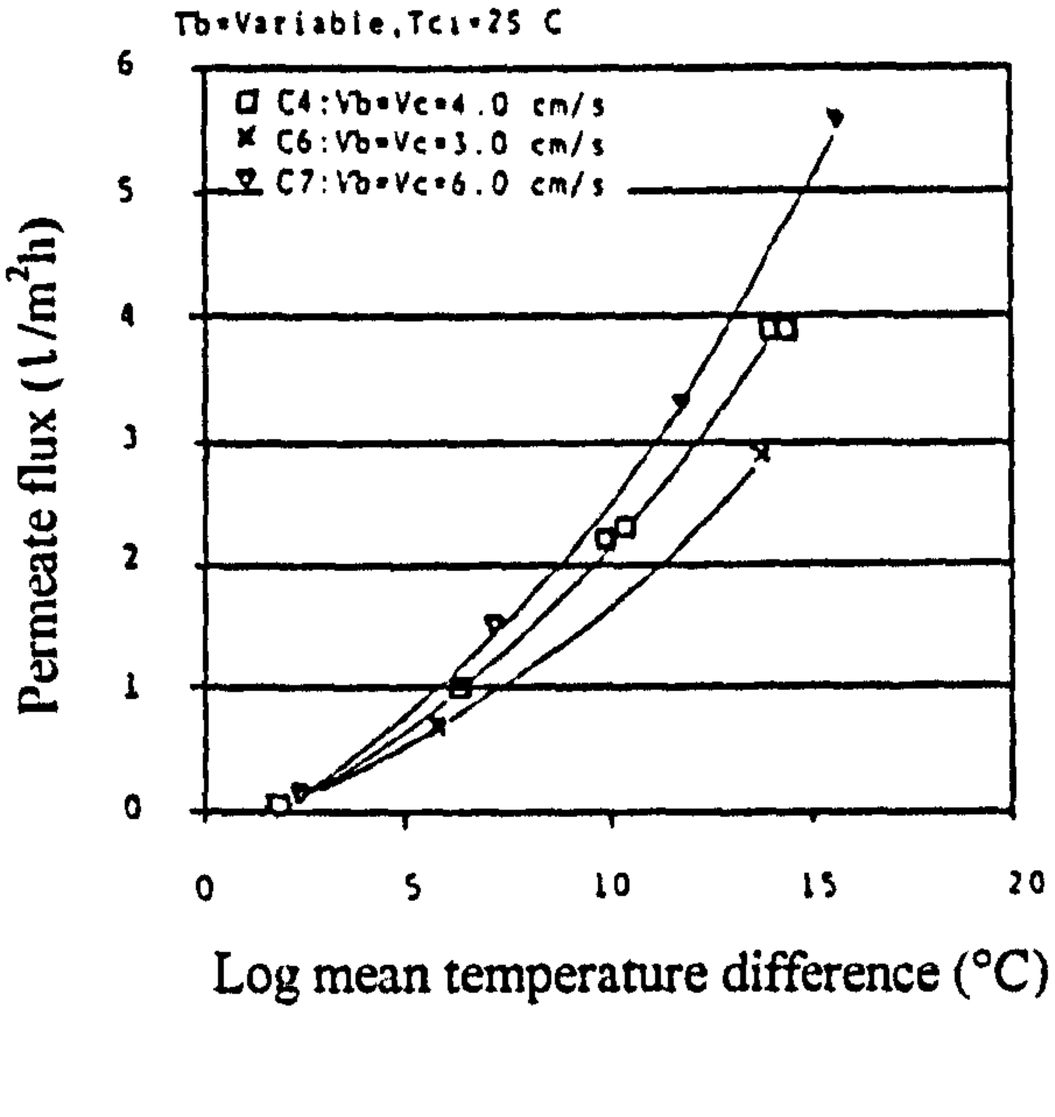

Figure 2.20: Variation of flux with temperature difference [28]

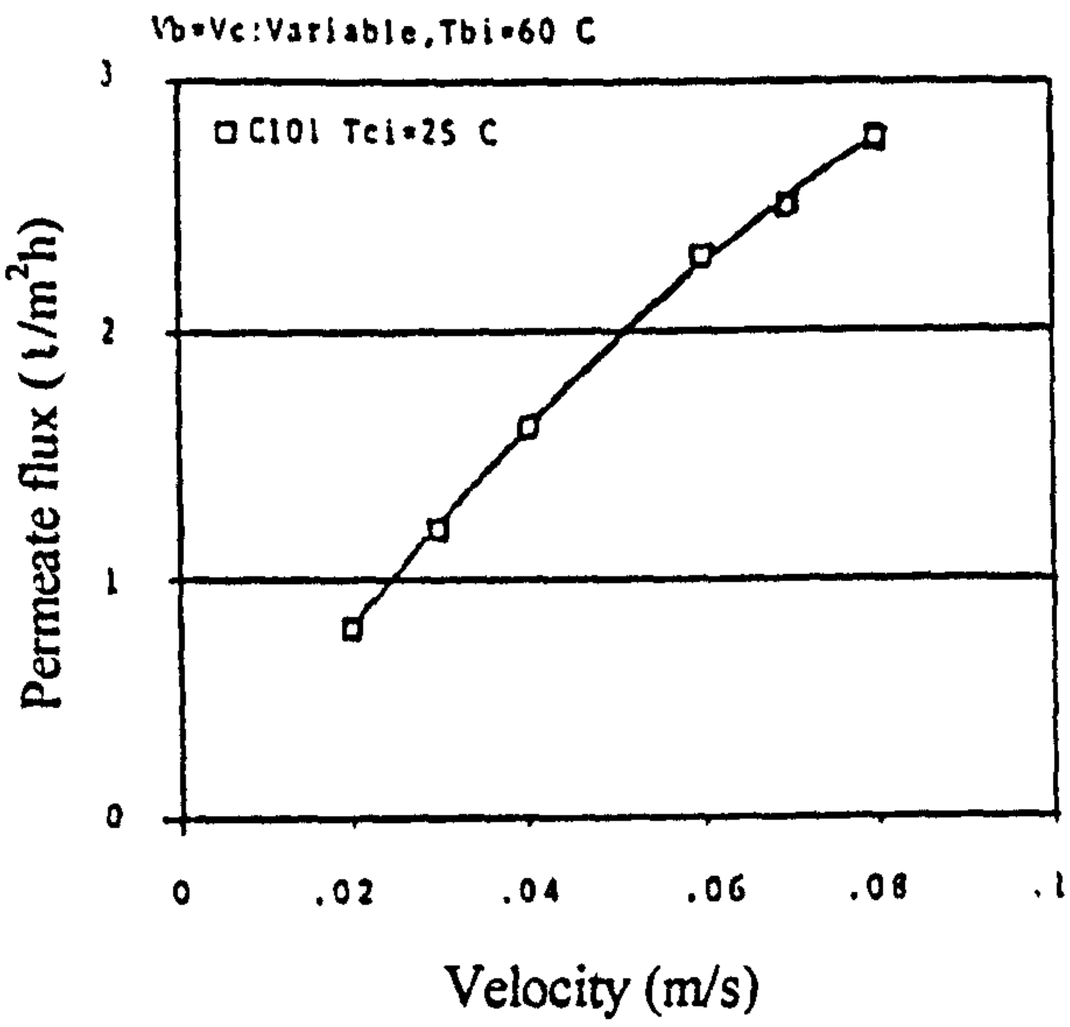

Figure 2.21: Effect of flow rate on permeate flux [28]

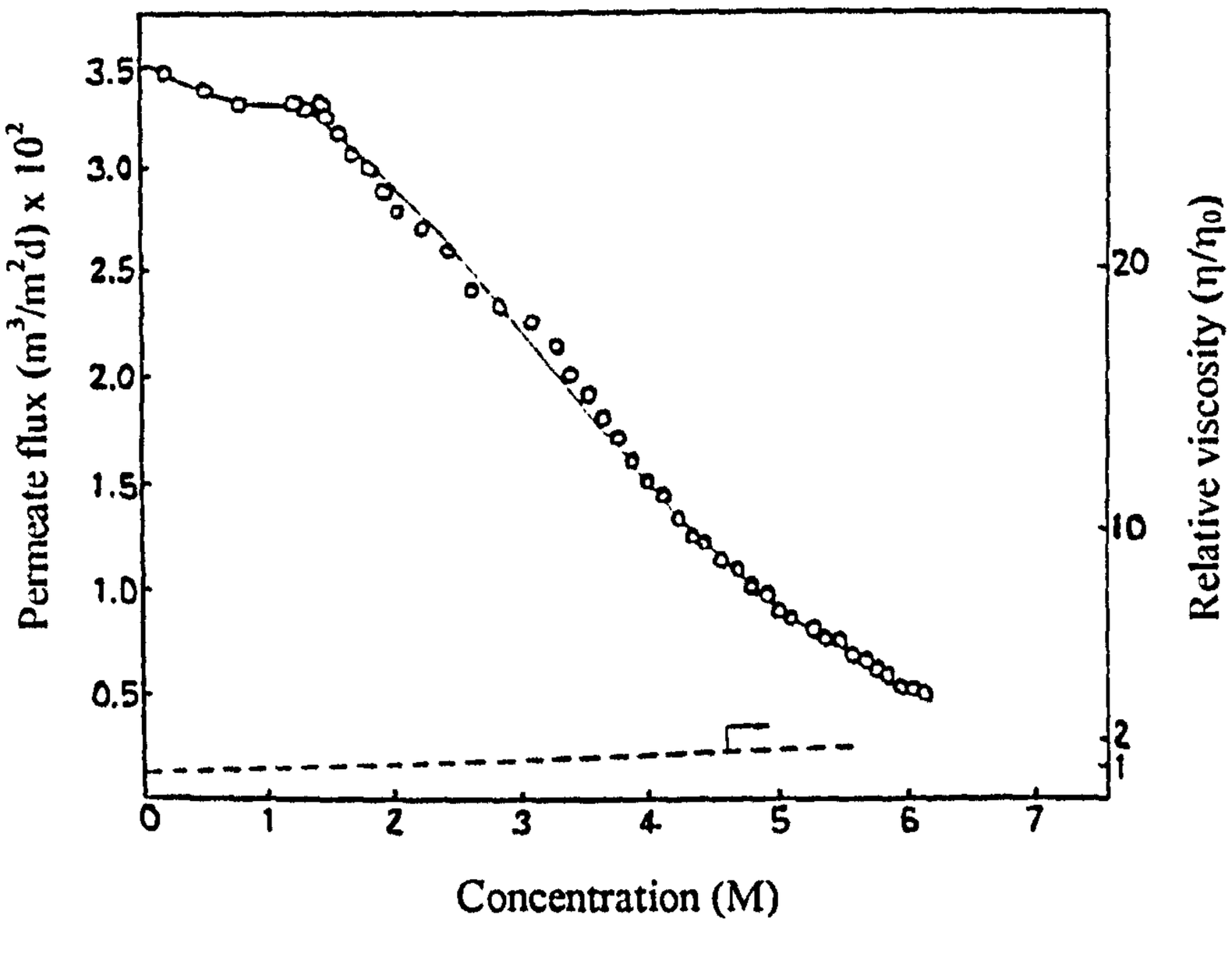

Figure 2.22: Variation of flux of a NaCl solution with concentration [18]

i) flux increases with increasing feed temperature,

ii) flux increases with increasing temperature difference across the membrane,

iii) flux increases with increasing fluid flow past the membrane surface and,

iv) flux decreases with increasing feed concentration.

Other trends found include that dearation increases flux by roughly 50% [5], increasing the stirring rate produces higher fluxes with hotter liquids [23], and flux increases with decreasing membrane thickness [46]. Also, as the hot and cold side heat transfer coefficients increase, flux increases and, as the membrane area increases, flux decreases due to closer temperature differences across the membrane [17]. Drioli *et al* [1] found that generally, as the porosity of the membrane increased, the flux increased.

Of course, not every situation for which membrane distillation is possible utilises just water and sodium chloride as feed solutions. Recovery of taurine from waste water was studied by Wu *et al* [45], who discovered that as the solids content in the feed approached 35%, then the flux was reduced to zero, but precipitation of taurine was obtained at temperature differences across the membrane of 12°C and higher. Recovery of blue and red dyes was the subject of an investigation by Calabro *et al* [11], where the rejection of the dye by the membrane was basically 100%. Van Gassel and Schneider [46] found that a slight reduction in the pressure on the permeate side increased the flux through the membrane, by increasing convective transport. A full list of specific feed solutions can be found in Table 2.4.

2.8 Membrane Wetting

Membrane wetting is a serious problem in membrane distillation as the process relies on the pores of the membrane being filled only with vapour. This means that the membrane must be highly hydrophobic and the wetting power of the liquids low [10]. Wetting causes membrane distillation to slow down, and in the worst cases, halt due to a liquid flux occurring in the liquid filled pores, in opposition to the vapour flux through the

Feed	Initial conc. (M)	Feed Temp. (°C)	Permeate Temp. (°C)	Stirring rate (rpm)	Temp. diff.	Max. flux (kg/m^2h)	Ref.
Glucose	0-5.3	30			10-15	5	48
Glucose	10, 30 g/l	50		n/a	4.5,8.5	5	1,14,18
Sucrose	0-5	61,71,81	21		41,51,61		5
NH_3Cl	0.1-0.5	40-70	20-50	n/a	0-20	0.36	35
Sulphuric acid	12 wt %	60	30	n/a	30	12.5	38
Sulphuric acid	10 wt%	60	20	n/a	40	12.5	12
HCl	0-30wt %	60	20	n/a	40	10.5	12
Citric acid	12 wt %	55	25	n/a	30	10.4	12
$NiSO_4$	0.1	40,50,60	15	n/a	25-45	18.7	6
$NiCl_2.6H_20$	0.1	40,50,60	15	n/a	25-45	18	6
$Ni(NO_3)_2.6H_2O$	0.1	40,50,60	15	n/a	25-45	20.1	6
Ethanol/water	0-7 wt %	30-60	0-20	n/a	10-40	4.7	19
Propanoic acid/water		60	30	n/a	30	22.1	41
Ethylene glycol		65	25-45	n/a	20-40		52
Gelatine	3-10 wt%	90	20	n/a	55-70	50	43
Orange juice	108-300g/l	25-45	20	n/a	5-25	10.8	8

Table 2.4: Experimental conditions used for specific solutions

vapour filled pores. Once the membrane is wetted, some pores will always contain liquid, and an hysterisis type effect has been noticed by Mengual *et al* [35]. Membrane wetting can occur due to various operating conditions. Repeated heating and cooling tend to wet the membrane [1], as do feeds containing organics [10], and membranes also become less hydrophobic with use [35]. The main reason for membrane wetting is the pressure of liquid on the feed side of the membrane. For a given pore size, there is a critical penetration pressure, above which the liquid will penetrate the membrane [1]. This pressure is known as the liquid entry pressure of water, LEPW. The mechanism for membrane wetting is that water enters the larger pores of the membrane by osmotic pressure, breaking the surface tension at the interface between liquid and vapour on the membrane surface [1]. The relationship between the pore size and pressure, given by the Kelvin Law [1] is,

$$P = 2\sigma \frac{\cos\phi}{r} \qquad (2.42)$$

Schofield *et al* [47] state that pore sizes must be less than 0.5μm to avoid wetting. For feed pressures greater than the LEPW, the relation between hydraulic flux and pressure depends on the degree of wetting [35].

Organics have the effect of reducing the LEPW. Water, and solutions of inorganics have high surface tensions (>72×10^{-3} N/m), but when organics are present, the surface tension falls rapidly until a critical value is reached. The membrane is then fully wetted and membrane distillation is no longer possible [10]. For example, Gostoli and Sarti [19] found that for mixtures of water and ethanol, the LEPW decreased linearly with ethanol concentration until the membrane was freely wetted at an ethanol concentration of 75wt%. This is shown by Figure 2.23.

Franken *et al* [10] looked at methods for calculating the penetration surface tension. The penetration surface tension is the surface tension of the liquid on the verge of penetrating into the membrane. From comparing experimental results with theoretical calculations, it was discovered that contact angle measurements on homogeneous smooth materials were unsuitable for determining the possibility of membrane wetting occurring during membrane distillation. However, the wettability criteria determined by

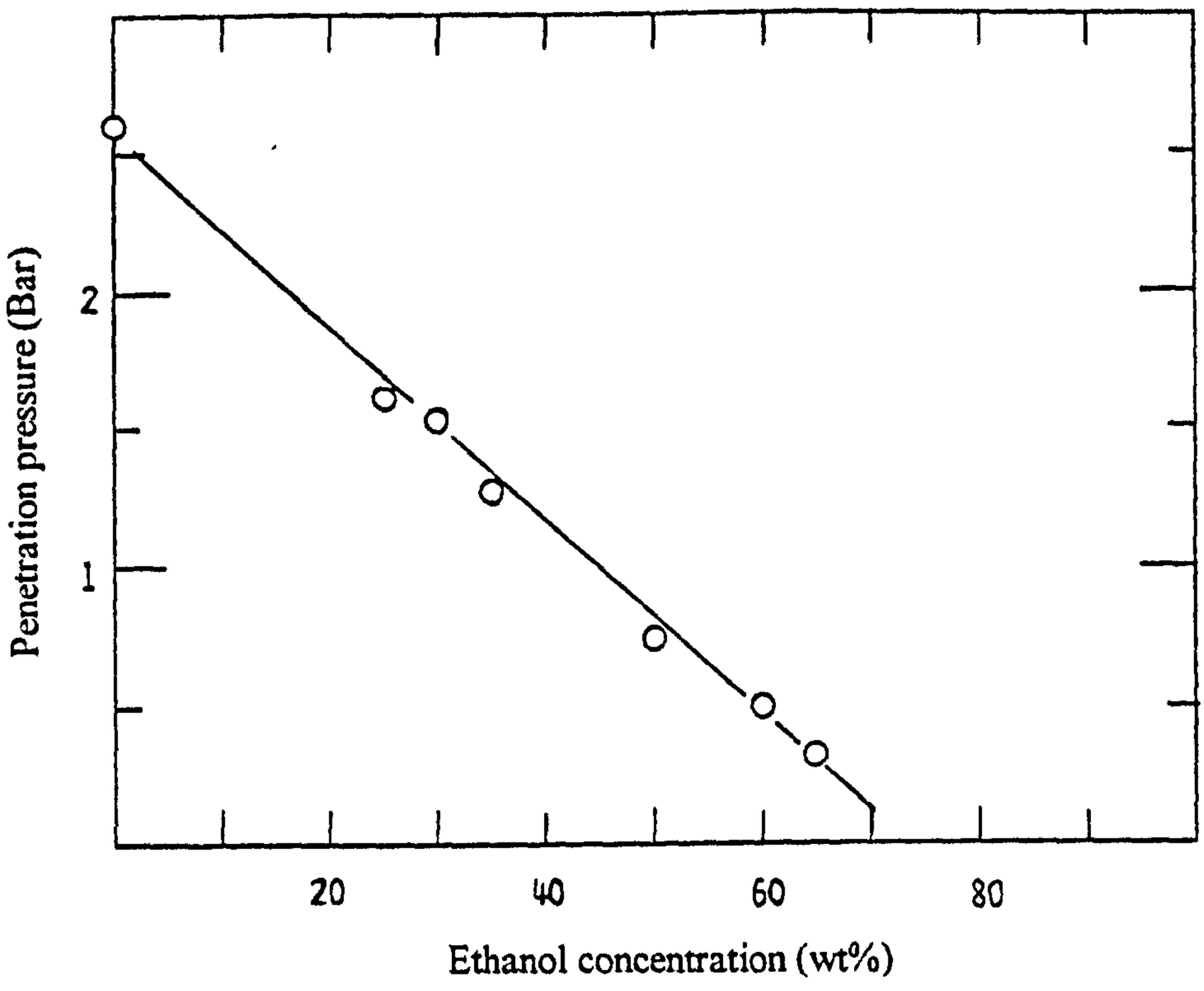

Figure 2.23: Minimum entry pressure of ethanol-water mixtures in a PTFE membrane, pore size = 0.2μm [19]

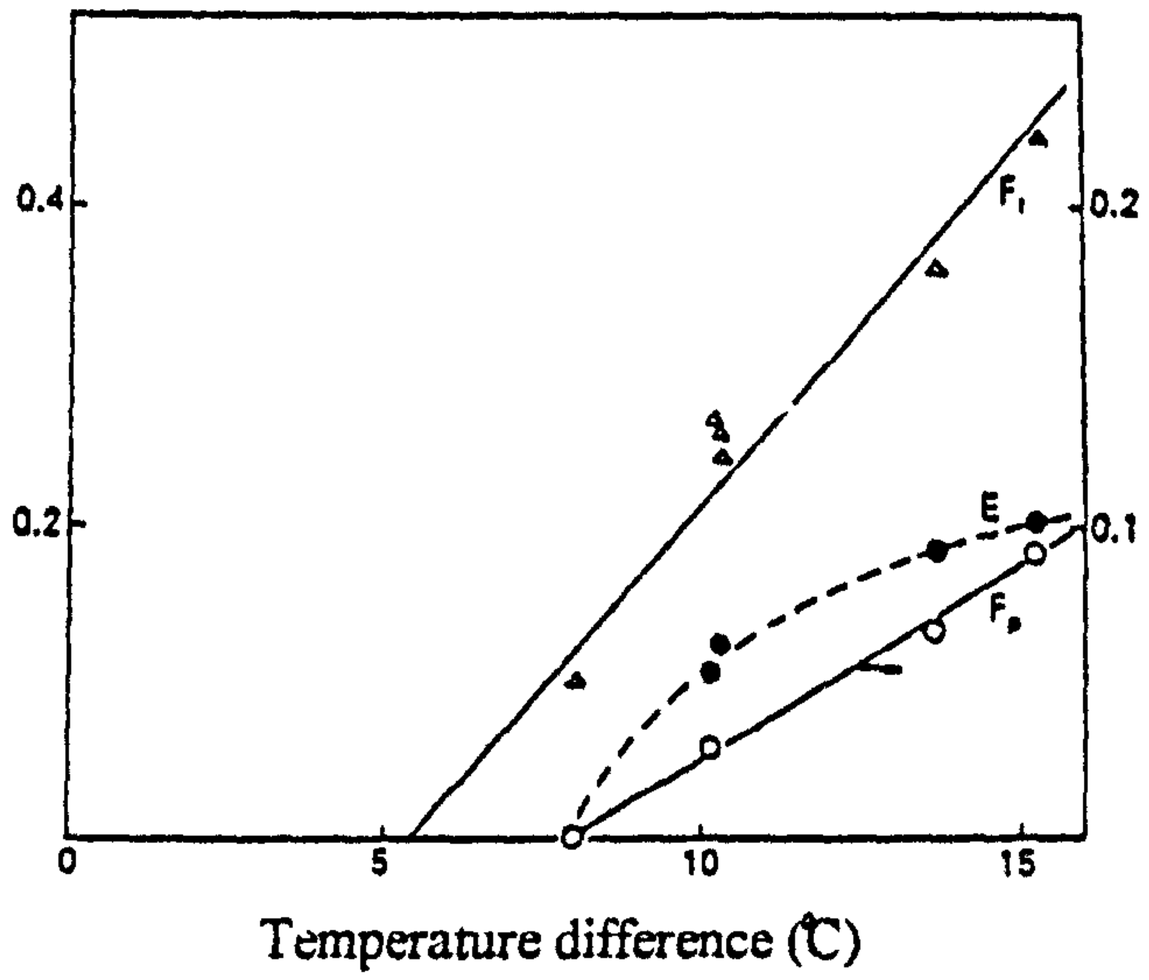

Figure 2.24: Distillation efficiency,E, and theoretical and practical transfer fractions, F_t and F_p as functions of temperature difference in the membrane distillation of 5.3M NaCl solutions [18]

the penetrating drop method showed a good agreement with the calculated values of the critical penetration surface tension. The penetrating drop method is where a droplet is brought into contact with the membrane. By trials with narrowing series of solution compositions, the composition of a liquid mixture on the verge of penetration into the membrane can be found. The surface tension belonging to this composition is the critical penetration surface tension. However, the maximum allowable concentration of organic material in water cannot be calculated and has to be determined for each organic [10]. The next stage of their work will concern the effect of the structure of the membranes on membrane wetting.

Lawson *et al* [55] have also conducted research on membrane wetting, and have looked at the effect of membrane compaction and permeability on wetting. Membrane compaction is usually neglected for most membrane processes, but this cannot be done for membrane distillation as the thickness of the membrane is an important consideration for the process. To compact the membrane in membrane distillation, the feed pressure can be increased, which increases the permeability and reduces the thermal energy requirement, without affecting the temperature driving force. Lawson *et al* [55] made certain assumptions about the effect of compaction. These are that porosity decreases while the volume remains constant, $r\varepsilon/\chi\delta$ decreases with decreasing porosity, and χ increases, it never decreases. The actual increase in flux caused by compaction is more than that calculated theoretically because of the three assumptions made, so further work is required. The results obtained show that permeability can increase up to 11% with membrane compaction.

2.9 Energy Analysis

Membrane distillation is energy intensive, and so heat economy is a most important issue [41]. Energy recovery, up to 75%, can be achieved by heat exchange between the feed and warmed distillate in counter-current flow [47].

Zotolarev *et al* [6] carried out a preliminary economic analysis which showed that under some conditions membrane distillation is competitive with reverse osmosis for production of distilled and potable water, but the exact conditions were not specified. The possibility of using solar and geothermal energy, or existing low temperature gradients available in industry is attractive, and was used by Hogan *et al* [48]. Jonsson *et al* [20] suggested that as membrane distillation requires the same heat addition for evaporation as a conventional one stage evaporator, low grade, or waste heat should be used.

The advantage of membrane distillation is the ability to recover latent heat for re-use [48]. Ohta *et al* [28] looked at the amount of heat brought into a membrane distillation system, and the heat actually used for the evaporation of the feed, and derived equation (2.43) for the thermal efficiency.

$$thermal\ \ efficiency\ \ \% = \frac{effective\ \ heat\ \ for\ \ evaporation}{heat\ \ input\ \ excluding\ \ emanation\ \ heat} \qquad (2.43)$$

The effective heat for evaporation is found from the permeate flux. The emanation heat is a loss that emanates from outside the module. An increase in flow rate does not increase the thermal efficiency very much. However, a higher feed temperature does result in a significant rise in the thermal efficiency. Efficiencies of up to 40% were calculated [29]. An expression for efficiency similar to that given by Ohta *et al* [28] was given by Calabro *et al* [11],

$$e = \frac{NA\lambda}{mC_p(T_{in} - T_{out})} \qquad (2.44)$$

Equation (2.44) shows that to increase the efficiency, the driving force must be increased. This can be accomplished, at constant feed temperature, by reducing the permeate temperature. This increases the temperature difference, improves the flux, but does not increase the amount of heat supplied in the feed. The efficiency has been increased from 8 to 14% by this method.

Wu and Drioli [18] defined a distillation efficiency for membrane distillation where,

$$e = \frac{F_{pr}}{F_{th}} \qquad (2.45)$$

F_{pr} is the practical transfer fraction,

$$F_{pr} = \frac{NA}{m} \tag{2.46}$$

and F_{th} is the theoretical transfer fraction,

$$F_{th} = \frac{P_H - P_C}{P^0} \tag{2.47}$$

F_{pr} and F_{th} are both proportional to the temperature difference, and F_{pr}, F_{th}, and e, all decrease with increasing concentration. The outcome of their work was that for solutions other than pure water, there was a certain temperature difference which had to be satisfied for membrane distillation to occur. For example in Figure 2.24, for 5.3M sodium chloride, F_{th} is 0 at ΔT equal to 5°C, and F_{pr} is 0 at ΔT equal to 8°C. These temperature differences had to be satisfied before the module could arrive at its normal distillation efficiency as given by equation (2.45).

In terms of modules, larger membrane surface areas and lower flow rates increase the contact time in the module, which gives closer approach temperatures and therefore more recoverable heat [48]. For hollow fibre modules, the flow regimes are important. For instance, for the shell side between the membranes and the module wall, it is better to have laminar flow than turbulent [47]. There should also be a balance between low liquid velocities and long flow passes, i.e. membrane length, to keep cost and pressure drop down, and to produce high fluxes [41].

Schofield *et al* [17] suggested various methods to minimise the heat lost by conduction across the membrane. The first was to increase the thickness of the membrane, which lowers the heat lost by conduction, but also affects the latent heat, therefore the overall effect is negligible. The situation might be different for feeds containing solutes. Another suggestion was to introduce an air gap, which would act as an insulating layer, but this could reduce the flux due to the lengthened diffusion path. The final suggestion was dearation, which would increase the latent heat. Normal heat loss in a membrane distillation module is 20-40% of the heat input. Dearation could reduce this to less than 10%.

Schofield *et al* [17] found that the energy cost of membrane distillation falls with increasing temperature as shown in Figure 2.25. For example, at 90°C, the cost could be as low as $2/tonne, using the heat recovery system shown in Figure 2.26.

2.10 Osmotic Distillation

Osmotic distillation is very closely related to membrane distillation. Instead of having a thermal vapour pressure driving force, osmotic distillation has a concentration driven vapour pressure driving force, i.e. a change in apparent osmotic pressures [56]. The typical trends for osmotic distillation are the same as for membrane distillation, but there is no temperature gradient required to produce the vapour pressure difference across the membrane. The process is suitable for concentration of heat sensitive feeds [54] and systems where product integrity and purity are important, i.e. the food and pharmaceutical industries [34].

The vapour pressure difference is obtained by a difference in the composition of the bulk phases adjoining the membrane. The process takes the advantage of the high osmotic pressure of a salt solution on the permeate side, to reduce the water vapour pressure according to [34],

$$\Pi = \frac{RT}{V} \ln \frac{P_w^0}{P_C^0} \qquad (2.48)$$

Osmotic pressures on the feed side decrease as the concentration increases [57]. The overall process is isothermal [54]. NaCl is usually used as the salt on the permeate side, as it is cheap and widely available, but higher osmotic pressures can be obtained using LiCl, $MgCl_2$, $CaCl_2$ or $MgSO_4$ [58].

Figure 2.27 shows a schematic of the process. The two heat fluxes are in opposition to each other, the opposite to that which is found in membrane distillation. Membranes should have high thermal conductivity to maximise the heat conduction through the membrane, Q_v, and should be thin to promote higher vapour flux [34].

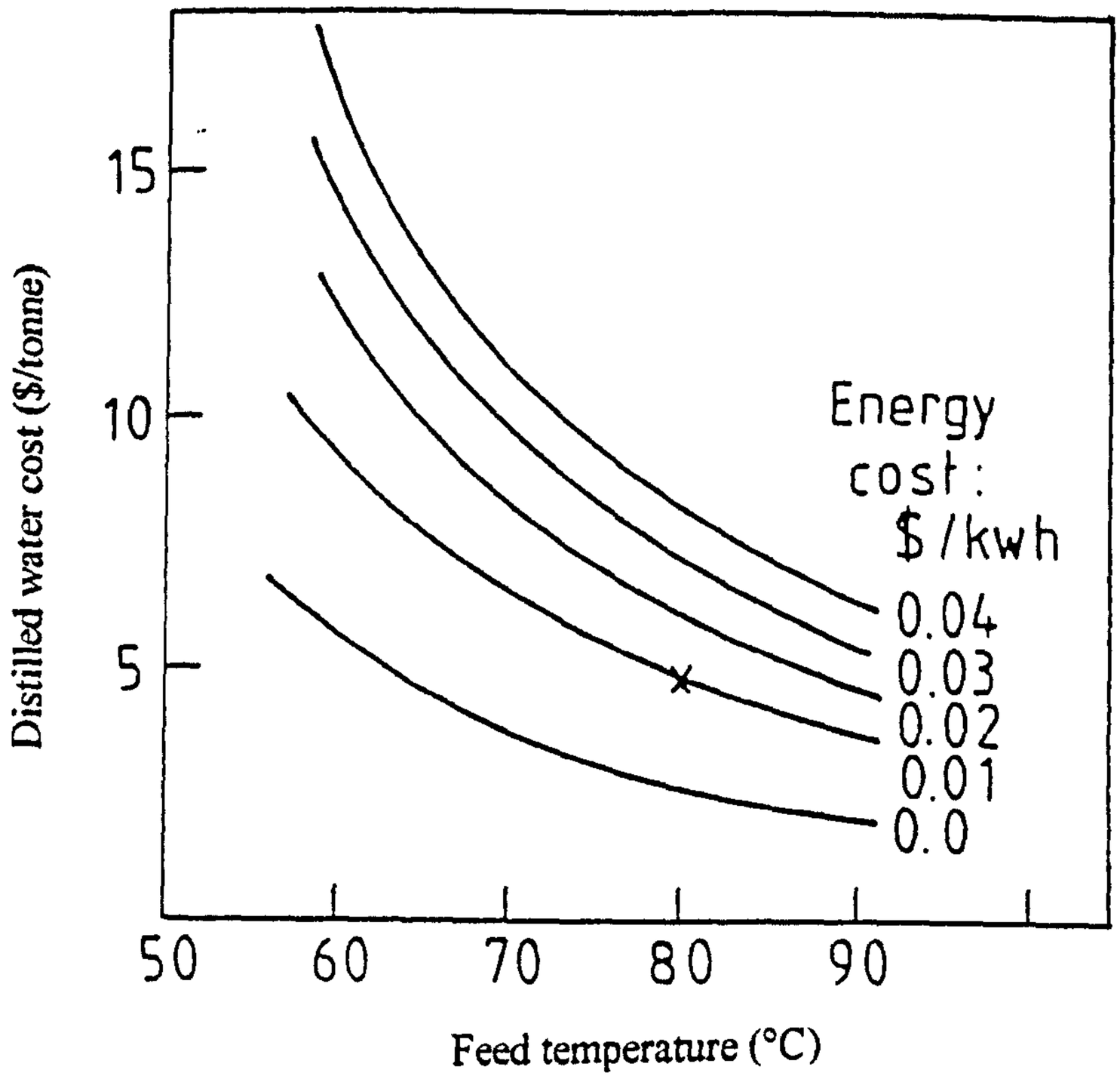

Figure 2.25: Effect of energy cost and feed temperature on distilled water cost (5000 kg/h distilled water) [16]

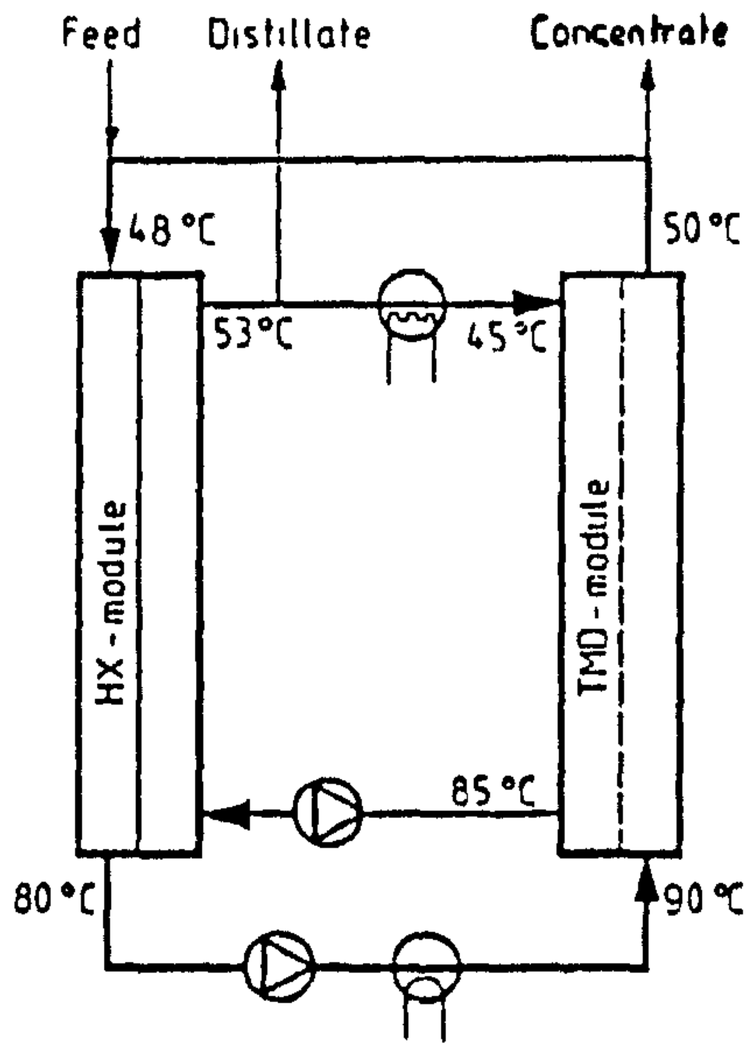

Figure 2.26: Membrane distillation with energy recovery by heat exchanger [16]

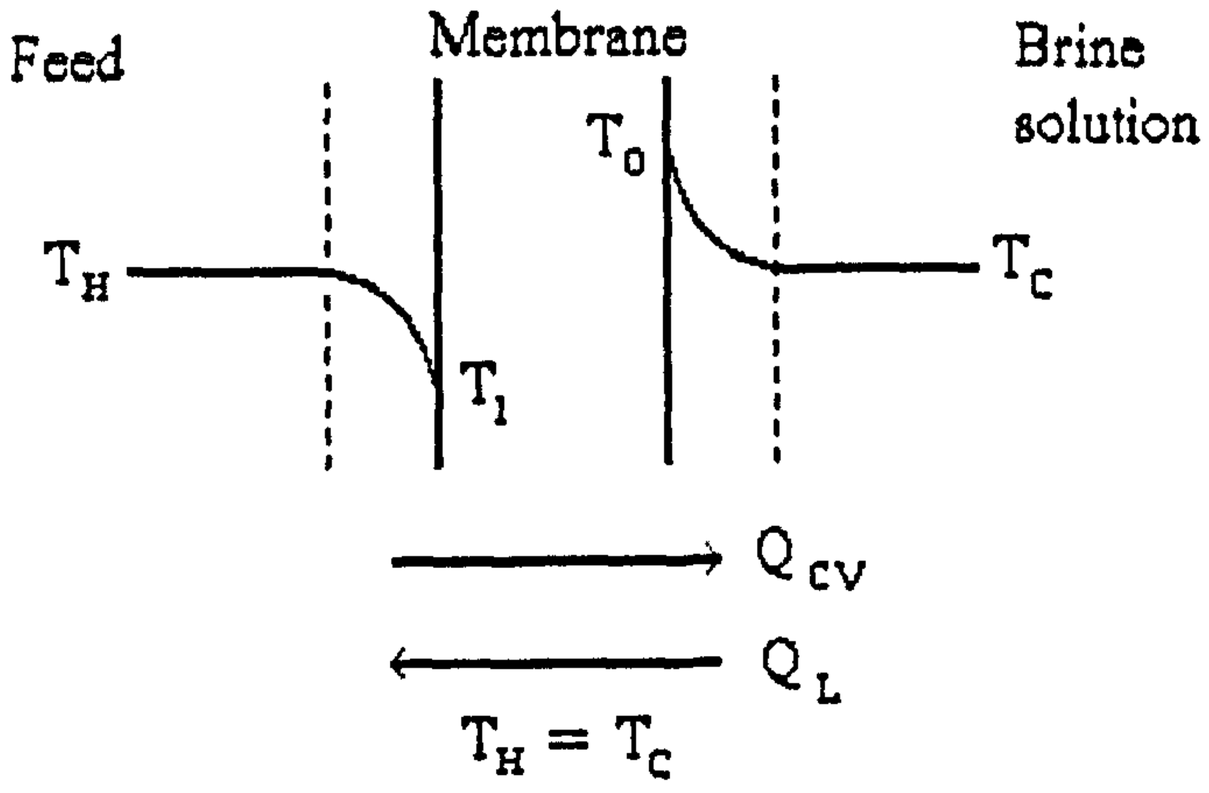

Figure 2.27: Osmotic distillation system [34]

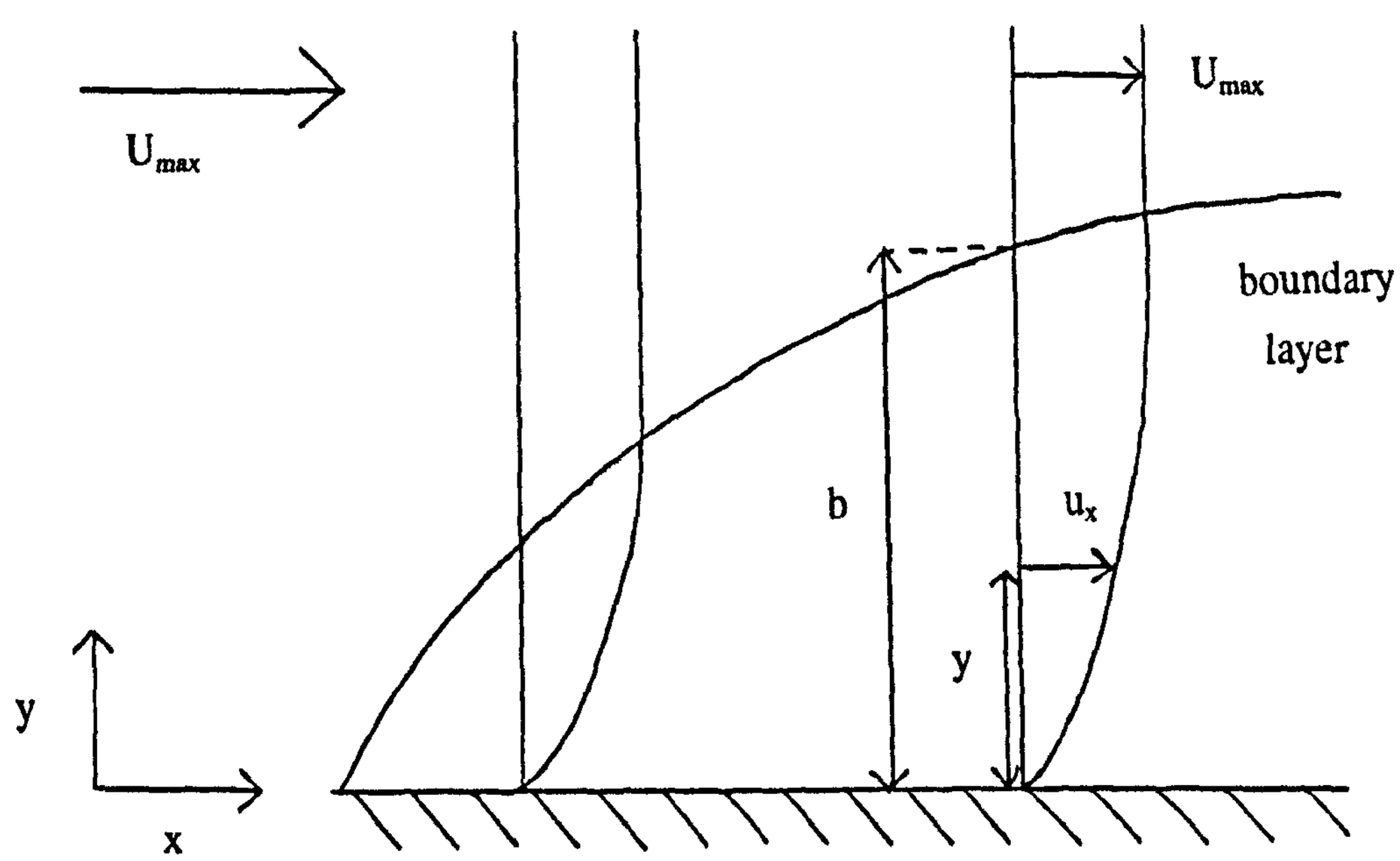

Figure 2.28: Velocity gradients next to a surface

Only direct contact modules can be used for osmotic distillation, as both sides of the membrane need to be in contact with a solution to achieve the concentration driven vapour pressure difference [57]. Modules used for osmotic distillation are mainly hollow fibre, as these can cope with high solids content, but spiral wound modules with suitable spacing material have also been used [34].

The permeate flux depends on the membrane type, concentration of the solutions, the stirring rate, and the temperature. There is an increases of flux with mean temperature because of an Arrhenius type relationship [54]. Increasing the overall temperature can increase flux as higher temperatures reduce viscosity and increase the mass transfer coefficient [56].

The mechanism of transport of water vapour through the membrane is a combination of convective and diffusive transport, the same as for membrane distillation. The process is also affected by polarisation layers. Like membrane distillation, there is temperature polarisation because of evaporation and condensation at the membrane surfaces, but concentration polarisation is a much bigger problem with this process. Temperature polarisation decreases the vapour pressure difference set up by the concentration difference between the feed and permeate streams. The temperature polarisation causes a membrane distillation flux, which is much smaller than the osmotic distillation flux. Mengual *et al* [54] assumed the decrease in vapour pressure difference caused by the membrane distillation flux was negligible, but a fixed temperature difference across the membrane should be avoided [58].

The polarisation layers can be reduced by stirring, and Mengual *et al* [54] found that the flux increased by up to 40-50% when stirring was introduced. The unstirred concentration layer can be modelled by the Nernst film model [54] assuming eddy diffusions are negligible, which limits the mass transfer through the layer to diffusion and convection mechanisms. The membrane concentration can be related to the bulk concentration by,

$$c_B = c_m \exp\left(\frac{N}{C}\right) \tag{2.49}$$

where, $C = D/\delta$ (2.50)

Equation (2.49) is equivalent to the equations used to describe concentration polarisation in ultrafiltration, microfiltration, and reverse osmosis [54].

PVDF and PTFE membranes have been used for concentrating orange, grape, apple and sugarcane juices as well as, skimmed milk, coffee, tea [34], and tomato puree [60]. Thompson [61] reported on industrial plants for the concentration of grape, pear, and apple juices. In 1991, a plant capable of handling 10,000 litres/day of juice was commisioned in Australia and was so successful that it was expanded to 23,000 liters/day. The physical parameters of the membrane control the flux and selectivity of the process, and the diffusion of water through the membrane controls the mass transfer [56]. Because of the high solids content of the feed, fouling of the membrane becomes an important consideration. Fats and proteins may foul the membrane, and alcohols and surfactants may penetrate, and cause leakage through the membrane [59]. Normal cleaning methods may affect the hydrophobicity of the membrane. Durham and Nguyen [60] studied this problem for the concentration of tomato puree. The fouling in this instance was by fatty substances blocking the pores. It was discovered that a cleaning agent had to be carefully selected which did not destroy the integrity of the membrane. In addition, the membrane was found to become less hydrophobic as the concentration of the feed solution increased [60]. High concentrations of dissolved solids can be handled, with solutions being concentrated up to 75-85% solids [34]. Typical fluxes are 1-10 kg/m^2h with operating temperatures of 10 - 50 °C.

In a review by Kunz *et al* [58], they state that there needs to be better comprehension of the important parameters in osmotic distillation in order to define and improve the process.

2.11 Boundary Layers

The modelling of boundary layers has been a major activity in fluid mechanics and has been extensively studied. Most studies have been concerned with flow through pipes

and over objects, such as aircraft wings. In membrane processes however, the flow is always enclosed, with transport occuring through one or two porous walls.

A simple boundary layer is a layer of fluid close to a surface where the velocity approaches zero at a solid surface, the no-slip condition, and approaches the bulk velocity at the edge of the boundary layer. The velocity gradients are large along the normal, near to the surface and are smaller in the direction of the flow (Figure 2.28). Boundary layer theory is used to predict the development of boundary layers. Heat and mass transfer rates can be predicted because the major resistances lie in the thermal and concentration boundary layers. The velocity, thermal and concentration boundary layers can develop and exist simultaneously.

This section is a concise review of studies concerned with ultrafiltraion, velocity profiles through modules, and prediction of boundary layer growth in membrane distillation. Because this work concerns a flat plate module, the review will concentrate on modelling in flat plate channels with one porous wall.

2.11.1 Boundary Layer Equations for Porous Channels

Belfort [62] pointed out that as mass transport to a membrane surface is dependant on the flow above the surface, understanding the fluid mechanics is a prerequisite to studying mass transport problems such as concentration polarisation and fouling. This reasoning can be extended to heat transfer and temperature polarisation.

The majority of models use the work of Berman [63] to describe the momentum transport. He used Navier-Stokes and continuity equations together with a stream function for a channel with two porous walls. For one porous wall, Kleinstrauer and Paller [65] developed similar equations. The equations referred to in this section are given in Table 2.5.

Bouchard [66] developed simplified equations, for one porous wall, in which the term,

$$\frac{v_r Y \rho}{2\mu}$$

was eliminated. This meant that only the average velocity was altered by the transport through the porous wall, and the velocity profile remained unchanged

Two porous walls:

$$v_{tp}(x) = v_{tp}(0) - \frac{2}{Y}\int_0^x v_f(x)dx$$

Complete equations (Berman [63])

$$v_t(x,\theta) = \tfrac{3}{2} v_{tp}(x)\left(1-\theta^2\right)\left[1 - \frac{Re_Y}{420}\left(2 - 7\theta^2 - 7\theta^4\right)\right]$$

$$\frac{v(\theta)}{v_f} = \frac{\theta}{2}\left(3-\theta^2\right) - \frac{Re_Y\,\theta}{280}\left(2 - 3\theta^2 + \theta^6\right)$$

Simplified equations (Brian [64])

$$v_t(x,\theta) = \frac{3}{2} v_{tp}(x)\left(1-\theta^2\right)$$

$$v(\theta) = v_f \frac{\theta}{2}\left(3-\theta^2\right)$$

One porous wall:

$$v_{tp}(x) = v_{tp}(0) - \frac{1}{Y}\int_0^x v_f(x)dx$$

Complete equations (Kleinstrauer and Paller [65])

$$v_t(x,\theta) = v_{tp}(x)\left[\frac{3}{2}\left(1-\theta^2\right) - \frac{Re_Y}{560}\left(-7\theta^6 - 140\theta^3 + 9\theta^2 + 140\theta - 2\right)\right]$$

$$\frac{v(\theta)}{v_f} = -\frac{1}{4}\left(\theta^3 - 3\theta - 2\right) + \frac{Re_Y}{1120}\left(-\theta^7 - 35\theta^4 + 3\theta^3 + 70\theta^2 - 2\theta - 35\right)$$

Simplified equations (Bouchard [66])

$$v_t(x,\theta) = \frac{3}{2} v_{tp}(x)\left(1-\theta^2\right)$$

$$\frac{v(\theta)}{v_f} = \frac{1}{4}\left(-\theta^3 + 3\theta + 2\right)$$

Where: $Re_Y = \dfrac{v_f Y \rho}{2\mu}$ and, $\theta = \dfrac{2y}{Y}$

Table 2.5: Solutions for velocity profiles in a rectangular channel with one or two porous walls

In most studies, a laminar velocity profile has been used as shown in Figure 2.29. Some have shown that the shape of the profile does not change, it remains parabolic, but the magnitude does change [67]. Probstein *et al* [68] formed equation (2.51) to allow for this change of magnitude caused by the flux through the membrane.

$$v = 3V\left[1 - N(x)\right]\left[\frac{2y}{Y} - \frac{1}{2}\left(\frac{2y}{Y}\right)^2 + ...\right] \qquad (2.51)$$

They modelled the boundary layer to form a model predicting the limiting flux in ultrafiltration.

2.11.2 Thermal Boundary Layer

Although the work by Lee and Ju [69] concerns the flow in a parallel plate channel with insulated walls (no membranes), they do give a methodology for determining the temperature distribution in the channel. The energy equation for the fluid in the channel is given by,

$$Q = \rho C_p v \frac{dT}{dx} \qquad (2.52)$$

which is Fourier's equation. As the fluid has a high Prandtl Number, the laminar velocity profile is assumed fully developed.

Whenever heat transfer is involved in fluid flow, the subject of buoyancy needs to be addressed. This was done by Naito [70] who looked at the effect of buoyancy on laminar flow and heat transfer between parallel plates. Two forms of heat transfer were studied, uniform wall temperature and uniform heat flux, and a numerical solution was developed using the SOR method. He found that buoyancy effects increased the entrance region where the velocity profile was developing. The problem with this work is that all calculations were carried out for air (Pr = 0.71), but in a water system at 273 K, Pr is around 12, so the effect may be different.

2.11.3 Concentration Boundary Layer

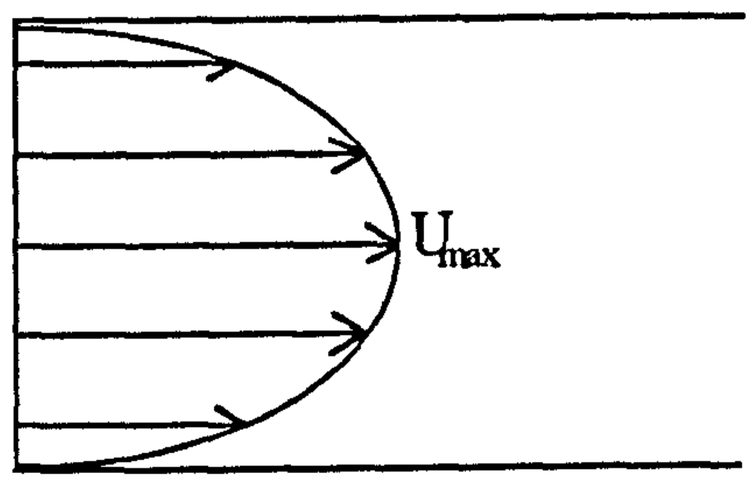

Figure 2.29: Laminar velocity profile

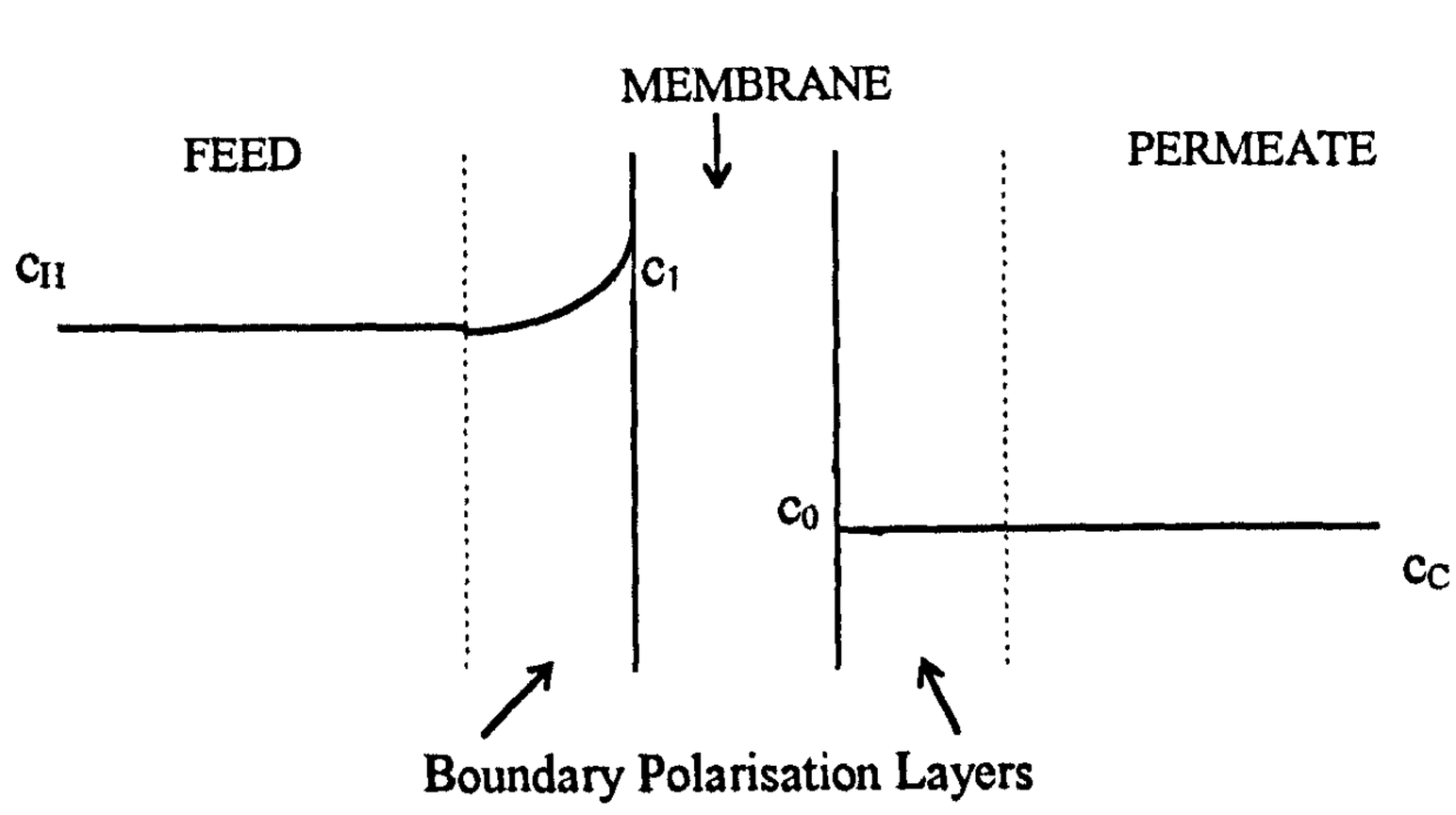

Figure 2.30: Concentration polarisation effect on the solute in membrane processes

Much of the work carried out on modelling boundary layers in membrane processes has concerned ultrafiltration and the formation of concentration polarisation layers. These layers are similar to temperature polarisation layers as described in Chapter 2.3, in that they change the concentration at the membrane surface from that of the bulk concentration. Figure 2.30 shows this effect.

Aimar *et al* [71] give a method for modelling the concentration boundary layer and Figure 2.31 shows the shape of the boundary layer calculated with increasing distance along the channel. The concentration profile is represented by,

$$c = c_B + (c_0 - c_B)\exp\left(\frac{-y}{\delta}\right) \tag{2.53}$$

A conclusion from their work is that the average flux of a module with a short channel is larger than that with a long channel.

Wu and Howell [72] considered calculating the entrance length of this concentration boundary layer. They state that a fully developed boundary layer should be avoided. A useful equation is given relating the viscosity as a function of concentration,

$$\mu = \mu_L \exp(Kc) \tag{2.54}$$

From their work, they found that increasing the feed pressure above 2.5 bar decreases the entrance length and when fouling is present, it is better to have the actual channel length shorter than the entrance length. Although increasing the Reynolds Number does not greatly increase the entrance length, it does increase the flux obtained over the entrance length. An empirical expression, equation (2.55), was obtained by dimensional analysis and compared with their numerical method to calculate the concentration boundary layer entrance length, L_e,

$$L_e = 1.178 \times 10^{-5} \times d\left(\frac{Zd}{\mu}\right)^{0.8363}\left(\frac{S_t\mu}{Pd^3}\right)^{0.1845} \tag{2.55}$$

Granger *et al* [67] looked at channels with both one and two porous walls. They found the axial and transverse flows using Navier-Stokes equations, but neglected the simplifying assumption of constant permeation rate along the channel. This assumption was neglected as constant permeation (permeate flux) is not obtained when combining

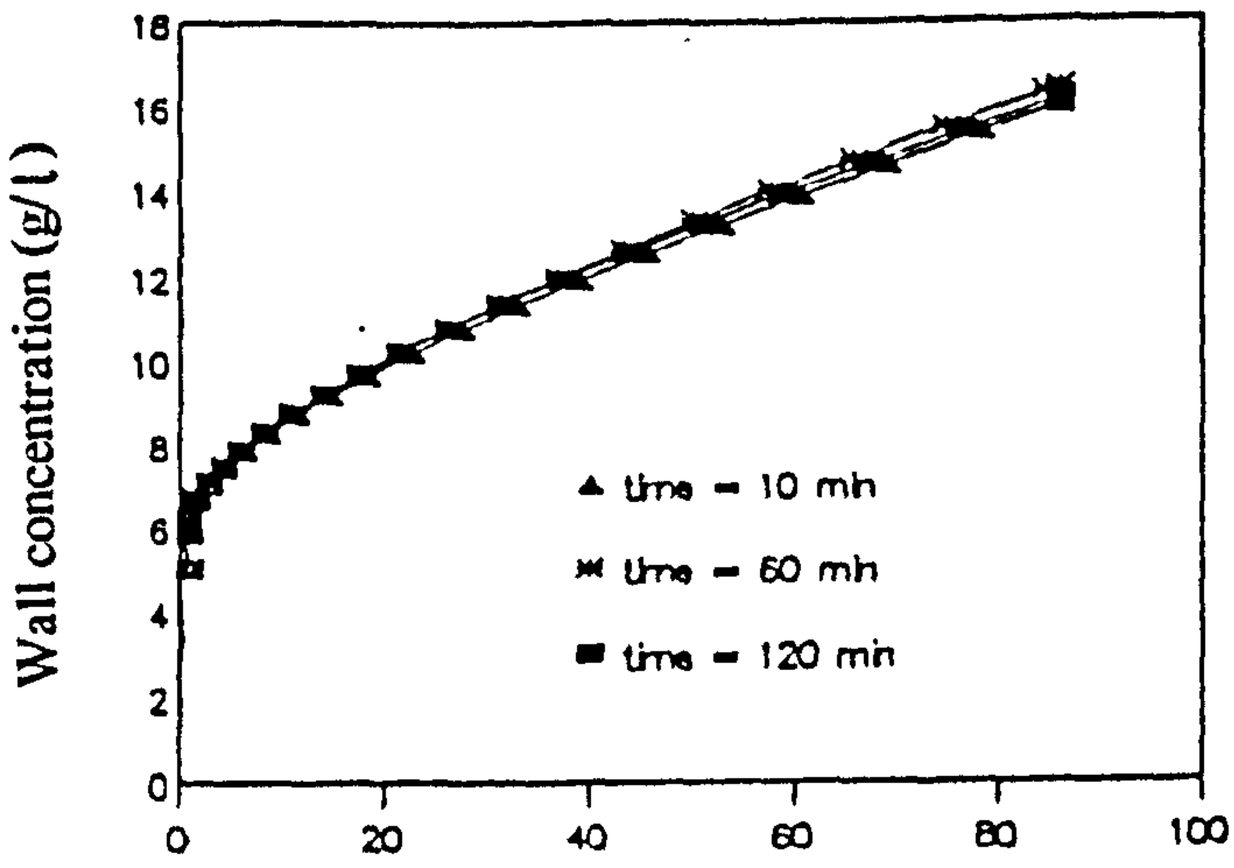

Figure 2.31: Calculated shape of concentration boundary layer along a channel [71]

(Re = 2200)

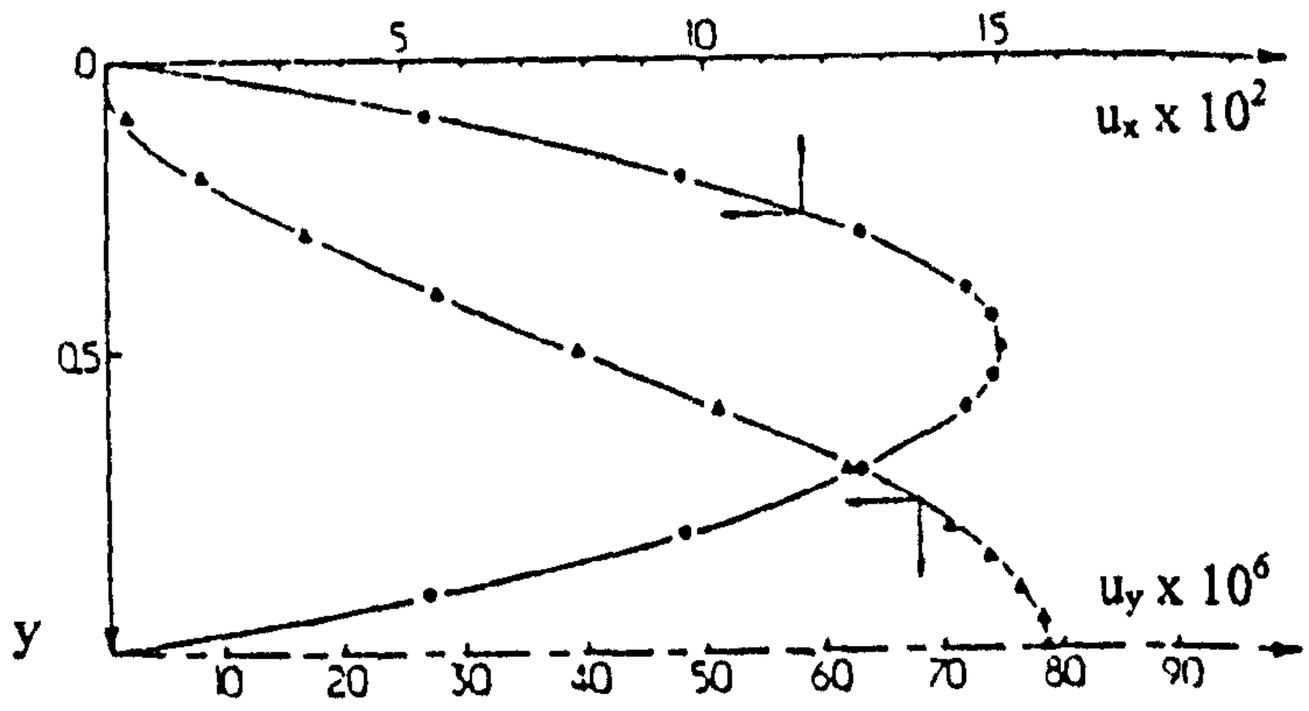

Figure 2.32: Shape of axial and transverse velocity profiles in a rectangular channel [67]

high permeability membranes with long channels. The assumption has been used in other studies, which leads to the simplification that the permeate flow through the membrane is independent of axial position. To be able to use this simplification, the pressure drop across the membrane must be constant along its total length to give uniform permeation flow.

The velocity and pressure layers described by Granger *et al* [67] are given by,

$$\langle v_x \rangle = \frac{1}{Y}\int_0^Y v_x(x,y)\,dy \tag{2.56}$$

$$\langle P \rangle = \frac{1}{Y}\int_0^Y P(x,y)\,dy \tag{2.57}$$

where the laminar profile was given by,

$$v_x(x,y) = 6V\left(\frac{y}{Y} - \frac{y^2}{Y^2}\right) \tag{2.58}$$

A mass balance over a slice, width δx, was carried out, and Poiseuilles Law then linked the pressure change to the mean axial velocity to give a second order differential equation. The Navier-Stokes equations and the equation of continuity were then solved using an iterative procedure assuming an incompressible fluid with constant density. The findings were that the axial velocity profile remained parabolic, and the pressure profile stayed flat across the width of the channel irrespective of the membrane permeability and height of the channel,. This means that the simplification that the flux is independent of axial position is generally valid. The maximum transverse velocity is located next to the porous wall as shown in Figure 2.32.

Bouchard *et al* [66] also tried to predict the effects of the concentration boundary layer in a rectangular channel with laminar flow. They state that using an assumption of mass conservation gives physical meaning to mass transfer numerical solutions. A comparison between a finite difference solution and an analytical solution for the mass transfer showed good agreement for large separations. Other membrane configurations studied include hollow fibre and tubular membranes [73,74]. A study by Kotzev [73] is purely theoretical, whereas the work of Mellis *et al* [74] includes experiments to confirm their

results, but only for situations in which the assumed parabolic velocity profile is not distorted by wall suction.

Wall suction is a phenomenon that occurs with most pressure driven processes with liquid in the pores of the membrane. Mellis *et al* [74] state that wall suction is important for Reynolds Numbers between 1000 and 15000, and affects the axial pressure drop.

Belfort [75] compared different membrane modules, where he mainly looked at porous tubes and the convective flow of fluids and the effect of particles for pressure driven processes. Flat plate modules were found to have a lower flowrate capacity than both hollow fibre and spiral wound modules, but are easier to clean. The onset of the transition region in porous channels is about 4000 compared to 2100 in a smooth walled channel.

2.11.4 Reducing Boundary Layers

Boundary layers are a problem with membrane processes, and many ways of reducing them have been investigated. Only a few are mentioned here, but they give the general ideas applied.

One method of reducing boundary layers is by laying a spacer in the channel [76-79]. This disturbs the flow of fluid at the membrane surface, creating turbulence. A problem with spacers is that they cause larger pressure drops over the module.

Another method is to use vortices, by manipulating module geometry. In the studies by Mallubhotla [80], Ophoff [81], and Kaminski and Stawczyk [82], Dean vortices have been used. It has been shown that this reduces the effect of concentration polarisation without requiring the energy for producing turbulence.

Forcing air slugs and bubbles through modules is another method which has shown an improvement in fluxes and has been investigated by Li *et al* [83] and Laborie *et al* [84]. Using pulsating flow [75] has also been shown to be effective.

2.11.5 Membrane distillation

Dubinski *et al* [85] decided that understanding the hydrodynamic conditions in their equipment would aid in the optimum construction of a module for membrane distillation. Their design was a circular disk with the permeate outlet in the centre. The fluid flows from one side to the other as shown in Figure 2.33. Their work concentrated on predicting where the fluid would flow using Laplace's equation (equation (2.59)).

$$\Delta\psi = 0 \tag{2.59}$$

where ψ is the flow through a cross section between ψ equal to 0 and any local value of ψ, i.e. it is a stream function.

As mentioned in Chapter 2.2.2, Agashichev and Sivakov [24] have carried out the only study to date which uses the theory of hydrodynamics and boundary layers to model membrane distillation. They used a velocity profile given by equation (2.60), and related the temperature and concentration profiles in fixed ratios to the velocity profile (equations (2.27) and (2.28)).

$$v_\eta = \frac{v_z}{v} = \sin\left(\frac{\pi}{2}\eta\right) \tag{2.60}$$

Their model took into account the energy interdependence between the flow in the feed and permeate channels. The model determines the temperature and concentration in both channels.

2.12 Literature Review Summary

This review has covered the research carried out on membrane distillation over the past 15 years. It considers theoretical modelling, polarisation effects, types of modules and membranes, experimental work and applications, the phenomenon of membrane wetting, osmotic distillation, and modelling of boundary layers along porous channels.

The modelling of membrane distillation has been the main area of investigation, which includes the effect of mass transfer, heat transfer and stirring rate. The initial feed concentration, temperature difference, membrane temperature and boundary layers are

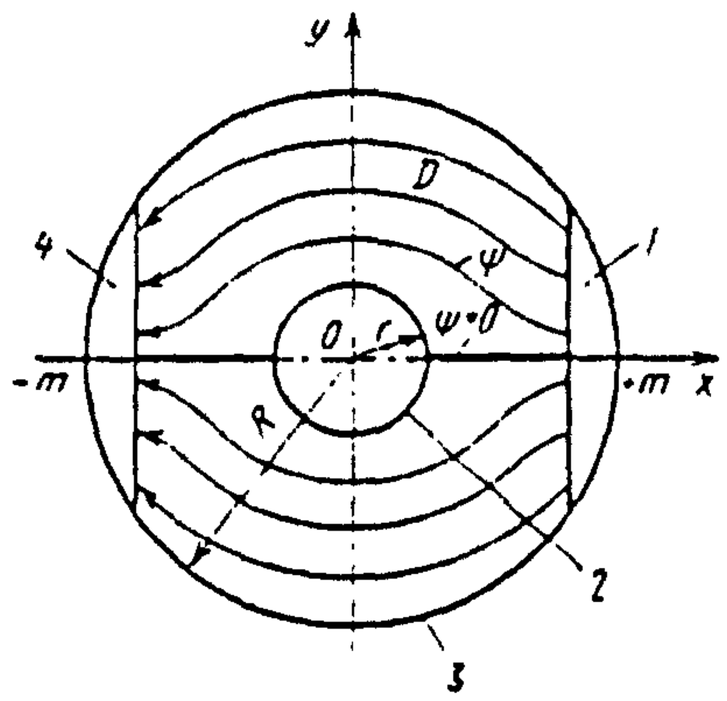

Figure 2.33: Diagram of flow over a circular plate for membrane distillation [85]

all factors that have to be accounted for in modelling membrane distillation. The equations developed have been shown to be accurate for specific operating conditions, using a small range of feed solutions. The most important effect that has to be considered with membrane distillation is temperature polarisation, which results in a reduction in the driving temperature difference. Any model for membrane distillation must include the effect of temperature polarisation and there is scope for further work in this area.

There are two types of module that have been used for experimental work on membrane distillation. These are flat plate, and hollow fibre modules. The majority of the flat plate work has used a Lewis cell which has facilities for stirring the bulk fluids. Membranes used in the modules must be hydrophobic, with a porosity of 70-80% and a mean pore size of around 0.2 μm.

Membrane distillation is suitable for a range of separations. They include processes where,

i) the permeate is the product (e.g. desalination, water reclamation),

ii) the concentrated feed is the product (e.g. food stuffs),

iii) both feed and permeate are products (e.g. azeotropic separation).

Studies which involved experimental work were concerned with two different systems. The first involved using water and sodium chloride to study the basic trends of membrane distillation and to confirm the theoretical modelling. The second involved using specific feed solutions to test the suitability of membrane distillation for each separation.

A number of studies found that when dealing with organics the problem of membrane wetting could be significant, producing a liquid flux in opposition to the required permeate flux.

Membrane distillation was found to be most suitable when the energy required is supplied by waste heat. This is because membrane distillation is energy intensive. Introducing a separate heat exchanger to recover heat has also been shown to improve the efficiency of the process.

This review has enabled the identification of some areas where further research could produce better understanding of membrane distillation. One area which could be further investigated is the production of specific membranes. Currently, commercial microfiltration and ultrafiltration membranes are used, but research has highlighted certain requirements of a membrane for membrane distillation. These requirements are that the membrane is hydrophobic, porous with pores sizes of 0.1 to 0.6 μm, has a low thermal conductivity and the thickness of the membrane is at a minimum.

The design of a module which could produce better heat and mass transfer could also be investigated. Again, commercial ultrafiltration and microfiltration modules are currently used for research into membrane distillation. These modules are designed to cope with pressure driven processes, but membrane distillation has a thermal driving force so the module requirements are fundamentally different. This means that to enhance membrane distillation, a module needs to be designed specifically for this process.

Another area of possible research concerns the effect of temperature polarisation. If this effect can be reduced, the efficiency of membrane distillation can be increased.

The overall objective of the research mentioned above is to improve the permeate flux so that membrane distillation becomes a viable option in industry.

Expanding the types of separations membrane distillation could be used for is another area of investigation. Testing different feed solutions could highlight a process in which membrane distillation could achieve higher purities and separation than other existing processes. For example, an interesting separation possibility is azeotropic distillation. Of course, all separations bring the problem of membrane fouling and flux decay. Very little work has looked at this area of membrane distillation, but it is important and needs to be studied in the near future.

A final area that needs further work concerns membrane wetting. Methods to accurately measure and prevent this phenomenon could extend the lifetime of the hydrophobic membranes, and expand the range of suitable separations.

This work is concerned with improving the overall flux of membrane distillation. As stated above, this also includes better module design and reducing temperature

polarisation. Understanding the fluid mechanics in a channel with porous walls is required before tackling mass transport and the problem of temperature polarisation. To carry out the research, the temperature and flow profiles in the module have to be studied.

The module type chosen to carry out the research consisted of flat plates. Consequently a review of boundary layers along flat plates and porous channels was carried out. The majority of the studies concerned with boundary layers in channels with porous walls are based on ultrafiltration. The equations developed to describe the flow through channels are based on Navier-Stokes equations and the Continuity equation. The method of solution is to develop the velocity profile, including the transverse, tangential, and permeate velocity components. Most studies using a laminar velocity profile have found that the shape of the velocity profile does not change, it remains parabolic, but the magnitude does change because of the permeate flux through the membrane. Wall suction is a phenomenon that occurs with most pressure driven processes with liquid in the pores of the membrane. As membrane distillation has only vapour in the pores of the membrane, wall suction can be neglected.

In the boundary layer studies carried out, the emphasis has been on the velocity and concentration profiles, with only a few taking account of temperature. The work carried out on ultrafiltration can only give a general indication of suitable modelling equations and methods, as membrane distillation has different transport processes and driving force. A fully developed boundary layer should be avoided and shorter channel lengths are better than long channels.

A method for reducing boundary layers is to place a spacer in the channel, creating turbulence. Another is to introduce vortices by manipulating module geometry. Utilising pulsed flow, bubbles and air slugs through the channel, are all other methods that have been successfully used. These work by introducing high shear through turbulence.

There has not been much work linking fluid mechanics with membrane distillation. One study has concentrated only on predicting where the fluid would flow over the module. Another study modelled the boundary layers. As stated before (Chapter 2.2.2), the work

by Agashichev and Sivakov [24] relates the temperature and concentration boundary layers by fixed ratio to the assumed velocity boundary layer, which may be inaccurate and does not allow the model to be flexible.

The modelling of boundary layers could be expanded to study the effect of module configuration on the process. Any model for membrane distillation would have to take the effect of velocity, temperature and concentration into account. The permeate flux through the membrane must also be included.

CHAPTER 3

FLOW DISTRIBUTION MODEL

3.1 Introduction

Initially, it was necessary to investigate the flow paths of the liquid through the existing module. This would then lead to improving the module design for membrane distillation by reducing the effects of boundary layers.

This first model relates the flow through the module to the pressure drop, and enables the determination of the flow path through the module.

3.2 The Flow Distribution Model

This section is an investigation into the flow paths of the liquid through the existing plate and spacer, shown in Figure 3.1.

Flow and pressure in a channel are related, i.e. the higher the pressure drop, for a given flowrate, the more the resistance to the flow. A series of equations to model the pressure drop in the module can be derived. For instance, if a flow of liquid is exposed

to two channels, with channel A having a larger resistance than channel B, the flow would go down channel B, and bypass channel A.

For laminar flow through a rectangular duct, assuming fully developed flow,

$$Eu = \frac{I}{Re}\,\frac{l}{d} \tag{3.1}$$

where;

$$Eu = \frac{\Delta P}{\frac{1}{2}\rho v^2} \tag{3.2}$$

$$Re = \frac{dv\rho}{\mu} \tag{3.3}$$

and,

$$d = \frac{4Yw}{(2Y+2w)} \tag{3.4}$$

I is a loss coefficient obtained from Figure 3.2, and is a function of the height to width ratio of the channel. Therefore, substituting equations (3.2), (3.3) and (3.4) into equation (3.1) gives an equation relating the pressure drop along a channel to the liquid velocity,

$$\Delta P = \frac{I\mu v l(2Y+2w)^2}{8Y^2w^2} \tag{3.5}$$

or, more simply,

$$\Delta P = \frac{I\mu v l}{8d^2} \tag{3.6}$$

The pressure measurement system used to investigate this problem is shown in Figure 3.3. To fully model the module, three different equations were required. One for the portion between the pressure tapping and the entrance to the main channel, one for the main channels, and one for the spacer gaps. The dimensions of the channels are given in Figure 3.1.

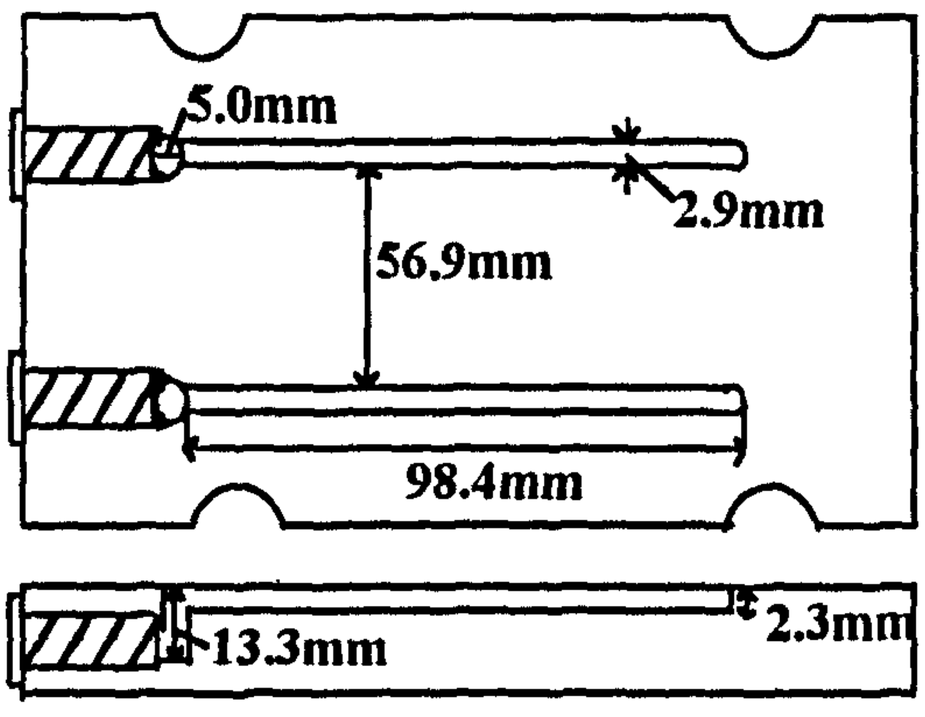

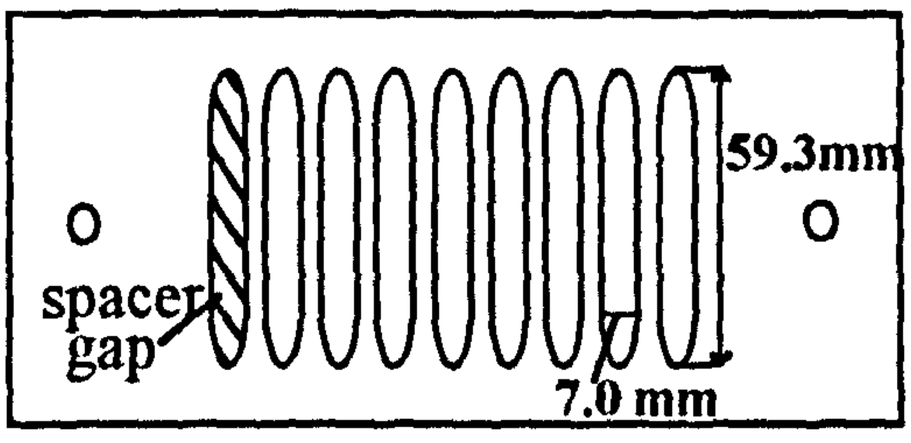

b) PLAIN PLATE

d) SPACER

0.45 mm thick

Figure 3.1: Plain plate and spacer

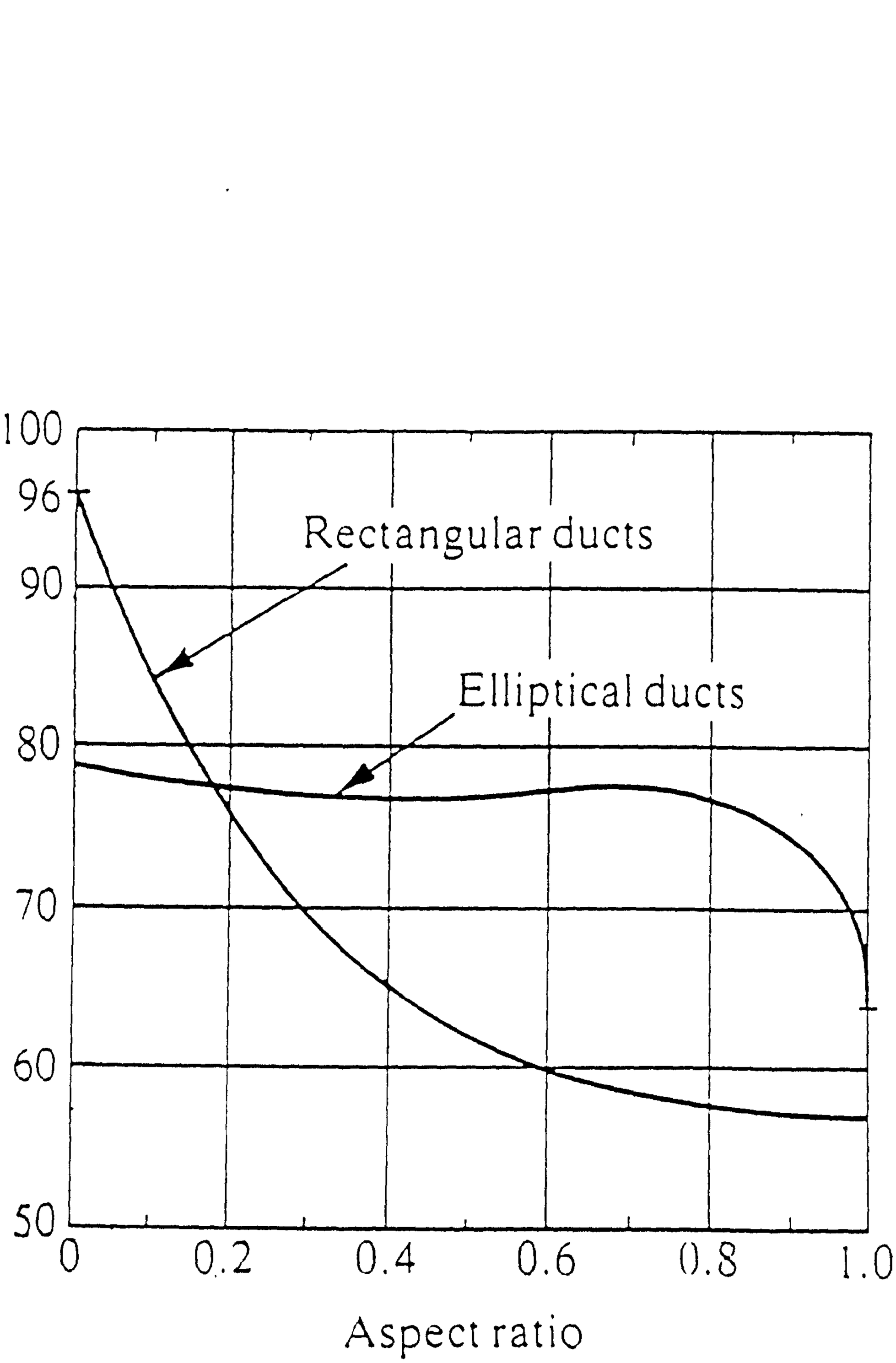

Figure 3.2: Loss coefficient I for laminar flow

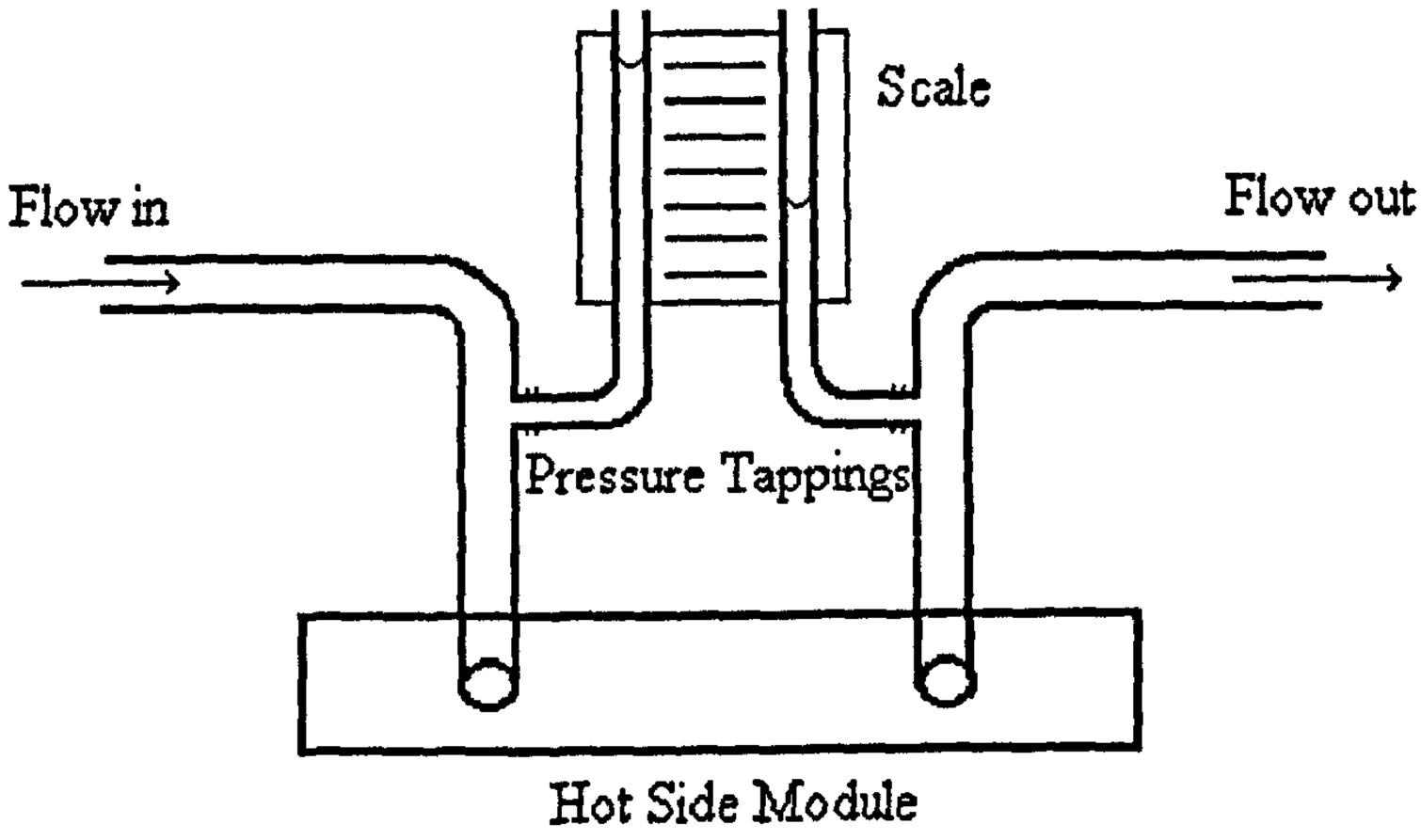

Figure 3.3: Pressure measurement of the hot side of the module

From equation (3.1), the equation for the initial section is;

$$\Delta P_e = \frac{28.5v\mu l}{d^2} \tag{3.7}$$

the main channel equation is;

$$\Delta P_{mc} = \frac{29v\mu l}{d^2} \tag{3.8}$$

and the spacer gap equation is;

$$\Delta P_{sg} = \frac{44v\mu l}{d^2} \tag{3.9}$$

The equations are required to be in the form of flowrates, so therefore equation (3.7) becomes;

$$\Delta P_e = \frac{114q\mu l}{\pi d^4} \tag{3.10}$$

equation (3.8) becomes;

$$\Delta P_{mc} = \frac{116q\mu l}{\pi d^4} \tag{3.11}$$

and equation (3.9) becomes;

$$\Delta P_{sg} = \frac{176q\mu l}{\pi d^4} \tag{3.12}$$

Once the equations were derived, then the calculation procedure had to be developed. The calculation procedure is very involved for this model, as each channel is related to the previous one. A cascade of equations have to be set up to solve the problem. The calculation can be arranged for any number of spacer gaps, which alters the area available for the liquid to flow through.

For instance, for a system where four spacer gaps are being utilised, the arrangement of pressures and resistances to flow are shown in Figure 3.4. The corresponding calculation procedure is shown in Figure 3.5. The resistance term, R_{sg}, is the pressure drop over the spacer gap.

Table 3.1 shows the values assumed for the density and viscosity of water at various temperatures that were used in the theoretical model.

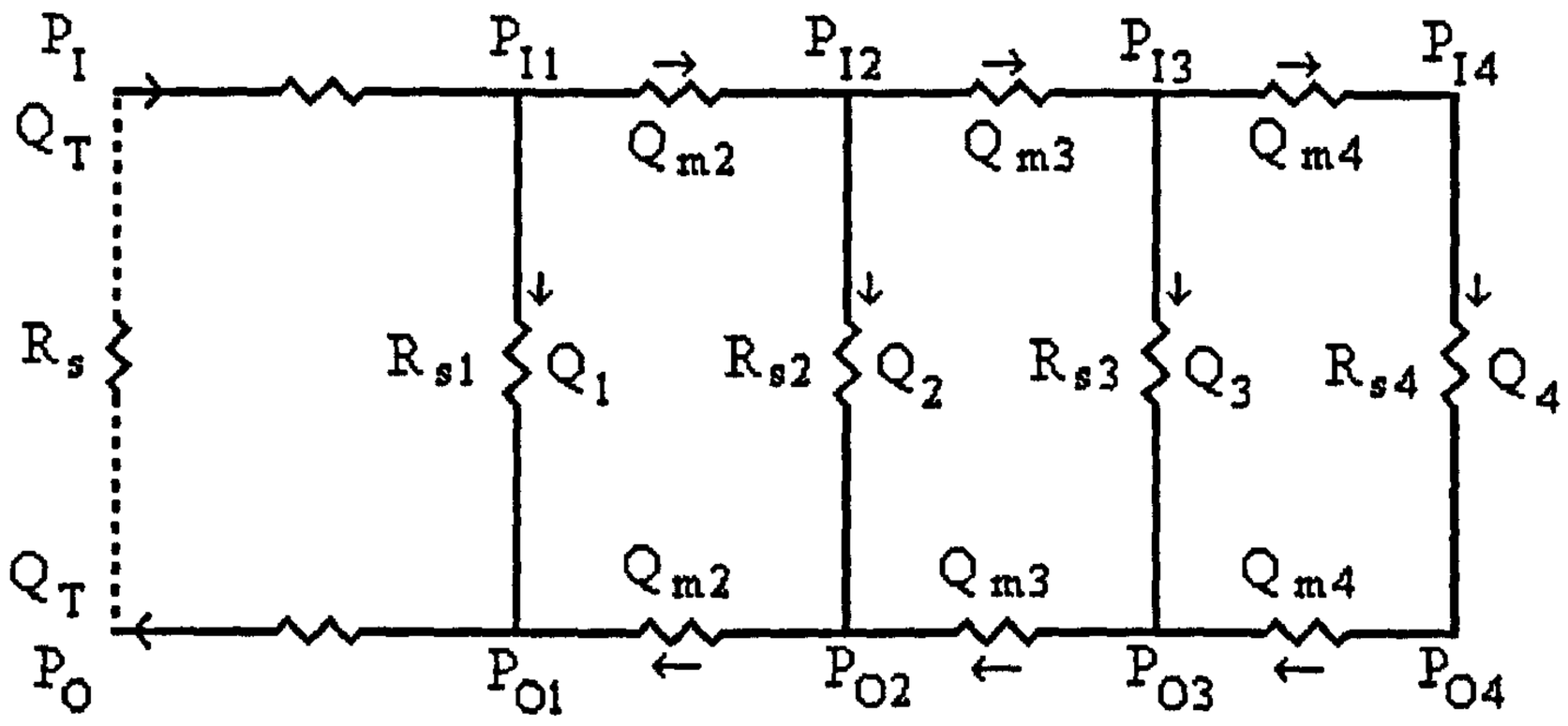

Figure 3.4: Pressure and resistance arrangement with 4 spacer gaps

Temperature (°C)	Density (kg/m^3)	Viscosity (Pa s)
15	999.099	1.15×10^{-3}
20	998.204	1.01×10^{-3}
25	997.045	9.3×10^{-4}
30	995.647	8.5×10^{-4}
35	994.032	7.7×10^{-4}

Table 3.1: Density and viscosity data for water [88]

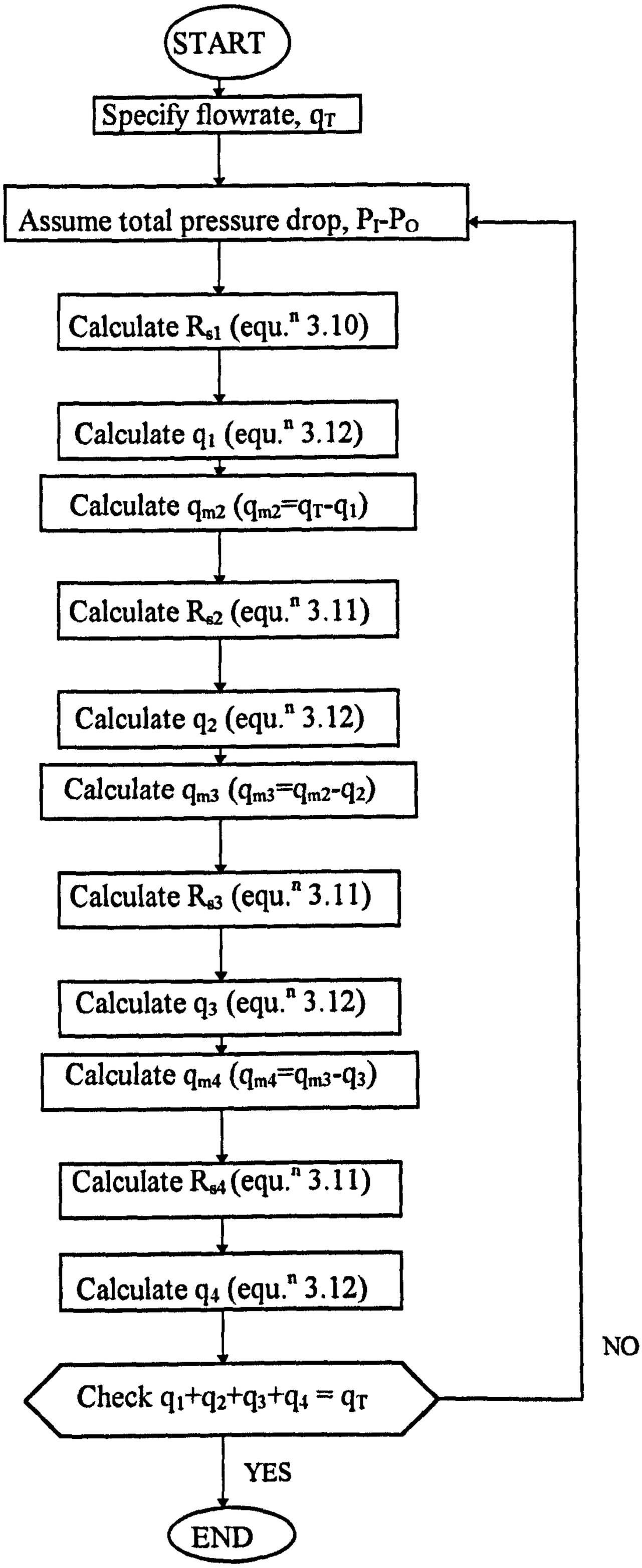

Figure 3.5: Calculation procedure for the 4 spacer gap example

3.3 Experimental Procedure

The experimental conditions and details of the experiments carried out for the flow distribution model can be found in Chapter 6.3.2

3.4 Results and Discussion

The theoretical and experimental results of the flow distribution model can be found in Chapter 7.3, together with a discussion of the findings.

CHAPTER 4

MEMBRANE DISTILLATION MODEL

4.1 Introduction

The aim of this second model is to use the basic equations of membrane distillation to model the effect that temperature, and temperature polarisation have on the permeate flux. This section of the work closely relates to the literature review given in Chapter 2.

4.2 The Membrane Distillation Model

The model developed here shows the relationship between temperature and permeate flux for membrane distillation. It will enable the prediction of flux given the bulk temperatures, channel height and type of membrane. The model was developed and expanded from earlier work [86].

The system of membrane distillation is illustrated in Figure 4.1, indicating the mass and heat fluxes, the temperatures, and water mole fraction in the bulk fluids and at the membrane surfaces.

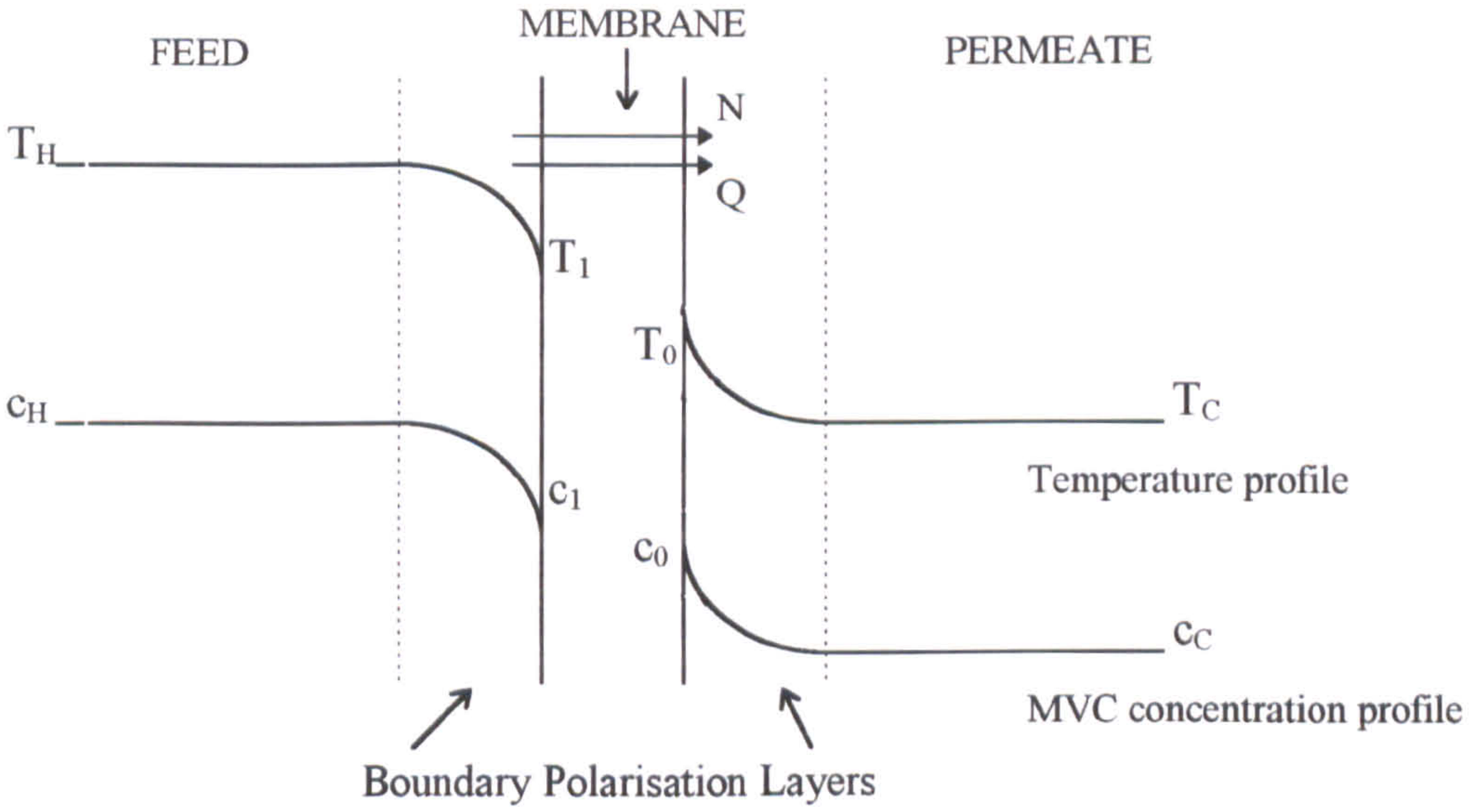

Figure 4.1: System of membrane distillation

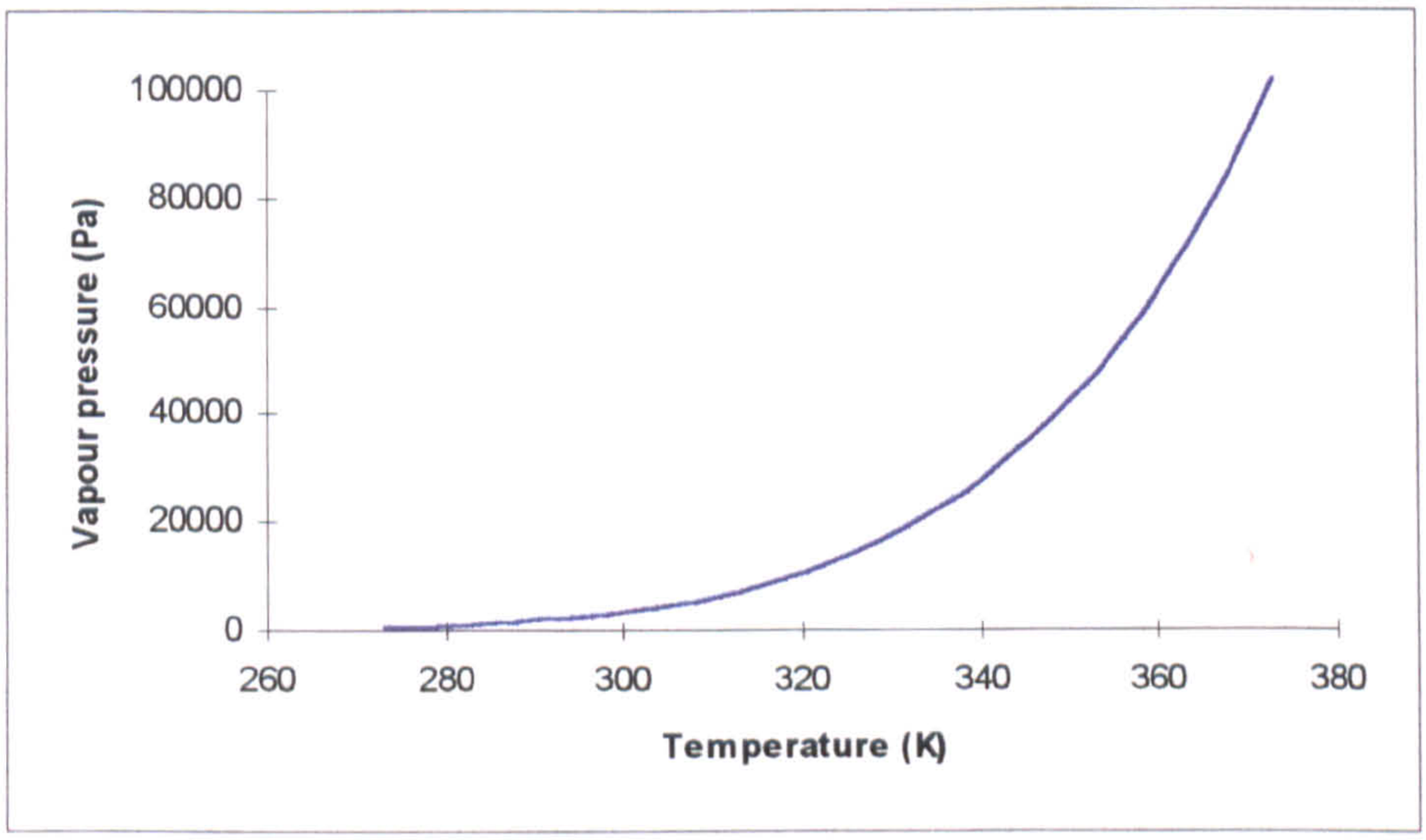

Figure 4.2: Variation of vapour pressure with temperature using the Antoine equation

The mass flux of permeate depends directly on the water vapour pressure difference across the membrane, and the effective overall membrane mass transfer coefficient given by:

$$N = C\,(P_1 y_1 - P_0 y_0) \tag{4.1}$$

Schofield *et al* [53] showed that the mass transfer coefficient, C, is determined by a combination of Knudsen diffusion resistance, Poiseuille flow resistance and molecular diffusion through any trapped air. For a membrane thickness of 0.11 mm, they state C as $9.0\text{x}10^{-7}$ kg/m^{2}sPa for a PVDF membrane. Table 4.1 shows the data used for the different membranes tested in this work. The membrane mass transfer coefficient depends on the membrane properties, thickness and, to a small extent, on temperature.

	PVDF	PTFE	Versapor
C (kg/m^{2}sPa)	$9.0\text{x}10^{-7}$	$4.3\text{x}10^{-7}$	$2.5\text{x}10^{-7}$
δ (mm)	0.13	0.06	0.17
k_m (W/mK)	0.05	0.05	0.05

Table 4.1: Membrane data used in the membrane distillation model

It is expected that increasing the temperature would increase the permeate flux exponentially due to the exponential increase of vapour pressure with temperature. This relationship is shown in Figure 4.2, in which the vapour pressure was calculated using the Antoine equation,

$$P = \exp\left(23.238 - \frac{3841}{(T_m - 45)}\right) \tag{4.2}$$

There are boundary layers either side of the membrane which affect the mass and heat transfer in membrane distillation. The equation for calculating the mass flux in the liquid boundary layers either side of the membrane is approximated by [71]:

$$N = \frac{DCM}{\delta}\Delta y \tag{4.3}$$

The largest effect on the fluxes obtained in membrane distillation is caused by temperature gradients across the membrane. Equation (4.2) shows that the vapour

pressure is affected by temperature. Consequently, from equation (4.1), the mass flux is linked to the temperature difference across the membrane.

The effect of temperature gradients on the heat flux is given by equations (4.4) and (4.5). The total heat flux between the bulk fluids, Q, is obtained by the addition of the two heat fluxes occurring in the system, Q_c and Q_v.

The conducted heat through the membrane, Q_c, is due to the temperature difference between the surfaces of the membrane and is given by:

$$Q_c = \frac{k_m}{\delta_m}(T_1 - T_0) \tag{4.4}$$

The membrane thermal conductivity, k_m, is typically 0.05 W/m K [71].

The second heat flux, Q_v, must occur through the liquid in the direction of the vapour flow to supply the required heat of evaporation, and to dissipate that heat in condensation on the other side of the membrane. This is:

$$Q_v = N\lambda \tag{4.5}$$

Combining equations (4.4) and (4.5) gives the total heat flux:

$$Q = Q_c + Q_v = \frac{k_m}{\delta_m}(T_1 - T_0) + N\lambda \tag{4.6}$$

At equilibrium the heat flux must also travel through the boundary layers. Assuming initially that the boundary layer thickness and liquid thermal conductivity are the same on both sides of the membrane:

$$Q = \frac{k}{\delta}(T_H - T_1) = \frac{k}{\delta}(T_0 - T_C) \tag{4.7}$$

The boundary layer thicknesses defined in this model are constrained by the height of the channels. At the conditions used for this work, the laminar boundary layers occupy the entire channel height.

Manipulating the above equations, the interfacial, i.e. at the membrane surface, conditions can be found. Using equations (4.6) and (4.7), the hot side interfacial temperature, T_1 is:

$$T_1 = \frac{T_H\left(\frac{k}{\delta}+\frac{k_m}{\delta_m}\right)+\frac{k_m}{\delta_m}T_C - N\lambda}{2\frac{k_m}{\delta_m}+\frac{k}{\delta}} \tag{4.8}$$

Then rearranging equation (4.7), the cold side interfacial temperature, T_0 is:

$$T_0 = T_H - T_1 + T_C \tag{4.9}$$

The hot side interfacial water mole fraction, y_1, is found using equations (4.1) and (4.3), by combining mass transfer through the membrane and boundary layers respectively:

$$y_1 = \frac{y_H\left(\frac{D_H CM}{\delta}+\frac{D_H}{D_C}CP_0\right)+y_C CP_0}{CP_1+\frac{D_H CM}{\delta}+\frac{D_H}{D_C}C\,P_0} \tag{4.10}$$

The cold side interfacial water mole fraction, y_0, is then found by rearranging equation (4.3):

$$y_0 = \frac{D_H}{D_C}(y_H - y_1)+y_C \tag{4.11}$$

An iterative procedure is then used to calculate the mass flux of permeate, as the latter is present in equations (4.3) and (4.5).

This model assumes that there is no membrane wetting, i.e. the membrane is 100% hydrophobic. If membrane wetting were present, the flux would decrease due to a liquid flux occurring in the liquid filled pores, in opposition to the vapour flux [11].

The boundary layers either side of the membrane were initially assumed to be equal. This would be acceptable in modules with the same characteristics either side, but for the majority of modules, the feed and permeate sides are different. This means that the boundary layer thicknesses would be different due to different channel dimensions and flow characteristics. Decreasing the boundary layer thickness leads to a larger flux.

Another simplifying assumption used in this model is that the membrane temperature is the average of the hot and cold temperatures, with no variation over the module. To predict the temperature profile more accurately, the module could be assumed to behave

like a heat exchanger, or a method found to provide the temperature profile through a module.

4.3 Experimental Procedure

The experimental conditions and details of the experiments carried out for the flow distribution model can be found in Chapter 6.3.3

4.4 Results and Discussion

The theoretical and experimental results of the flow distribution model can be found in Chapter 7.4, together with a discussion of the findings.

CHAPTER 5

BOUNDARY LAYER ANALYSIS

5.1 Introduction

The development of the temperature and concentration profiles in the flow along the two surfaces of the membrane are the key to the mass transfer performance of a membrane unit. As stated before in Chapter 2, membrane distillation is limited by temperature and concentration polarisation which are boundary layer effects. Therefore it is necessary to study the behaviour of the boundary layers next to the membrane surface.

Boundary layer theory is an approximation to the full Navier-Stokes form of the fluid flow equations. Simplifications are justifiably made by neglecting terms which are small due to the small gradients in the direction of flow along a boundary relative to the large gradients perpendicular to the boundary. This idea is developed with detailed examples by Schlichting [89]. As stated in Chapter 2.11, although various researchers have looked at modelling boundary layers in channels with porous walls, only one group, Agaschiev *et al* [24] have looked specifically at membrane distillation. The problem with the work carried out by Agaschiev *et al* [24] is that they relate the growth of the temperature and concentration boundary layers in fixed ratios to a velocity boundary layer obtained from

the flow along a solid wall in the absence of heat and mass transfer. It is therefore an approximation of doubtful accuracy. Also they do not present any practically useful results. It would be an advantage to develop a more appropriate analysis.

The method chosen for this work was to develop differential equations describing the boundary layers on both sides of the membrane which were then coupled by a term to take into account the process of mass and heat transfer through the membrane. These simultaneous ordinary differential equations were solved by a Runge-Kutta numerical procedure.

5.2 Level One: Plug Flow, Single Component

The theory was developed in a number of levels, from simple to more realistic. The first step was to develop a model to analyse the thermal boundary layer in plug flow with a single component. This avoided, at first, the complications of the velocity and concentration boundary layers, yet because the temperature difference is the most important factor for membrane distillation it gave a good indication of the membrane unit performance.

The initial assumptions used were,

i) steady state

ii) velocities of liquids on both sides of the membrane are uniform and equal

iii) co-current flow

iv) no conduction in the direction of flow

v) no convection perpendicular to the flow

vi) no concentration effects

For two dimensional flow, the method of Karman and Pohlhausen [89,90] further simplifies the boundary layer theory by assuming a functional form for the velocity profile.

The boundary layer growth can be divided into two parts, as shown in Figure 5.1. In the entrance region, the boundary layer is growing in the channel between the membrane and the wall. In the constant region, the boundary layer has reached the wall opposite the membrane, and occupies the width of the channel. Figure 5.1 shows the nomenclature used in this analysis.

Enthalpy balances were then developed on an element of unit width (1m), height y_1, and length of δx, as shown in Figure 5.2. The bulk temperature of the hot feed, T_{01}, was taken as the datum for the enthalpy changes.

The steady state enthalpy balance on the control volume was developed as follows, with the form,

$$Convection\ In + Condutcion\ In = Convection\ Out + Conduction\ Out \qquad (5.1)$$

Convection In

The convection into the control volume at x is given by,

$$Q_{cvi} = \int_{y=0}^{y=y_1} C_p \rho v T \, dy + \delta x C_p T(y_1) \frac{d}{dx} \int_{y=0}^{y=y_1} \rho v \, dy \qquad (5.2)$$

The first term is the convection through the control face at x, the second term accounts for the heat convected into the top of the control volume.

Convection Out

The convection out through the control face at x + δx is related to the convection through the control face at x by a Taylor Series expansion (given by equation (5.3)).

$$f(x+h) = f(x) + hf'(x) + \frac{h^2}{2!} f''(x) + \frac{h^3}{3!} f'''(x) + \ldots\ldots \qquad (5.3)$$

Applying equation (5.3) to the first RHS term in equation (5.2) and neglecting higher order terms as $h = \delta x \rightarrow 0$ gives,

$$Q_{cvo} = \int_{y=0}^{y=y_1} C_p \rho v T \, dy + \delta x \frac{d}{dx} \int_{y=0}^{y=y_1} C_p \rho v T \, dy \qquad (5.4)$$

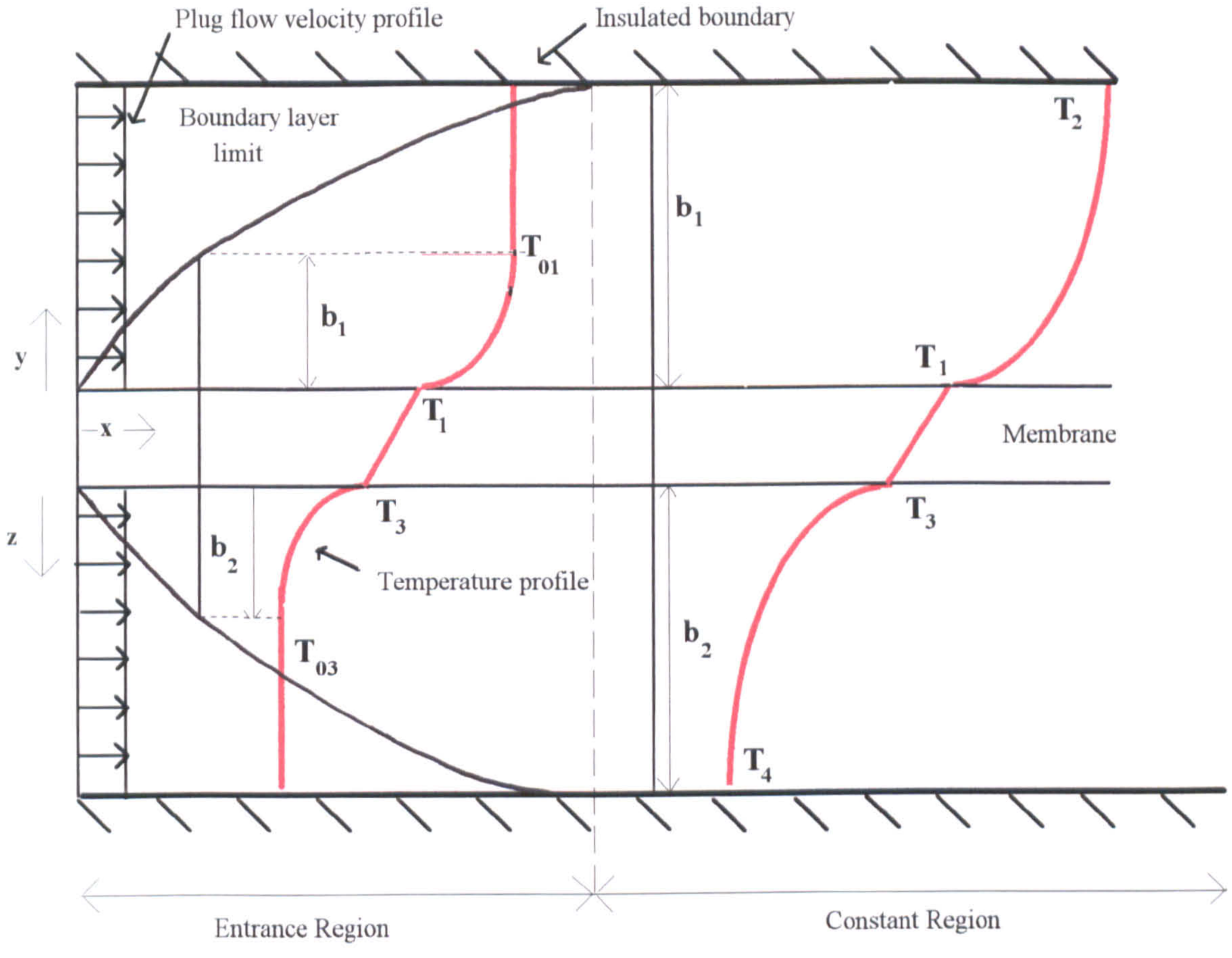

Figure 5.1: Boundary layer profiles

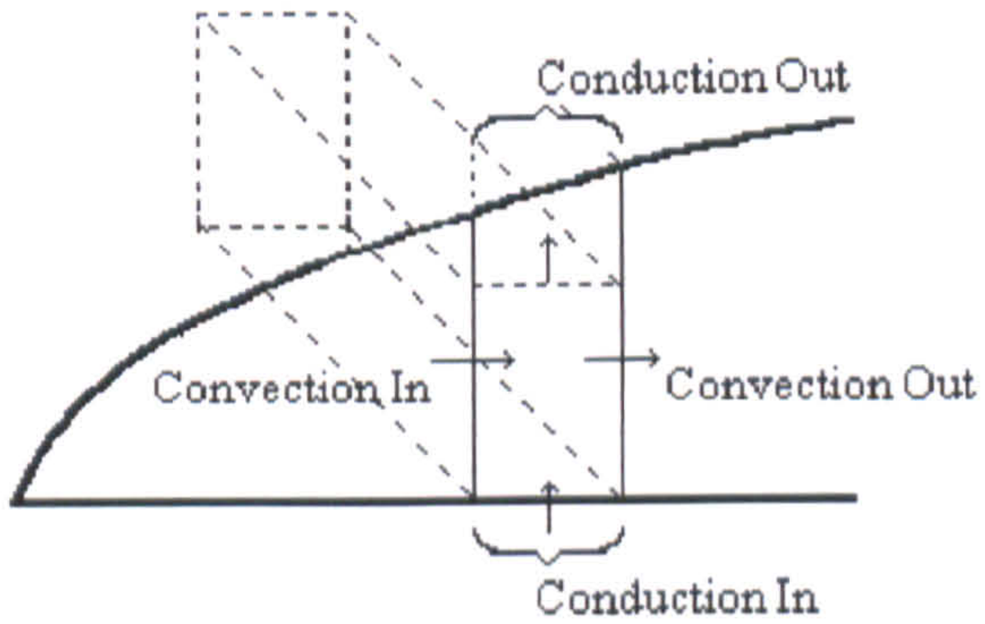

Figure 5.2: The control volume in a boundary layer

Conduction In

The heat conducted into the control volume from the membrane surface is given by Fouriers equation,

$$Q_{cni} = -\delta x\, k \left.\frac{dT}{dy}\right|_{y=0} \tag{5.5}$$

The rate of heat transfer through the membrane, as mentioned in Chapter 2.1.1, is represented by,

$$Q = E(T_1 - T_3) \tag{5.6}$$

and for the control volume in the analysis,

$$Q_{cni} = -\delta x\, E(T_1 - T_3) \tag{5.7}$$

This relates the temperatures on both sides of the membrane, T_1 and T_3.

Conduction Out

At the top of the control volume the conduction is again represented by Fouriers equation of heat conduction and is

$$Q_{cno} = -\delta x\, k \left.\frac{dT}{dy}\right|_{y=y_1} \tag{5.8}$$

5.2.1 The General Integral Equation for the Thermal Boundary Layer

Collecting all these terms into the enthalpy balance, equation (5.1), and cancelling terms and dividing through by δx gives an integral equation for the thermal boundary layer,

$$C_p \rho \frac{d}{dx} \int_{y=0}^{y=y_1} v(y)\left[T(y) - T(y_1)\right] dy = k \left.\frac{dT}{dy}\right|_{y=y_1} - k \left.\frac{dT}{dy}\right|_{y=0} \tag{5.9}$$

The Solution Procedure

The temperature profiles in equation (5.9) can be represented by third order polynomials,

$$T = a_0 + a_1 y + a_2 y^2 + a_3 y^3 \tag{5.10}$$

in which a_0 ,a_1 ,a_2, and a_3 are specified by the boundary conditions. For example, the temperature profile for the hot side with the boundary layer growing has the following boundary conditions: @ y = 0, T = T_1 and dT/dy = -E(T_1-T_3)/k and @ y = y_1,
T = T_{01} and dT/dy = 0, which gives,

$$T = T_1 + \frac{E(T_1 - T_3)}{k} y + \left[\frac{3(T_{01} - T_1)}{b^2} - \frac{2E(T_1 - T_3)}{kb}\right] y^2 + \left[\frac{E(T_1 - T_3)}{kb^2} - \frac{2(T_{01} - T_1)}{b^3}\right] y^3 \qquad (5.11)$$

For each side of the membrane, and for each region, two integrations of equation (5.9) were carried out. These were from y = 0 to y = b_1 and from y = 0 to y = b_1/2 for the hot side, and from z = 0 to z = b_2 and z = 0 to z = b_2/2 for the cold side. For the entrance region balances, the conduction out term is zero (equation (5.11)) as the energy is utilised in increasing the width of the boundary layer. For the constant region balances, the second term in equation (5.4), representing the convection in, is zero as the boundary layer is at constant width.

The enthalpy balances give four differential equations with four unknowns. The integrations, and rearrangement of the equations are given in detail in Appendix A. The equations have been solved by a Runge Kutta numerical integral procedure (See Appendix B), to give the temperatures and boundary layer thicknesses versus x, the distance along the channel.

For the Level One analysis, the four enthalpy balances for the entrance region where the thermal boundary layer thickness, b_1 = y_1, is growing, are given in the left column of Table 5.1. For the constant region where the thermal boundary layer thickness b_1 has grown to fill the channel so that b_1 = constant = Y_1, the four enthalpy balances are in the right column of Table 5.1.

Each of the enthalpy balance equations in Table 5.1 have three differential terms. They can be rearranged as simultaneous first order differential equations. For instance, for the hot side, entrance region at y = b_1,

$$a_1 \frac{db_1}{dx} + a_2 \frac{dT_1}{dx} + a_3 \frac{dT_3}{dx} + a_4 = 0 \qquad (5.12)$$

where,

	ENTRANCE REGION	CONSTANT REGION
HOT SIDE		
$y=b_1$	$C_p v\rho\left[\left(\frac{Eb_1T_1}{6k}-\frac{Eb_1T_3}{6k}+\frac{T_1}{2}-\frac{T_{01}}{2}\right)\frac{db_1}{dx}+\left(\frac{Eb_1^2}{12k}+\frac{b_1}{2}\right)\frac{dT_1}{dx}-\frac{Eb_1^2}{12k}\frac{dT_3}{dx}\right]$ $+E(T_1-T_3)=0$	$C_p v\rho\left[\left(\frac{b_1}{2}+\frac{Eb_1^2}{12k}\right)\frac{dT_1}{dx}+\frac{b_1}{2}\frac{dT_2}{dx}-\frac{Eb_1^2}{12k}\frac{dT_3}{dx}\right]+E(T_1-T_3)=0$
$y=b_1/2$	$C_p v\rho\left[\left(\frac{5T_1}{32}-\frac{5T_{01}}{32}-\frac{Eb_1T_1}{96k}+\frac{Eb_1T_3}{96k}\right)\frac{db_1}{dx}+\left(\frac{5b_1}{32}-\frac{Eb_1^2}{192k}\right)\frac{dT_1}{dx}+\frac{Eb_1^2}{192k}\frac{dT_3}{dx}\right]$ $+\frac{5E(T_1-T_3)}{4}-\frac{3k(T_{01}-T_1)}{2b_1}=0$	$C_p v\rho\left[\left(\frac{13b_1}{32}+\frac{11Eb_1^2}{192}\right)\frac{dT_1}{dx}+\frac{3b_1}{32}\frac{dT_2}{dx}-\frac{11Eb_1^2}{192}\frac{dT_3}{dx}\right]$ $+\frac{3k(T_1-T_2)}{2b_1}+\frac{5E(T_1-T_3)}{4}=0$
COLD SIDE		
$z=b_3$	$C_p v\rho\left[\left(\frac{Eb_3T_3}{6k}-\frac{Eb_3T_1}{6k}+\frac{T_1}{2}-\frac{T_{03}}{2}\right)\frac{db_3}{dx}+\left(\frac{Eb_3^2}{12k}+\frac{b_3}{2}\right)\frac{dT_3}{dx}-\frac{Eb_3^2}{12k}\frac{dT_1}{dx}\right]$ $-E(T_1-T_3)=0$	$C_p v\rho\left[\left(\frac{b_3}{2}+\frac{Eb_3^2}{12k}\right)\frac{dT_3}{dx}+\frac{b_3}{2}\frac{dT_4}{dx}-\frac{Eb_3^2}{12k}\frac{dT_1}{dx}\right]+E(T_3-T_1)=0$
$z=b_3/2$	$C_p v\rho\left[\left(\frac{5T_3}{32}-\frac{5T_{03}}{32}-\frac{Eb_3T_3}{96k}+\frac{Eb_3T_1}{96k}\right)\frac{db_3}{dx}+\left(\frac{5b_3}{32}-\frac{Eb_3^2}{192k}\right)\frac{dT_3}{dx}+\frac{Eb_3^2}{192k}\frac{dT_1}{dx}\right]$ $+\frac{5E(T_3-T_1)}{4}-\frac{3k(T_{03}-T_3)}{2b_3}=0$	$C_p v\rho\left[\left(\frac{13b_3}{32}+\frac{11Eb_3^2}{192}\right)\frac{dT_3}{dx}+\frac{3b_3}{32}\frac{dT_4}{dx}-\frac{11Eb_3^2}{192}\frac{dT_1}{dx}\right]$ $+\frac{3k(T_3-T_4)}{2b_1}+\frac{5E(T_3-T_1)}{4}=0$

Table 5.1 : Level One enthalpy balances

$$a_1 = C_p \rho v \left(\frac{Eb_1 T_1}{6k} - \frac{Eb_1 T_3}{6k} + \frac{T_1}{2} - \frac{T_{01}}{2} \right) \tag{5.13}$$

$$a_2 = C_p \rho v \left(\frac{Eb_1^2}{12k} + \frac{b_1}{2} \right) \tag{5.14}$$

$$a_3 = C_p \rho v \left(-\frac{Eb_1^2}{12k} \right) \tag{5.15}$$

$$a_4 = E(T_1 - T_3) \tag{5.16}$$

The simultaneous equation terms for the Level One enthalpy balances are given in Table 5.2.

The general formulation of simultaneous first order differential equations used in all the Fortran programmes developed for this analysis is shown in Appendix C. The resulting differential equations for T_3, T_1, b_1 and b_3 in the entrance region are,

$$\frac{dT_3}{dx} = \frac{(G_1 H_3 - G_3 H_2)}{(G_2 H_2 - G_1 H_1)} = F3 \tag{5.17}$$

$$\frac{dT_1}{dx} = \frac{(G_2 H_3 - G_3 H_1)}{(G_1 H_1 - G_2 H_2)} = F2 \tag{5.18}$$

where,

$$G_1 = a_2 c_1 - a_1 c_2$$

$$G_2 = a_3 c_1 - a_1 c_3$$

$$G_3 = a_4 c_1 - a_1 c_4$$

$$H_1 = m_2 n_1 - m_1 n_2$$

$$H_2 = m_3 n_1 - m_1 n_3$$

$$H_3 = m_4 n_1 - m_1 n_4$$

and,

$$\frac{db_1}{dx} = -\left(\frac{a_2 F2 + a_3 F3 + a_4}{a_1} \right) = F1 \tag{5.19}$$

$$\frac{db_3}{dx} = -\left(\frac{m_2 F3 + m_3 F1 + m_4}{m_1} \right) = F4 \tag{5.20}$$

Similar equations are obtained for T_1, T_2, T_3, and T_4 in the constant thickness region where the boundary layers fill the channels.

ENTRANCE REGION - HOT SIDE	
$y = b_1$	$y = b_1/2$
$a_1 = C_p\rho v\left(\frac{Eb_1T_1}{6k} - \frac{Eb_1T_3}{6k} + \frac{T_1}{2} - \frac{T_{01}}{2}\right)$	$c_1 = C_p\rho v\left(\frac{5T_1}{32} - \frac{5T_{01}}{32} - \frac{Eb_1T_1}{96k} + \frac{Eb_1T_3}{96k}\right)$
$a_2 = C_p\rho v\left(\frac{Eb_1^2}{12k} + \frac{b_1}{2}\right)$	$c_2 = C_p\rho v\left(\frac{5b_1}{32} - \frac{Eb_1^2}{192k}\right)$
$a_3 = C_p\rho v\left(-\frac{Eb_1^2}{12k}\right)$	$c_3 = C_p\rho v\left(\frac{Eb_1^2}{192k}\right)$
$a_4 = E(T_1 - T_3)$	$c_4 = \frac{5E(T_1 - T_3)}{4} - \frac{3k(T_{01} - T_1)}{2b_1}$

ENTRANCE REGION - COLD SIDE	
$z = b_3$	$z = b_3/2$
$m_1 = C_p\rho v\left(\frac{Eb_3T_3}{6k} - \frac{Eb_3T_1}{6k} + \frac{T_3}{2} - \frac{T_{03}}{2}\right)$	$n_1 = C_p\rho v\left(\frac{5T_3}{32} - \frac{5T_{03}}{32} - \frac{Eb_3T_3}{96k} + \frac{Eb_3T_1}{96k}\right)$
$m_2 = C_p\rho v\left(\frac{Eb_3^2}{12k} + \frac{b_3}{2}\right)$	$n_2 = C_p\rho v\left(\frac{5b_3}{32} - \frac{Eb_3^2}{192k}\right)$
$m_3 = C_p\rho v\left(-\frac{Eb_3^2}{12k}\right)$	$n_3 = C_p\rho v\left(\frac{Eb_3^2}{192k}\right)$
$m_4 = E(T_3 - T_1)$	$n_4 = \frac{5E(T_3 - T_1)}{4} - \frac{3k(T_{03} - T_3)}{2b_3}$

CONSTANT REGION - HOT SIDE	
$a_1 = C_p\rho v\left(\frac{Eb_1^2}{12k} + \frac{b_1}{2}\right)$	$c_1 = C_p\rho v\left(\frac{13b_1}{32} + \frac{11Eb_1^2}{192k}\right)$
$a_2 = C_p\rho v\left(\frac{b_1}{2}\right)$	$c_2 = C_p\rho v\left(\frac{3b_1}{32}\right)$
$a_3 = C_p\rho v\left(-\frac{Eb_1^2}{12k}\right)$	$c_3 = C_p\rho v\left(-\frac{11Eb_1^2}{192k}\right)$
$a_4 = E(T_1 - T_3)$	$c_4 = \frac{5E(T_1 - T_3)}{4} - \frac{3k(T_2 - T_1)}{2b_1}$

CONSTANT REGION - COLD SIDE	
$m_1 = C_p\rho v\left(\frac{Eb_3^2}{12k} + \frac{b_3}{2}\right)$	$n_1 = C_p\rho v\left(\frac{13b_3}{32} + \frac{11Eb_3^2}{192k}\right)$
$m_2 = C_p\rho v\left(\frac{b_3}{2}\right)$	$n_2 = C_p\rho v\left(\frac{3b_3}{32}\right)$
$m_3 = C_p\rho v\left(-\frac{Eb_3^2}{12k}\right)$	$n_3 = C_p\rho v\left(-\frac{11Eb_3^2}{192k}\right)$
$m_4 = E(T_3 - T_1)$	$n_4 = \frac{5E(T_3 - T_1)}{4} - \frac{3k(T_4 - T_3)}{2b_3}$

Table 5.2 : Level One simultaneous equation terms

The Runge Kutta calculation starts with the entrance region enthalpy balances, and once the boundary height equals the channel height, then the values of T calculated are used as the initial conditions for the constant region balances.

5.2.2 Circumventing the singularity at x = 0

The initial condition of y = 0 at x = 0 cannot be implemented in Fortran as it comprises a singularity which needs to be circumvented. Appropriate initial conditions were found by assuming a linear variation of y with x in the vicinity of the singularity and applying an energy balance to the first incremental step to give the new initial conditions.

An initial length of the boundary layer, x, where x is a very small distance was considered. It was assumed that between 0 and x, the boundary layer is linear as shown by Figure 5.3.

The heat transferred in the system satisfies three conditions,

i) conduction through the membrane,

$$Q = -E(T_1 - T_3)x \approx -E(T_{01} - T_{03})x \tag{5.21}$$

ii) conduction through the boundary layer,

$$Q \approx \frac{-2k(T_{01} - T_1)x}{b/2} \approx \frac{-4k(T_{01} - T_1)x}{b} \tag{5.22}$$

or,

$$Q \approx \frac{-2k(T_{01} - T_1)x}{b} \tag{5.23}$$

and, iii) convection through the boundary layer.

$$Q \approx C_p v \rho b\left(\frac{T_{01} + T_1}{2} - T_{01}\right) \approx C_p v \rho b\left(\frac{T_1 - T_{01}}{2}\right) \tag{5.24}$$

Combining equations (5.21) and (5.23) gives,

$$b \approx \frac{2k(T_{01} - T_1)}{E(T_{01} - T_{03})} \tag{5.25}$$

and equations (5.21) and (5.24) gives,

$$x \approx -\frac{C_p v \rho b(T_1 - T_{01})}{2E(T_{01} - T_{03})} \tag{5.26}$$

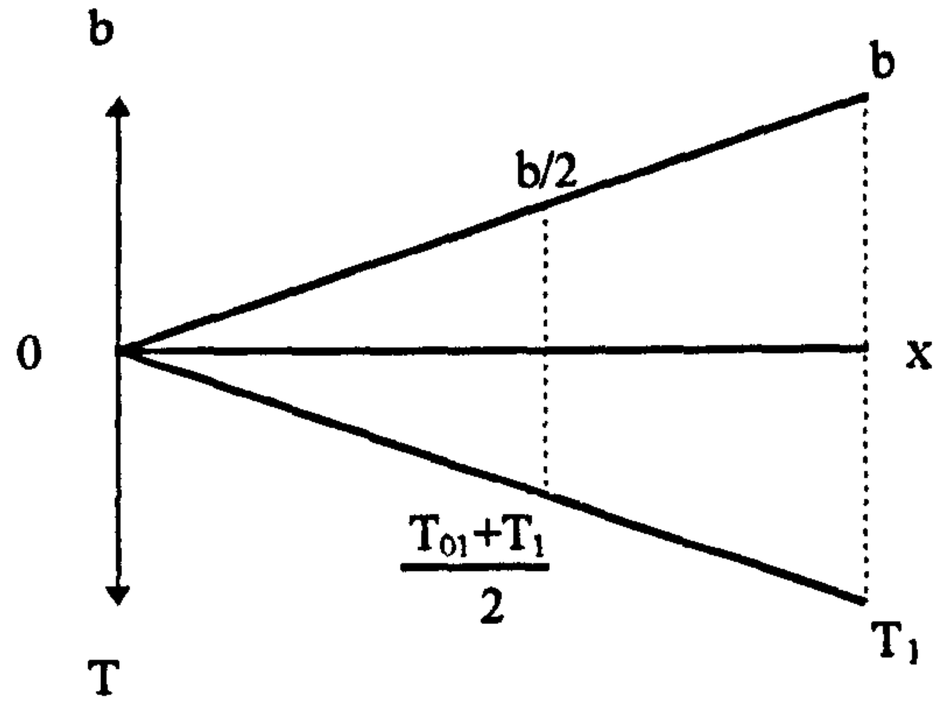

Figure 5.3: Removal of the singularity in the initial conditions

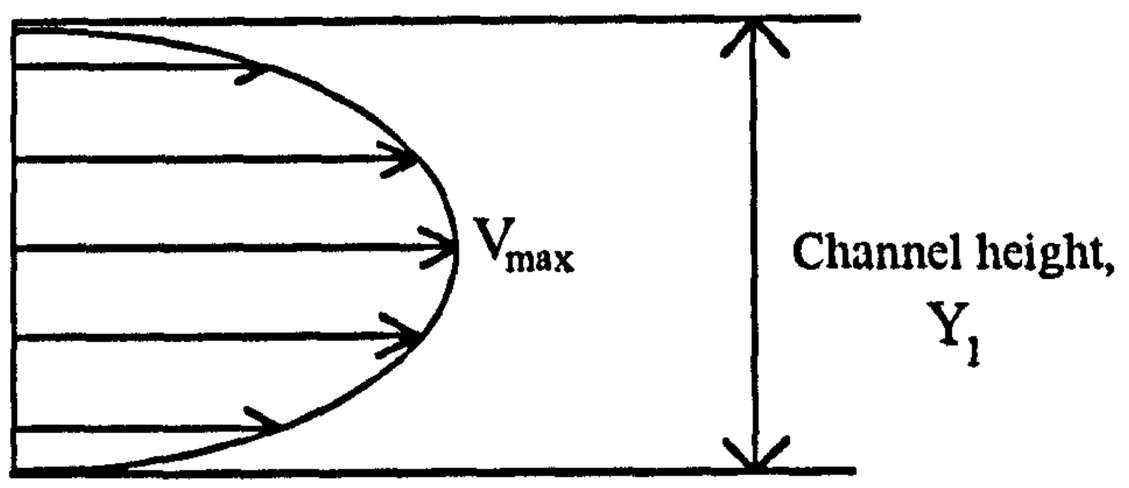

Figure 5.4: The laminar velocity profile

Equations (5.25) and (5.26) give initial values of x and y for specified temperature differences (T_1-T_{01}) that can be used in the Fortran programme. The Fortran programme for the Level One analysis is given in Appendix D.

5.2.3 Experimental Procedure

The experimental work which was carried out in order to provide corroborating data for this analysis is given in Chapter 6.3.4.

5.2.4 Results and Discussion

The Level One model was run with various starting conditions given in Chapter 7.5. The actual results and graphs are also given together with a discussion of the results.

5.3 Level Two: Laminar Velocity Profile, Single Component

The next stage of the work was to introduce a velocity profile to more accurately model the actual flow found in the module.

As the velocity in the channel was low (1 m/s) and the Reynolds Number was also low (25 - 200), the flow in the channel was laminar. This meant that, apart from the entrance region of the velocity boundary layer, the logical velocity profile to introduce was a laminar velocity profile as shown in Figure 5.4 and represented by equation (5.27) [89].

$$v_x = 4V_{max}\left[\frac{y}{Y_1} - \left(\frac{y}{Y_1}\right)^2\right] = 6\bar{V}\left[\frac{y}{Y_1} - \left(\frac{y}{Y_1}\right)^2\right] \qquad (5.27)$$

The enthalpy balances developed for Level Two are given in Appendix E, and the differential equations used in the Fortran programme are given in Tables 5.3 and 5.4.

5.3.1 Effect of permeate flux on the velocity profile

The velocity profile given by equation (5.27) represents a laminar profile with constant mass flowrate. With membrane distillation, this is not the case, as there is a mass flux

ENTRANCE REGION		
	$y = b_1$	$y = b_1/2$
HOT SIDE	$a_1 = 6C_p\rho\bar{v}\left(\frac{3T_1b_1}{10Y_1} - \frac{3T_{01}b_1}{10Y_1} - \frac{T_1b_1^2}{5Y_1^2} + \frac{T_{01}b_1^2}{5Y_1^2} + \frac{Eb_1^2T_1}{10Y_1k} - \frac{Eb_1^2T_3}{10Y_1k} - \frac{Eb_1^3T_1}{15Y_1^2k} + \frac{Eb_1^3T_3}{15Y_1^2k}\right)$ $a_2 = 6C_p\rho\bar{v}\left(\frac{3b_1^2}{20Y_1} - \frac{b_1^3}{15Y_1^2} + \frac{Eb_1^3}{30Y_1k} - \frac{Eb_1^4}{60Y_1^2k}\right)$ $a_3 = 6C_p\rho\bar{v}\left(\frac{Eb_1^3}{30Y_1k} - \frac{Eb_1^4}{60Y_1^2k}\right)$ $a_4 = E(T_1 - T_3)$	$c_1 = 6C_p\rho\bar{v}\left(\frac{9T_1b_1}{160Y_1} - \frac{9T_{01}b_1}{160Y_1} - \frac{7T_1b_1^2}{320Y_1^2} + \frac{7T_{01}b_1^2}{320Y_1^2} + \frac{ET_1b_1^2}{320Y_1k} - \frac{ET_3b_1^2}{320Y_1k} - \frac{ET_1b_1^3}{480Y_1^2k} + \frac{ET_3b_1^3}{480Y_1^2k}\right)$ $c_2 = 6C_p\rho\bar{v}\left(\frac{9b_1^2}{320Y_1} - \frac{7b_1^3}{960Y_1^2} + \frac{Eb_1^3}{960Y_1k} - \frac{Eb_1^4}{1920Y_1^2k}\right)$ $c_3 = 6C_p\rho\bar{v}\left(\frac{Eb_1^4}{1920Y_1^2k} - \frac{Eb_1^3}{960Y_1k}\right)$ $c_4 = \frac{5E(T_1 - T_3)}{4} - \frac{3k(T_{01} - T_1)}{2b_1}$
	$z = b_3$	$z = b_3/2$
COLD SIDE	$m_1 = 6C_p\rho\bar{v}\left(\frac{3T_3b_3}{10Y_3} - \frac{3T_{03}b_3}{10Y_3} - \frac{T_3b_3^2}{5Y_3^2} + \frac{T_{03}b_3^2}{5Y_3^2} + \frac{Eb_3^2T_3}{10Y_3k} - \frac{Eb_3^2T_1}{10Y_3k} - \frac{Eb_3^3T_3}{15Y_3^2k} + \frac{Eb_3^3T_1}{15Y_3^2k}\right)$ $m_2 = 6C_p\rho\bar{v}\left(\frac{3b_3^2}{20Y_3} - \frac{b_3^3}{15Y_3^2} + \frac{Eb_3^3}{30Y_3k} - \frac{Eb_3^4}{60Y_3^2k}\right)$ $m_3 = 6C_p\rho\bar{v}\left(\frac{Eb_3^3}{30Y_3k} - \frac{Eb_3^4}{60Y_3^2k}\right)$ $m_4 = E(T_3 - T_1)$	$n_1 = 6C_p\rho\bar{v}\left(\frac{9T_3b_3}{160Y_3} - \frac{9T_{03}b_3}{160Y_3} - \frac{7T_3b_3^2}{320Y_3^2} + \frac{7T_{03}b_3^2}{320Y_3^2} + \frac{ET_3b_3^2}{320Y_3k} - \frac{ET_1b_3^2}{320Y_3k} - \frac{ET_3b_3^3}{480Y_3^2k} + \frac{ET_1b_3^3}{480Y_3^2k}\right)$ $n_2 = 6C_p\rho\bar{v}\left(\frac{9b_3^2}{320Y_3} - \frac{7b_3^3}{960Y_3^2} + \frac{Eb_3^3}{960Y_3k} - \frac{Eb_3^4}{1920Y_3^2k}\right)$ $n_3 = 6C_p\rho\bar{v}\left(\frac{Eb_3^4}{1920Y_3^2k} - \frac{Eb_3^3}{960Y_3k}\right)$ $n_4 = \frac{5E(T_3 - T_1)}{4} - \frac{3k(T_{03} - T_3)}{2b_3}$

Table 5.3 : Level Two simultaneous equation terms - entrance region

CONSTANT REGION		
	$y = b_1$	$y = b_1/2$
HOT SIDE	$a_1 = 6C_p\rho\bar{v}\left(\frac{b_1}{12} + \frac{Eb_1^2}{60k}\right)$ $a_2 = 6C_p\rho\bar{v}\left(\frac{b_1}{12}\right)$ $a_3 = 6C_p\rho\bar{v}\left(-\frac{Eb_1^2}{60k}\right)$ $a_4 = E(T_1 - T_3)$	$c_1 = 6C_p\rho\bar{v}\left(\frac{b_1}{16} + \frac{21Eb_1^2}{1920k}\right)$ $c_2 = 6C_p\rho\bar{v}\left(\frac{b_1}{48}\right)$ $c_3 = 6C_p\rho\bar{v}\left(-\frac{21Eb_1^2}{1920k}\right)$ $c_4 = \frac{3k(T_1 - T_2)}{2b_1} + \frac{5E(T_1 - T_3)}{4}$
	$z = b_3$	$z = b_3/2$
COLD SIDE	$m_1 = 6C_p\rho\bar{v}\left(\frac{b_3}{12} + \frac{Eb_3^2}{60k}\right)$ $m_2 = 6C_p\rho\bar{v}\left(\frac{b_3}{12}\right)$ $m_3 = 6C_p\rho\bar{v}\left(-\frac{Eb_3^2}{60k}\right)$ $m_4 = E(T_3 - T_1)$	$n_1 = 6C_p\rho\bar{v}\left(\frac{b_3}{16} + \frac{21Eb_3^2}{1920k}\right)$ $n_2 = 6C_p\rho\bar{v}\left(\frac{b_3}{48}\right)$ $n_3 = 6C_p\rho\bar{v}\left(-\frac{21Eb_3^2}{1920k}\right)$ $n_4 = \frac{3k(T_3 - T_4)}{2b_3} + \frac{5E(T_3 - T_1)}{4}$

Table 5.4 : Level Two simultaneous equation terms - constant region

that occurs from the feed to the permeate. This meant that the effect of the permeate flux on the laminar velocity profile had to be considered.

The critical arguement was that if the momentum flux normal to the membrane caused by the shear stress in laminar flow was much greater than the momentum flux of the transferred material, then the deviation from the assumed parabolic velocity profile would be negligable.

The first step was to calculate the momentum flux due to the shear stress in laminar flow (equation (5.28)).

$$L_l \approx \mu \frac{\Delta v}{\Delta x} = \mu \frac{\Delta v}{Y/2} \qquad (5.28)$$

The second step was to calculate the momentum flux due to the flux of liquid through the membrane (equation (5.29)).

$$L_m \approx (\rho v) v \qquad (5.29)$$

Typical values in the membrane distillation system used,

$V_{max} = 1$ m/s

$Y = 0.45 \times 10^{-3}$ m

$\mu = 1 \times 10^{-3}$ Ns/m^2

$N = 4$ kg/m^{2}h

$\therefore v$ @ membrane (normal) $= N/3600\rho = 1.1 \times 10^{-6}$ m/s

Substituting these values into equations (5.28) and (5.29) gives,

$L_l = 5.4$ N/m^2

$L_m = 1.1 \times 10^{-9}$ N/m^2

L_l is much greater than L_m, and so the effect of the permeate flux on the velocity profile would be negligible, even if the flux and viscosity were both increased by 100. This means that equation (5.27) remains valid for the entire length of the channel, only the magnitude of velocity would alter.

The alteration in the magnitude of the velocity could be integrated into the analysis (See Appendix F), but as the mass transfer rates studied in this thesis were low, the magnitude

of the velocity profile was assumed constant. The Level Two Fortran programme is given in Appendix G.

5.3.2 Level Two Extension - Level Three

An extension to the Level Two model was made to allow the model to take into account different velocities and channel dimensions on either side of the membrane. This means that the structure of the Fortran programme becomes more complex. This is because for the first two models there are only two possible regions, the entrance region and the constant region. Introducing different velocities and channel dimensions means that there are three possible regions. These are,

1) both boundary layers growing i.e. entrance region,

2) one boundary layer has reached the opposite wall and the other is still growing, and

3) both boundary layers have reached the opposite wall i.e. constant region.

The logic for this expanded model is given in Figure 5.5. There can be situations where the hot boundary layer is the one which has grown to fill the channel in advance of the cold boundary layer, or situations in which the cold boundary layer is the first to fill the channel. This means that four sets of enthalpy balances need to be developed in order to take into account every situation.

Other factors which are included in this expanded model are the effect of temperature on the specific heat and densities of the two sides, as well as the variation of E, the membrane transfer coefficient.

5.3.3 Variation with temperature

Specific Heat

The specific heat varies with temperature, but for liquids the difference is not large at temperatures below the critical temperature [91]. The temperature difference along the channel is 10°C, which is small. At the minimum and maximum temperatures used in the system [91],

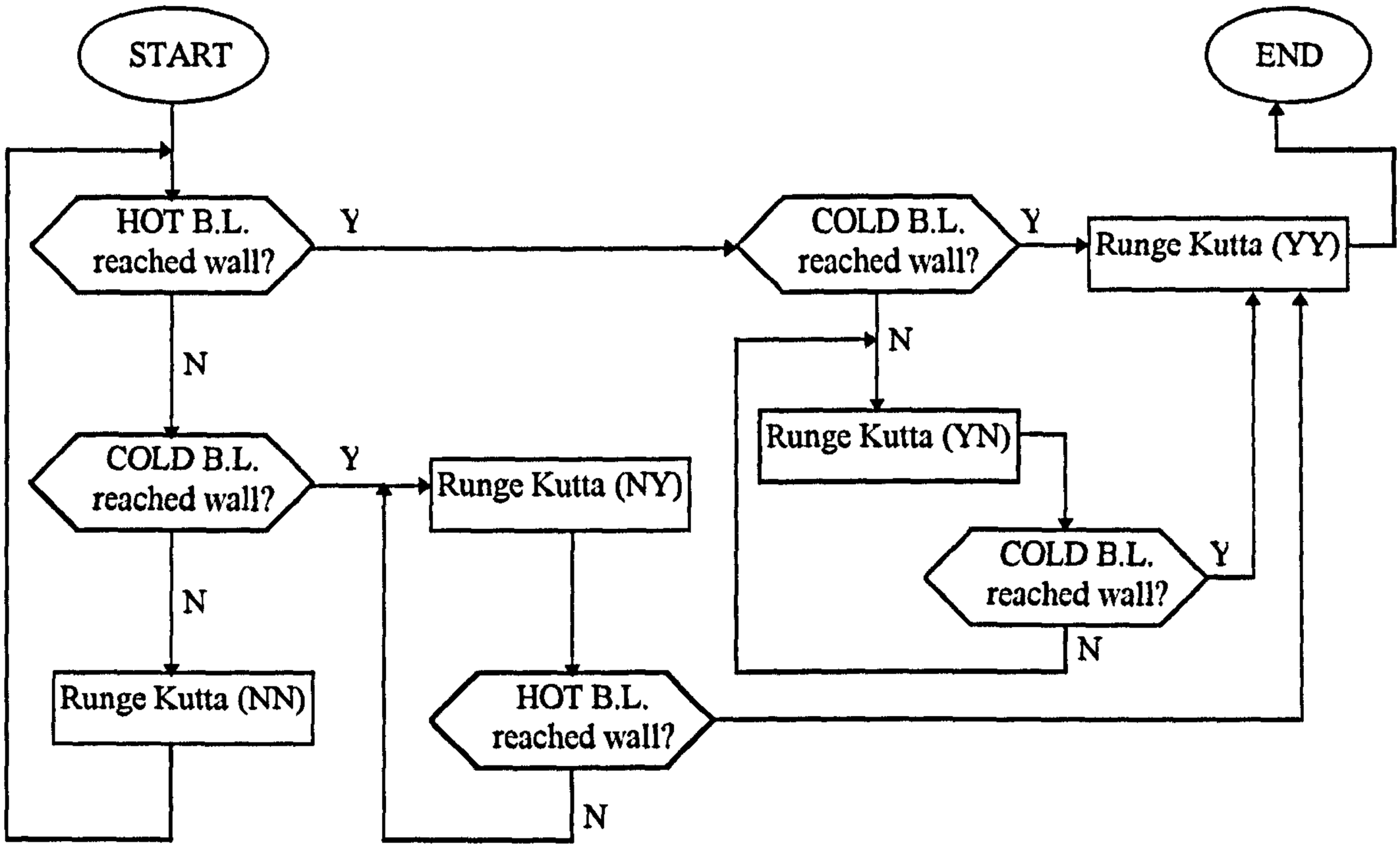

Figure 5.5: Logic diagram for expanded Level Two model

@ 10°C $C_p = 5.194$ kJ/kg K

@ 60°C $C_p = 5.185$ kJ/kg K

So the difference in specific heat is 9 J/kg K, which is negligible, 0.22% of the value at 60°C. Therefore it was assumed that the specific heat was the average of the values stated above and was constant along the module, and on both sides of the membrane.

$\therefore C_p = 5.1895$ kJ/kg K error = 0.0045 kJ/kg K ≡ 0.11 %

Density

The density also varies with temperature. At the minimum and maximum temperatures used in the system [91],

@ 10°C $\rho = 999.699$ kg/m^3

@ 60°C $\rho = 983.200$ kg/m^3

This gives a difference in density of 16.499 kg/m^3. Again, the difference is small compared to the actual values, 1.68% of the density at 60°C. Assuming the density is the average of the values stated and is constant along the module, and on both sides of the membrane,

$\rho = 991.4495$ kg/m^3 error = 8.2495 kg/m^3 ≡ 0.84 %

Membrane Transfer Coefficient

The membrane transfer coefficient, E, is given by equation (5.30) [3]

$$E = C\left.\frac{dP}{dT}\right|_{T_m} \lambda + \frac{k_m}{\delta} \qquad (5.30)$$

where, by the Clausius-Clapeyron equation,

$$\left.\frac{dP}{dT}\right|_{T_m} = \left.\frac{P\lambda M}{RT^2}\right|_{T_m} \qquad (5.31)$$

so,

$$E = C\left.\frac{P\lambda M}{RT^2}\right|_{T_m} \lambda + \frac{k_m}{\delta} \qquad (5.32)$$

In equation (5.32), the latent heat, vapour pressure and membrane mass transfer coefficient all vary with temperature. Table 5.5 gives all the terms relating to equation (5.32).

Term	Variation	Notes
λ	according to $\lambda = \lambda_b \left[\frac{T_c - T}{T_c - T_b}\right]^{0.38}$	(5.33)
P	according to $P = \exp\left(23.238 - \frac{3841}{T_m - 45}\right)$	(5.34)
k_m	constant at 0.05	varies only with type of membrane
M	18	constant
R	8314 J/kmol K	constant
C	according to type of membrane and operating conditions	
δ	constant at 0.13mm	varies only with type of membrane

Table 5.5: Terms from equation (5.32) variation with temperature

It is necessary to determine whether the variation of latent heat is going to have a large effect on the heat transfer. From steam tables, the following values were obtained at the miniumum and maximum temperatures used in the system.

lowest T =10°C $\lambda = 2477.2$ kJ/kg

highest T = 60°C $\lambda = 2357.9$ kJ/kg

$$\therefore \Delta\lambda = 119.3 \text{ kJ/kg}$$

Calculating the percentage error, taking an average of the minimum and maximum values,

$\lambda = 2420$ kJ/kg error = $\pm$ 60 kJ/kg $\equiv$ 2.48%

Figure 5.6 shows the difference between using accurate values of λ and assuming an average value of 2420 kJ/kg, on E, the membrane transfer coefficient. At the temperatures selected, using a constant value of λ does not alter E to a large degree, but as the temperature is increased past 333K, accurate values of λ would have to be used. The maximum difference, assuming a constant average value of λ, at 333K is 55.484 kJ/kg, which is equivalent to an increase of 3.90% from using the accurate value.

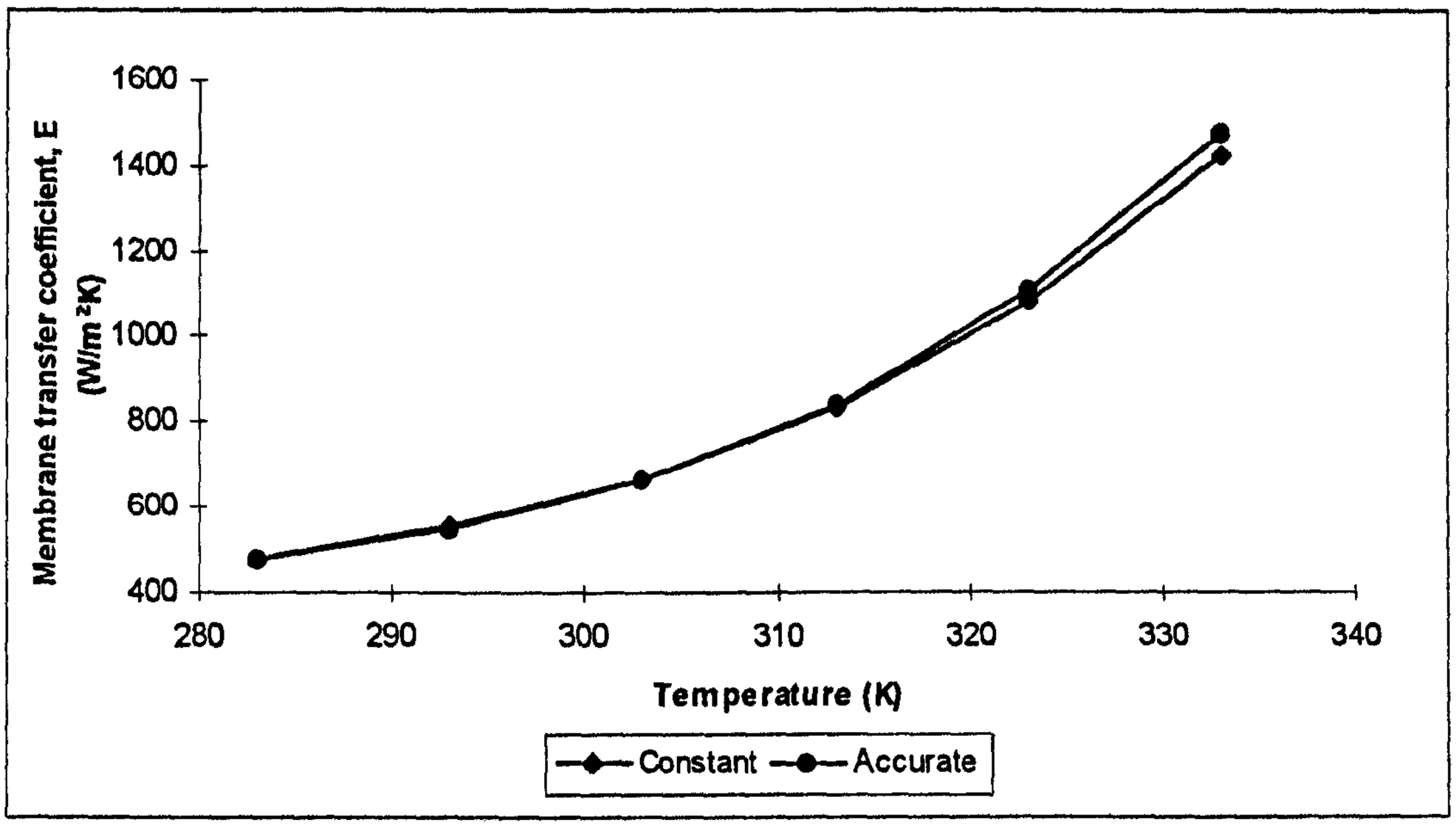

Figure 5.6: Effect of temperature variation of the latent heat on the membrane transfer coefficient

Therefore for this work it was assumed λ is constant at 2420 kJ/kg.

The membrane mass transfer coefficient, C, varies with temperature according to the type of membrane used and the operating conditions. Schofield *et al* [3] carried out experiments with water vapour at temperatures and pressure similar to those used in the experiments for this work, with the same type of membrane. The value of membrane mass transfer coefficient, C, for a Millipore 0.45μm PVDF membrane is 5.8×10^{-7} kg/m^2sPa [3].

Once the latent heat and membrane mass transfer coefficient had been assumed constant over the range of temperatures used for this work, the next step was to look at the membrane transfer coefficent, E.

From equation (5.32), assuming C and λ constant,

$$E = \left.\frac{CP\lambda^2 M}{RT^2}\right|_{T_m} + \frac{k_m}{\delta} \qquad (5.35)$$

Putting in values,

$$E = \frac{4.8\times10^{-7}\left(2420\times10^3\right)^2 \times 18 \times P}{8314 \times T^2} + \frac{0.05}{0.13\times10^{-3}}$$

$$E = 6086.035\frac{P}{T^2} + 384.615 \qquad (5.36)$$

For the Fortran programme, for each full iteration, equations (5.39) and (5.40) had to be calculated at the mean membrane temperature T_m, assuming

$$T_m = \frac{T_1 + T_3}{2} \qquad (5.37)$$

This was done to take account of temperature variation along the module. Equations (5.38), (5.39), and (5.40) are written as they appear in the programme.

$$\therefore \quad Tm = (T10+T30)/2 \qquad (5.38)$$

$$P = EXP(23.238-(3841/(Tm-45))) \qquad (5.39)$$

$$E=((6086.035\times P)/(Tm\times Tm))+385.615 \qquad (5.40)$$

The enthalpy balance equations developed are basically the same as for the simple Level Two model. The Fortran programme for Level Three is given in Appendix H.

5.3.4 Results and Discussion

The Level Three model was run with the same starting conditions as the Level One model. The results, graphs and discussion can be found in Chapter 7.5.

5.4 Level Four: Laminar Velocity Profile, Single Component, Wall Heat Transfer

All earlier models assumed insulated walls opposite the membrane. From the results (given in Chapter 7.3) it can be seen that the temperature decreases as the fluid flows down the channel. To overcome this, the next step was to introduce heat through the channel wall. This meant extra heat conduction terms had to be included in the enthalpy balances. The diagram describing the situation and nomenclature is shown in Figure 5.7.

5.4.1 The Entrance Region

The balance terms are the same as for the previous Levels, but in the entrance region there are two more independant thermal boundary layers developing from the walls. The development of the related enthalpy balances follow the same method described in Chapter 5.2 so that the general balance is,

$$C_p \rho \frac{d}{dx} \int_{w=0}^{w=w_1} v(w)\left[T(w) - T(w_1)\right] dw = k \left.\frac{dT}{dw}\right|_{w=w_1} - k \left.\frac{dT}{dw}\right|_{w=0} \qquad (5.41)$$

The Solution Procedure

For the entrance region, the Level Three balances are used, together with the independant wall thermal boundary layers. The wall boundary layers require their own temperature profile, again developed as before. For example, the temperature profile for

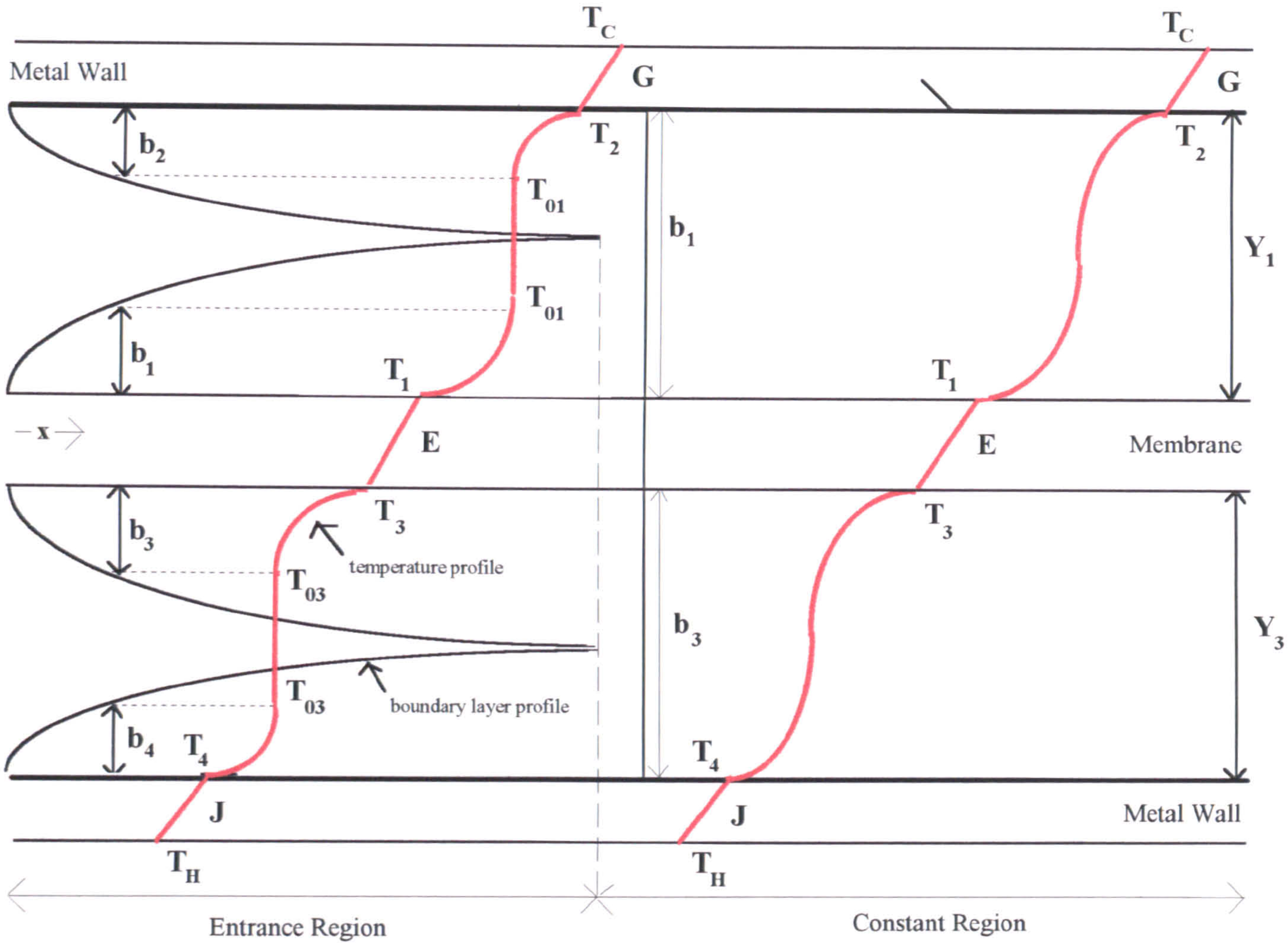

Figure 5.7: Level Four boundary layer schematic including nomenclature

the hot side with the boundary layer growing from the wall, has the following boundary conditions: @ w = 0, T = T_2 and dT/dw = -G(T_C-T_2)/k and @ w = w_1, T = T_{01} and dT/dw = 0, which gives,

$$T = T_2 + \frac{G(T_2 - T_C)}{k}w + \left[\frac{3(T_{01} - T_2)}{b_2^{\,2}} - \frac{2G(T_2 - T_C)}{kb_2}\right]w^2 + \left[\frac{G(T_2 - T_C)}{kb_2^{\,2}} - \frac{2(T_{01} - T_2)}{b_2^{\,3}}\right]w^3 \qquad (5.42)$$

In total there are 8 enthalpy balances for the entrance region, which can be found in Appendix E. The differential equations that were solved in the Fortran programme are given in Tables 5.6 and 5.7. The entrance region ends when $b_1 + b_2 = Y_1$.

5.4.2 The Constant Region

The constant region is much simpler than the entrance region. Again the enthalpy balances are developed in the same manner. The temperature profile for the constant region had to include the effect of the heat transfer through the wall.

For example, for the hot side the boundary conditions of the temperature profile are,:

@ y = 0, T = T_1 and dT/dy = -E(T_1-T_3)/k and @ y = y_1, T = T_2 and dT/dy = -G(T_C-T_2)/k

which gives,

$$T = T_1 + \frac{E(T_1 - T_3)}{k}y + \left[\frac{3(T_2 - T_1)}{b_1^{\,2}} - \frac{2E(T_1 - T_3)}{kb_1} - \frac{2G(T_C - T_2)}{kb_1}\right]y^2 + \left[\frac{G(T_C - T_2)}{kb_1^{\,2}} + \frac{E(T_1 - T_3)}{kb_1^{\,2}} - \frac{2(T_2 - T_1)}{b_1^{\,3}}\right]y^3 \qquad (5.43)$$

There are four enthalpy balances for the constant region, which can be found in Appendix E. The differential equation terms that were solved in the Fortran programme are given in Table 5.8. The full Fortran programme is given in Appendix I.

5.4.3 Supply and Removal of Heat

The aim is to maintain constant temperatures on the outside walls of the channels along the entire channel length. A way of realising this is to use boiling and condensing heat transfer. For instance, when a gas is condensing, it gives out its latent heat of

ENTRANCE REGION		
	$w=b_2$	$w=b_2/2$
HOT SIDE	$a_1 = 6C_p\rho\bar{v}\left(\frac{3T_{01}b_2}{10Y_1} - \frac{3T_2b_2}{10Y_1} + \frac{T_2b_2^2}{5Y_1^2} - \frac{T_{01}b_2^2}{5Y_1^2} + \frac{Gb_2^2T_C}{10Y_1k} - \frac{Gb_2^2T_2}{10Y_1k} - \frac{Gb_2^3T_C}{15Y_1^2k} + \frac{Gb_2^3T_2}{15Y_1^2k}\right)$ $a_2 = 6C_p\rho\bar{v}\left(\frac{b_2^3}{15Y_1^2} - \frac{3b_2^2}{20Y_1} - \frac{Gb_2^3}{30Y_1k} + \frac{Gb_2^4}{60Y_1^2k}\right)$ $a_3 = G(T_C - T_2)$	$c_1 = 6C_p\rho\bar{v}\left(\frac{9T_{01}b_2}{160Y_1} - \frac{9T_2b_2}{160Y_1} - \frac{7T_{01}b_2^2}{320Y_1^2} + \frac{7T_2b_2^2}{320Y_1^2} + \frac{GT_Cb_2^2}{320Y_1k} - \frac{GT_2b_2^2}{320Y_1k} - \frac{GT_Cb_2^3}{480Y_1^2k} + \frac{GT_2b_2^3}{480Y_1^2k}\right)$ $c_2 = 6C_p\rho\bar{v}\left(\frac{7b_2^3}{960Y_1^2} - \frac{9b_2^2}{320Y_1} - \frac{Gb_2^3}{960Y_1k} + \frac{Gb_2^4}{1920Y_1^2k}\right)$ $c_4 = \frac{5G(T_C - T_2)}{4} + \frac{3k(T_{01} - T_2)}{2b_2}$
	$u=b_4$	$u=b_4/2$
COLD SIDE	$m_1 = 6C_p\rho\bar{v}\left(\frac{3T_{03}b_4}{10Y_3} - \frac{3T_4b_4}{10Y_3} - \frac{T_{03}b_4^2}{5Y_3^2} + \frac{T_4b_4^2}{5Y_3^2} + \frac{Jb_4^2T_H}{10Y_3k} - \frac{Jb_4^2T_4}{10Y_3k} - \frac{Jb_4^3T_H}{15Y_3^2k} + \frac{Jb_4^3T_4}{15Y_3^2k}\right)$ $m_2 = 6C_p\rho\bar{v}\left(\frac{b_4^3}{15Y_3^2} - \frac{3b_4^2}{20Y_3} - \frac{Jb_4^3}{30Y_3k} + \frac{Jb_4^4}{60Y_3^2k}\right)$ $m_3 = J(T_4 - T_H)$	$n_1 = 6C_p\rho\bar{v}\left(\frac{9T_{03}b_4}{160Y_3} - \frac{9T_4b_4}{160Y_3} - \frac{7T_{03}b_4^2}{320Y_3^2} + \frac{7T_4b_4^2}{320Y_3^2} + \frac{JT_Hb_4^2}{320Y_3k} - \frac{JT_4b_4^2}{320Y_3k} - \frac{JT_Hb_4^3}{480Y_3^2k} + \frac{JT_4b_4^3}{480Y_3^2k}\right)$ $n_2 = 6C_p\rho\bar{v}\left(\frac{7b_4^3}{960Y_3^2} - \frac{9b_4^2}{320Y_3} - \frac{Jb_4^3}{960Y_3k} + \frac{Jb_4^4}{1920Y_3^2k}\right)$ $n_4 = \frac{5J(T_4 - T_H)}{4} + \frac{3k(T_{03} - T_4)}{2b_4}$

Table 5.6 : Level Four wall simultaneous equation terms - entrance region

ENTRANCE REGION		
	$y = b_1$	$y = b_1/2$
HOT SIDE	$a_1 = 6C_p\rho\bar{v}\left(\frac{3T_1b_1}{10Y_1} - \frac{3T_{01}b_1}{10Y_1} - \frac{T_1b_1^2}{5Y_1^2} + \frac{T_{01}b_1^2}{5Y_1^2} + \frac{Eb_1^2T_1}{10Y_1k} - \frac{Eb_1^2T_3}{10Y_1k} - \frac{Eb_1^3T_1}{15Y_1^2k} + \frac{Eb_1^3T_3}{15Y_1^2k}\right)$ $a_2 = 6C_p\rho\bar{v}\left(\frac{3b_1^2}{20Y_1} - \frac{b_1^3}{15Y_1^2} + \frac{Eb_1^3}{30Y_1k} - \frac{Eb_1^4}{60Y_1^2k}\right)$ $a_3 = 6C_p\rho\bar{v}\left(\frac{Eb_1^3}{30Y_1k} - \frac{Eb_1^4}{60Y_1^2k}\right)$ $a_4 = E(T_1 - T_3)$	$c_1 = 6C_p\rho\bar{v}\left(\frac{9T_1b_1}{160Y_1} - \frac{9T_{01}b_1}{160Y_1} - \frac{7T_1b_1^2}{320Y_1^2} + \frac{7T_{01}b_1^2}{320Y_1^2} + \frac{ET_1b_1^2}{320Y_1k} - \frac{ET_3b_1^2}{320Y_1k} - \frac{ET_1b_1^3}{480Y_1^2k} + \frac{ET_3b_1^3}{480Y_1^2k}\right)$ $c_2 = 6C_p\rho\bar{v}\left(\frac{9b_1^2}{320Y_1} - \frac{7b_1^3}{960Y_1^2} + \frac{Eb_1^3}{960Y_1k} - \frac{Eb_1^4}{1920Y_1^2k}\right)$ $c_3 = 6C_p\rho\bar{v}\left(\frac{Eb_1^4}{1920Y_1^2k} - \frac{Eb_1^3}{960Y_1k}\right)$ $c_4 = \frac{5E(T_1 - T_3)}{4} - \frac{3k(T_{01} - T_1)}{2b_1}$
	$z = b_3$	$z = b_3/2$
COLD SIDE	$m_1 = 6C_p\rho\bar{v}\left(\frac{3T_3b_3}{10Y_3} - \frac{3T_{03}b_3}{10Y_3} - \frac{T_3b_3^2}{5Y_3^2} + \frac{T_{03}b_3^2}{5Y_3^2} + \frac{Eb_3^2T_3}{10Y_3k} - \frac{Eb_3^2T_1}{10Y_3k} - \frac{Eb_3^3T_3}{15Y_3^2k} + \frac{Eb_3^3T_1}{15Y_3^2k}\right)$ $m_2 = 6C_p\rho\bar{v}\left(\frac{3b_3^2}{20Y_3} - \frac{b_3^3}{15Y_3^2} + \frac{Eb_3^3}{30Y_3k} - \frac{Eb_3^4}{60Y_3^2k}\right)$ $m_3 = 6C_p\rho\bar{v}\left(\frac{Eb_3^3}{30Y_3k} - \frac{Eb_3^4}{60Y_3^2k}\right)$ $m_4 = E(T_3 - T_1)$	$n_1 = 6C_p\rho\bar{v}\left(\frac{9T_3b_3}{160Y_3} - \frac{9T_{03}b_3}{160Y_3} - \frac{7T_3b_3^2}{320Y_3^2} + \frac{7T_{03}b_3^2}{320Y_3^2} + \frac{ET_3b_3^2}{320Y_3k} - \frac{ET_1b_3^2}{320Y_3k} - \frac{ET_3b_3^3}{480Y_3^2k} + \frac{ET_1b_3^3}{480Y_3^2k}\right)$ $n_2 = 6C_p\rho\bar{v}\left(\frac{9b_3^2}{320Y_3} - \frac{7b_3^3}{960Y_3^2} + \frac{Eb_3^3}{960Y_3k} - \frac{Eb_3^4}{1920Y_3^2k}\right)$ $n_3 = 6C_p\rho\bar{v}\left(\frac{Eb_3^4}{1920Y_3^2k} - \frac{Eb_3^3}{960Y_3k}\right)$ $n_4 = \frac{5E(T_3 - T_1)}{4} - \frac{3k(T_{03} - T_3)}{2b_3}$

Table 5.7 : Level Four membrane simultaneous equation terms - entrance region

CONSTANT REGION		
	$y=b_1$	$y=b_1/2$
HOT SIDE	$a_1 = 6C_p\rho\bar{v}\left(\frac{b_1}{12}+\frac{Eb_1^2}{60k}\right)$ $a_2 = 6C_p\rho\bar{v}\left(\frac{b_1}{12}+\frac{Gb_1^2}{60k}\right)$ $a_3 = 6C_p\rho\bar{v}\left(-\frac{Eb_1^2}{60k}\right)$ $a_4 = E(T_1-T_3)-G(T_C-T_2)$	$c_1 = 6C_p\rho\bar{v}\left(\frac{b_1}{16}+\frac{21Eb_1^2}{1920k}\right)$ $c_2 = 6C_p\rho\bar{v}\left(\frac{b_1}{48}+\frac{11Gb_1^2}{1920k}\right)$ $c_3 = 6C_p\rho\bar{v}\left(-\frac{21Eb_1^2}{1920k}\right)$ $c_4 = \frac{3k(T_1-T_2)}{2b_1}+\frac{5E(T_1-T_3)}{4}+\frac{G(T_C-T_2)}{4}$
	$z=b_3$	$z=b_3/2$
COLD SIDE	$m_1 = 6C_p\rho\bar{v}\left(\frac{b_3}{12}+\frac{Eb_3^2}{60k}\right)$ $m_2 = 6C_p\rho\bar{v}\left(\frac{b_3}{12}+\frac{Jb_3^2}{60k}\right)$ $m_3 = 6C_p\rho\bar{v}\left(-\frac{Eb_3^2}{60k}\right)$ $m_4 = E(T_3-T_1)-J(T_H-T_4)$	$n_1 = 6C_p\rho\bar{v}\left(\frac{b_3}{16}+\frac{21Eb_3^2}{1920k}\right)$ $n_2 = 6C_p\rho\bar{v}\left(\frac{b_3}{48}+\frac{11Jb_3^2}{1920k}\right)$ $n_3 = 6C_p\rho\bar{v}\left(-\frac{21Eb_3^2}{1920k}\right)$ $n_4 = \frac{3k(T_3-T_4)}{2b_3}+\frac{5E(T_3-T_1)}{4}+\frac{J(T_H-T_4)}{4}$

Table 5.8 : Level Four simultaneous equation terms - constant region

vapourisation i.e. it is a source of heat. Similarly, boiling requires heat and is a source of cooling.

These principles have been utilised in heat pumps (see Figure 5.8) in which a suitable refrigerant is pumped round a system consisting of both boiling and condensing surfaces. The associated pressure-enthalpy diagram is given in Figure 5.9.

Although in Figure 5.7, T_C and T_H are shown as the wall temperatures, they are in fact, the bulk gas temperatures. The heat transfer through the liquid layers has been incorporated into the wall heat transfer coefficients, G and J respectively. This was done to reduce and simplify the outer wall variables in the analysis. This is because the detail necessary for this stage only required a constant wall temperature, not detailed knowledge of the heat transfer rate through the wall.

Sample Wall Heat Transfer Rates

There are various refrigerants suitable for use in a heat pump, and a selection are given in Table 5.9.

Chemical	Refrigerant Identification	Density (liquid) (kg/m^3)	Density (vapour) (kg/m^3)	Viscosity (Pa s)	Specific Heat (kJ/kg K)	Thermal Conductivity (W/m K)	Latent Heat (kJ/kg K)
Methyl Chloride	R40	90.66	13.83	2.51E-04	1.605	0.156	374
Propane	R290	489.24	21.692	1.10E-04	2.76	0.091	333.3
n-Butane	R600	570.78	6.523	1.62E-04	2.437	0.116	359.59
Isobutane	R600a	548.25	9.615	1.59E-04	2.53	0.106	327.3
Ammonia	R717	600.24	8.264	1.41E-04	5.82	0.477	1157.5
Propylene	R1270	503.27	25.707	8.70E-05	2.694	0.11	329.4
Water		997.01	0.0256	8.55E-04	5.179	0.613	2437.5
* All data taken at 300K							

Table 5.9: Physical properties of various refrigerants

To work out suitable heat transfer coefficients, equations describing the boiling and condensing film coefficients were found and are,

for condensing on horizontal tubes,

$$h_f\left(\frac{\mu^2}{k^3\rho^2 g}\right)^{\frac{1}{3}} = 1.51\left(\frac{4m}{l\mu}\right)^{-\frac{1}{3}} \qquad (5.44)$$

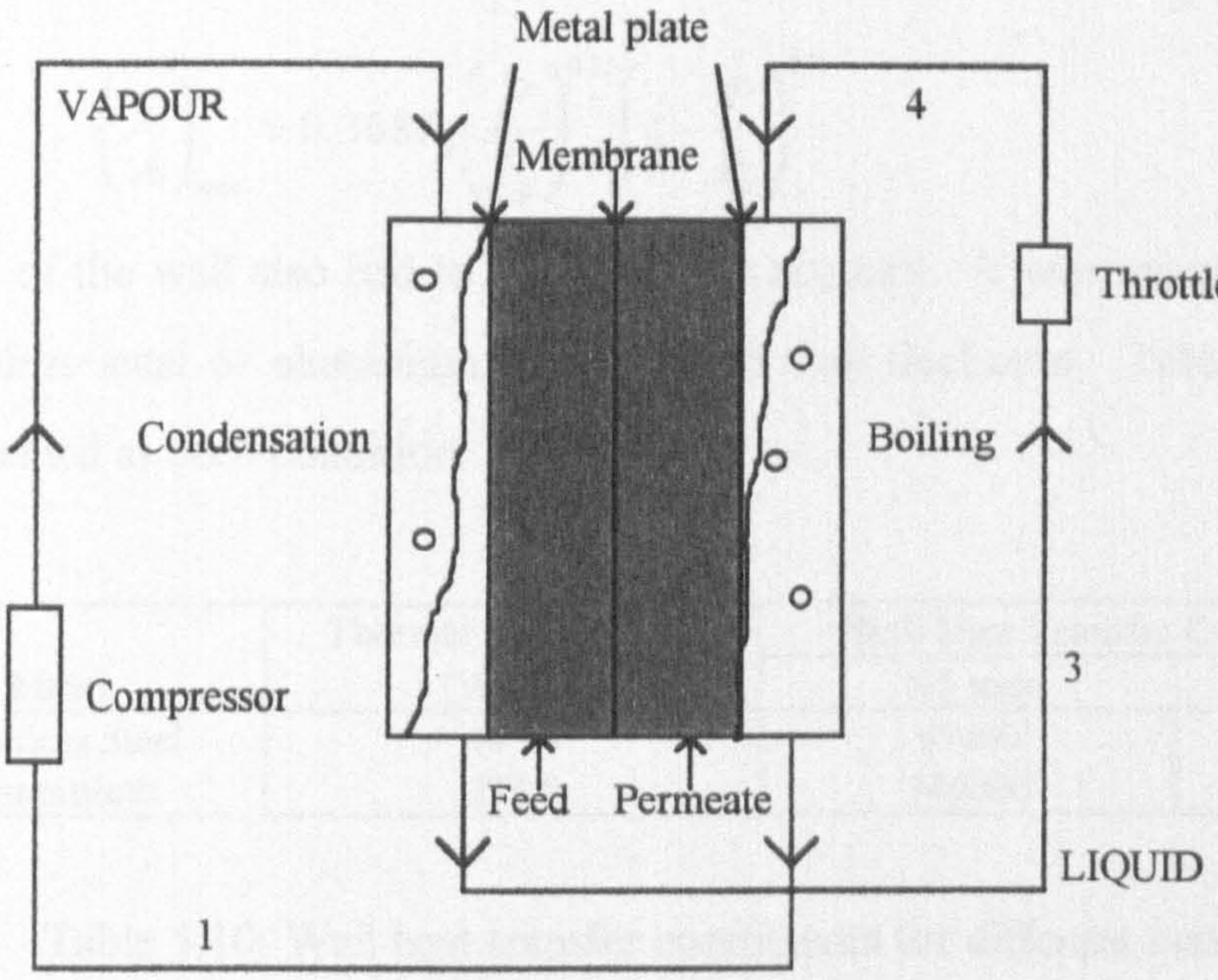

Figure 5.8: Heat pump circuit

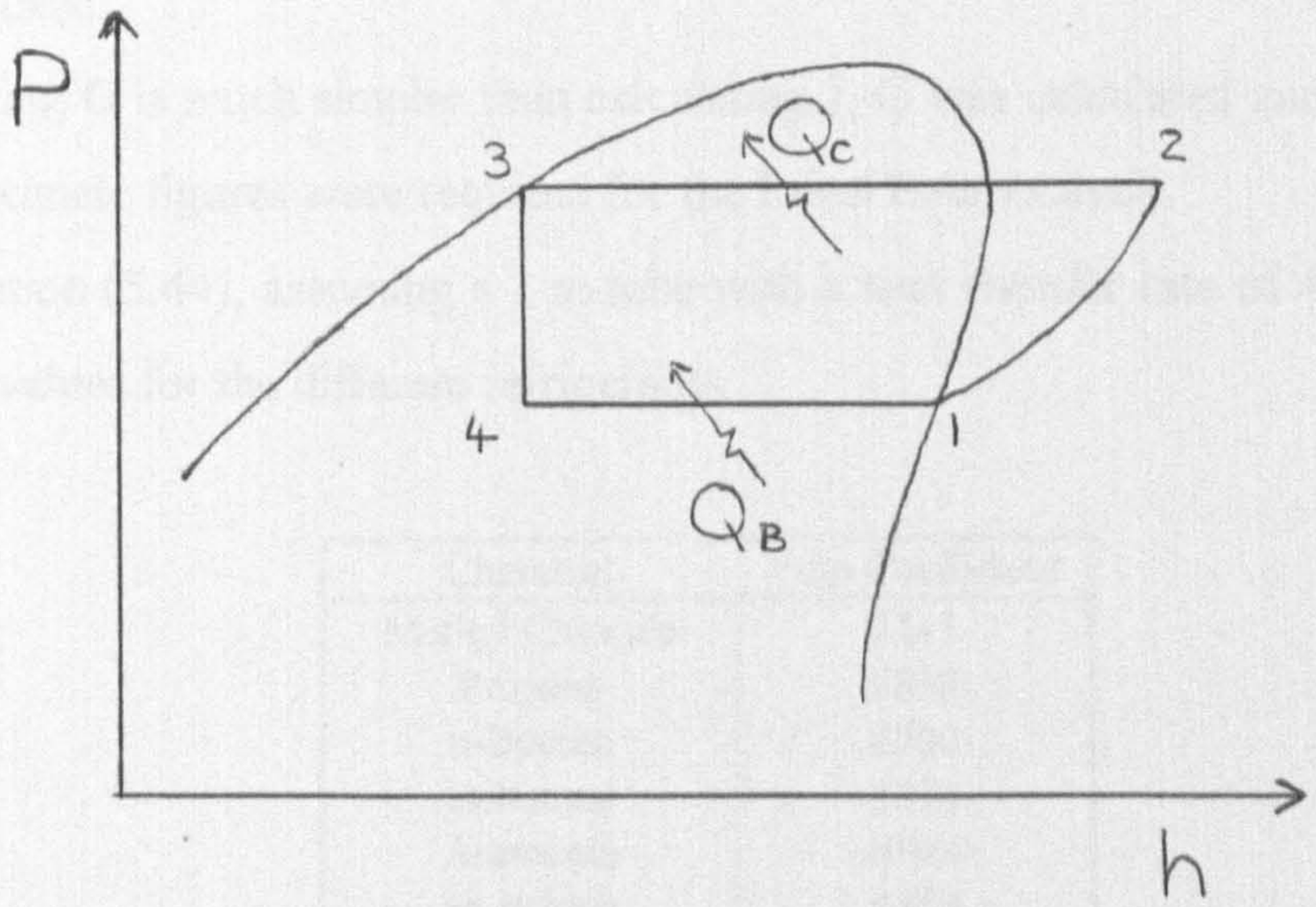

Figure 5.9: Pressure-Enthalpy diagram for the heat pump circuit

for nucleate boiling on a single tube, or flat surface [88],

$$h_g = 3.75\times10^{-5} P_d^{0.69}\left(\frac{q}{A}\right)^{0.7}\left[1.8\left(\frac{P}{P_d}\right)^{0.17} + 4\left(\frac{P}{P_d}\right)^{1.2} + 10\left(\frac{P}{P_d}\right)^{10}\right] \qquad (5.45)$$

where,
$$\left(\frac{q}{A}\right)_{max} = 0.368 P_d\left(\frac{P}{P_d}\right)^{0.35}\left(1-\frac{P}{P_d}\right)^{0.9} \qquad (5.46)$$

The effect of the wall also had to be taken into account. It was assumed that the walls were stainless steel or aluminium of 1.0 or 0.5 mm thickness. Table 5.10 shows the values obtained at each condition.

Metal	Thermal Conductivity (W/mK)	Wall Heat Transfer Coefficient, h_w	
		0.5 mm	1.0 mm
Stainless Steel	46.76	93460	46730
Aluminium	273.0	546000	273000

Table 5.10: Wall heat transfer coefficients for different materials

As it can be seen from Table 5.10, aluminium gives much higher wall heat transfer coefficients, but when included with the film coefficients, it does not produce such a great difference.

As calculating G is much simpler than calculating J, G was calculated and J assumed, as only approximate figures were required for the Level Four analysis.

Using equation (5.44), assuming a 1 m tube with a heat transfer rate of 40 W/m^2, Table 5.11 gives values for the different refrigerants.

Chemical	Film Coefficient
Methyl Chloride	2141
Propane	4868
n-Butane	6200
Isobutane	5378
Ammonia	40769
Propylene	6459
Water	51651

Table 5.11: Film heat transfer coefficients for different refrigerants

Now, the overall heat transfer rate is,

$$\frac{1}{G} = \frac{1}{h_f} + \frac{1}{h_w} \tag{5.47}$$

and Table 5.12 gives the values of G for the different wall types as given in Table 5.10.

Chemical	Overall Coefficient, G (W/m^2K)			
	Stainless steel 1.0 mm	Stainless steel 0.5 mm	Aluminium 1.0 mm	Aluminium 0.5 mm
Methyl Chloride	2047	2093	2124	2133
Propane	4409	4627	4783	4825
n-Butane	5473	5814	6062	6130
Isobutane	4823	5086	5274	5326
Ammonia	21773	28386	35472	37936
Propylene	5675	6041	6310	6383
Water	24534	33266	43434	47187

Table 5.12: Values of G for different refrigerants and wall types

For the Level Four analysis, a value of 2000 W/m^2 K was taken as G. J was assumed to be the same.

5.4.4 Results and Discussion

The Level Four model was run with the same starting conditions as previous levels, and the results, graphs and discussion can be found in Chapter 7.5.

CHAPTER 6

EXPERIMENTAL PROCEDURE

6.1 Introduction

Various experiments were carried out in order to investigate membrane distillation and to characterise the performance of the flat plate module used. The experiments included varying the temperature, flow rate and types of membrane, and noting the effect on the permeate flux. Experiments were also conducted to provide corroborating data for the theoretical models described in Chapters 3, 4 and 5.

In this Chapter, the experimental rig and the tests conducted, are described.

6.2 The Experimental Rig

The experimental rig used consisted of a flat plate module, with a maximum exposed membrane surface area of 36.4 cm^2. The components of the module are shown in Figure 6.1. The exposed area could be reduced by decreasing the number of spacer gaps available for flow. A diagram of the complete experimental rig is shown in Figure 6.2. On the hot, feed side of the rig, the bulk fluid was heated in a container situated in a water bath. The liquid was then pumped to the module. From the module it was returned to the bulk fluid container. On the cold, permeate side of the rig, the fluid was cooled by passing it through a coil located in a refrigerated water bath. It was then pumped into the module. After leaving the module, the fluid entered a container located on a balance which recorded the weight increase of permeate. From the bulk container the fluid passed into the cooling coil. Peristaltic pumps, producing pulsed flow, were used to pump the fluids through the gap produced by the spacers either side of the membrane. The spacers also supported the membrane.

Distilled water was used on both sides of the membrane for all the experiments conducted. This allowed the fundamental temperature dependant process involved in membrane distillation to be studied, but eliminated the effects of variation of concentration.

6.2.1 Configuration Of The Module

Various module plates were used, all with slightly different channel dimensions. Figure 6.3 shows the modules plates used, as well as a spacer. The main channels on Plate C were twice as wide as those on Plate A, and the minor channels on Plate D were smaller than those on Plate A. The silicone spacers used had a thickness of 0.45 mm. A complete module was made up of a module plate, a spacer, the membrane, a spacer, and then another module plate as shown in Figure 6.1.

6.2.2 Types Of Membranes Used

The membranes used were all hydrophobic and porous and the details are summarised in Table 6.1. PVDF is Poly vinyldiflouride, PTFE is Poly tetrafluoroethylene, and Versapor

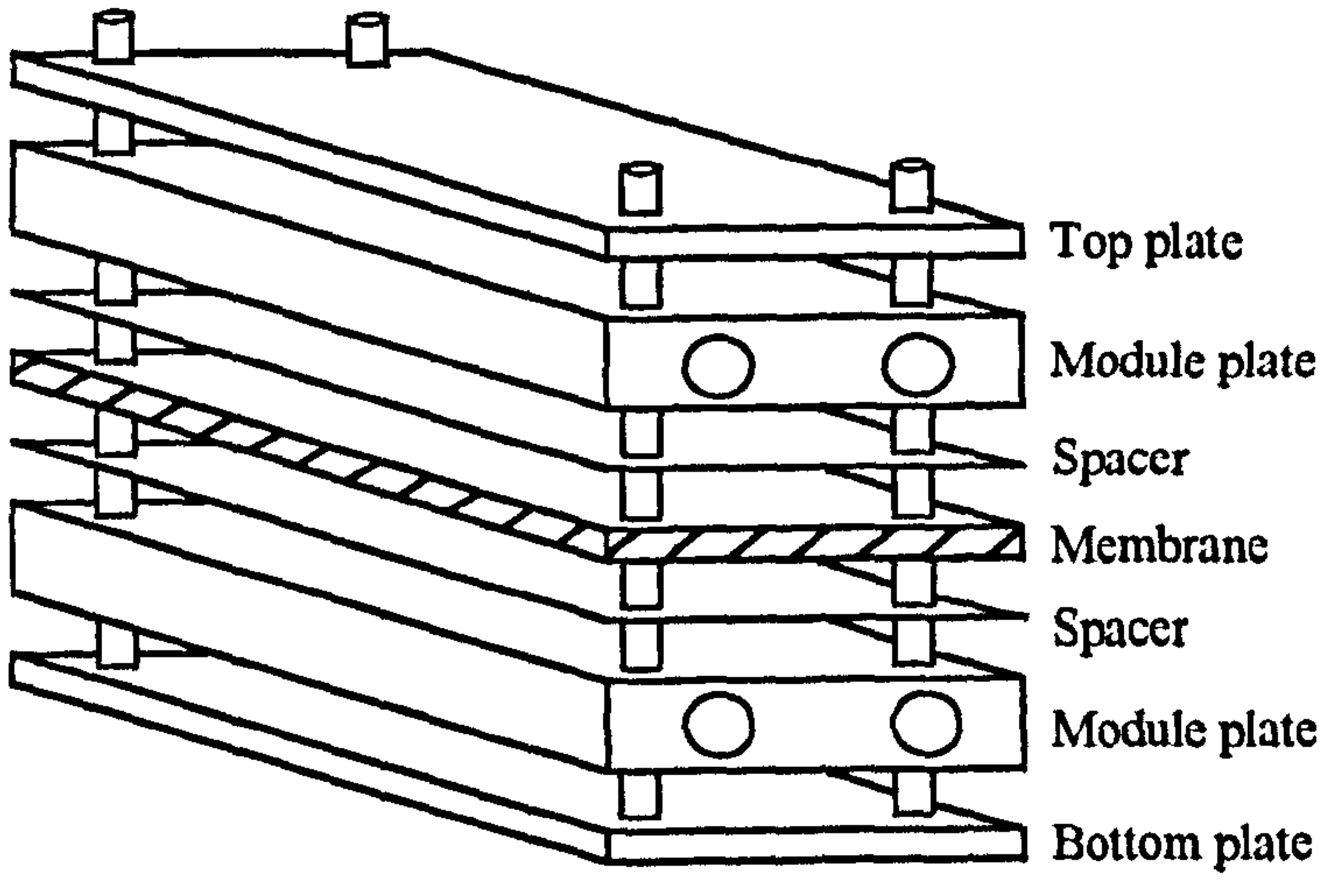

Figure 6.1: Module construction

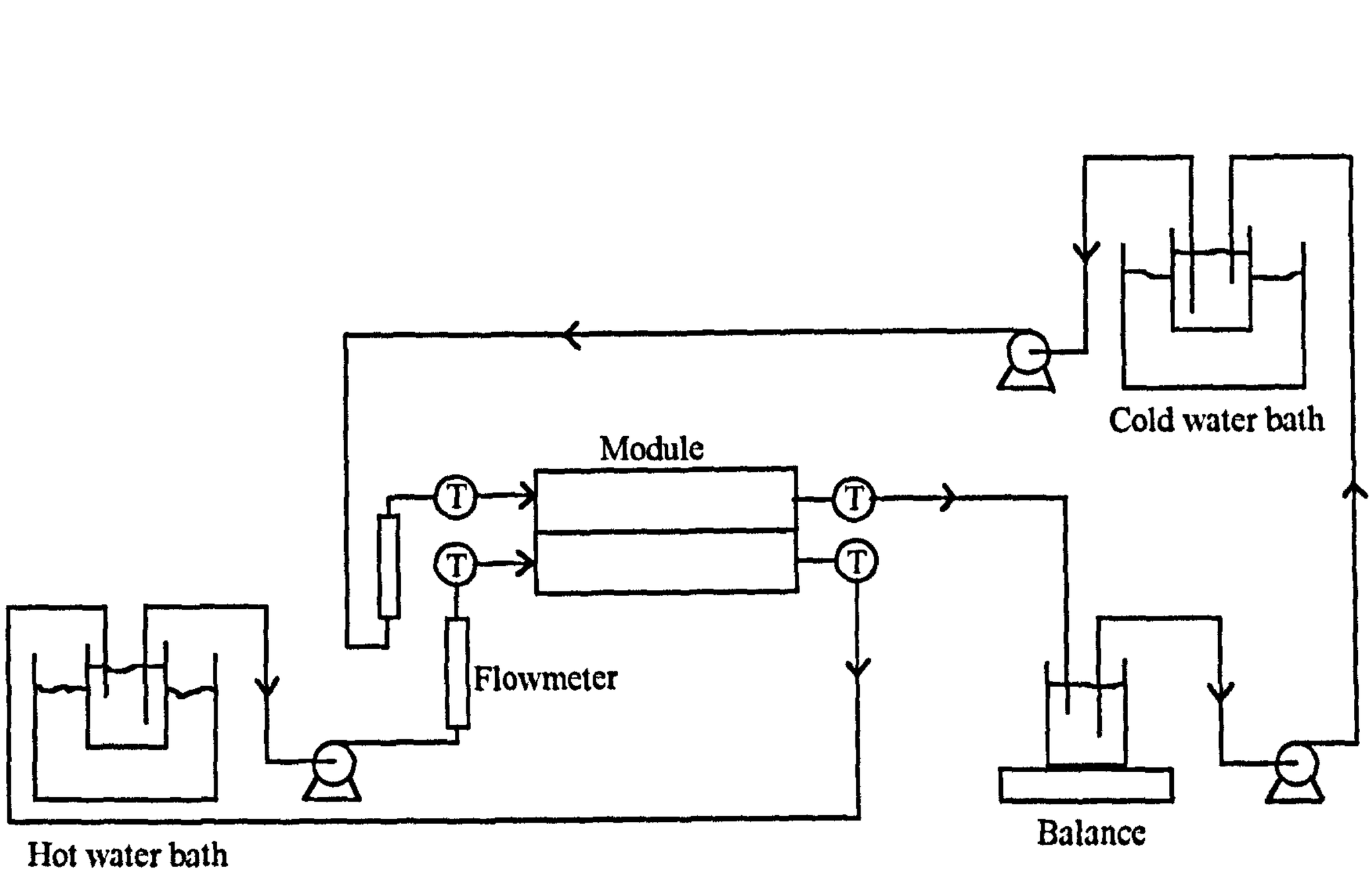

Figure 6.2: Experimental rig

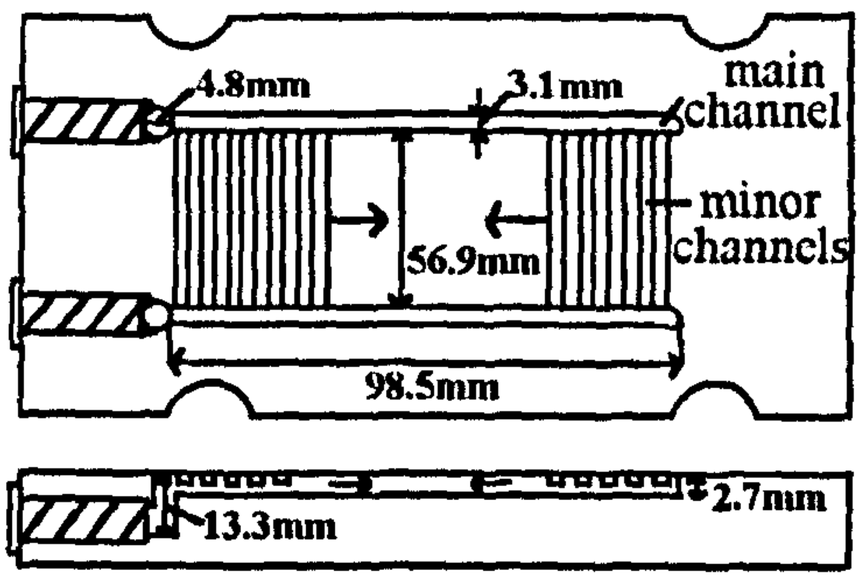

a) CHANNELLED

43 active minor channels - 0.85 x 0.85

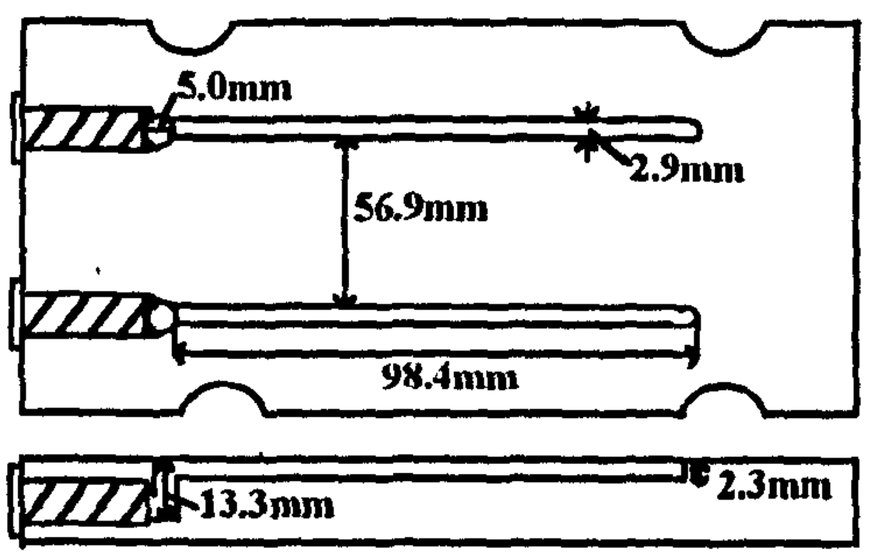

b) PLAIN PLATE

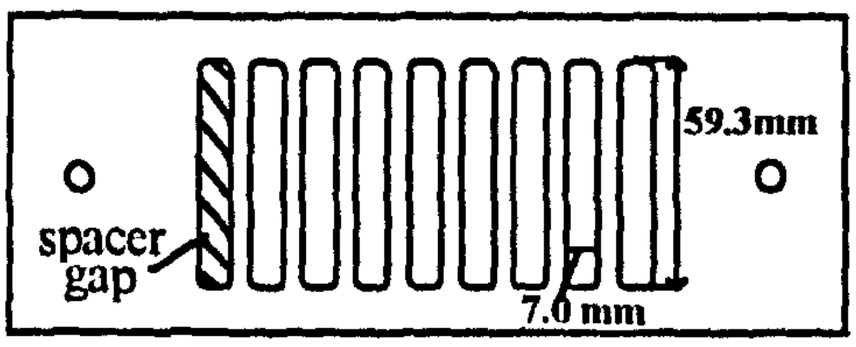

e) SPACER

0.45 mm thick

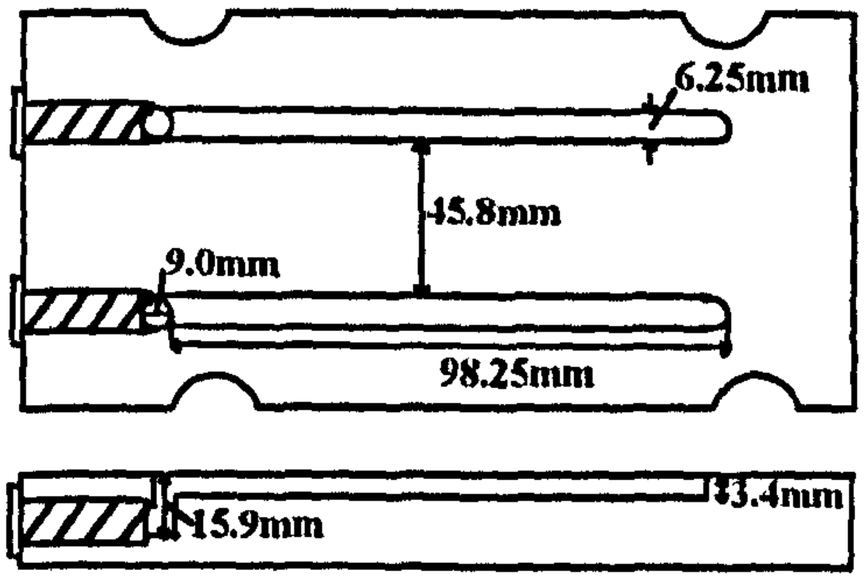

c) WIDE PLATE

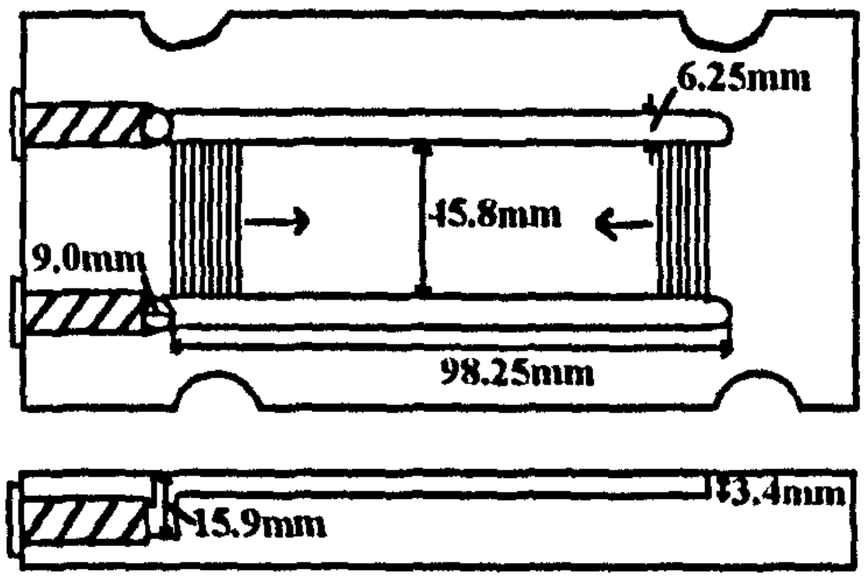

d) WIDE CHANNELLED

60 active minor channels - 0.5 x 0.5

Figure 6.3: Module components

is a composite membrane made of modified acrylic polymer cast on a nonwoven nylon support. A new membrane was used for each experiment. The active membrane area was equal to the total area of the spacer gaps.

Membrane	Pore Size (μm)	Porosity (%)	Thickness (mm)
PVDF	0.45	75	0.13
PTFE	0.2	80	0.06
Versapor	0.2	-	0.17

Table 6.1 : Membranes used in the experiments

Plate 6.1 shows the surface of a PTFE membrane by a Scanning Electron Microscope at a magnification of 5000. Plate 6.2 is of a PVDF membrane and Plate 6.3 is of a Versapor membrane. As it can be seen, the PTFE pores show the stretched characteristic caused by the membrane formation process. The Versapor membrane has better defined pores, but the structure is 'spongy'. The PVDF membrane is the membrane used for the majority of this work, and has a well defined pore structure. Plate 6.4 is of a used PVDF membrane. Comparing Plate 6.4 with Plate 6.1, the pore openings on the used membrane have been deformed. The surface has a squashed texture, altering the size of the entrances to the pores.

6.3 Experimental Work

6.3.1 Determination of the Basic Performance

For these experiments, the full range of module plates were used. The temperatures entering and leaving the module were recorded by K-type thermocouples. The increase in the weight of the permeate with time was also recorded in order to measure the permeate flux. The aim was to observe the effect of the flowrate and module geometry on the flux. Each run lasted between 1 and 2 hours, with temperature readings taken

Plate 5.1: SEM of a PTFE membrane - magnification x 5000

Plate 5.2: SEM of a new PVDF membrane - magnification x 5000

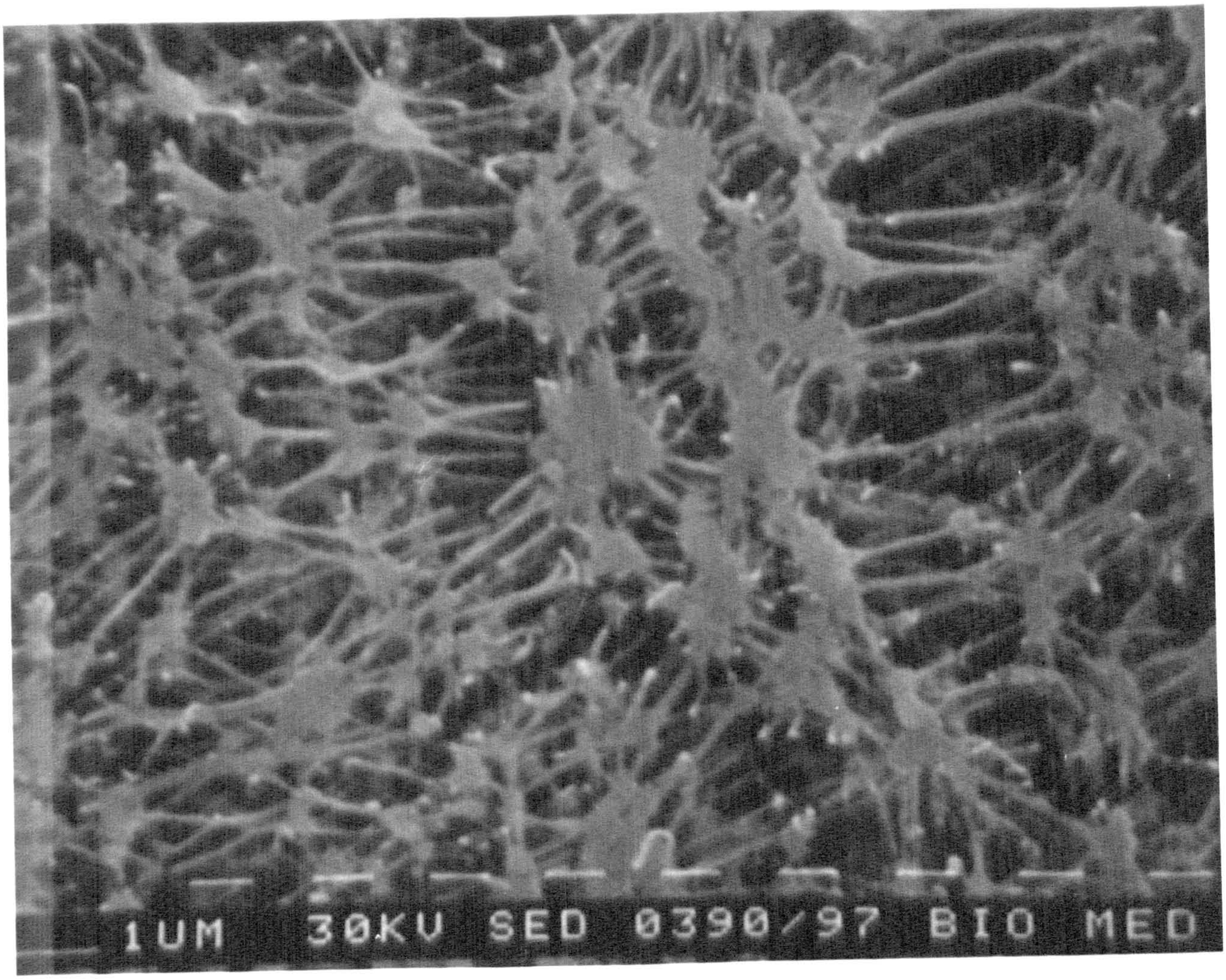
1UM 30.0KV SED 0390/97 BIO MED

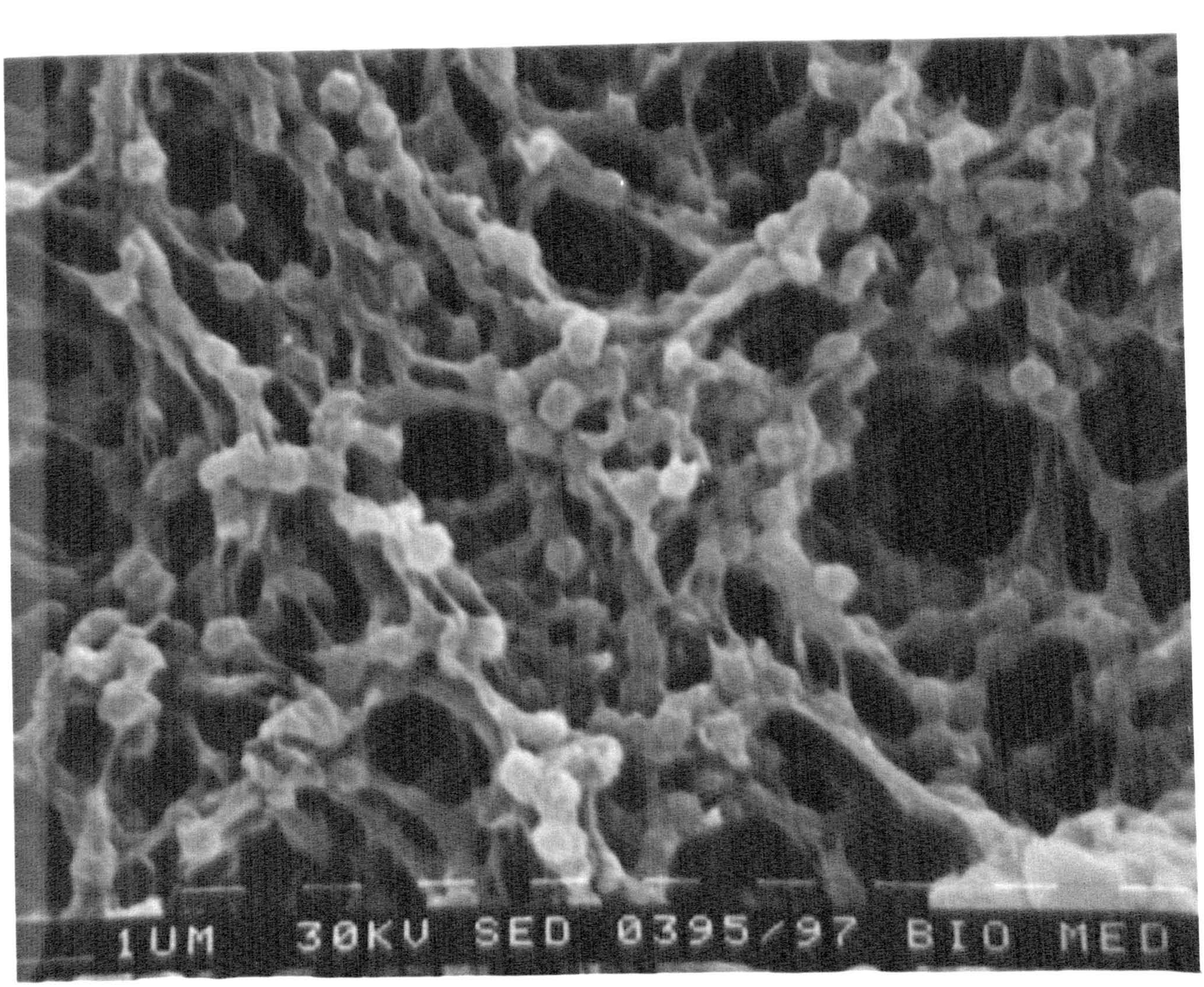
1UM 30KV SED 0395/97 BIO MED

Plate 5.3: SEM of a Versapor membrane - magnification x 5000

Plate 5.4: SEM of a used PVDF membrane - magnification x 5000

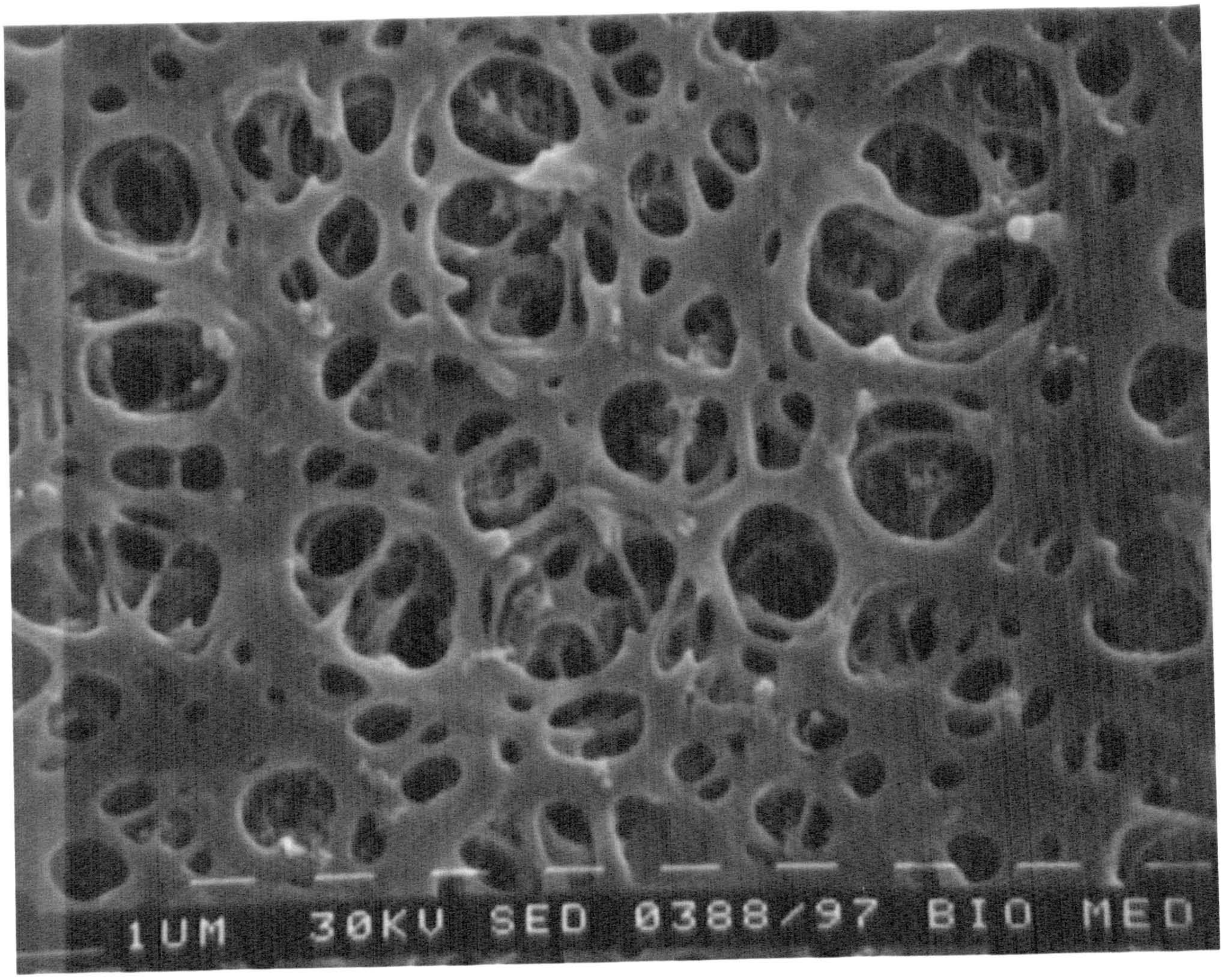
1UM 30KV SED 0388/97 BIO MED

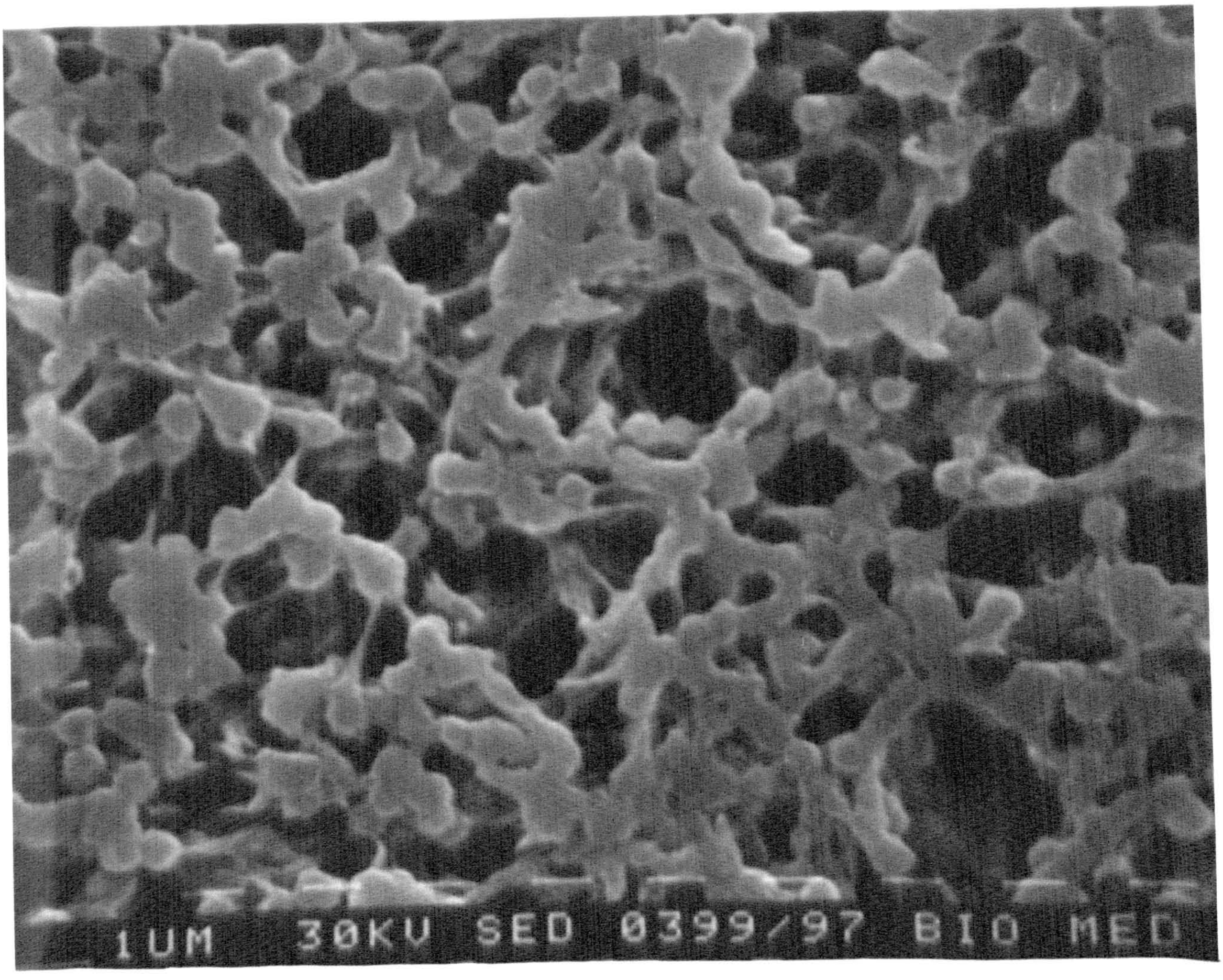
1UM 30KV SED 0399/97 BIO MED

every ten minutes. It was possible to carry out these short runs because water was used on both sides of the membrane.

For the initial study carried out, the flow rates were constant at 100 ml/min. The hot side inlet temperature was maintained at 38°C, and the cold side inlet temperature was maintained at 12°C. This meant that the membrane temperature was 25°C, and the maximum temperature difference (i.e. at the inlet) across the membrane was 26°C.

The first study was to investigate the relationship between membrane surface area and flux. This was accomplished by progressively blocking the main channels on the plates, limiting the number of spacer gaps used, and hence reducing the membrane surface area. A spacer is shown in Figure 6.3E. The main channels were blocked so that experiments could be carried out utilising 9, 7, 5 and 4 spacer gaps, corresponding to surface areas of 36.4, 28.3, 20.2, and 16.2 cm^2 respectively.

The second study investigated the relationship between the different plate geometries (shown in Figure 6.3) on the permeate flux. These included the main channel width, and minor channels cut into the plate surface between the inlet and outlet main channels. The main channels on Plate C were twice as wide as those on Plate A. The minor channels on Plate A were 0.85 mm by 0.85 mm. It should be noted that increasing the main channel width also caused a decrease in the distance travelled by the liquid over the surface of the membrane between the inlet and outlet main channels.

To look at the effect of different module geometries on the permeate flux, the feed temperature was varied from 38°C to 60°C, the permeate temperature was varied from 12°C to 30°C, and the flowrate varied from 90 to 230 ml/min. The module combinations used in the study are given in Table 6.2.

6.3.2 Flow Distribution Experiments

These experiments were carried out in order to compare the results with those obtained from the flow and distribution model (Chapter 3).

The experimental rig used Plain plates, Plate B, shown in Figure 6.3B. In place of the membrane, a blank plate was inserted to remove the effect of the flux through the

Feed Side	Permeate Side
Plate B	Plate B
Plate B	Plate A
Plate A	Plate B
Plate B	Plate C
Plate C	Plate B
Plate B	Plate D
Plate D	Plate B
Plate C	Plate A
Plate A	Plate C

Table 6.2: Module configurations used in the basic performance study

membrane. Pressure tappings were placed just outside the module to measure the pressure difference over the plate, as shown in Figure 6.4. A flowmeter was used to measure the total flowrate of the liquid.

The main channels were progressively blocked off to vary the area available for flow from 36.4 to 16.2 cm^2. This corresponded to utilising nine, through to four, spacer gaps in the experiments. Varying the area available for flow altered the flow distribution down each spacer gap. Distilled water was used for all the experiments and the flowrates were varied from 37.5 to 265 ml/min. The temperature of the water was maintained at 23°C for the majority of the experiments. Some experiments were carried out with the water temperature at 15 and then 35°C, to study the effect of the liquid temperature on the pressure drop.

6.3.3 Membrane Distillation Experiments

These experiments were carried out in order to compare the results with those obtained from the membrane distillation model (Chapter 4).

A basic module system of two Plain plates was used initially (Plate B in Figure 6.3), with a PVDF membrane. The flowrate was varied from 90 to 227 ml/min, the feed temperature was varied from 37 to 60°C and the permeate temperature was varied from 12 to 30°C. Some experiments were carried out using two and three spacers on either

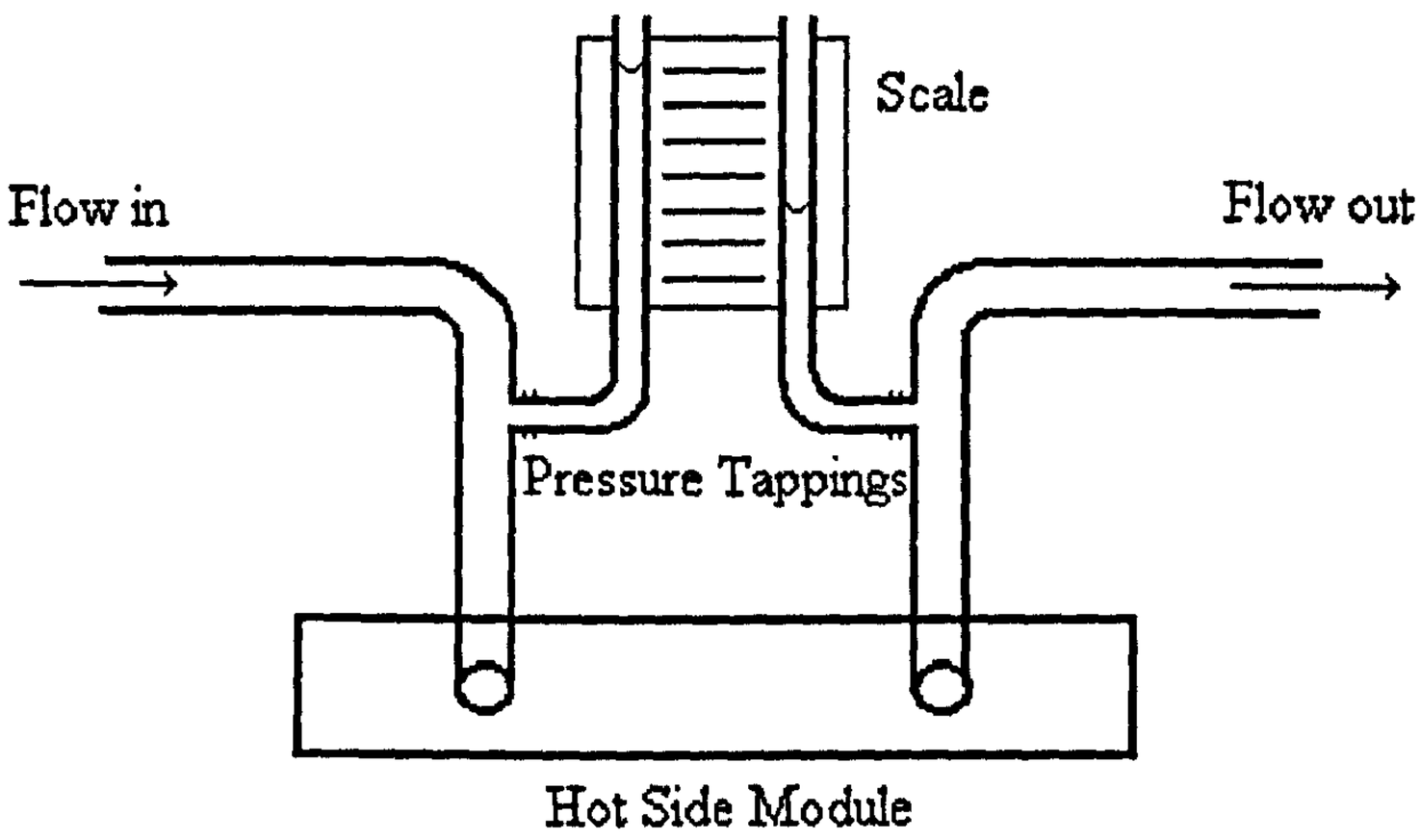

Figure 6.4: Pressure measurement of the hot side of the module

side of the membrane, varying the height of the liquid channels. Therefore there were a wide range of experimental conditions.

Next, a PTFE membrane was used to check that the model would predict fluxes for a different membrane. The flowrate was varied from 152 to 227 ml/min, the feed temperature was maintained at 57°C and the permeate temperature was varied slightly between 21 and 26°C. A Versapor membrane was then used. Similar flowrates were used as for the PTFE membrane, with a feed temperature of 56°C and a permeate temperature of 20°C.

Finally, the permeate plate of the module was changed to Plate A, with the 0.85 mm square minor channels. A PVDF membrane was used, and the flowrate was kept constant at 90 ml/min. The feed temperature was varied between 36 and 45°C, and the permeate temperature was varied between 12 and 21°C.

6.3.4 Boundary Layer Experiments

These experiments were carried out in order to compare the results with those obtained from the boundary layer model (Chapter 5).

For these experiments, thermocouples were placed at the inlet and outlet of a single spacer gap on both the feed and permeate sides. The module used two Plain plates (Figure 6.3B) with a PVDF membrane, and the temperature, flowrate and number of spacers were varied. The experimental conditions used are shown in Table 6.3.

6.4 Errors

The experimental system, designed to be simple, was expected to have a number of small errors. These included the accuracy and measurement of the weight of permeate, the temperatures, the flowrates, and the pressures.

These possible sources of errors are discussed in more detail in the following sections.

Experiment	Flowrate (ml/min)	No. of Spacers	T_{Hin} (°C)	T_{Cin} (°C)
64	152	1	29.5	24.3
65	227	1	30.6	22.1
66	152	1	41.2	18.1
67	190	1	42.4	17.1
68	227	1	33.7	24.8
69	152	1	41.9	30.9
70	227	1	48.4	22.9
71	152	1	51.0	31.2
72	152	1	46.3	29.6
73	190	1	51.5	31.2
74	227	1	51.7	31.6
75	152	2	35.1	26.5
76	152	2	42.2	23.8
77	90	2	38.2	18.5
78	90	3	38.9	18.6
79	90	3	38.4	18.8

Table 6.3: Experimental conditions for the boundary layer analysis

6.4.1 Weight of Permeate

A Metler balance was used and was connected to a datalogging system. The permeate was held in a container placed on the balance and the balance was zeroed at the start of each experiment. The balance could read to an accuracy of 0.005 g and the data was transferred to the datalogger as shown in Table 6.4.

Time (s)	No. of readings per second
up to 4	64
4 - 8	32
8 - 16	16
16 - 32	8
etc.	etc.

Table 6.4: Data transferrence rate from balance to datalogger

This system of measuring the quantity of permeate was suitable for the purpose of this thesis as the flux was constant with only small fluctuations in all of the experiments. The range of weights measured were between 0 and 100 g.

6.4.2 Temperatures

The temperatures, either at the inlet and outlet of the feed and permeate streams, or at either end of a spacer gap, were measured using K-type thermocouples linked to a datalogger. The thermocouples had an accuracy of ± 0.5°C. The diameter of the probes was 1.5 mm which, for the boundary layer experiments was large compared to the channel diameter. Therefore the probes represented an obstruction to the flow in this case as they occupied 20% of the available area of 7.8 mm^2. In order to cover the measuring surface of the thermocouples with liquid, the airtight seal over the thermocouple pockets was broken. This produced a small controlled flow of liquid, which was collected to account for any change in the flowrate of the stream concerned.

6.4.3 Flowrates

The flowrates were measured using rotameters in the range 1 to 5 gal/h, which correspond to 76 to 379 ml/min. Graduations were marked every 0.5 gal/h, so reading the rotameters involved an error of ± 0.25 gal/h (± 19 ml/min).

6.4.4 Pressure

For the pressure and flow model, the pressure drop was measured using a manometer set-up as shown in Figure 6.4. Tubing was attached to the pressure tappings and laid against a scale. The smallest graduation was 1 mm, which corresponds to 9.81 Pa. As the pressure drops recorded were small (see Chapter 6.2), there might have been a margin of error in reading the scale.

Overall, the effect of pressure over the module was small and for the rest of the work was assumed negligible.

6.4.5 The Overall Effect of the Experimental Errors

The overall effect of the experimental errors was small. Given here is an example of the typical error in calculating the permeate flux, which was the main result obtained for this work.

Data:

$$\text{width} = 7.0\ \text{mm} \pm 0.05\ \text{mm} \quad = 7\times10^{-3}\ \text{m} \pm 5\times10^{-5}\ \text{m}$$

$$\text{length} = 59.3\ \text{mm} \pm 0.05\ \text{mm} \quad = 0.0593\ \text{m} \pm 5\times10^{-5}\ \text{m}$$

$$\text{weight} = 32.61\ \text{g} \pm 0.005\ \text{g} \quad = 0.03261\ \text{kg} \pm 5\times10^{-6}\ \text{kg}$$

$$\text{time} = 3024\ \text{s} \pm 0.5\ \text{s} \quad = 0.84\ \text{h} \pm 1.389\times10^{-4}\ \text{h}$$

The first step in calculating the permeate flux was to calculate the membrane area.

<u>error in calculating area</u>

$$\frac{\text{error}_{\text{Area}}}{3.64\times10^{-3}} = \sqrt{\left(\frac{5\times10^{-5}}{0.0593}\right)^2 + \left(\frac{5\times10^{-5}}{7\times10^{-3}}\right)^2} \tag{6.1}$$

$$\therefore \text{error}_{\text{Area}} = \mathbf{2.618\times10^{-5}\ m^2}$$

So the area is $3.64\times10^{-3}\ \text{m}^2 \pm 2.62\times10^{-5}$

The permeate flux was calculated by,

$$\text{Flux} = \frac{\text{Weight}}{\text{Time}\times\text{Area}} \tag{6.2}$$

<u>Error in calculation of permeate flux</u>

$$\frac{\text{error}_{\text{Flux}}}{10.665} = \sqrt{\left(\frac{5\times10^{-6}}{0.03261}\right)^2 + \left(\frac{1.389\times10^{-4}}{0.84}\right)^2 + \left(\frac{2.618\times10^{-5}}{3.64\times10^{-3}}\right)^2} \tag{6.3}$$

$$\therefore \text{error}_{\text{Flux}} = \mathbf{0.077\ kg/m^2h}$$

So the permeate flux is $10.67\ \text{kg/m}^2\text{h} \pm 0.08$

CHAPTER 7

RESULTS AND DISCUSSION

7.1 Introduction

This work has been concerned with improving the overall flux of membrane distillation. This included reducing temperature polarisation by understanding heat and mass transfer, describing the flow of fluids through a flat plate module and designing a better module for membrane distillation.

This work was concerned with the development of three mathematical models. These included, flow distribution, membrane distillation, and boundary layer analysis. Before any work could be carried out on the models, the basic performance of the flat plate module was studied.

7.2 Basic Performance of the System

These experiments were concerned with the determination of the basic performance of the experimental system and membrane distillation. All experiments were run using distilled water in order to remove the effect of concentration, and to highlight thermal effects. The different plate types are shown in Figure 5.3.

An example of the increase in the weight of permeate obtained from an experimental run is given in Figure 7.1. This graph shows the increase in weight of the permeate measured by the balance datalogging system. The increase is linear, and Figure 7.2 shows the related permeate flux, which is basically constant at 11 kg/m^2h. The experiments showed only a fluctuation of $\pm$ 0.2 kg/m^2h flux with time. This is because distilled water gives the maximum possible permeate flux as there is no reduction in flux due to fouling.

The first study was to look at varying the membrane surface area in order to investigate its effect on the permeate flux. From Figure 7.3, it can be seen that increasing the membrane area available in the module, decreases the flux. This is because decreasing the membrane area increases the flow rate (i.e. Reynolds Number) across the remainder of the surface which in turn increases the flux.

The next study was to discover the effect of different module plate configurations. The experimental results for the second study are given in Tables 7.1 and 7.2. Figure 7.4 shows the permeate flux obtained with the different module configurations. The first set of experiments, Set A, were carried out with the feed at 38°C, the permeate at 12°C both at a flow rate of 90 ml/min. From Figure 7.4 it can be observed that the best module configuration was a plain plate on the feed side with a wide plate on the permeate side. The worst module configuration was with the channelled plate on the feed side and the plain plate on the permeate side. The difference of permeate flux between these two configurations was 1.328 kg/m^2h for a feed temperature of 38°C and a permeate temperature of 12°C. The second set of experiments, Set B, used a feed temperature of 55°C, a permeate temperature of 20°C, and flow rates of 152 ml/min.

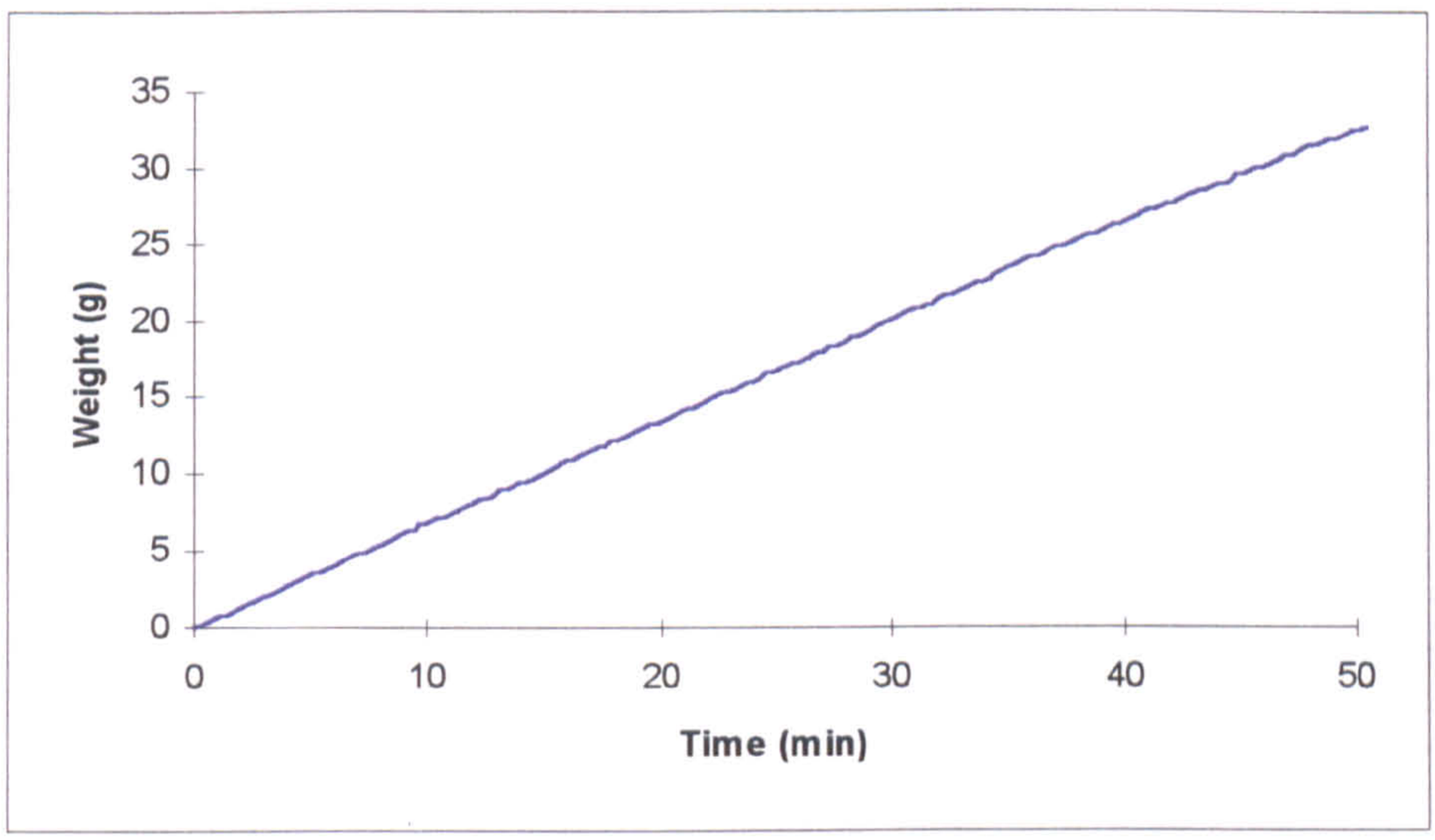

Figure 7.1: Increase in the weight of permeate during an experiment
(T_H = 30.6°C, T_C = 22.1°C, v = 152 ml/min)

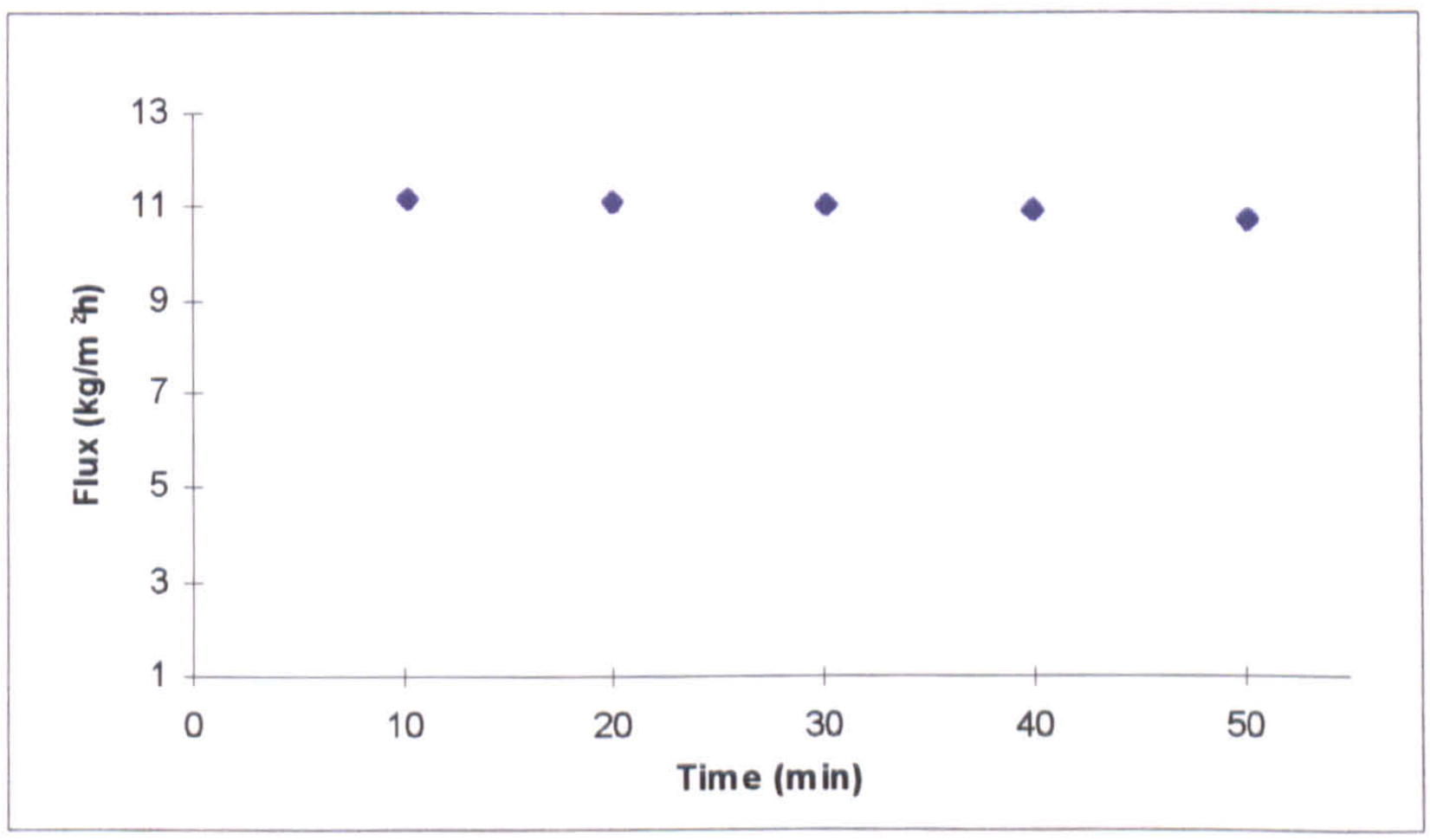

Figure 7.2: Permeate flux from data in Figure 7.1
(T_H = 30.6°C, T_C = 22.1°C, v = 152 ml/min)

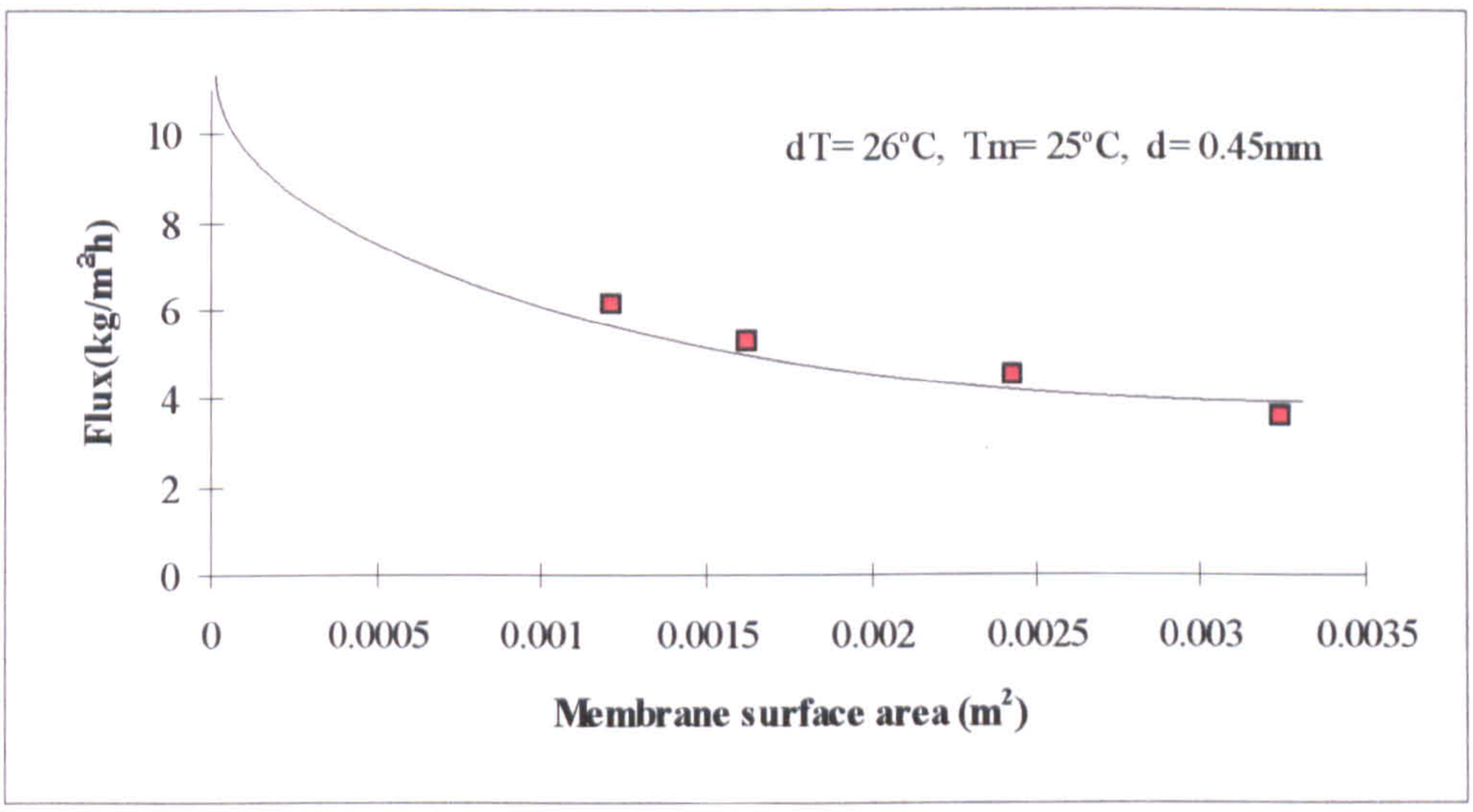

Figure 7.3: Trend of flux versus membrane surface area
($dT = 26°C$, $T_m = 25°C$, $Y = 0.45$ mm)

Experiment	Feed Plate	Permeate Plate	Permeate Flux (kg/m^2h)	Experiment Set
1	B	B	3.345	A
2	B	A	3.577	
3	A	B	2.653	
4	B	C	3.981	
5	C	B	3.543	
6	C	A	3.839	
7	A	C	3.056	
8	B	B	9.224	B
9	B	A	10.551	
10	A	B	8.18	
11	A	B	7.76	
12	B	D	12.937	
13	B	D	11.363	
14	D	B	9.039	
15	D	B	9.14	

Table 7.1: Experimental results for different module geometries

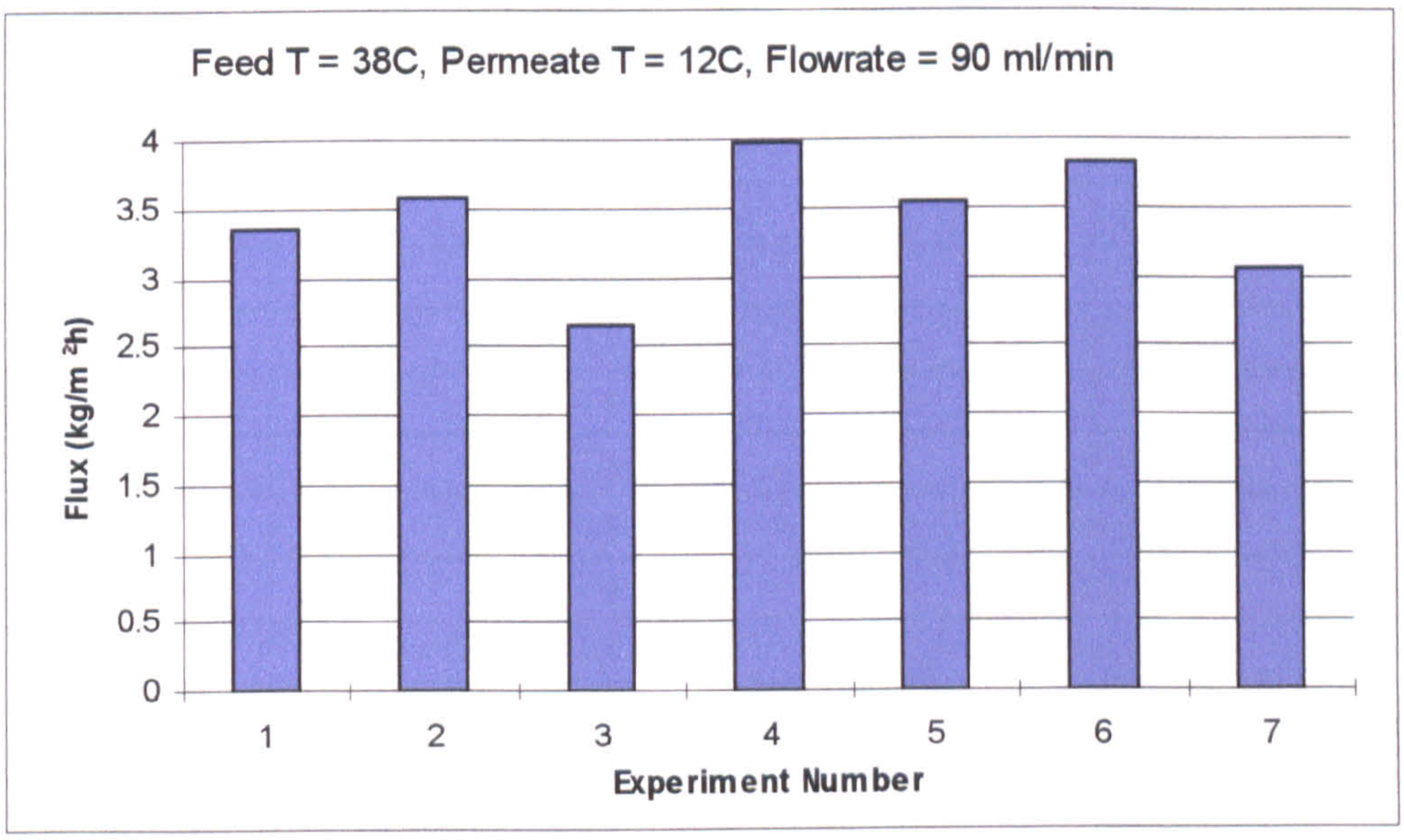

Figure 7.4: Graph to show the flux obtained using different module geometries

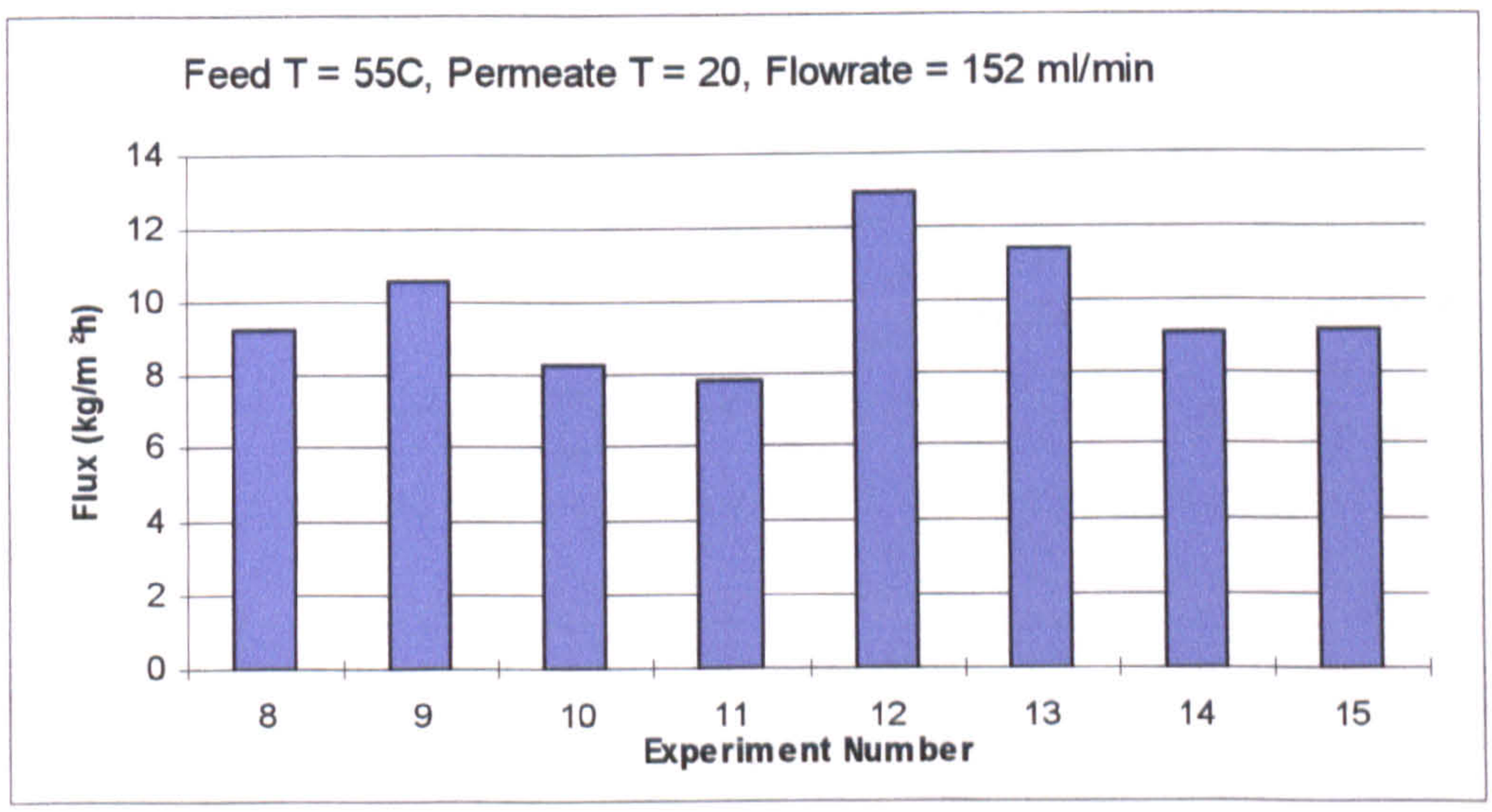

Figure 7.5: Graph to show the flux obtained using different module geometries

Experiment	Feed T (°C)	Permeate T (°C)	Flowrate (ml/min)	Permeate Flux (kg/m^2h)	
16	60	30	152	9.76	Set C
17	60	30	190	11.005	
18	60	30	227	13.458	
19	40	13	152	4.693	Set D
20	40	13	190	7.236	
21	40	13	227	10.959	
22	60	14	114	5.611	Set E
23	60	14	152	7.406	
24	60	14	190	9.061	
25	60	14	227	12.084	
25	46	13	114	4.512	Set F
23	46	13	152	5.473	
24	46	13	190	7.103	
25	46	13	227	7.066	

Table 7.2: Experimental results for different flowrates at various temperatures

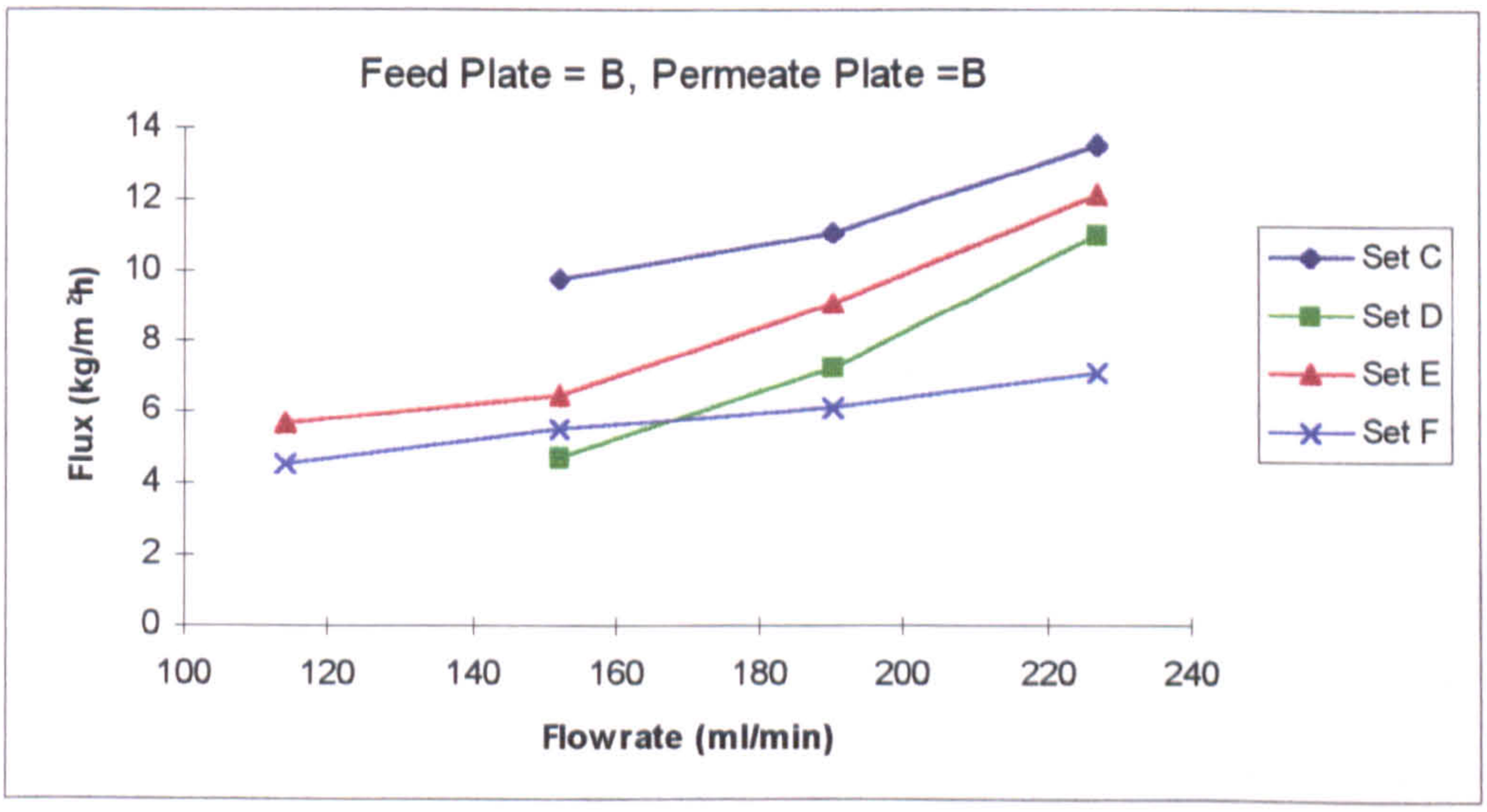

Figure 7.6: Graph to show the flux obtained using different flowrates

The corresponding graph of results is shown in Figure 7.5. At the higher feed and permeate temperatures of 55 and 20°C, the difference in permeate flux between the best and worst configurations was 4.180 kg/m^{2}h. Again the configuration with the lowest flux consisted of a channelled plate on the feed side and a plain plate on the permeate side. The flux increased by increasing the temperature because the vapour pressure increases exponentially with temperature. For the experiments shown in Table 7.1, the flux increase was around 6 kg/m^{2}h. Overall, putting a channelled plate on the feed side reduced fluxes, whilst using a wide plate on any side improved fluxes compared to a reference configuration of two plain plates. The reason for this behaviour concerns the ease of the flow of fluid through the module, especially on the permeate side. In the process of membrane distillation, there is transfer of liquid from the feed to the permeate side, i.e. the flow rate of the feed reduces while there is an increase in flow rate on the permeate side. Introducing channels cut into the plate surface between the inlet and outlet main channels allows the permeate flux to be transported from the membrane surface. The wide plate decreases the pressure drop across the plate, thereby maintaining the vapour pressure difference driving force created by the temperature difference. In addition, according to the Leveque solution of laminar mass transfer theory, the wide channel also decreases the effective transfer channel length, thereby increasing the transfer coefficient, and therefore the flux.

Incorporating both wide channels, and minor channels across the plate surface (see Figure 7.3) take advantage of these effects and achieves the maximum flux as shown in Figure 7.5.

The results for the third set of experiments, Set C through to Set F, showing the effect of flow rate on flux using normal plates, are given in Table 7.2 and are shown graphically in Figure 7.7. For all temperature conditions, the flux increased with increasing flow rate. The range of flow rates used were from 114 to 227 ml/min which correspond to $1.9\text{x}10^{-6}$ and $3.78\text{x}10^{-6}$ m^3/s respectively. Only experimental Set F show a much shallower trend with flow rate than the other experiments. Set C has higher fluxes than Set E due to a colder permeate temperature creating a larger temperature difference, and Set E has higher fluxes than Set D due to the feed temperature being higher. Sets D and F should

have roughly the same fluxes due to similar operating conditions, which they do at lower flow rates. At higher flow rates, I believe the Set F results are incorrect due to experimental error as they do not follow the trend set by the other experimental results.

7.3 Flow Distribution Model

Once a basic understanding of the behaviour of membrane distillation had been reached, then a closer look at the flow profiles through the module could be carried out. The approach for this model was to use the relationship between flow and pressure drop. A series of equations were developed for all the channels in a module, taking into account the different dimensions.

7.3.1 Experimental Results

Table 7.3 shows the experimental results for the flow distribution model. Various effects of temperature, membrane surface area and flow rates were studied experimentally, before adding in the theoretical model. The experiments carried out for this section of the work, utilised a plain:plain plate configuration with the membrane replaced by a blank plate. This was done to remove the effect the permeate flux would have on the pressure drop. If the permeate flux needed to be accounted for, the model could be expanded, though this would make it more complicated.

The first group of experiments varied the flow rates and membrane surface area and studied how they affected the overall pressure drop. The membrane surface area was varied by blocking off spacer gaps, reducing the area for flow of the liquid. The experimental results for this are shown in Figure 7.7. Figure 7.7 shows the pressure drops measured at different flow rates for different numbers of spacer gaps available for flow in the module. It can be seen that increasing the flow rate increases the pressure drop, though the pressures involved are very low, around 1600 Pa (16 mbar) at the highest flow rate used. Decreasing the number of spacer gaps being utilised for flow also increases the

No. of spacer gaps	Membrane surface area (cm^2)	Temp. (°C)	Flowrate (ml/min)	Flowrate (m^3/s)	P (mmH_20)			P (mmH_20)	P (Pa)
9	36.41	35	152	2.53E-06	53	53	52	52.67	516.66
9	36.41	35	190	3.17E-06	83	84	83	83.33	817.5
9	36.41	35	227	3.78E-06	116	115	116	115.67	1134.69
9	36.41	35	265	4.42E-06	150	150	151	150.33	1474.77
9	36.41	15	152	2.53E-06	49	47	49	48.33	474.15
9	36.41	15	190	3.17E-06	76	77	77	76.67	752.1
9	36.41	15	227	3.78E-06	101	102	103	102.00	1000.62
9	36.41	15	265	4.42E-06	123	122	122	122.33	1200.09
9	36.41	23	37.5	6.25E-07	5	9	8	7.33	71.94
9	36.41	23	75	1.25E-06	15	16	15	15.33	150.42
9	36.41	23	152	2.53E-06	51	52	50	51.00	500.31
9	36.41	23	190	3.17E-06	79	78	78	78.33	768.45
9	36.41	23	227	3.78E-06	108	107	106	107.00	1049.67
9	36.41	23	265	4.42E-06	135	136	137	136.00	1334.16
7	28.3	23	37.5	6.25E-07	7	8	7	7.33	71.94
7	28.3	23	75	1.25E-06	17	16	18	17.00	166.77
7	28.3	23	152	2.53E-06	50	54	53	52.33	513.39
7	28.3	23	190	3.17E-06	78	78	76	77.33	758.64
7	28.3	23	227	3.78E-06	109	106	105	106.67	1046.4
7	28.3	23	265	4.42E-06	139	140	140	139.67	1370.13
5	20.2	23	37.5	6.25E-07	9	9	8	8.67	85.02
5	20.2	23	75	1.25E-06	19	18	19	18.67	183.12
5	20.2	23	152	2.53E-06	59	54	53	55.33	542.82
5	20.2	23	190	3.17E-06	84	80	81	81.67	801.15
5	20.2	23	227	3.78E-06	110	110	110	110.00	1079.1
5	20.2	23	265	4.42E-06	139	141	141	140.33	1376.67
3	16.2	23	37.5	6.25E-07	11	12	10	11.00	107.91
3	16.2	23	75	1.25E-06	21	22	21	21.33	209.28
3	16.2	23	152	2.53E-06	63	63	62	62.67	614.76
3	16.2	23	190	3.17E-06	97	95	94	95.33	935.22
3	16.2	23	227	3.78E-06	128	129	129	128.67	1262.22
3	16.2	23	265	4.42E-06	171	165	168	168.00	1648.08

Table 7.3: Experimental results for the flow distribution model

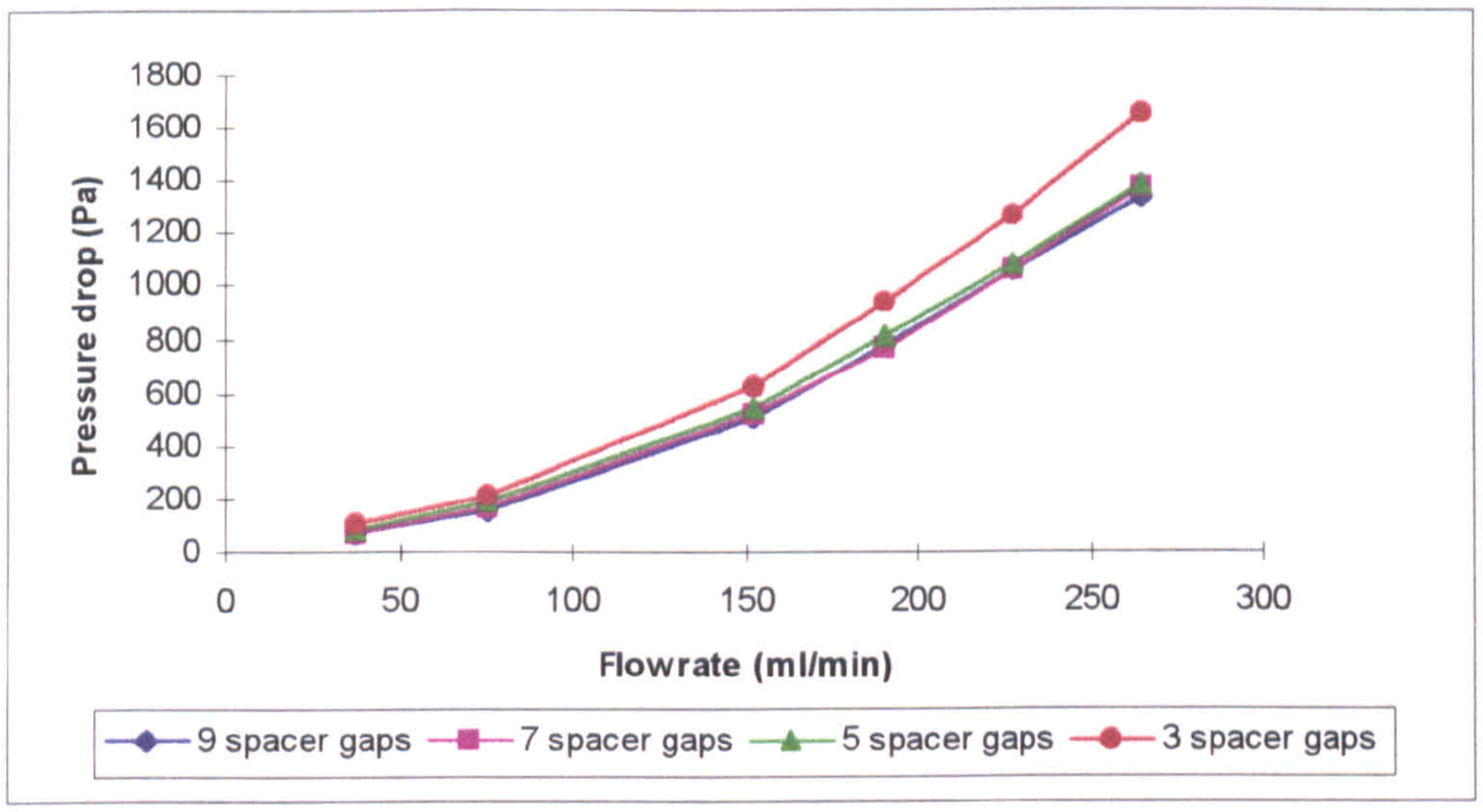

Figure 7.7: Experimental results for varying number of available spacer gaps and flow rate

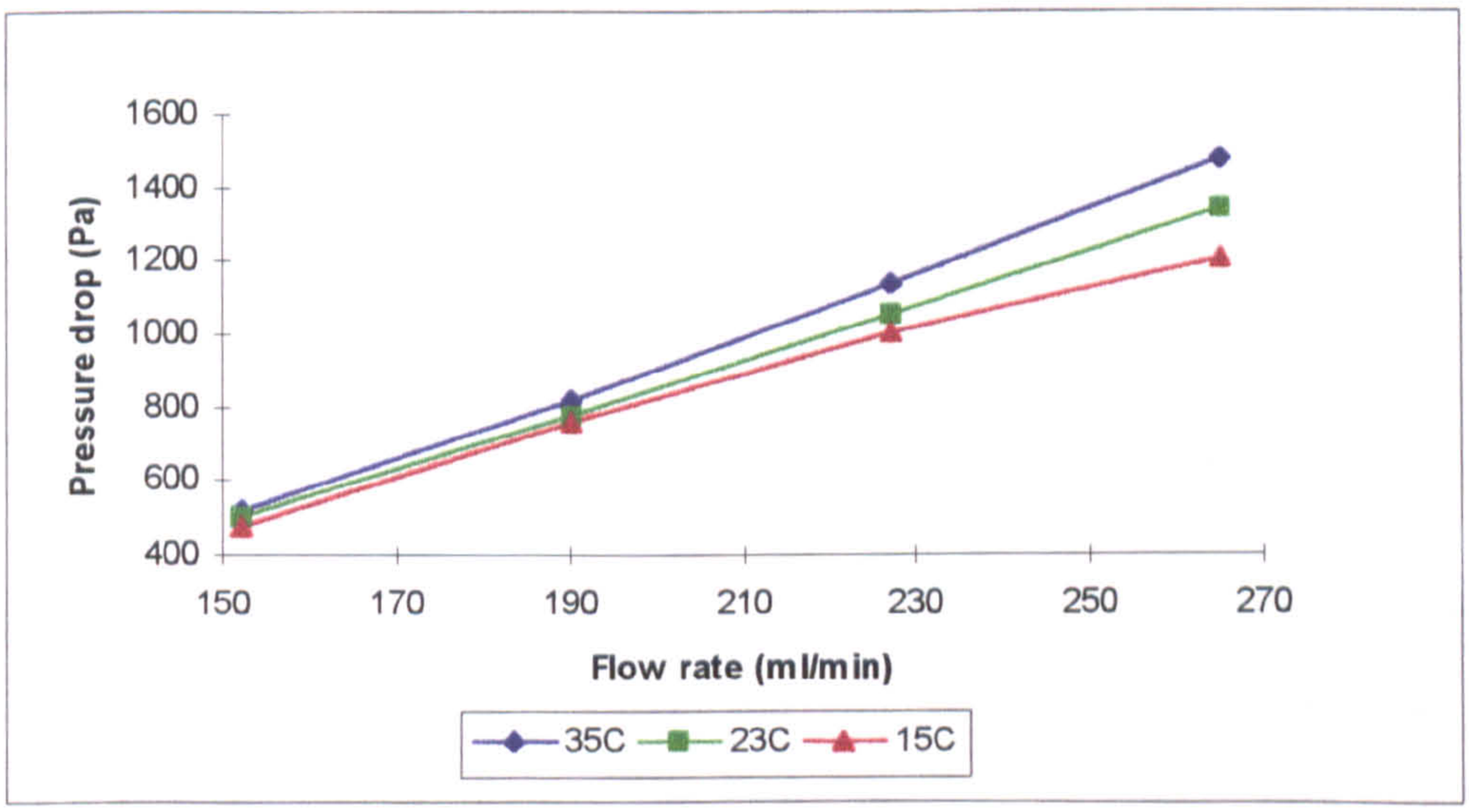

Figure 7.8: Experimental results for varying temperature and flow rate

pressure drop. This is because decreasing the number of spacer gaps increases the flow rate down each remaining spacer gap thereby increasing the pressure drop.

The second group of experiments used temperatures of 15, 25 and 35°C, a membrane surface area of 37.41 cm^2 and flow rates ranging from 150 ml/min to 260 ml/min. This was to study the effect of temperature on the overall module pressure drop. The results are shown in Figure 7.8, which again shows that as the flow rate increases, the pressure drop increases. Also shown is that decreasing the temperature of the liquid flowing through the module decreases the pressure drop. This result is opposite to what was expected, as decreasing the temperature would increase the liquid viscosity, thereby increasing the pressure drop.

7.3.2 Theoretical Results

The next step was to simulate the experiments using the model described in Chapter 3.2. Table 7.4 shows an example of the results obtained from the model for a total flow of 150 ml/min ($2.5x10^{-6}$ m^3/s) at a fluid temperature of 23°C.

The theoretical model could be calculated for any number of spacer gaps (i.e. membrane area), but only a maximum of nine spacer gaps were used.

Figure 7.9 shows the results for varying number of spacer gaps. Figure 7.9 shows a linear trend of increasing pressure drop with increasing flow rate, and with increasing the number of spacer gap channels utilised for flow in a module. As can be seen, as the number of spacer gaps available for flow is reduced from nine to three, the overall pressure drop of the module increases by 83% with a flow rate of 150 ml/min. Comparing the results from the flow distribution model, and those obtained experimentally, (Figure 7.11) there is fairly good agreement. The maximum deviation is 500 Pa (51 mmH_2O) which may be due to the method of pressure measurement and entrance effects. The theory does predict a linear trend, when the experimental data show a shallow curve with increasing flow rate. The deviation of the theory could be an unaccounted pressure loss due to entrance effects, or bend. The relationship between the flowrate and pressure drop then becomes based on $1/2\rho v^2$. However, both theory and experiment show that

Formation of Equations

Section A		*Section B*		*Section C*	
L=	0.5723 m	L=	0.004 m	L=	0.05 m
h=	0.004 m	h=	0.0023 m	h=	0.00045 m
w=	0.004 m	w=	0.0029 m	w=	0.007 m
d=	0.004 m	d=	2.57E-03 m	d=	8.46E-04 m
C_f=	57	C_f=	58	C_f=	88

			dP (v)	dP (Q)
Temperature	23 C	Section A	988.8271	6.18E+07
Viscosity	9.70E-04 Ns/m^2	Section B	17.03584	2.55E+06
Density	997.538 kg/m^3	Section C	2981.63	9.47E+08

Iterative Calculation

9 Spacer Gaps

Q (m^3/s)	2.50E-06
dP (Pa)	**603**

spacer gap	Rs	Q	
1	2.94E+02	3.11E-07	
2	2.83E+02	2.99E-07	
3	2.73E+02	2.89E-07	
4	2.65E+02	2.8E-07	
5	2.58E+02	2.73E-07	
6	2.53E+02	2.67E-07	
7	2.49E+02	2.63E-07	
8	2.46E+02	2.6E-07	
9	2.45E+02	2.59E-07	
sum		2.5E-06	m^3/s

7 Spacer Gaps

Q (m^3/s)	2.50E-06
dP (Pa)	**670**

spacer gap	Rs	Q	
1	3.61E+02	3.81E-07	
2	3.50E+02	3.7E-07	
3	3.41E+02	3.61E-07	
4	3.34E+02	3.53E-07	
5	3.29E+02	3.47E-07	
6	3.25E+02	3.44E-07	
7	3.24E+02	3.42E-07	
sum		2.5E-06	m^3/s

5 Spacer Gaps

Q (m^3/s)	2.50E-06
dP (Pa)	**797**

spacer gap	Rs	Q	
1	4.88E+02	5.16E-07	
2	4.78E+02	5.05E-07	
3	4.70E+02	4.97E-07	
4	4.65E+02	4.92E-07	
5	4.63E+02	4.89E-07	
sum		2.5E-06	m^3/s

3 Spacer Gaps

Q (m^3/s)	2.50E-06
dP (Pa)	**1105**

spacer gap	Rs	Q	
1	7.96E+02	8.41E-07	
2	7.88E+02	8.32E-07	
3	7.83E+02	8.28E-07	
sum		2.5E-06	m^3/s

Table 7.4: Example of model calculating the flow distribution and pressure drop for various numbers of spacer gaps available for flow (Q_T = 150 ml/min, T = 23°C)

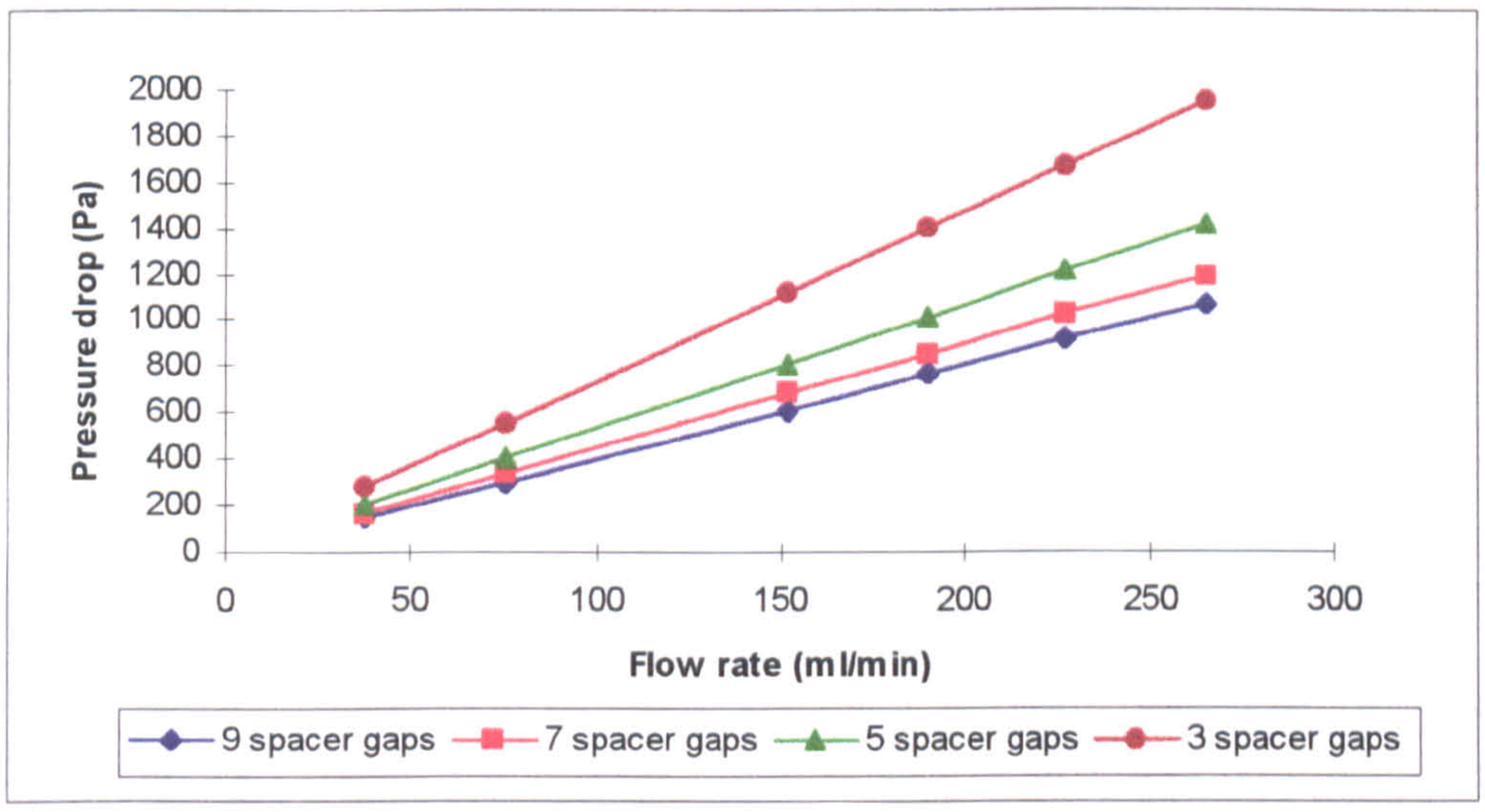

Figure 7.9: Pressure drop values calculated by the theoretical model for varying the number of spacer gaps available and flow rates

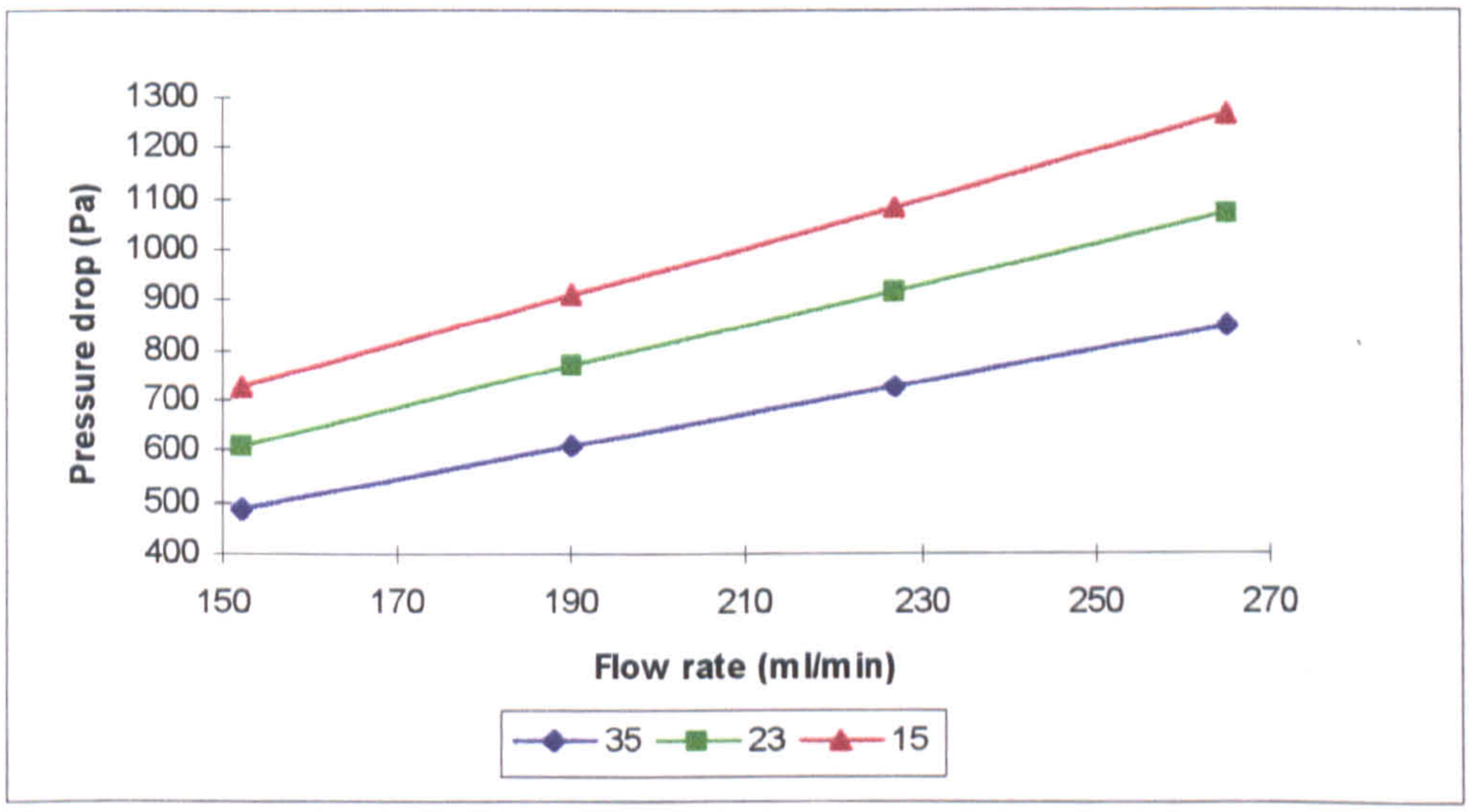

Figure 7.10: Pressure drop results from the theoretical model for varying temperature and flow rates

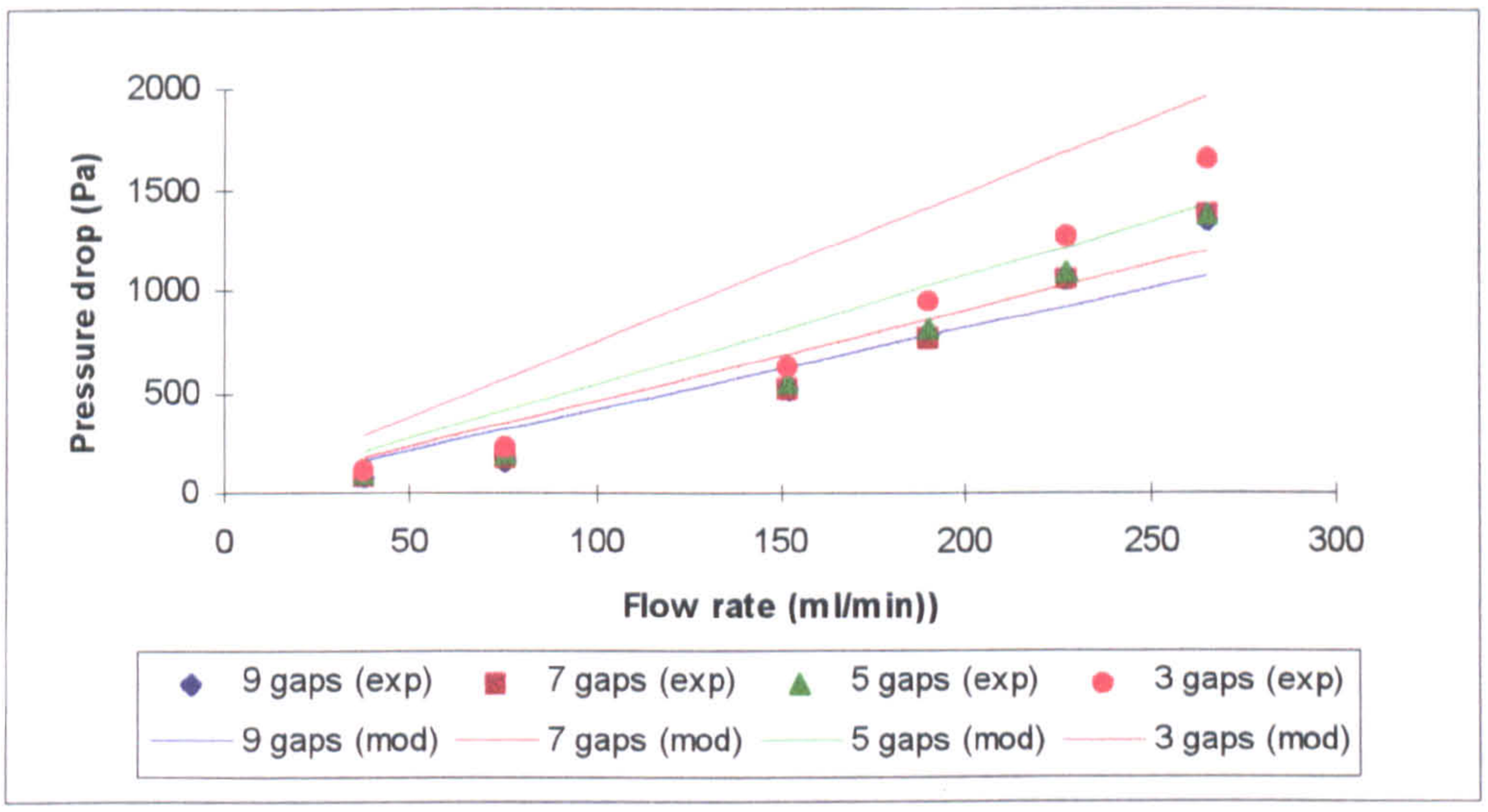

Figure 7.11: Comparison between the theoretical model and experimental results for varying number of spacer gaps and flow rates

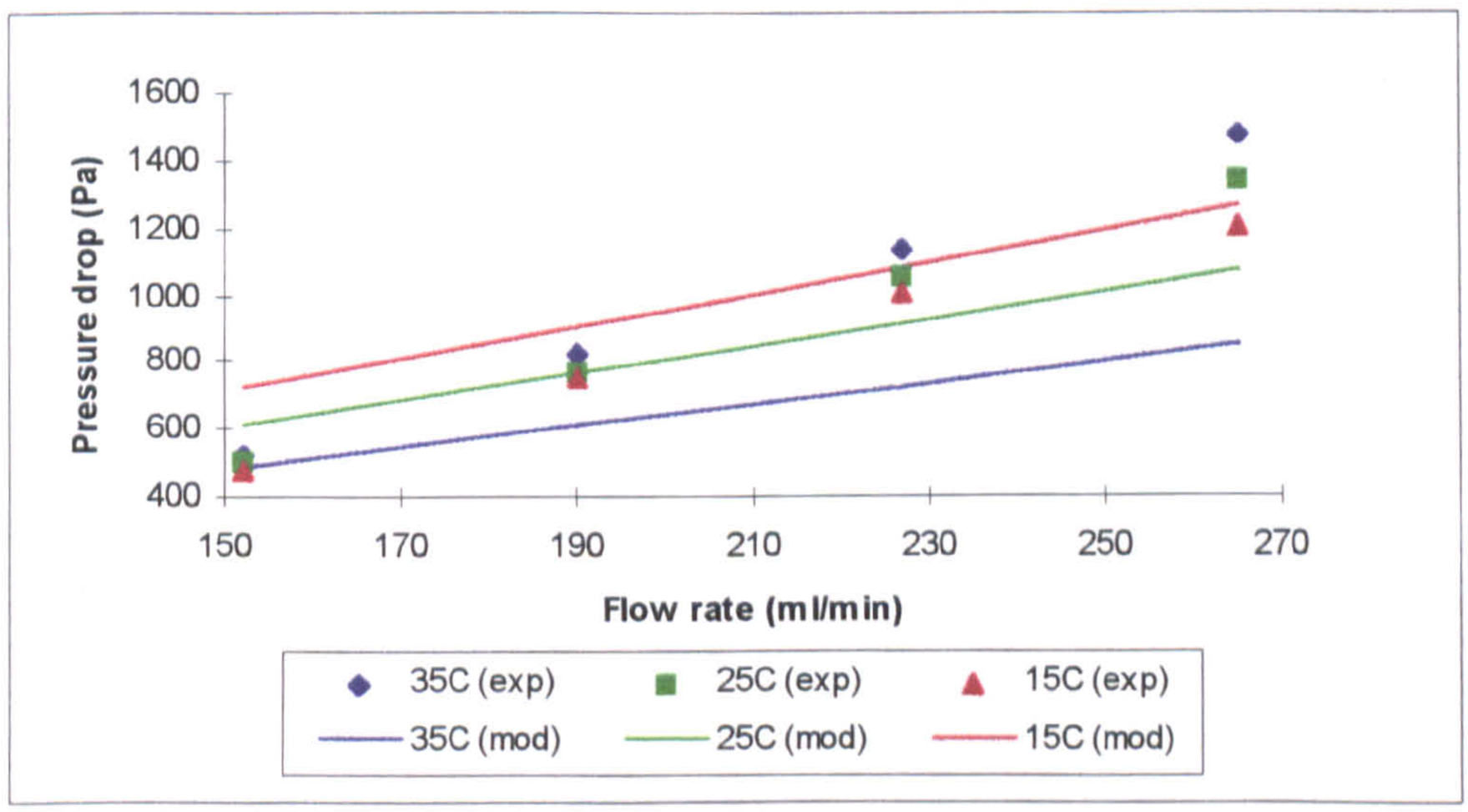

Figure 7.12: Comparison between the theoretical model and experimental results for varying temperatures and flow rates

increasing the number of spacer gap channels available for flow increases the pressure drop.

Looking at the effect of temperature on the pressure drop (Figure 7.10) the model predicts a decrease of pressure drop with temperature. This is because as the liquid temperature is increased, the viscosity decreases, thereby reducing the resistance to flow, and pressure drop. For instance, at a flow rate of 3.78×10^{-6} m^3/s (227 ml/min) increasing the liquid temperature from 15 to 35°C, decreases the pressure drop by 357 Pa from 1081 Pa. Comparing these with the experimental data, shown in Figure 7.12, both are linear trends and are reasonably accurate, but the theoretical trends are shallower than the experimental trends. If the flow is turbulent instead of laminar, the pressure drop is not dependant on viscosity. This might explain the difference seen in Figure 7.12.

The conclusions to be drawn from the comparisons are that the flow distribution model can adequately predict the effect of liquid temperature, area available for flow and flow rate on the pressure drop across the module. The flow distribution model can be used to predict the liquid flow rate through a module plate. Figure 7.13 shows the pressure drop across each spacer gap which is then related to the flow rate of liquid down each spacer gap as shown in Figure 7.14. Spacer gap 1 is nearest the main inlet and outlet and spacer gap 9 is the farthest. The graph shows that on moving from the first to the ninth spacer gap, the pressure drop decreases from 294 to 245 Pa. This corresponds to a decrease in the liquid flow rate down each spacer gap, shown in Figure 7.14, which is 3.11×10^{-7} to 2.59×10^{-7} m^3/s (18.7 to 15.5 ml/min).

7.4 Membrane Distillation Model

This model aimed to predict the flux obtained with known bulk temperatures taking into account the membrane used and the channel height (i.e. boundary layer thickness).

7.4.1 Experimental Results

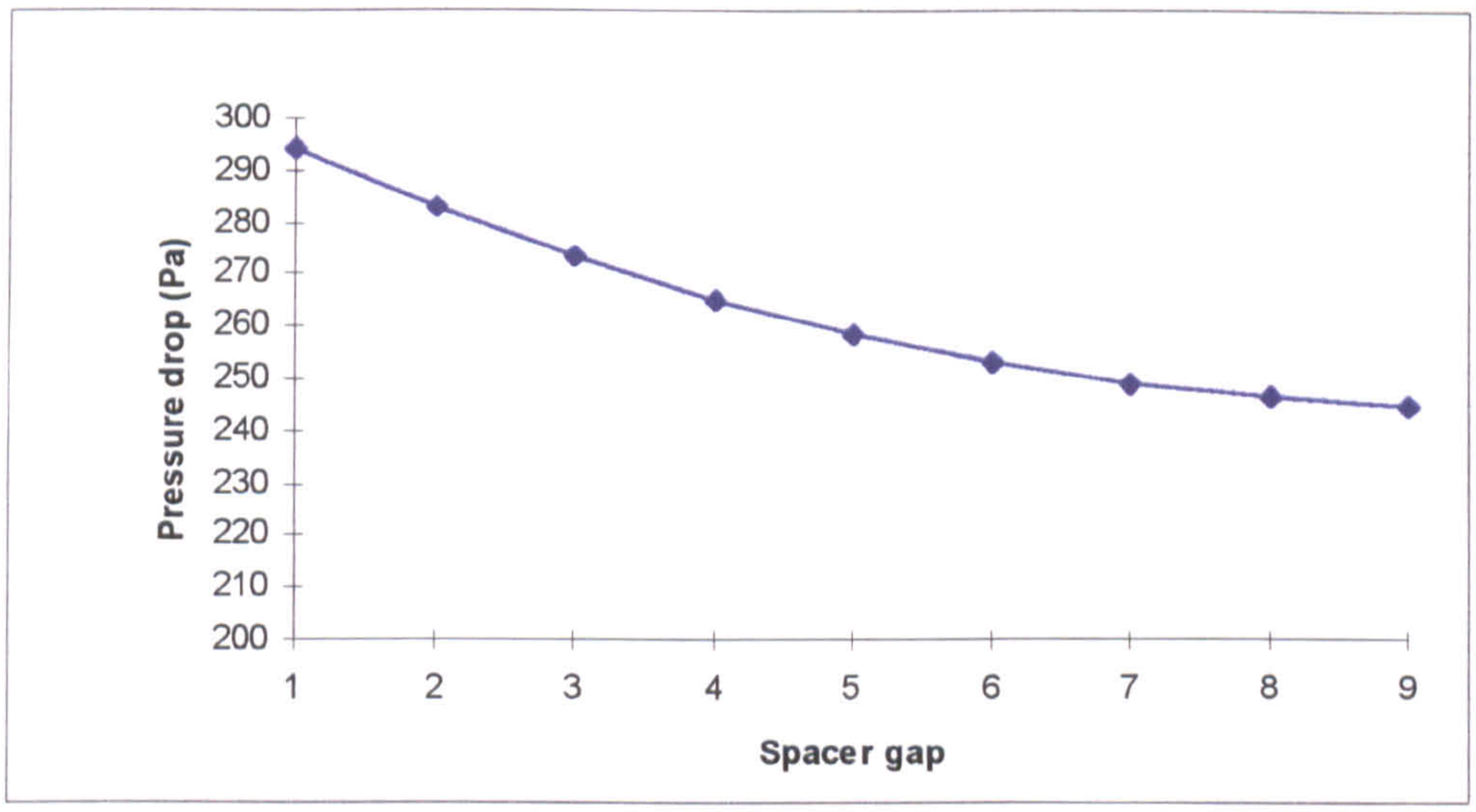

Figure 7.13: Calculated pressure drop down each spacer gap in a module with 9 spacer gaps (W_T=2.5x10^{-6} m^3/s, T=23°C)

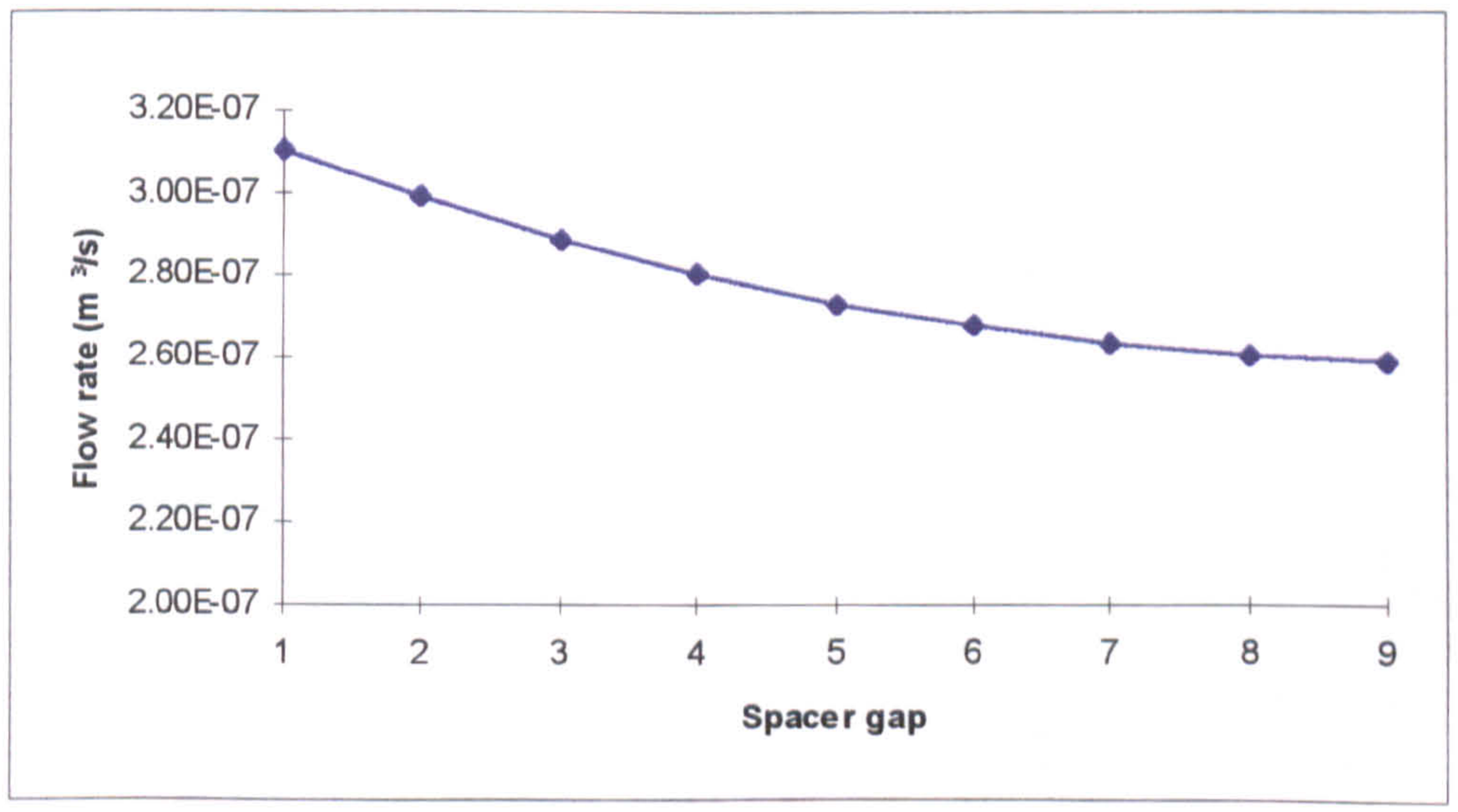

Figure 7.14: Calculated flowrate down each spacer gap in a module with 9 spacer gaps (W_T=2.5x10^{-6} m^3/s, T=23°C)

Experiment	No. of Spacers	Feed T (°C)	Permeate T (°C)	Tm (°C)	dT (°C)	Flowrate (ml/min)	Permeate Flux (kg/m²h)
26	1	55.6	21.1	38.35	34.5	152	8.271
27	1	44.4	20.3	32.35	24.1	152	5.591
28	1	37.5	12.4	24.95	25.1	90	3.342
29	1	59.6	14.4	37.00	45.2	190	9.464
30	1	60.9	15.0	37.95	45.9	152	9.640
31	1	60.1	22.1	41.10	38	152	10.969
32	1	60.7	22.6	41.65	38.1	227	11.803
33	1	60.3	30.9	45.60	29.4	227	12.927
34	1	58.5	29.1	43.80	29.4	152	9.983
35	1	39.9	13.9	27.90	26	152	4.693
36	1	47.0	13.3	29.65	32.7	152	5.881
37	1	47.6	12.9	29.75	33.7	190	7.103
38	1	45.5	13.0	29.25	32.5	227	7.973
39	3	54.0	19.3	37.65	34.7	152	7.208
40	2	55.5	18.4	37.95	37.1	152/227	8.599
41	2	55	18.7	37.85	37.3	152	7.974
42	1	55.1	17.7	37.40	37.4	152	8.517
43	1	51.5	19.8	35.65	31.7	227	10.706
44	1	51.5	18.5	35.00	33	152	7.095

Table 7.5: Experimental Results for Plain:Plain plate configuration, PVDF membrane

Experiment	Feed T (°C)	Permeate T (°C)	Tm (°C)	dT (°C)	Flowrate (ml/min)	Permeate Flux (kg/m²h)
45	57.6	22.5	39.55	34.1	152	12.710
46	57.4	23.4	40.40	34	190	11.478
47	57.0	24.5	40.75	32.5	152	10.541
48	57.8	25.7	41.75	32.1	227	11.775
49	57.7	21.3	39.00	35.4	152	12.106
50	57.4	23.5	40.45	33.9	227	13.119

Table 7.6: Experimental Results for Plain:Plain plate configuration, PTFE membrane

There were various studies carried out for this section of work, as explained in Chapter 6.3.3.

The results using two normal plates and a PVDF membrane are given in Table 7.5. The experiments using PTFE and Versapor membranes are given in Tables 7.6 and 7.7 respectively, and Table 7.8 shows the results for a channelled plate on the permeate side of the module, with a PVDF membrane. The experimental data used for comparison using a PVDF membrane are shown in Figure 7.15. As can be seen, there is a trend in that as the mean membrane temperature increases, the permeate flux increases. In this figure, there can not be a more defined trend as the data points concern different temperature differences. If the temperature differences were equal, then the trend would be parabolic because of the relationship of vapour pressure and temperature (shown in Figure 5.6).

An aspect of the module, was the ability to alter the number of spacers either side of the membrane. This affected the channel height through which the feed and permeate flowed. Isolating these experiments and displaying them in Table 7.9 shows the results obtained with the relevant experimental conditions, and Figure 7.16 shows the overall trends. Figure 7.16 shows that as the number of spacers is increased, the permeate flux decreases. This is probably due to the formation of thicker boundary layers which will affect the driving force temperature difference. Set G are for a low flow rate and temperature difference. Increasing the temperature difference by 5°C (Set H) slightly increases the permeate flux. The final set (Set I) are at a higher flow rate and almost double the temperature difference of Set G. Correspondingly, the permeate flux is much higher, but still follows the trend of decreasing flux with increasing channel height.

Three membranes were available for this work, PVDF, PTFE and Versapor, and experiments were carried out to obtain information about the fluxes produced. The results given in Table 7.10, enables a graphical representation to be drawn (Figure 7.17). From Figure 7.17, it can be observed that PTFE produces the highest fluxes, with Versapor producing the lowest. All the membranes follow the trend of increasing flux with increasing flow rate.

This work was the first time a Versapor membrane was used for membrane distillation, and it was difficult to obtain consistent experimental runs. A lot of the data could not be

Experiment	Feed T (°C)	Permeate T (°C)	Tm (°C)	dT (°C)	Flowrate (ml/min)	Permeate Flux (kg/m^{2}h)
51	54.9	19.4	37.15	35.5	152	4.730
52	57.0	19.7	37.85	37.3	190	5.864
53	57.6	19.8	38.20	37.8	227	7.284
54	57.4	20.3	38.35	37.1	152	4.404
55	57.7	20.2	38.45	37.5	227	5.230

Table 7.7: Experimental Results for Plain:Plain plate configuration, Versapor membrane

Experiment	No. of Spacers	Feed T (°C)	Permeate T (°C)	Tm (°C)	dT (°C)	Flowrate (ml/min)	Permeate Flux (kg/m^{2}h)
56	1	52.7	20.1	37.40	32.6	152	10.600
57	1	39.0	27.0	33.00	12	90	2.131
58	1	37.9	20.8	28.85	17.1	90	3.088
59	1	37.5	18.1	27.30	18.4	90	3.825
60	1	44.5	20.9	32.70	23.6	90	7.306
61	1	37.7	17.1	27.40	20.6	90	4.542
62	1	37.3	12.0	24.65	25.3	90	3.583
63	2	37.8	12.3	25.05	25.5	90	3.071
64	2	38.2	18.5	28.35	19.7	90	2.581
65	3	38.9	18.6	28.75	20.3	90	2.595
66	1	37.0	18.8	27.90	18.2	90	3.600
67	2	38.0	18.9	28.45	19.1	90	2.531
68	3	38.4	18.8	28.60	19.6	90	2.452

Table 7.8: Experimental Results for Plain:Channelled plate configuration, PVDF membrane

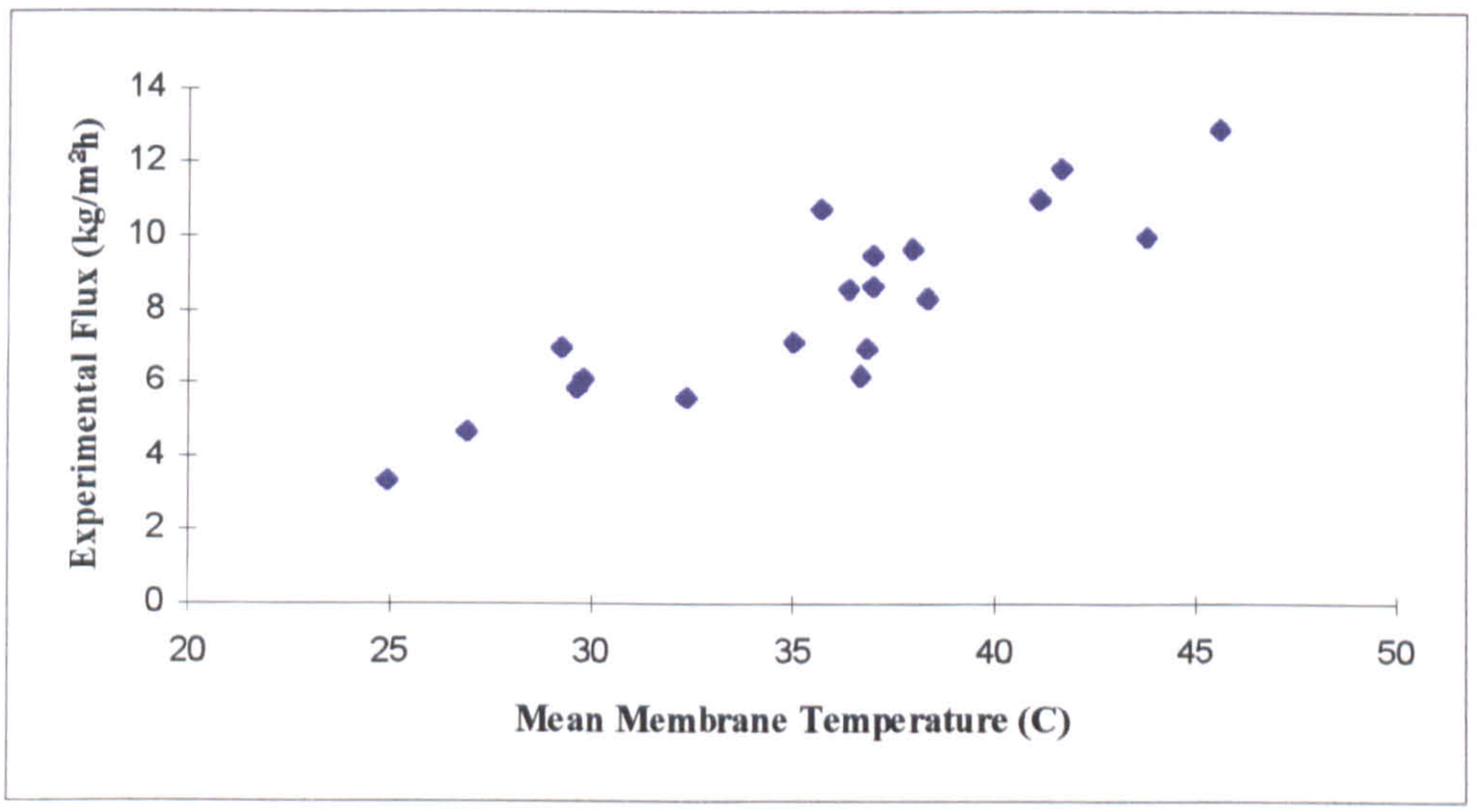

Figure 7.15: Graphical representation of the experimental results for Plain:Plain plate configuration, PVDF membrane

Experiment	Feed T (°C)	Permeate T (°C)	dT (°C)	Speed (ml/min)	Permeate Plate	No. of spacers	Permeate Flux (kg/m^{2}h)	Experiment Set
59	36.5	18.1	18.4	90	A	1	3.825	G
66	37	18.8	18.2	90	A	1	3.6	
64	38.2	18.5	19.7	90	A	2	2.581	
67	38	18.9	19.1	90	A	2	2.531	
65	38.9	18.6	20.3	90	A	3	2.595	
68	38.4	18.8	19.6	90	A	3	2.452	
62	37.3	12	25.3	90	A	1	3.583	H
63	37.8	12.3	25.5	90	A	2	3.071	
42	55.1	17.7	37.4	152	B	1	10.357	
26	55.6	21.1	34.5	152	B	1	9.224	
41	55	18.7	36.3	152	B	2	7.974	
39	54	19.3	34.7	152	B	3	7.608	

Table 7.9: Experimental results for varying number of spacers

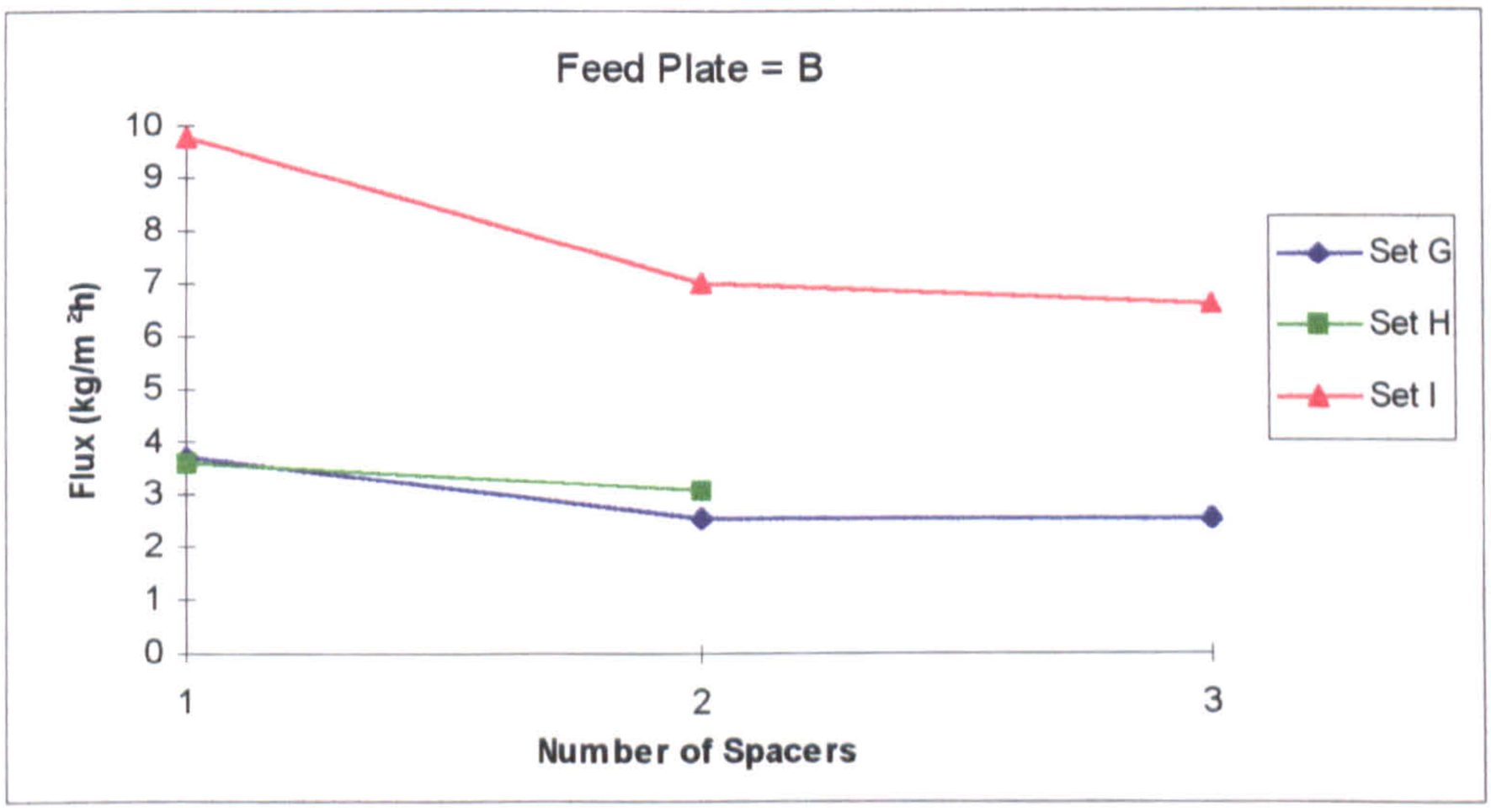

Figure 7.16: Experimental Results for varying number of spacers at different conditions

Experiment	Feed T (°C)	Permeate T (°C)	dT (°C)	Speed (ml/min)	Membrane	Permeate Flux (kg/m^2h)
49	56.7	21.3	35.4	152	PTFE	12.106
47	57.0	24.5	32.5	152	PTFE	10.541
45	56.6	22.5	34.1	152	PTFE	12.71
42	55.1	17.7	37.4	152	PVDF	8.517
44	51.5	18.5	33.0	152	PVDF	7.095
26	55.6	21.1	34.5	152	PVDF	8.271
51	54.9	19.4	35.5	152	Versapor	4.730
46	56.4	23.4	34.0	190	PTFE	11.478
29	59.6	14.4	45.2	190	PVDF	9.464
54	56.4	20.3	37.1	152	Versapor	4.404
52	56.0	19.7	36.3	190	Versapor	5.864
50	57.4	23.5	33.9	227	PTFE	13.119
48	57.8	25.7	32.1	227	PTFE	11.775
43	51.5	19.8	31.7	227	PVDF	10.706
53	56.6	19.8	36.8	227	Versapor	7.284
55	56.7	20.2	36.5	227	Versapor	5.230

Table 7.10: Experimental results for different membranes at different flowrates

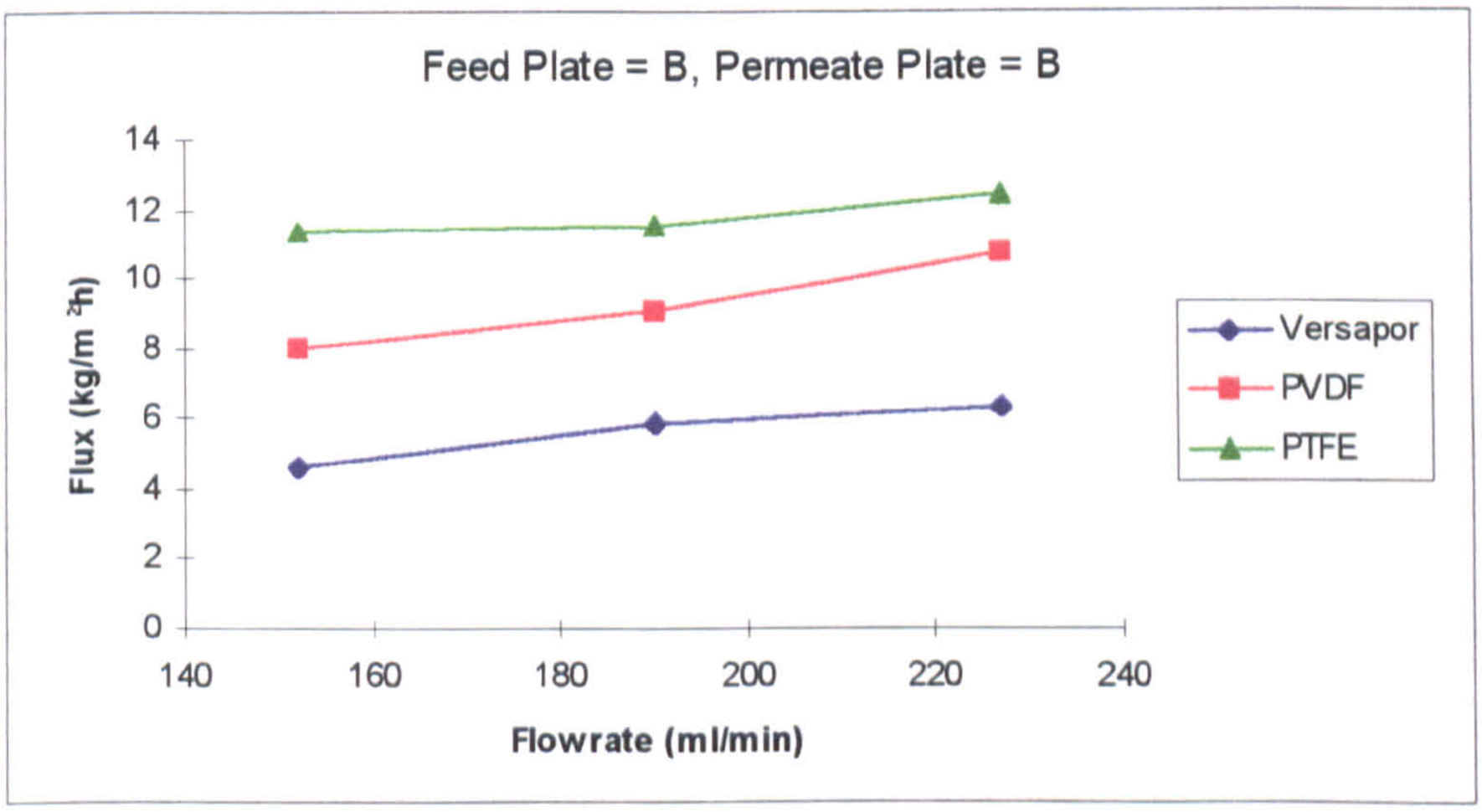

Figure 7.17: Average experimental results for different membranes at various flowrates

relied upon, and therefore it was concluded that this membrane material was not suitable for this work.

7.4.2 Theoretical Results

The theoretical model was run with all the experimental conditions. An example of the output from the model is shown in Table 7.11 for a PVDF membrane. As the calculation procedure was iterative, the model was run until the flux error was less than 0.0001 kg/m^2h. Table 7.12 through to Table 7.15 give the fluxes calculated by the model for all the experimental conditions.

7.4.3 Comparison Of The Membrane Distillation Model With Experiments

Once the theoretical model had been run at all the experimental conditions, the results were compared to the experimental results, to measure the accuracy of the model.

Figure 7.18 shows the comparison for a Plain:Plain plate configuration and a PVDF membrane. The line on this graph (and on later graphs) represents the 'direct correlation' situation i.e. the predicted model permeate flux is the same as the experimental flux. If a point lies above the line, the model overpredicts the flux, and if a point lies below the line, the model underpredicts the flux. The points are all in close proximation to the direct correlation line with the worst point having an error of 31% based on the experimental flux. Half of the results have an error of less than 10%. Figure 7.19 is the comparison for a PTFE membrane in a Plain:Plain module. All of the results, but one, are within 5% of the direct correlation line which shows that the model accurately predicts permeate flux when using a PTFE membrane.

The attempt to model membrane distillation using a Versapor membrane is shown in Figure 7.20. As it can be seen, the experimental and theoretical results do not agree. This is because the experiments, while they were carried out at very similar temperatures, did not produce consistent fluxes. This is probably due to the membrane not maintaining 100% hydrophobicity during the process, altering the permeate flux through the membrane. This confirms that the Versapor membrane is not suitable for this work on membrane distillation.

PVDF membrane
Coef,C = 4.5E-07
Dh/Dc = 100
km/dm = 384.62

Channel height mm	kliquid /delta	HotMTC DhMC/d	Tm °C	dT °C	Feed T °C	Permeate T °C	Estimate Flux kg/m²hr	Latent heat w/m²	Hot side int.temp °C	Cold side int.temp °C	Hot side V.Press N/m²	Cold side V.Press N/m²	Hot side interface mol. frac	Cold side Interface mol. frac.	Calculate Flux kg/m²hr	Flux error kg/m²hr
0.05	12400	1.998	25	25	37.5	12.5	7.34	4600	37.42	13.58	6075	1538	0.999	1.001	7.34	1.02E-06
0.15	4133	0.666	25	25	37.5	12.5	7.16	3864	34.75	15.25	5539	1716	0.997	1.003	7.16	1.07E-06
0.25	2480	0.400	25	25	37.5	12.5	5.32	3336	33.51	17.49	5169	1858	0.996	1.004	5.32	9.27E-07
0.35	1771	0.285	25	25	37.5	12.5	4.68	2937	32.56	17.44	4898	1976	0.995	1.005	4.68	7.75E-07
0.45	1378	0.222	25	25	37.5	12.5	4.18	2623	31.80	18.20	4692	2073	0.995	1.005	4.18	4.38E-07

Coef,C = 4.5E-07
Dh/Dc = 100
km/dm = 384.62

0.45	1378	0.222	25	25	37.5	12.5	4.18	2623	31.80	18.20	4692	2073	0.995	1.005	4.18	4.32E-07
0.9	689	0.111	25	25	37.5	12.5	2.83	1771	29.69	20.31	4157	2367	0.993	1.007	2.83	5.21E-08
1.35	460	0.074	25	25	37.5	12.5	2.13	1333	28.59	21.41	3899	2535	0.992	1.008	2.13	2.35E-07

Table 7.11: Example of Membrane Distillation Model for a PVDF Membrane

Experiment for comparison	Channel Height (mm)	Feed T (°C)	Permeate T (°C)	Tm (°C)	dT (°C)	Calculated Permeate Flux (kg/m²h)
26	0.45	55.6	21.1	38.35	34.5	9.673
27	0.45	44.4	20.3	32.35	24.1	5.422
28	0.45	37.5	12.4	24.95	25.1	4.192
29	0.45	59.6	14.4	37.00	45.2	12.234
30	0.45	60.9	15.0	37.95	45.9	12.829
31	0.45	60.1	22.1	41.10	38	11.665
32	0.45	60.7	22.6	41.65	38.1	11.897
33	0.45	60.3	30.9	45.60	29.4	10.266
34	0.45	58.5	29.1	43.80	29.4	9.745
35	0.45	39.9	13.9	27.90	26	4.721
36	0.45	47.0	13.3	29.65	32.7	7.684
37	0.45	47.6	12.9	29.75	33.7	7.924
38	0.45	45.5	13.0	29.25	32.5	7.538
39	1.35	54.0	19.3	37.65	34.7	4.354
40	0.9	55.5	18.4	37.95	37.1	7.400
41	0.9	55.0	18.7	37.85	37.3	7.242
42	0.45	55.1	17.7	37.40	37.4	9.844
43	0.45	51.5	19.8	35.65	31.7	8.090
44	0.45	51.5	18.5	35.00	33	8.240

Table 7.12: Theoretical results obtained at experimental conditions for Plain: Plain plate configuration and a PVDF membrane

Experiment for comparison	Feed T (°C)	Permeate T (°C)	Tm (°C)	dT (°C)	Calculated Permeate Flux (kg/m²h)
45	57.6	22.5	39.55	34.1	12.322
46	57.4	23.4	40.40	34	12.587
47	57.0	24.5	40.75	32.5	12.146
48	57.8	25.7	41.75	32.1	12.331
49	57.7	21.3	39.00	35.4	12.594
50	57.4	23.5	40.45	33.9	12.567

Table 7.13: Theoretical results obtained at experimental conditions for Plain: Plain plate configuration and a PTFE membrane

Experiment for comparison	Feed T (°C)	Permeate T (°C)	Tm (°C)	dT (°C)	Calculated Permeate Flux (kg/m^2h)
51	54.9	19.4	37.15	35.5	7.542
52	57.0	19.7	37.85	37.3	7.875
53	57.6	19.8	38.20	37.8	7.065
54	57.4	20.3	38.35	37.1	7.963
55	57.7	20.2	38.45	37.5	7.070

Table 7.14: Theoretical results obtained at experimental conditions for Plain: Plain plate configuration and a Versapor membrane

Experiment for comparison	Channel Height (mm)	Feed T (°C)	Permeate T (°C)	Tm (°C)	dT (°C)	Calculated Permeate Flux (kg/m^2h)
56	0.45	52.7	20.1	37.40	32.6	8.545
57	0.45	39.0	27.0	33.00	12	2.748
58	0.45	37.9	20.8	28.85	17.1	3.141
59	0.45	37.5	18.1	27.30	18.4	3.374
60	0.45	44.5	20.9	32.70	23.6	5.378
61	0.45	37.7	17.1	27.40	20.6	3.644
62	0.45	37.3	12.0	24.65	25.3	4.172
63	0.9	37.8	12.3	25.05	25.5	2.888
64	0.9	38.2	18.5	28.35	19.7	2.528
65	1.35	38.9	18.6	28.75	20.3	1.979
66	0.45	37.0	18.8	27.90	18.2	3.421
67	0.9	38.0	18.9	28.45	19.1	2.460
68	1.35	38.4	18.8	28.60	19.6	1.900

Table 7.15: Theoretical results obtained at experimental conditions for Plain: Channelled plate configuration and a PVDF membrane

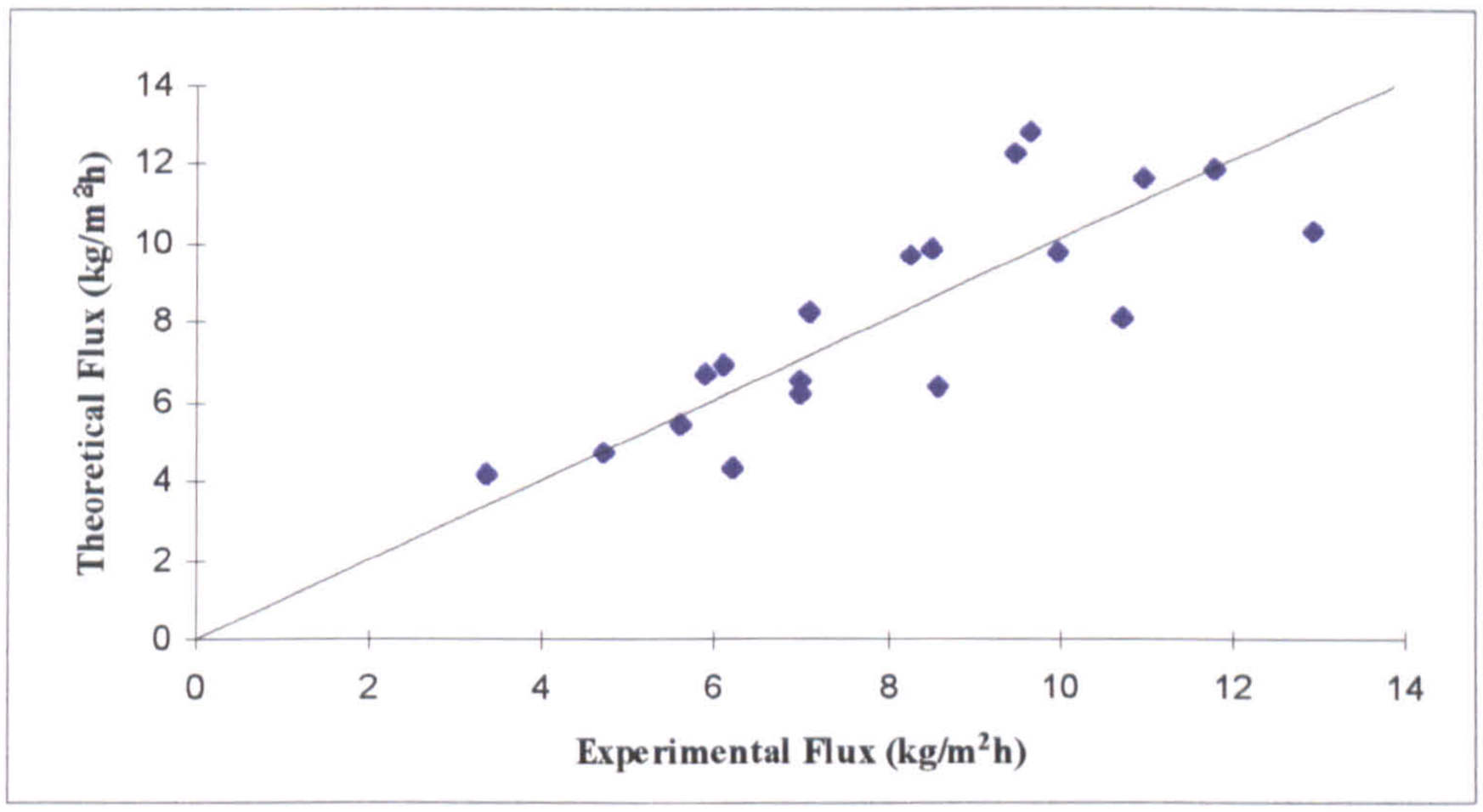

Figure 7.18: Comparison between the theoretical model and experimental results for Plain:Plain plate configuration and a PVDF membrane

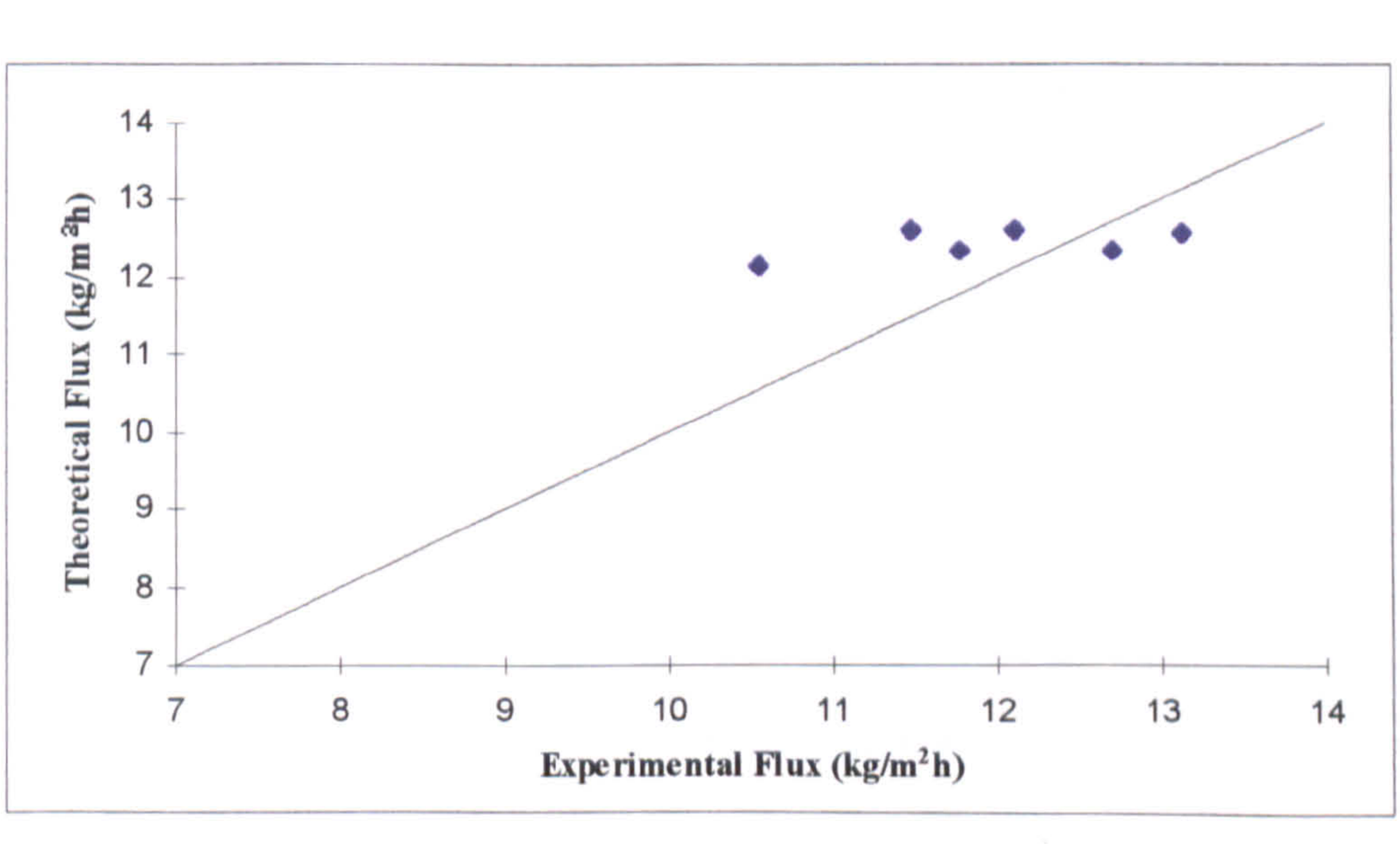

Figure 7.19: Comparison between the theoretical model and experimental results for Plain:Plain plate configuration and a PTFE membrane

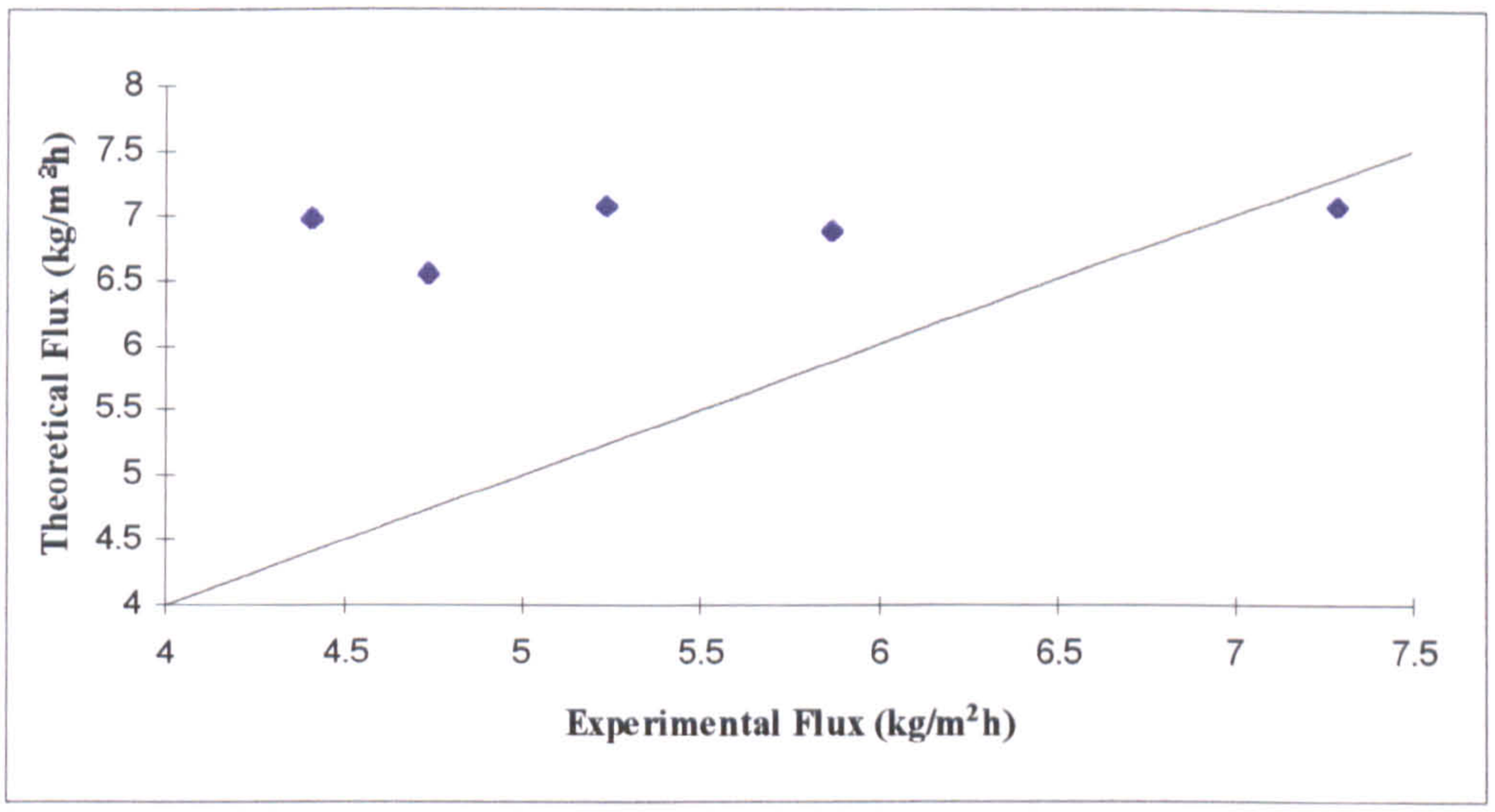

Figure 7.20: Comparison between the theoretical model and experimental results for Plain:Plain plate configuration and a Versapor membrane

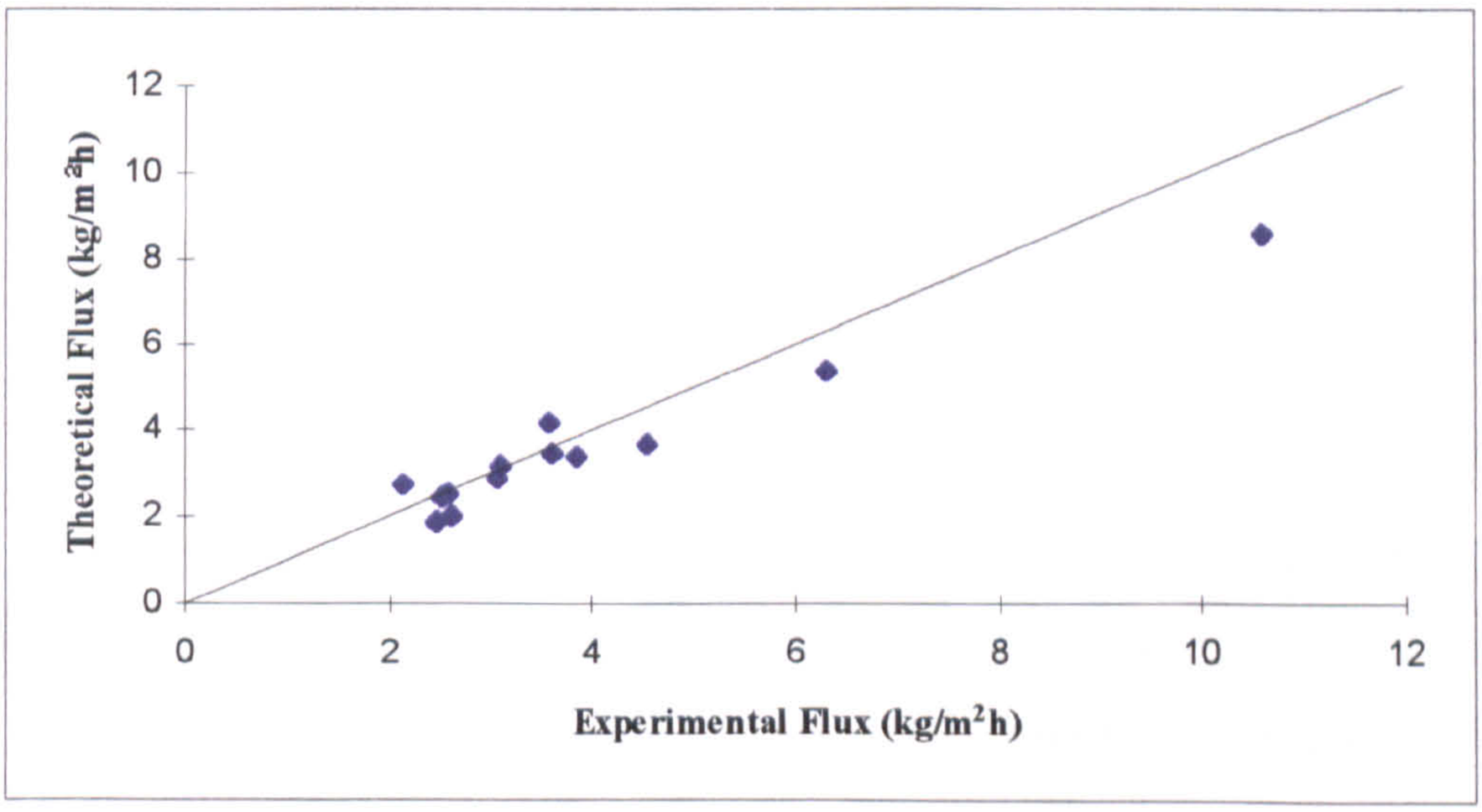

Figure 7.21: Comparison between the theoretical model and experimental results for Plain:Channelled plate configuration and a PVDF membrane

The next comparison was for introducing a channelled plate on the permeate side for a PVDF membrane and is shown in Figure 7.21. Again the points lie close to the direct correlation line with about half of the points within 5% of the line. Looking closer at the effect of boundary layer thickness on the permeate flux, Figure 7.22 shows the comparison for a PVDF membrane, with varied boundary layer thickness. The theory matches closely to the experimental results.

All the comparisons so far concern the mass flux. For another comparison, the heat flux (Q) through the membrane was compared with that calculated from the model. The comparison is shown in Figure 7.23. The experimental heat flux was calculated from,

$$Q = mC_p\Delta T \tag{7.1}$$

The theoretical heat flux was calculated using the membrane distillation model to find the membrane interfacial temperatures. The temperature difference is represented by equation (7.2),

$$\Delta T_{lm} = \frac{(T_{Hin} - T_{Cin}) - (T_{Hout} - T_{Cout})}{ln\left[\frac{(T_{Hin} - T_{Cout})}{(T_{Hout} - T_{Cout})}\right]} \tag{7.2}$$

The theoretical heat flux consists of two parts which are,

$$Q_v = \frac{k_m}{\delta_m}(\Delta T_{lm}) \tag{7.3}$$

$$Q_c = N\lambda \tag{7.4}$$

$N\lambda$ is obtained from the membrane distillation model. Q_v and Q_c are calculated and combined to give the theoretical heat flux.

Figure 7.23 compares the heat flux found experimentally for various temperatures, with those calculated by the model, utilising a PVDF membrane. For instance, the heat flux calculated from an experiment was 37.8 W for hot inlet and outlet temperatures of 37 and 31°C, and cold inlet and outlet temperatures of 12 and 18°C respectively. Values for the interfacial temperatures and Q_V were taken from the model and, using equations (4.12) and (4.6), Q was found to be 38.2 W, a very small variation from the experimental value. This means the model also gives an accurate representation of the heat transfer in the membrane module.

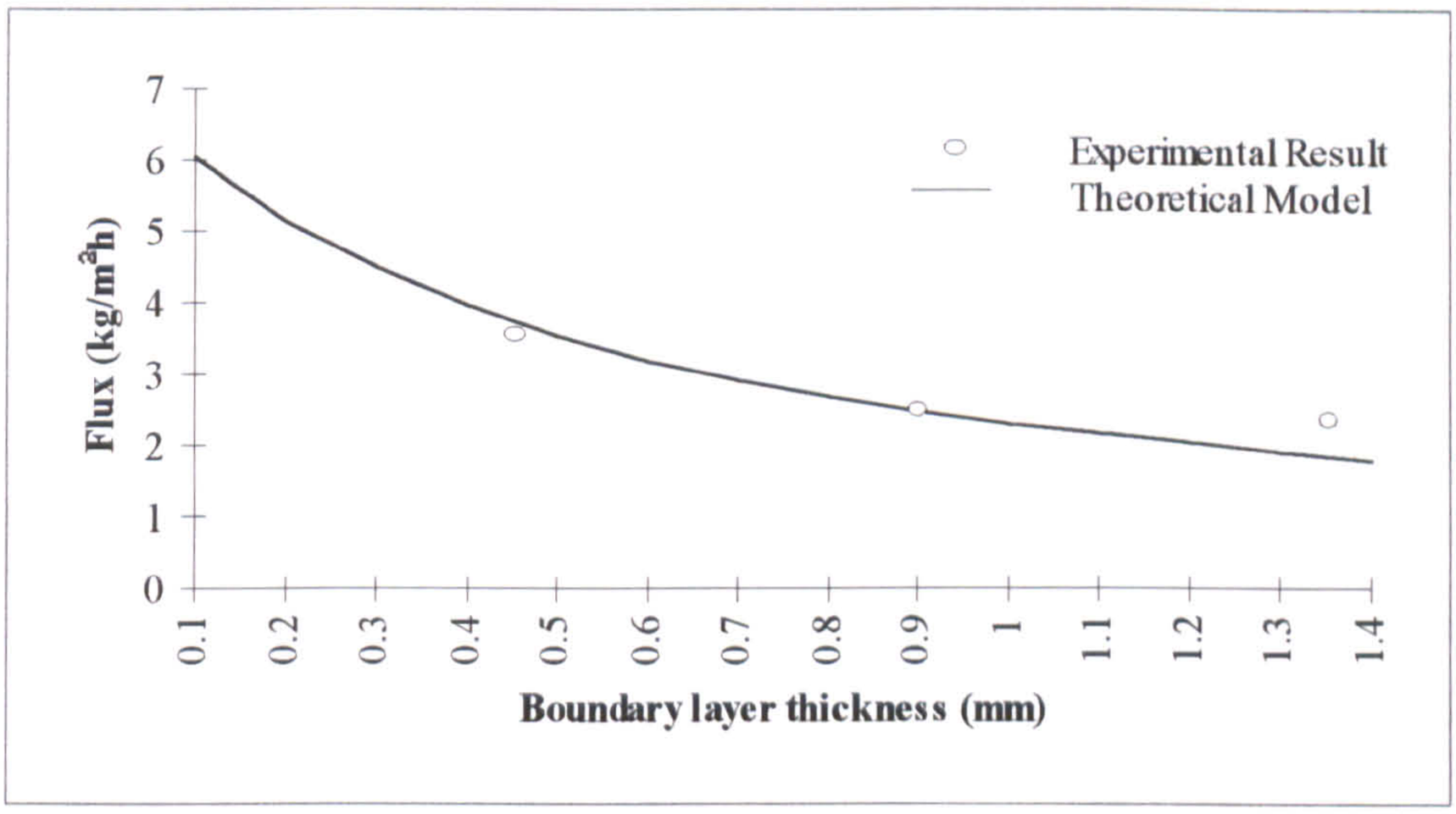

Figure 7.22: Comparison between experimental results and the membrane distillation model - Trend of flux with boundary layer thickness (PVDF membrane)

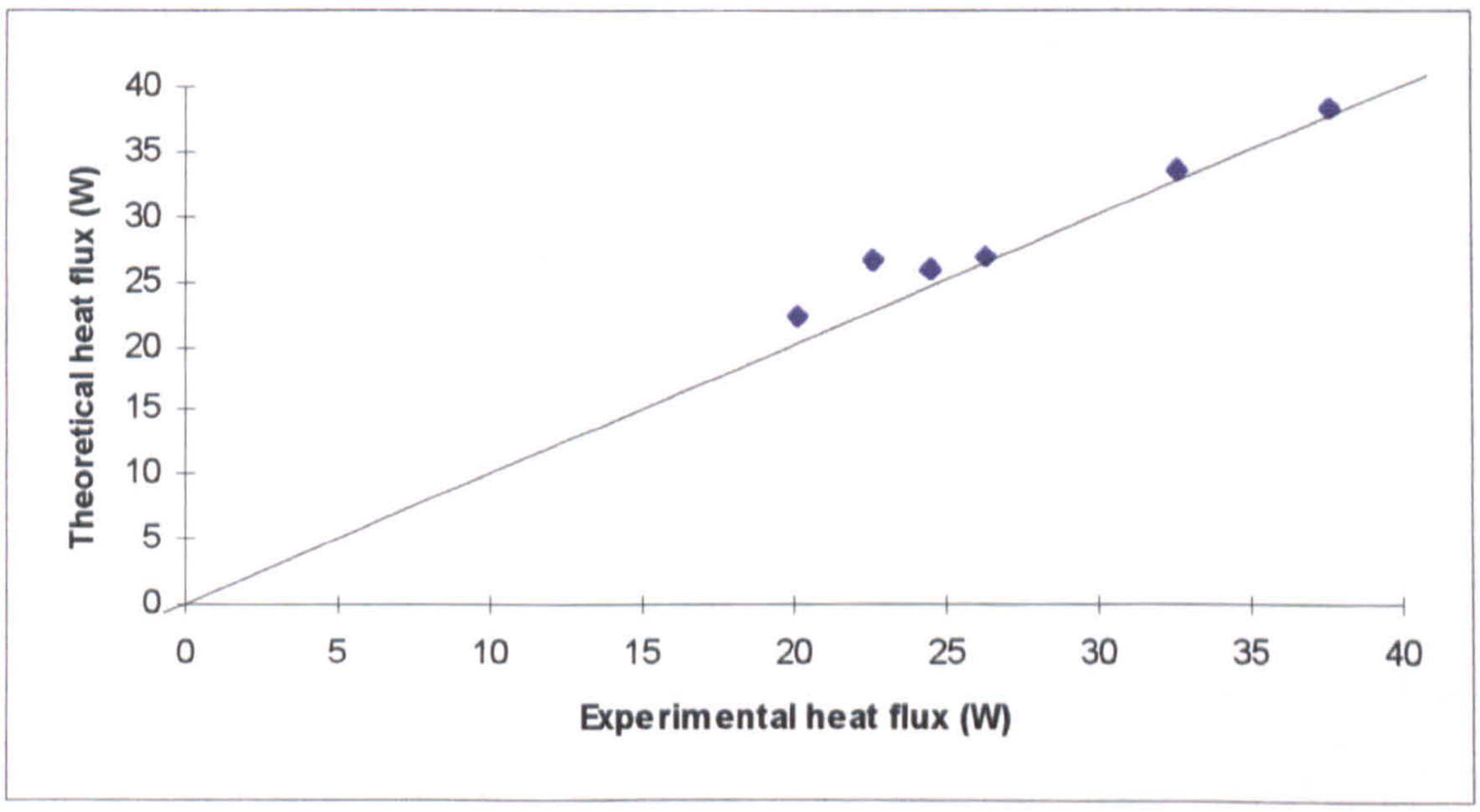

Figure 7.23: Comparison of the heat flux between experimental values and the membrane distillation model

7.4.4 Further Theoretical Results

As the comparison carried out in Chapter 7.3.3 shows that the membrane distillation model can accurately predict the permeate flux, further investigation was carried out. The theoretical model was run at other various conditions, to obtain graphs of the trends calculated for membrane distillation. The factors altered were, temperature difference, mean membrane temperature, feed temperature, permeate temperature, channel height and type of membrane. The graphs obtained are shown in Figures 7.24 to 7.27.

Figures 7.24 and 7.25 concern a PVDF membrane. Bulk temperatures were varied to obtain flux predictions for a constant mean membrane temperature (Figure 7.24), with various temperature differences. It can be seen that increasing the temperature difference increases the permeate flux, and the effect is enhanced when decreasing the boundary layer thickness. Decreasing the boundary layer thickness also enhances the effect of increasing the mean membrane temperature, shown in Figure 7.25. From the two graphs it can be seen that increasing the mean membrane temperature has a greater effect on the flux than increasing the temperature difference. For instance, from Figure 7.24, increasing the temperature difference from 25 to 30°C at a mean membrane temperature of 25°C increases the flux (at a boundary layer thickness of 0.05 mm) from 7.5 to 9.1 kg/m^{2}h, a difference of 1.6 kg/m^{2}h. From Figure 7.25, increasing the mean membrane temperature from 20 to 25°C at a temperature difference of 30°C, increases the flux by 2 kg/m^{2}h.

Similar treatment is given for a PTFE membrane in Figures 7.26 and 7.27. The same trends are observed, but the fluxes involved are much higher. The maximum flux in Figure 7.26 is 17.2 kg/m^{2}h while for the PVDF membrane it is 9.1 kg/m^{2}h. The maximum flux in Figure 7.27 is 76% larger then the PVDF value from Figure 7.25.

From this section of work it can be summarised that for membrane distillation, a PTFE membrane produces the highest fluxes due to its very hydrophobic nature and small membrane thickness. PVDF is also suitable for use in membrane distillation, but produces lower fluxes mainly due to the fact that it is twice as thick as the PTFE membrane. The permeate flux increases with increasing temperature difference and mean membrane temperature, with the latter being more dominant. The flux also increases with decreasing

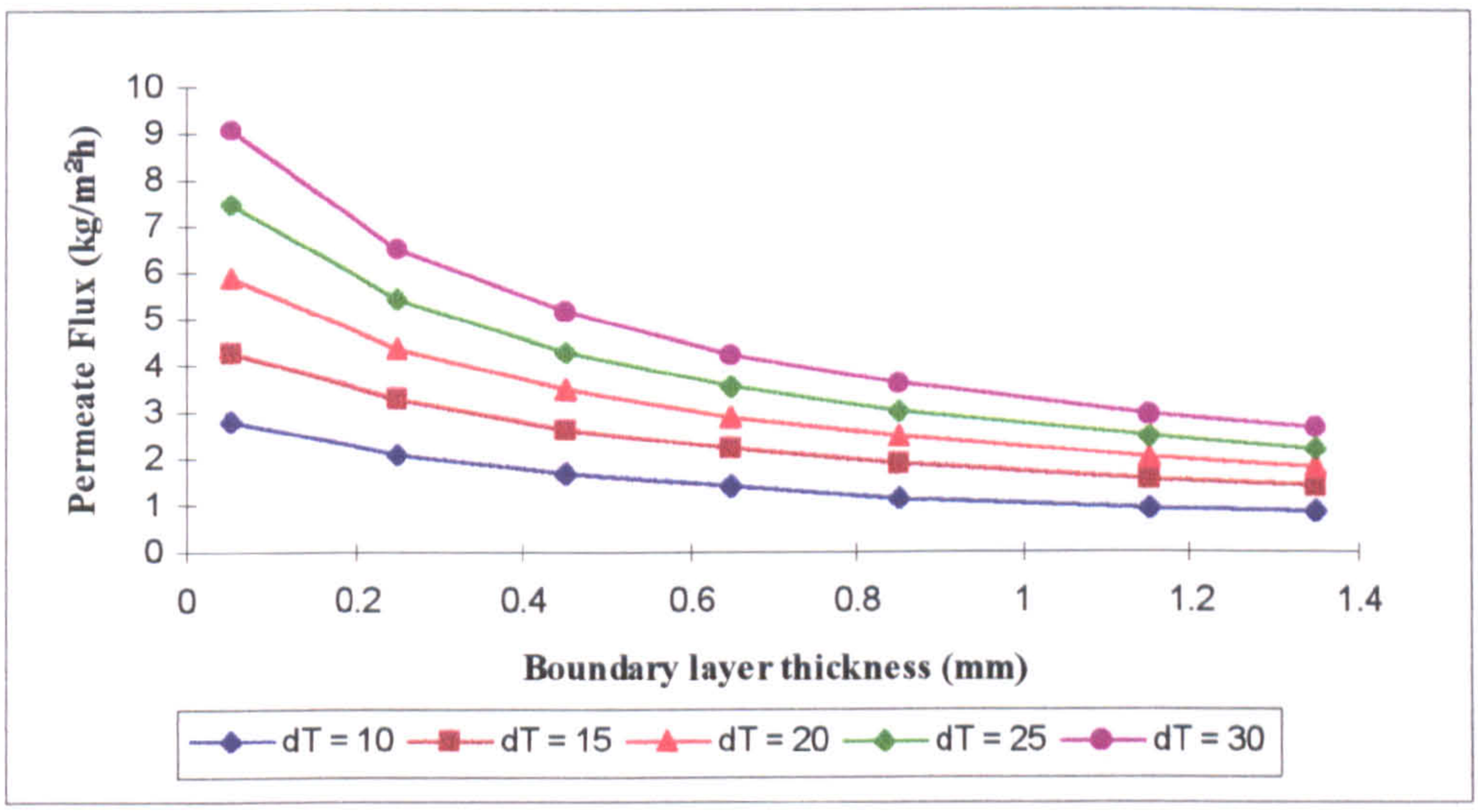

Figure 7.24: Trends calculated by the theoretical model for a PVDF membrane with a membrane temperature of 25°C

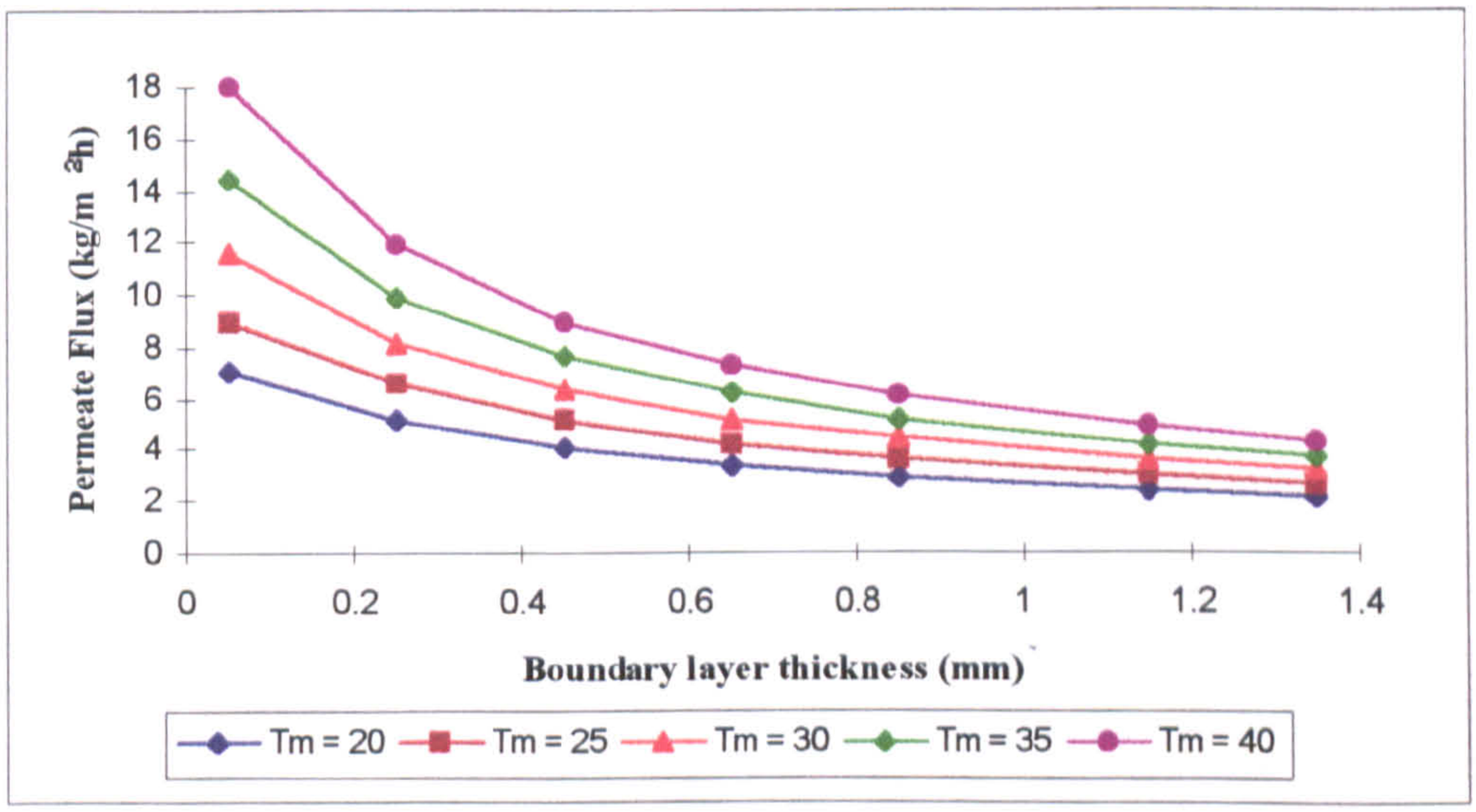

Figure 7.25: Trends calculated by the theoretical model for a PVDF membrane with a temperature difference of 30°C

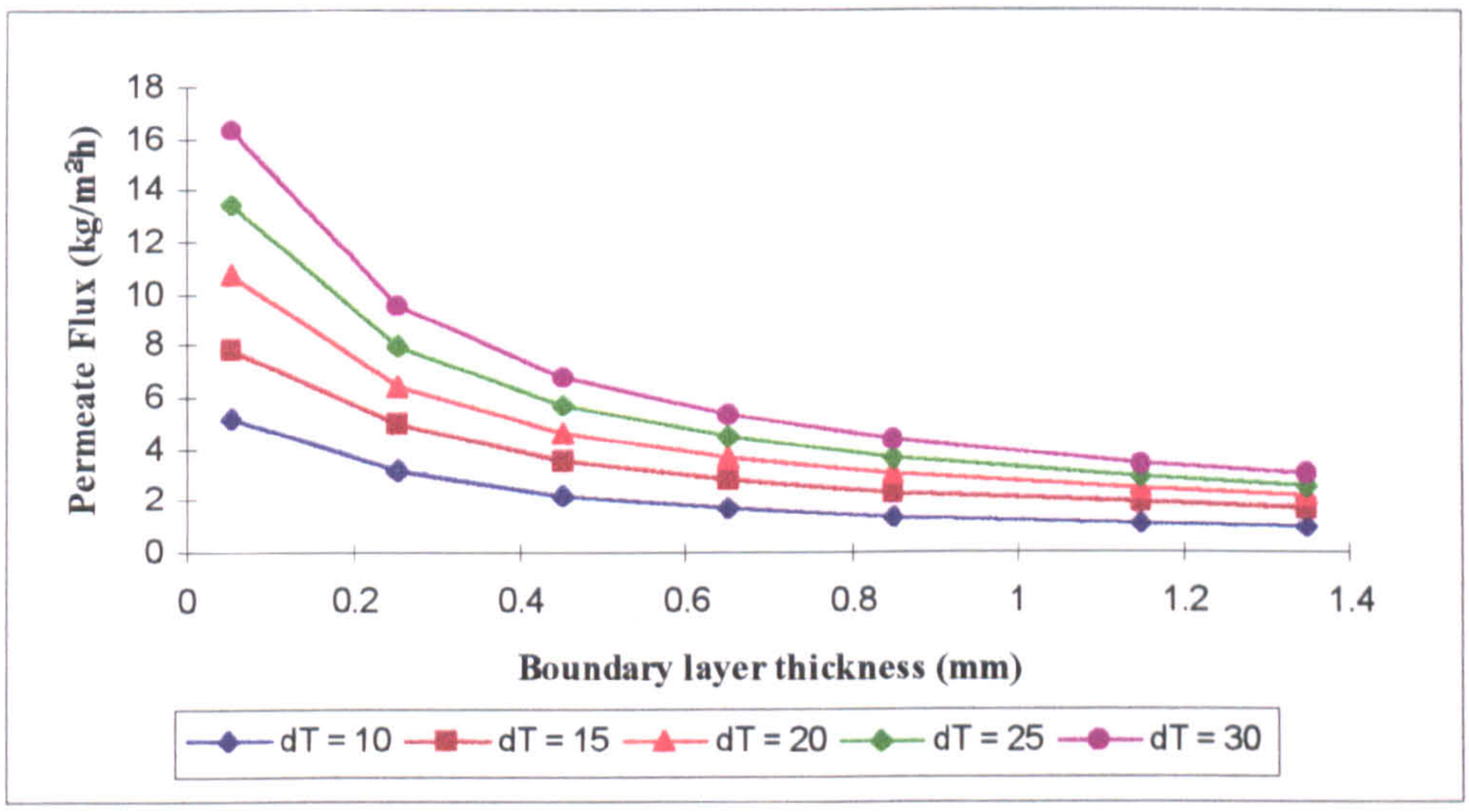

Figure 7.26: Trends calculated by the theoretical model for a PTFE membrane with a membrane temperature of 25°C

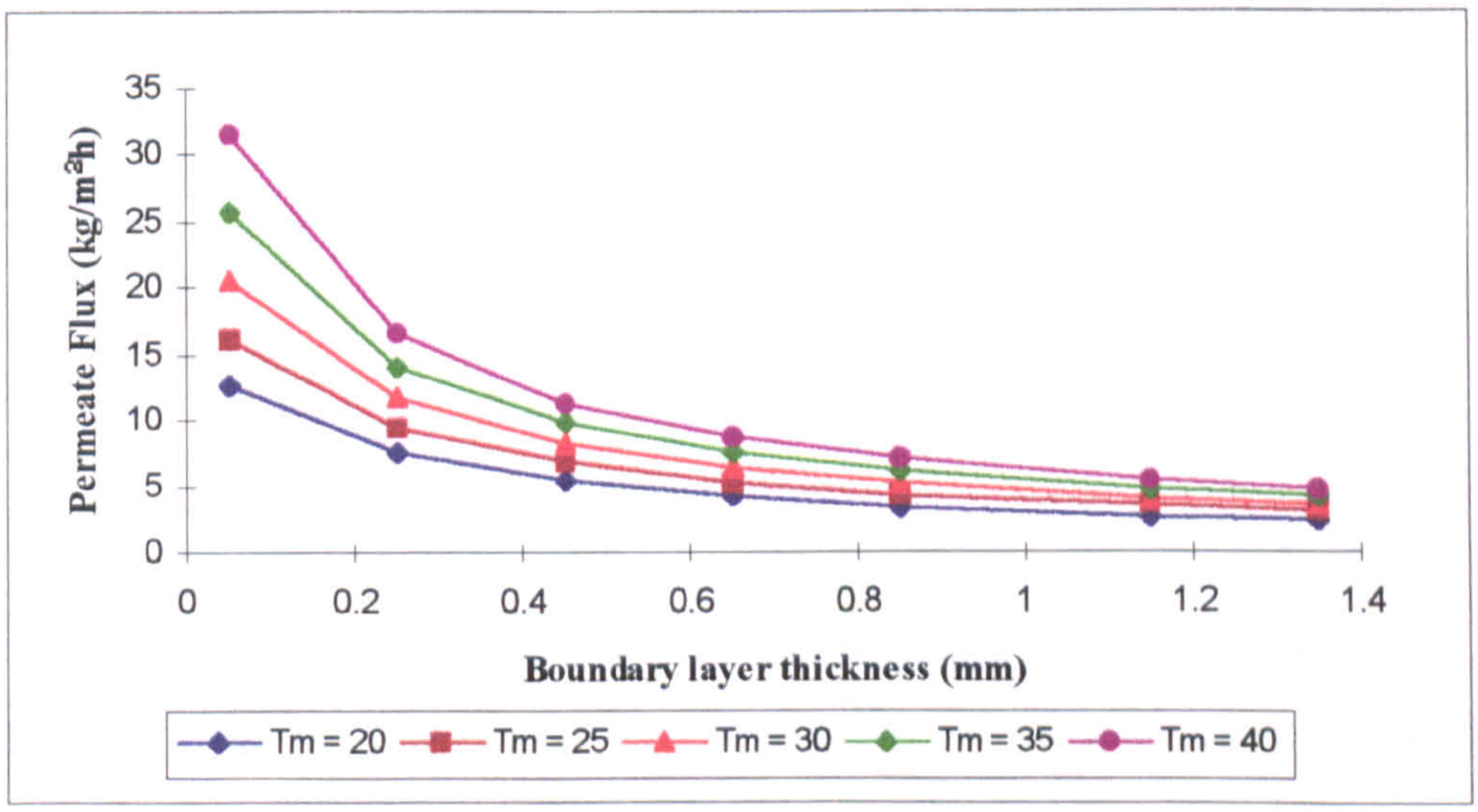

Figure 7.27: Trends calculated by the theoretical model for a PTFE membrane with a temperature difference of 30°C

boundary layer thickness, as this reduces the effect of temperature polarisation i.e. it keeps the membrane interfacial temperatures close to the bulk fluid temperatures.

The membrane distillation model formed in Chapter 4 has been shown to be accurate for the experimental conditions used in this work and aids in the prediction of permeate flux with a wide range of conditions.

7.5 Boundary Layer Analysis

The aim of this section of the work was to model the growth of the thermal boundary layer along a module channel to predict the exit temperatures. As membrane distillation is driven by a temperature induced vapour pressure difference this is an important consideration. This work was mainly theoretical. The experiments carried out were used for comparison for all Levels of the model.

7.5.1 Experimental Results

The experimental results for the boundary layer analysis are given in Table 7.16. These results were only used for comparison with those obtained from the boundary layer analysis model.

7.5.2 Theoretical Results

Level 1

The analysis was started by assuming a plug flow velocity distribution and single component stream (Level One). This was to achieve a basic working model to find the main relationships of boundary layer growth in a symmetrical module channel. The first study was to see how the liquid velocity would affect the thermal boundary layer growth. This is shown in Figure 7.28. The dotted line represents the experimental channel height of 0.45 mm. As the velocity is increased, the growth rate decreases. Doubling the velocity roughly doubles the distance taken for the boundary layer to grow to 0.45 mm.

Experiment	Flowrate (ml/min)	No. of Spacers	T_{Hin} (°C)	T_{Cin} (°C)	T_{Hout} (°C)	T_{Cout} (°C)
64	152	1	29.5	24.3	28.4	25.1
65	227	1	30.6	22.1	29.9	23.7
66	152	1	41.2	18.1	36.2	22.9
67	190	1	42.4	17.1	37.6	20.0
68	227	1	33.7	24.8	22.1	25.9
69	152	1	41.9	30.9	24.6	33.5
70	227	1	48.4	22.9	41.0	26.6
71	152	1	51.0	31.2	46.0	34.5
72	152	1	46.3	29.6	42.3	31.6
73	190	1	51.5	31.2	40.8	27.1
74	227	1	51.7	31.6	50.4	34.2
75	152	2	35.1	26.5	32.5	29.1
76	152	2	42.2	23.8	41.0	25.2
77	90	2	38.2	18.5	37.3	23.1
78	90	3	38.9	18.6	37.0	23.9
79	90	3	38.4	18.8	36.6	24.3

Table 7.16: Experimental results for comparison with the boundary layer analysis model

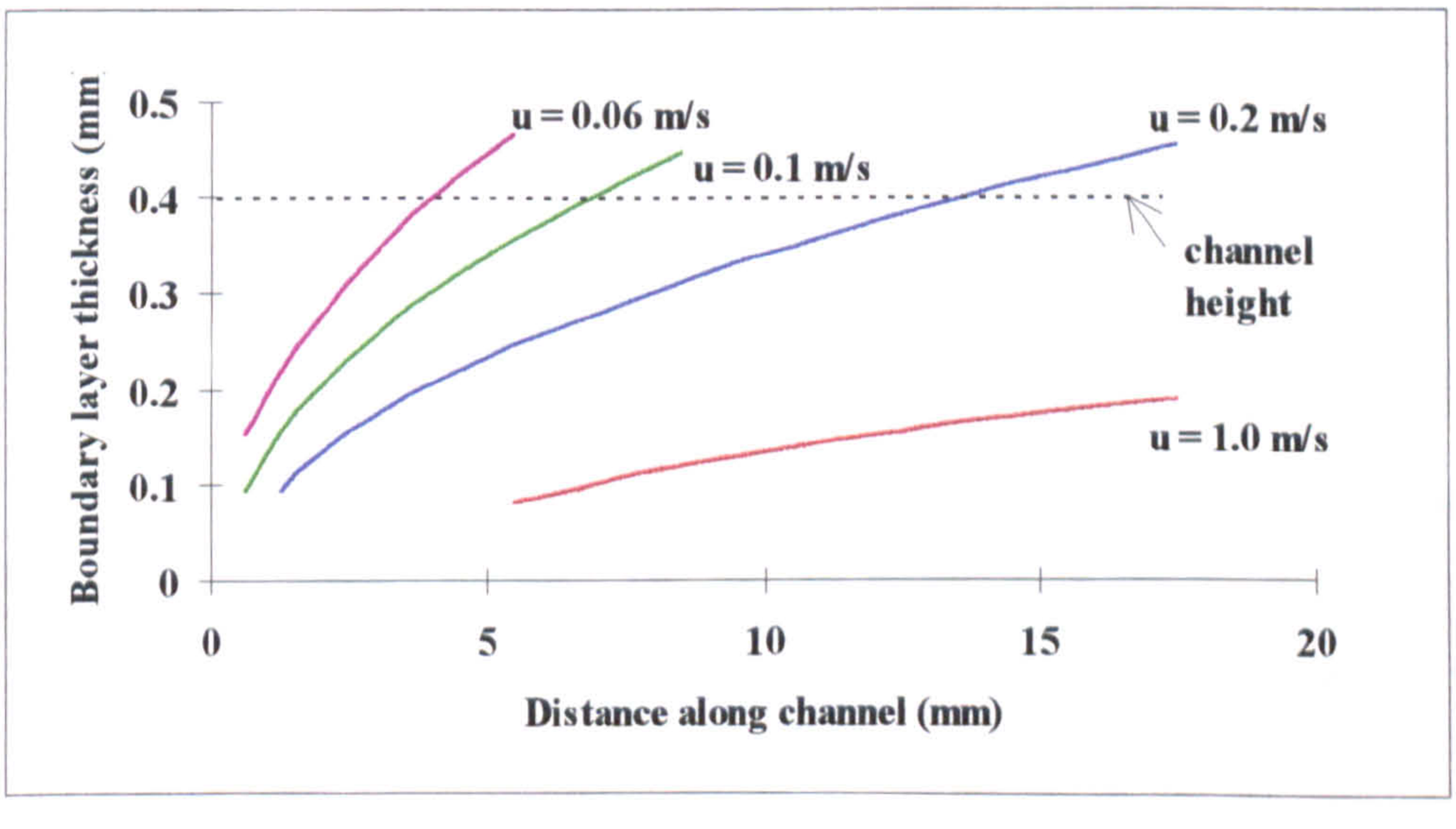

Figure 7.28: Growth of boundary layer at various liquid velocities - Level One
($Y = 0.45$ mm, $T_H = 318$ K, $T_C = 291$ K)

In the experiments, the total channel length was 60 mm, so the entrance region of the channel, where the boundary layer is growing is relatively small. This is shown in Figure 7.29 for a velocity of 0.0894 m/s. There are clearly two areas of boundary layer development as described in the theory (Chapter 4). The entrance region where the boundary layer is growing, and the constant region where the boundary layer has grown to fill the channel. For this example, the boundary layer grows to fill the channel in 6.9 mm, roughly a tenth of the entire channel length. This means that the constant region, where the thermal boundary layer completely fills the channel, is the dominant region. The model also allows the determination of temperatures along the module. Figure 7.30 gives the temperatures relating to the feed side wall and membrane temperatures, T_2 and T_1 respectively. From Figure 7.29, it can be observed that the entrance region is from 0 to 6.9 mm, and Figure 7.30 shows that the wall temperature, T_2, is constant in this region. This is because the heat of the bulk fluid is providing the temperature difference required by membrane distillation and the heat of liquid at the wall is not being utilised and is still at the bulk temperature. The membrane temperature falls rapidly in the entrance region as the thermal boundary layer is growing. Once the boundary layer fills the channel, the heat is provided from the whole of the bulk fluid and the membrane surface temperature falls less rapidly. Unfortunately, the wall temperature also starts to fall as the process of membrane distillation continues. In fact, once the constant region has taken over, the temperature fall on the feed side is linear.

Looking at the same format of graphs, but for a higher velocity of 0.117 m/s, Figures 7.31 and 7.32 show that the entrance region is slightly longer due to the higher velocity. The constant region starts 8.8 mm from the start of the channel. The same traits as in Figures 7.29 and 7.30 are shown in these figures. The Figures shown here are for the feed side only, but the permeate side trends are similar, with a temperature rise, not a fall, as the liquid flows along the module.

The model also produces the permeate side temperature profiles. An example of the full temperature profiles is given in Figure 7.33, with the experimental data plotted for comparison. The actual temperature difference between T_1 and T_2 is 1.38 K which is very small. The measured experimental outlet feed temperature was 302.9 K, which is between

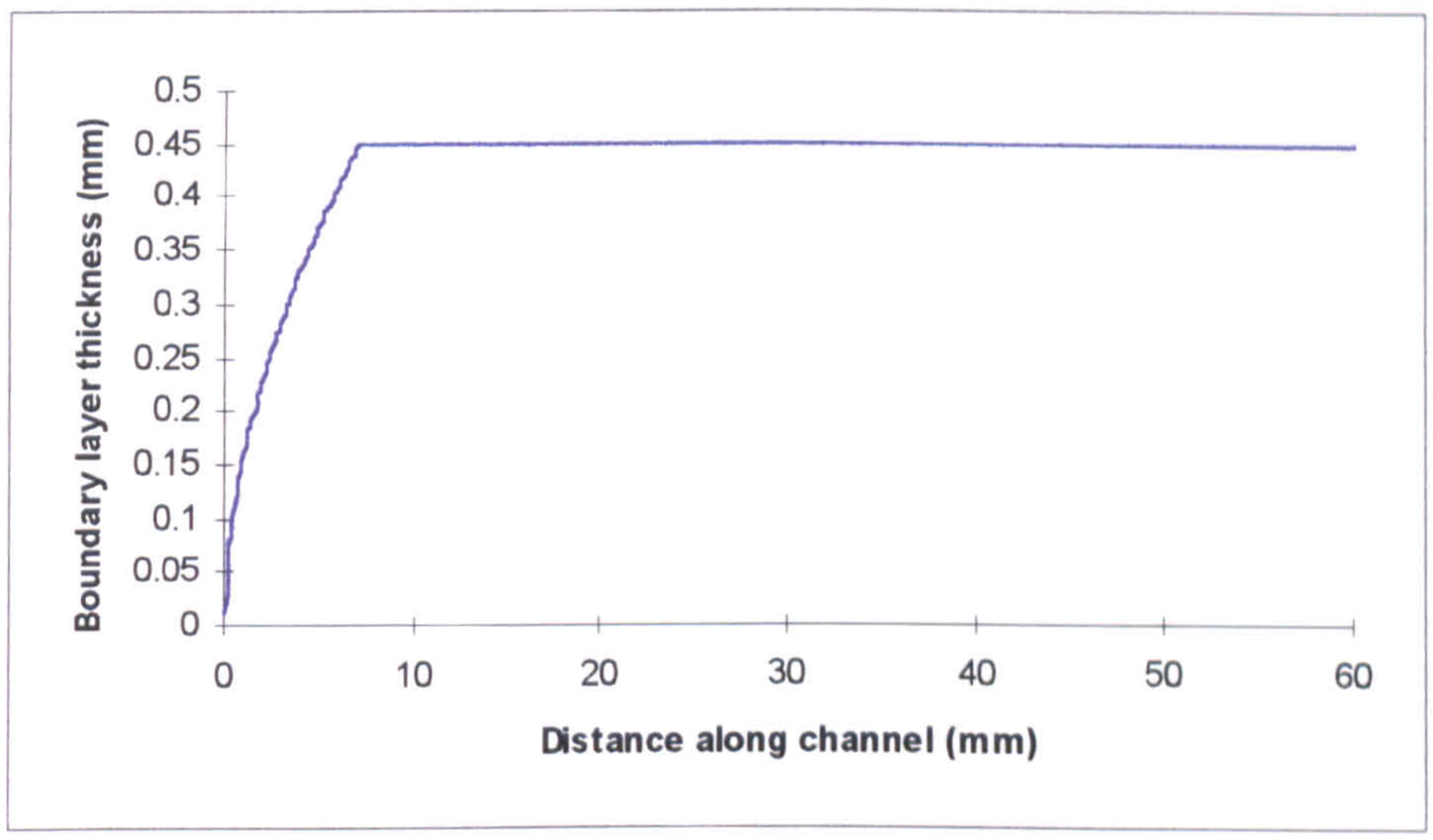

Figure 7.29: Level One thermal boundary layer development
($Y = 0.45$ mm, $v = 0.0894$ m/s, $T_H = 314.2$ K, $T_C = 291.1$ K)

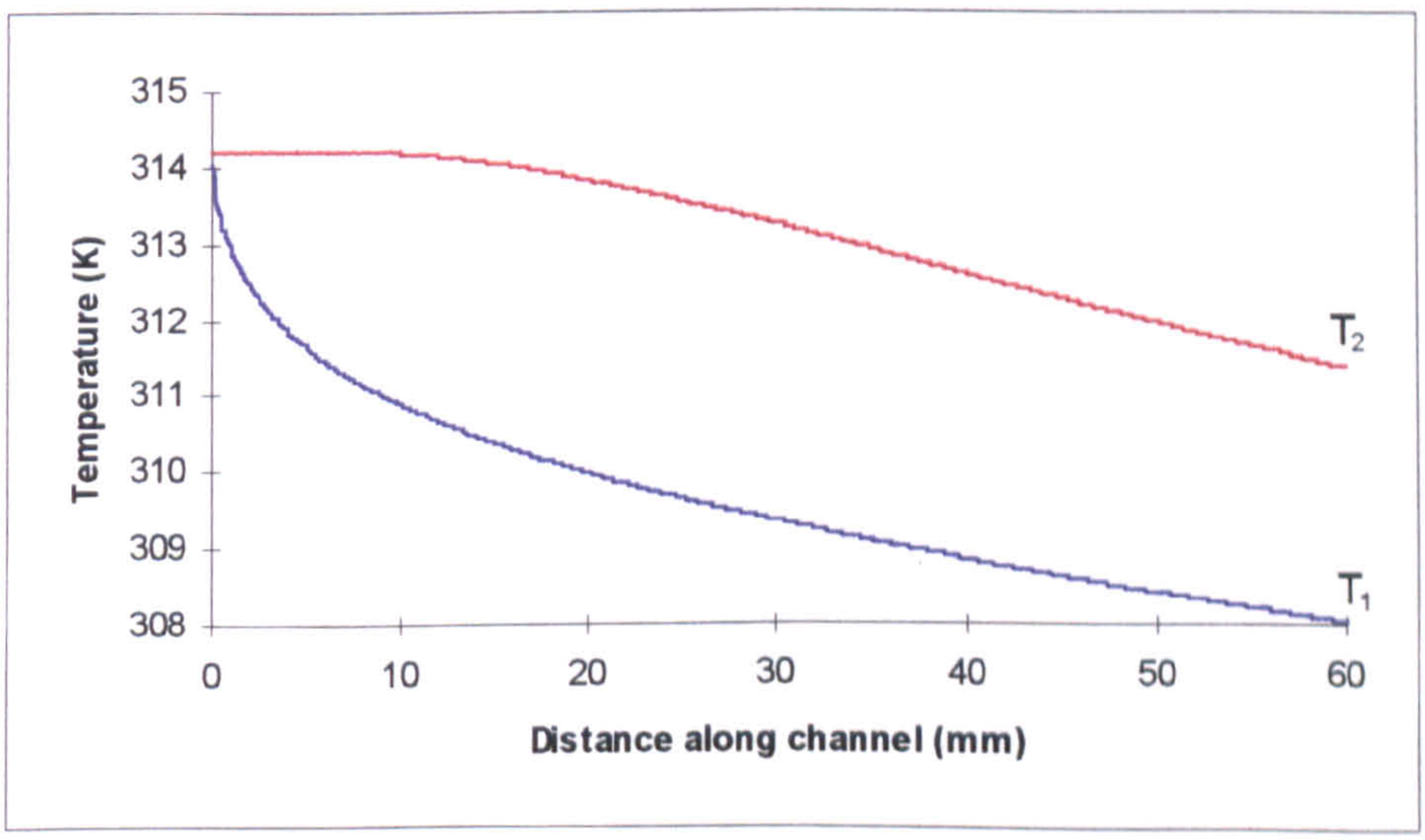

Figure 7.30: Level One feed side temperature profiles
($Y = 0.45$ mm, $v = 0.0894$ m/s, $T_H = 314.2$ K, $T_C = 291.1$ K)

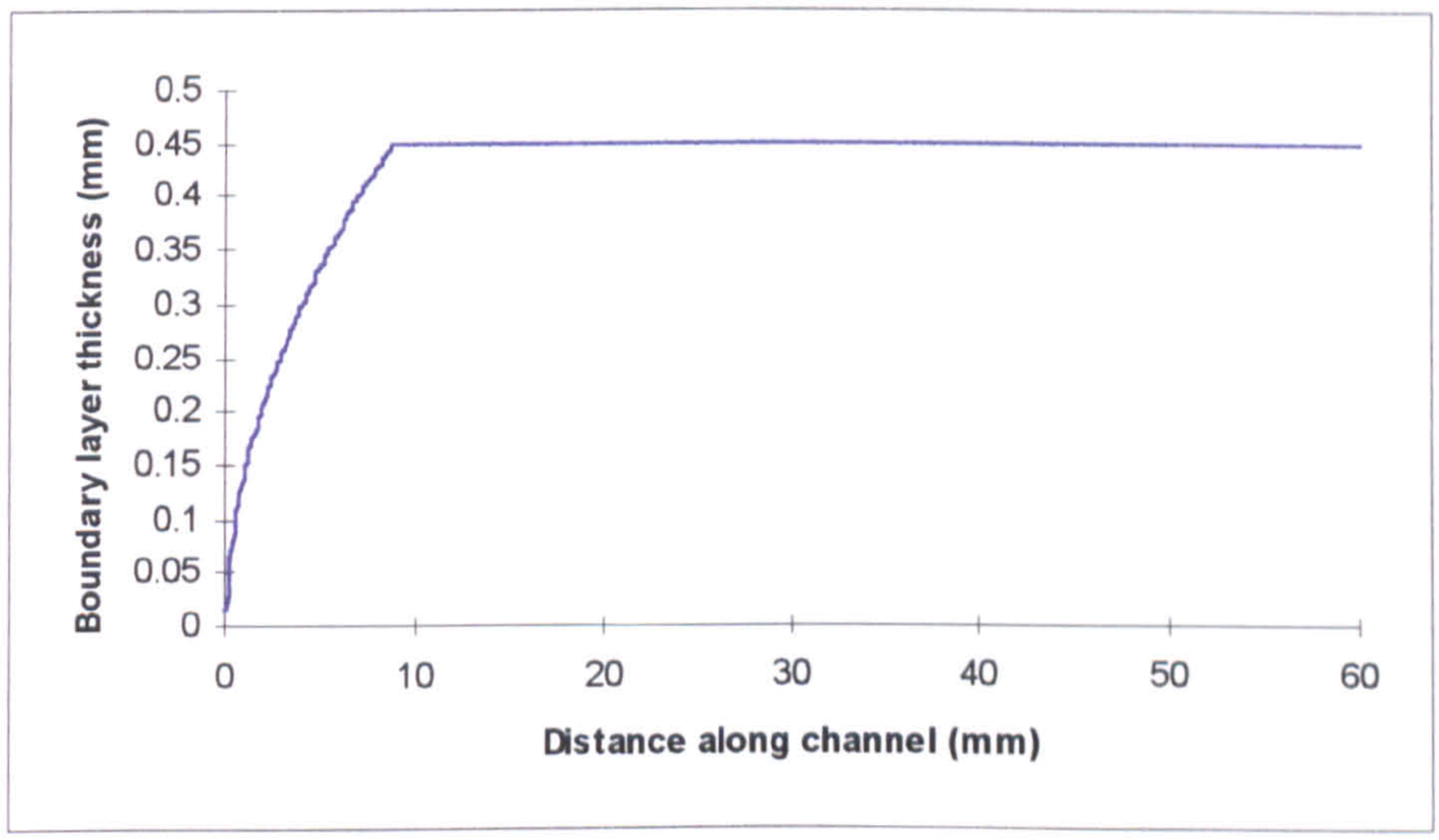

Figure 7.31: Level One thermal boundary layer development
(Y = 0.45 mm, v = 0.1117 m/s , T_H = 315.4 K, T_C = 290.1 K)

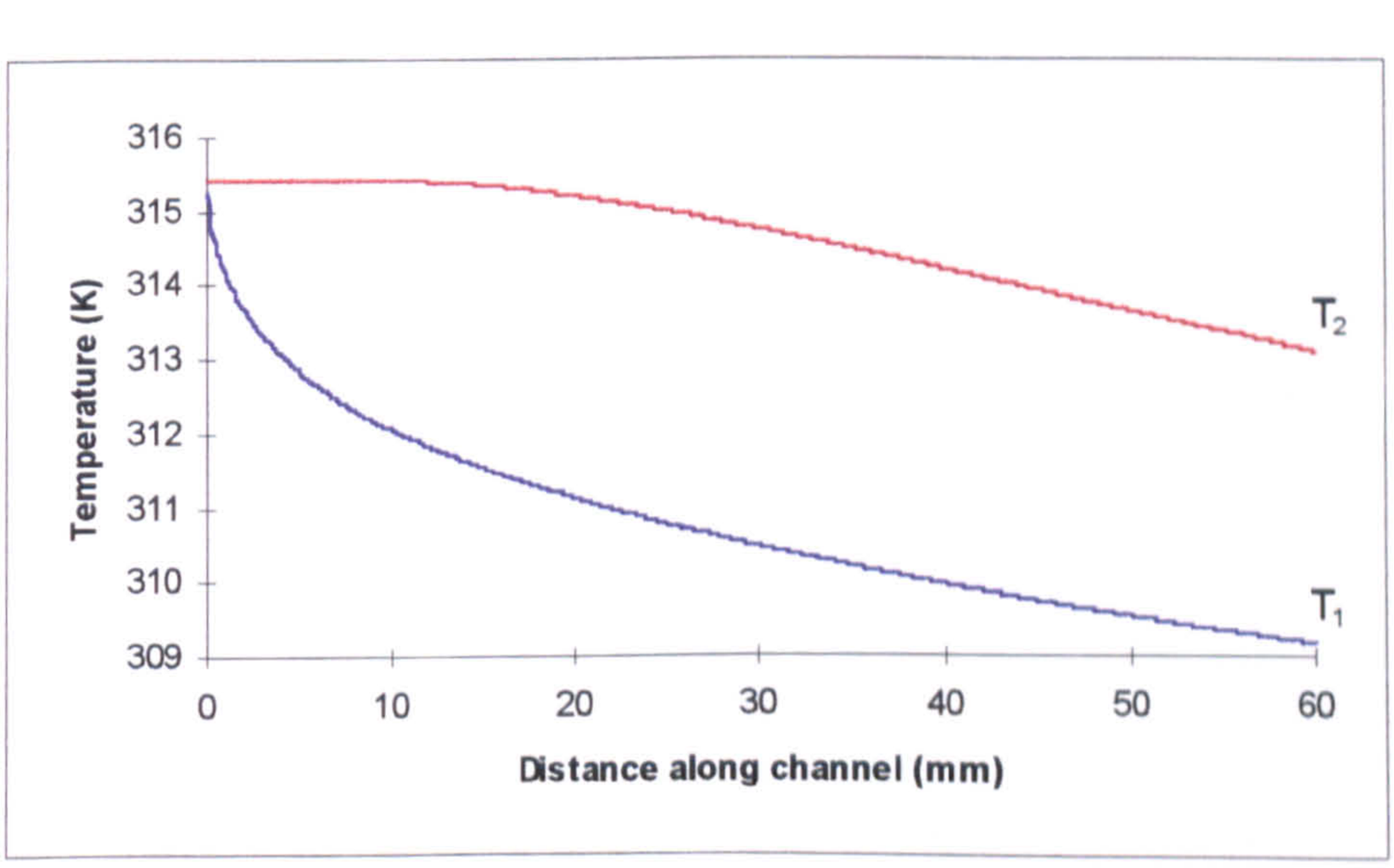

Figure 7.32: Level One feed side temperature profiles
(Y = 0.45 mm, v = 0.1117 m/s , T_H = 315.4 K, T_C = 290.1 K)

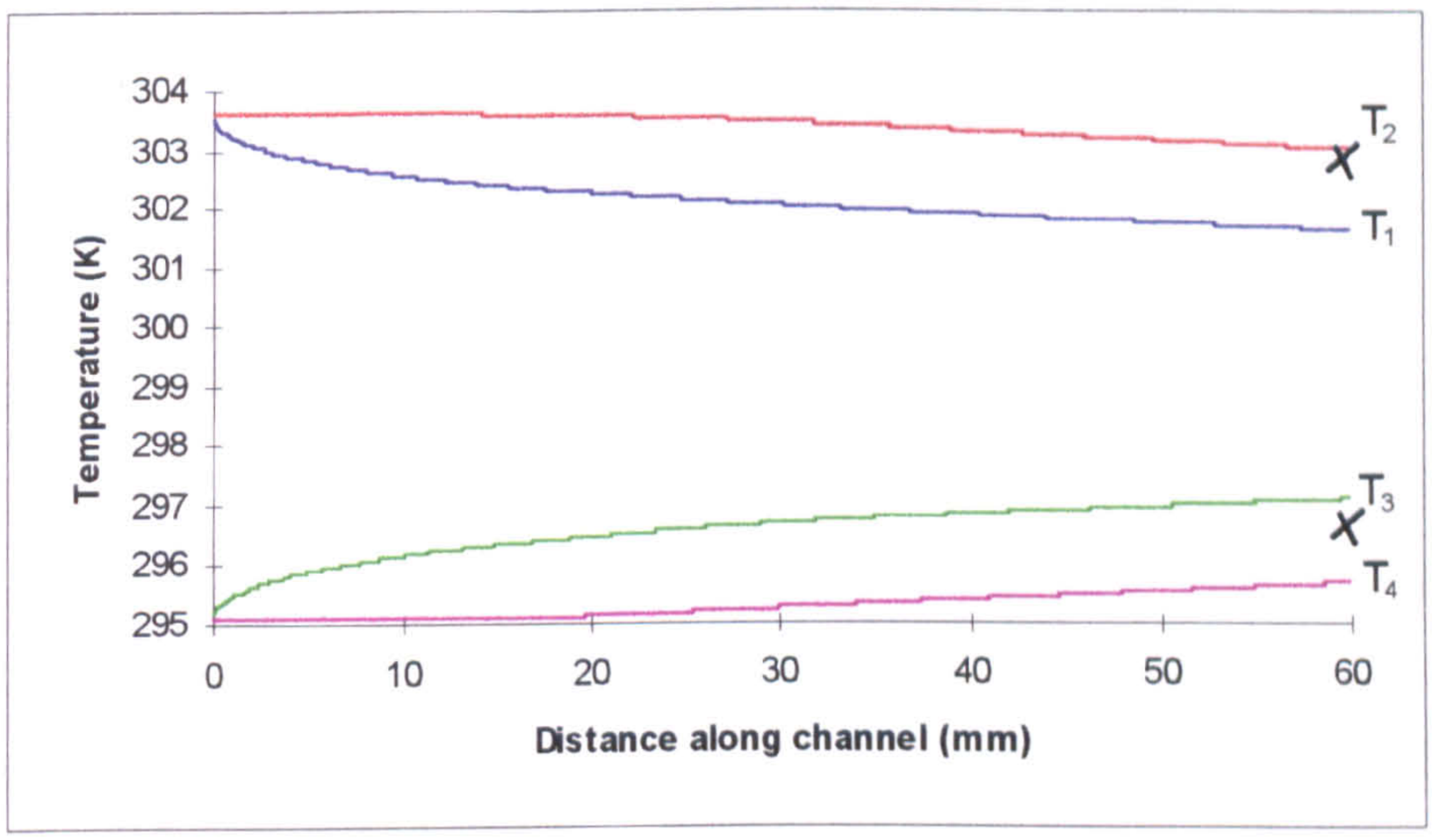

Figure 7.33: Level One full temperature profiles with experimental data
(Y = 0.45 mm, v = 0.1334 m/s, T_H = 303.6 K, T_C = 295.2 K)

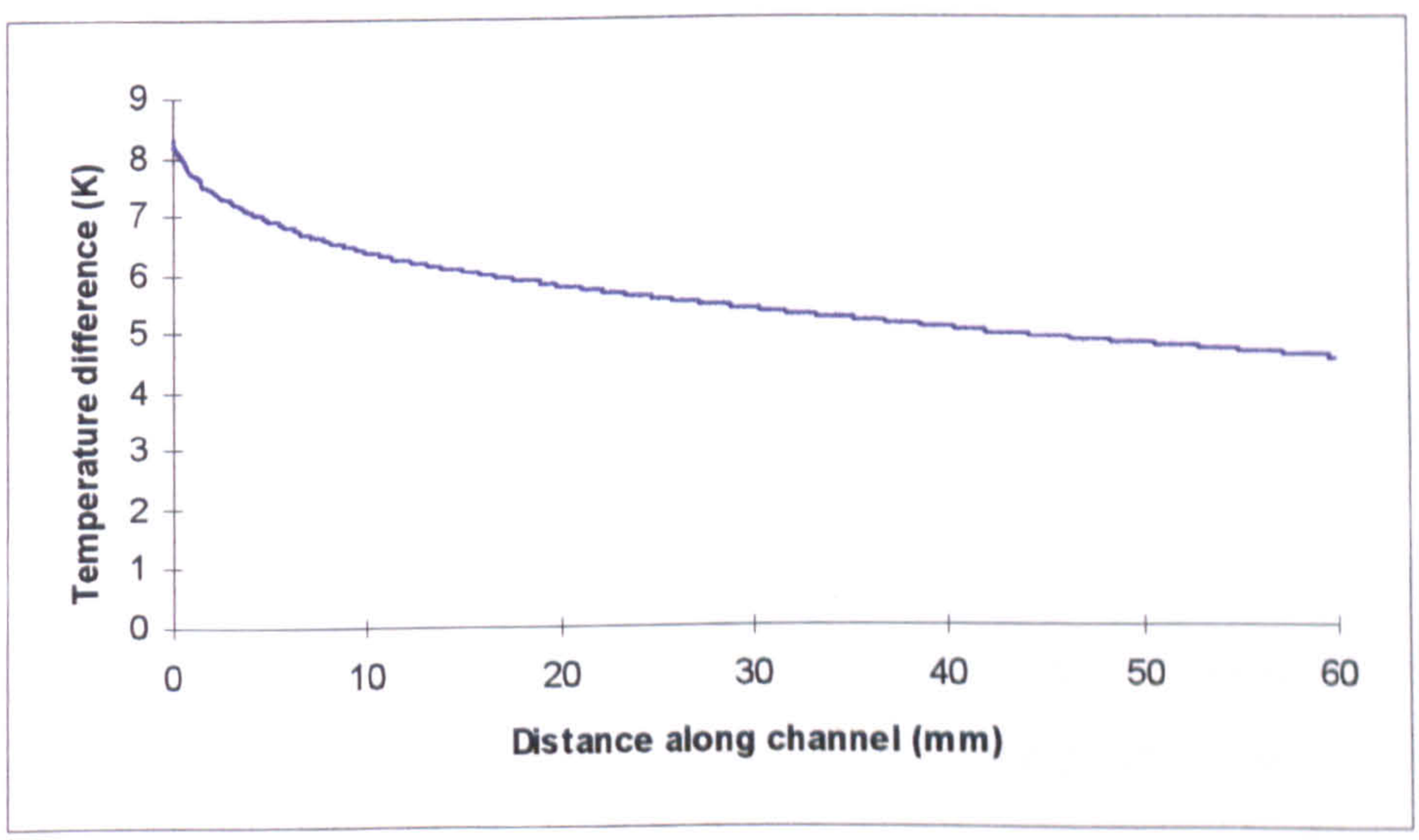

Figure 7.34: Level One variation of driving force temperature difference along a channel
(Y = 0.45 mm, v = 0.1334 m/s, T_H = 303.6 K, T_C = 295.2 K)

the temperatures of the wall and membrane calculated by the boundary layer model. This is to be expected as the thermocouples could only measure an average temperature. Trying to accurately measure the temperatures next to the wall and membrane surfaces is very difficult due to the small scales involved. The actual driving force of membrane distillation is the membrane interfacial temperatures. The trend of this temperature difference along the module is given in Figure 7.34. which shows the driving force temperature difference i.e. T_1-T_3. The entrance region is in the first 12.5 mm of the channel and causes a large initial drop in temperature difference. Over the entire channel the temperature difference from inlet to outlet is 3.74 °C, so although the entrance region has a large effect on the temperature difference, it is only over a short distance and is minimised due to the temperature of the liquid at the wall surfaces being equal to the bulk temperatures in the entrance region.. As the constant region is very long, the slow linear decrease in temperature difference eventually contributes greatly to the loss in driving force temperature difference. Looking at another set of experimental conditions on the temperature profiles, Figure 7.35 again shows the two regions of boundary layer growth. The experimental results lie within the outlet temperatures predicted by the model. Using the comparison of the Level One theoretical and experimental outlet temperatures, Figure 7.36 shows that the agreement is good.

Once the model had been shown to allow the determination of the temperature profiles in a flat plate module, a look at some of the variables involved was carried out. The liquid velocity and channel height both affect the temperature drop along the module, and the effects are shown in Figures 7.37 and 7.38 respectively. Figure 7.37 shows that as the velocity increased, the feed outlet temperature also increased. This is because the entrance region was longer due to the reduced rate of boundary layer growth, thereby decreasing the temperature drop along the channel. Once a velocity of around 0.5 m/s was reached for the conditions shown, increasing the velocity further did not really increase the outlet temperature. This was because the entrance region dominated the channel length i.e. the boundary layer only just filled the channel, and the wall temperature was the original bulk temperature. Looking at the effect of channel height on the average feed outlet temperature (Figure 7.38), increasing the channel height also increased

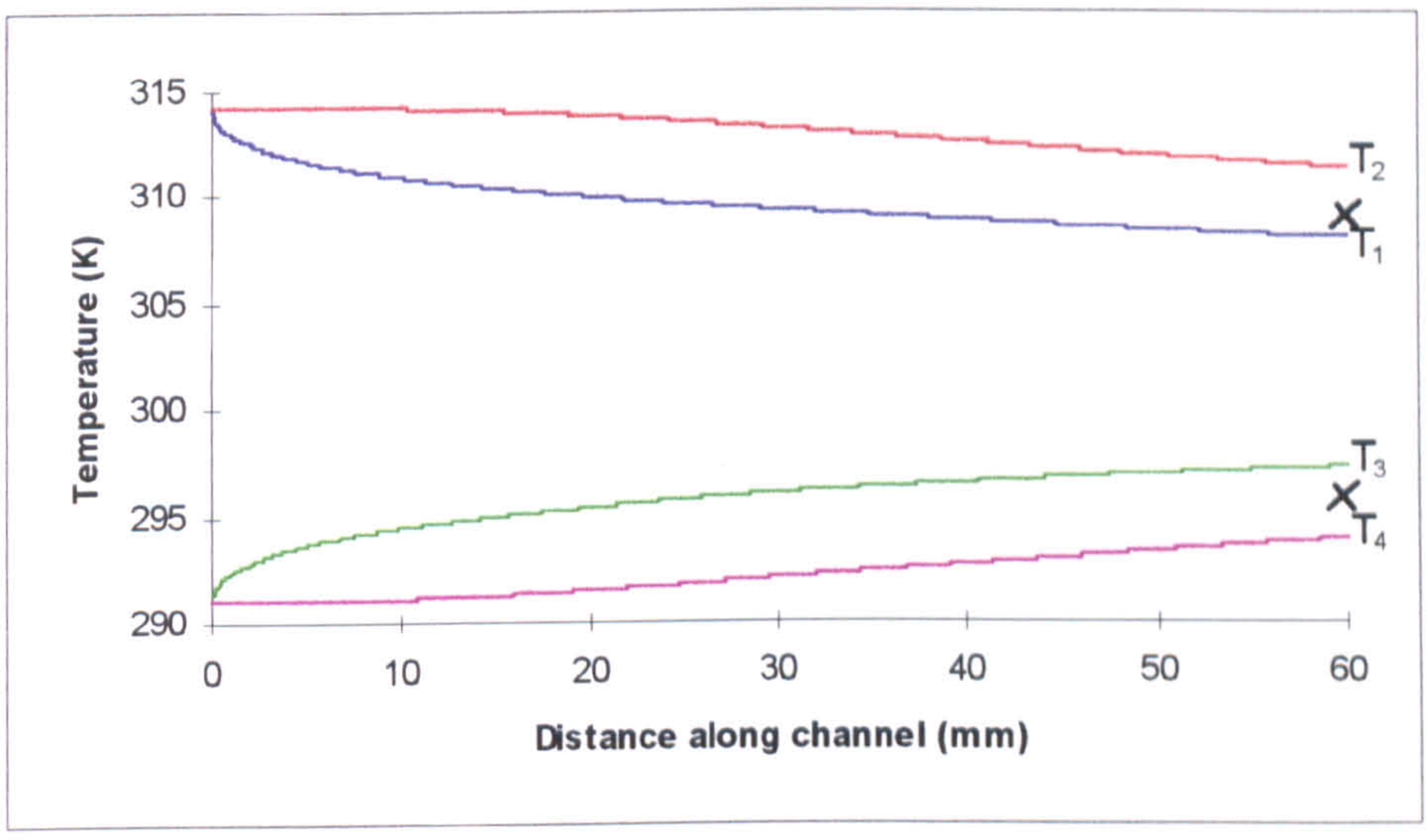

Figure 7.35: Level One full temperature profiles with experimental data
(Y = 0.45 mm, v = 0.0894 m/s, T_H = 314.2 K, T_C = 291.1 K)

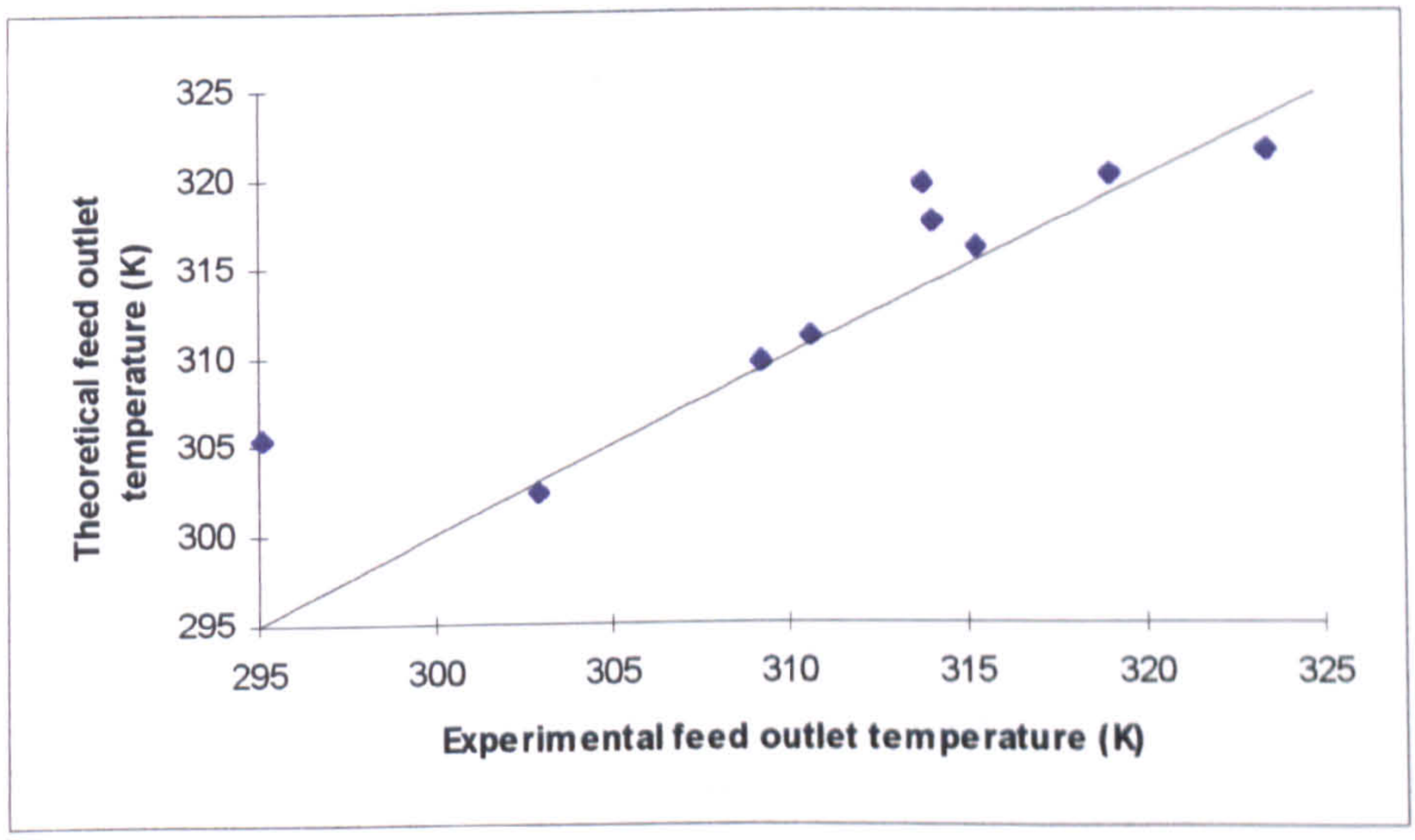

Figure 7.36: Level One comparison between theoretical model and experimental results

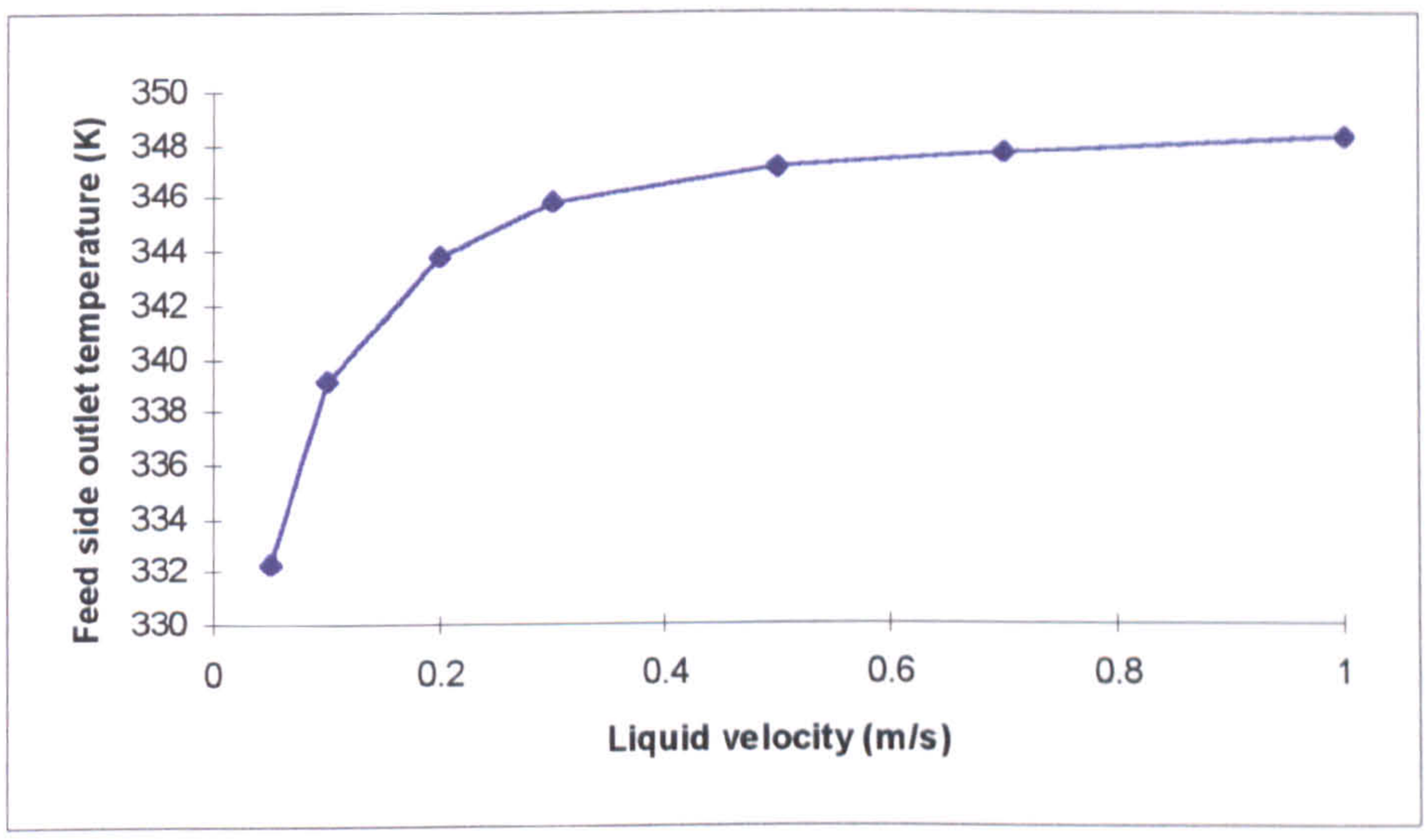

Figure 7.37: Level One effect of liquid velocity on the feed side outlet temperature ($Y = 0.45$ mm, $T_H = 353$ K, $T_C = 285$ K)

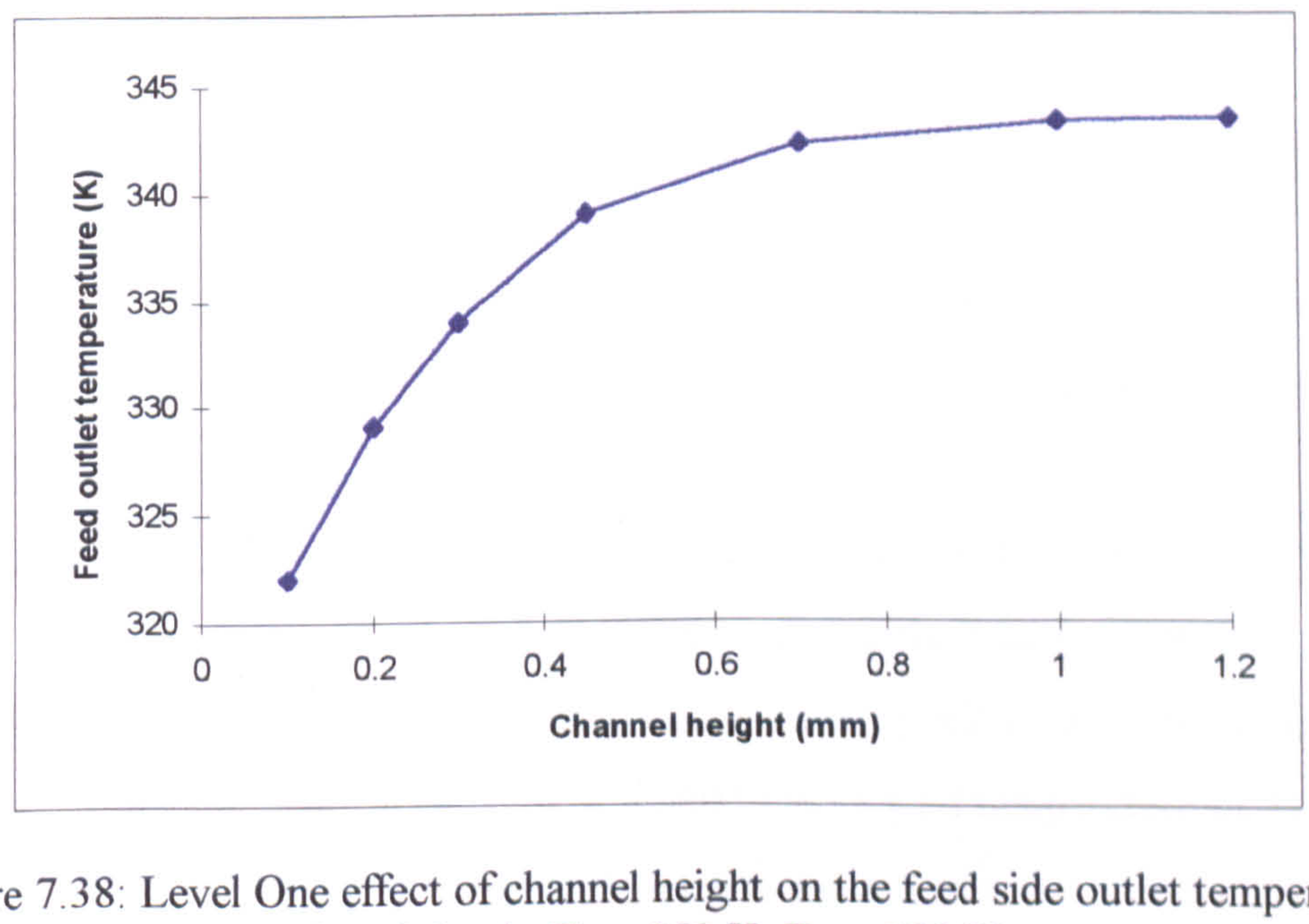

Figure 7.38: Level One effect of channel height on the feed side outlet temperature ($v = 0.1$ m/s, $T_H = 353$ K, $T_C = 285$ K)

the outlet temperature. This was due to the entrance region again being longer with the larger channel heights. Figure 7.39 looks at how increasing the channel height affects the distance taken for the boundary layer to fill the channel.

The work on the Level One model allowed the Fortran programme and a basic understanding of the boundary layer growth to be developed with a plug flow velocity profile. The next stage was to introduce a more realistic laminar flow velocity profile.

Level Two

The next stage utilised a laminar velocity distribution. Figure 7.40 shows the boundary layer development with Figure 7.41 being the related feed temperature profiles. Again, the two distinct areas of boundary layer growth can be seen. Figure 7.41 shows the fall in wall and membrane surface temperatures on the feed side of the module. There is a slight increase of T_2 when the constant region begins. This is because of the way in which the Fortran programme reacts when switching from the entrance to the constant region differential equations. This increase in temperature has only a minor effect on the final wall temperature.

Comparison of the full temperature profiles with experimental results is shown in Figure 7.42. Both the feed and permeate experimental points fall in-between the wall and membrane temperatures. Looking at the temperature difference for this run, Figure 7.43, the overall temperature drop over the entire channel is 3.68 °C. For the same initial conditions, the Level One temperature drop was 3.74 °C. The difference is caused only by the change in assumed velocity profile. Figures 7.40 to 7.43 utilised the same operating conditions as for Figures 7.33 and 7.34.

As the change between Level One and Two is the velocity profile, Figure 7.44 is a comparison of the growth rate of the boundary layer utilising the two profiles. As it can be seen the laminar boundary layer fills the channel much quicker than the plug flow boundary layer. For example, for a velocity of 0.0894 m/s, a feed temperature of 41.2 °C and a permeate temperature of 18.1 °C, the difference is about 5 mm.

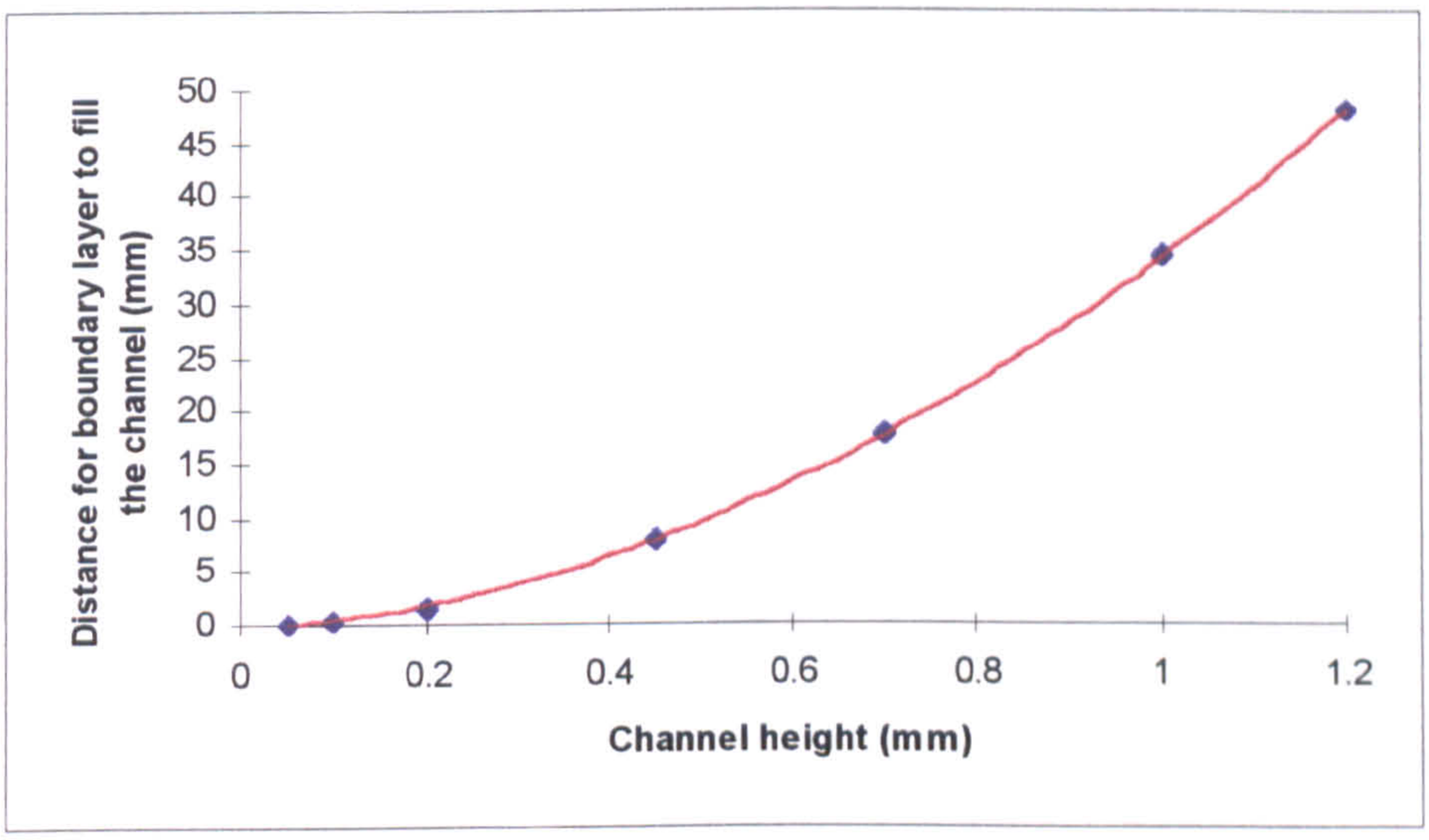

Figure 7.39: Level One effect of channel height on the distance taken by the boundary layer to fill the channel ($v = 0.1$ m/s, $T_H = 353$ K, $T_C = 285$ K)

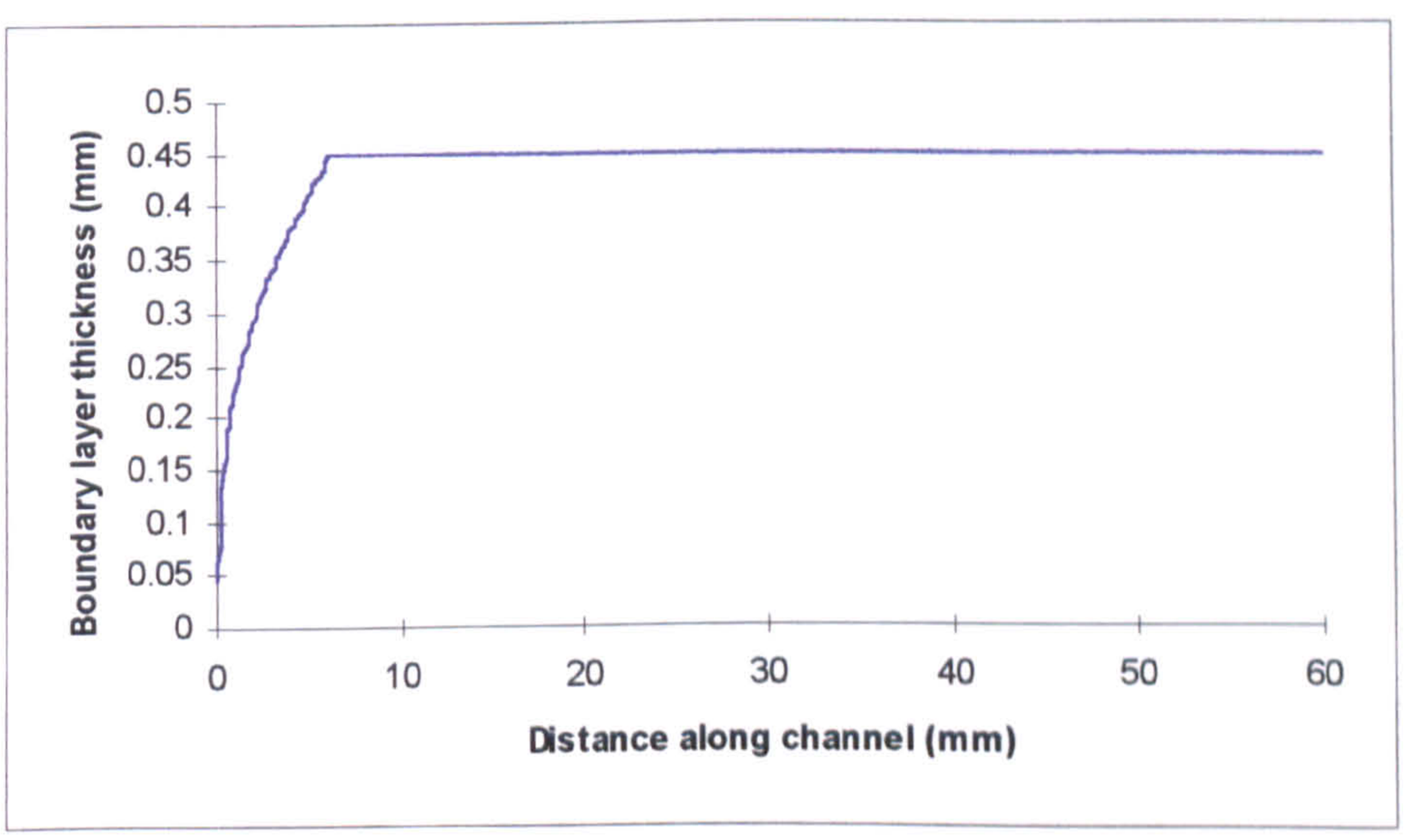

Figure 7.40: Level Two thermal boundary layer development
($Y = 0.45$ mm, $v = 0.1334$ m/s, $T_H = 303.6$ K, $T_C = 295.2$ K)

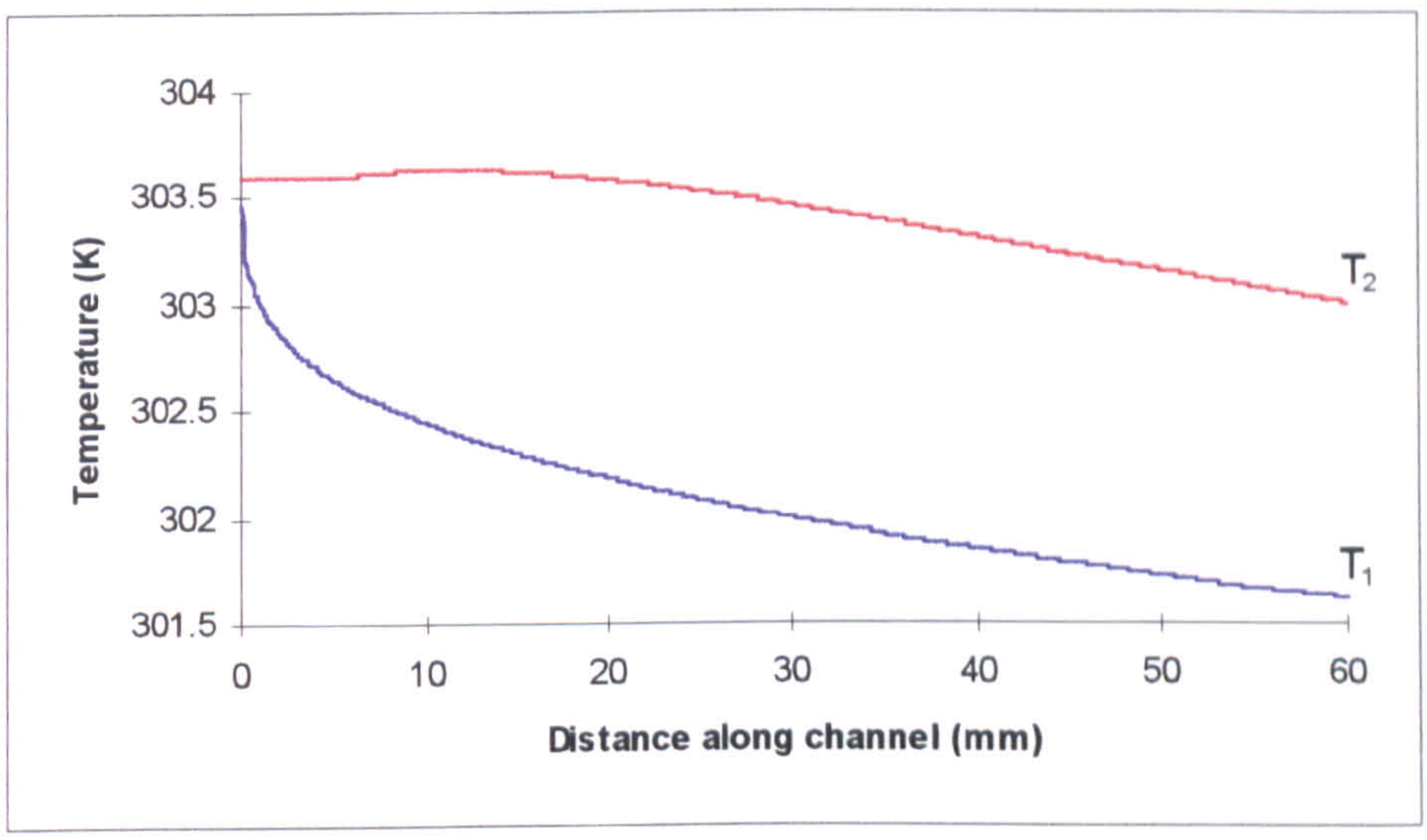

Figure 7.41: Level Two feed side temperature profiles
(Y = 0.45 mm, v = 0.1334 m/s, T_H = 303.6 K, T_C = 295.2 K)

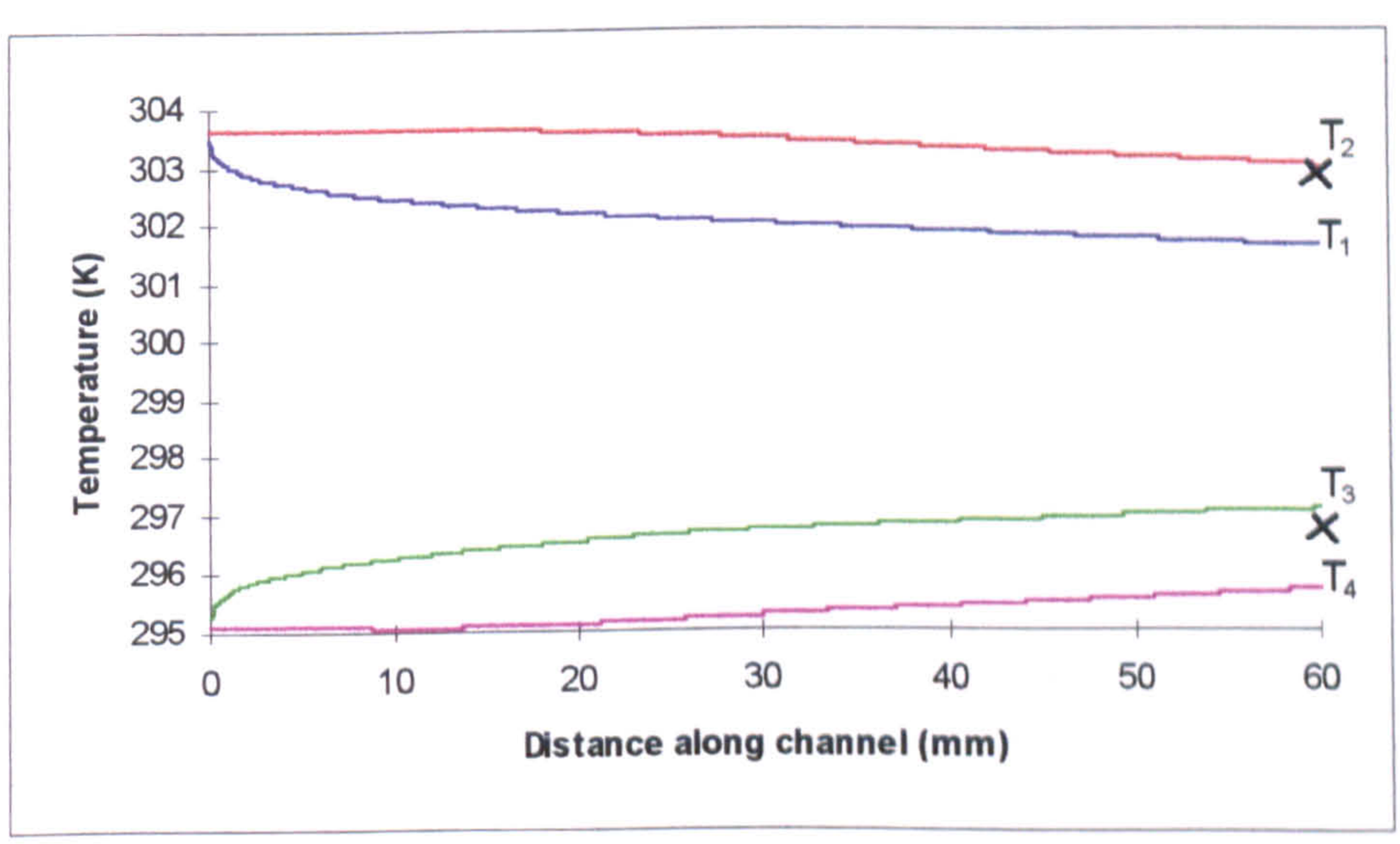

Figure 7.42: Level Two full temperature profiles with experimental data
(Y = 0.45 mm, v = 0.1334 m/s, T_H = 303.6 K, T_C = 295.1 K)

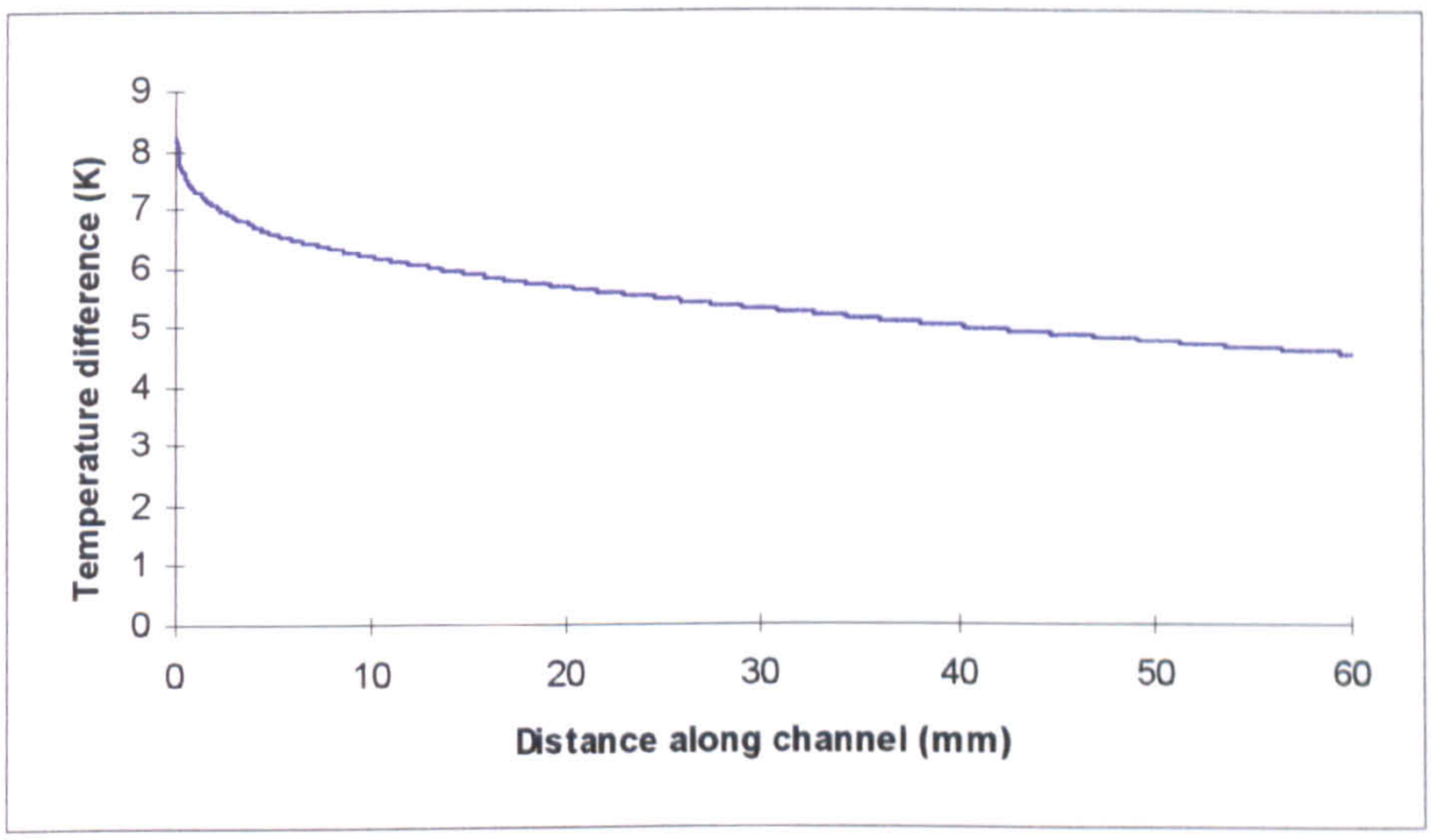

Figure 7.43: Level Two variation of driving force temperature difference along a channel
(Y = 0. 45 mm, v = 0.1334 m/s, T_H = 303.6 K, T_C = 295.1 K)

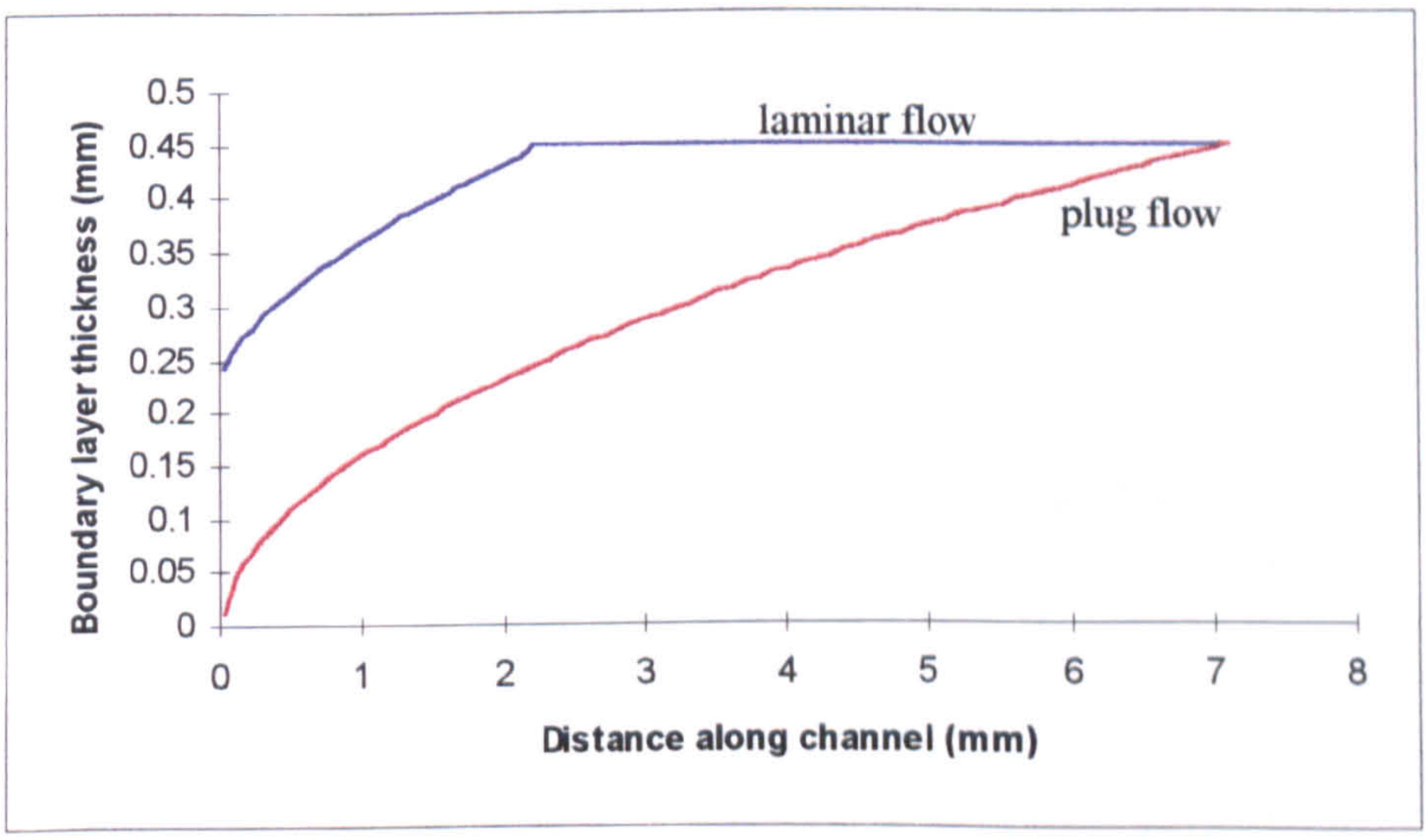

Figure 7.44: Effect of velocity profile on boundary layer growth
(Y = 0.45 mm, v = 0.0894 m/s, T_H = 314.2 K, T_C = 291.1 K)

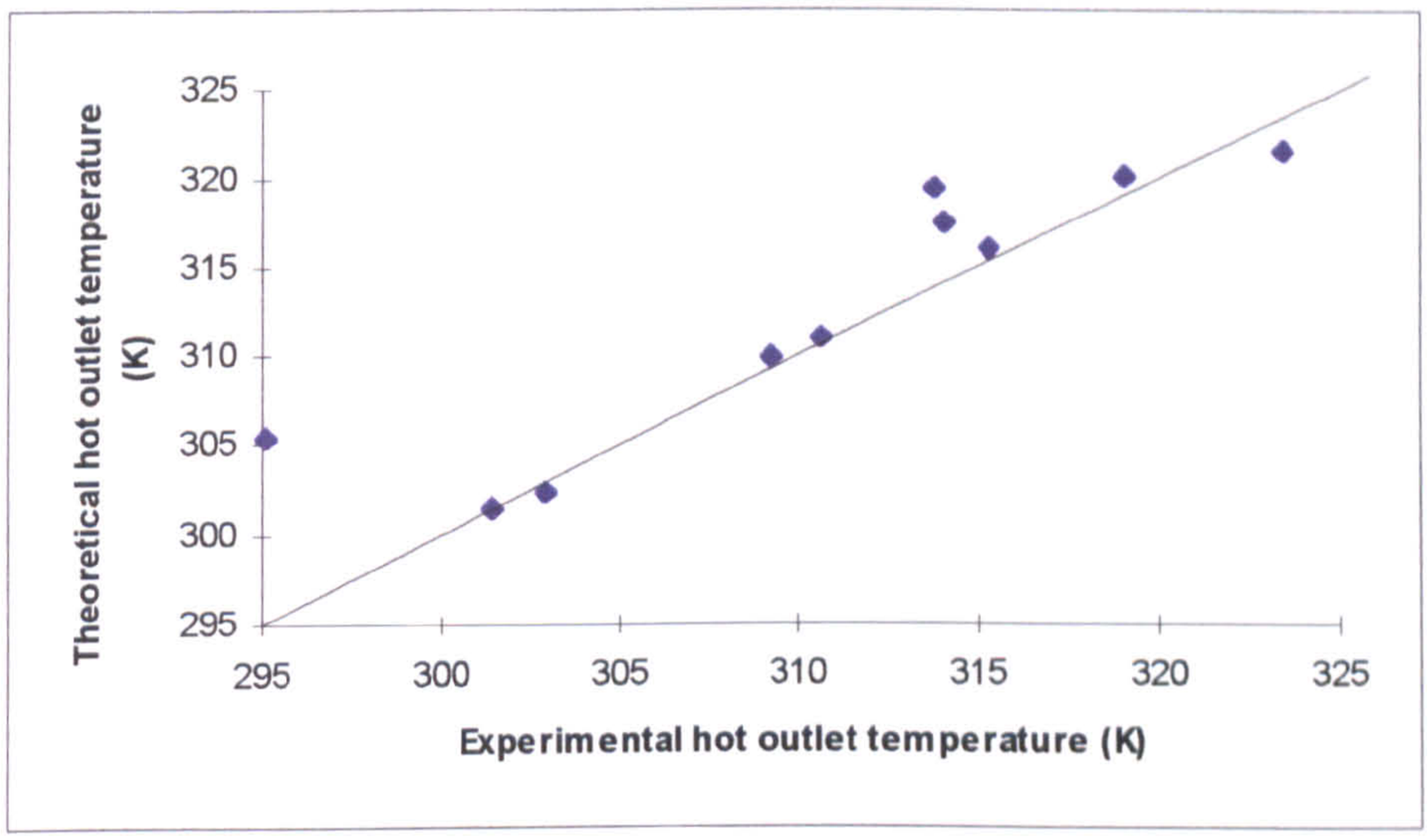

Figure 7.45: Level Two comparison between the theoretical model and experimental results

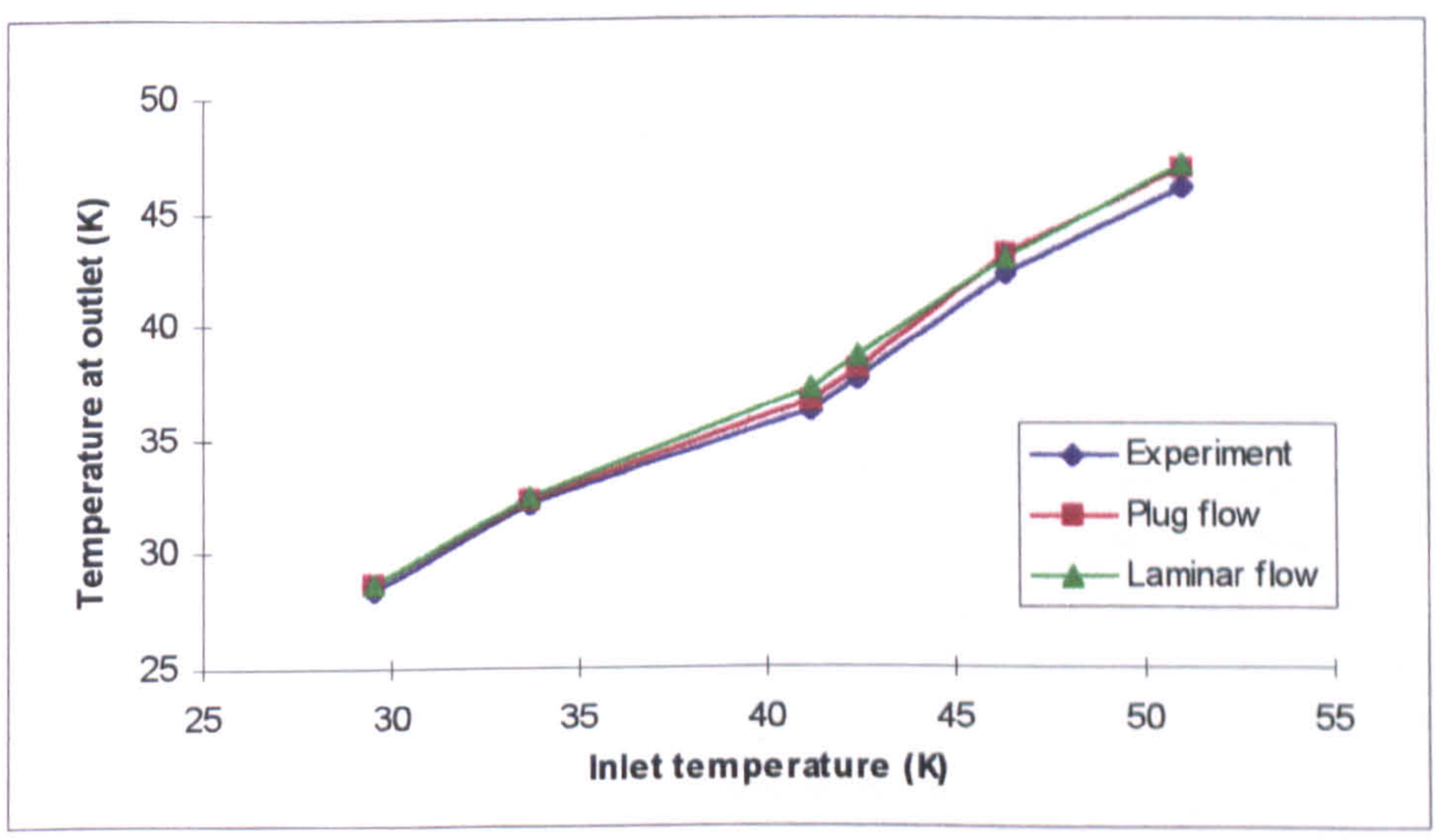

Figure 7.46: Comparison between inlet to outlet channel temperatures, for plug, laminar and experimental velocity profiles

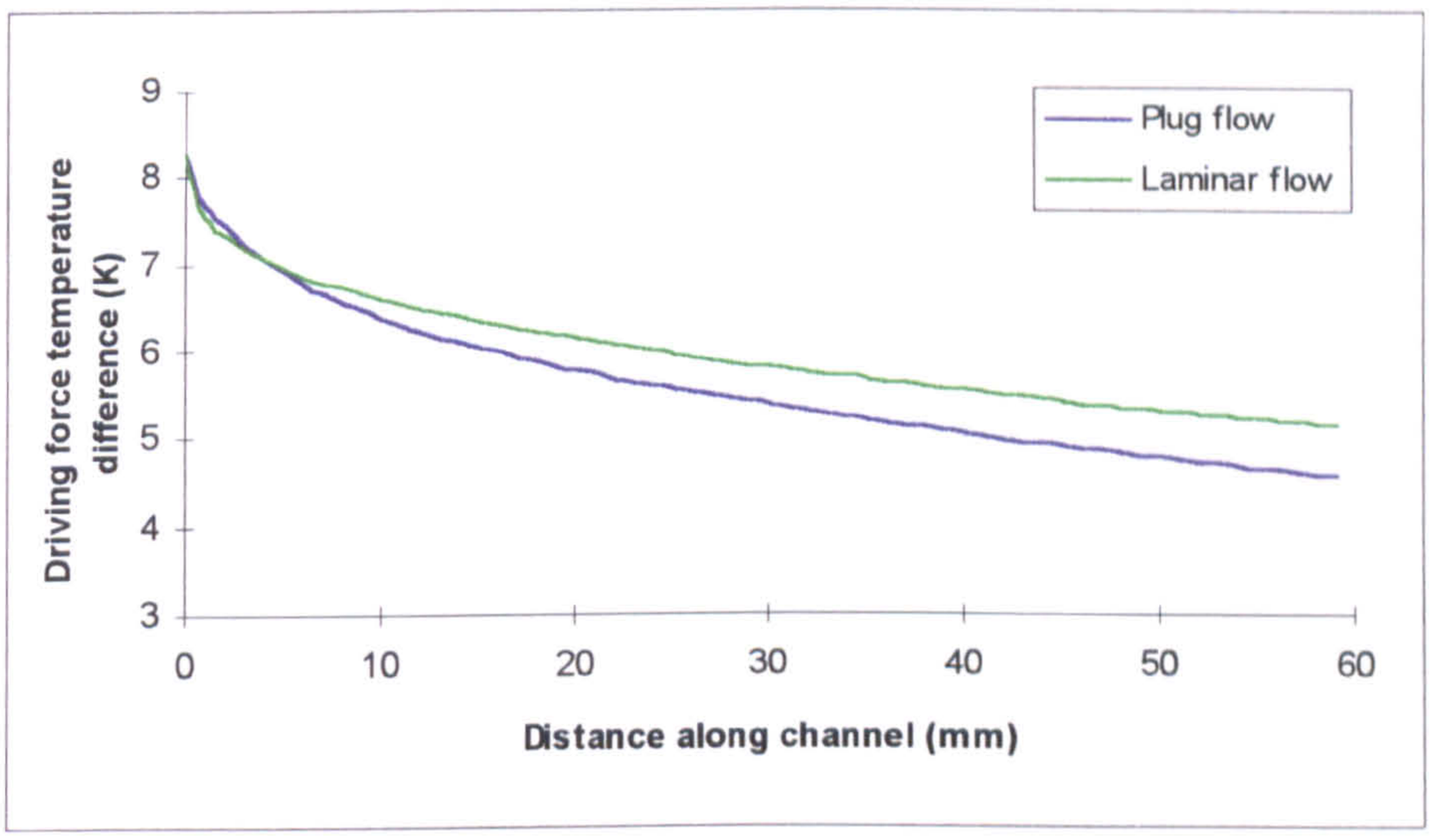

Figure 7.46a: Comparison of plug and laminar veloicty profiles on the driving force temperature difference

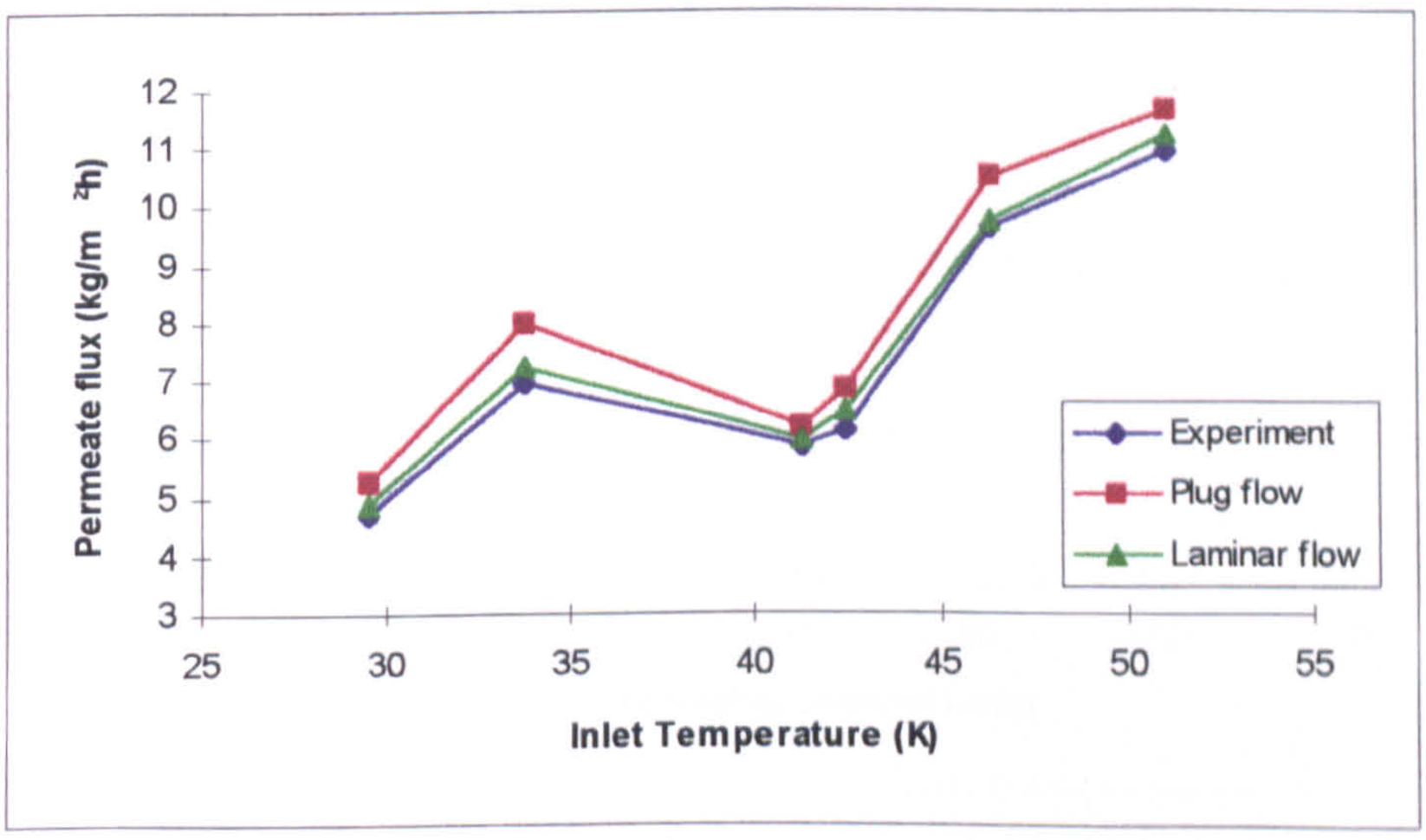

Figure 7.46b: Comparison of the permeate flux obtained using plug flow and laminar velocity profiles with experimental values

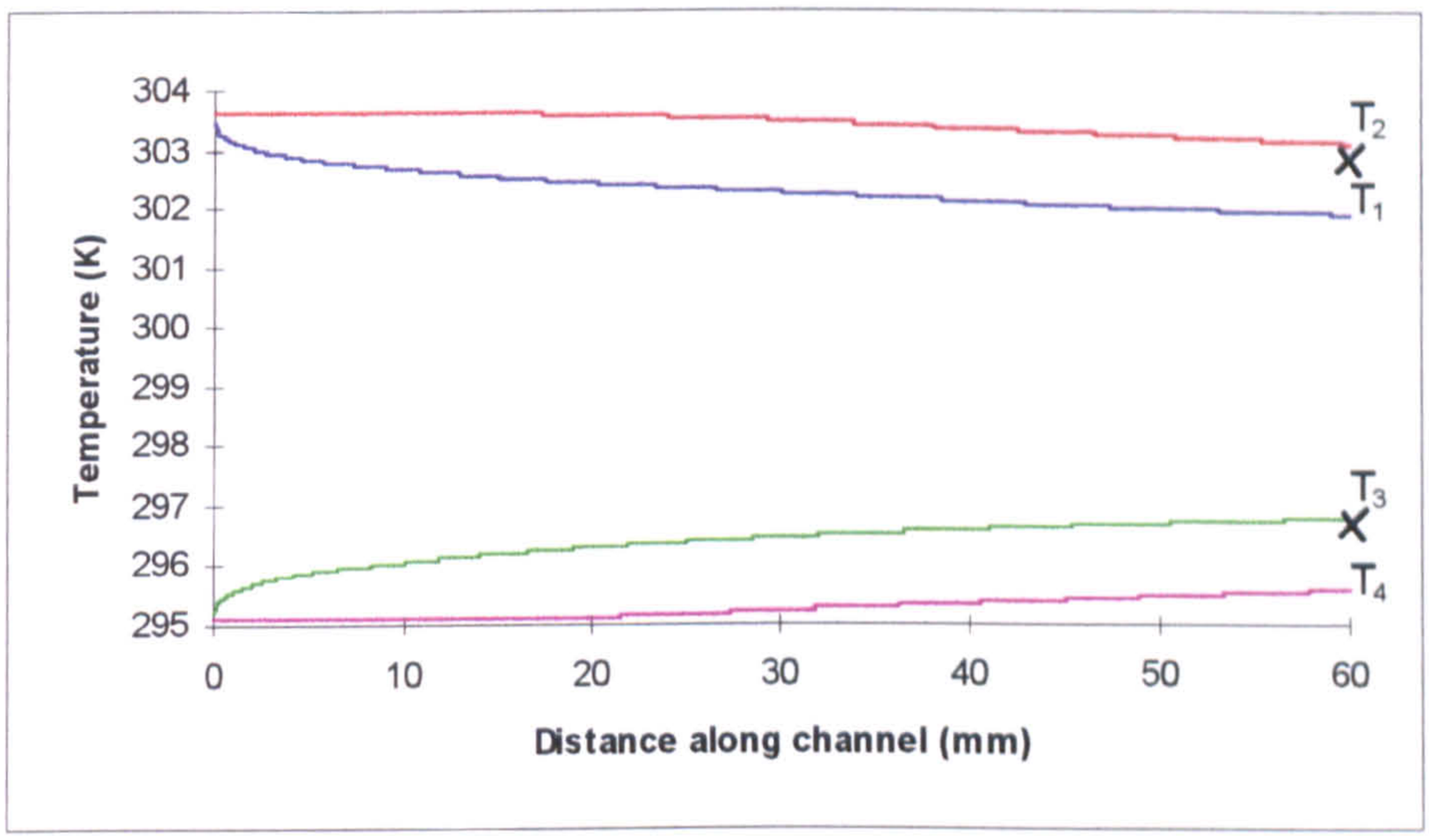

Figure 7.47: Level Three full temperature profiles with experimental data (Y = 0.45 mm, v = 0.1334 m/s, T_H = 303.6 K, T_C = 295.1 K)

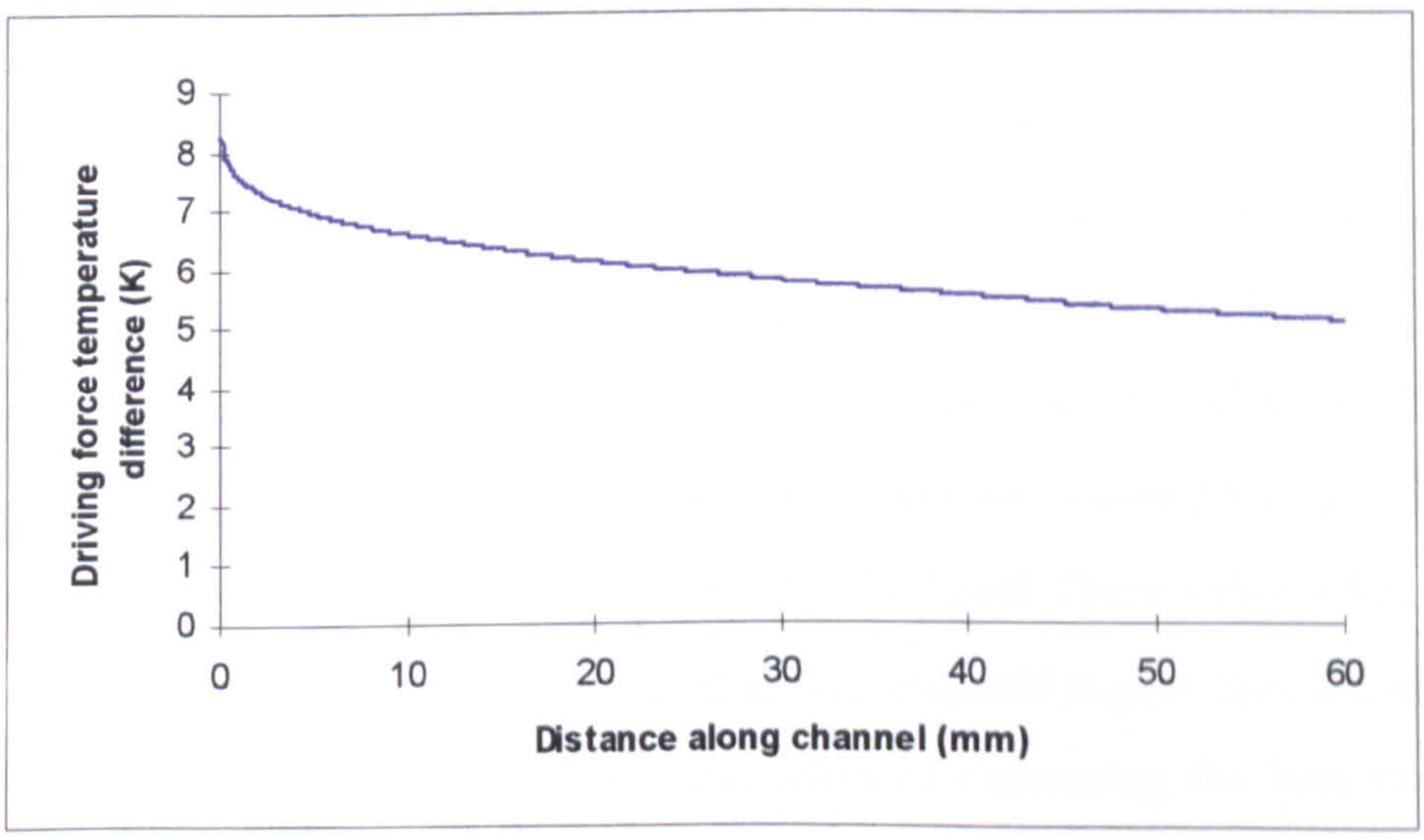

Figure 7.48: Level Three variation of driving force temperature difference along a channel (Y = 0. 45 mm, v = 0.1334 m/s, T_H = 303.6 K, T_C = 295.1 K)

Comparing the Level Two model and experimental results, Figure 7.45 shows good agreement between the theoretical and experimental outlet temperatures. All of the points are within 1.5% of the direct correlation line.

Figure 7.46 then compares the outlet temperatures obtained experimentally with the Level One and Level Two models using the inlet temperature as the basis. As can be seen, the models show good agreement with the trend of the experimental results. Figure 7.46a shows the difference of driving force temperature difference along a channel with the two velocity profiles. The laminar temperature profile maintains a higher temperature difference than the plug flow profile. Going one step further, Figure 7.46b shows the flux relationship. Again, both velocity profiles show good agreement with experimental results. The laminar flow assumption however, more closely represents the experimental values.

Level Three

The next stage of the work was to extend the Level Two model to take into account different velocities and channel dimensions either side of the membrane (Level Three). As the basis of the programme was essentially the same, similar graphs to Level Two were obtained for symmetrical situations. A more accurate method of obtaining E, the membrane transfer coefficient was used for this level. To document the effect of this more accurate calculation of E, Figures 7.47 and 7.48 give the full temperature profiles and driving force temperature difference along the channel for the same conditions as for Figures 7.42 and 7.43. The temperature drop along the channel is 3.13 °C which is less than for the Level Two value of 3.68 °C. The difference between Level Three and Level Two for this set of experimental conditions is 0.55 °C. The Level Three value is less than the Level Two value because the Level Two E value was assumed higher than the actual, calculated value. The accurate value of E had the effect of decreasing the heat transfer across the membrane causing a lower temperature drop on the feed side and temperature rise on the permeate side. Overall, although calculating a more accurate membrane transfer coefficient leads to a more accurate model, the values of E assumed in the previous levels were close to the calculated values. This means that the comparison

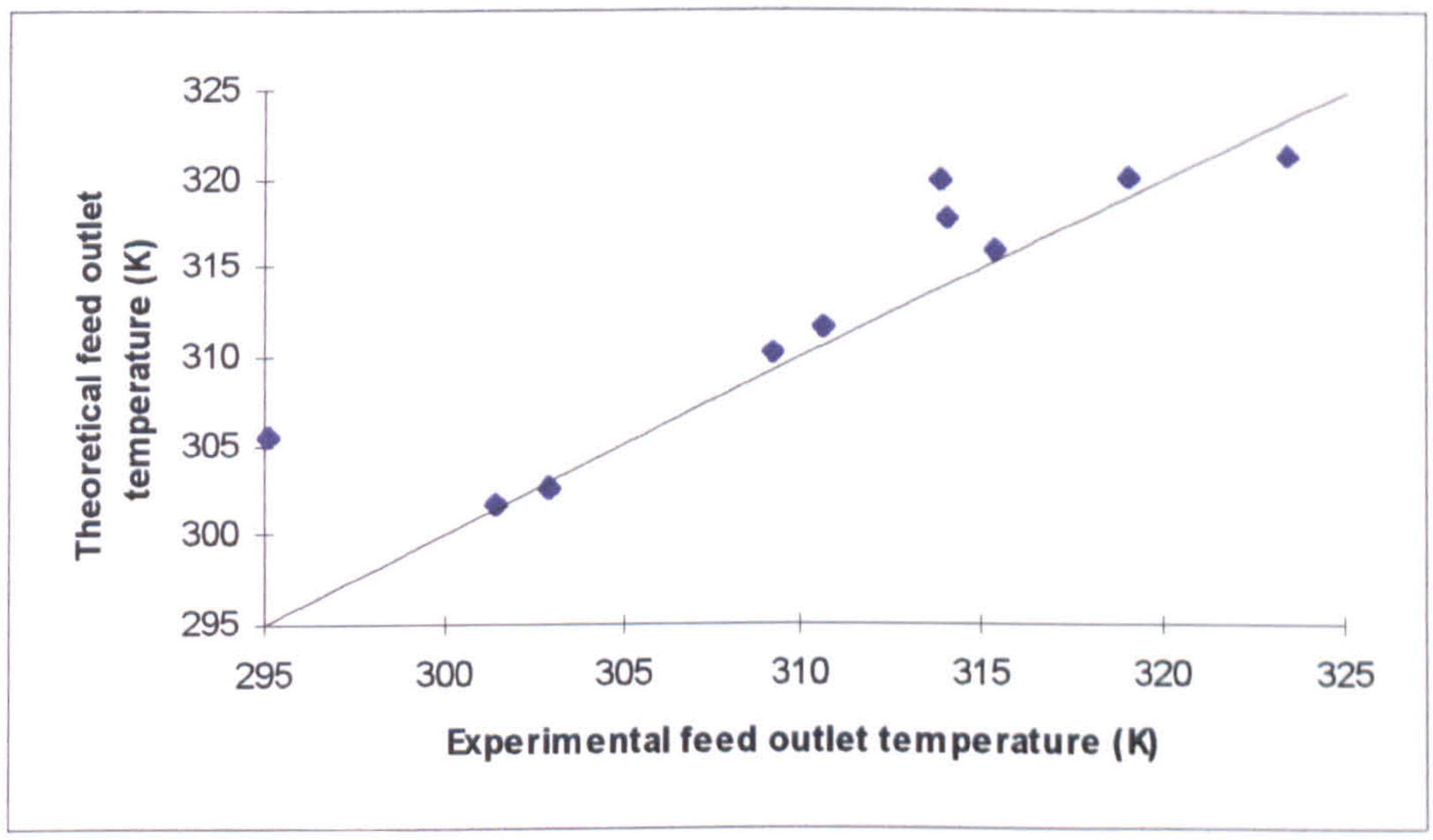

Figure 7.49: Level Three comparison between the theoretical model and experimental results

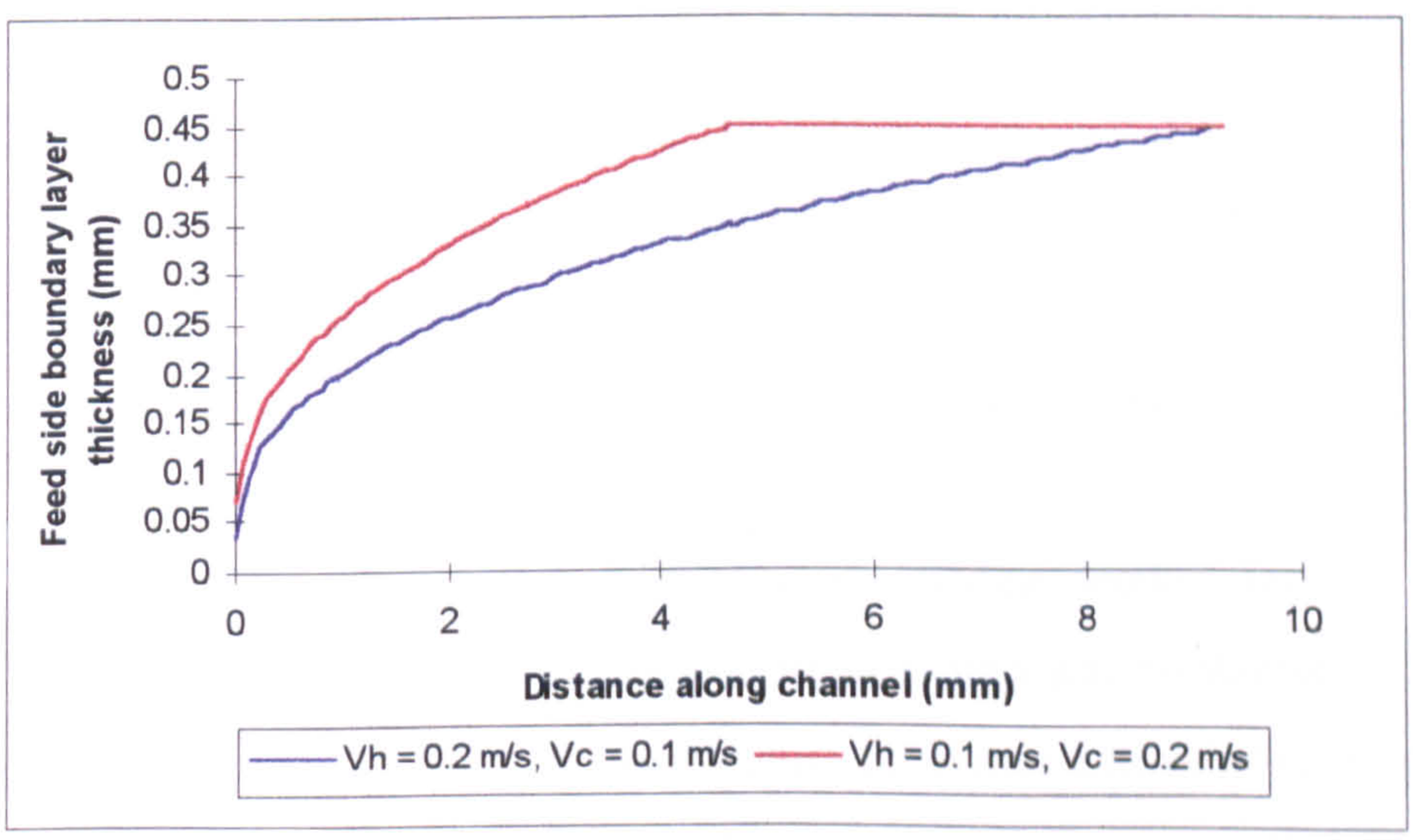

Figure 7.50: Level Three effect of liquid velocities either side of the membrane on the boundary layer growth (T_H = 333K, T_C = 290 K)

between theoretical and experimental results shown in Figure 7.49 is very similar to Figure 7.45, and there is still good agreement.

Non-symmetrical conditions can be investigated using the Level Three model. Figure 7.50 introduces non-symmetrical velocities either side of the membrane and compares the boundary layer growth where the feed side has a higher velocity than the permeate, and where the permeate has a higher velocity than the feed. This figure only shows the effect of velocity on the feed side boundary layer. Having a higher velocity on the feed side makes the feed side boundary layer grow quicker to fill the channel height, than when the permeate has a higher velocity. Figure 7.51 gives the full temperature profiles for a module having a feed velocity greater than the permeate velocity. In this case the feed velocity is higher than the permeate velocity. This has the effect of increasing the length of the entrance region on the feed side. The permeate entrance length occupies 4.31 mm of the channel, whereas the feed entrance region occupies 6.37 mm. The experimental points show the accuracy of this more complete model. Figure 7.52 shows the effect of non-symmetrical velocities on the driving force temperature difference compared to equal velocities either side of the membrane of 0.0894 and 0.1334 m/s. The temperature difference profile for the non-symmetrical velocities lies between the profiles for the symmetrical velocities. Figure 7.53 shows the full temperature profiles for the opposite non-symmetrical situation as for Figure 7.51, i.e. the permeate velocity is higher than the feed velocity. The feed side profiles react in the wrong manner when switching from the entrance region equations to the constant region equations. After trying various methods to amend this problem, it was concluded that a further development of the temperature profile in the theory would be required.

All the work carried out on the boundary layer analysis models showed that accurate representation of the temperatures was obtained. The next step was to introduce more extreme conditions such as large membrane temperature difference and velocity, to study the limits of using flat channels for membrane distillation.

The feed side temperature was taken as 70°C with the permeate temperature of 15°C. The first graph, Figure 7.54 utilised a velocity of 0.1 m/s to study the boundary layer growth, with the temperature difference profile along the channel shown in Figure 7.55.

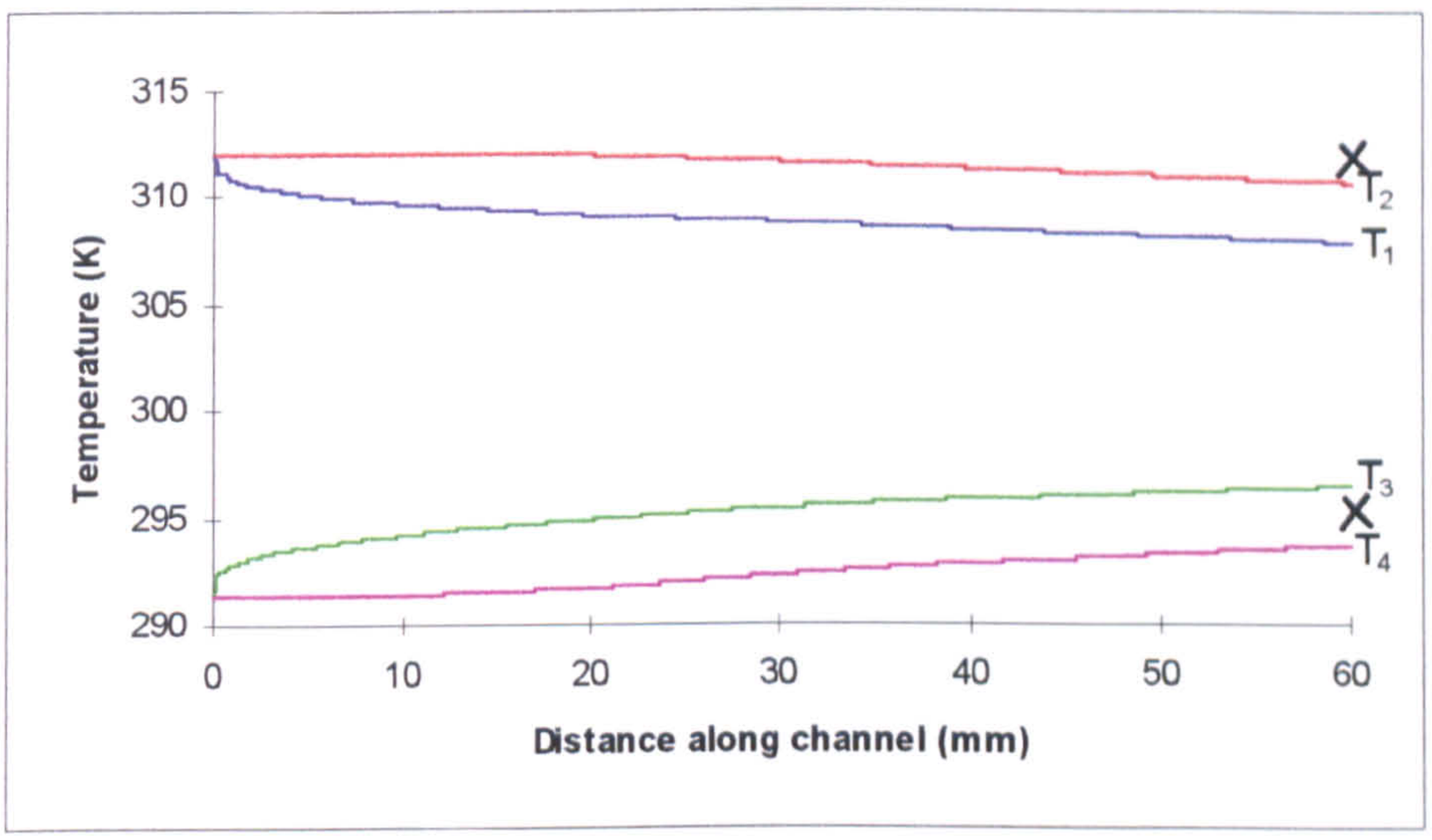

Figure 7.51: Level Three full temperature profiles with experimental data (Y = 0.45 mm, v_H = 0.1334 m/s, v_C = 0.0894 m/s, T_H = 312 K, T_C = 291.4 K)

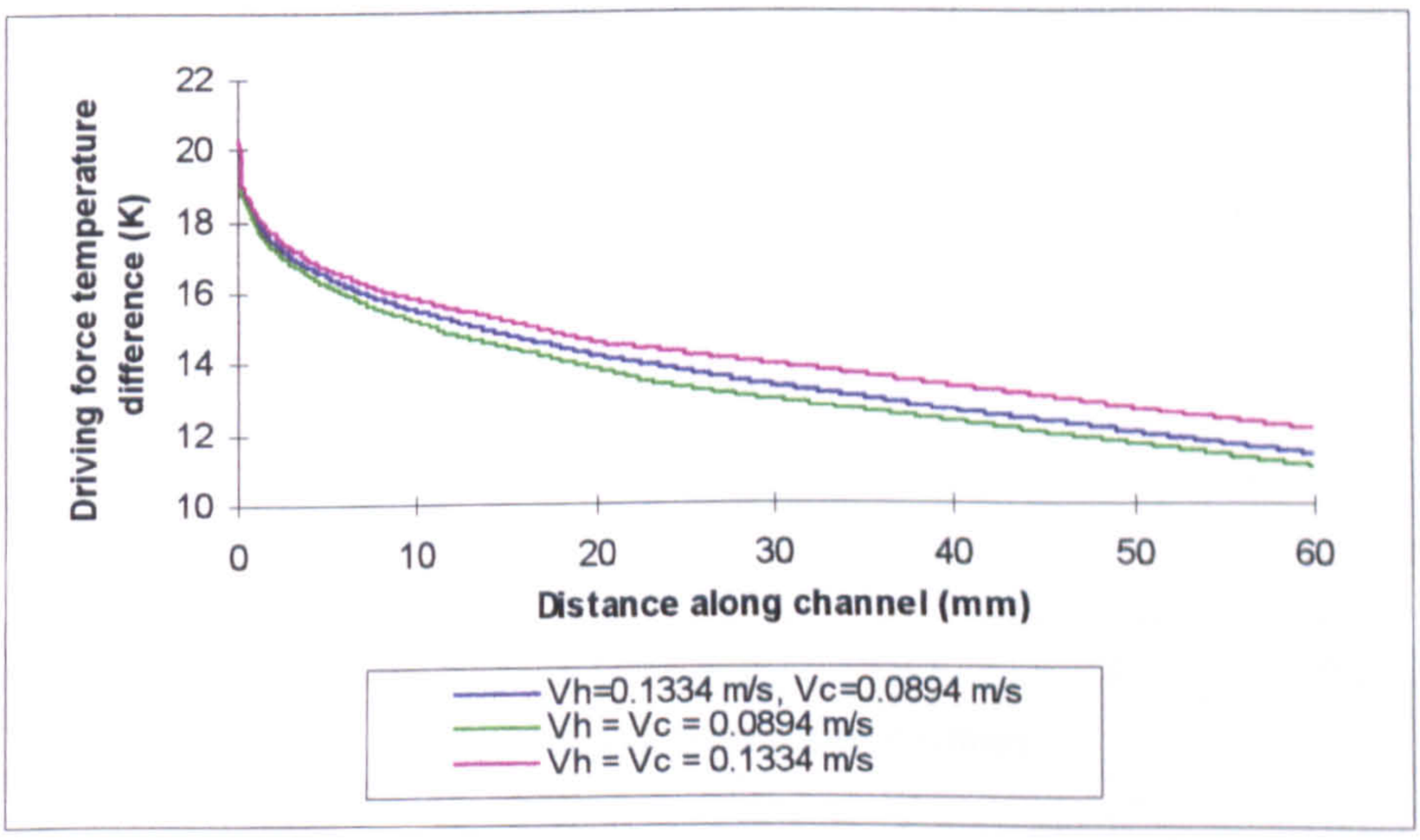

Figure 7.52: Level Three variation of driving force temperature difference along a channel (Y = 0.45 mm, v_H = 0.1334 m/s, v_C = 0.0894 m/s, T_H = 312 K, T_C = 291.4 K)

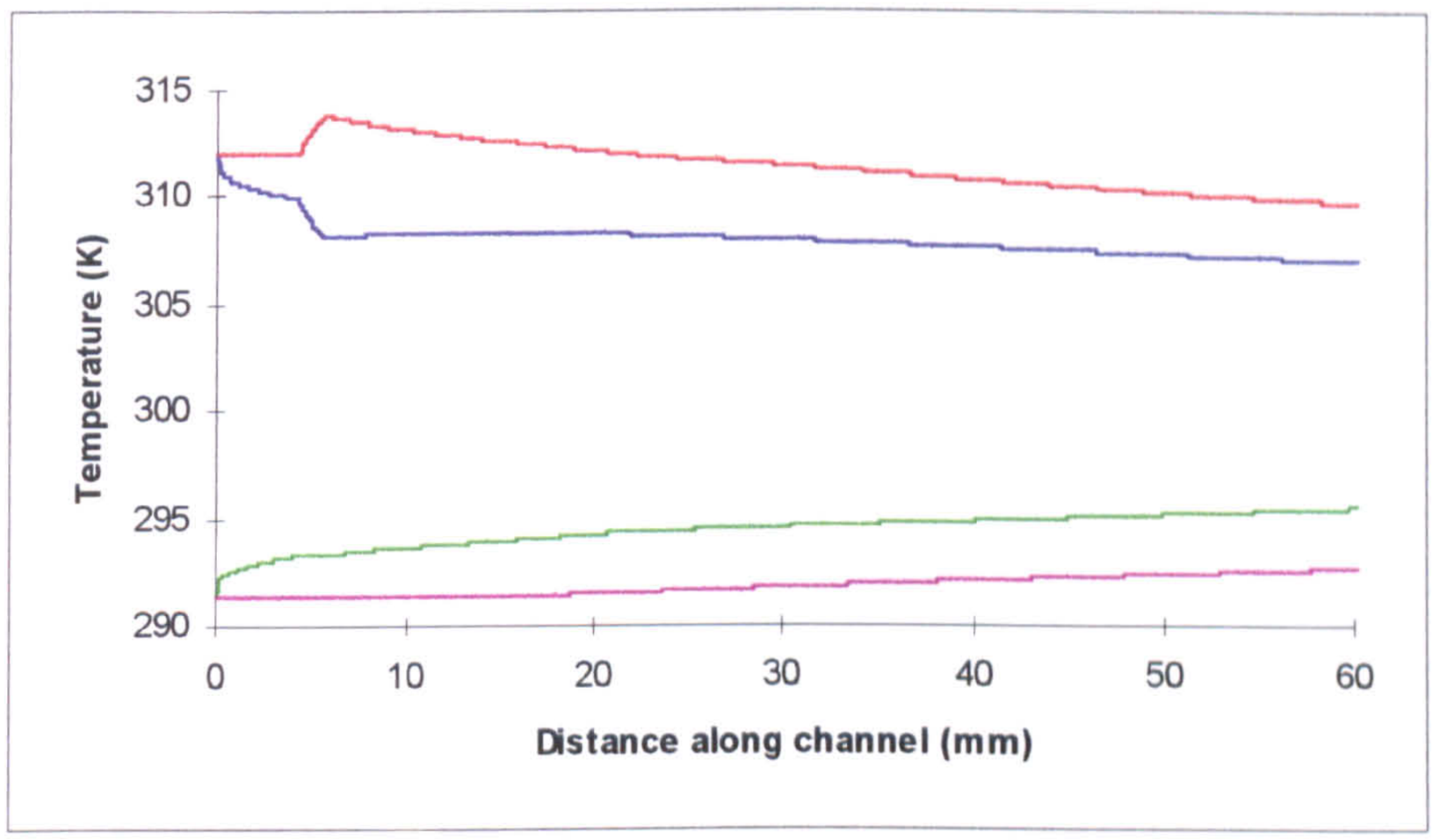

Figure 7.53: Level Three full temperature profiles with experimental data
($Y = 0.45$ mm, $v_H = 0.0894$ m/s, $v_C = 0.1334$ m/s, $T_H = 312$ K, $T_C = 291.4$ K)

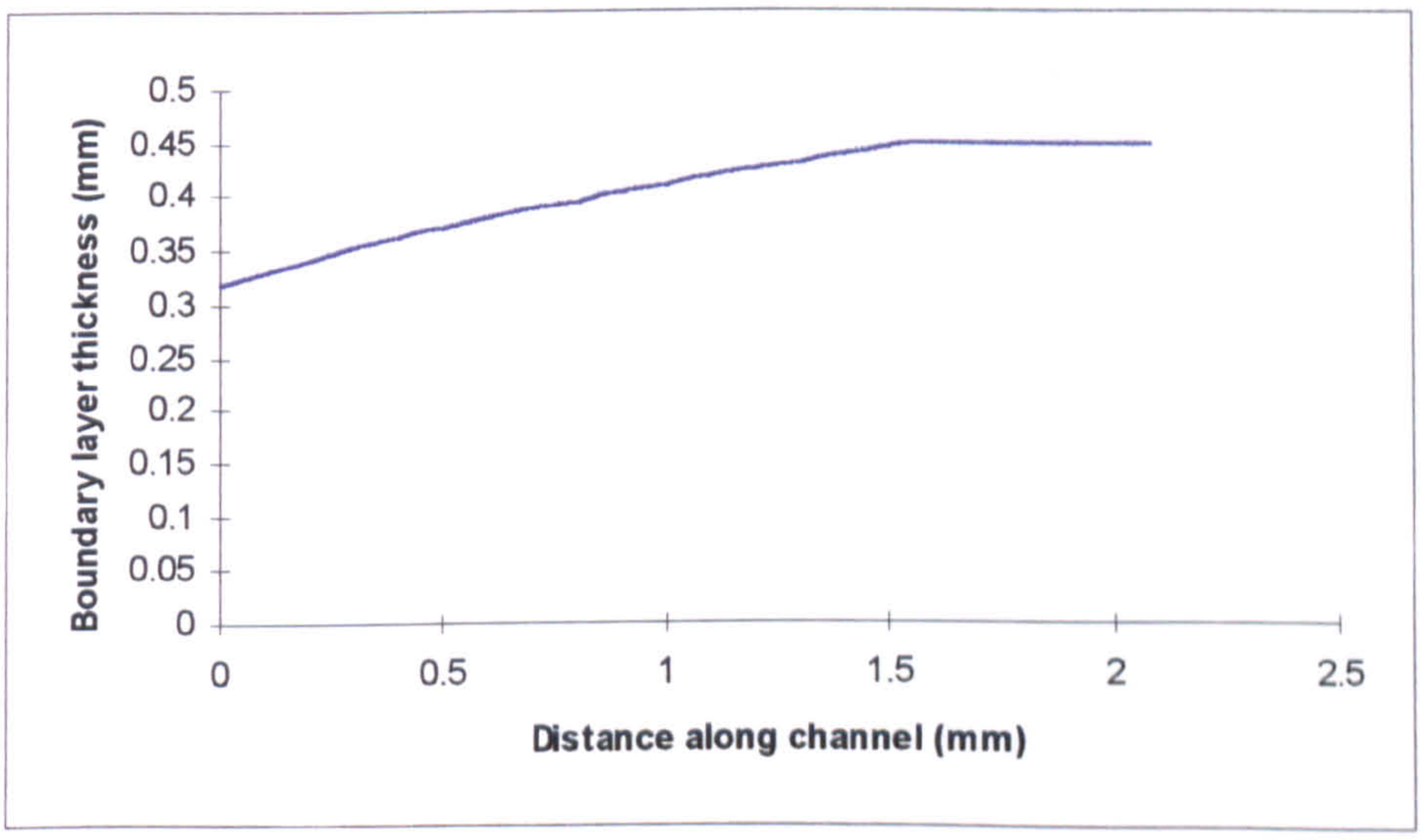

Figure 7.54: Level Three boundary layer profile along a channel
($Y = 0.45$ mm, $v_H = 0.1$ m/s, $v_C = 0.1$ m/s, $T_H = 353$ K, $T_C = 285$ K)

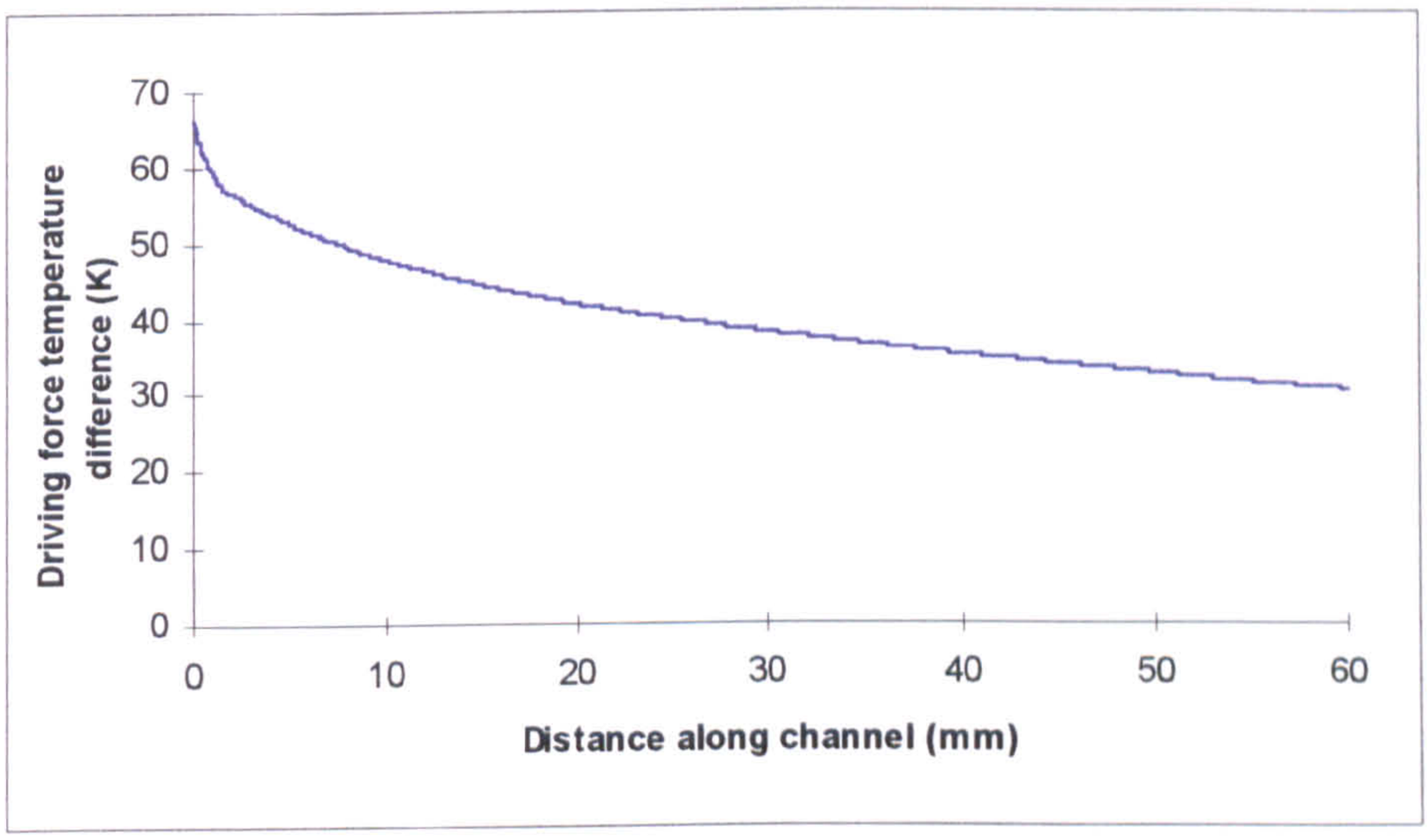

Figure 7.55: Level Three variation of driving force temperature difference along a channel (Y = 0.45mm, v_H = 0.1 m/s, v_C = 0.1 m/s, T_H = 353 K, T_C = 285 K)

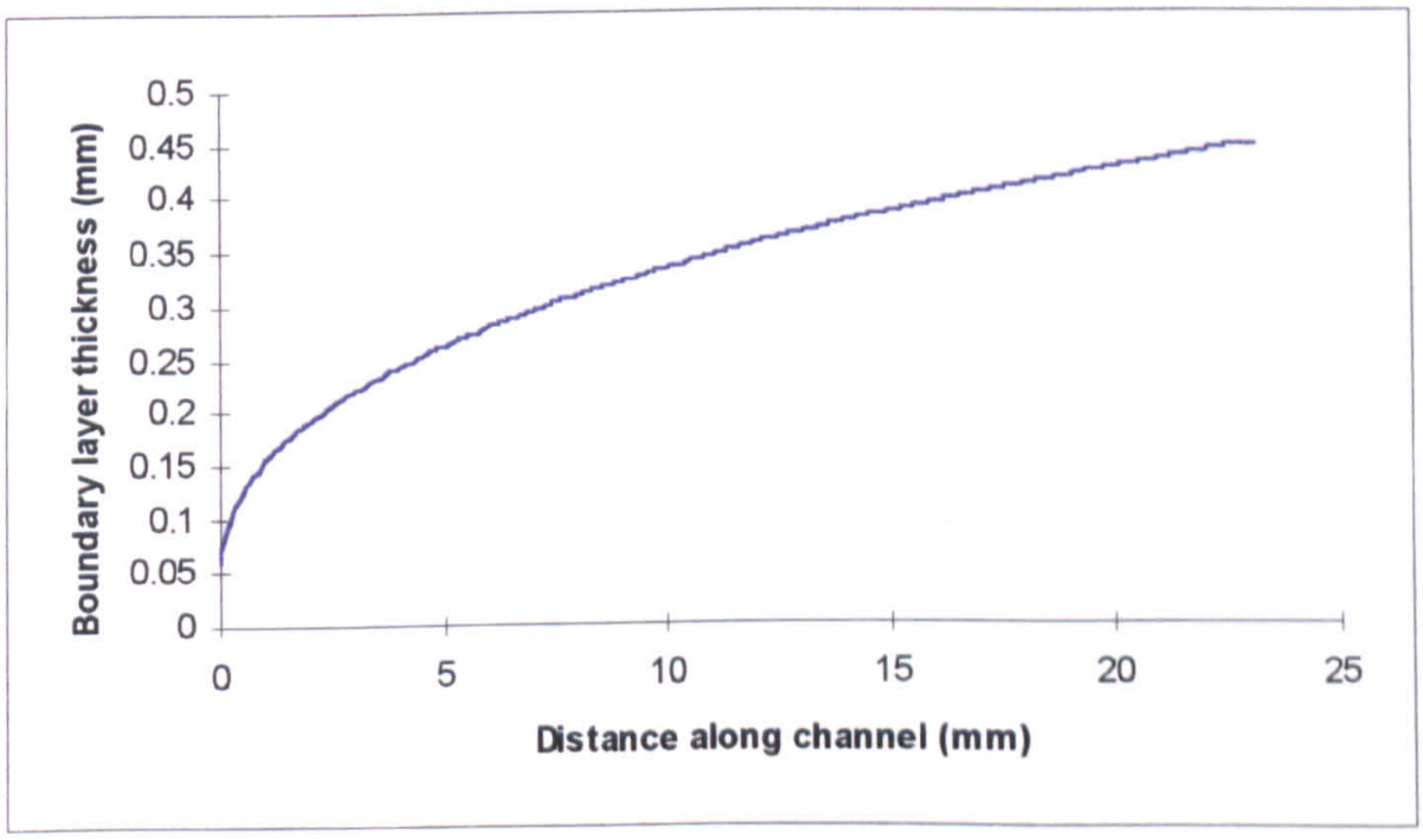

Figure 7.56: Level Three boundary layer profile along a channel (Y = 0.45 mm, v_H = 1 m/s, v_C = 1 m/s, T_H = 353 K, T_C = 285 K)

Figure 7.54 shows that at very high feed temperatures the entrance region is very short, about 1.6 mm. This means that the driving force temperature difference, Figure 7.55, is controlled much more by the constant region causing a much greater temperature drop from inlet to outlet. For instance, for the conditions specified in Figure 7.55, the temperature drop is 35.35 °C.

Figures 7.56 and 7.57 are for the same extreme temperatures, but for a velocity of 1 m/s. They show a much slower growth of boundary layer than for Figure 7.53 due to the higher velocity. This translates to a much lower temperature drop as shown in Figure 7.57 which is 20.11 °C. This shows that increasing the length of the entrance region decreases the loss of the driving force temperature difference. This must be the objective when designing flat plate modules for membrane distillation. The results of using the same extreme conditions, but varying the liquid velocities are shown in Figure 7.58. This shows that increasing the velocity increases the feed outlet temperature. Once high velocities of around 0.6 m/s are reached, the increase in outlet temperature is negligible. This is due to the entrance region dominating the channel length, creating a lower temperature drop along the channel.

Figure 7.59 shows the effect of the channel height on the outlet temperature of the feed. As the channel height is increased, the outlet temperature increases. Again this is due to the growth rate of the boundary layer causing the entrance region to be dominant. The distance for the boundary layer to reach the channel wall is shown in Figure 7.60 where the larger the channel height, the longer it takes for the boundary layer to grow to fill the channel. The final outlet temperature relies on the liquid velocity and channel height as well as the temperature difference between the feed and permeate.

Linked Model

The boundary layer analysis model only produced data on the thermal boundary layer profiles and temperatures through a flat plate module. To study the process of membrane distillation through the module, the boundary layer model was linked to the membrane distillation model. The temperatures calculated in the boundary layer model were used in the membrane distillation model to calculate the permeate flux obtained along the channel.

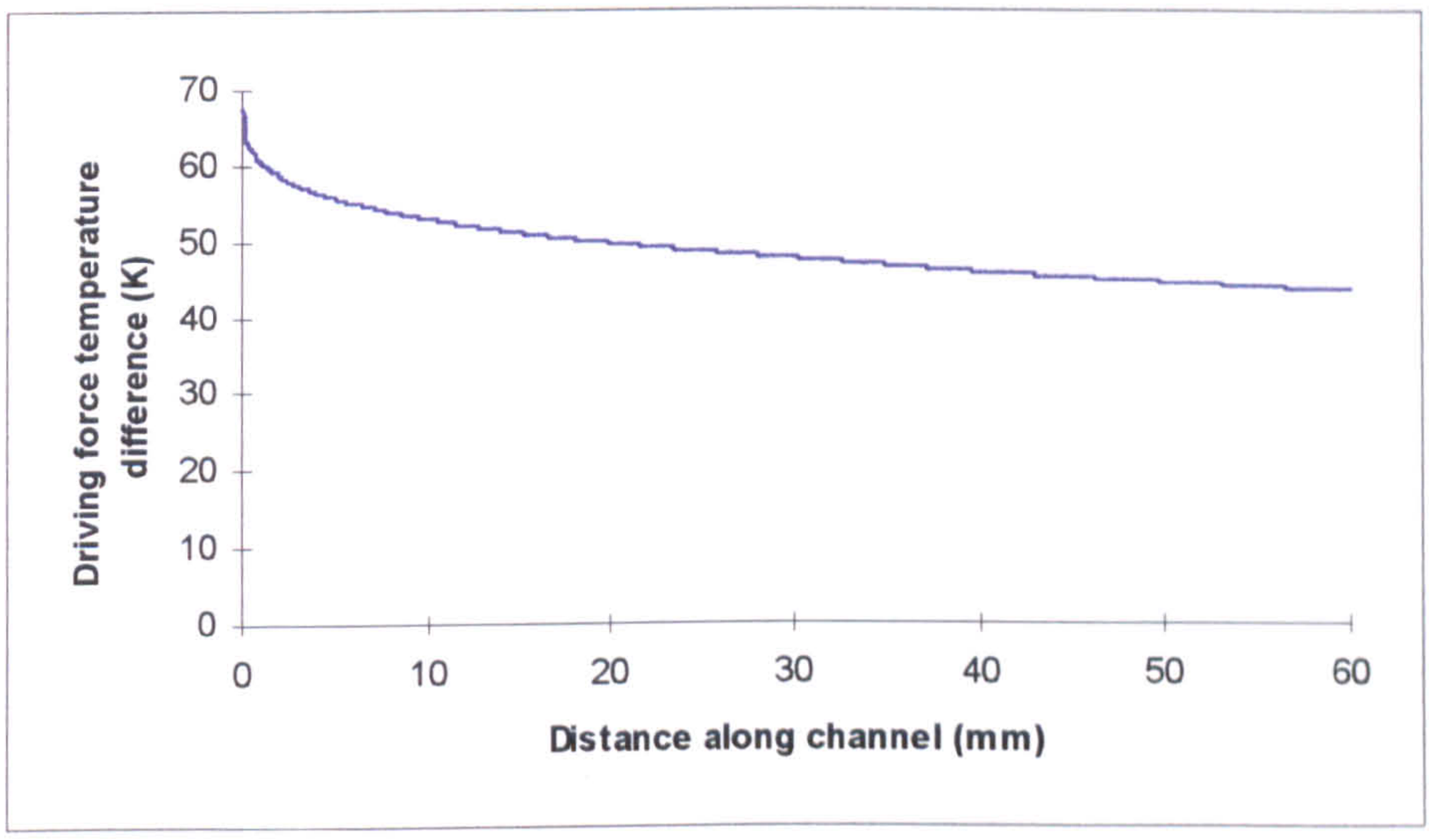

Figure 7.57: Level Three variation of driving force temperature difference along a channel (Y = 0.45 mm, v_H = 1 m/s, v_C = 1 m/s, T_H = 353 K, T_C = 285 K)

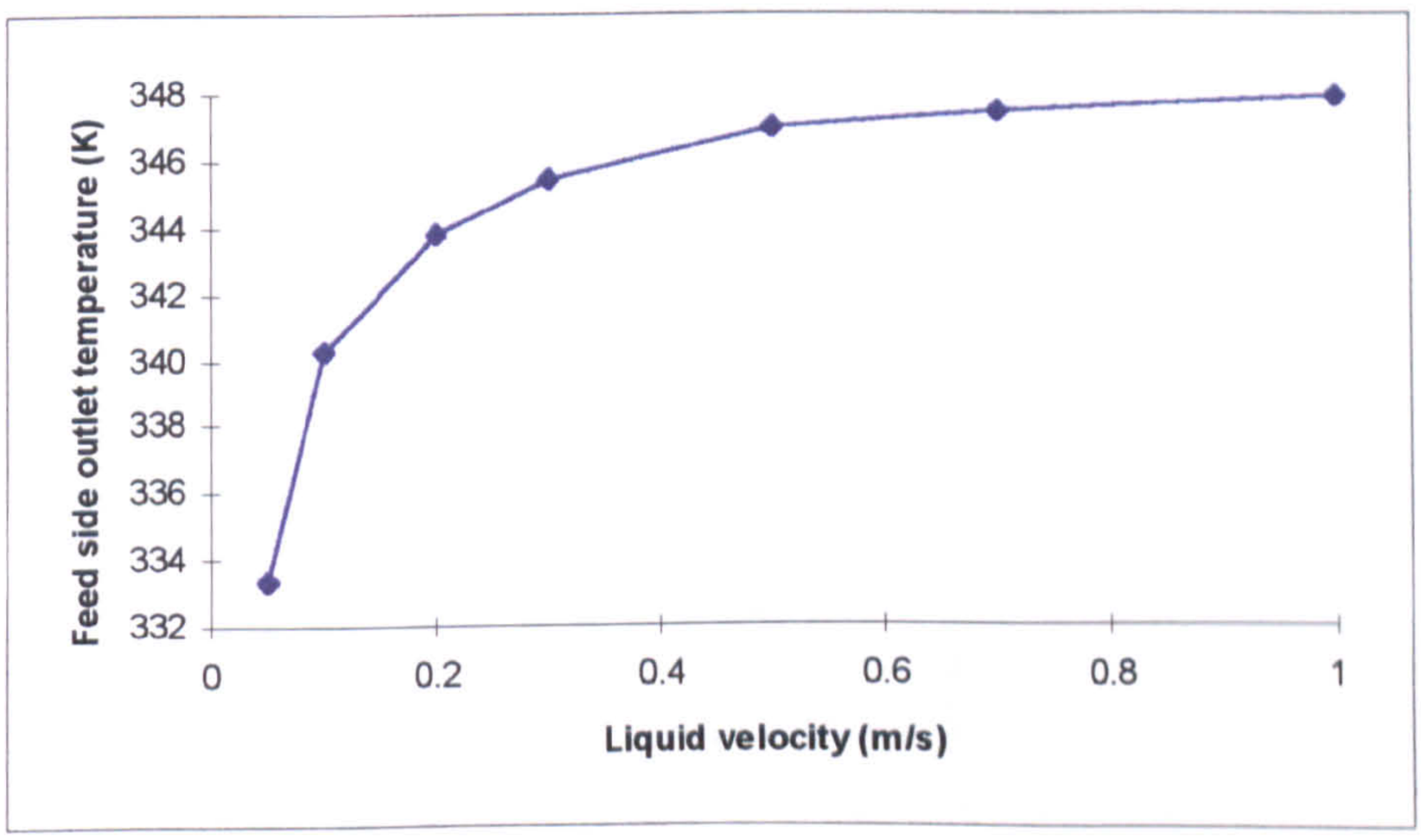

Figure 7.58: Level Three effect of liquid velocity on the feed outlet temperature (Y = 0.45 mm, T_H = 353 K, T_C = 285 K)

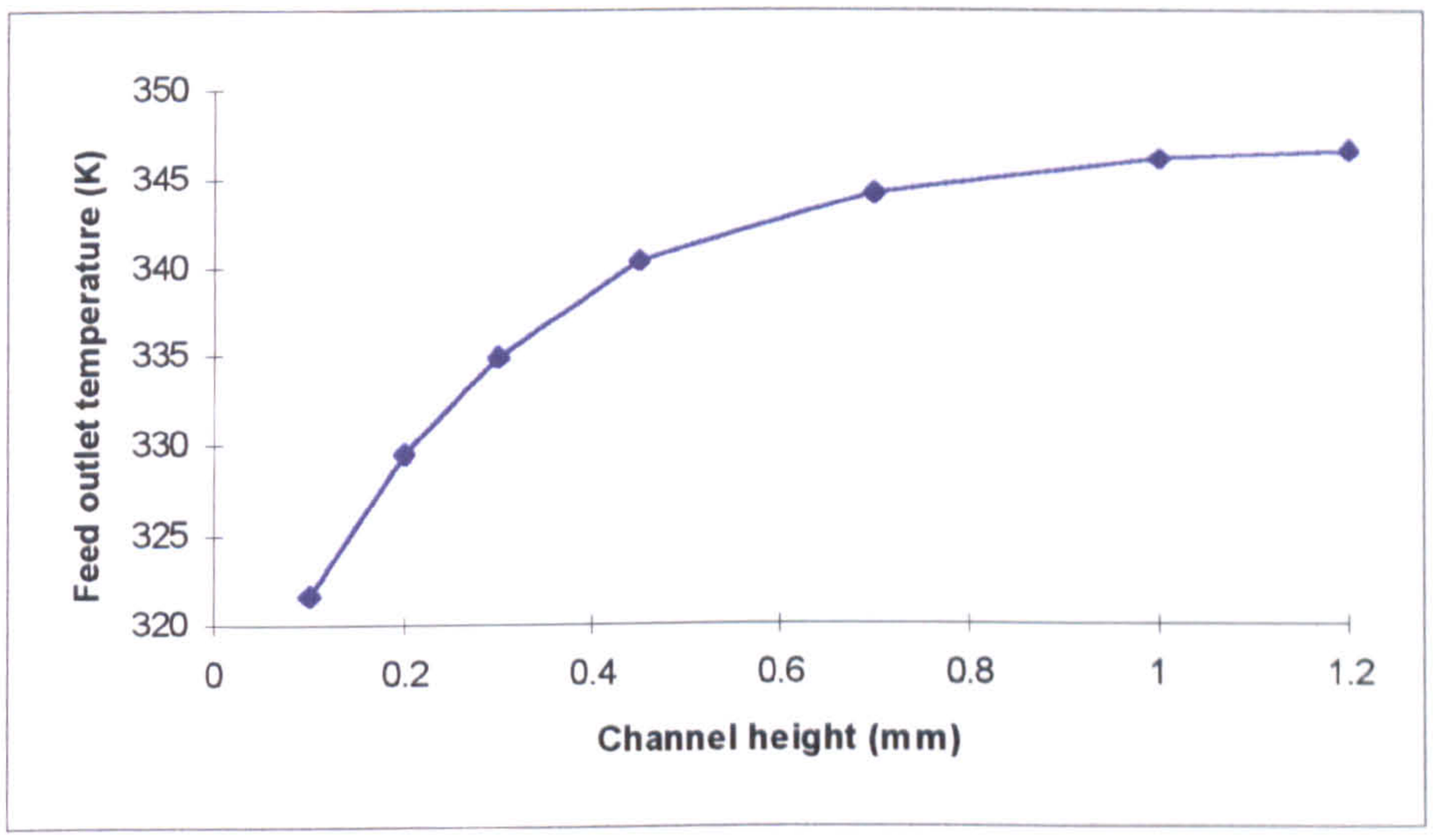

Figure 7.59: Level Three effect of channel height on the feed outlet temperature ($v_H = 0.1$ m/s, $v_C = 0.1$ m/s, $T_H = 353$ K, $T_C = 285$ K)

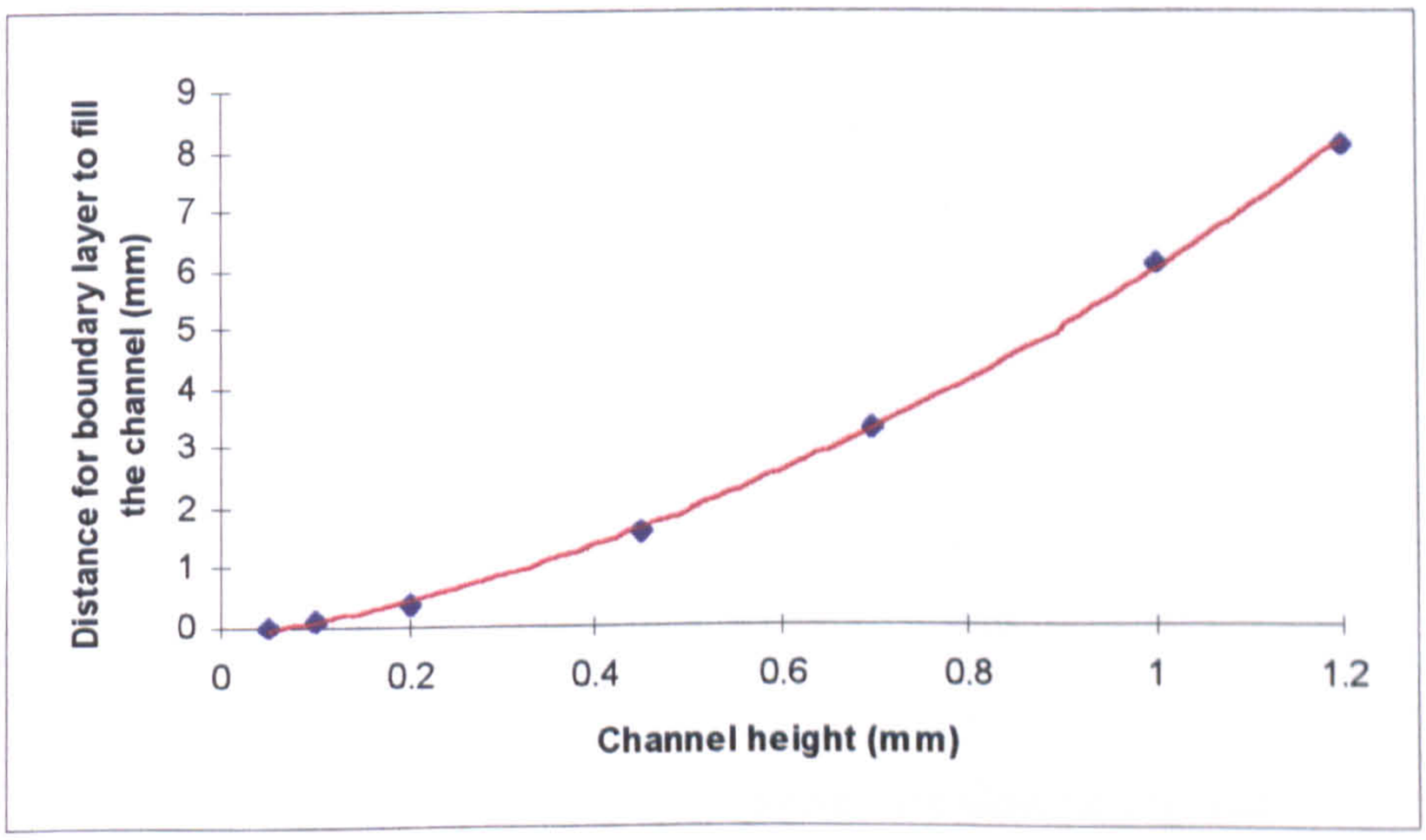

Figure 7.60: Level Three effect of channel height on the distance of the boundary layer to fill the channel ($v_H = 0.1$ m/s, $v_C = 0.1$ m/s, $T_H = 353$ K, $T_C = 285$ K)

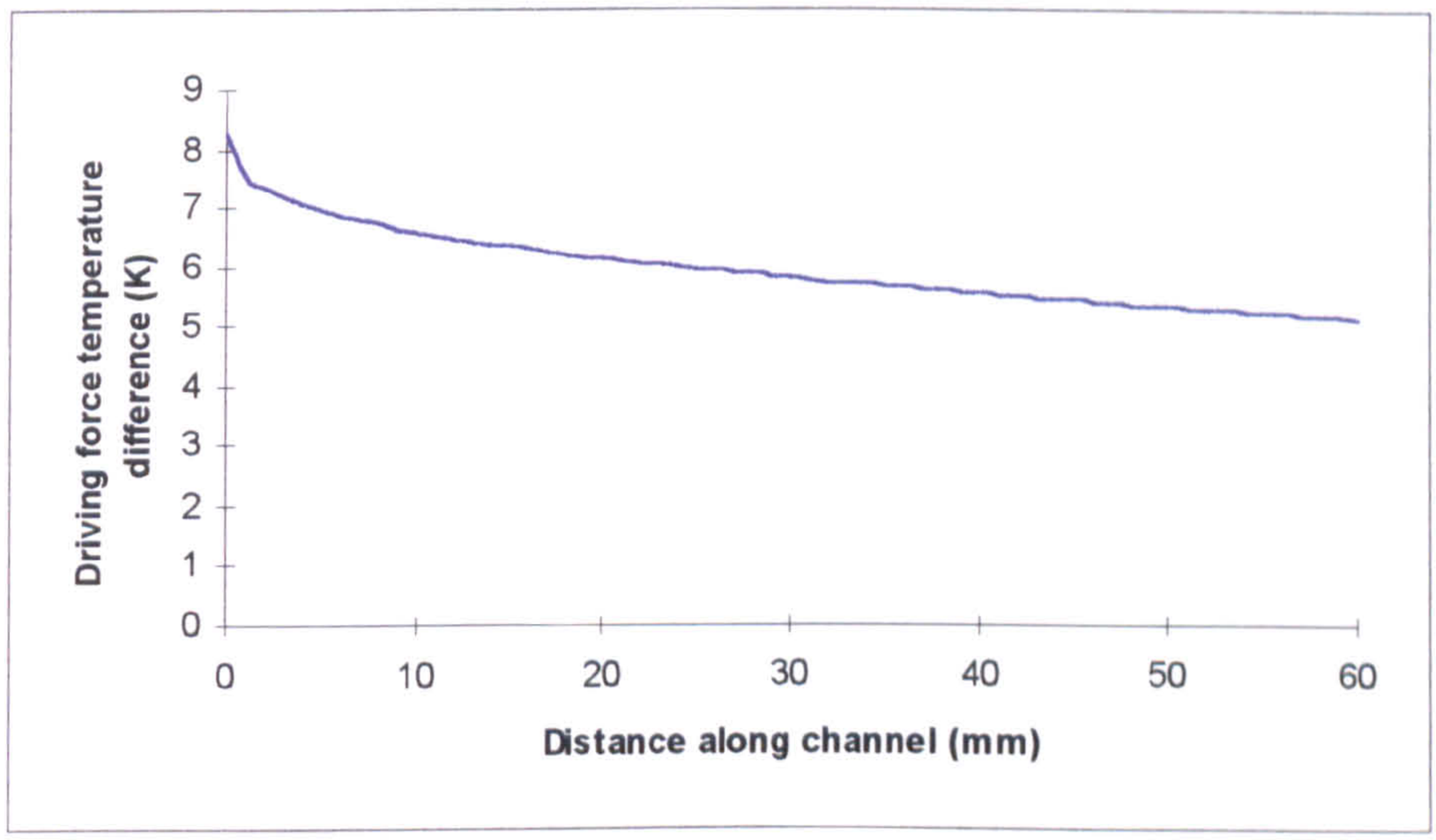

Figure 7.61: Variation of driving force temperature difference along a channel
(Y= 0.45 mm , v = 0.1334, T_H = 303.6 K, T_C = 295.1 K)

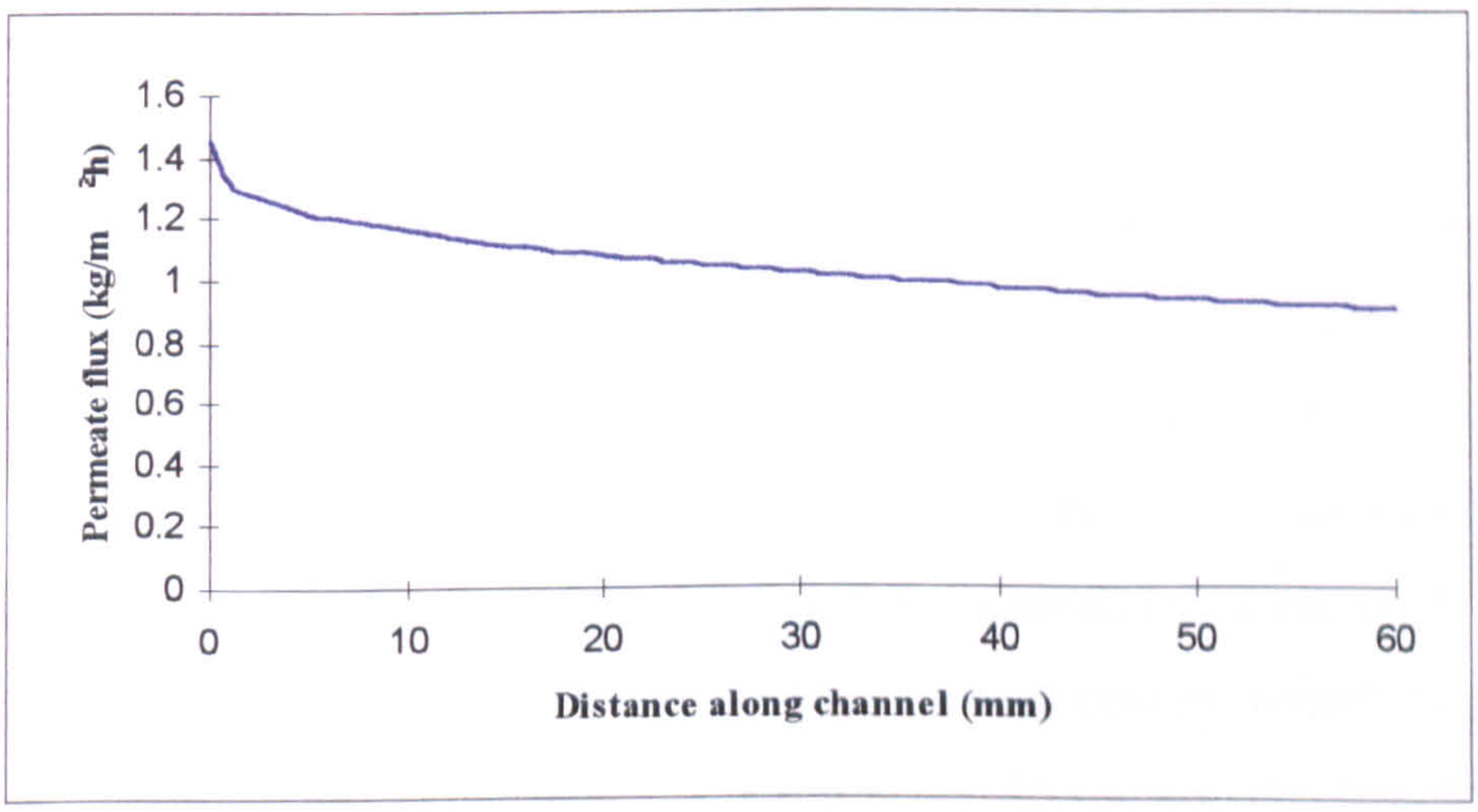

Figure 7.62: Variation of permeate flux along a channel
(Y= 0.45 mm, v = 0.1334 m/s, T_H = 303.6 K, T_C = 295.1 K)

Figure 7.61 shows a temperature difference profile calculated by Level Three of the boundary layer model. Using this data, the membrane distillation model has been used to calculate the related permeate flux profile along a channel (Figure 7.62). As it can be seen, the permeate flux decreases as the temperature difference decreases. This is as expected. The drop in flux over the channel is 0.55 kg/m^{2}h, i.e. the flux is reduced by 62%.

Further examples using the same extreme conditions as for Figures 7.54 to 7.57 are given in Figures 7.63 to 7.65, to study the permeate flux along the module channel. Figure 7.63 shows that for a velocity of 0.1 m/s, the permeate flux decreased by 12.99 kg/m^{2}h (54.4 %) over the channel. Increasing the velocity to 1 m/s (Figure 7.64) decreased the permeate flux drop to 7.53 kg/m^{2}h (30.8 %). This is due to the increased velocity increasing the entrance region length, which decreases the overall drop in temperature difference over the channel, and hence the flux. Decreasing the channel height to 0.2 mm, Figure 7.65, increases the permeate flux drop to 49.2 kg/m^{2}h (73.3 %). Again this is due to the length of the entrance region. Decreasing the channel height reduces the length taken by the boundary layer to fill the channel.

A more detailed study of the effect of channel height on the permeate flux is shown in Figure 7.66. Figure 7.66 takes the average permeate flux of a channel from the permeate flux profile, and collates them to study the effect of channel height and membrane temperature difference on the flux for a velocity of 0.1 m/s. This graph shows an unexpected and exciting development. For a specific velocity, there is an optimum channel height which would produce the maximum possible permeate flux over the channel. From Figure 7.66, for a liquid velocity of 0.1 m/s at the conditions stated, the optimum channel height is around 0.2 mm. Altering the temperature difference, though not the mean membrane temperature, does not alter the optimum channel height, but does affect the actual maximum flux obtainable. For instance, decreasing the temperature difference by 10 °C, lowers the maximum possible flux by 2.83 kg/m^{2}h.

Figure 7.67 keeps the initial membrane temperature difference constant and varies the channel height and velocity. Figure 7.67 shows that increasing the velocity increases the permeate flux, but only for smaller channel heights. With a channel height of 0.7 mm, the

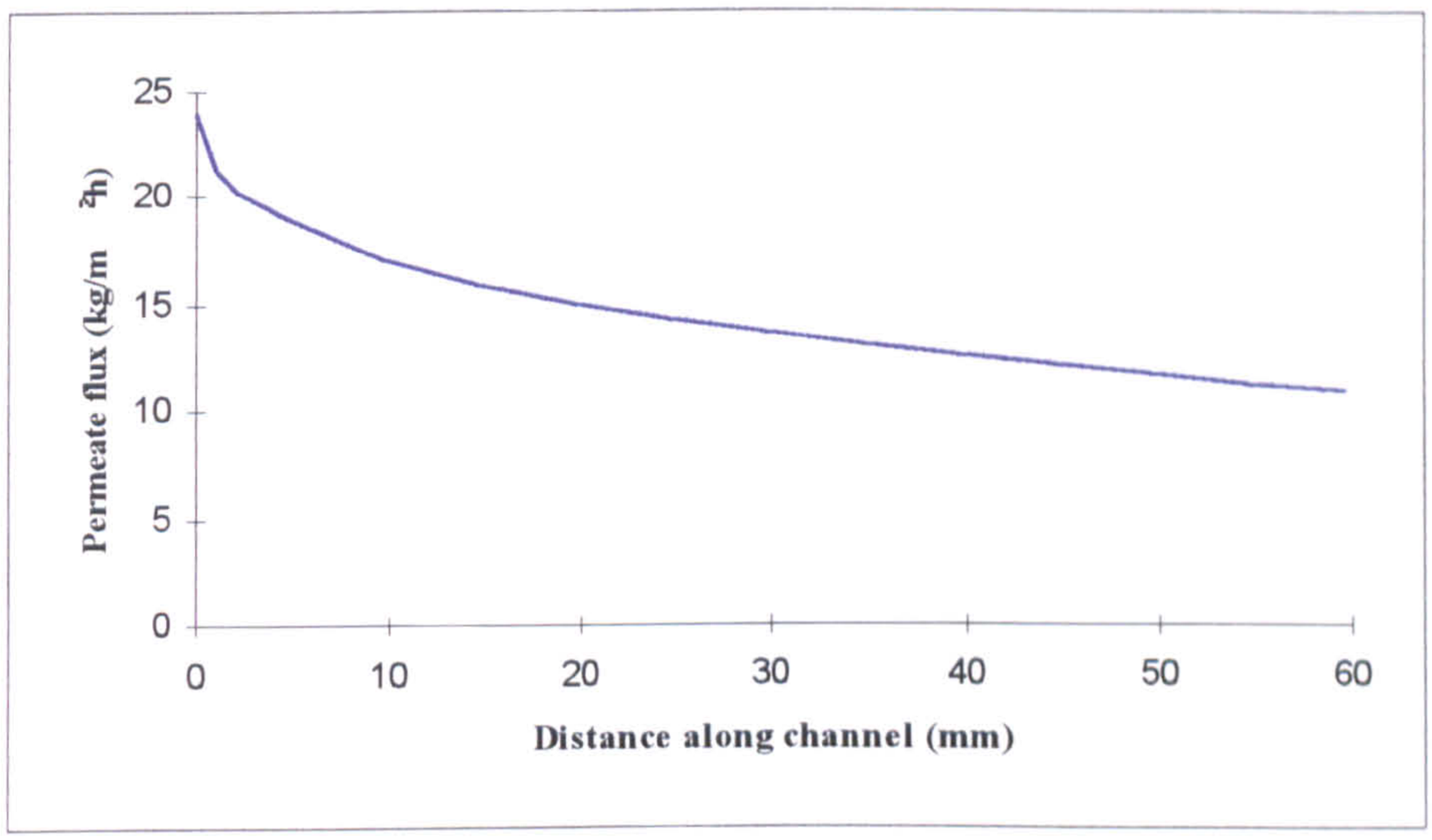

Figure 7.63: Variation of permeate flux along a channel
(Y = 0.45 mm, v = 0.1 m/s, T_H = 353 K, T_C = 285 K)

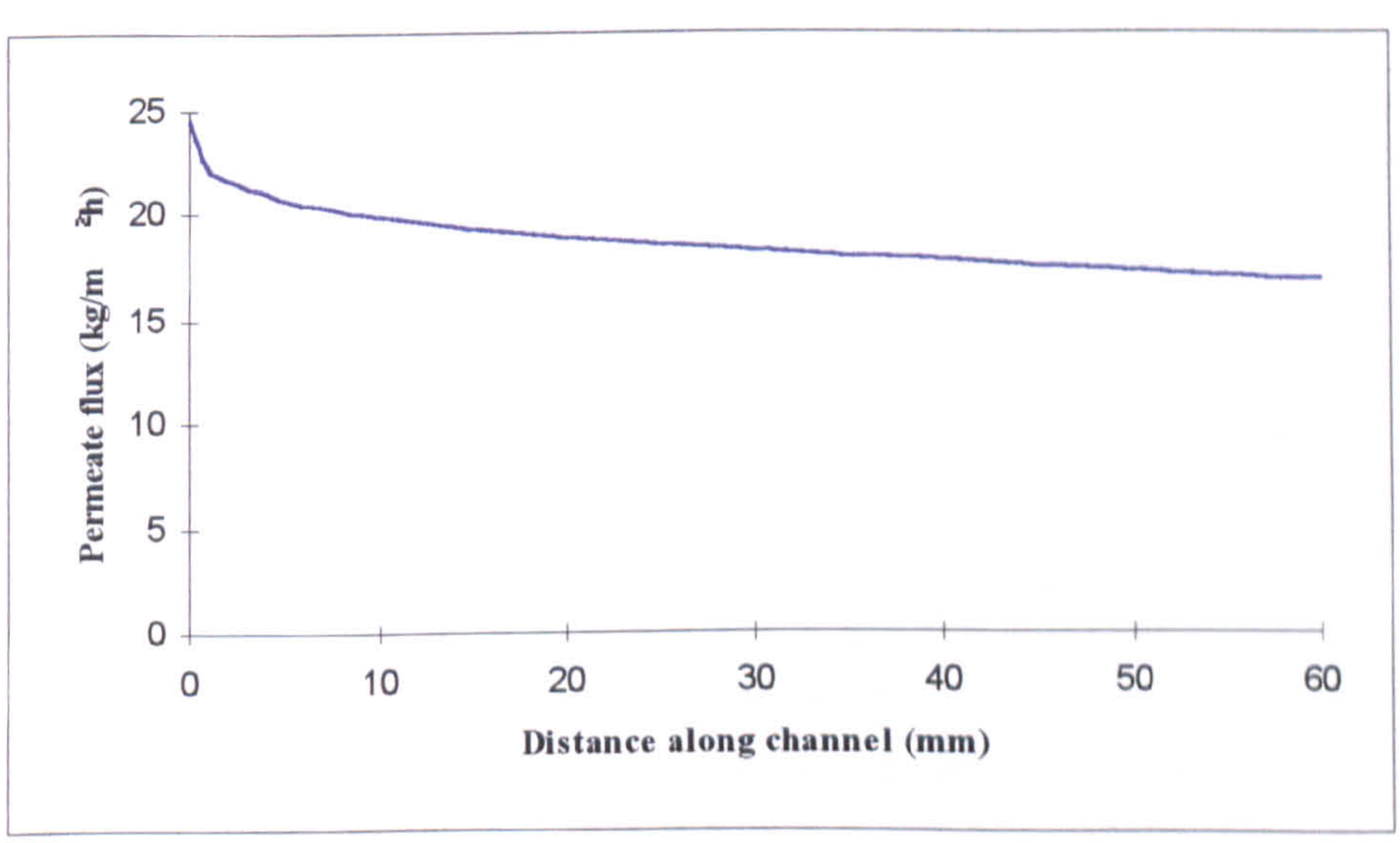

Figure 7.64: Variation of permeate flux along a channel
(Y = 0.45 mm, v = 1 m/s, T_H = 353 K, T_C = 285 K)

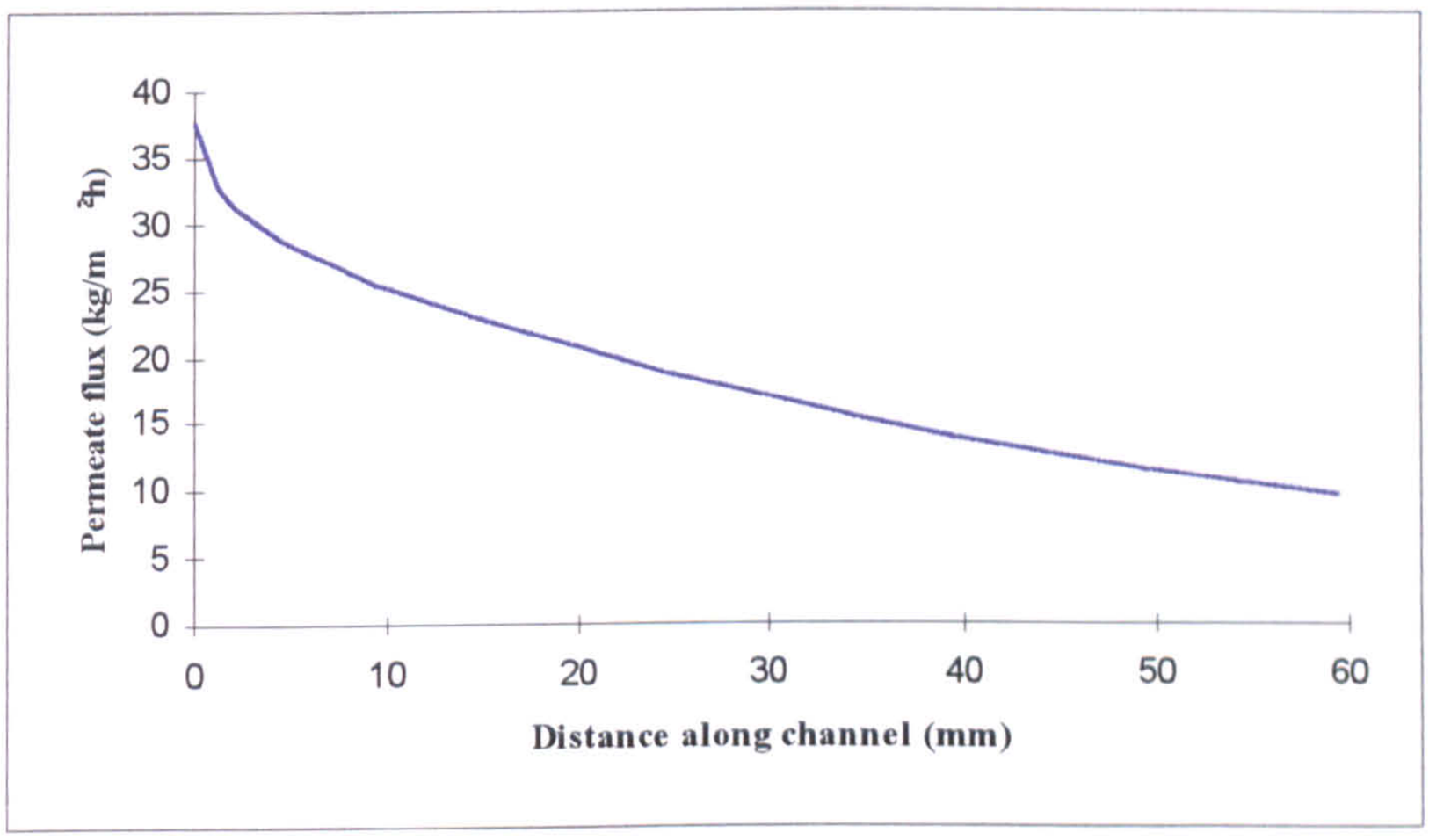

Figure 7.65: Variation of permeate flux along a channel
(Y = 0.2 mm, v = 0.1 m/s, T_H = 353 K, T_C = 285 K)

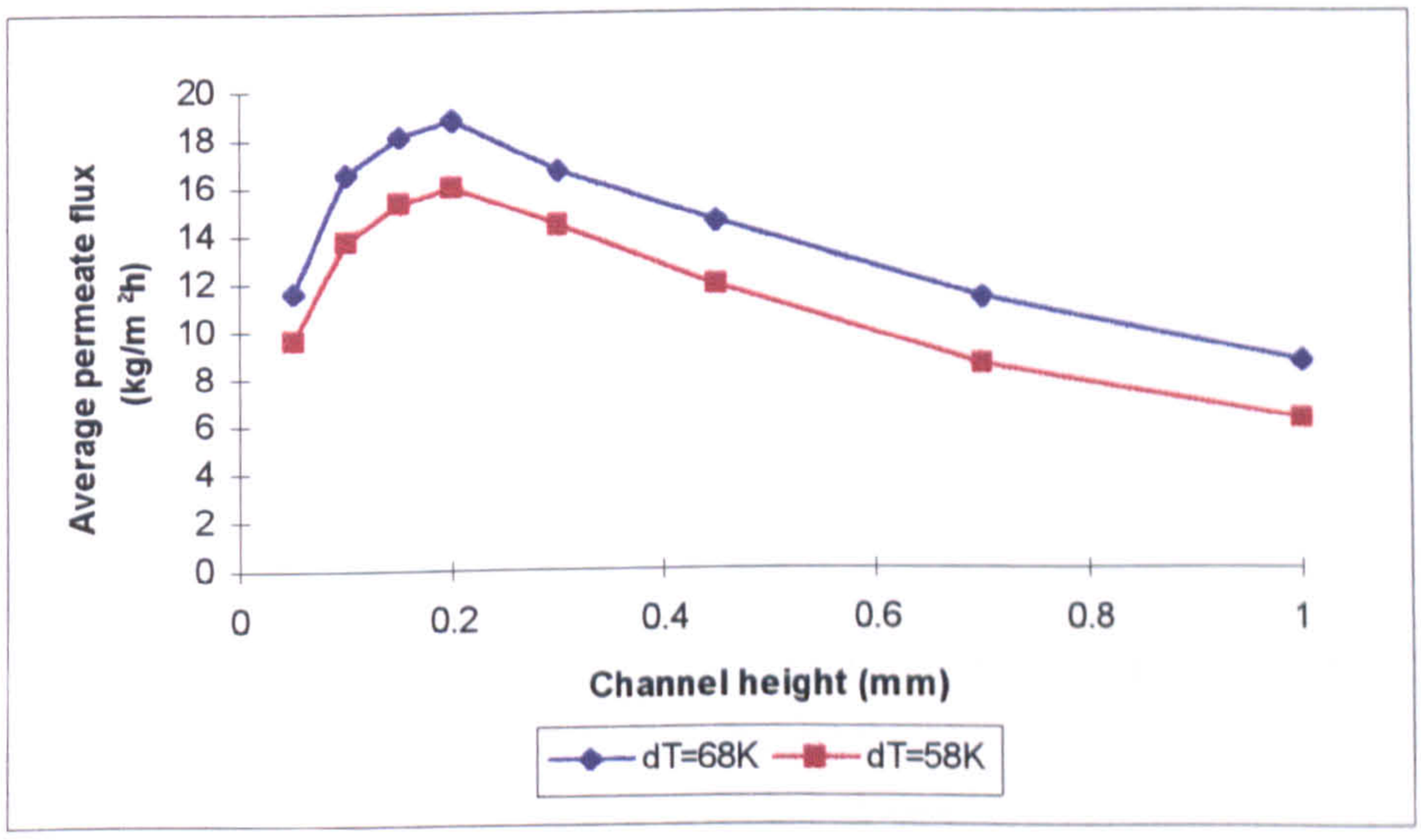

Figure 7.66: Effect of channel height and temperature difference on permeate flux
(v = 0.1 m/s, T_m = 319 K)

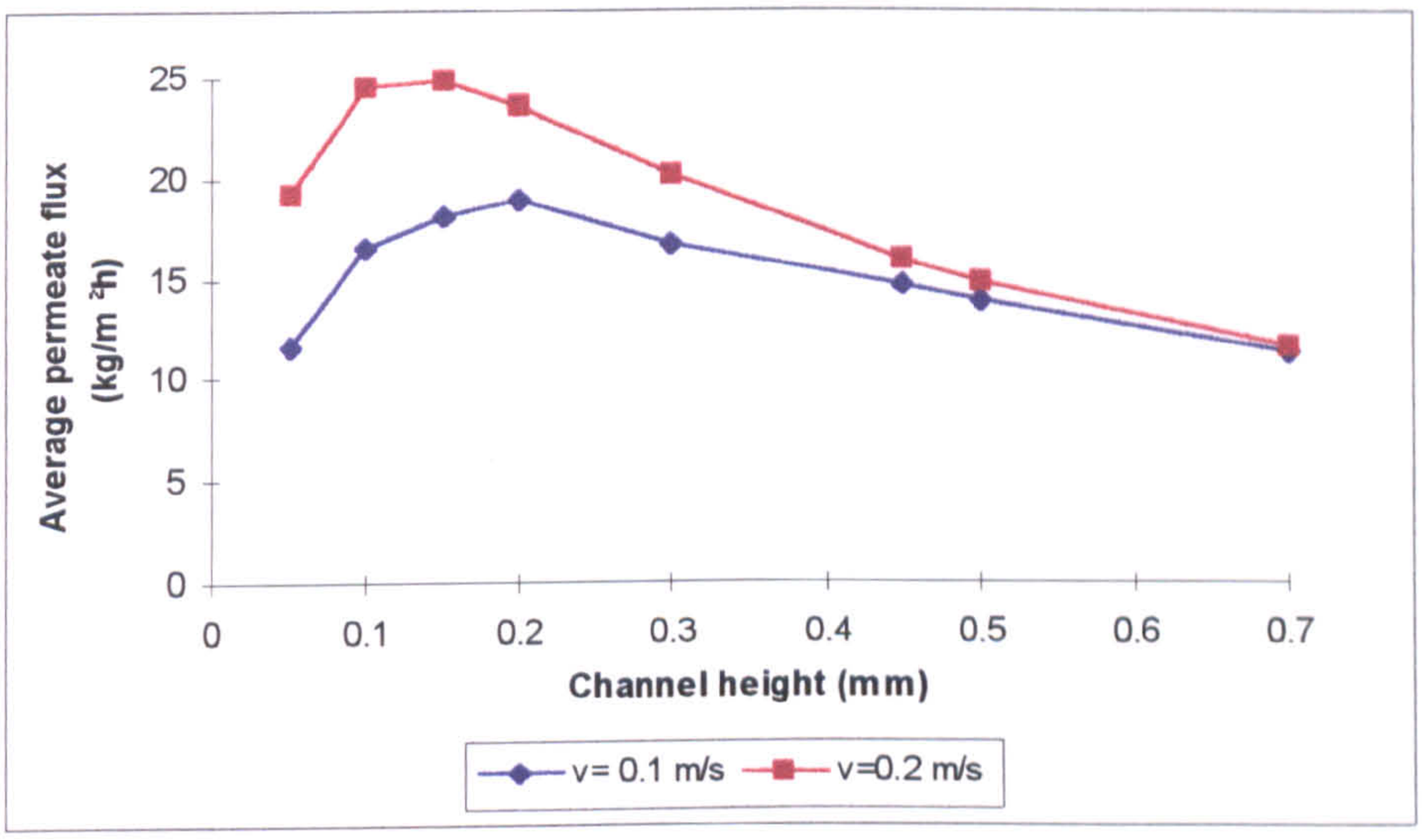

Figure 7.67: Effect of channel height and liquid velocity on permeate flux (T_m = 319 K, dT = 68 K)

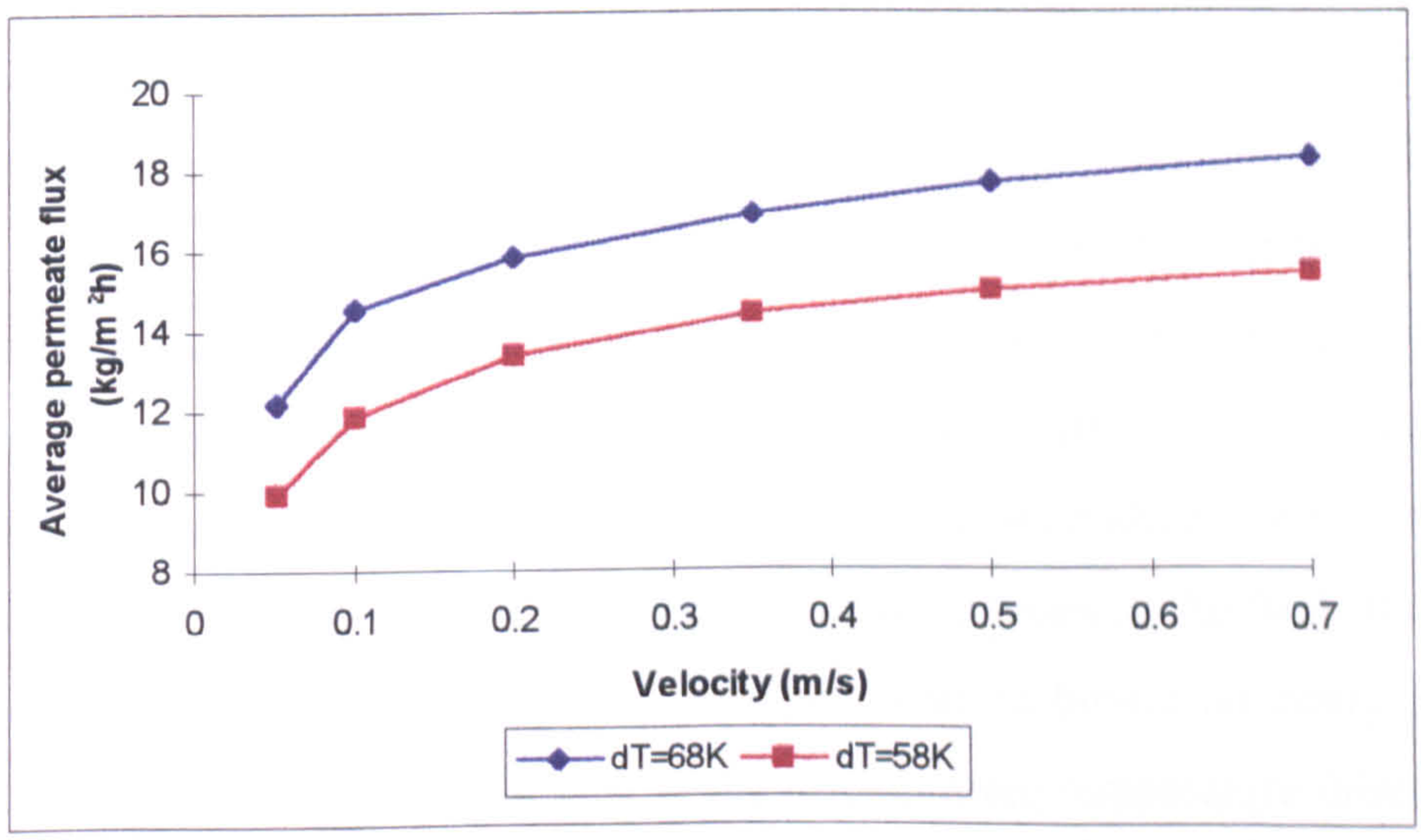

Figure 7.68: Effect of liquid velocity and temperature difference on permeate flux (Y = 0.45 mm, T_m = 319 K)

difference in flux caused by the increase in velocity is negligible. With the smaller channel heights, increasing the velocity reduces the optimum channel height. In Figure 7.67 the optimum channel height is 0.2 mm for a velocity of 0.1 m/s, and is 0.15 mm for a velocity of 0.2 m/s. The shape of the graph suggests that decreasing the channel height beyond the optimum height has a more detrimental effect than using a slightly bigger channel height.

Finally, for this linked model, Figure 7.68 for a channel height of 0.45 mm, shows that increasing the velocity increases the permeate flux, and that this effect increases with an increase in the temperature difference over the membrane.

Level Four

The final level of the boundary layer analysis carried out for this work was formed to try and overcome the drop in driving force temperature difference along the flat plate channel. The idea was to introduce boiling and condensing surfaces either side of the module to remove and provide heat respectively. Level Three was modified to take into account the heat transfer at the walls of the channel (Level Four). Various theoretical runs were made. There were no experimental results to compare with this level of the analysis, as the analysis was carried out purely on a theoretical investigative basis.

The first graph, Figure 7.69 shows the development of the two feed side boundary layers. b_1 is the membrane surface boundary layer, and b_2 is the channel wall boundary layer formed by the transfer of heat through the channel wall from a condensing liquid. The constant region is reached when the two boundary layers meet to fill the channel. For the extreme conditions given in Figure 7.69, the constant region begins 0.36 mm along the channel. The full temperature profiles along the module for these conditions are shown in Figure 7.70. The wall heat transfer has the effect of initially increasing the feed side wall temperature, and decreasing the permeate side wall temperature before returning to the trends observed for previous levels. Looking at the driving force temperature difference, Figure 7.71, the drop along the channel is 23.97 °C. This compares with 35.35 °C for the Level Three analysis at these conditions.

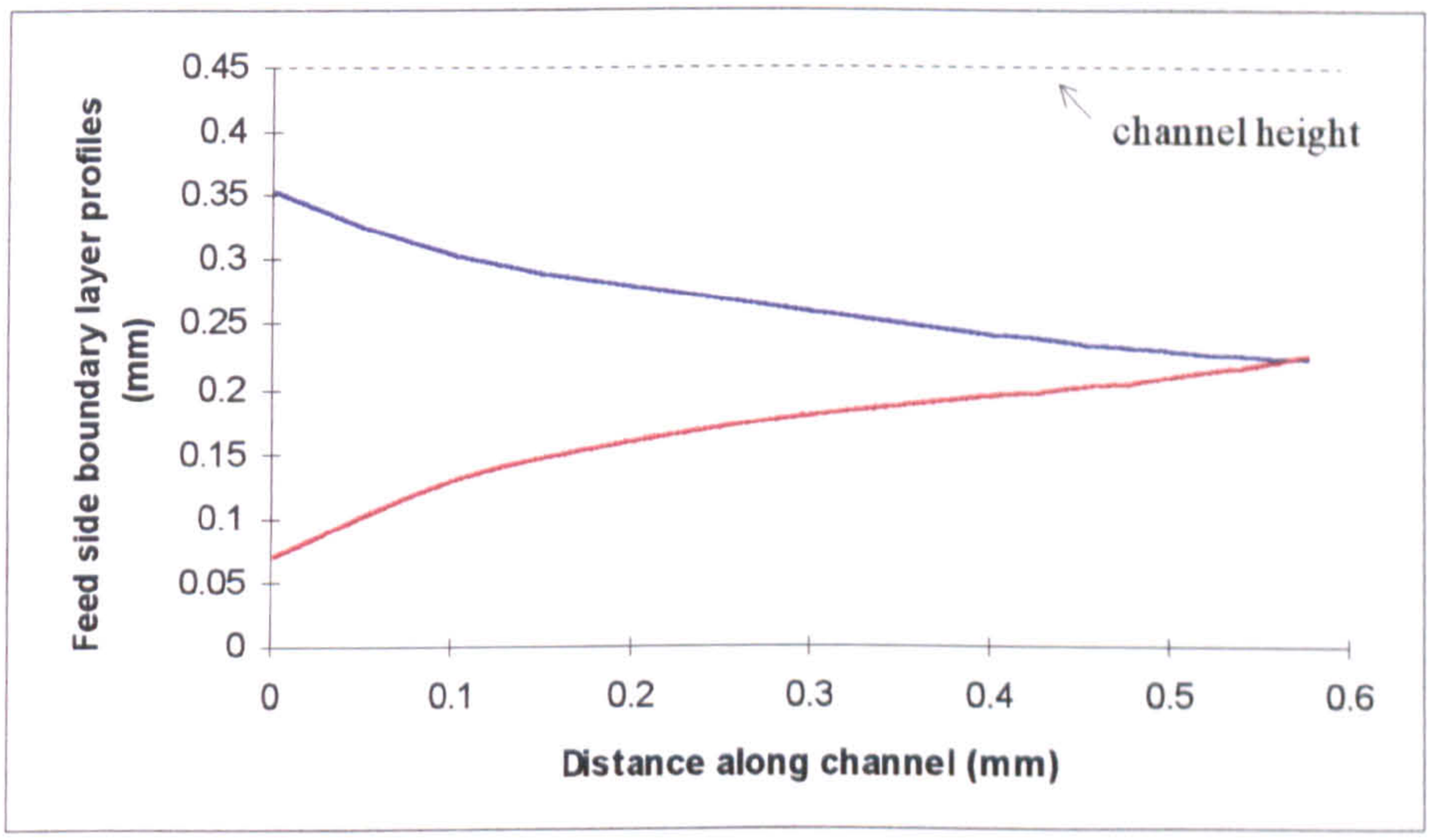

Figure 7.69: Level Four feed side dual boundary layer development
(Y = 0.45 mm, v = 0.1 m/s, T_H = 353 K, T_C = 285 K)

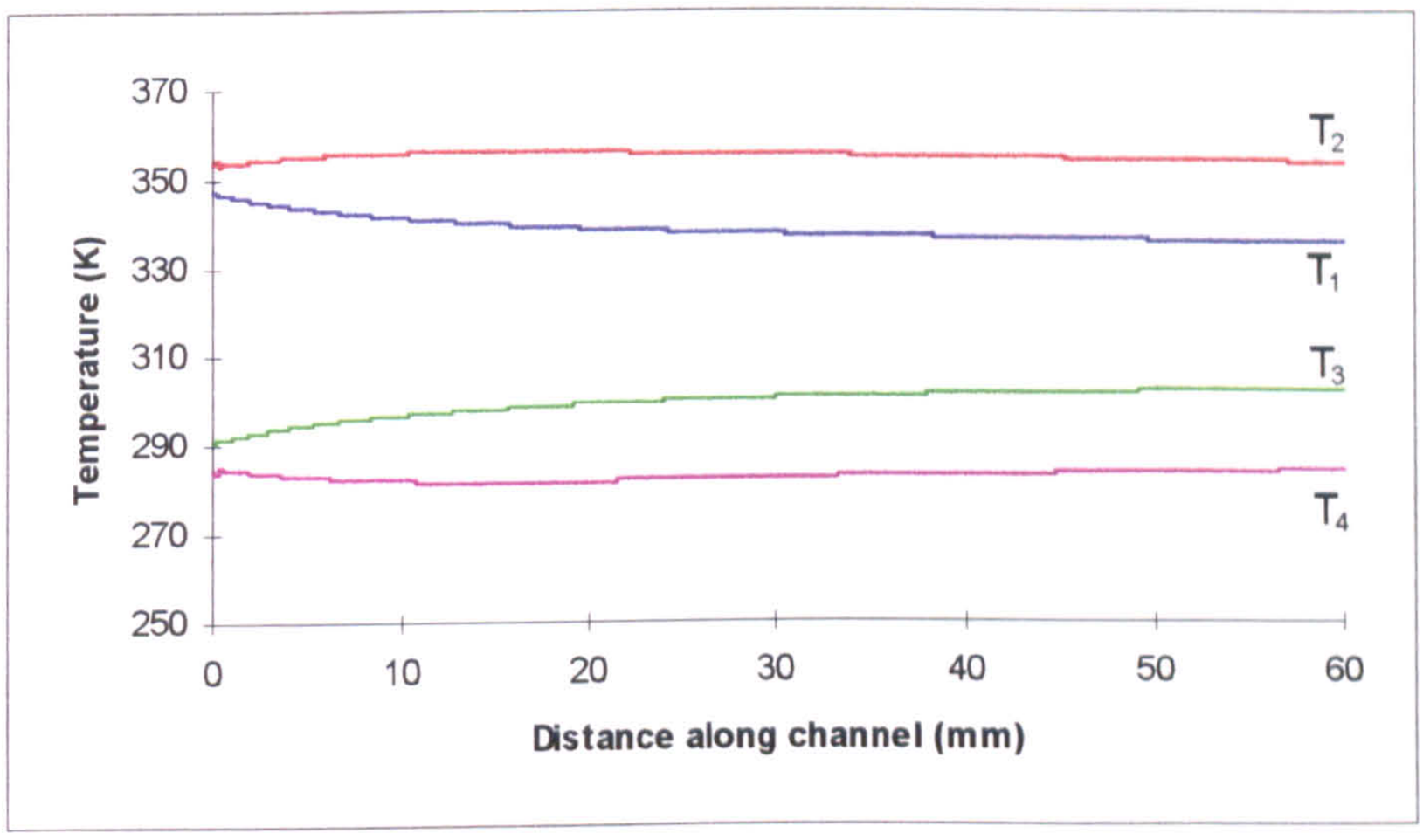

Figure 7.70: Level Four full temperature profiles compared with experiment
(Y = 0.45 mm, v = 0.1 m/s, T_H = 353 K, T_C = 285 K)

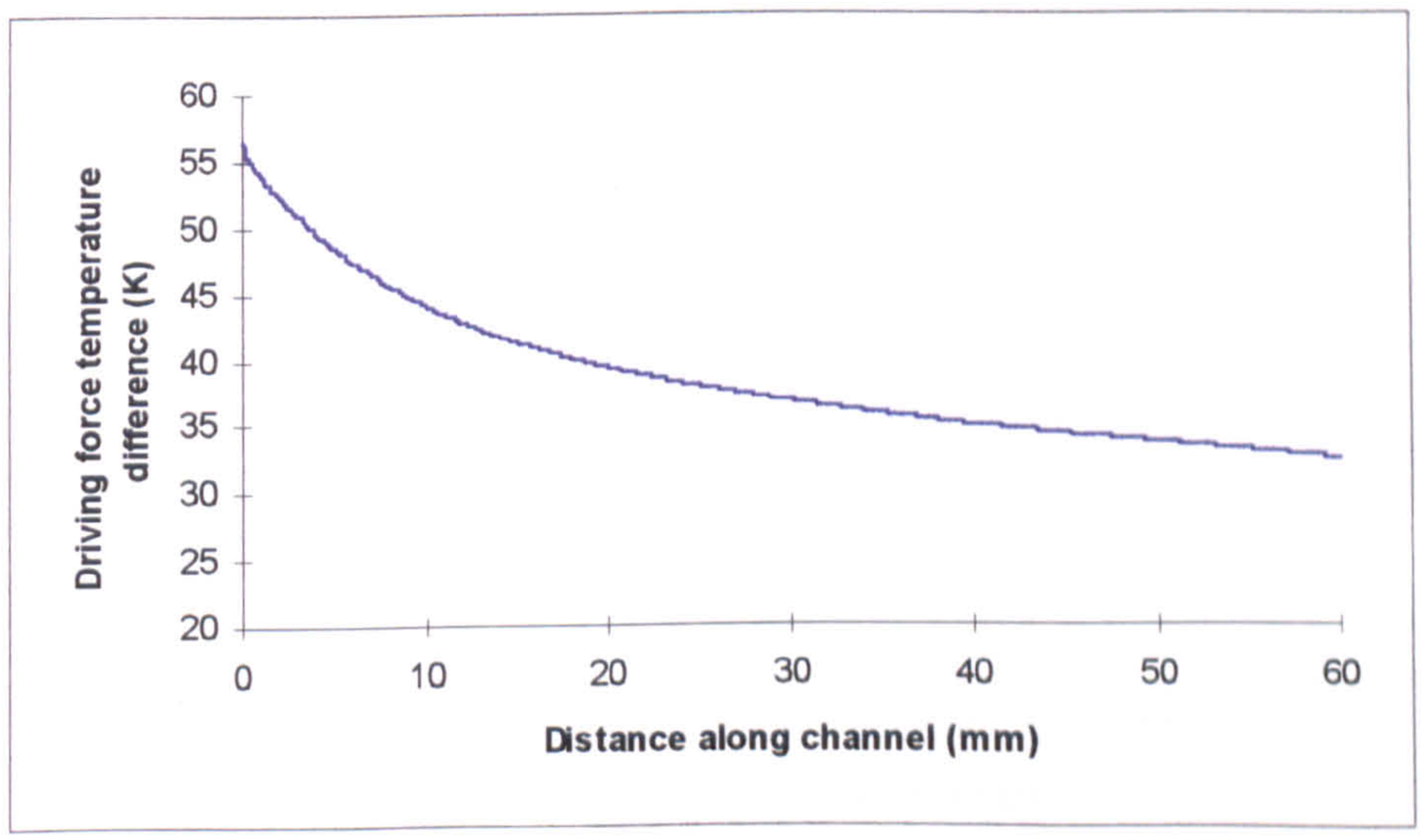

Figure 7.71: Level Four variation of driving force temperature difference along a channel
(Y = 0.45 mm, v = 0.1 m/s, T_H = 353 K, T_C = 285 K)

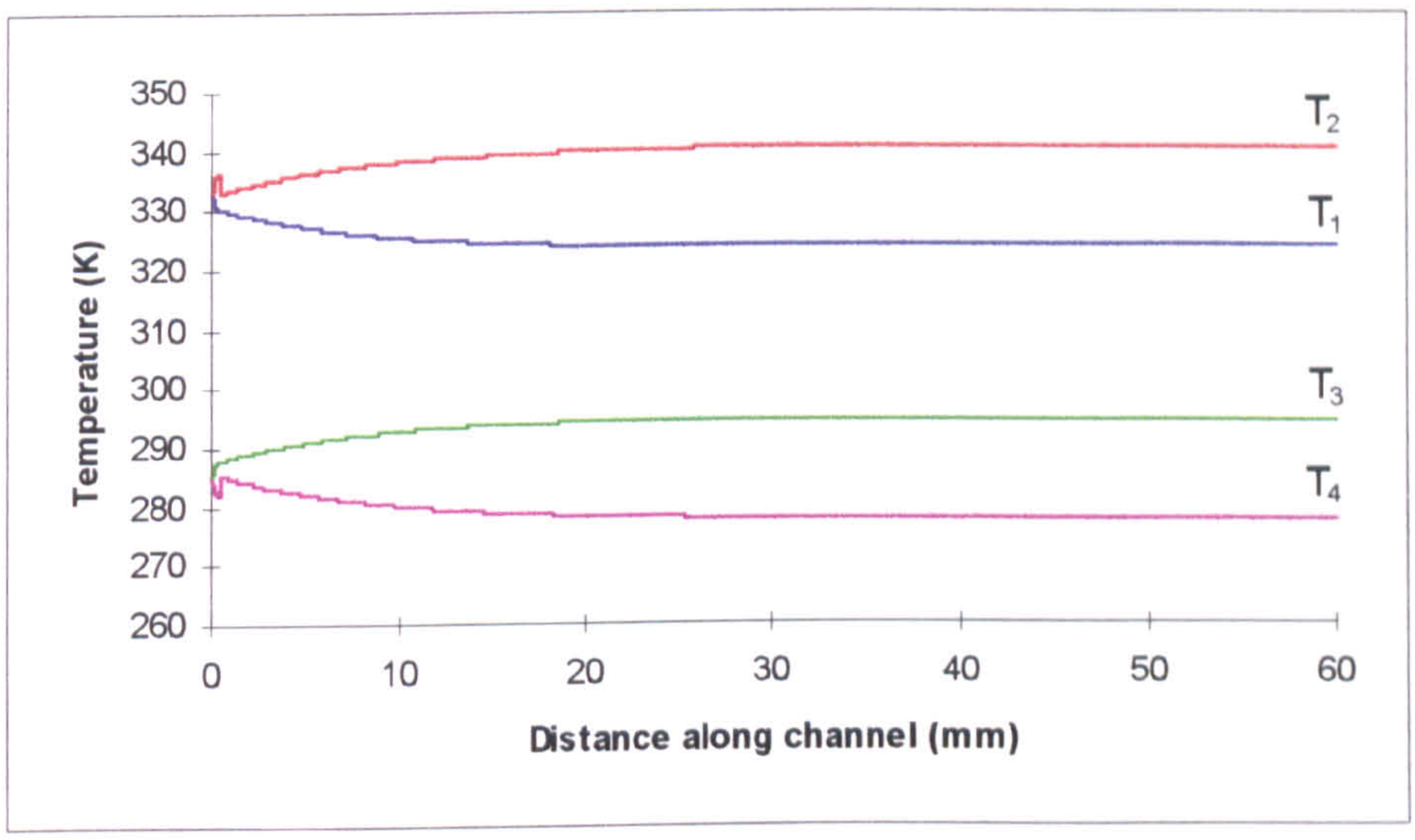

Figure 7.72: Level Four full temperature profiles compared with experiment
(Y = 0.45 mm, v = 0.1 m/s, T_H = 333 K, T_C = 285 K)

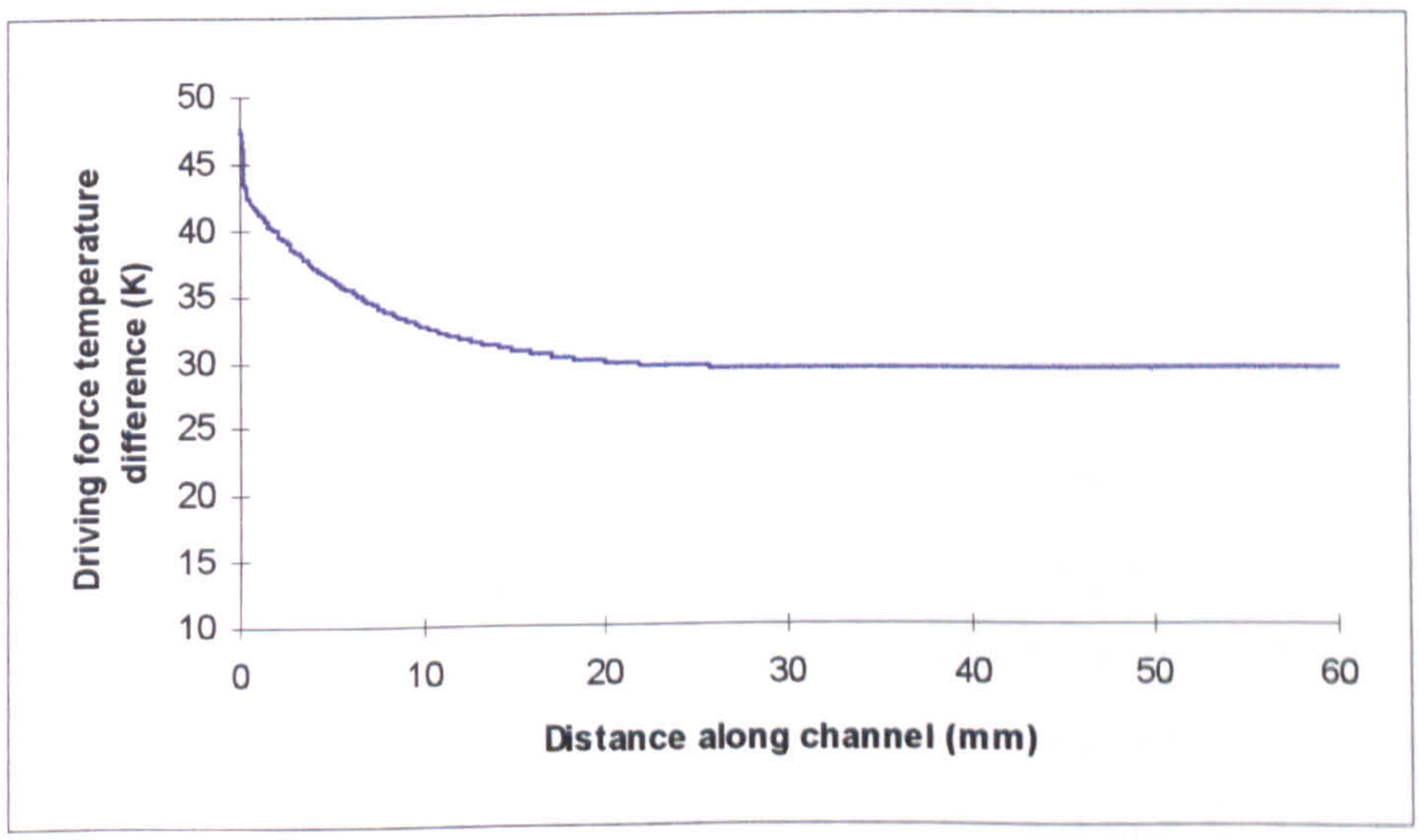

Figure 7.73: Level Four variation of driving force temperature difference along a channel
(Y = 0.45 mm, v = 0.1 m/s, T_H = 333 K, T_C = 285 K)

Using a feed temperature 20 °C lower, Figure 7.72 shows the calculated full temperature profiles. The main point from this graph is that halfway along the channel, the temperature profiles reach constant values. This means that the temperature difference shown in Figure 7.73 remains constant. This would be the best situation for membrane distillation as this would mean that the system reaches thermal equilibrium. Extending the channel length further (i.e. increasing the membrane surface area) would not affect the temperature as the boundary layer effects are at equilibrium. This means that the permeate flux would be predictable and constant along the constant temperature section. For the conditions used in Figure 7.73, the temperature drop along the channel is 18.35 °C.

Collating the results obtained with the Level Four model, various graphical relationships were found. From the theory, it can be assumed that increasing the channel height would increase the length of the entrance region. The effect of the channel height on the distance taken by the boundary layers to fill the channel is shown in Figure 7.74, which is for a liquid velocity of 0.1 m/s. The increase in length of the entrance region is due to the increased flow of liquid causing the heat to travel through more fluid before transport through the membrane. For example, using channel dimensions from the experimental rig, for a channel height of 0.1 mm the flowrate would be 7×10^{-8} m^3/s, and for a channel height of 0.45 mm the flowrate would be 3.15×10^{-7} m^3/s. This relationship is linear. The relationship overall however is not linear due to the nature of boundary layer growth (see Figure 7.28). Another assumption was that increasing the liquid velocity would also increase the entrance region. This reduces the time the liquid is in the channel and so reduces heat transfer. This is shown in Figure 7.75, and the relationship is generally linear. The next step was to study how the temperature driving force was affected by the liquid velocity and channel height. For Figures 7.76 and 7.77 the inlet conditions were the same and only the outlet temperature differences are reported. In Figure 7.76 the curve approaches zero at low velocities. This is because at infinitely low velocities, all the available heat is transferred through the liquid and through the membrane. At infinitely high velocities, the liquid would travel so fast through the channel that no heat transfer would occur and the outlet temperature driving force would be the same as the inlet driving force. Basically, at the conditions chosen, the outlet temperature difference

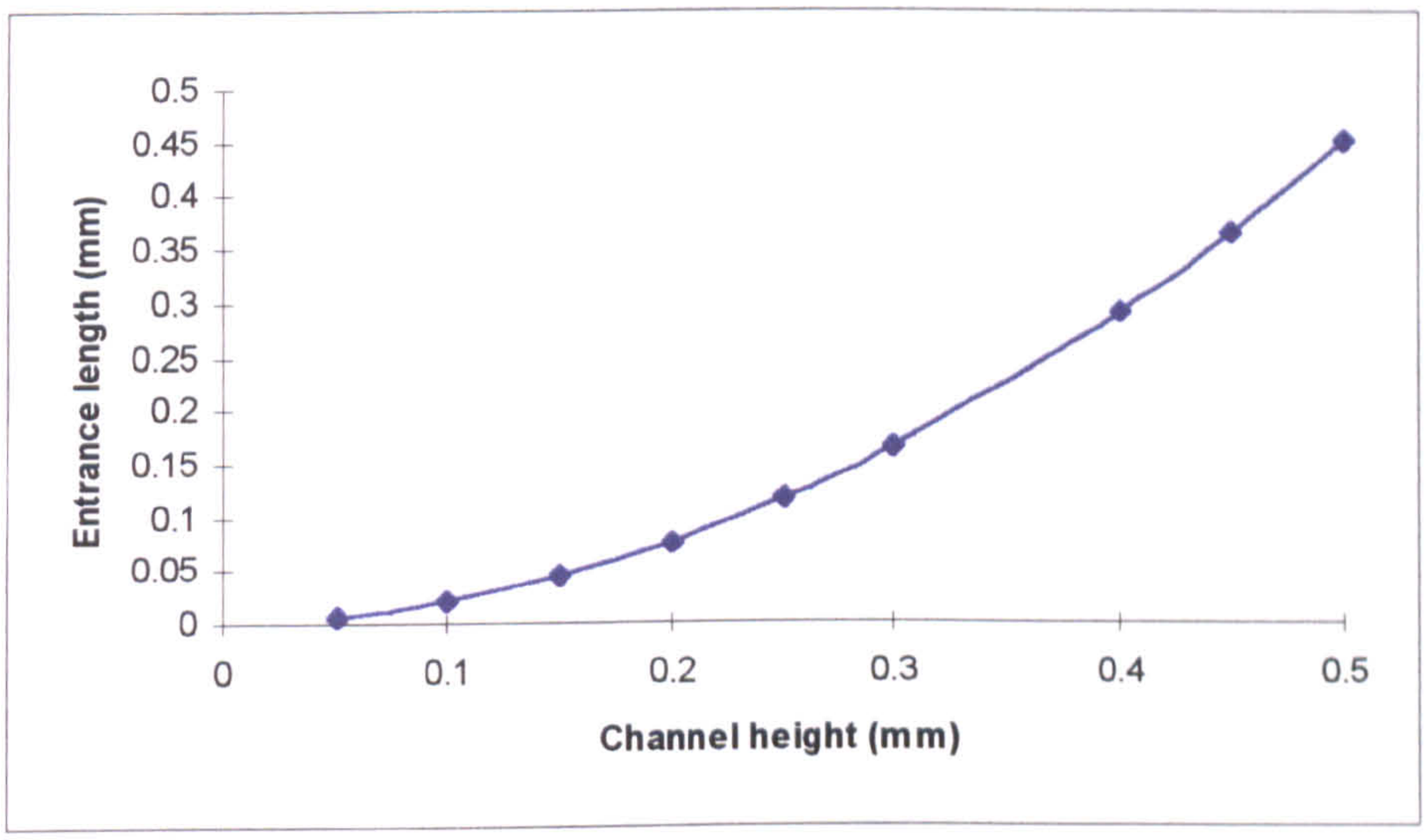

Figure 7.74: Level Four effect of channel height on the boundary layer entrance length (v = 0.1 m/s)

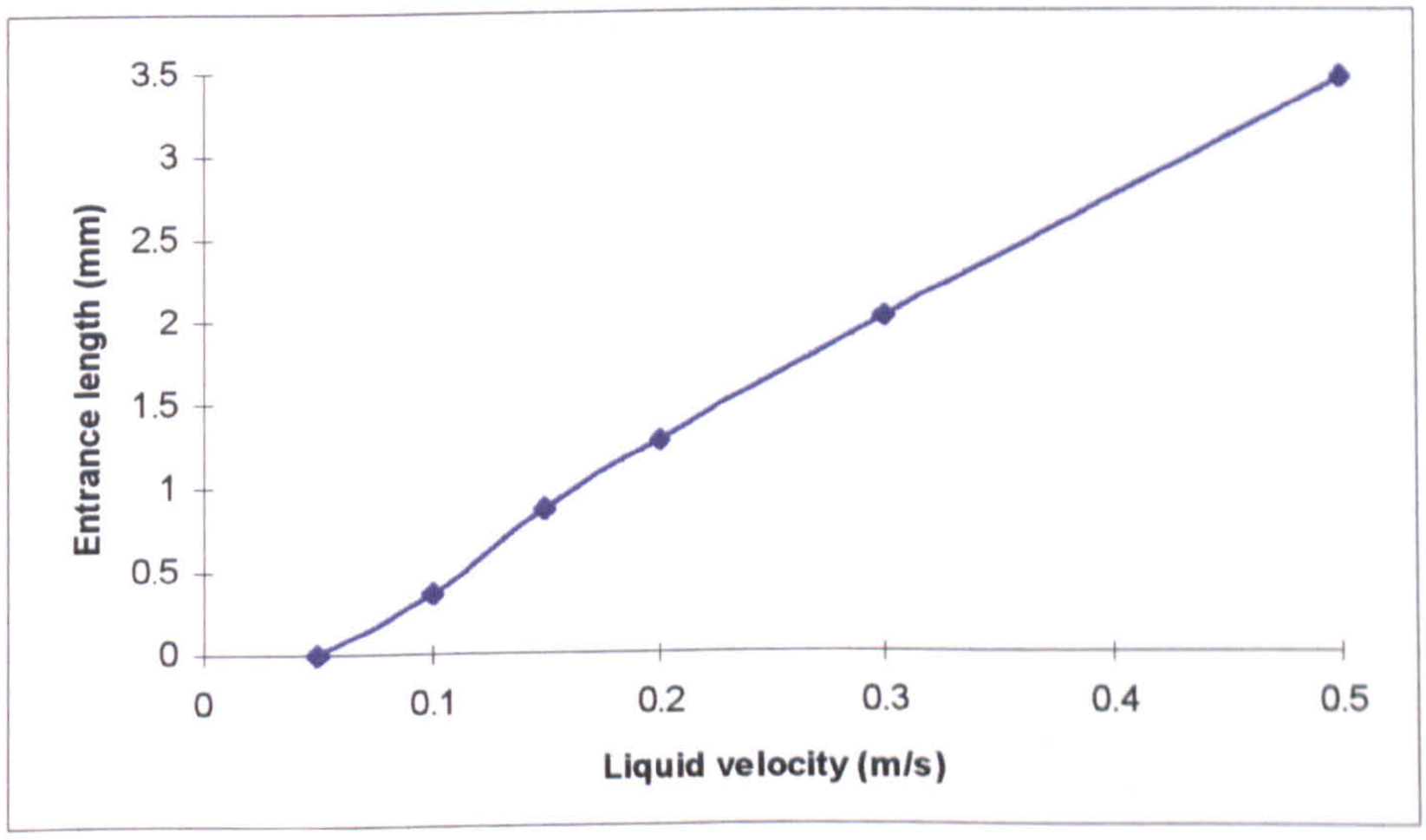

Figure 7.75: Level Four effect of liquid velocity on the boundary layer entrance length (Y = 0.45 mm)

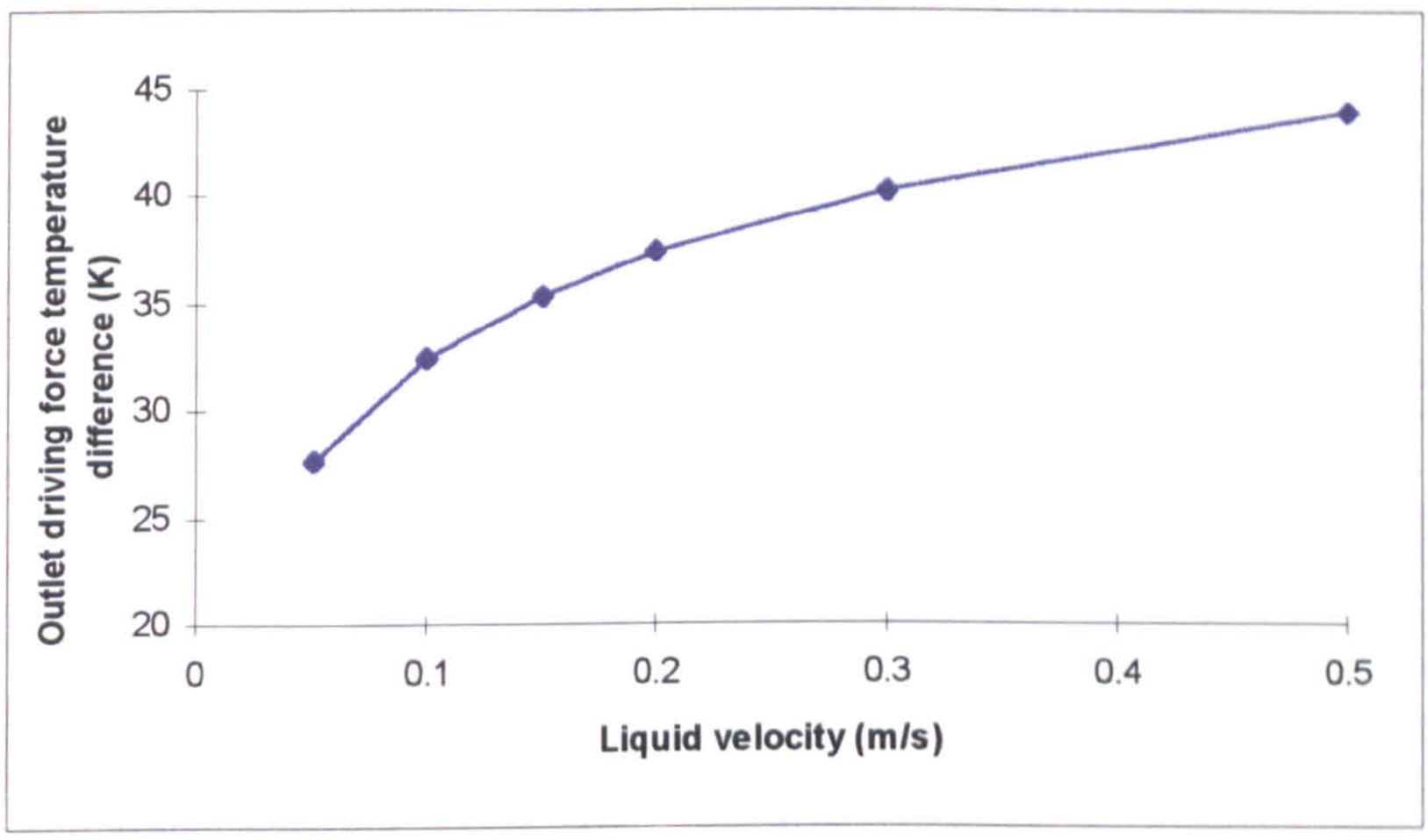

Figure 7.76: Level Four effect of liquid velocity on the drop of driving force channel temperature difference (Y = 0.45 mm)

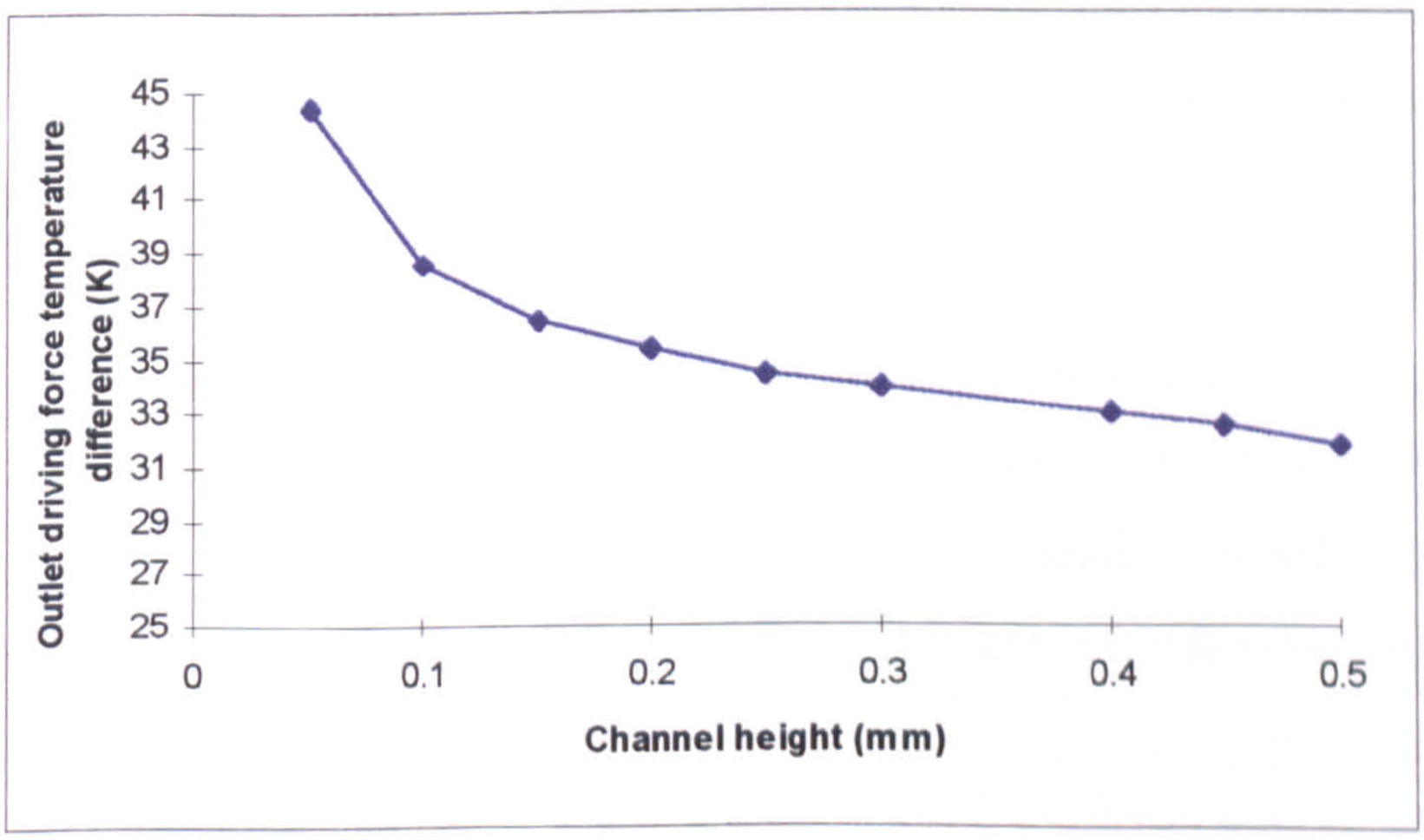

Figure 7.77: Level Four effect of channel height on the outlet driving force temperature difference (v = 0.1 m/s)

increases with an increase in velocity. The effect of channel height is shown in Figure 7.77. In this situation, as the channel height is increased, the outlet temperature difference decreases. This is due to the flowrate increasing with increasing channel height at a constant velocity. At very large channel heights, the heat transfer through the feed wall from the condensing vapour has only a small effect. Most of the heat required by membrane distillation is taken from the fluid itself thereby reducing the available temperature difference across the membrane. At very small channel heights, the heat transfer through the wall is the controlling factor and it is this heat which is used for membrane distillation. The heat of the fluids are maintained. Therefore, at very small channel heights, the outlet temperature difference is very close to the inlet temperature difference. Ofcourse, these effects can be translated to effects on the permeate flux to show that very large velocities and very small channel heights would maximise the flux when using boiling and condensing heat transfer surfaces.

Finally, conditions from two Level Three runs (Figure 7.78: T_H = 353 K, T_C = 285 K, v = 0.2 m/s, Y = 0.45 mm, Figure 7.79: T_H = 333 K, T_C = 285 K, v = 0.1 m/s, Y = 0.45 mm) were chosen at random to use in the Level Four model. The final two graphs concern the comparison between a flat plate module, with (Level Four) and without (Level Three) heat transfer surfaces along the channel walls. The membrane distillation model was used to calculate the flux along the channel for both systems. The figures show the effect heating and cooling surfaces along the channel walls had on the permeate flux, compared to the current flat plate module.

In Figure 7.78 it can be seen that there is not much difference in the permeate flux profiles obtained along a 60 mm channel. Initially, the Level Three case produces a higher flux, but overall the Level Four case does manage to produce better fluxes. If the channel length were extended then the difference between the two modules would become apparent. This is because at the end of the current channel length, the difference between the two modules is increasing.

Looking at another set of conditions, the Level Four analysis produces a more definite result. Again, in the initial distance of the channel, the Level Three case produces higher fluxes, but after 28 mm the Level Four case is better. At these conditions, the flux has

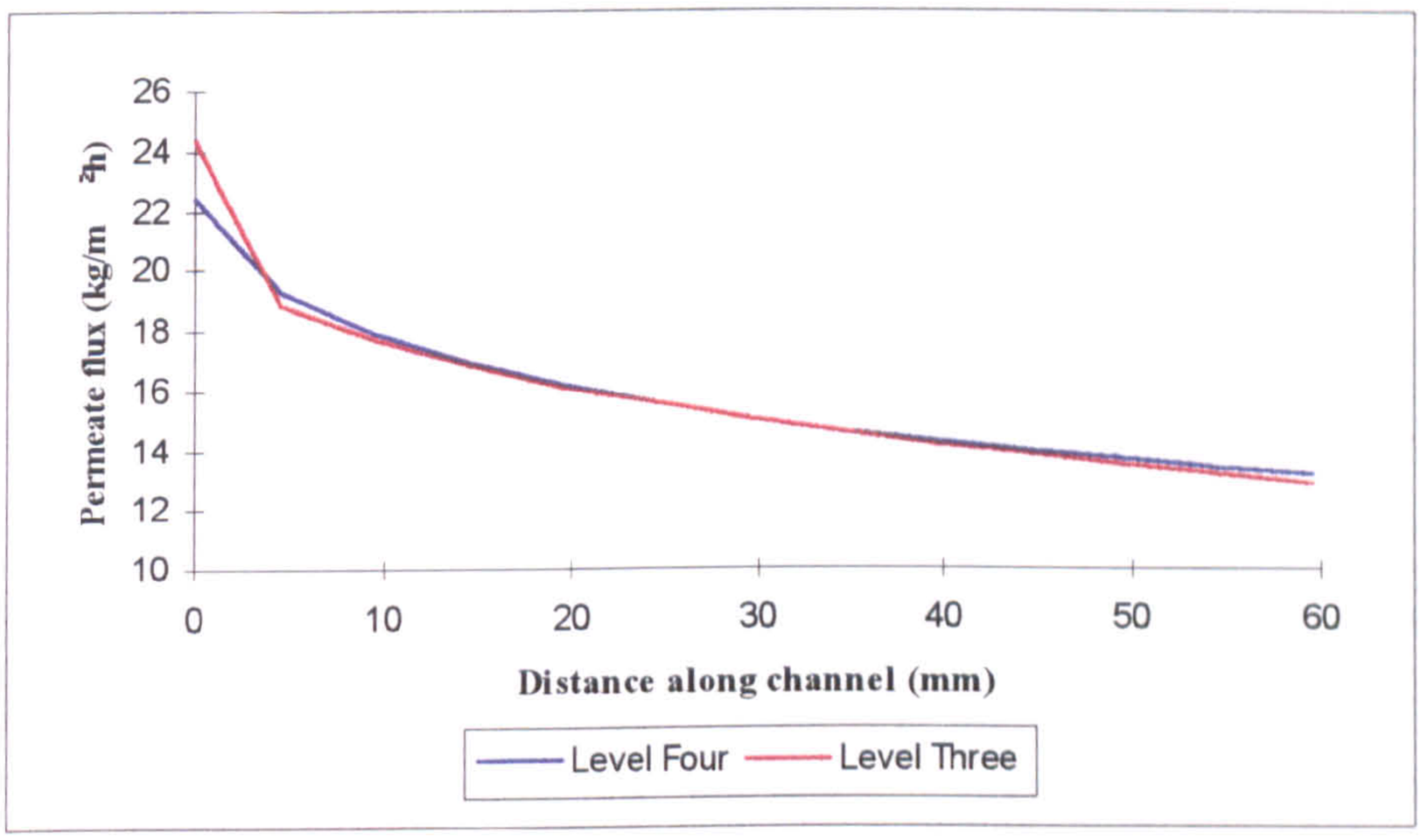

Figure 7.78: Comparison of permeate flux between insulated wall assumption and wall heat transfer ($Y = 0.45$ mm, $v = 0.2$ m/s, $T_H = 353$ K, $T_C = 285$ K)

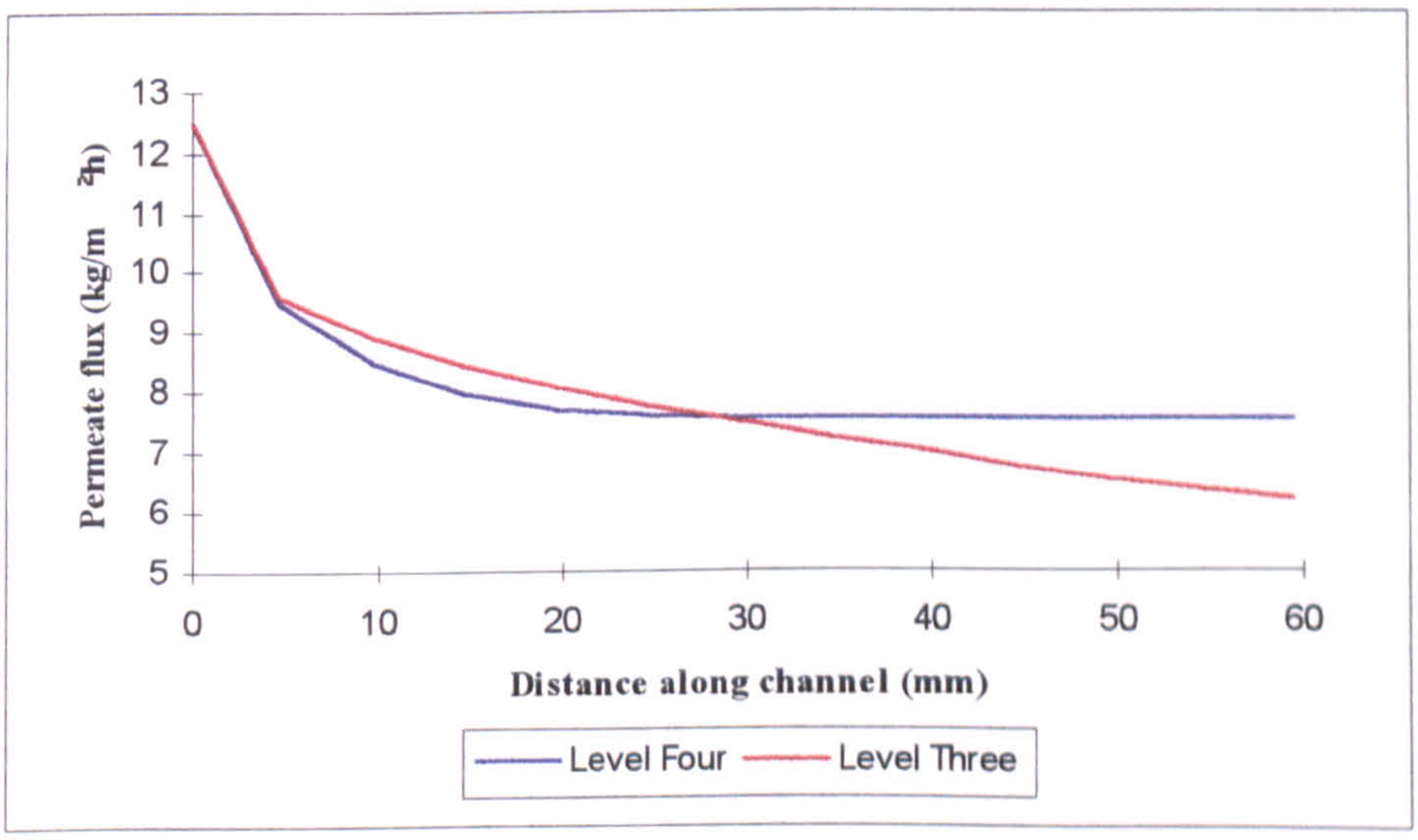

Figure 7.79: Comparison of permeate flux between insulated wall assumption and wall heat transfer ($Y = 0.45$ mm, $v = 0.1$ m/s, $T_H = 333$ K, $T_C = 285$ K)

reached a permanent value for the Level Four case, as explained earlier for Figure 7.73, whilst the Level Three values continue to fall. It is much easier to see in this analysis that using boiling and condensing heat transfer at the channel walls improves and stabilises the performance of membrane distillation in flat plate modules.

In summary for this Level of the boundary layer analysis, introducing boiling and condensing heat transfer at the channel walls complicates the analysis. In the entrance region there are two more boundary layers to model. The entrance region is much shorter than for a simple flat plate channel, and the temperatures of the feed and permeate are less affected by the membrane distillation. This causes lower drops in the driving force temperature difference over the length of the channel. Under some conditions the temperatures, and hence the permeate flux, reach equilibrium and so increasing the channel length would not decrease the permeate flux further. To maximise the flux, a module should utilise large velocities and very small channel heights. Comparing a simple module with a module incorporating boiling and condensing heat transfer, the second module produces better fluxes which become prominent in longer channels. Unfortunately the second module would cost more because of the boiling/condensing circuit so would only be suitable for cases where the module would produce much higher and constant fluxes.

CHAPTER 8

CONCLUSION

8.1 Conclusions

Membrane distillation is a process which utilises a temperature induced vapour pressure difference to transport vapour through a porous hydrophobic membrane. The membrane acts only as a surface for vapour-liquid interfaces to exist.

This work has been concerned with the understanding and modelling of membrane distillation in a flat plate module. The conclusions reached from the four distinct parts of work carried out are outlined below.

From the experimental determination of the basic performance of the module, it was found that;

- the permeate flux increased with increasing flow rate,
- it was advantageous to keep the pressure drop over the module to a minimum, to maintain the vapour pressure difference across the membrane.

Maintaining a low pressure drop over the module was accomplished in this work by increasing the main channel width, and introducing minor channels across the plates between the main channels.

The second study was concerned with the flow distribution model. This utilised flow and pressure relationships to investigate the way in which the flow was distributed through the module. It was found that;

- the pressure drop over the module was increased by increasing the flow rate,
- reducing the surface area of the membrane, produced higher pressure drops again due to increased flow rate,
- the pressure drop, and therefore flow rate, was highest at the main inlet and outlet of the module,
- the experimental module was shown to have good flow distribution.

The work up to this point was concerned with understanding the basics of membrane distillation and the module characteristics. Once these had been established, the next step was to model membrane distillation in order to allow the prediction of the permeate flux. Using the model developed, the following were determined;

- the model accurately predicted both heat and mass transfer,
- increasing the mean membrane temperature was more effective at increasing the permeate flux than increasing the temperature difference over the membrane,
- decreasing the channel height reduced the effect of temperature polarisation, and consequently increased the permeate flux,
- the largest fluxes for membrane distillation were obtained when using PTFE membranes, which agreed with the findings of other researchers working in this area,
- PVDF membranes also resulted in acceptable fluxes, and was used throughout this work,
- Versapor, had never been tested for use in membrane distillation. It was concluded that this membrane was not suitable due to inconsistent experimental results.

The main part of this work was concerned with modelling thermal boundary layers to study temperature polarisation in a flat plate module. The findings were;

- as the velocity of the liquid streams were increased, the length of the entrance region increased. This had the effect of decreasing the temperature difference over the channel,
- increasing the channel height also decreased the temperature drop over the channel,
- in the constant boundary layer region, the reduction in the temperature difference driving force over the module was linear This was shown to seriously affect the final outlet temperatures,
- when the entrance region almost equalled the channel length, then increasing the velocity did not alter the reduction in the temperature difference any further.

Two different velocity profiles were assumed. The first was a plug flow velocity profile (Level One), and the second was a laminar profile (Level Two). Comparing the two profiles;

- the laminar thermal boundary layer developed faster than the plug flow boundary layer,
- the temperature drop over the channel was lower for the laminar profile,

For the laminar profile, the boundary layer equations were linked to the velocity profile. For situations where the velocities either side of the membrane were different, the Level Three model showed that the temperature reduction over the module lay between the profiles obtained with equal velocities. There was a fluctuation in the temperature profile when the entrance region on the feed side developed more rapidly than the permeate side. This was because the differential equations were developed using a third order temperature profile. The model was therefore forced to adjust the temperatures to maintain the heat and mass transfer across the membrane.

The main findings from this model were that;

- increasing the entrance length decreased the temperature drop over the channel,

the final outlet temperatures of feed and permeate depended on the liquid velocity, channel height, and the initial temperature difference between feed and permeate.

The next stage of this work forged the membrane distillation and the boundary layer analysis models together. The two models were linked to provide a more complete and detailed understanding of membrane distillation. The results from this linked model were;

- the permeate flux along the channel decreased with decreasing temperature difference,
- increasing the velocity decreased the reduction in flux over the channel,
- increasing the channel height decreased the reduction in flux over the channel.

These results were due to the length where the boundary layer was still growing, being increased.

The linked model also provided an unexpected development. It was thought previously, that decreasing the channel height would always increase the flux due to a reduction in temperature polarisation. However, it was shown in this work that for a specific velocity, there was an optimum channel height which produced the maximum possible flux. Decreasing the channel height beyond this optimum height was more detrimental than increasing it beyond the optimum height. Due to the relationship between the velocity profile and the thermal boundary layer, increasing the liquid velocity increased the maximum possible flux. At the same time, increasing the velocity decreased the channel height at which the maximum flux was obtained.

The final level of the boundary layer analysis model introduced boiling and condensing heat transfer at the channel walls. The entrance region was found to be much shorter than for a simple flat plate channel, and the temperatures of the feed and permeate were less affected by the process of membrane distillation. This resulted in a reduction in the rate at which the driving force temperature difference decreased over the length of the channel. Under some conditions, the temperatures, and hence the permeate flux, reached equilibrium and so increasing the channel length did not result in any further decrease in the permeate flux. To maximise the flux, a module should utilise large velocities and optimum channel heights. Comparing a simple module, with a module incorporating boiling and condensing heat transfer, the latter module was shown to produce better

fluxes, which become prominent in longer channels. Unfortunately, such a module would cost more because of the boiling/condensing circuit which needs to be included. This means that it would only be suitable for cases where the module would be required to produce much higher, and consistant fluxes.

In summary, to enhance the performance of membrane distillation in flat plate modules, the following factors must be included in the design considerations;

- small channel heights and larger velocities should be utilised,
- the reduction in driving force temperature difference along the module should be minimised,
- the optimum channel height at specific operating conditions should be determined.
- the region where boundary layers are still growing should be increased by increasing the channel height and velocity,
- large temperature differences across the membrane, and hotter membrane temperatures should be used,
- good flow distribution should be ensured, keeping the pressure drop low, by modifying flat plate geometries,
- boiling and condensing surfaces should be used.

8.2 Further Work

This work has highlighted areas that could benefit from further study. These are outlined below.

- Further study is required in order to provide a more flexible temperature profile in the boundary layer analysis model to remove the 'glitch' when changing from the entrance, to constant region equations, and to introduce a concentration boundary

layer. This would enable the model to be applied to actual liquids and to study the joint effect of temperature and concentration polarisation.

- The Flow Distribution model could be linked to the membrane distillation and Boundary Layer Analysis to provide a 3D graph to accurately observe the temperature and flux profiles through a module. This would lead to the ability to evaluate more complex geometries.
- A module should be designed and constructed that utilises boiling and condensing surfaces to help maintain the temperature difference along the module as supported by Level Four of the boundary layer analysis model in this work. Linked to this would be an economic analysis to provide data concerning the viability of such a module.

NOMENCLATURE

A	membrane surface area	m^2
b	boundary layer thickness	m
B	net non-isothermal coefficient	-
B′	global non-isothermal coefficient	-
c	concentration	kg/m^3
C	membrane mass transfer coefficient	kg/m^2sPa
C_p	specific heat	J/kg K
d	diameter	m
D	diffusion coefficient	m^2/s
e	distillation efficiency	-
E	membrane transfer coefficient	W/m^2
Eu	Euler Number	-
F	transfer fraction	-
g	gravity constant	m/s^2
G	Heat transfer coefficient	W/m^2 K
h	heat transfer coefficient	W/m^2 K
H	overall heat transfer coefficient	W/m^2 K
i	Taylor series expansion coefficient	-
I	Loss coefficient	-
J	Heat transfer coefficient	W/m^2 K
k	thermal conductivity	W/m K
K	constant in equation (2.54)	m^3/kg
l	length	m
L	momentum flux	kg/m s^2
m	mass flow rate	kg/s
M	molecular weight	kg/mol
N	mass flux	kg/m^2s

P	pressure	Pa
P^o	vapour pressure	Pa
q	volumetric flow rate	m^3/s
Q	heat transfer rate	W/m^2 K
r	membrane pore radius	m
R	gas constant	J/molK
Re	Reynolds Number	-
S	flow rate	ml/min
T	temperature	K
U	wall coefficient	W/m^2
v	velocity	m/s
V	volume	m^3
w	width	m
W	adjustment factor	-
X	adjustment factor	-
x	mole fraction	-
y	co-ordinate perpendicular to membrane	m
Y	channel height	m
Y_{ln}	mol fraction of air (log mean)	-
z	physical distance	m
Z	membrane hydraulic resistance	Pa s/m
β	dimensionless channel distance	-
χ	tortuosity factor	-
δ	membrane thickness	m
ε	porosity	-
ϕ	contact angle	^{o}
γ	factor in equation (2.25)	-
η	dimensionless channel distance	-
λ	latent heat of vapourisation	J/kg

ν	kinematic viscosity	m^2/s
μ	viscosity	Pa s
Π	osmotic pressure	Pa
θ	dimensionless channel distance	-
ρ	density	kg/m^3
σ	surface tension	N/m
ϖ	stirring rate	rpm

Subscripts

B	bulk
c	conduction
C	cold bulk
d	critical
e	entrance
f	flux
g	gas
h	hydraulic
H	hot bulk
i	initial value
K	Knudsen flow
l	laminar
L	solvent
m	membrane
mc	main channel
p	pore
P	Pouseuille flow
s	solid
sg	spacer gap
t	tangential

tp	tangential profile
v	latent heat
w	water
x	axial
Y	co-ordinate perpendicular to membrane
ϖ	with stirring
1	interfacial hot side
0	interfacial cold side

REFERENCES

1 ***Microporous membranes in membrane distillation***
Drioli, E., Calabro, V., Wu, Y.
Pure and Applied Chemistry, 1986, **58**(12), 1657 - 1662

2 ***Transport mode of membrane distillation process and the VMD method to determine the membrane configurational number***
Xu, S.C., Wang, Y.X., Wang, S.C.
Journal of Membrane Science, Dec 1994, **97**, 1 - 6

3 ***Heat and mass transfer in membrane distillation***
Schofield, R.W., Fane, A.G., Fell, C.J.D.
Journal of Membrane Science, 1987, **33**, 299 - 313

4 ***Non-isothermal water transport through hydrophobic membranes in a stirred cell***
Vazquez-Gonzalez, M.I., Martinez, L.
Separation Science and Technology, 1994, **29**(15), 1957 - 1966

5 ***Factors affecting flux in membrane distillation***
Schofield, R.W., Fane, A.G., Fell, C.J.D., Macoun, R.G.
Desalination, Mar. 1990, **77**(1-3), 279 - 294

6 ***Treatment of wastewater for removing heavy metals by membrane distillation***
Zotolarev, P.P., Ugrozov, V.V., Volkina, I.B., Nikulin, V.N.
Journal of Hazardous Materials, Apr. 1994. **37**(1), 77-82

7 ***Gas and vapour transport through microporous membranes I: Knudsen - Poiseuille transition***
Schofield, R.W., Fane, A.G., Fell, C.J.D.
Journal of Membrane Science, Oct. 1990, **53**(1-2), 159 - 171

8 ***Theoretical and experimental study on membrane distillation in the concentration of orange juice***
Calabro, V., Jiao, B.L., Drioli, E.
Industrial and Engineering Chemistry Research, 1994, **33**, 1803 - 1808

9 ***Non-isothermal solute transport through PTFE membranes.***
Ortiz de Zarate, J. M., Velazquez, A., Pena, L., Garcia-Lopez, F., Mengual, J. I.
Journal of Membrane Science, Apr. 24 1992, **69**(1-2), 169-178

10 *Wetting criteria for the applicability of membrane distillation*
Franken, A.C.M., Nolten, J.A.M., Mulder, M.H.V., Bargeman, D., Smolders, C.A.
Journal of Membrane Science, Oct. 1987, **33**(3), 315 - 328

11 *Membrane distillation in the textile wastewater treatment.*
Calabro,V., Drioli, E., Matera, F.
Desalination, Sept. 1991, **83**(1-3), 209-224

12 *Study of the concentration of acids by membrane distillation*
Tomaszewska, M., Gryta, M., Morawski, A.W.
Journal of Membrane Science **102**, 1995, 113 - 122

13 *Temperature polarisation coefficients in membrane distillation*
Velazquez, A., Mengual, J.I.
Industrial Engineering Chemistry Research, 1995, **34**(2), 585 - 590

14 *Membrane distillation in the treatment of aqueous solutions*
Drioli, E., Wu, Y., Calabro, V.
Journal of Membrane Science, 1987, **33**, 277 - 284

15 *Non- isothermal water transport through membranes*
Ortiz-Zarate, J.M., Garcia Lopez, F., Mengual, J.I.
Journal of Membrane Science, Feb. 15 1991, **56**(2), 181 - 194

16 *Gas and vapour transport through microporous membranes II: Membrane distillation*
Schofield, R.W., Fane, A.G., Fell, C.J.D.
Journal of Membrane Science, Oct. 1990, **53**(1-2), 173 - 185

17 *The efficient use of energy in membrane distillation*
Fane, A.G., Schofield, R.W., Fell, C.J.D.
Desalination, 1987, **64**, 231-243

18 *The behaviour of membrane distillation of concentrated aqueous solution*
Wu, Y., Drioli, E.
Water Treatment, Oct. 1989, 4(4), 399 - 415

19 *Separation of liquid mixtures by membrane distillation*
Gostoli, C., Sarti, G.C.
Journal of Membrane Science, Feb. 1989, **41**, 211 - 224

20 ***Membrane Distillation - a theoretical study of evaporation through microporous membranes***
Jonsson, A.S., Wimmerstedt, R., Harrysson, A.C.
Desalination, 1985, **56**, 237 - 249

21 ***Membrane distillation - an assessment***
Hanbury, W.T., Hodgkiess, T.
Desalination, 1985, **56**, 287 - 297

22 ***Analytical method for calculating the process of contact membrane distillation in a flow-through membrane module***
Ugrozov, V.V., Nikulin, V.N., Elkina, I.B., Zolotarev, P.P.
Theoretical Foundations of Chmeical Engineering, 1995, **29**(6), 535 - 540

23 ***Influence of temperature polarisation on separation by membrane distillation***
Ortiz de Zarate, J.M., Velazuquez, A., Pena, L., Mengual, J.I.
Separation Science and Technology , May 1993, **28**(7), 1421 - 1436

24 ***Modelling and calculation of temperature-concentration polarisation in the membrane distillation process (MD)***
Agashichev, S., Sivakov, A.V.
Desalination, Aug. 1993, **93**(1-3), 245-258

25 ***Multistage process of deuterium and heavy oxygen enrichment by membrane distillation***
Chmielewski, A.G., Zakrzewska-Trznadel, G.
Separaton Science and Technology, 1997, **32**(1-4), 527 - 539

26 ***Parameters that may influence the correction factor in membranes subjected to thermal gradients***
Vazquez-Gonzalez, M.I., Serrano, F.
Separation Science and Technology, Jul.1992, **27**(8-9), 1115-1123

27 ***Terminology for membrane distillation***
Smolders, K., Franken, A.C.M.
Desalination, Dec. 1989, **72**(3), 249 - 262

28 ***Experiments on seawater desalination by membrane distillation***
Ohta, K., Kikuchi, K., Hayano, I., Okabe, T., Goto, T., Kimura, S., Ohya, H.
Desalination, Aug. 1990, **78**(2), 177 - 185

29 ***Membrane distillation with fluro-carbon membranes***
Otha, K., Hayano, I., Okabe, T., Goto, T., Kimura, S., Ohya, H.
Desalination, Jul. 1994, **81**(1-3), 107 - 115

30 *Characterisation of membrane distillation membranes prepared by phase inversion*
Ortiz de Zarate, J.M., Pena, L. Mengual, J.I.
Desalination, 1995, **100**(1-3), 139 - 148

31 *Preparation and properties of flat sheet membranes from PVDF for membrane distillation*
Tomaszewska, M.
Desalination, 1996, **104**(1-2), 1-11

32 *Surface modified hydrophilic membranes in membrane distillation*
Wu, Y., Kong, Y., Lin, X., Liu, W., Xu, J.
Journal of Membrane Science, 1992, **72**, 189 - 196

33 *Separation of mineral acids by temperature driven membrane processes*
Elkina, I.B., Ugrozov, V.V., Gilman, A.B., Nikulin, V.N., Volkov, V.V.
Euromembrane '97, University of Twente, The Netherlands, 1997, 341

34 *Osmotic distillation - a low temperature concentration technique*
Johnson, R.A., Valks, R.H., Lefebvre, M.S.
Australian Journal of Biotechnology, July 1989, **3**(3), 215 - 217

35 *Steady state in membrane distillation : influence of membrane wetting*
Pena, L., Ortiz de Zarate, J.M., Mengual, J.I.
J. Chem Soc., Faraday Trans., 21 Dec. 1993, **89**(24), 4333-4338

36 *Low energy cost desalination processes using hydrophobic membranes*
Sarti, G.C., Gostoli, C., Matulli, S.
Desalination, 1985, **56**, 277 - 286

37 *Membrane distillation: Theory and experiments*
Godino, P., Pena, L., Mengual, J.I.
Journal of Membrane Science, 1996, **121**, 83 - 93

38 *Low temperature distillation through hydrophobic membranes*
Gostoli, C., Sarti, G.C., Matulli, S.
Separation Science and Technology, Feb - Mar 1987, **22**(2-3), 855 - 872

39 *Concentration of the extraction fluid from sulphuric acid treatment of phosphogypsum by membrane distillation*
Tomaszewska, M.
Journal of Membrane Science, Apr. 1993, **78**(3), 277 - 282

40 ***Reducing boundary layer effects in membrane osmotic distillation***
Vahdati, M.M., Priestman, G.H.
IChemE 1994 Research Event

41 ***Transport phenomena in membrane distillation***
Kimura, S., Nakao, S.
Journal of Membrane Science, Oct. 1987, **33**(3), 285 - 298

42 ***Azeotropic mixtures may be broken by membrane distillation***
Udriot, H. Araque, A., on Stockar, U.
The Chem. Eng. Journal, 1994, **54**(2), 87 - 93

43 ***Membranes and modules for transmembrane distillation***
Schneider, K., Holz, W. Wollbeck, R.
Journal of Membrane Science, 1988, **39**, 25 -42

44 ***Non-isothermal mass transport of organic aqueous solution in hydrophobic porous membrane***
Honda, Z., Komada, H., Okamoto, K., Kai, M.
Separation Science and Technology, 587 - 594

45 ***An Experimental study on membrane distillation crystallisation for treating waste water in taurine production***
Wu, Y., Kong, Y., Liu, J., Zhang, J., Xu, J.
Desalination, May 1991, **80**(2-3), 235 - 242

46 ***An energy efficient membrane distillation process***
Van Gassel, T.J., Schneider, K.
Separation Science and Technology , 343 - 348

47 ***Developments in membrane distillation***
Schofield, R.W., Hogan, P.A., Fane, A.G., Fell, C.J.D.
Desalination, 1987, **62**, 1987, 728 - 729

48 ***Desalination by solar heated membrane distillation***
Hogan, P.A., Sudjito, Fane, A.G., Morrison, G.L.
Desalination, Jul. 1991, **81**(1-3), 81 - 90

49 ***Membrane distillation***
Lawson, K.W., Lloyd, D.R.
Journal of Membrane Science, 1997, **124**, 1 - 25

50 ***An influence of salt in solutions on hydrochloric acid recovery by membrane distillation***
Tomaszewska, M
Euromembrane '97, University of Twente, The Netherlands, 1997, 320-322

51 ***Concentration of fluosilicic acid liquor by membrane distillation***
Tomaszewska, M
Euromembrane '97, University of Twente, The Netherlands, 1997, 360

52 ***Non-linear fluxes in membrane distillation of water-ethylene glycol mixtures***
Rincon, C., Jansa, B., Ortiz de Zarate, J.M., Mengual, J.I.
Euromembrane '97, University of Twente, The Netherlands, 1997, 357

53 ***Selectivity and characteristics of direct contact membrane distillation type experiment I. Permeability and selectivity through dried hydrophobic fine porous membranes***
Fujii, Y., Kigoshi, S. Iwatani, H., Aoyama, M.
Journal of Membrane Science, 1992, **72**, 53 - 72

54 ***Osmotic distillation through porous hydrophobic membranes***
Mengual, J.I., Ortiz de Zarate, J.M., Pena, L., Velasquez, A.
Journal of Membrane Science, Jul 15 1993, **82**(1-2), 129-140

55 ***Compaction of microporous membranes used in membrane distillation. I. Effect on gas permeability***
Lawson, K.W., Hall, M.S., Lloyd, D.R.
Journal of Membrane Science, 1995, **101**, 99 - 108

56 ***Method of performing osmotic distillation***
Lefebvre, M.S.M.
United States Patent, 1988, **4,781,837**

57 ***Mass and heat transfer mechanisms in the osmotic distillation process***
Sheng, J., Johnson, R.A., Lefebvre, M.S.
Desalination, May 1991, **80**(2-3), 113 - 121

58 ***Osmotic evaporation through macroporous hydrophobic membranes: A survey of current research and applications***
Kunz, W., Benhabiles, A., Ben-Aim, R.
Journal of Membrane Science, 1996, **121**, 25 - 36

59 ***Osmotic distillation***
Uniersity of Bath
Membrane Applications Centre

60 ***Hydrophobic membrane evaluation and cleaning for osmotic distillation of tomato puree***
Durham, R.J., Nguyen, M.H.
Journal of Membrane Science, Feb 23 1994, **87**(1-2), 181-189

61 ***The application of osmotic distillation for the wine industry***
Thompson, D.
Australian Grapegrower and Winemaker, 1991, **328**, 11 - 13

62 ***Fluid mechanics in membrane filtration: Recent developments***
Belfort, G.
Journal of Membrane Science, 1989, **40**, 123 - 147

63 ***Laminar flow in channels with porous walls***
Berman, A.S.
Journal of Applied Physics, Sept. 1953, **24**(9), 1232-1235

64 ***Concentration polarisation in reverse osmosis desalination with variable flux and incomplete salt rejection***
Brian, P.L.T.
Industrial Engineering Chemistry Fundamentals, **4**, 1965, 439-445

65 ***Laminar dilute suspension flows in plate and frame ultrafiltration units***
Kleinstreuer, K., Paller, S.
AIChE Journal, 29, 1983, 529-533

66 ***Modelling of ultrafiltration: predictions of concentration polarisation effects***
Bouchard, C.R., Carreau, P.J., Matsuura, T., Sourirajan, S.
Journal of Membrane Science, Dec. 1994, **97**, 215 - 229

67 ***Laminar flow in channels with porous walls***
Granger, J., Dodds, J., Midoux,N.
Chem. Eng. J. (Lausanne), Dec. 1989, **42**(3), 193 - 204

68 ***Ultrafiltration of macromolecular solutions at high polarisation in laminar channel flow***
Probstein, R.F., Shen, J.S., Leung, W.F.
Desalination, 1978, **24**, 1-16

69 ***Conjugate Leveque solution for Newtonian fluid in a parallel plate channel***
Lee, W.C., Ju, Y.H.
International Journal of Heat and Mass Transfer, 1986, **29**(6), 941 - 947

70 ***The effect of buoyancy on laminar flow and heat transfer in the entrance region between horizontal parallel plates***
Naito, E.
International Chemical Engineer, 1985, **25**(2), 315 - 323

71 ***Effects of concentration boundary layer development on the flux limitations in ultrafiltration***
Aimar, P., Howell, J.A., Turner, M.
Chemical Engineering Reasearch and Design, 1989, **67**, 255-261

72 ***Calculation of the entrance length of the concentration boundary layer in ultrafiltration and its influence on scale-up***
Wu, D., Howell, J.A.
Journal of Membrane Science, 1992, **74**, 37 - 49

73 ***Numerical study of the fluid dynamics and mass transfer of an ultrafiltration performance in a tube membrane module***
Kotzev, T.
International Journal of Engineering Science, Feb. 1994, **32**(2), 359-368

74 ***Fluid dynamics in a tubular membrane: Theory and experiment***
Mellis, R., Gill, W. N., Belfort, G.
Chemical Engineering Communications, 1993, **122**, 103-125

75 ***Membrane modules: comparison of different configurations using fluid mechanics***
Belfort, G.
Journal of Membrane Science, 1988, **35**, 245 - 270

76 ***Description of fluid flow through spacers in flat channel filtration systems***
Geissler, S., Heits, H., Werner, U.
Filtration and Separation, 1995, **32**(6), 530 - 544

77 ***The role of turbulence promoters in hyperfiltration plant optimisation***
Thomas, D.G., Griffith, W.L., Keller, R.M.
Desalination, 1971, **9**, 33-50

78 ***Mass transfer in narrow channels in the presence of turbulence promoters***
Winograd, Y., Solan, A., Toren, M.
Desalination, 1973, **13**, 171-186

79 ***Optimal channel spacer design for ultrafiltration***
Da Costa, A.R., Fane, A.G., Fell, C.J.D., Franken, A.C.M.
Journal of Membrane Science, 1991, **62**, 275 - 291

80 *Membrane filtration with self-cleaning spiral vortices*
Mallubhotla, H., Luque, S., Belfort, G.
Euromembrane '97, University of Twente, The Netherlands, 1997, 385-387

81 *Flux enhancement by reduction of concentration polarisation due to secondary flow in twisted membrane tubes*
Ophoff, J., Vos, G.S., Racz, I.G., Reith, T.
Euromembrane '97, University of Twente, The Netherlands, 1997, 400-402

82 *An effect of vortex flow on fluxes in ultrafiltration plate-frame modules*
Kaminski, W., Stawczyk, J.
Journal of Membrane Science, 1997, **123**, 157-164

83 *Enhancement of UF with flat sheet membrane modules by gas sparging*
Li, Q.Y., Ghosh, R., Cui, Z.F., Pepper, D.S.
Euromembrane '97, University of Twente, The Netherlands, 1997, 92-94

84 *Flux enhancement by air slug flow in ultrafiltration hollow fibres - hydrodynamics characterisation*
Laborie, S., Cabassud, C., Laine, J.M., Durand-Bourlier, L.
Euromembrane '97, University of Twente, The Netherlands, 1997, 406-408

85 *Investigation of the flow dynamics at the surface of a flat membrane element*
Dubinskii, G.Ya., Kote, A.A., Chernyako, I.E., Noitskii, E.G.
Chemical and Petroleum Engineering, Nov. 1991, **27**(3-4), 130-134

86 *Developments in membrane and osmotic distillation*
Vahdati, M.M; Priestman, G.H.
New Directions in Distillation and Absorption meeting, IChemE Fluid Separation Processes Group, 3rd November 1993, Sheffield.

87 *Internal Flow Systems*
Miller, D.S.
1990, 2nd Edition, BHRA

88 *Perry's Chemical Engineers Handbook*
Perry, R.H., Green, D.W.
1984, 6th Edition, McGraw-Hill, London

89 *Boundary Layer Theory*
Schlichting, H.
1979, 7th Edition, McGraw-Hill, New York

90 ***Mathematical Methods in Chemical Engineering***
Jenson, V.G., Jeffreys, G.V.
1981, 2nd Edition, Academic Press, London

91 ***Chemical Engineering Volume VI - Design***
Coulson, J.M., Richardson, J.F., Sinnott, R.K.
1991, 1st Edition, Pergamon Press, Oxford

APPENDICIES

APPENDIX A

Development of the Boundary Layer Equations: Level One

1. Boundary layer growing, hot side

Third Order Temperature Profile:

$$T = a_0 + a_1 y + a_2 y^2 + a_3 y^3 \qquad \text{(A1)}$$

differentiating,

$$\frac{dT}{dy} = a_1 + 2a_2 y + 3a_3 y^2 \qquad \text{(A2)}$$

Boundary conditions;

@ $y = b_1$	$T = T_{01}$	$dT/dy = 0$
@ $y = 0$	$T = T_1$	$dT/dy = E(T_1-T_3)/k$

Using equation (A1),

@ $y = 0$	$T_1 = a_0$
@ $y = b_1$	$T_{01} = a_0 + a_1 b_1 + a_2 b_1^2 + a_3 b_1^3$

Using equation (A2),

@ $y = 0$	$\frac{E}{k}(T_1 - T_3) = a_1$
@ $y = b_1$	$0 = a_1 + 2a_2 b_1 + 3a_3 b_1^2$

Solving for terms,

$$a_2 = \frac{3(T_{01} - T_1)}{b_1^2} - \frac{2E(T_1 - T_3)}{kb_1} \qquad a_3 = \frac{E(T_1 - T_3)}{kb_1^2} - \frac{2(T_{01} - T_1)}{b_1^3}$$

Substituting terms into equation (A1),

$$\boxed{T = T_1 + \frac{E(T_1 - T_3)}{k} y + \left[\frac{3(T_{01} - T_1)}{b_1^{\,2}} - \frac{2E(T_1 - T_3)}{kb_1}\right] y^2 + \left[\frac{E(T_1 - T_3)}{kb_1^{\,2}} - \frac{2(T_{01} - T_1)}{b_1^{\,3}}\right] y^3} \qquad \text{(A3)}$$

Enthalpy Balance

From Chapter 5.2, the enthalpy balance is,

$$\text{Convection In} + \text{Condutcion In} = \text{Convection Out} + \text{Conduction Out} \qquad \text{(A4)}$$

where, Convection In, when the boundary layer is growing, is given by,

$$Q_{cvi} = \int_{y=0}^{y=b} C_p \rho v T \, dy + \delta x C_p T(y) \frac{d}{dx} \int_{y=0}^{y=b} \rho v \, dy \qquad \text{(A5)}$$

Convection Out, is

$$Q_{cvo} = \int_{y=0}^{y=b} C_p \rho v T \, dy + \delta x \frac{d}{dx} \int_{y=0}^{y=b} C_p \rho v T \, dy \qquad \text{(A6)}$$

the Conduction In is,

$$Q_{cni} = -\delta x \, E(T_1 - T_3) \qquad \text{(A7)}$$

and the Conduction Out is,

$$Q_{cno} = -\delta x \, k \left.\frac{dT}{dy}\right|_{y=b} \qquad \text{(A8)}$$

Forming the enthalpy balance for the entrance region at $y = b_1$,

$$\int_{y=0}^{y=b_1} C_p \rho v T \, dy + \delta x C_p T(y) \frac{d}{dx} \int_{y=0}^{y=b_1} \rho v \, dy - \delta x E(T_1 - T_3) = \int_{y=0}^{y=b_1} C_p \rho v T \, dy + \delta x \frac{d}{dx} \int_{y=0}^{y=b_1} C_p \rho v T \, dy + 0$$

which reduces to,

$$\boxed{C_p \rho v \int_{y=0}^{y=b_1} \big(T - T(y)\big) \, dy + E(T_1 - T_3) = 0} \qquad \text{(A9)}$$

Equation Development

Using the temperature profile, equation (A3), and that @ $y = b_1$, $T(y) = T_{01}$,

$$T - T(y) = T_1 - T_{01} + \frac{E(T_1 - T_3)}{k}y + \left[\frac{3(T_{01} - T_1)}{b_1^2} - \frac{2E(T_1 - T_3)}{kb_1}\right]y^2 + \left[\frac{E(T_1 - T_3)}{kb_1^2} - \frac{2(T_{01} - T_1)}{b_1^3}\right]y^3$$

$$\int_{y=0}^{y=b_1}(T - T(y))dy = \left[T_1 y - T_{01}y + \frac{E(T_1 - T_3)y^2}{2k} + \frac{3(T_{01} - T_1)y^3}{3b_1^2} - \frac{2E(T_1 - T_3)y^3}{3kb_1} + \frac{E(T_1 - T_3)y^4}{4kb_1^2} - \frac{2(T_{01} - T_1)y^4}{4b_1^3}\right]_0^{b_1}$$

$$\int_{y=0}^{y=b_1}(T - T(y))dy = T_1 b_1 - T_{01}b_1 + \frac{E(T_1 - T_3)b_1^2}{2k} + \frac{(T_{01} - T_1)b_1^3}{b_1^2} - \frac{2E(T_1 - T_3)b_1^3}{3kb_1} + \frac{E(T_1 - T_3)b_1^4}{4kb_1^2} - \frac{(T_{01} - T_1)b_1^4}{2b_1^3}$$

$$\int_{y=0}^{y=b_1}(T - T(y))dy = T_1 b_1 - T_{01}b_1 + \frac{ET_1 b_1^2}{2k} - \frac{ET_3 b_1^2}{2k} + T_{01}b_1 - T_1 b_1 - \frac{2ET_1 b_1^2}{3k} + \frac{2ET_3 b_1^2}{3k} + \frac{ET_1 b_1^4}{4kb_1^2} - \frac{ET_3 b_1^4}{4kb_1^2} - \frac{T_{01}b_1}{2} + \frac{T_1 b_1}{2}$$

$$\int_{y=0}^{y=b_1}(T - T(y))dy = \frac{ET_1 b_1^2}{2k} - \frac{ET_3 b_1^2}{2k} - \frac{2ET_1 b_1^2}{3k} + \frac{2ET_3 b_1^2}{3k} + \frac{ET_1 b_1^4}{4kb_1^2} - \frac{ET_3 b_1^4}{4kb_1^2} - \frac{T_{01}b_1}{2} + \frac{T_1 b_1}{2}$$

$$\int_{y=0}^{y=b_1}(T - T(y))dy = \frac{6ET_1 b_1^2}{12k} - \frac{8ET_1 b_1^2}{12k} + \frac{3ET_1 b_1^4}{12kb_1^2} - \frac{3ET_3 b_1^2}{12k} + \frac{8ET_3 b_1^2}{12k} - \frac{3ET_3 b_1^4}{12kb_1^2} - \frac{T_{01}b_1}{2} + \frac{T_1 b_1}{2}$$

$$\int_{y=0}^{y=b_1}(T - T(y))dy = \frac{ET_1 b_1^2}{12k} - \frac{ET_3 b_1^2}{12k} - \frac{T_{01}b_1}{2} + \frac{T_1 b_1}{2}$$

$$\frac{d}{dx}\int_{y=0}^{y=b_1}(T - T(y))dy = \frac{d}{dx}\left[\frac{ET_1 b_1^2}{12k} - \frac{ET_3 b_1^2}{12k} - \frac{T_{01}b_1}{2} + \frac{T_1 b_1}{2}\right]$$

$$\frac{d}{dx}\int_{y=0}^{y=b_1}(T - T(y))dy = \frac{Eb_1^2}{12k}\frac{dT_1}{dx} + \frac{2ET_1 b_1}{12k}\frac{db_1}{dx} - \frac{Eb_1^2}{12k}\frac{dT_3}{dx} - \frac{2ET_3 b_1}{12k}\frac{db_1}{dx} - \frac{T_{01}}{2}\frac{db_1}{dx} + \frac{b_1}{2}\frac{dT_1}{dx} + \frac{T_1}{2}\frac{db_1}{dx}$$

$$\frac{d}{dx}\int_{y=0}^{y=b_1}(T-T(y))dy=\left(\frac{ET_1b_1}{6k}-\frac{ET_3b_1}{6k}-\frac{T_{01}}{2}+\frac{T_1}{2}\right)\frac{db_1}{dx}+\left(\frac{Eb_1^2}{12k}+\frac{b_1}{2}\right)\frac{dT_1}{dx}-\frac{Eb_1^2}{12k}\frac{dT_3}{dx}$$

Therefore, substituting this result into equation (A9)

@ $y = b_1$

$$\boxed{C_p\rho v\left[\left(\frac{ET_1b_1}{6k}-\frac{ET_3b_1}{6k}-\frac{T_{01}}{2}+\frac{T_1}{2}\right)\frac{db_1}{dx}+\left(\frac{Eb_1^2}{12k}+\frac{b_1}{2}\right)\frac{dT_1}{dx}-\frac{Eb_1^2}{12k}\frac{dT_3}{dx}\right]+E(T_1-T_3)=0} \quad \text{(A10)}$$

Forming the second enthalpy balance for the entrance region, at $y = b_1/2$,

$$\int_{y=0}^{y=b_1/2}C_p\rho vT\,dy+\delta xC_pT(y)\frac{d}{dx}\int_{y=0}^{y=b_1/2}\rho v\,dy-\delta xE(T_1-T_3)$$

$$=\int_{y=0}^{y=b_1/2}C_p\rho vT\,dy+\delta x\frac{d}{dx}\int_{y=0}^{y=b_1/2}C_p\rho vT\,dy-\delta xk\left.\frac{dT}{dy}\right|_{y=b_1/2}$$

which reduces to,

$$\boxed{C_p\rho v\int_{y=0}^{y=b_1/2}(T-T(y))\,dy-k\left.\frac{dT}{dy}\right|_{y=b_1/2}+E(T_1-T_3)=0} \quad \text{(A11)}$$

Equation Development

Using the temperature profile, equation (A3),

@ $y = b_1/2$,

$$T(y)=T_1+\frac{E(T_1-T_3)b_1}{2k}+\left[\frac{3(T_{01}-T_1)}{b_1^2}-\frac{2E(T_1-T_3)}{kb_1}\right]\frac{b_1^2}{4}+\left[\frac{E(T_1-T_3)}{kb_1^2}-\frac{2(T_{01}-T_1)}{b_1^3}\right]\frac{b_1^3}{8}$$

$$T(y)=T_1+\frac{ET_1b_1}{2k}-\frac{ET_3b_1}{2k}+\frac{3T_{01}}{4}-\frac{3T_1}{4}-\frac{2Eb_1T_1}{4k}+\frac{2Eb_1T_3}{4k}+\frac{Eb_1T_1}{8k}-\frac{Eb_1T_1}{8k}-\frac{2T_{01}}{8}+\frac{2T_1}{8}$$

$$T(y)=\frac{4T_1}{4}+\frac{T_1}{4}-\frac{3T_1}{4}-\frac{T_{01}}{4}+\frac{3T_{01}}{4}+\frac{ET_1b_1}{2k}-\frac{Eb_1T_1}{2k}+\frac{Eb_1T_1}{8k}-\frac{ET_3b_1}{2k}+\frac{Eb_1T_3}{2k}-\frac{Eb_1T_3}{8k}$$

$$T(y)=\frac{T_1}{2}+\frac{T_{01}}{2}+\frac{Eb_1T_1}{8k}-\frac{Eb_1T_3}{8k}$$

so,

$$T-T(y)=T_1-T_{01}-\frac{T_1}{2}-\frac{T_{01}}{2}-\frac{Eb_1T_1}{8k}+\frac{Eb_1T_3}{8k}+\frac{E(T_1-T_3)}{k}y+\left[\frac{3(T_{01}-T_1)}{b_1^{\,2}}-\frac{2E(T_1-T_3)}{kb_1}\right]y^2$$
$$+\left[\frac{E(T_1-T_3)}{kb_1^{\,2}}-\frac{2(T_{01}-T_1)}{b_1^{\,3}}\right]y^3$$

$$\int_{y=0}^{y=b_1/2}(T-T(y))dy=\left[\frac{T_1y}{2}-\frac{T_{01}y}{2}-\frac{Eb_1T_1y}{8k}+\frac{Eb_1T_3y}{8k}+\frac{E(T_1-T_3)y^2}{2k}+\frac{3(T_{01}-T_1)y^3}{3b_1^{\,2}}\right.$$
$$\left.-\frac{2E(T_1-T_3)y^3}{3kb_1}+\frac{E(T_1-T_3)y^4}{4kb_1^{\,2}}-\frac{2(T_{01}-T_1)y^4}{4b_1^{\,3}}\right]_0^{b_1/2}$$

$$\int_{y=0}^{y=b_1/2}(T-T(y))dy=\frac{T_1b_1}{4}-\frac{T_{01}b_1}{4}-\frac{ET_1b_1^{\,2}}{16k}+\frac{ET_3b_1^{\,2}}{16k}+\frac{E(T_1-T_3)b_1^{\,2}}{8k}+\frac{(T_{01}-T_1)b_1^{\,3}}{8_1^{\,2}}$$
$$-\frac{2E(T_1-T_3)b_1^{\,3}}{24kb_1}+\frac{E(T_1-T_3)b_1^{\,4}}{64kb_1^{\,2}}-\frac{2(T_{01}-T_1)b_1^{\,4}}{64b_1^{\,3}}$$

$$\int_{y=0}^{y=b_1/2}(T-T(y))dy=\frac{T_1b_1}{4}-\frac{T_{01}b_1}{4}-\frac{ET_1b_1^{\,2}}{16k}+\frac{ET_3b_1^{\,2}}{16k}+\frac{ET_1b_1^{\,2}}{8k}-\frac{ET_3b_1^{\,2}}{8k}+\frac{T_{01}b_1}{8}-\frac{T_1b_1}{8}$$
$$-\frac{ET_1b_1^{\,2}}{12k}+\frac{ET_3b_1^{\,2}}{12k}+\frac{ET_1b_1^{\,2}}{64k}-\frac{ET_3b_1^{\,2}}{64k}-\frac{T_{01}b_1}{32}+\frac{T_1b_1}{32}$$

$$\int_{y=0}^{y=b_1/2}(T-T(y))dy=\frac{8T_1b_1}{32}-\frac{4T_1b_1}{32}+\frac{T_1b_1}{32}-\frac{8T_{01}b_1}{32}+\frac{4T_{01}b_1}{32}-\frac{T_{01}b_1}{32}-\frac{12ET_1b_1^{\,2}}{192k}+\frac{24ET_1b_1^{\,2}}{192k}$$
$$-\frac{16ET_1b_1^{\,2}}{192k}+\frac{3ET_1b_1^{\,2}}{192k}+\frac{12ET_3b_1^{\,2}}{192k}-\frac{24ET_3b_1^{\,2}}{192k}+\frac{16ET_3b_1^{\,2}}{192k}-\frac{3ET_3b_1^{\,2}}{192k}$$

$$\int_{y=0}^{y=b_1/2}(T-T(y))dy=\frac{5T_1b_1}{32}-\frac{5T_{01}b_1}{32}-\frac{ET_1b_1^{\,2}}{192k}-\frac{ET_3b_1^{\,2}}{192k}$$

$$\frac{d}{dx}\int_{y=0}^{y=b_1/2}(T-T(y))dy=\frac{d}{dx}\left[\frac{5T_1b_1}{32}-\frac{5T_{01}b_1}{32}-\frac{ET_1b_1^2}{192k}-\frac{ET_3b_1^2}{192k}\right]$$

$$\frac{d}{dx}\int_{y=0}^{y=b_1/2}(T-T(y))dy=\frac{5b_1}{32}\frac{dT_1}{dx}+\frac{5T_1}{32}\frac{db_1}{dx}-\frac{5T_{01}}{32}\frac{db_1}{dx}-\frac{Eb_1^2}{192k}\frac{dT_1}{dx}-\frac{2ET_1b_1}{192k}\frac{db_1}{dx}$$
$$+\frac{Eb_1^2}{192k}\frac{dT_3}{dx}+\frac{2ET_3b_1}{192k}\frac{db_1}{dx}$$

$$\frac{d}{dx}\int_{y=0}^{y=b_1/2}(T-T(y))dy=\left(\frac{5T_1}{32}-\frac{5T_{01}}{32}-\frac{2ET_1b_1}{192k}+\frac{2ET_3b_1}{192k}\right)\frac{db_1}{dx}+\left(\frac{5b_1}{32}-\frac{Eb_1^2}{192k}\right)\frac{dT_1}{dx}+\frac{Eb_1^2}{192k}\frac{dT_3}{dx}$$

Therefore, substituting this result into equation (A11)

@ $y = b_1/2$

$$C_p\rho v\left[\left(\frac{5T_1}{32}-\frac{5T_{01}}{32}-\frac{2ET_1b_1}{192k}+\frac{2ET_3b_1}{192k}\right)\frac{db_1}{dx}+\left(\frac{5b_1}{32}-\frac{Eb_1^2}{192k}\right)\frac{dT_1}{dx}+\frac{Eb_1^2}{192k}\frac{dT_3}{dx}\right]$$
$$-k\left.\frac{dT}{dy}\right|_{y=b_1/2}+E(T_1-T_3)=0 \qquad \text{(A12)}$$

Calculating the conduction out term,

From the temperature profile, equation (A3),

$$\frac{dT}{dy}=\frac{E(T_1-T_3)}{k}+2\left[\frac{3(T_{01}-T_1)}{b_1^2}-\frac{2E(T_1-T_3)}{kb_1}\right]y+3\left[\frac{E(T_1-T_3)}{kb_1^2}-\frac{2(T_{01}-T_1)}{b_1^3}\right]y^2$$

@ $y = b_1/2$,

$$\frac{dT}{dy}=\frac{E(T_1-T_3)}{k}+\frac{6(T_{01}-T_1)b_1}{2b_1^2}-\frac{4E(T_1-T_3)b_1}{2kb_1}+\frac{3E(T_1-T_3)b_1^2}{4kb_1^2}-\frac{6(T_{01}-T_1)b_1^2}{4b_1^3}$$

$$\frac{dT}{dy}=\frac{E(T_1-T_3)}{k}+\frac{3(T_{01}-T_1)}{b_1}-\frac{2E(T_1-T_3)}{k}+\frac{3E(T_1-T_3)}{4k}-\frac{3(T_{01}-T_1)}{2b_1}$$

$$\frac{dT}{dy}=\frac{4E(T_1-T_3)}{4k}-\frac{8E(T_1-T_3)}{4k}+\frac{3E(T_1-T_3)}{4k}+\frac{6(T_{01}-T_1)}{2b_1}-\frac{3(T_{01}-T_1)}{2b_1}$$

$$\frac{dT}{dy}=-\frac{E(T_1-T_3)}{4k}+\frac{3(T_{01}-T_1)}{2b_1}$$

Therefore,

$$-\delta x\frac{dT}{dy}\bigg|_{y=b_1/2}=\frac{E(T_1-T_3)}{4k}-\frac{3(T_{01}-T_1)}{2b_1}$$

and,

$$-\delta x\frac{dT}{dy}\bigg|_{y=b_1/2}+E(T_1-T_3)=\frac{E(T_1-T_3)}{4k}-\frac{3(T_{01}-T_1)}{2b_1}+E(T_1-T_3)$$

$$-\delta x\frac{dT}{dy}\bigg|_{y=b_1/2}+E(T_1-T_3)=\frac{5E(T_1-T_3)}{4k}-\frac{3(T_{01}-T_1)}{2b_1}$$

Therefore the complete balance @ $y = b_1/2$ is,

$$C_p\rho v\left[\left(\frac{5T_1}{32}-\frac{5T_{01}}{32}-\frac{2ET_1b_1}{192k}+\frac{2ET_3b_1}{192k}\right)\frac{db_1}{dx}+\left(\frac{5b_1}{32}-\frac{Eb_1^2}{192k}\right)\frac{dT_1}{dx}+\frac{Eb_1^2}{192k}\frac{dT_3}{dx}\right]$$
$$+\frac{5E(T_1-T_3)}{4}-\frac{3k(T_{01}-T_1)}{2b_1}=0 \qquad \text{(A13)}$$

2. Boundary layer growing, cold side

The method of equation development for the cold side is exactly the same as shown for the hot side, but with the following transposition of terms;

hot side	cold side
T_1	T_3
T_{01}	T_{03}
b_1	b_3
T_3	T_1

This results in the following enthalpy balance equations,

@ $z = b_2$

$$C_p\rho v\left[\left(\frac{ET_3b_3}{6k}-\frac{ET_1b_3}{6k}-\frac{T_{03}}{2}+\frac{T_3}{2}\right)\frac{db_3}{dx}+\left(\frac{Eb_3^{\,2}}{12k}+\frac{b_3}{2}\right)\frac{dT_3}{dx}-\frac{Eb_3^{\,2}}{12k}\frac{dT_1}{dx}\right]+E(T_3-T_1)=0 \qquad \text{(A14)}$$

@ $z = b_2/2$

$$C_p\rho v\left[\left(\frac{5T_3}{32}-\frac{5T_{03}}{32}-\frac{2ET_3b_3}{192k}+\frac{2ET_1b_3}{192k}\right)\frac{db_3}{dx}+\left(\frac{5b_3}{32}-\frac{Eb_3^{\,2}}{192k}\right)\frac{dT_3}{dx}+\frac{Eb_3^{\,2}}{192k}\frac{dT_1}{dx}\right] +\frac{5E(T_3-T_1)}{4}-\frac{3k(T_{03}-T_3)}{2b_3}=0 \qquad \text{(A15)}$$

3. Constant boundary layer region, hot side

Third Order Temperature Profile:

$$T = a_0 + a_1 y + a_2 y^2 + a_3 y^3 \tag{A16}$$

differentiating,

$$\frac{dT}{dy} = a_1 + 2a_2 y + 3a_3 y^2 \tag{A17}$$

Boundary conditions;

@ $y = b_1$	$T = T_2$	$dT/dy = 0$
@ $y = 0$	$T = T_1$	$dT/dy = E(T_1-T_3)/k$

Using equation (A16),

@ $y = 0$	$T_1 = a_0$
@ $y = b_1$	$T_2 = a_0 + a_1 b_1 + a_2 b_1^2 + a_3 b_1^3$

Using equation (A17),

@ $y = 0$	$\frac{E}{k}(T_1 - T_3) = a_1$
@ $y = b_1$	$0 = a_1 + 2a_2 b_1 + 3a_3 b_1^2$

Solving for terms,

$$a_2 = \frac{3(T_2 - T_1)}{b_1^2} - \frac{2E(T_1 - T_3)}{kb_1} \qquad a_3 = \frac{E(T_1 - T_3)}{kb_1^2} - \frac{2(T_2 - T_1)}{b_1^3}$$

Substituting terms into equation (A16),

$$\boxed{T = T_1 + \frac{E(T_1 - T_3)}{k} y + \left[\frac{3(T_2 - T_1)}{b_1^2} - \frac{2E(T_1 - T_3)}{kb_1}\right] y^2 + \left[\frac{E(T_1 - T_3)}{kb_1^2} - \frac{2(T_2 - T_1)}{b_1^3}\right] y^3} \tag{A18}$$

Enthalpy Balance

From Chapter 5.2, the enthalpy balance is,

$$\text{Convection In} + \text{Condutcion In} = \text{Convection Out} + \text{Conduction Out} \tag{A19}$$

where, Convection In, when the boundary layer is constant, is given by,

$$Q_{cvi} = \int_{y=0}^{y=b} C_p \rho v T \, dy \tag{A20}$$

Convection Out, is

$$Q_{cvo} = \int_{y=0}^{y=b} C_p \rho v T \, dy + \delta x \frac{d}{dx} \int_{y=0}^{y=b} C_p \rho v T \, dy \tag{A21}$$

the Conduction In is,

$$Q_{cni} = -\delta x \, E(T_1 - T_3) \tag{A22}$$

and the Conduction Out is,

$$Q_{cno} = -\delta x \, k \left. \frac{dT}{dy} \right|_{y=b} \tag{A23}$$

Forming the enthalpy balance for the entrance region at $y = b_1$,

$$\int_{y=0}^{y=b_1} C_p \rho v T \, dy - \delta x E(T_1 - T_3) = \int_{y=0}^{y=b_1} C_p \rho v T \, dy + \delta x \frac{d}{dx} \int_{y=0}^{y=b_1} C_p \rho v T \, dy + 0$$

which reduces to,

$$\boxed{C_p \rho v \int_{y=0}^{y=b_1} T \, dy + E(T_1 - T_3) = 0} \tag{A24}$$

Equation Development

Using the temperature profile, equation (A18),

$$\int_{y=0}^{y=b_1} Tdy = \left[T_1 y + \frac{E(T_1 - T_3)y^2}{2k} + \frac{3(T_2 - T_1)y^3}{3b_1^2} - \frac{2E(T_1 - T_3)y^3}{3kb_1} + \frac{E(T_1 - T_3)y^4}{4kb_1^2} - \frac{2(T_2 - T_1)y^4}{4b_1^3} \right]_0^{b_1}$$

$$\int_{y=0}^{y=b_1} Tdy = T_1 b_1 + \frac{E(T_1 - T_3)b_1^2}{2k} + \frac{(T_2 - T_1)b_1^3}{b_1^2} - \frac{2E(T_1 - T_3)b_1^3}{3kb_1} + \frac{E(T_1 - T_3)b_1^4}{4kb_1^2} - \frac{(T_2 - T_1)b_1^4}{2b_1^3}$$

$$\int_{y=0}^{y=b_1} Tdy = T_1 b_1 + \frac{ET_1 b_1^2}{2k} - \frac{ET_3 b_1^2}{2k} + T_2 b_1 - T_1 b_1 - \frac{2ET_1 b_1^2}{3k} + \frac{2ET_3 b_1^2}{3k} + \frac{ET_1 b_1^4}{4kb_1^2} - \frac{ET_3 b_1^4}{4kb_1^2} - \frac{T_2 b_1}{2} + \frac{T_1 b_1}{2}$$

$$\int_{y=0}^{y=b_1} Tdy = \frac{ET_1 b_1^2}{2k} - \frac{ET_3 b_1^2}{2k} - \frac{2ET_1 b_1^2}{3k} + \frac{2ET_3 b_1^2}{3k} + \frac{ET_1 b_1^4}{4kb_1^2} - \frac{ET_3 b_1^4}{4kb_1^2} + \frac{T_2 b_1}{2} + \frac{T_1 b_1}{2}$$

$$\int_{y=0}^{y=b_1} Tdy = \frac{6ET_1 b_1^2}{12k} - \frac{8ET_1 b_1^2}{12k} + \frac{3ET_1 b_1^4}{12kb_1^2} - \frac{3ET_3 b_1^2}{12k} + \frac{8ET_3 b_1^2}{12k} - \frac{3ET_3 b_1^4}{12kb_1^2} + \frac{T_2 b_1}{2} + \frac{T_1 b_1}{2}$$

$$\int_{y=0}^{y=b_1} Tdy = \frac{ET_1 b_1^2}{12k} - \frac{ET_3 b_1^2}{12k} + \frac{T_2 b_1}{2} + \frac{T_1 b_1}{2}$$

$$\frac{d}{dx}\int_{y=0}^{y=b_1} Tdy = \frac{d}{dx}\left[\frac{ET_1 b_1^2}{12k} - \frac{ET_3 b_1^2}{12k} + \frac{T_2 b_1}{2} + \frac{T_1 b_1}{2} \right]$$

$$\frac{d}{dx}\int_{y=0}^{y=b_1} Tdy = \frac{Eb_1^2}{12k}\frac{dT_1}{dx} - \frac{Eb_1^2}{12k}\frac{dT_3}{dx} + \frac{b_1}{2}\frac{dT_1}{dx} + \frac{b_1}{2}\frac{dT_2}{dx}$$

$$\frac{d}{dx}\int_{y=0}^{y=b_1} Tdy = \left(\frac{Eb_1^2}{12k} + \frac{b_1}{2} \right)\frac{dT_1}{dx} + \frac{b_1}{2}\frac{dT_2}{dx} - \frac{Eb_1^2}{12k}\frac{dT_3}{dx}$$

Therefore, substituting this result into equation (A24)

@ $y = b_1$

$$\boxed{C_p\rho v\left[\left(\frac{Eb_1^{\,2}}{12k}+\frac{b_1}{2}\right)\frac{dT_1}{dx}+\left(\frac{b_1}{2}\right)\frac{dT_2}{dx}-\frac{Eb_1^{\,2}}{12k}\frac{dT_3}{dx}\right]+E(T_1-T_3)=0} \qquad \text{(A25)}$$

Forming the second enthalpy balance for the constant region, at $y = b_1/2$,

$$\int_{y=0}^{y=b_1/2} C_p\rho vT\,dy-\delta xE(T_1-T_3)=\int_{y=0}^{y=b_1/2} C_p\rho vT\,dy+\delta x\frac{d}{dx}\int_{y=0}^{y=b_1/2} C_p\rho vT\,dy-\delta xk\left.\frac{dT}{dy}\right|_{y=b_1/2}$$

which reduces to,

$$\boxed{C_p\rho v\int_{y=0}^{y=b_1/2} T\,dy-k\left.\frac{dT}{dy}\right|_{y=b_1/2}+E(T_1-T_3)=0} \qquad \text{(A26)}$$

<u>Equation Development</u>

Using the temperature profile, equation (A18),

$$\int_{y=0}^{y=b_1/2} Tdy=\left[T_1y+\frac{E(T_1-T_3)y^2}{2k}+\frac{3(T_2-T_1)y^3}{3b_1^{\,2}}-\frac{2E(T_1-T_3)y^3}{3kb_1}+\frac{E(T_1-T_3)y^4}{4kb_1^{\,2}}-\frac{2(T_2-T_1)y^4}{4b_1^{\,3}}\right]_0^{b_1/2}$$

$$\int_{y=0}^{y=b_1/2} Tdy=\frac{T_1b_1}{2}+\frac{E(T_1-T_3)b_1^{\,2}}{8k}+\frac{(T_2-T_1)b_1^{\,3}}{8b_1^{\,2}}-\frac{2E(T_1-T_3)b_1^{\,3}}{24kb_1}+\frac{E(T_1-T_3)b_1^{\,4}}{64kb_1^{\,2}}-\frac{(T_2-T_1)b_1^{\,4}}{32b_1^{\,3}}$$

$$\int_{y=0}^{y=b_1/2} Tdy=\frac{16T_1b_1}{32}-\frac{4T_1b_1}{32}+\frac{T_1b_1}{32}+\frac{4T_2b_1}{32}-\frac{T_2b_1}{32}+\frac{T_1b_1}{32}-\frac{16ET_1b_1^{\,2}}{192k}+\frac{24ET_1b_1^{\,2}}{192k}+\frac{3ET_1b_1^{\,2}}{192k}-\frac{24ET_3b_1^{\,2}}{192k}+\frac{16ET_3b_1^{\,2}}{192k}-\frac{3ET_3b_1^{\,2}}{192k}$$

$$\int_{y=0}^{y=b_1/2} Tdy = \frac{13T_1b_1}{32} - \frac{3T_2b_1}{32} - \frac{11ET_3b_1^2}{192k} + \frac{11ET_1b_1^2}{192k}$$

$$\frac{d}{dx}\int_{y=0}^{y=b_1/2} Tdy = \frac{d}{dx}\left[\frac{13T_1b_1}{32} - \frac{3T_2b_1}{32} + \frac{11ET_1b_1^2}{192k} - \frac{11ET_3b_1^2}{192k}\right]$$

$$\frac{d}{dx}\int_{y=0}^{y=b_1/2} Tdy = \frac{13b_1}{32}\frac{dT_1}{dx} + \frac{3b_1}{32}\frac{dT_2}{dx} + \frac{11Eb_1^2}{192k}\frac{dT_1}{dx} - \frac{11Eb_1^2}{192k}\frac{dT_3}{dx}$$

$$\frac{d}{dx}\int_{y=0}^{y=b_1/2} Tdy = \left(\frac{13b_1}{32} + \frac{11Eb_1^2}{192k}\right)\frac{dT_1}{dx} + \left(\frac{3b_1}{32}\right)\frac{dT_2}{dx} - \frac{11Eb_1^2}{192k}\frac{dT_3}{dx}$$

Therefore, substituting this result into equation (A26)

@ $y = b_1/2$

$$\boxed{C_p\rho v\left[\left(\frac{13b_1}{32} + \frac{11Eb_1^2}{192k}\right)\frac{dT_1}{dx} + \left(\frac{3b_1}{32}\right)\frac{dT_2}{dx} - \frac{11Eb_1^2}{192k}\frac{dT_3}{dx}\right] - k\left.\frac{dT}{dy}\right|_{y=b_1/2} + E(T_1 - T_3) = 0} \qquad \text{(A27)}$$

Calculating the conduction out term,

From the temperature profile, equation (A18),

$$\frac{dT}{dy} = \frac{E(T_1 - T_3)}{k} + 2\left[\frac{3(T_2 - T_1)}{b_1^2} - \frac{2E(T_1 - T_3)}{kb_1}\right]y + 3\left[\frac{E(T_1 - T_3)}{kb_1^2} - \frac{2(T_2 - T_1)}{b_1^3}\right]y^2$$

@ $y = b_1/2$,

$$\frac{dT}{dy} = \frac{E(T_1 - T_3)}{k} + \frac{6(T_2 - T_1)b_1}{2b_1^2} - \frac{4E(T_1 - T_3)b_1}{2kb_1} + \frac{3E(T_1 - T_3)b_1^2}{4kb_1^2} - \frac{6(T_2 - T_1)b_1^2}{4b_1^3}$$

$$\frac{dT}{dy} = \frac{E(T_1 - T_3)}{k} + \frac{3(T_2 - T_1)}{b_1} - \frac{2E(T_1 - T_3)}{k} + \frac{3E(T_1 - T_3)}{4k} - \frac{3(T_2 - T_1)}{2b_1}$$

$$\frac{dT}{dy} = \frac{4E(T_1 - T_3)}{4k} - \frac{8E(T_1 - T_3)}{4k} + \frac{3E(T_1 - T_3)}{4k} + \frac{6(T_2 - T_1)}{2b_1} - \frac{3(T_2 - T_1)}{2b_1}$$

$$\frac{dT}{dy} = -\frac{E(T_1 - T_3)}{4k} + \frac{3(T_2 - T_1)}{2b_1}$$

Therefore,

$$-\delta x \frac{dT}{dy}\bigg|_{y=b_1/2} = \frac{E(T_1 - T_3)}{4k} - \frac{3(T_2 - T_1)}{2b_1}$$

and,

$$-\delta x \frac{dT}{dy}\bigg|_{y=b_1/2} + E(T_1 - T_3) = \frac{E(T_1 - T_3)}{4k} - \frac{3(T_2 - T_1)}{2b_1} + E(T_1 - T_3)$$

$$-\delta x \frac{dT}{dy}\bigg|_{y=b_1/2} + E(T_1 - T_3) = \frac{5E(T_1 - T_3)}{4k} - \frac{3(T_2 - T_1)}{2b_1}$$

Therefore the complete balance @ $y = b_1/2$ is,

$$C_p \rho v \left[\left(\frac{13b_1}{32} + \frac{11Eb_1^2}{192k} \right) \frac{dT_1}{dx} + \left(\frac{3b_1}{32} \right) \frac{dT_2}{dx} - \frac{11Eb_1^2}{192k} \frac{dT_3}{dx} \right] + \frac{5E(T_1 - T_3)}{4} - \frac{3k(T_2 - T_1)}{2b_1} = 0 \qquad \text{(A28)}$$

4. Boundary layer constant, cold side

The method of equation development for the cold side is exactly the same as shown for the hot side, but with the following transposition of terms;

hot side	cold side
T_1	T_3
T_2	T_4
b_1	b_3
T_3	T_1

This results in the following enthalpy balance equations,

@ $z = b_2$

$$C_p\rho v\left[\left(\frac{Eb_3^{\,2}}{12k}+\frac{b_3}{2}\right)\frac{dT_3}{dx}+\left(\frac{b_3}{2}\right)\frac{dT_4}{dx}-\frac{Eb_3^{\,2}}{12k}\frac{dT_1}{dx}\right]+E(T_3-T_1)=0 \tag{A29}$$

@ $z = b_2/2$

$$C_p\rho v\left[\left(\frac{13b_3}{32}+\frac{11Eb_3^{\,2}}{192k}\right)\frac{dT_3}{dx}+\left(\frac{3b_3}{32}\right)\frac{dT_4}{dx}-\frac{11Eb_3^{\,2}}{192k}\frac{dT_1}{dx}\right]+\frac{5E(T_3-T_1)}{4}-\frac{3k(T_4-T_3)}{2b_3}=0 \tag{A30}$$

APPENDIX B

Method of Runge Kutta

The method of Runge Kutta enables the numerical solution of a set of first order differential equations,

$$\frac{dy_n}{dx} = f_n(x, y_1, y_2, y_3 \ldots) \tag{B1}$$

for n = 1, 2, 3...,

by calculating the increment of y_n corresponding to an increment in x by a set of formulae, which are, for the entrance region in this work,

$$k_1 = f(x_0, T_{10}, b_{10}, T_{30}, b_{30})\Delta x \tag{B2}$$

$$k_2 = f\left(x_0 + \frac{\Delta x}{2}, T_{10} + \frac{k_1}{2}, b_{10} + \frac{k_1}{2}, T_{30} + \frac{k_1}{2}, b_{30} + \frac{k_1}{2}\right)\Delta x \tag{B3}$$

$$k_3 = f\left(x_0 + \frac{\Delta x}{2}, T_{10} + \frac{k_2}{2}, b_{10} + \frac{k_2}{2}, T_{30} + \frac{k_2}{2}, b_{30} + \frac{k_2}{2}\right)\Delta x \tag{B4}$$

$$k_4 = f(x_0 + \Delta x, T_{10} + k_3, b_{10} + k_3, T_{30} + k_3, b_{30} + k_3)\Delta x \tag{B5}$$

$$\Delta T_1 = \tfrac{1}{6}(k_1 + 2k_2 + 2k_3 + k_4) \tag{B6}$$

and,

$$x_1 = x_0 + \Delta x \tag{B7}$$

$$T_1 = T_{10} + \Delta T_1 \tag{B8}$$

The next incremental step is calculated by replacing x_0, T_{10} etc. with x_1, T_1 etc.

This method is well suited to solution utilising a Fortran programme, which has been written specifically for the boundary analysis in Chapter 5. The error in this method is of the same order as Simpson's rule and can be explored by repeating the numerical integration with small values of the increment, Δx.

APPENDIX C

The Rearrangement of the Enthalpy Balances into a set of First Order Differential Simultaneous Equations

From the hot side enthalpy balances,

$$(C1) \qquad a_1\frac{db_1}{dx}+a_2\frac{dT_1}{dx}+a_3\frac{dT_3}{dx}+a_4=0$$

$$(C2) \qquad c_1\frac{db_1}{dx}+c_2\frac{dT_1}{dx}+c_3\frac{dT_3}{dx}+c_4=0$$

Remove db_1/dx term,

$$(C1)\times c_1 \qquad a_1c_1\frac{db_1}{dx}+a_2c_1\frac{dT_1}{dx}+a_3c_1\frac{dT_3}{dx}+a_4c_1=0 \qquad (C3)$$

$$(C2)\times a_1 \qquad a_1c_1\frac{db_1}{dx}+a_1c_2\frac{dT_1}{dx}+a_1c_3\frac{dT_3}{dx}+a_1c_4=0 \qquad (C4)$$

$$(C3)-(C4) \qquad (a_2c_1-a_1c_2)\frac{dT_1}{dx}+(a_3c_1-a_1c_3)\frac{dT_3}{dx}+a_4c_1-a_1c_4=0 \qquad (C5)$$

which simplifies to,

$$G_1\frac{dT_1}{dx}+G_2\frac{dT_3}{dx}+G_3=0 \qquad (C6)$$

From the cold side enthalpy balances,

$$(C7) \qquad m_1\frac{db_3}{dx}+m_2\frac{dT_3}{dx}+m_3\frac{dT_1}{dx}+m_4=0$$

$$(C8) \qquad n_1\frac{db_3}{dx}+n_2\frac{dT_3}{dx}+n_3\frac{dT_1}{dx}+n_4=0$$

Remove db_3/dx term,

$$(C7)\times n_1 \qquad m_1n_1\frac{db_3}{dx}+m_2n_1\frac{dT_3}{dx}+m_3n_1\frac{dT_1}{dx}+m_4n_1=0 \qquad (C9)$$

$$(C8)\times m_1 \qquad m_1n_1\frac{db_3}{dx}+m_1n_2\frac{dT_3}{dx}+m_1n_3\frac{dT_1}{dx}+m_1n_4=0 \qquad (C10)$$

$$(C9)-(C10) \qquad (m_2n_1-m_1n_2)\frac{dT_3}{dx}+(m_3n_1-m_1n_3)\frac{dT_1}{dx}+m_4n_1-m_1n_4=0 \qquad (C11)$$

which simplifies to,

$$H_1\frac{dT_3}{dx}+H_2\frac{dT_1}{dx}+H_3=0 \qquad \text{(C12)}$$

Remove dT_1/dx term,

(C6) x H_2 $$G_1H_2\frac{dT_1}{dx}+G_2H_2\frac{dT_3}{dx}+G_3H_2=0 \qquad \text{(C13)}$$

(C12) x G_1 $$G_1H_1\frac{dT_3}{dx}+G_1H_2\frac{dT_1}{dx}+G_1H_3=0 \qquad \text{(C14)}$$

(C13) - (C14) $$(G_2H_2-G_1H_1)\frac{dT_3}{dx}+(G_3H_2-G_1H_3)=0 \qquad \text{(C15)}$$

Rearranging for dT_3/dx,

$$\boxed{\frac{dT_3}{dx}=\frac{(G_1H_3-G_3H_2)}{(G_2H_2-G_1H_1)}=F3} \qquad \text{(C16)}$$

Remove dT_3/dx term,

(C6) x H_1 $$G_1H_1\frac{dT_1}{dx}+G_2H_1\frac{dT_3}{dx}+G_3H_1=0 \qquad \text{(C17)}$$

(C12) x G_2 $$G_2H_1\frac{dT_3}{dx}+G_2H_2\frac{dT_1}{dx}+G_2H_3=0 \qquad \text{(C18)}$$

(C17) - (C18) $$(G_1H_1-G_2H_2)\frac{dT_1}{dx}+(G_3H_1-G_2H_3)=0 \qquad \text{(C19)}$$

Rearranging for dT_1/dx,

$$\boxed{\frac{dT_1}{dx}=\frac{(G_2H_3-G_3H_1)}{(G_1H_1-G_2H_2)}=F2} \qquad \text{(C20)}$$

Finding db_1/dx term,

(C1) $$a_1\frac{db_1}{dx}+a_2\frac{dT_1}{dx}+a_3\frac{dT_3}{dx}+a_4=0$$

$$a_1 \frac{db_1}{dx} + a_2 F2 + a_3 F3 + a_4 = 0 \qquad \text{(C21)}$$

Rearranging for db_1/dx term,

$$\boxed{\frac{db_1}{dx} = -\left(\frac{a_2 F2 + a_3 F3 + a_4}{a_1}\right) = F1} \qquad \text{(C22)}$$

Finding db_3/dx term,

(C7) $$m_1 \frac{db_3}{dx} + m_2 \frac{dT_3}{dx} + m_3 \frac{dT_1}{dx} + m_4 = 0$$

$$m_1 \frac{db_3}{dx} + m_2 F3 + m_3 F1 + m_4 = 0 \qquad \text{(C23)}$$

Rearranging for db_3/dx term,

$$\boxed{\frac{db_3}{dx} = -\left(\frac{m_2 F3 + m_3 F1 + m_4}{m_1}\right) = F4} \qquad \text{(C24)}$$

APPENDIX D

Level One Fortran Programme
Plug Flow Profile, Single Component

```
c     INITIAL SECTION
c     defining variables
      REAL Cp, RHO, V, T01, k, T3, E, TOTX, X0, T10, B10, DX, X, T1, B1,
     1K1, L1, K2, L2, K3, L3, K4, L4, F1, F2, DT1, DB1, A1, A2, A3, A4,
     1C1, C2, C3, M1, M2, M3, N1, N2, N3, B3, DT3, DB3, F3, F4,P1, P2,
     1P3, P4, Q1, Q2, Q3, Q4, T30, T03, G1, G2, G3, H1, H2, H3, C4, M4,
     1N4, T20, T40, T2, T4, B30, DT2, DT4
      INTEGER TOT, BOT, I, BUZZ
      BUZZ=1

c     inputting data from a file
      OPEN(UNIT=8,FILE='11d.DAT')
      READ(8,*)Cp,RHO,V,T01,T03,k,E,TOTX,X0,T10,T30,B10,B30,DX
c     opening output file
      OPEN(UNIT=9,FILE='11r.DAT')
      WRITE(9,*)
      WRITE(9,800)
800   FORMAT(8X,'X',10X,'T1',10X,'B1',12X,'T3',11X,'B3')

c     number of repititions
      TOT=NINT(TOTX/dX)-1
      DO 100 I=1,TOT

c     ENTRANCE REGION
c     Runge Kutta equations
      X=X0
      T1=T10
      B1=B10
      T3=T30
      B3=B30
      CALL HNCN(A1,A2,A3,A4,C1,C2,C3,C4,M1,M2,M3,M4,N1,N2,N3,N4,G1,G2
     1,G3,H1,H2,H3,F3,F4,T1,B1,B3,F1,F2,k,T3,E,T01,T03,RHO,Cp,V)
      K1=F1*dX
      L1=F2*dX
      P1=F3*DX
      Q1=F4*DX

      X=X0+(dX/2)
      T1=T10+(K1/2)
      B1=B10+(L1/2)
      T3=T30+(P1/2)
```

```
      B3=B30+(Q1/2)
      CALL HNCN(A1,A2,A3,A4,C1,C2,C3,C4,M1,M2,M3,M4,N1,N2,N3,N4,G1,G2
     1,G3,H1,H2,H3,F3,F4,T1,B1,B3,F1,F2,k,T3,E,T01,T03,RHO,Cp,V)
      K2=F1*dX
      L2=F2*dX
      P2=F3*DX
      Q2=F4*DX

      T1=T10+(K2/2)
      B1=B10+(L2/2)
      T3=T30+(P2/2)
      B3=B30+(Q2/2)
      CALL HNCN(A1,A2,A3,A4,C1,C2,C3,C4,M1,M2,M3,M4,N1,N2,N3,N4,G1,G2
     1,G3,H1,H2,H3,F3,F4,T1,B1,B3,F1,F2,k,T3,E,T01,T03,RHO,Cp,V)
      K3=F1*dX
      L3=F2*dX
      P3=F3*DX
      Q3=F4*DX

      X=X0+dX
      T1=T10+K3
      B1=B10+L3
      T3=T30+P3
      B3=B30+Q3
      CALL HNCN(A1,A2,A3,A4,C1,C2,C3,C4,M1,M2,M3,M4,N1,N2,N3,N4,G1,G2
     1,G3,H1,H2,H3,F3,F4,T1,B1,B3,F1,F2,k,T3,E,T01,T03,RHO,Cp,V)
      K4=F1*dX
      L4=F2*dX
      P4=F3*DX
      Q4=F4*DX

      DT1=(K1+(2*K2)+(2*K3)+K4)/6
      DB1=(L1+(2*L2)+(2*L3)+L4)/6
      DT3=(P1+(2*P2)+(2*P3)+P4)/6
      DB3=(Q1+(2*Q2)+(2*Q3)+Q4)/6

c     resetting initial values for next loop
      X0=X
      T10=T10+DT1
      B10=B10+DB1
      T30=T30+DT3
      B30=B30+DB3

c     output results to a file
      IF(I.EQ.BUZZ)THEN
       BUZZ=BUZZ+10
       WRITE(9,200)X0,T10,B10,T30,B30
200    FORMAT(3X,F8.6,3X,F10.4,3X,F10.8,3X,F10.4,3X,F11.8)
      END IF
```

```
c     check to see if constant section conditions are met
      IF(B10.GT.0.00044999) GOTO 1000

100   CONTINUE
      GOTO 2000

c     CONSTANT REGION
1000  T20=T01
      T40=T03
      B10=0.00045
      B30=0.00045
      BUZZ=1
      WRITE(9,*)
      WRITE(9,900)
900   FORMAT(6X,'X',11X,'T1',11X,'T2',11X,'T3',11X,'T4')
      WRITE(9,901)X0,T10,T20,T30,T40
901   FORMAT(3X,F8.6,5X,F8.4,5X,F8.4,5X,F8.4,5X,F8.4)

c     number of repititions
      BOT=TOT-I
      DO 101 I=1,BOT

c     Runge Kutta equations
      X=X0
      T1=T10
      T2=T20
      T3=T30
      T4=T40
      CALL HYCY(T1,T2,T3,T4,F1,F2,F3,F4,k,E,RHO,Cp,V,B10,B30)
      K1=F1*dX
      L1=F2*dX
      P1=F3*DX
      Q1=F4*DX

      X=X0+(dX/2)
      T1=T10+(K1/2)
      T2=T20+(L1/2)
      T3=T30+(P1/2)
      T4=T40+(Q1/2)
      CALL HYCY(T1,T2,T3,T4,F1,F2,F3,F4,k,E,RHO,Cp,V,B10,B30)
      K2=F1*dX
      L2=F2*dX
      P2=F3*DX
      Q2=F4*DX

      T1=T10+(K2/2)
      T2=T20+(L2/2)
      T3=T30+(P2/2)
```

```
T4=T40+(Q2/2)
CALL HYCY(T1,T2,T3,T4,F1,F2,F3,F4,k,E,RHO,Cp,V,B10,B30)
K3=F1*dX
L3=F2*dX
P3=F3*DX
Q3=F4*DX

X=X0+dX
T1=T10+K3
T2=T20+L3
T3=T30+P3
T4=T40+Q3
CALL HYCY(T1,T2,T3,T4,F1,F2,F3,F4,k,E,RHO,Cp,V,B10,B30)
K4=F1*dX
L4=F2*dX
P4=F3*DX
Q4=F4*DX

DT1=(K1+(2*K2)+(2*K3)+K4)/6
DT2=(L1+(2*L2)+(2*L3)+L4)/6
DT3=(P1+(2*P2)+(2*P3)+P4)/6
DT4=(Q1+(2*Q2)+(2*Q3)+Q4)/6

c   resetting initial values for next loop
    X0=X
    T10=T10+DT1
    T20=T20+DT2
    T30=T30+DT3
    T40=T40+DT4

c   output results to a file
    IF (I.EQ.BUZZ) THEN
     BUZZ=BUZZ+10
     WRITE(9,600)X0,T10,T20,T30,T40
600   FORMAT(3X,F8.6,5X,F8.4,5X,F8.4,5X,F8.4,5X,F8.4)
    END IF

101  CONTINUE
2000 WRITE(6,*)'YOUR RESULTS CAN BE FOUND IN "11r.DAT"'
    WRITE(6,*)
    WRITE(6,*)'END'
    CLOSE(UNIT=8)
    CLOSE(UNIT=9)
    STOP
    END

c   calculation of entrance region functions
    SUBROUTINE HNCN(A1,A2,A3,A4,C1,C2,C3,C4,M1,M2,M3,M4,N1,N2,N3,N4,
```

```
1,G1,G2,G3,H1,H2,H3,F3,F4,T1,B1,B3,F1,F2,k,T3,E,T01,T03,RHO,Cp,V)
 REAL A1,A2,A3,A4,C1,C2,C3,C4,M1,M2,M3,M4,N1,N2,N3,N4,F3,F4,T1,B1,
1F1,F2,G1,G2,G3,H1,H2,H3,k,T3,E,T01,RHO,Cp,V,T03,B3

  A1=Cp*V*RHO*((T1/2)+((E*T1*B1)/(6*k))-((E*T3*B1)/(6*k))-(T01/2))
  A2=Cp*V*RHO*((B1/2)+((E*B1*B1)/(12*k)))
  A3=Cp*V*RHO*(((-1)*E*B1*B1)/(12*k))
  A4=E*(T1-T3)

  C1=Cp*V*RHO*(((5*T1)/32)-((5*T01)/32)-((E*B1*T1)/(96*k))+
1((E*B1*T3)/(96*k)))
  C2=Cp*V*RHO*(((5*B1)/32)-((E*B1*B1)/(192*k)))
  C3=Cp*V*RHO*((E*B1*B1)/(192*k))
  C4=((5*E*(T1-T3))/4)-((3*k*(T01-T1))/(2*B1))

  G1=(A2*C1)-(A1*C2)
  G2=(A3*C1)-(A1*C3)
  G3=(A4*C1)-(A1*C4)

  M1=Cp*V*RHO*((T3/2)+((E*T3*B3)/(6*k))-((E*T1*B3)/(6*k))-(T03/2))
  M2=Cp*V*RHO*((B3/2)+((E*B3*B3)/(12*k)))
  M3=Cp*V*RHO*(((-1)*E*B3*B3)/(12*k))
  M4=E*(T3-T1)

  N1=Cp*V*RHO*(((5*T3)/32)-((5*T03)/32)+((E*B3*T1)/(96*k))-
1((E*B3*T3)/(96*k)))
  N2=Cp*V*RHO*(((5*B3)/32)-((E*B3*B3)/(192*k)))
  N3=Cp*V*RHO*((E*B3*B3)/(192*k))
  N4=((5*E*(T3-T1))/4)-((3*k*(T03-T3))/(2*B3))

  H1=(M2*N1)-(M1*N2)
  H2=(M3*N1)-(M1*N3)
  H3=(M4*N1)-(M1*N4)

  F3=((G1*H3)-(G3*H2))/((G2*H2)-(G1*H1))
  F1=((G2*H3)-(G3*H1))/((G1*H1)-(G2*H2))
  F2=(-1)*(((A2*F1)+(A3*F3)+A4)/A1)
  F4=(-1)*(((M2*F3)+(M3*F1)+M4)/M1)

RETURN
END
```

c calculation of constant region functions

```
      SUBROUTINE HYCY(T1,T2,T3,T4,F1,F2,F3,F4,k,E,RHO,Cp,V,B10,B30)
      REAL T1,T2,T3,T4,F1,F2,F3,F4,k,E,RHO,Cp,V,B10,B30

       A1=Cp*V*RHO*((B10/2)+((E*B10*B10)/(12*k)))
       A2=Cp*V*RHO*(B10/2)
       A3=Cp*V*RHO*(((-1)*E*B10*B10)/(12*k))
```

```
A4=E*(T1-T3)

C1=Cp*V*RHO*(((13*B10)/32)+((11*E*B10*B10)/(192*k)))
C2=Cp*V*RHO*((3*B10)/32)
C3=Cp*V*RHO*(((-1)*11*E*B10*B10)/(192*k))
C4=((5*E*(T1-T3))/4)+((3*k*(T1-T2))/(2*B10))

G1=(A1*C2)-(A2*C1)
G2=(A3*C2)-(A2*C3)
G3=(A4*C2)-(A2*C4)

M1=Cp*V*RHO*((B30/2)+((E*B30*B30)/(12*k)))
M2=Cp*V*RHO*(B30/2)
M3=Cp*V*RHO*(((-1)*E*B30*B30)/(12*k))
M4=E*(T3-T1)

N1=Cp*V*RHO*(((13*B30)/32)+((11*E*B30*B30)/(192*k)))
N2=Cp*V*RHO*((3*B30)/32)
N3=Cp*V*RHO*(((-1)*11*E*B30*B30)/(192*k))
N4=((5*E*(T3-T1))/4)+((3*k*(T3-T4))/(2*B30))

H1=(M1*N2)-(M2*N1)
H2=(M3*N2)-(M2*N3)
H3=(M4*N2)-(M2*N4)

F3=((G1*H3)-(G3*H2))/((G2*H2)-(G1*H1))
F1=((G2*H3)-(G3*H1))/((G1*H1)-(G2*H2))
 F2=(-1)*(((A1*F1)+(A3*F3)+A4)/A2)
 F4=(-1)*(((M1*F3)+(M3*F1)+M4)/M2)

RETURN
END
```

APPENDIX E

Enthalpy Balances for the Boundary Layer Analysis Models

	ENTRANCE REGION	CONSTANT REGION
HOT SIDE		
$y= b_1$	$C_p v\rho\left[\left(\frac{Eb_1T_1}{6k}-\frac{Eb_1T_3}{6k}+\frac{T_1}{2}-\frac{T_{01}}{2}\right)\frac{db_1}{dx}+\left(\frac{Eb_1^2}{12k}+\frac{b_1}{2}\right)\frac{dT_1}{dx}-\frac{Eb_1^2}{12k}\frac{dT_3}{dx}\right]$ $+E(T_1-T_3)=0$	$C_p v\rho\left[\left(\frac{b_1}{2}+\frac{Eb_1^2}{12k}\right)\frac{dT_1}{dx}+\frac{b_1}{2}\frac{dT_2}{dx}-\frac{Eb_1^2}{12k}\frac{dT_3}{dx}\right]+E(T_1-T_3)=0$
$y= b_1/2$	$C_p v\rho\left[\left(\frac{5T_1}{32}-\frac{5T_{01}}{32}-\frac{Eb_1T_1}{96k}+\frac{Eb_1T_3}{96k}\right)\frac{db_1}{dx}+\left(\frac{5b_1}{32}-\frac{Eb_1^2}{192k}\right)\frac{dT_1}{dx}+\frac{Eb_1^2}{192k}\frac{dT_3}{dx}\right]$ $+\frac{5E(T_1-T_3)}{4}-\frac{3k(T_{01}-T_1)}{2b_1}=0$	$C_p v\rho\left[\left(\frac{13b_1}{32}+\frac{11Eb_1^2}{192}\right)\frac{dT_1}{dx}+\frac{3b_1}{32}\frac{dT_2}{dx}-\frac{11Eb_1^2}{192}\frac{dT_3}{dx}\right]$ $+\frac{3k(T_1-T_2)}{2b_1}+\frac{5E(T_1-T_3)}{4}=0$
COLD SIDE		
$z= b_3$	$C_p v\rho\left[\left(\frac{Eb_3T_3}{6k}-\frac{Eb_3T_1}{6k}+\frac{T_1}{2}-\frac{T_{03}}{2}\right)\frac{db_3}{dx}+\left(\frac{Eb_3^2}{12k}+\frac{b_3}{2}\right)\frac{dT_3}{dx}-\frac{Eb_3^2}{12k}\frac{dT_1}{dx}\right]$ $-E(T_1-T_3)=0$	$C_p v\rho\left[\left(\frac{b_3}{2}+\frac{Eb_3^2}{12k}\right)\frac{dT_3}{dx}+\frac{b_3}{2}\frac{dT_4}{dx}-\frac{Eb_3^2}{12k}\frac{dT_1}{dx}\right]+E(T_3-T_1)=0$
$z= b_3/2$	$C_p v\rho\left[\left(\frac{5T_3}{32}-\frac{5T_{03}}{32}-\frac{Eb_3T_3}{96k}+\frac{Eb_3T_1}{96k}\right)\frac{db_3}{dx}+\left(\frac{5b_3}{32}-\frac{Eb_3^2}{192k}\right)\frac{dT_3}{dx}+\frac{Eb_3^2}{192k}\frac{dT_1}{dx}\right]$ $+\frac{5E(T_3-T_1)}{4}-\frac{3k(T_{03}-T_3)}{2b_3}=0$	$C_p v\rho\left[\left(\frac{13b_3}{32}+\frac{11Eb_3^2}{192}\right)\frac{dT_3}{dx}+\frac{3b_3}{32}\frac{dT_4}{dx}-\frac{11Eb_3^2}{192}\frac{dT_1}{dx}\right]$ $+\frac{3k(T_3-T_4)}{2b_1}+\frac{5E(T_3-T_1)}{4}=0$

Level One enthalpy balances

	ENTRANCE REGION
$w = b_2$	$6C_p\rho\overline{V}\left[\left(\frac{3T_{01}b_2}{10Y_1}-\frac{3T_2b_2}{10Y_1}+\frac{T_2b_2^{\,2}}{5Y_1^{\,2}}-\frac{T_{01}b_2^{\,2}}{5Y_1^{\,2}}+\frac{Gb_2^{\,2}T_C}{10Y_1k}-\frac{Gb_2^{\,2}T_2}{10Y_1k}-\frac{Gb_2^{\,3}T_C}{15Y_1^{\,2}k}+\frac{Gb_2^{\,3}T_2}{15Y_1^{\,2}k}\right)\frac{db_2}{dx}+\left(\frac{b_2^{\,3}}{15Y_1^{\,2}}-\frac{3b_2^{\,2}}{20Y_1}-\frac{Gb_2^{\,3}}{30Y_1k}+\frac{Gb_2^{\,4}}{60Y_1^{\,2}k}\right)\frac{dT_2}{dx}\right]+G(T_C-T_2)=0$
$w = b_2/2$	$6C_p\rho\overline{V}\left[\left(\frac{9T_{01}b_2}{160Y_1}-\frac{9T_2b_2}{160Y_1}-\frac{7T_{01}b_2^{\,2}}{320Y_1^{\,2}}+\frac{7T_2b_2^{\,2}}{320Y_1^{\,2}}+\frac{Gb_2^{\,2}T_C}{320Y_1k}-\frac{Gb_2^{\,2}T_2}{320Y_1k}-\frac{Gb_2^{\,3}T_C}{480Y_1^{\,2}k}+\frac{Gb_2^{\,3}T_2}{480Y_1^{\,2}k}\right)\frac{db_2}{dx}+\left(\frac{7b_2^{\,3}}{960Y_1^{\,2}}-\frac{9b_2^{\,2}}{320Y_1}-\frac{Gb_2^{\,3}}{960Y_1k}+\frac{Gb_2^{\,4}}{1920Y_1^{\,2}k}\right)\frac{dT_2}{dx}\right]+\frac{5G(T_C-T_2)}{4}+\frac{3k(T_{01}-T_2)}{2b_2}=0$
$u = b_4$	$6C_p\rho\overline{V}\left[\left(\frac{3T_{03}b_4}{10Y_3}-\frac{3T_4b_4}{10Y_3}-\frac{T_{03}b_4^{\,2}}{5Y_3^{\,2}}+\frac{T_4b_4^{\,2}}{5Y_3^{\,2}}+\frac{Jb_4^{\,2}T_H}{10Y_3k}-\frac{Jb_4^{\,2}T_4}{10Y_3k}-\frac{Jb_4^{\,3}T_H}{15Y_3^{\,2}k}+\frac{Jb_4^{\,3}T_4}{15Y_3^{\,2}k}\right)\frac{db_4}{dx}+\left(\frac{b_4^{\,3}}{15Y_3^{\,2}}-\frac{3b_4^{\,2}}{20Y_3}-\frac{Jb_4^{\,3}}{30Y_3k}+\frac{Jb_4^{\,4}}{60Y_3^{\,2}k}\right)\frac{dT_4}{dx}\right]+J(T_4-T_H)=0$
$u = b_4/2$	$6C_p\rho\overline{V}\left[\left(\frac{9T_{03}b_4}{160Y_3}-\frac{9T_4b_4}{160Y_3}-\frac{7T_{03}b_4^{\,2}}{320Y_3^{\,2}}+\frac{7T_4b_4^{\,2}}{320Y_3^{\,2}}+\frac{Jb_4^{\,2}T_H}{320Y_3k}-\frac{Jb_4^{\,2}T_4}{320Y_3k}-\frac{Jb_4^{\,3}T_H}{480Y_3^{\,2}k}+\frac{Jb_4^{\,3}T_4}{480Y_3^{\,2}k}\right)\frac{db_4}{dx}+\left(\frac{7b_4^{\,3}}{960Y_3^{\,2}}-\frac{9b_4^{\,2}}{320Y_3}-\frac{Jb_4^{\,3}}{960Y_3k}+\frac{Jb_4^{\,4}}{1920Y_3^{\,2}k}\right)\frac{dT_4}{dx}\right]+\frac{5J(T_4-T_H)}{4}+\frac{3k(T_{03}-T_4)}{2b_4}=0$

Level Four wall enthalpy balances

	ENTRANCE REGION
$y = b_1$	$6C_p\rho\overline{V}\left[\left(\frac{3T_1b_1}{10Y_1}-\frac{3T_{01}b_1}{10Y_1}-\frac{T_1b_1^2}{5Y_1^2}+\frac{T_{01}b_1^2}{5Y_1^2}+\frac{Eb_1^2T_1}{10Y_1k}-\frac{Eb_1^2T_3}{10Y_1k}-\frac{Eb_1^3T_1}{15Y_1^2k}+\frac{Eb_1^3T_3}{15Y_1^2k}\right)\frac{db_1}{dx}\right.$ $\left.+\left(\frac{3b_1^2}{20Y_1}-\frac{b_1^3}{15Y_1^2}+\frac{Eb_1^3}{30Y_1k}-\frac{Eb_1^4}{60Y_1^2k}\right)\frac{dT_1}{dx}-\left(\frac{Eb_1^4}{60Y_1^2k}-\frac{Eb_1^3}{30Y_1k}\right)\frac{dT_3}{dx}\right]+E(T_1-T_3)=0$
$y = b_1/2$	$6C_p\rho\overline{V}\left[\left(\frac{9T_1b_1}{160Y_1}-\frac{9T_{01}b_1}{160Y_1}-\frac{7T_1b_1^2}{320Y_1^2}+\frac{7T_{01}b_1^2}{320Y_1^2}+\frac{Eb_1^2T_1}{320Y_1k}-\frac{Eb_1^2T_3}{320Y_1k}-\frac{Eb_1^3T_1}{480Y_1^2k}+\frac{Eb_1^3T_3}{480Y_1^2k}\right)\frac{db_1}{dx}\right.$ $\left.+\left(\frac{9b_1^2}{320Y_1}-\frac{7b_1^3}{960Y_1^2}+\frac{Eb_1^3}{960Y_1k}-\frac{Eb_1^4}{1920Y_1^2k}\right)\frac{dT_1}{dx}+\left(\frac{Eb_1^4}{1920Y_1^2k}-\frac{Eb_1^3}{960Y_1k}\right)\frac{dT_3}{dx}\right]$ $+\frac{5E(T_1-T_3)}{4}-\frac{3k(T_{01}-T_1)}{2b_1}=0$
$z = b_3$	$6C_p\rho\overline{V}\left[\left(\frac{3T_3b_3}{10Y_3}-\frac{3T_{03}b_3}{10Y_3}-\frac{T_3b_3^2}{5Y_3^2}+\frac{T_{03}b_3^2}{5Y_3^2}+\frac{Eb_3^2T_3}{10Y_3k}-\frac{Eb_3^2T_1}{10Y_3k}-\frac{Eb_3^3T_3}{15Y_3^2k}+\frac{Eb_3^3T_1}{15Y_3^2k}\right)\frac{db_3}{dx}\right.$ $\left.+\left(\frac{3b_3^2}{20Y_3}-\frac{b_3^3}{15Y_3^2}+\frac{Eb_3^3}{30Y_3k}-\frac{Eb_3^4}{60Y_3^2k}\right)\frac{dT_3}{dx}-\left(\frac{Eb_3^4}{60Y_3^2k}-\frac{Eb_3^3}{30Y_3k}\right)\frac{dT_1}{dx}\right]+E(T_3-T_1)=0$
$z = b_3/2$	$6C_p\rho\overline{V}\left[\left(\frac{9T_3b_3}{160Y_3}-\frac{9T_{03}b_3}{160Y_3}-\frac{7T_3b_3^2}{320Y_3^2}+\frac{7T_{03}b_3^2}{320Y_3^2}+\frac{Eb_3^2T_3}{320Y_3k}-\frac{Eb_3^2T_1}{320Y_3k}-\frac{Eb_3^3T_3}{480Y_3^2k}+\frac{Eb_3^3T_1}{480Y_3^2k}\right)\frac{db_3}{dx}\right.$ $\left.+\left(\frac{9b_3^2}{320Y_3}-\frac{7b_3^3}{960Y_3^2}+\frac{Eb_3^3}{960Y_3k}-\frac{Eb_3^4}{1920Y_3^2k}\right)\frac{dT_3}{dx}+\left(\frac{Eb_3^4}{1920Y_3^2k}-\frac{Eb_3^3}{960Y_3k}\right)\frac{dT_1}{dx}\right]$ $+\frac{5E(T_3-T_1)}{4}-\frac{3k(T_{03}-T_3)}{2b_3}=0$

Level Four membrane enthalpy balances

	CONSTANT REGION
$y= b_1$	$6C_p\rho\bar{V}\left[\left(\frac{b_1}{12}+\frac{Eb_1^2}{60k}\right)\frac{dT_1}{dx}+\left(\frac{b_1}{12}+\frac{Gb_1^2}{60k}\right)\frac{dT_2}{dx}-\frac{Eb_1^2}{60k}\frac{dT_3}{dx}\right]$ $+E(T_1-T_3)-G(T_C-T_2)=0$
$y= b_1/2$	$6C_p\rho\bar{V}\left[\left(\frac{b_1}{16}+\frac{21Eb_1^2}{1920k}\right)\frac{dT_1}{dx}+\left(\frac{b_1}{48}+\frac{11Gb_1^2}{1920k}\right)\frac{dT_2}{dx}-\frac{21Eb_1^2}{1920k}\frac{dT_3}{dx}\right]$ $+\frac{3k(T_1-T_2)}{2b_1}+\frac{5E(T_1-T_3)}{4}+\frac{G(T_C-T_2)}{4}=0$
$z= b_3$	$6C_p\rho\bar{V}\left[\left(\frac{b_3}{12}-\frac{Eb_3^2}{60k}\right)\frac{dT_3}{dx}+\left(\frac{b_3}{12}+\frac{Jb_3^2}{60k}\right)\frac{dT_4}{dx}-\frac{Eb_3^2}{60k}\frac{dT_1}{dx}\right]$ $+E(T_3-T_1)-J(T_H-T_4)=0$
$z= b_3/2$	$6C_p\rho\bar{V}\left[\left(\frac{b_3}{16}+\frac{21Eb_3^2}{1920k}\right)\frac{dT_3}{dx}+\left(\frac{b_3}{48}+\frac{11Jb_3^2}{1920k}\right)\frac{dT_4}{dx}-\frac{21Jb_3^2}{1920k}\frac{dT_1}{dx}\right]$ $+\frac{3k(T_3-T_4)}{2b_3}+\frac{5E(T_3-T_1)}{4}+\frac{J(T_H-T_4)}{4}=0$

Level Four enthalpy balances

APPENDIX F

Variation of Velocity Profile Magnitude

Assuming a laminar velocity profile, as given in Chapter 5.3,

$$v_x = 4V_{max}\left[\frac{y}{Y_1} - \left(\frac{y}{Y_1}\right)^2\right] = 6\overline{V}\left[\frac{y}{Y_1} - \left(\frac{y}{Y_1}\right)^2\right] \qquad \text{(F1)}$$

The mass flow along the channel is given by,

$$\dot{M} = \overline{V}\rho_f Y_1 \qquad \text{(F2)}$$

and the mass flow through the membrane per unit time and area at position x is given by,

$$m(x)$$

Carrying out a mass balance on an element in a channel of unit width in steady state

$$IN = OUT$$

$$\overline{V}\rho Y_1\big|_x = \overline{V}\rho Y_1\big|_{x+\delta x} + \dot{m}\delta x \qquad \text{(F3)}$$

Using a Taylors Series expansion equation (F3) becomes,

$$\overline{V}\rho Y_1\big|_x + \delta x\frac{d}{dx}\overline{V}\rho Y_1\big|_x + \dot{m}\delta x = 0 \qquad \text{(F4)}$$

Y_1 and ρ_f are constant, whereas v(x) and m(x) vary along the channel, therefore,

$$\frac{d}{dx}(\overline{V}\rho Y_1) = -\dot{m} \qquad \text{(F5)}$$

$$\rho Y_1\frac{d\overline{V}}{dx} = -\dot{m} \qquad \text{(F6)}$$

$$\frac{d\overline{V}}{dx} = -\frac{\dot{m}}{\rho Y_1} \tag{F7}$$

$$\int_{V(0)}^{V(x)} d\overline{V}(x) = -\int_{x=0}^{x} \frac{\dot{m}(x)}{\rho Y_1} dx \tag{F8}$$

$$\overline{V}_x - \overline{V}_0 = -\frac{1}{\rho Y_1} \int_0^x \dot{m}(x) dx \tag{F9}$$

In order to incorporate this equation into the anaylsis, the entrance boundary layers must have merged. This is to satisfy the assumption of a laminar velocity profile. m(x) can be integrated numerically by Simpsons Rule, simultaneously with the enthalpy balances given in Chapter 5.

PAGE NUMBERING AS ORIGINAL

APPENDIX G

Level Two Fortran Programme
Laminar Velocity Profile, Single Component

```
c     defining variables
      REAL Cp, RHO, V, T01, k, T3, E, TOTX, X0, T10, B10, DX, X, T1, B1,
     1K1, L1, K2, L2, K3, L3, K4, L4, F1, F2, DT1, DB1, A1, A2, A3, A4,
     1C1, C2, C3, M1, M2, M3, N1, N2, N3, B3, DT3, DB3, F3, F4, P1, P2,
     1P3, P4, Q1, Q2, Q3, Q4, T30, T03, G1, G2, G3, H1, H2, H3, C4, M4,
     1N4, Y1, Y3, T20, T40, T2, T4, B30, DT2, DT4, D
      INTEGER TOT, BOT, I, BUZZ
      BUZZ=1

c     inputting data from a file
      OPEN(UNIT=8,FILE='l2d.DAT')
      READ(8,*)Cp,RHO,V,T01,T03,k,E,TOTX,X0,T10,T30,B10,B30,DX,Y1,Y3
c     opening output file
      OPEN(UNIT=9,FILE='l2r.DAT')
      WRITE(9,*)
      WRITE(9,800)
800   FORMAT(8X,'X',10X,'T1',10X,'B1',12X,'T3',11X,'B3')

c     number of repititions
      TOT=NINT(TOTX/dX)-1
      DO 100 I=1,TOT

c     ENTRANCE REGION
c     Runge Kutta equations
      X=X0
      T1=T10
      B1=B10
      T3=T30
      B3=B30
      CALL HNCN(A1,A2,A3,A4,C1,C2,C3,C4,M1,M2,M3,M4,N1,N2,N3,N4,G1,G2
     1,G3,H1,H2,H3,F3,F4,T1,B1,B3,F1,F2,k,T3,E,T01,T03,RHO,Cp,V,Y1,Y3)
      K1=F1*dX
      L1=F2*dX
      P1=F3*DX
      Q1=F4*DX

      X=X0+(dX/2)
      T1=T10+(K1/2)
      B1=B10+(L1/2)
      T3=T30+(P1/2)
      B3=B30+(Q1/2)
```

```
      CALL HNCN(A1,A2,A3,A4,C1,C2,C3,C4,M1,M2,M3,M4,N1,N2,N3,N4,G1,G2
     1,G3,H1,H2,H3,F3,F4,T1,B1,B3,F1,F2,k,T3,E,T01,T03,RHO,Cp,V,Y1,Y3)
      K2=F1*dX
      L2=F2*dX
      P2=F3*DX
      Q2=F4*DX

      T1=T10+(K2/2)
      B1=B10+(L2/2)
      T3=T30+(P2/2)
      B3=B30+(Q2/2)
      CALL HNCN(A1,A2,A3,A4,C1,C2,C3,C4,M1,M2,M3,M4,N1,N2,N3,N4,G1,G2
     1,G3,H1,H2,H3,F3,F4,T1,B1,B3,F1,F2,k,T3,E,T01,T03,RHO,Cp,V,Y1,Y3)
      K3=F1*dX
      L3=F2*dX
      P3=F3*DX
      Q3=F4*DX

      X=X0+dX
      T1=T10+K3
      B1=B10+L3
      T3=T30+P3
      B3=B30+Q3
      CALL HNCN(A1,A2,A3,A4,C1,C2,C3,C4,M1,M2,M3,M4,N1,N2,N3,N4,G1,G2
     1,G3,H1,H2,H3,F3,F4,T1,B1,B3,F1,F2,k,T3,E,T01,T03,RHO,Cp,V,Y1,Y3)
      K4=F1*dX
      L4=F2*dX
      P4=F3*DX
      Q4=F4*DX

      DT1=(K1+(2*K2)+(2*K3)+K4)/6
      DB1=(L1+(2*L2)+(2*L3)+L4)/6
      DT3=(P1+(2*P2)+(2*P3)+P4)/6
      DB3=(Q1+(2*Q2)+(2*Q3)+Q4)/6

c     resetting initial values for next loop
      X0=X
      T10=T10+DT1
      B10=B10+DB1
      T30=T30+DT3
      B30=B30+DB3

c     output results to a file
      IF(I.EQ.BUZZ)THEN
       BUZZ=BUZZ+10
       WRITE(9,200)X0,T10,B10,T30,B30
200    FORMAT(3X,F8.6,3X,F10.4,3X,F10.8,3X,F10.4,3X,F11.8)
      END IF
```

```
c     check to see if constant section conditions are met
      D=Y1-0.00001
      IF(B10.GT.D) GOTO 1000
100   CONTINUE
      GOTO 2000

c     CONSTANT REGION
1000  T20=T01
      T40=T03
      B10=Y1
      B30=Y3
      BUZZ=1
      WRITE(9,*)
      WRITE(9,900)
900   FORMAT(6X,'X',11X,'T1',11X,'T2',11X,'T3',11X,'T4')
      WRITE(9,901)X0,T10,T20,T30,T40
901   FORMAT(3X,F8.6,5X,F8.4,5X,F8.4,5X,F8.4,5X,F8.4)

c     number of repititions
      BOT=TOT-I
      DO 101 I=1,BOT

c     Runge Kutta equations
      X=X0
      T1=T10
      T2=T20
      T3=T30
      T4=T40
      CALL HYCY(A1,A2,A3,C1,C2,C3,M1,M2,M3,N1,N2,N3,T1,T2,T3,T4,F1,F2,
     1F3,F4,k,E,RHO,Cp,V,B10,B30)
      K1=F1*dX
      L1=F2*dX
      P1=F3*DX
      Q1=F4*DX

      X=X0+(dX/2)
      T1=T10+(K1/2)
      T2=T20+(L1/2)
      T3=T30+(P1/2)
      T4=T40+(Q1/2)
      CALL HYCY(A1,A2,A3,C1,C2,C3,M1,M2,M3,N1,N2,N3,T1,T2,T3,T4,F1,F2,
     1F3,F4,k,E,RHO,Cp,V,B10,B30)
      K2=F1*dX
      L2=F2*dX
      P2=F3*DX
      Q2=F4*DX

      T1=T10+(K2/2)
      T2=T20+(L2/2)
```

```
  T3=T30+(P2/2)
  T4=T40+(Q2/2)
  CALL HYCY(A1,A2,A3,C1,C2,C3,M1,M2,M3,N1,N2,N3,T1,T2,T3,T4,F1,F2,
1F3,F4,k,E,RHO,Cp,V,B10,B30)
  K3=F1*dX
  L3=F2*dX
  P3=F3*DX
  Q3=F4*DX

  X=X0+dX
  T1=T10+K3
  T2=T20+L3
  T3=T30+P3
  T4=T40+Q3
  CALL HYCY(A1,A2,A3,C1,C2,C3,M1,M2,M3,N1,N2,N3,T1,T2,T3,T4,F1,F2,
1F3,F4,k,E,RHO,Cp,V,B10,B30)
  K4=F1*dX
  L4=F2*dX
  P4=F3*DX
  Q4=F4*DX

  DT1=(K1+(2*K2)+(2*K3)+K4)/6
  DT2=(L1+(2*L2)+(2*L3)+L4)/6
  DT3=(P1+(2*P2)+(2*P3)+P4)/6
  DT4=(Q1+(2*Q2)+(2*Q3)+Q4)/6

c   resetting initial values for next loop
      X0=X
      T10=T10+DT1
      T20=T20+DT2
      T30=T30+DT3
      T40=T40+DT4

c   output results to a file
      IF (I.EQ.BUZZ) THEN
        BUZZ=BUZZ+10
        WRITE(9,600)X0,T10,T20,T30,T40
600    FORMAT(3X,F8.6,5X,F8.4,5X,F8.4,5X,F8.4,5X,F8.4)
      END IF

101   CONTINUE
2000  WRITE(6,*)'YOUR RESULTS CAN BE FOUND IN "12r.DAT"'
      WRITE(6,*)
      WRITE(6,*)'END'

    CLOSE(UNIT=8)
    CLOSE(UNIT=9)
    STOP
    END
```

```
c     calculation of entrance region functions
      SUBROUTINE HNCN(A1,A2,A3,A4,C1,C2,C3,C4,M1,M2,M3,M4,N1,N2,N3,N4,
     1G1,G2,G3,H1,H2,H3,F3,F4,T1,B1,B3,F1,F2,k,T3,E,T01,T03,RHO,Cp,V,
     1Y1,Y3)
      REAL A1,A2,A3,A4,C1,C2,C3,C4,M1,M2,M3,M4,N1,N2,N3,N4,F3,F4,T1,B1,
     1F1,F2,G1,G2,G3,H1,H2,H3,k,T3,E,T01,RHO,Cp,V,T03,B3,Y1,Y3

        A1=(Cp*RHO*6*V)*((3*T1*B1/(10*Y1))-(3*T01*B1/(10*Y1))-(T1*B1*
     1  B1/(5*Y1*Y1))+(T01*B1*B1/(5*Y1*Y1))+(E*T1*B1*B1/(10*Y1*K))-(E*
     1  T3*B1*B1/(10*Y1*K))-(E*T1*B1*B1*B1/(15*Y1*Y1*K))+(E*T3*B1*B1*
     1  B1/(15*Y1*Y1*K)))
        A2=(Cp*RHO*6*V)*((3*B1*B1/(20*Y1))-(B1*B1*B1/(15*Y1*Y1))+(E*B1
     1  *B1*B1/(30*Y1*K))-((E*B1*B1*B1*B1)/(60*Y1*Y1*K)))
        A3=(Cp*RHO*6*V)*(((-1)*E*B1*B1*B1/(30*Y1*K))+((E*B1*B1*B1*B1)/
     1  (60*Y1*Y1*K)))
        A4=E*(T1-T3)

        C1=(Cp*RHO*6*V)*((9*T1*B1/(160*Y1))-(9*T01*B1/(160*Y1))-(7*T1*
     1  B1*B1/(320*Y1*Y1))+(7*T01*B1*B1/(320*Y1*Y1))+(E*T1*B1*B1/(320*
     1  Y1*K))-(E*T3*B1*B1/(320*Y1*K))-(E*T1*B1*B1*B1/(480*Y1*Y1*K))+(E
     1  *T3*B1*B1*B1/(480*Y1*Y1*K)))
        C2=(Cp*RHO*6*V)*((9*B1*B1/(320*Y1))-(7*B1*B1*B1/(960*Y1*Y1))+
     1  (E*B1*B1*B1/(960*Y1*K))-(E*B1*B1*B1*B1/(1920*Y1*Y1*K)))
        C3=(Cp*RHO*6*V)*((E*B1*B1*B1*B1/(1920*Y1*Y1*K))-(E*B1*B1*B1/(
     1  960*Y1*K)))
        C4=((5*E*(T1-T3))/4)-((3*k*(T01-T1))/(2*B1))

        G1=(A2*C1)-(A1*C2)
        G2=(A3*C1)-(A1*C3)
        G3=(A4*C1)-(A1*C4)

        M1=(Cp*RHO*6*V)*((3*T3*B3/(10*Y3))-(3*T03*B3/(10*Y3))-(T3*B3*
     1  B3/(5*Y3*Y3))+(T03*B3*B3/(5*Y3*Y3))+(E*T3*B3*B3/(10*Y3*K))-(E*
     1  T1*B3*B3/(10*Y3*K))-(E*T3*B3*B3*B3/(15*Y3*Y3*K))+(E*T1*B3*B3*
     1  B3/(15*Y3*Y3*K)))
        M2=(Cp*RHO*6*V)*((3*B3*B3/(20*Y3))-(B3*B3*B3/(15*Y3*Y3))+(E*B3
     1  *B3*B3/(30*Y3*K))-(E*B3*B3*B3*B3/(60*Y3*Y3*K)))
        M3=(Cp*RHO*6*V)*(((-1)*E*B3*B3*B3/(30*Y3*K))+(E*B3*B3*B3*B3/(60
     1  *Y3*Y3*K)))
        M4=E*(T3-T1)

        N1=(Cp*RHO*6*V)*((9*T3*B3/(160*Y3))-(9*T03*B3/(160*Y3))-(7*T3*
     1  B3*B3/(320*Y3*Y3))+(7*T03*B3*B3/(320*Y3*Y3))+(E*T3*B3*B3/(320*
     1  Y3*K))-(E*T1*B3*B3/(320*Y3*K))-(E*T3*B3*B3*B3/(480*Y3*Y3*K))+(E
     1  *T1*B3*B3*B3/(480*Y3*Y3*K)))
        N2=(Cp*RHO*6*V)*((9*B3*B3/(320*Y3))-(7*B3*B3*B3/(960*Y3*Y3))+
     1  (E*B3*B3*B3/(960*Y3*K))-(E*B3*B3*B3*B3/(1920*Y3*Y3*K)))
        N3=(Cp*RHO*6*V)*(((E*B3*B3*B3*B3)/(1920*Y3*Y3*K))-((E*B3*B3
     1  *B3)/(960*Y3*K)))
```

```
N4=((5*E*(T3-T1))/4)-((3*k*(T03-T3))/(2*B3))

H1=(M2*N1)-(M1*N2)
H2=(M3*N1)-(M1*N3)
H3=(M4*N1)-(M1*N4)

F3=((G1*H3)-(G3*H2))/((G2*H2)-(G1*H1))
F1=((G2*H3)-(G3*H1))/((G1*H1)-(G2*H2))
F2=(-1)*(((A2*F1)+(A3*F3)+A4)/A1)
F4=(-1)*(((M2*F3)+(M3*F1)+M4)/M1)

RETURN
END

c   calculation of constant region functions
    SUBROUTINE HYCY(A1,A2,A3,C1,C2,C3,M1,M2,M3,N1,N2,N3,T1,T2,T3,T4,
   1F1,F2,F3,F4,k,E,RHO,Cp,V,B10,B30)
    REAL A1,A2,A3,C1,C2,C3,M1,M2,M3,N1,N2,N3,T1,T2,T3,T4,F1,F2,F3,F4
   1,k,E,RHO,Cp,V,B10,B30

    A1=(Cp*RHO*6*V)*((B10/12)+((E*B10*B10)/(60*k)))
    A2=(Cp*RHO*6*V)*(B10/12)
    A3=(Cp*RHO*6*V)*((-1)*((E*B10*B10)/(60*k)))
    A4=E*(T1-T3)

    C1=(Cp*RHO*6*V)*((B10/16)+((21*E*B10*B10)/(1920*k)))
    C2=(Cp*RHO*6*V)*(B10/48)
    C3=(Cp*RHO*6*V)*((-1)*((21*E*B10*B10)/(1920*k)))
    C4=((3*k*(T1-T2))/(2*B10))+((5*E*(T1-T3))/4)

     G1=(A1*C2)-(A2*C1)
     G2=(A3*C2)-(A2*C3)
     G3=(A4*C2)-(A2*C4)

    M1=(Cp*RHO*6*V)*((B30/12)+((E*B30*B30)/(60*k)))
    M2=(Cp*RHO*6*V)*(B30/12)
    M3=(Cp*RHO*6*V)*((-1)*((E*B30*B30)/(60*k)))
    M4=E*(T3-T1)

    N1=(Cp*RHO*6*V)*((B30/16)+(21*E*B30*B30/(1920*k)))
    N2=(Cp*RHO*6*V)*(B30/48)
    N3=(Cp*RHO*6*V)*((-1)*((21*E*B30*B30)/(1920*k)))
    N4=((3*k*(T3-T4))/(2*B30))+((5*E*(T3-T1))/4)

     H1=(M1*N2)-(M2*N1)
     H2=(M3*N2)-(M2*N3)
     H3=(M4*N2)-(M2*N4)

     F3=((G1*H3)-(G3*H2))/((G2*H2)-(G1*H1))
```

```
  F1=((G2*H3)-(G3*H1))/((G1*H1)-(G2*H2))
  F2=(-1)*(((A1*F1)+(A3*F3)+A4)/A2)
  F4=(-1)*(((M1*F3)+(M3*F1)+M4)/M2)

RETURN
END
```

APPENDIX H

Level Three Fortran Programme
Laminar Velocity Profile, Full Program

```
c     defining variables
      REAL Cp, RHO, VH, VC, T01, k, T3, E, TOTX, X0, T10, DT4, P, Tm,
     1B10, DX, X, T1, B1, K1, L1, K2, L2, K3, L3, K4, L4, F1, F2, DT1,
     1DB1, A1, A2, A3, A4, C1, C2, C3, M1, M2, M3, N1, N2, N3, B3, DT3,
     1DB3, F3, F4, P1, P2, P3, P4, Q1, Q2, Q3, Q4, T30, T03, G1, G2, G3,
     1H1, H2, H3, C4, M4, N4, Y1, Y3, T20, T40, T2, T4, B30, DT2 , D, C
      INTEGER TOT, BOT, I, BUZZ
      BUZZ=1

c     inputting data from a file
      OPEN(UNIT=8,FILE='l3d.DAT')
      READ(8,*)Cp,RHO,VH,VC,T01,T03,k,TOTX,X0,T10,T30,B10,B30,DX,Y1,Y3
c     opening output file
      OPEN(UNIT=9,FILE='l3r.DAT')
      WRITE(9,*)
      WRITE(9,800)
800   FORMAT(8X,'X',10X,'T1',10X,'B1',12X,'T3',11X,'B3')

c     number of repititions
      TOT=NINT(TOTX/dX)-1
      DO 100 I=1,TOT

c     ENTRANCE REGION
c     Runge Kutta equations
      X=X0
      T1=T10
      B1=B10
      T3=T30
      B3=B30
      CALL CALCE(P,Tm,E,T10,T30)
      CALL HNCN(A1,A2,A3,A4,C1,C2,C3,C4,M1,M2,M3,M4,N1,N2,N3,N4,G1,
     1G2,G3,H1,H2,H3,F3,F4,T1,B1,B3,F1,F2,k,T3,E,T01,T03,RHO,Cp,VH,VC,
     1Y1,Y3)
      K1=F1*dX
      L1=F2*dX
      P1=F3*DX
      Q1=F4*DX

      X=X0+(dX/2)
      T1=T10+(K1/2)
      B1=B10+(L1/2)
      T3=T30+(P1/2)
```

```
  B3=B30+(Q1/2)
  CALL HNCN(A1,A2,A3,A4,C1,C2,C3,C4,M1,M2,M3,M4,N1,N2,N3,N4,G1,
1G2,G3,H1,H2,H3,F3,F4,T1,B1,B3,F1,F2,k,T3,E,T01,T03,RHO,Cp,VH,VC,
1Y1,Y3)
  K2=F1*dX
  L2=F2*dX
  P2=F3*DX
  Q2=F4*DX

  T1=T10+(K2/2)
  B1=B10+(L2/2)
  T3=T30+(P2/2)
  B3=B30+(Q2/2)
  CALL HNCN(A1,A2,A3,A4,C1,C2,C3,C4,M1,M2,M3,M4,N1,N2,N3,N4,G1,
1G2,G3,H1,H2,H3,F3,F4,T1,B1,B3,F1,F2,k,T3,E,T01,T03,RHO,Cp,VH,VC,
1Y1,Y3)
  K3=F1*dX
  L3=F2*dX
  P3=F3*DX
  Q3=F4*DX

  X=X0+dX
  T1=T10+K3
  B1=B10+L3
  T3=T30+P3
  B3=B30+Q3
  CALL HNCN(A1,A2,A3,A4,C1,C2,C3,C4,M1,M2,M3,M4,N1,N2,N3,N4,G1,
1G2,G3,H1,H2,H3,F3,F4,T1,B1,B3,F1,F2,k,T3,E,T01,T03,RHO,Cp,VH,VC,
1Y1,Y3)
  K4=F1*dX
  L4=F2*dX
  P4=F3*DX
  Q4=F4*DX

  DT1=(K1+(2*K2)+(2*K3)+K4)/6
  DB1=(L1+(2*L2)+(2*L3)+L4)/6
  DT3=(P1+(2*P2)+(2*P3)+P4)/6
  DB3=(Q1+(2*Q2)+(2*Q3)+Q4)/6

c   resetting initial values for next loop
  X0=X
  T10=T10+DT1
  B10=B10+DB1
  T30=T30+DT3
  B30=B30+DB3

c   output results to a file
  IF(I.EQ.BUZZ)THEN
    BUZZ=BUZZ+10
```

```
      WRITE(9,200)X0,T10,B10,T30,B30,E
200   FORMAT(3X,F8.6,3X,F10.4,3X,F10.8,3X,F10.4,3X,F11.8,2X,F8.2)
      END IF

c     check to see if constant section conditions are met
      D=Y1-0.0000001
      C=Y3-0.0000001
      IF(B10.GT.D) GOTO 3000
      IF(B30.GT.C) GOTO 6000

100   CONTINUE
      GOTO 2000

c     Hot - Entrance, Cold - Constant
6000  T40=T03
      B30=Y3
      BUZZ=1
      WRITE(9,801)
801   FORMAT(6X,'X',11X,'T1',11X,'B1',11X,'T3',11X,'T4')
      WRITE(9,802)X0,T10,B10,T30,T40
802   FORMAT(3X,F8.6,5X,F8.4,5X,F8.6,5X,F8.4,5X,F8.4)
      COT=TOT-I
      DO 101 I=1,COT

c     Runge Kutta equations
      X=X0
      T1=T10
      B1=B10
      T3=T30
      T4=T40
      CALL CALCE(P,Tm,E,T10,T30)
      CALL HNCY(A1,A2,A3,A4,C1,C2,C3,C4,M1,M2,M3,M4,N1,N2,N3,N4,G1,G2,
     1G3,F3,F4,T1,B1,B30,F1,F2,k,T3,T4,E,T01,RHO,Cp,VH,VC,Y1,Y3)
      K1=F1*dX
      L1=F2*dX
      P1=F3*DX
      Q1=F4*DX

      X=X0+(dX/2)
      T1=T10+(K1/2)
      B1=B10+(L1/2)
      T3=T30+(P1/2)
      T4=T40+(Q1/2)
      CALL HNCY(A1,A2,A3,A4,C1,C2,C3,C4,M1,M2,M3,M4,N1,N2,N3,N4,G1,G2,
     1G3,F3,F4,T1,B1,B30,F1,F2,k,T3,T4,E,T01,RHO,Cp,VH,VC,Y1,Y3)
      K2=F1*dX
      L2=F2*dX
      P2=F3*DX
      Q2=F4*DX
```

```
      T1=T10+(K2/2)
      B1=B10+(L2/2)
      T3=T30+(P2/2)
      T4=T40+(Q2/2)
      CALL HNCY(A1,A2,A3,A4,C1,C2,C3,C4,M1,M2,M3,M4,N1,N2,N3,N4,G1,G2,
     1G3,F3,F4,T1,B1,B30,F1,F2,k,T3,T4,E,T01,RHO,Cp,VH,VC,Y1,Y3)
      K3=F1*dX
      L3=F2*dX
      P3=F3*DX
      Q3=F4*DX

      X=X0+dX
      T1=T10+K3
      B1=B10+L3
      T3=T30+P3
      T4=T40+Q3
      CALL HNCY(A1,A2,A3,A4,C1,C2,C3,C4,M1,M2,M3,M4,N1,N2,N3,N4,G1,G2,
     1G3,F3,F4,T1,B1,B30,F1,F2,k,T3,T4,E,T01,RHO,Cp,VH,VC,Y1,Y3)
      K4=F1*dX
      L4=F2*dX
      P4=F3*DX
      Q4=F4*DX

      DT1=(K1+(2*K2)+(2*K3)+K4)/6
      DB1=(L1+(2*L2)+(2*L3)+L4)/6
      DT3=(P1+(2*P2)+(2*P3)+P4)/6
      DT4=(Q1+(2*Q2)+(2*Q3)+Q4)/6

c     resetting initial values for next loop
      X0=X
      T10=T10+DT1
      B10=B10+DB1
      T30=T30+DT3
      T40=T40+DT4

c     output results to a file
      IF(I.EQ.BUZZ)THEN
        BUZZ=BUZZ+10
        WRITE(9,300)X0,T10,B10,T30,T40,E
300    FORMAT(3X,F8.6,3X,F10.4,3X,F10.8,3X,F10.4,3X,F10.4,2X,F8.2)
      END IF

c     check to see if constant section conditions are met
      D=Y1-0.0000001
      IF(B10.GT.D) GOTO 4000
101   CONTINUE
      GOTO 2000
```

```
c       Hot - Constant, Cold - Entrance
3000  C=Y3-0.0000001
      IF(B30.GT.C) GOTO 4000

      T20=T01
      B10=Y1
      BUZZ=1
      WRITE(9,803)
803   FORMAT(6X,'X',11X,'T1',11X,'T2',11X,'T3',11X,'B2')
      WRITE(9,804)X0,T10,T20,T30,B30
804   FORMAT(3X,F8.6,5X,F8.4,5X,F8.4,5X,F8.4,5X,F8.4)

c     Number of repititions
      DOT=TOT-I
      DO 102 I=1,DOT

c     Runge Kutta equations
      X=X0
      T1=T10
      T2=T20
      T3=T30
      B3=B30
      CALL CALCE(P,Tm,E,T10,T30)
      CALL HYCN(A1,A2,A3,C1,C2,C3,M1,M2,M3,N1,N2,N3,T1,T2,T3,T4,F1,F2,
     1F3,F4,k,E,RHO,Cp,VH,VC,Y1,Y3,B10,B3,H1,H2,H3,T03)
      K1=F1*dX
      L1=F2*dX
      P1=F3*DX
      Q1=F4*DX

      X=X0+(dX/2)
      T1=T10+(K1/2)
      T2=T20+(L1/2)
      T3=T30+(P1/2)
      B3=B30+(Q1/2)
      CALL HYCN(A1,A2,A3,C1,C2,C3,M1,M2,M3,N1,N2,N3,T1,T2,T3,T4,F1,F2,
     1F3,F4,k,E,RHO,Cp,VH,VC,Y1,Y3,B10,B3,H1,H2,H3,T03)
      K2=F1*dX
      L2=F2*dX
      P2=F3*DX
      Q2=F4*DX

      T1=T10+(K2/2)
      T2=T20+(L2/2)
      T3=T30+(P2/2)
      B3=B30+(Q2/2)
      CALL HYCN(A1,A2,A3,C1,C2,C3,M1,M2,M3,N1,N2,N3,T1,T2,T3,T4,F1,F2,
     1F3,F4,k,E,RHO,Cp,VH,VC,Y1,Y3,B10,B3,H1,H2,H3,T03)
      K3=F1*dX
```

```
      L3=F2*dX
      P3=F3*DX
      Q3=F4*DX

      X=X0+dX
      T1=T10+K3
      T2=T20+L3
      T3=T30+P3
      B3=B30+Q3
      CALL HYCN(A1,A2,A3,C1,C2,C3,M1,M2,M3,N1,N2,N3,T1,T2,T3,T4,F1,F2,
     1F3,F4,k,E,RHO,Cp,VH,VC,Y1,Y3,B10,B3,H1,H2,H3,T03)
      K4=F1*dX
      L4=F2*dX
      P4=F3*DX
      Q4=F4*DX

      DT1=(K1+(2*K2)+(2*K3)+K4)/6
      DT2=(L1+(2*L2)+(2*L3)+L4)/6
      DT3=(P1+(2*P2)+(2*P3)+P4)/6
      DB3=(Q1+(2*Q2)+(2*Q3)+Q4)/6

c     resetting initial values for next loop
      X0=X
      T10=T10+DT1
      T20=T20+DT2
      T30=T30+DT3
      B30=B30+DB3

c     output results to a file
      IF(I.EQ.BUZZ)THEN
       BUZZ=BUZZ+10
       WRITE(9,400)X0,T10,T20,T30,B30,E
400    FORMAT(3X,F8.6,3X,F10.4,3X,F10.4,3X,F10.4,3X,F11.8,2X,F8.2)
      END IF

c     check to see if constant region conditions are met
      C=Y3-0.0000001
      IF(B30.GT.C) GOTO 4000
102   CONTINUE
      GOTO 2000

c     CONSTANT REGION
4000  T20=T01
      T40=T03
      B10=Y1
      B30=Y3
      BUZZ=1
      WRITE(9,*)
      WRITE(9,900)
```

```
900   FORMAT(6X,'X',11X,'T1',11X,'T2',11X,'T3',11X,'T4')
      WRITE(9,901)X0,T10,T20,T30,T40
901   FORMAT(3X,F8.6,5X,F8.4,5X,F8.4,5X,F8.4,5X,F8.4)

c     number of repititions
      BOT=TOT-I
      DO 103 I=1,BOT

c     Runge Kutta equations
      X=X0
      T1=T10
      T2=T20
      T3=T30
      T4=T40
      CALL CALCE(P,Tm,E,T10,T30)
      CALL HYCY(A1,A2,A3,C1,C2,C3,M1,M2,M3,N1,N2,N3,T1,T2,T3,T4,F1,F2,
     1F3,F4,k,E,RHO,Cp,VH,VC,B10,B30,G1,G2,G3,H1,H2,H3,M4,N4)
      K1=F1*dX
      L1=F2*dX
      P1=F3*DX
      Q1=F4*DX

      X=X0+(dX/2)
      T1=T10+(K1/2)
      T2=T20+(L1/2)
      T3=T30+(P1/2)
      T4=T40+(Q1/2)
      CALL HYCY(A1,A2,A3,C1,C2,C3,M1,M2,M3,N1,N2,N3,T1,T2,T3,T4,F1,F2,
     1F3,F4,k,E,RHO,Cp,VH,VC,B10,B30,G1,G2,G3,H1,H2,H3,M4,N4)
      K2=F1*dX
      L2=F2*dX
      P2=F3*DX
      Q2=F4*DX

      T1=T10+(K2/2)
      T2=T20+(L2/2)
      T3=T30+(P2/2)
      T4=T40+(Q2/2)
      CALL HYCY(A1,A2,A3,C1,C2,C3,M1,M2,M3,N1,N2,N3,T1,T2,T3,T4,F1,F2,
     1F3,F4,k,E,RHO,Cp,VH,VC,B10,B30,G1,G2,G3,H1,H2,H3,M4,N4)
      K3=F1*dX
      L3=F2*dX
      P3=F3*DX
      Q3=F4*DX

      X=X0+dX
      T1=T10+K3
      T2=T20+L3
      T3=T30+P3
```

```
  T4=T40+Q3
  CALL HYCY(A1,A2,A3,C1,C2,C3,M1,M2,M3,N1,N2,N3,T1,T2,T3,T4,F1,F2,
1F3,F4,k,E,RHO,Cp,VH,VC,B10,B30,G1,G2,G3,H1,H2,H3,M4,N4)
  K4=F1*dX
  L4=F2*dX
  P4=F3*DX
  Q4=F4*DX

  DT1=(K1+(2*K2)+(2*K3)+K4)/6
  DT2=(L1+(2*L2)+(2*L3)+L4)/6
  DT3=(P1+(2*P2)+(2*P3)+P4)/6
  DT4=(Q1+(2*Q2)+(2*Q3)+Q4)/6

c     resetting initial values for next loop
      X0=X
      T10=T10+DT1
      T20=T20+DT2
      T30=T30+DT3
      T40=T40+DT4

c     output results to a file
      IF (I.EQ.BUZZ) THEN
        BUZZ=BUZZ+10
        WRITE(9,500)X0,T10,T20,T30,T40,E
500     FORMAT(3X,F8.6,5X,F8.4,5X,F8.4,5X,F8.4,5X,F8.4,2X,F8.2)
      END IF

103   CONTINUE
2000  WRITE(6,*)'YOUR RESULTS CAN BE FOUND IN "l3r.DAT"'
      WRITE(6,*)
      WRITE(6,*)'END'

    CLOSE(UNIT=8)
    CLOSE(UNIT=9)
    STOP
    END

c     calculation of E
    SUBROUTINE CALCE(P,Tm,E,T10,T30)
    REAL P,Tm,E,T10,T30

    Tm=(T10+T30)/2
    P=EXP(23.238-(3841/(Tm-45)))
    E=((6086.035*P)/(Tm*Tm))+384.615

    RETURN
    END
```

```
c    calculation of functions
c    hot-entrance, cold-entrance
     SUBROUTINE HNCN(A1,A2,A3,A4,C1,C2,C3,C4,M1,M2,M3,M4,N1,N2,N3,N4,G1
    1,G2,G3,H1,H2,H3,F3,F4,T1,B1,B3,F1,F2,k,T3,E,T01,T03,RHO,Cp,VH,VC,
    1Y1,Y3)
     REAL A1,A2,A3,A4,C1,C2,C3,C4,M1,M2,M3,M4,N1,N2,N3,N4,F3,F4,T1,B1,
    1F1,F2,G1,G2,G3,H1,H2,H3,k,T3,E,T01,RHO,Cp,VH,VC,T03,B3,Y1,Y3

      A1=((Cp*RHO*6*VH))*((3*T1*B1/(10*Y1))-(3*T01*B1/(10*Y1))-(T1*
    1  B1*B1/(5*Y1*Y1))+(T01*B1*B1/(5*Y1*Y1))+(E*T1*B1*B1/(10*Y1*K))-
    1  (E*T3*B1*B1/(10*Y1*K))-(E*T1*B1*B1*B1/(15*Y1*Y1*K))+(E*T3*B1*
    1  B1*B1/(15*Y1*Y1*K)))
      A2=((Cp*RHO*6*VH))*((3*B1*B1/(20*Y1))-(B1*B1*B1/(15*Y1*Y1))+
    1  (E*B1*B1*B1/(30*Y1*K))-(E*B1*B1*B1*B1/(60*Y1*Y1*K)))
      A3=((Cp*RHO*6*VH))*((((-1)*E*B1*B1*B1)/(30*Y1*K))+((E*B1*B1*B1*
    1  B1)/(60*Y1*Y1*K)))
      A4=E*(T1-T3)

      C1=((Cp*RHO*6*VH))*((9*T1*B1/(160*Y1))-(9*T01*B1/(160*Y1))-(7
    1  *T1*B1*B1/(320*Y1*Y1))+(7*T01*B1*B1/(320*Y1*Y1))+(E*T1*B1*B1/
    1  (320*Y1*K))-(E*T3*B1*B1/(320*Y1*K))-(E*T1*B1*B1*B1/(480*Y1*Y1*
    1  K))+(E*T3*B1*B1*B1/(480*Y1*Y1*K)))
      C2=((Cp*RHO*6*VH))*((9*B1*B1/(320*Y1))-(7*B1*B1*B1/(960*Y1*Y1
    1  ))+(E*B1*B1*B1/(960*Y1*K))-(E*B1*B1*B1*B1/(1920*Y1*Y1*K)))
      C3=((Cp*RHO*6*VH))*(((E*B1*B1*B1*B1)/(1920*Y1*Y1*K))-((E*B1*B1*
    1  B1)/(960*Y1*K)))
      C4=((5*E*(T1-T3))/4)-((3*k*(T01-T1))/(2*B1))

      G1=(A2*C1)-(A1*C2)
      G2=(A3*C1)-(A1*C3)
      G3=(A4*C1)-(A1*C4)

      M1=((Cp*RHO*6*VC))*((3*T3*B3/(10*Y3))-(3*T03*B3/(10*Y3))-(T3*
    1  B3*B3/(5*Y3*Y3))+(T03*B3*B3/(5*Y3*Y3))+(E*T3*B3*B3/(10*Y3*K))-
    1  (E*T1*B3*B3/(10*Y3*K))-(E*T3*B3*B3*B3/(15*Y3*Y3*K))+(E*T1*B3*
    1  B3*B3/(15*Y3*Y3*K)))
      M2=((Cp*RHO*6*VC))*((3*B3*B3/(20*Y3))-(B3*B3*B3/(15*Y3*Y3))+
    1  (E*B3*B3*B3/(30*Y3*K))-(E*B3*B3*B3*B3/(60*Y3*Y3*K)))
      M3=((Cp*RHO*6*VC))*((((-1)*E*B3*B3*B3)/(30*Y3*K))+((E*B3*B3*B3*
    1  B3)/(60*Y3*Y3*K)))
      M4=E*(T3-T1)

      N1=((Cp*RHO*6*VC))*((9*T3*B3/(160*Y3))-(9*T03*B3/(160*Y3))-(7
    1  *T3*B3*B3/(320*Y3*Y3))+(7*T03*B3*B3/(320*Y3*Y3))+(E*T3*B3*B3/
    1  (320*Y3*K))-(E*T1*B3*B3/(320*Y3*K))-(E*T3*B3*B3*B3/(480*Y3*Y3*
    1  K))+(E*T1*B3*B3*B3/(480*Y3*Y3*K)))
      N2=((Cp*RHO*6*VC))*((9*B3*B3/(320*Y3))-(7*B3*B3*B3/(960*Y3*Y3
    1  ))+(E*B3*B3*B3/(960*Y3*K))-(E*B3*B3*B3*B3/(1920*Y3*Y3*K)))
      N3=((Cp*RHO*6*VC))*(((E*B3*B3*B3*B3)/(1920*Y3*Y3*K))-((E*B3
```

```
1   *B3*B3)/(960*Y3*K)))
    N4=((5*E*(T3-T1))/4)-((3*k*(T03-T3))/(2*B3))

    H1=(M2*N1)-(M1*N2)
    H2=(M3*N1)-(M1*N3)
    H3=(M4*N1)-(M1*N4)

    F3=((G1*H3)-(G3*H2))/((G2*H2)-(G1*H1))
    F1=((G2*H3)-(G3*H1))/((G1*H1)-(G2*H2))
    F2=(-1)*(((A2*F1)+(A3*F3)+A4)/A1)
    F4=(-1)*(((M2*F3)+(M3*F1)+M4)/M1)

    RETURN
    END

c   hot-constant, cold-entrance
    SUBROUTINE HYCN(A1,A2,A3,C1,C2,C3,M1,M2,M3,N1,N2,N3,T1,T2,T3,T4,
   1F1,F2,F3,F4,k,E,RHO,Cp,VH,VC,Y1,Y3,B10,B3,H1,H2,H3,T03)
    REAL A1,A2,A3,C1,C2,C3,M1,M2,M3,N1,N2,N3,T1,T2,T3,T4,F1,F2,F3,F4
   1,k,E,RHO,Cp,VH,VC,Y1,Y3,B10,B3,H1,H2,H3,T03

    A1=((Cp*RHO*6*VH))*((B10/12)+(E*B10*B10/(60*k)))
    A2=((Cp*RHO*6*VH))*(B10/12)
    A3=((Cp*RHO*6*VH))*((-1)*((E*B10*B10)/(60*k)))
    A4=E*(T1-T3)

    C1=((Cp*RHO*6*VH))*((B10/16)+((21*E*B10*B10)/(1920*k)))
    C2=((Cp*RHO*6*VH))*(B10/48)
    C4=((Cp*RHO*6*VH))*((-1)*(21*E*B10*B10)/(1920*k))
    C3=((3*k*(T1-T2))/(2*B10))+((5*E*(T1-T3))/4)

     G1=(A1*C2)-(A2*C1)
     G2=(A3*C2)-(A2*C3)
     G3=(A4*C2)-(A2*C4)

     M1=((Cp*RHO*6*VC))*((3*T3*B3/(10*Y3))-(3*T03*B3/(10*Y3))-(T3*
   1  B3*B3/(5*Y3*Y3))+(T03*B3*B3/(5*Y3*Y3))+(E*T3*B3*B3/(10*Y3*K))-
   1  (E*T1*B3*B3/(10*Y3*K))-(E*T3*B3*B3*B3/(15*Y3*Y3*K))+(E*T1*B3*
   1  B3*B3/(15*Y3*Y3*K)))
     M2=((Cp*RHO*6*VC))*((3*B3*B3/(20*Y3))-(B3*B3*B3/(15*Y3*Y3))+
   1  (E*B3*B3*B3/(30*Y3*K))-(E*B3*B3*B3*B3/(60*Y3*Y3*K)))
     M3=((Cp*RHO*6*VC))*(((-1)*E*B3*B3*B3/(30*Y3*K))+(E*B3*B3*B3*B3/
   1  (60*Y3*Y3*K)))
     M4=E*(T3-T1)

     N1=((Cp*RHO*6*VC))*((9*T3*B3/(160*Y3))-(9*T03*B3/(160*Y3))-(7
   1  *T3*B3*B3/(320*Y3*Y3))+(7*T03*B3*B3/(320*Y3*Y3))+(E*T3*B3*B3/
   1  (320*Y3*K))-(E*T1*B3*B3/(320*Y3*K))-(E*T3*B3*B3*B3/(480*Y3*Y3*
   1  K))+(E*T1*B3*B3*B3/(480*Y3*Y3*K)))
```

```
 N2=((Cp*RHO*6*VC))*((9*B3*B3/(320*Y3))-(7*B3*B3*B3/(960*Y3*Y3
1  ))+(E*B3*B3*B3/(960*Y3*K))-(E*B3*B3*B3*B3/(1920*Y3*Y3*K)))
 N3=((Cp*RHO*6*VC))*(((E*B3*B3*B3*B3)/(1920*Y3*Y3*K))-((E*B3
1  *B3*B3)/(960*Y3*K)))
 N4=((5*E*(T3-T1))/4)-((3*k*(T03-T3))/(2*B3))

  H1=(M2*N1)-(M1*N2)
  H2=(M3*N1)-(M1*N3)
  H3=(M4*N1)-(M1*N4)

  F3=((G1*H3)-(G3*H2))/((G2*H2)-(G1*H1))
  F1=((G2*H3)-(G3*H1))/((G1*H1)-(G2*H2))
  F2=(-1)*(((A1*F1)+(A3*F3)+A4)/A2)
  F4=(-1)*(((M2*F3)+(M3*F1)+M4)/M1)

 RETURN
 END

c    hot-entrance, cold-constant
 SUBROUTINE HNCY(A1,A2,A3,A4,C1,C2,C3,C4,M1,M2,M3,M4,N1,N2,N3,N4,
1 G1,G2,G3,F3,F4,T1,B1,B30,F1,F2,k,T3,T4,E,T01,RHO,Cp,VH,VC,Y1,Y3)
 REAL A1,A2,A3,A4,C1,C2,C3,C4,M1,M2,M3,M4,N1,N2,N3,N4,F3,F4,T1,B1,
1F1,F2,G1,G2,G3,k,T3,E,T01,RHO,Cp,VH,VC,B30,Y1,Y3,T4

  A1=((Cp*RHO*6*VH))*((3*T1*B1/(10*Y1))-(3*T01*B1/(10*Y1))-(T1*
1  B1*B1/(5*Y1*Y1))+(T01*B1*B1/(5*Y1*Y1))+(E*T1*B1*B1/(10*Y1*K))-
1  (E*T3*B1*B1/(10*Y1*K))-(E*T1*B1*B1*B1/(15*Y1*Y1*K))+(E*T3*B1*
1  B1*B1/(15*Y1*Y1*K)))
  A2=((Cp*RHO*6*VH))*((3*B1*B1/(20*Y1))-(B1*B1*B1/(15*Y1*Y1))+
1  (E*B1*B1*B1/(30*Y1*K))-(E*B1*B1*B1*B1/(60*Y1*Y1*K)))
  A3=((Cp*RHO*6*VH))*(((-1)*E*B1*B1*B1/(30*Y1*K))+(E*B1*B1*B1*B1/
1  (60*Y1*Y1*K)))
  A4=E*(T1-T3)

  C1=((Cp*RHO*6*VH))*((9*T1*B1/(160*Y1))-(9*T01*B1/(160*Y1))-(7
1  *T1*B1*B1/(320*Y1*Y1))+(7*T01*B1*B1/(320*Y1*Y1))+(E*T1*B1*B1/
1  (320*Y1*K))-(E*T3*B1*B1/(320*Y1*K))-(E*T1*B1*B1*B1/(480*Y1*Y1*
1  K))+(E*T3*B1*B1*B1/(480*Y1*Y1*K)))
  C2=((Cp*RHO*6*VH))*((9*B1*B1/(320*Y1))-(7*B1*B1*B1/(960*Y1*Y1
1  ))+(E*B1*B1*B1/(960*Y1*K))-(E*B1*B1*B1*B1/(1920*Y1*Y1*K)))
  C3=((Cp*RHO*6*VH))*((E*B1*B1*B1*B1/(1920*Y1*Y1*K))-(E*B1*B1*
1  B1/(960*Y1*K)))
  C4=((5*E*(T1-T3))/4)-((3*k*(T01-T1))/(2*B1))

  G1=(A2*C1)-(A1*C2)
  G2=(A3*C1)-(A1*C3)
  G3=(A4*C1)-(A1*C4)

 M1=((Cp*RHO*6*VC))*((B30/12)+((E*B30*B30)/(60*k)))
```

```
M2=((Cp*RHO*6*VC))*(B30/12)
M3=((Cp*RHO*6*VC))*((-1)*(E*B30*B30)/(60*k))
M4=E*(T3-T1)

N1=((Cp*RHO*6*VC))*((B30/16)+((21*E*B30*B30)/(1920*k)))
N2=((Cp*RHO*6*VC))*(B30/48)
N3=((Cp*RHO*6*VC))*((-1)*(21*E*B30*B30)/(1920*k))
N4=((3*k*(T3-T4))/(2*B30))+((5*E*(T3-T1))/4)

 H1=(M1*N2)-(M2*N1)
 H2=(M3*N2)-(M2*N3)
 H3=(M4*N2)-(M2*N4)

  F3=((G1*H3)-(G3*H2))/((G2*H2)-(G1*H1))
  F1=((G2*H3)-(G3*H1))/((G1*H1)-(G2*H2))
  F2=(-1)*(((A2*F1)+(A3*F3)+A4)/A1)
  F4=(-1)*(((M1*F3)+(M3*F1)+M4)/M2)

 RETURN
 END

c   hot-constant, cold-constant
 SUBROUTINE HYCY(A1,A2,A3,C1,C2,C3,M1,M2,M3,N1,N2,N3,T1,T2,T3,T4,
1F1,F2,F3,F4,k,E,RHO,Cp,VH,VC,B10,B30,G1,G2,G3,H1,H2,H3,M4,N4)
 REAL A1,A2,A3,C1,C2,C3,M1,M2,M3,N1,N2,N3,T1,T2,T3,T4,F1,F2,F3,F4
1,k,E,RHO,Cp,VH,VC,B10,B30,G1,G2,G3,H1,H2,H3,M4,N4

A1=((Cp*RHO*6*VH))*((B10/12)+(E*B10*B10/(60*k)))
A2=((Cp*RHO*6*VH))*(B10/12)
A3=(-1)*((Cp*RHO*6*VH))*(E*B10*B10/(60*k))
A4=E*(T1-T3)

C1=((Cp*RHO*6*VH))*((B10/16)+(21*E*B10*B10/(1920*k)))
C2=((Cp*RHO*6*VH))*(B10/48)
C3=(-1)*((Cp*RHO*6*VH))*(21*E*B10*B10/(1920*k))
C4=((3*k/(2*B10))*(T1-T2))+((5*E/4)*(T1-T3))

 G1=(A1*C2)-(A2*C1)
 G2=(A3*C2)-(A2*C3)
 G3=(A4*C2)-(A2*C4)

M1=((Cp*RHO*6*VC))*((B30/12)+(E*B30*B30/(60*k)))
M2=((Cp*RHO*6*VC))*(B30/12)
M3=(-1)*((Cp*RHO*6*VC))*(E*B30*B30/(60*k))
M4=E*(T3-T1)

N1=((Cp*RHO*6*VC))*((B30/16)+(21*E*B30*B30/(1920*k)))
N2=((Cp*RHO*6*VC))*(B30/48)
N3=(-1)*((Cp*RHO*6*VC))*(21*E*B30*B30/(1920*k))
```

```
N4=((3*k/(2*B30))*(T3-T4))+((5*E/4)*(T3-T1))

 H1=(M1*N2)-(M2*N1)
 H2=(M3*N2)-(M2*N3)
 H3=(M4*N2)-(M2*N4)

 F1=((G2*H3)-(G3*H1))/((G1*H1)-(G2*H2))
 F3=((G1*H3)-(G3*H2))/((G2*H2)-(G1*H1))
 F2=(-1)*(((A1*F1)+(A3*F3)+A4)/A2)
 F4=(-1)*(((M1*F3)+(M3*F1)+M4)/M2)

RETURN
END
```

APPENDIX I

Level Four Fortran Programme
Laminar Velocity Profile, Boiling and Condensing Surfaces

```
c     defining variables
      REAL Cp,RHO,VH,VC,T01,T03,E,G,J,TOTX,X0,P,Tm,k,B10,B20,B30,B40,B1,
     1B2,B3,B4,DB1,DB2,DB3,DB4,DX,X,T1,T2,T3,T4,T10,T20,T30,T40,DT1,DT2,
     1DT3,DT4,TH,TC,A1,A2,A3,A4,C1,C2,C3,C4,M1,M2,M3,M4,N1,N2,N3,N4,K1,
     1K2,K3,K4,L1,L2,L3,L4,F1,F2,F3,F4,F5,F6,F7,F8,P1,P2,P3,P4,Q1,Q2,Q3,
     1Q4,G1,G2,G3,H1,H2,H3,Y1,Y3,O1,O2,O3,O4,R1,R2,R3,R4,S1,S2,S3,S4,Z1,
     1Z2,Z3,Z4,D,C,BH,BC
      INTEGER TOT, COT, DOT, I, BUZZ
      BUZZ=1

c     inputting data from a file
      OPEN(UNIT=8,FILE='14d.DAT')
      READ(8,*)Cp,RHO,VH,VC,T01,T03,k,TOTX,X0,T10,T20,T30,T40,B10,
     1B20,B30,B40,DX,Y1,Y3,TH,TC,G,J

c     opening output file
      OPEN(UNIT=9,FILE='14r.DAT')
      WRITE(9,*)
      WRITE(9,800)
800   FORMAT(4X,'X',10X,'T2',7X,'B2',7X,'T1',7X,'B1',7X,'T3',7X,'B3',7X
     1,'B4',7X,'T4')

c     number of repititions
      TOT=NINT(TOTX/dX)-1
      DO 100 I=1,TOT

c     ENTRANCE REGION

c     Runge Kutta equations
      X=X0
      T1=T10
      B1=B10
      T3=T30
      B3=B30
      T2=T20
      B2=B20
      T4=T40
      B4=B40
      CALL CALCE(P,Tm,E,T10,T30)
      CALL HNCN(A1,A2,A3,A4,C1,C2,C3,C4,M1,M2,M3,M4,N1,N2,N3,
     1N4,G1,G2,G3,H1,H2,H3,F3,F4,T1,B1,B3,F1,F2,T3,E,T01,T03,RHO,
     1Cp,VH,VC,Y1,Y3,k)
```

```
  CALL WALL(A1,A2,A3,C1,C2,C3,M1,M2,M3,N1,N2,N3,Cp,RHO,VH,VC,
1B2,B4,T01,T03,T2,T4,Y1,Y3,G,J,K,TH,TC,F5,F6,F7,F8)
  K1=F1*dX
  L1=F2*dX
  P1=F3*DX
  Q1=F4*DX
  O1=F5*DX
  R1=F6*DX
  S1=F7*DX
  Z1=F8*DX

  X=X0+(dX/2)
  T1=T10+(K1/2)
  B1=B10+(L1/2)
  T3=T30+(P1/2)
  B3=B30+(Q1/2)
  T2=T20+(O1/2)
  B2=B20+(R1/2)
  T4=T40+(S1/2)
  B4=B40+(Z1/2)

  CALL HNCN(A1,A2,A3,A4,C1,C2,C3,C4,M1,M2,M3,M4,N1,N2,N3,
1N4,G1,G2,G3,H1,H2,H3,F3,F4,T1,B1,B3,F1,F2,T3,E,T01,T03,RHO,
1Cp,VH,VC,Y1,Y3,k)
  CALL WALL(A1,A2,A3,C1,C2,C3,M1,M2,M3,N1,N2,N3,Cp,RHO,VH,VC,
1 B2,B4,T01,T03,T2,T4,Y1,Y3,G,J,K,TH,TC,F5,F6,F7,F8)

  K2=F1*dX
  L2=F2*dX
  P2=F3*DX
  Q2=F4*DX
  O2=F5*DX
  R2=F6*DX
  S2=F7*DX
  Z2=F8*DX

  T1=T10+(K2/2)
  B1=B10+(L2/2)
  T3=T30+(P2/2)
  B3=B30+(Q2/2)
  T2=T20+(O2/2)
  B2=B20+(R2/2)
  T4=T40+(S2/2)
  B4=B40+(Z2/2)

  CALL HNCN(A1,A2,A3,A4,C1,C2,C3,C4,M1,M2,M3,M4,N1,N2,N3,
1N4,G1,G2,G3,H1,H2,H3,F3,F4,T1,B1,B3,F1,F2,T3,E,T01,T03,RHO,
1Cp,VH,VC,Y1,Y3,k)
  CALL WALL(A1,A2,A3,C1,C2,C3,M1,M2,M3,N1,N2,N3,Cp,RHO,VH,VC,
```

```
1 B2,B4,T01,T03,T2,T4,Y1,Y3,G,J,K,TH,TC,F5,F6,F7,F8)

  K3=F1*dX
  L3=F2*dX
  P3=F3*DX
  Q3=F4*DX
  O3=F5*DX
  R3=F6*DX
  S3=F7*DX
  Z3=F8*DX

  X=X0+dX
  T1=T10+K3
  B1=B10+L3
  T3=T30+P3
  B3=B30+Q3
  T2=T20+O3
  B2=B20+R3
  T4=T40+S3
  B4=B40+Z3

  CALL HNCN(A1,A2,A3,A4,C1,C2,C3,C4,M1,M2,M3,M4,N1,N2,N3,
1N4,G1,G2,G3,H1,H2,H3,F3,F4,T1,B1,B3,F1,F2,T3,E,T01,T03,RHO,
1Cp,VH,VC,Y1,Y3,k)
  CALL WALL(A1,A2,A3,C1,C2,C3,M1,M2,M3,N1,N2,N3,Cp,RHO,VH,VC,
1 B2,B4,T01,T03,T2,T4,Y1,Y3,G,J,K,TH,TC,F5,F6,F7,F8)

  K4=F1*dX
  L4=F2*dX
  P4=F3*DX
  Q4=F4*DX
  O4=F5*DX
  R4=F6*DX
  S4=F7*DX
  Z4=F8*DX

  DT1=(K1+(2*K2)+(2*K3)+K4)/6
  DB1=(L1+(2*L2)+(2*L3)+L4)/6
  DT3=(P1+(2*P2)+(2*P3)+P4)/6
  DB3=(Q1+(2*Q2)+(2*Q3)+Q4)/6
  DT2=(O1+(2*O2)+(2*O3)+O4)/6
  DB2=(R1+(2*R2)+(2*R3)+R4)/6
  DT4=(S1+(2*S2)+(2*S3)+S4)/6
  DB4=(Z1+(2*Z2)+(2*Z3)+Z4)/6

c   resetting initial values for next loop
  X0=X
  T10=T10+DT1
  B10=B10+DB1
```

```
      T30=T30+DT3
      B30=B30+DB3
      T20=T20+DT2
      B20=B20+DB2
      T40=T40+DT4
      B40=B40+DB4

c     output results to a file
      IF(I.EQ.BUZZ)THEN
       BUZZ=BUZZ+100
       WRITE(9,200)X0,T20,B20,T10,B10,T30,B30,T40,B40,E
200     FORMAT(1X,F8.6,1X,F10.3,1X,F8.6,1X,F8.3,1X,F8.6,1X,F8.3,1X,
     1F8.6,1X,F10.3,1X,F8.6,1X,F7.2)
       END IF

c     check to see if constant section conditions are met
      D=Y1-0.0000001
      C=Y3-0.0000001
      BH=B10+B20
      BC=B30+B40
      IF(BH.GT.D) GOTO 3000
      IF(BC.GT.C) GOTO 6000

100   CONTINUE
      GOTO 2000

c     Hot - Entrance, Cold - Constant

6000  T40=T03
      B30=Y3
      BUZZ=1
      WRITE(9,801)
801   FORMAT(6X,'X',6X,'T2',6X,'B2',6X,'T1',6X,'B1',6X,'T3',6X,'T4')
      WRITE(9,802)X0,T20,B20,T10,B10,T30,T40
802   FORMAT(3X,F8.6,3X,F8.4,3X,F10.8,3X,F8.4,3X,F10.8,3X,F8.4,3X,F8.4)
      COT=TOT-I
      DO 101 I=1,COT

c     Runge Kutta equations
      X=X0
      T1=T10
      B1=B10
      T3=T30
      T4=T40
      T2=T20
      B2=B20
      CALL CALCE(P,Tm,E,T10,T30)
      CALL HNCY(A1,A2,A3,A4,C1,C2,C3,C4,M1,M2,M3,M4,N1,N2,N3,N4,G1,G2
     1,G3,F3,F4,T1,B1,B30,F1,F2,k,T3,T4,E,T01,RHO,Cp,VH,VC,Y1,Y3,J,TH)
```

```
  CALL WALLH(A1,A2,A3,C1,C2,C3,Cp,RHO,VH,B2,Y1,G,k,T01,TC,F5,
1F6,T2)
  K1=F1*dX
  L1=F2*dX
  P1=F3*DX
  Q1=F4*DX
  O1=F5*DX
  R1=F6*DX

  X=X0+(dX/2)
  T1=T10+(K1/2)
  B1=B10+(L1/2)
  T3=T30+(P1/2)
  T4=T40+(Q1/2)
  T2=T20+(O1/2)
  B2=B20+(R1/2)
  CALL HNCY(A1,A2,A3,A4,C1,C2,C3,C4,M1,M2,M3,M4,N1,N2,N3,N4,G1,G2
1,G3,F3,F4,T1,B1,B30,F1,F2,k,T3,T4,E,T01,RHO,Cp,VH,VC,Y1,Y3,J,TH)
  CALL WALLH(A1,A2,A3,C1,C2,C3,Cp,RHO,VH,B2,Y1,G,k,T01,TC,F5,
1F6,T2)
  K2=F1*dX
  L2=F2*dX
  P2=F3*DX
  Q2=F4*DX
  O2=F5*DX
  R2=F6*DX

  T1=T10+(K2/2)
  B1=B10+(L2/2)
  T3=T30+(P2/2)
  T4=T40+(Q2/2)
  T2=T20+(O2/2)
  B2=B20+(R2/2)
  CALL HNCY(A1,A2,A3,A4,C1,C2,C3,C4,M1,M2,M3,M4,N1,N2,N3,N4,G1,G2
1,G3,F3,F4,T1,B1,B30,F1,F2,k,T3,T4,E,T01,RHO,Cp,VH,VC,Y1,Y3,J,TH)
  CALL WALLH(A1,A2,A3,C1,C2,C3,Cp,RHO,VH,B2,Y1,G,k,T01,TC,F5,
1F6,T2)
  K3=F1*dX
  L3=F2*dX
  P3=F3*DX
  Q3=F4*DX
  O3=F5*DX
  R3=F6*DX

  X=X0+dX
  T1=T10+K3
  B1=B10+L3
  T3=T30+P3
  T4=T40+Q3
```

```
      T2=T20+O3
      B2=B20+R1
      CALL HNCY(A1,A2,A3,A4,C1,C2,C3,C4,M1,M2,M3,M4,N1,N2,N3,N4,G1,G2
     1,G3,F3,F4,T1,B1,B30,F1,F2,k,T3,T4,E,T01,RHO,Cp,VH,VC,Y1,Y3,J,TH)
      CALL WALLH(A1,A2,A3,C1,C2,C3,Cp,RHO,VH,B2,Y1,G,k,T01,TC,F5,
     1F6,T2)
      K4=F1*dX
      L4=F2*dX
      P4=F3*DX
      Q4=F4*DX
      O4=F5*DX
      R4=F6*DX

      DT1=(K1+(2*K2)+(2*K3)+K4)/6
      DB1=(L1+(2*L2)+(2*L3)+L4)/6
      DT3=(P1+(2*P2)+(2*P3)+P4)/6
      DT4=(Q1+(2*Q2)+(2*Q3)+Q4)/6
      DT2=(O1+(2*O2)+(2*O3)+O4)/6
      DB2=(R1+(2*R2)+(2*R3)+R4)/6

c     resetting initial values for next loop
      X0=X
      T10=T10+DT1
      B10=B10+DB1
      T30=T30+DT3
      T40=T40+DT4
      T20=T20+DT2
      B20=B20+DB2

c     output results to a file
      IF(I.EQ.BUZZ)THEN
       BUZZ=BUZZ+100
       WRITE(9,300)X0,T20,B20,T10,B10,T30,T40,E
300     FORMAT(2X,F7.6,2X,F8.3,2X,F10.8,2X,F8.3,2X,F10.8,2X,F8.3,2X,
     1F8.3,2X,F7.2)
      END IF

c     check to see if constant section conditions are met
      D=Y1-0.0000001
      BH=B10+B20
      IF(BH.GT.D) THEN
       T20=T01
       B10=Y1
       GOTO 4000
      END IF
101    CONTINUE
      GOTO 2000

c     Hot - Constant, Cold - Entrance
```

```
3000   T20=T01
       B10=Y1
       C=Y3-0.0000001
       IF(BC.GT.C) THEN
        T40=T03
        B30=Y3
        GOTO 4000
       END IF

      BUZZ=1
      WRITE(9,803)
803    FORMAT(4X,'X',4X,'T1',4X,'T2',4X,'T3',4X,'B3',4X,'T4',4X,'B4',4X
     1 ,'E')
       WRITE(9,804)X0,T10,T20,T30,B30,T40,B40,E
804    FORMAT(2X,F7.6,2X,F8.3,2X,F8.3,2X,F8.3,2X,F10.8,2X,F8.3,2X,F10.8,
     1 2X,F7.2)

       DOT=TOT-I
       DO 102 I=1,DOT

c      Runge Kutta equations
       X=X0
       T1=T10
       T2=T20
       T3=T30
       B3=B30
       T4=T40
       B4=B40
       CALL CALCE(P,Tm,E,T10,T30)
       CALL HYCN(A1,A2,A3,C1,C2,C3,M1,M2,M3,N1,N2,N3,T1,T2,T3,T4,
     1F1,F2,F3,F4,k,E,RHO,Cp,VH,VC,Y1,Y3,B10,B3,H1,H2,H3,T03,G,TC)
       CALL WALLC(M1,M2,M3,N1,N2,N3,Cp,RHO,VC,B4,Y3,J,k,T03,TH,F5,
     1F6,T4)
       K1=F1*dX
       L1=F2*dX
       P1=F3*DX
       Q1=F4*DX
       O1=F5*DX
       R1=F6*DX

       X=X0+(dX/2)
       T1=T10+(K1/2)
       T2=T20+(L1/2)
       T3=T30+(P1/2)
       B3=B30+(Q1/2)
       T4=T40+(O1/2)
       B4=B40+(R1/2)
       CALL HYCN(A1,A2,A3,C1,C2,C3,M1,M2,M3,N1,N2,N3,T1,T2,T3,T4,
```

```
1F1,F2,F3,F4,k,E,RHO,Cp,VH,VC,Y1,Y3,B10,B3,H1,H2,H3,T03,G,TC)
  CALL WALLC(M1,M2,M3,N1,N2,N3,Cp,RHO,VC,B4,Y3,J,k,T03,TH,F5,
1F6,T4)
  K2=F1*dX
  L2=F2*dX
  P2=F3*DX
  Q2=F4*DX
  O2=F5*DX
  R2=F6*DX

  T1=T10+(K2/2)
  T2=T20+(L2/2)
  T3=T30+(P2/2)
  B3=B30+(Q2/2)
  T4=T40+(O2/2)
  B4=B40+(R2/2)
  CALL HYCN(A1,A2,A3,C1,C2,C3,M1,M2,M3,N1,N2,N3,T1,T2,T3,T4,
1F1,F2,F3,F4,k,E,RHO,Cp,VH,VC,Y1,Y3,B10,B3,H1,H2,H3,T03,G,TC)
  CALL WALLC(M1,M2,M3,N1,N2,N3,Cp,RHO,VC,B4,Y3,J,k,T03,TH,F5,
1F6,T4)
  K3=F1*dX
  L3=F2*dX
  P3=F3*DX
  Q3=F4*DX
  O3=F5*DX
  R3=F6*DX

  X=X0+dX
  T1=T10+K3
  T2=T20+L3
  T3=T30+P3
  B3=B30+Q3
  T4=T40+O3
  B4=B40+R3
  CALL HYCN(A1,A2,A3,C1,C2,C3,M1,M2,M3,N1,N2,N3,T1,T2,T3,T4,
1F1,F2,F3,F4,k,E,RHO,Cp,VH,VC,Y1,Y3,B10,B3,H1,H2,H3,T03,G,TC)
  CALL WALLC(M1,M2,M3,N1,N2,N3,Cp,RHO,VC,B4,Y3,J,k,T03,TH,F5,
1F6,T4)
  K4=F1*dX
  L4=F2*dX
  P4=F3*DX
  Q4=F4*DX
  O4=F5*DX
  R4=F6*DX

  DT1=(K1+(2*K2)+(2*K3)+K4)/6
  DT2=(L1+(2*L2)+(2*L3)+L4)/6
  DT3=(P1+(2*P2)+(2*P3)+P4)/6
  DB3=(Q1+(2*Q2)+(2*Q3)+Q4)/6
```

```
      DT4=(O1+(2*O2)+(2*O3)+O4)/6
      DB4=(R1+(2*R2)+(2*R3)+R4)/6

c     resetting initial values for next loop
      X0=X
      T10=T10+DT1
      T20=T20+DT2
      T30=T30+DT3
      B30=B30+DB3
      T40=T40+DT4
      B40=B40+DB4

c     output results to a file
       IF(I.EQ.BUZZ)THEN
        BUZZ=BUZZ+100
        WRITE(9,400)X0,T10,T20,T30,B30,T40,B40,E
400     FORMAT(2X,F7.6,2X,F8.3,2X,F8.3,2X,F8.3,2X,F10.8,2X,F8.3,2X,
     1F10.8,2X,F7.2)
       END IF

c     check to see if constant section conditions are met
       C=Y3-0.0000001
       BC=B30+B40
       IF(BC.GT.C) THEN
        T40=T03
        B30=Y3
        GOTO 4000
       END IF
102    CONTINUE
      GOTO 2000

c     CONSTANT REGION

4000  BUZZ=1
      WRITE(9,*)
      WRITE(9,900)
900   FORMAT(8X,'X',11X,'T1',11X,'T2',11X,'T3',11X,'T4',8X,'E')
      WRITE(9,901)X0,T10,T20,T30,T40,E
901   FORMAT(3X,F8.6,5X,F8.3,5X,F8.3,5X,F8.3,5X,F8.3,2X,F7.2)

c     number of repititions
      COT=TOT-I
      DO 103 I=1,COT

c     Runge Kutta equations
       X=X0
       T1=T10
       T2=T20
       T3=T30
```

```
  T4=T40
  CALL CALCE(P,Tm,E,T10,T30)
  CALL HYCY (A1,A2,A3,C1,C2,C3,M1,M2,M3,N1,N2,N3,T1,T2,T3,T4,F1,F2,
1F3,F4,B10,B30,E,RHO,Cp,VH,VC,G,J,TH,TC,k,H1,H2,H3,G1,G2,G3,A4,C4,
1M4,N4)
  K1=F1*dX
  L1=F2*dX
  P1=F3*DX
  Q1=F4*DX

  X=X0+(dX/2)
  T1=T10+(K1/2)
  T2=T20+(L1/2)
  T3=T30+(P1/2)
  T4=T40+(Q1/2)
  CALL HYCY (A1,A2,A3,C1,C2,C3,M1,M2,M3,N1,N2,N3,T1,T2,T3,T4,F1,F2,
1F3,F4,B10,B30,E,RHO,Cp,VH,VC,G,J,TH,TC,k,H1,H2,H3,G1,G2,G3,A4,C4,
1M4,N4)
  K2=F1*dX
  L2=F2*dX
  P2=F3*DX
  Q2=F4*DX

  T1=T10+(K2/2)
  T2=T20+(L2/2)
  T3=T30+(P2/2)
  T4=T40+(Q2/2)
  CALL HYCY (A1,A2,A3,C1,C2,C3,M1,M2,M3,N1,N2,N3,T1,T2,T3,T4,F1,F2,
1F3,F4,B10,B30,E,RHO,Cp,VH,VC,G,J,TH,TC,k,H1,H2,H3,G1,G2,G3,A4,C4,
1M4,N4)
  K3=F1*dX
  L3=F2*dX
  P3=F3*DX
  Q3=F4*DX

  X=X0+dX
  T1=T10+K3
  T2=T20+L3
  T3=T30+P3
  T4=T40+Q3
  CALL HYCY (A1,A2,A3,C1,C2,C3,M1,M2,M3,N1,N2,N3,T1,T2,T3,T4,F1,F2,
1F3,F4,B10,B30,E,RHO,Cp,VH,VC,G,J,TH,TC,k,H1,H2,H3,G1,G2,G3,A4,C4,
1M4,N4)
  K4=F1*dX
  L4=F2*dX
  P4=F3*DX
  Q4=F4*DX

  DT1=(K1+(2*K2)+(2*K3)+K4)/6
```

```
      DT2=(L1+(2*L2)+(2*L3)+L4)/6
      DT3=(P1+(2*P2)+(2*P3)+P4)/6
      DT4=(Q1+(2*Q2)+(2*Q3)+Q4)/6

c     resetting initial values for next loop
      X0=X
      T10=T10+DT1
      T20=T20+DT2
      T30=T30+DT3
      T40=T40+DT4

c     output results to a file
       IF (I.EQ.BUZZ) THEN
        BUZZ=BUZZ+100
        WRITE(9,600)X0,T10,T20,T30,T40,E
600      FORMAT(3X,F8.6,5X,F8.3,5X,F8.3,5X,F8.3,5X,F8.3,2X,F7.2)
       END IF

103   CONTINUE
2000  WRITE(6,*)'YOUR RESULTS CAN BE FOUND IN "l4r.DAT"'
      WRITE(6,*)
      WRITE(6,*)'END'

     CLOSE(UNIT=8)
     CLOSE(UNIT=9)

     STOP
     END

c    calculation of E
     SUBROUTINE CALCE(P,Tm,E,T10,T30)
     REAL P,Tm,E,T10,T30

     Tm=(T10+T30)/2
     P=EXP(23.238-(3841/(Tm-45)))
     E=((6086.035*P)/(Tm*Tm))+384.615

     RETURN
     END

c    calculation of functions
c    hot-no, cold-no

     SUBROUTINE HNCN(A1,A2,A3,A4,C1,C2,C3,C4,M1,M2,M3,M4,N1,N2,N3,
    1N4,G1,G2,G3,H1,H2,H3,F3,F4,T1,B1,B3,F1,F2,T3,E,T01,T03,RHO,
    1Cp,VH,VC,Y1,Y3,k)
     REAL A1,A2,A3,A4,C1,C2,C3,C4,M1,M2,M3,M4,N1,N2,N3,N4,F3,F4,T1,B1,
    1F1,F2,G1,G2,G3,H1,H2,H3,T3,E,T01,RHO,Cp,VH,VC,T03,B3,Y1,Y3,k
```

```
      A1=(6*Cp*RHO*VH)*((3*T1*B1/(10*Y1))-(3*T01*B1/(10*Y1))-(T1*
     1  B1*B1/(5*Y1*Y1))+(T01*B1*B1/(5*Y1*Y1))+(E*T1*B1*B1/(10*Y1*K))-
     1  (E*T3*B1*B1/(10*Y1*K))-(E*T1*B1*B1*B1/(15*Y1*Y1*K))+(E*T3*B1*
     1  B1*B1/(15*Y1*Y1*K)))
      A2=(6*Cp*RHO*VH)*((3*B1*B1/(20*Y1))-(B1*B1*B1/(15*Y1*Y1))+
     1  (E*B1*B1*B1/(30*Y1*K))-(E*B1*B1*B1*B1/(60*Y1*Y1*K)))
      A3=(Cp*RHO*6*VH)*((E*B1*B1*B1*B1/(60*Y1*Y1*K))-(E*B1*B1*B1/
     1  (30*Y1*K)))
      A4=E*(T1-T3)

      C1=(Cp*RHO*6*VH)*((9*T1*B1/(160*Y1))-(9*T01*B1/(160*Y1))-(7
     1  *T1*B1*B1/(320*Y1*Y1))+(7*T01*B1*B1/(320*Y1*Y1))+(E*T1*B1*B1/
     1  (320*Y1*K))-(E*T3*B1*B1/(320*Y1*K))-(E*T1*B1*B1*B1/(480*Y1*Y1*
     1  K))+(E*T3*B1*B1*B1/(480*Y1*Y1*K)))
      C2=(Cp*RHO*6*VH)*((9*B1*B1/(320*Y1))-(7*B1*B1*B1/(960*Y1*Y1
     1  ))+(E*B1*B1*B1/(960*Y1*K))-(E*B1*B1*B1*B1/(1920*Y1*Y1*K)))
      C3=(Cp*RHO*6*VH)*((E*B1*B1*B1*B1/(1920*Y1*Y1*K))-(E*B1*B1*
     1  B1/(960*Y1*K)))
      C4=((5*E*(T1-T3))/4)-((3*k*(T01-T1))/(2*B1))

      G1=(A2*C1)-(A1*C2)
      G2=(A3*C1)-(A1*C3)
      G3=(A4*C1)-(A1*C4)

      M1=(Cp*RHO*6*VC)*((3*T3*B3/(10*Y3))-(3*T03*B3/(10*Y3))-(T3*
     1  B3*B3/(5*Y3*Y3))+(T03*B3*B3/(5*Y3*Y3))+(E*T3*B3*B3/(10*Y3*K))-
     1  (E*T1*B3*B3/(10*Y3*K))-(E*T3*B3*B3*B3/(15*Y3*Y3*K))+(E*T1*B3*
     1  B3*B3/(15*Y3*Y3*K)))
      M2=(Cp*RHO*6*VC)*((3*B3*B3/(20*Y3))-(B3*B3*B3/(15*Y3*Y3))+
     1  (E*B3*B3*B3/(30*Y3*K))-(E*B3*B3*B3*B3/(60*Y3*Y3*K)))
      M3=(Cp*RHO*6*VC)*((E*B3*B3*B3*B3/(60*Y3*Y3*K))-(E*B3*B3*B3/
     1  (30*Y3*K)))
      M4=E*(T3-T1)

      N1=(Cp*RHO*6*VC)*((9*T3*B3/(160*Y3))-(9*T03*B3/(160*Y3))-(7
     1  *T3*B3*B3/(320*Y3*Y3))+(7*T03*B3*B3/(320*Y3*Y3))+(E*T3*B3*B3/
     1  (320*Y3*K))-(E*T1*B3*B3/(320*Y3*K))-(E*T3*B3*B3*B3/(480*Y3*Y3*
     1  K))+(E*T1*B3*B3*B3/(480*Y3*Y3*K)))
      N2=(Cp*RHO*6*VC)*((9*B3*B3/(320*Y3))-(7*B3*B3*B3/(960*Y3*Y3
     1  ))+(E*B3*B3*B3/(960*Y3*K))-(E*B3*B3*B3*B3/(1920*Y3*Y3*K)))
      N3=(Cp*RHO*6*VC)*(((E*B3*B3*B3*B3)/(1920*Y3*Y3*K))-((E*B3
     1  *B3*B3)/(960*Y3*K)))
      N4=((5*E*(T3-T1))/4)-((3*k*(T03-T3))/(2*B3))

      H1=(M2*N1)-(M1*N2)
      H2=(M3*N1)-(M1*N3)
      H3=(M4*N1)-(M1*N4)

      F3=((G1*H3)-(G3*H2))/((G2*H2)-(G1*H1))
```

```
  F1=((G2*H3)-(G3*H1))/((G1*H1)-(G2*H2))
  F2=(-1)*(((A2*F1)+(A3*F3)+A4)/A1)
  F4=(-1)*(((M2*F3)+(M3*F1)+M4)/M1)

 RETURN
 END

 SUBROUTINE WALL(A1,A2,A3,C1,C2,C3,M1,M2,M3,N1,N2,N3,Cp,RHO,VH,VC,
1 B2,B4,T01,T03,T2,T4,Y1,Y3,G,J,K,TH,TC,F5,F6,F7,F8)
 REAL A1,A2,A3,C1,C2,C3,M1,M2,M3,N1,N2,N3,Cp,RHO,VH,VC,B2,B4,T01,
1 T03,T2,T4,Y1,Y3,G,J,K,TH,TC,F5,F6,F7,F8

  A1=(6*Cp*RHO*VH)*((3*T01*B2/(10*Y1))-(T01*B2*B2/(5*Y1*Y1))-
1  (3*T2*B2/(10*Y1))+(T2*B2*B2/(5*Y1*Y1))-(G*T2*B2*B2/(10*Y1*K))+
1  (G*T2*B2*B2*B2/(15*Y1*Y1*K))+(G*TC*B2*B2/(10*Y1*K))-(G*TC*B2*
1  B2*B2/(15*Y1*Y1*K)))
  A2=(6*Cp*RHO*VH)*((B2*B2*B2/(15*Y1*Y1))-(3*B2*B2/(20*Y1))-
1  (G*B2*B2*B2/(30*Y1*K))+(G*B2*B2*B2*B2/(60*Y1*Y1*K)))
  A3=G*(TC-T2)

  C1=(6*Cp*RHO*VH)*((9*T01*B2/(160*Y1))-(9*T2*B2/(160*Y1))-(7
1  *T01*B2*B2/(320*Y1*Y1))+(7*T2*B2*B2/(320*Y1*Y1))-(G*T2*B2*B2/
1  (320*Y1*K))+(G*TC*B2*B2/(320*Y1*K))+(G*T2*B2*B2*B2/(480*Y1*Y1*
1  K))-(G*TC*B2*B2*B2/(480*Y1*Y1*K)))
  C2=(6*Cp*RHO*VH)*((7*B2*B2*B2/(960*Y1*Y1))-(9*B2*B2/(320*Y1
1  ))-(G*B2*B2*B2/(960*Y1*K))+(G*B2*B2*B2*B2/(1920*Y1*Y1*K)))
  C3=((5*G*(TC-T2))/4)+((3*k*(T01-T2))/(2*B2))

  F5=((A1*C3)-(A3*C1))/((A2*C1)-(A1*C2))
  F6=((A2*C3)-(A3*C2))/((A1*C2)-(A2*C1))

  M1=(6*Cp*RHO*VC)*((3*T03*B4/(10*Y3))-(T03*B4*B4/(5*Y3*Y3))-
1  (3*T4*B4/(10*Y3))+(T4*B4*B4/(5*Y3*Y3))-(J*T4*B4*B4/(10*Y3*K))+
1  (J*T4*B4*B4*B4/(15*Y3*Y3*K))+(J*TH*B4*B4/(10*Y3*K))-(J*TH*B4*
1  B4*B4/(15*Y3*Y3*K)))
  M2=(6*Cp*RHO*VC)*((B4*B4*B4/(15*Y3*Y3))-(3*B4*B4/(20*Y3))-
1  (J*B4*B4*B4/(30*Y3*K))+(J*B4*B4*B4*B4/(60*Y3*Y3*K)))
  M3=J*(TH-T4)

  N1=(6*Cp*RHO*VC)*((9*T03*B4/(160*Y3))-(9*T4*B4/(160*Y3))-(7
1  *T03*B4*B4/(320*Y3*Y3))+(7*T4*B4*B4/(320*Y3*Y3))-(J*T4*B4*B4/
1  (320*Y3*K))+(J*TH*B4*B4/(320*Y3*K))+(J*T4*B4*B4*B4/(480*Y3*Y3*
1  K))-(J*TH*B4*B4*B4/(480*Y3*Y3*K)))
  N2=(6*Cp*RHO*VC)*((7*B4*B4*B4/(960*Y3*Y3))-(9*B4*B4/(320*Y3
1  ))-(J*B4*B4*B4/(960*Y3*K))+(J*B4*B4*B4*B4/(1920*Y3*Y3*K)))
  N3=((5*J*(TH-T4))/4)+((3*k*(T03-T4))/(2*B4))

  F7=((M1*N3)-(M3*N1))/((M2*N1)-(M1*N2))
  F8=((M2*N3)-(M3*N2))/((M1*N2)-(M2*N1))
```

```
      RETURN
      END

c     hot-yes, cold-no

      SUBROUTINE HYCN(A1,A2,A3,C1,C2,C3,M1,M2,M3,N1,N2,N3,T1,T2,T3,T4,
     1F1,F2,F3,F4,k,E,RHO,Cp,VH,VC,Y1,Y3,B10,B3,H1,H2,H3,T03,G,TC)
      REAL A1,A2,A3,C1,C2,C3,M1,M2,M3,N1,N2,N3,T1,T2,T3,T4,F1,F2,F3,F4
     1,k,E,RHO,Cp,VH,VC,Y1,Y3,B10,B3,H1,H2,H3,T03,G,TC

      A1=((Cp*RHO*6*VH))*((B10/12)+(E*B10*B10/(60*k)))
      A2=((Cp*RHO*6*VH))*((B10/12)+(G*B10*B10/(60*k)))
      A3=((Cp*RHO*6*VH))*((-1)*((E*B10*B10)/(60*k)))
      A4=E*(T1-T3)-(G*(TC-T2))

      C1=((Cp*RHO*6*VH))*((B10/16)+((21*E*B10*B10)/(1920*k)))
      C2=((Cp*RHO*6*VH))*((B10/48)+((11*G*B10*B10)/(1920*k)))
      C4=((Cp*RHO*6*VH))*((-1)*(21*E*B10*B10)/(1920*k))
      C3=((3*k*(T1-T2))/(2*B10))+((5*E*(T1-T3))/4)+((G*(TC-T2))/4)

       G1=(A1*C2)-(A2*C1)
       G2=(A3*C2)-(A2*C3)
       G3=(A4*C2)-(A2*C4)

      M1=((Cp*RHO*6*VC))*((3*T3*B3/(10*Y3))-(3*T03*B3/(10*Y3))-(T3*
     1  B3*B3/(5*Y3*Y3))+(T03*B3*B3/(5*Y3*Y3))+(E*T3*B3*B3/(10*Y3*K))-
     1  (E*T1*B3*B3/(10*Y3*K))-(E*T3*B3*B3*B3/(15*Y3*Y3*K))+(E*T1*B3*
     1  B3*B3/(15*Y3*Y3*K)))
       M2=((Cp*RHO*6*VC))*((3*B3*B3/(20*Y3))-(B3*B3*B3/(15*Y3*Y3))+
     1  (E*B3*B3*B3/(30*Y3*K))-(E*B3*B3*B3*B3/(60*Y3*Y3*K)))
       M3=((Cp*RHO*6*VC))*((((-1)*E*B3*B3*B3)/(30*Y3*K))+((E*B3*B3*B3*
     1  B3)/(60*Y3*Y3*K)))
       M4=E*(T3-T1)

       N1=((Cp*RHO*6*VC))*((9*T3*B3/(160*Y3))-(9*T03*B3/(160*Y3))-(7
     1  *T3*B3*B3/(320*Y3*Y3))+(7*T03*B3*B3/(320*Y3*Y3))+(E*T3*B3*B3/
     1  (320*Y3*K))-(E*T1*B3*B3/(320*Y3*K))-(E*T3*B3*B3*B3/(480*Y3*Y3*
     1  K))+(E*T1*B3*B3*B3/(480*Y3*Y3*K)))
       N2=((Cp*RHO*6*VC))*((9*B3*B3/(320*Y3))-(7*B3*B3*B3/(960*Y3*Y3
     1  ))+(E*B3*B3*B3/(960*Y3*K))-(E*B3*B3*B3*B3/(1920*Y3*Y3*K)))
       N3=((Cp*RHO*6*VC))*(((E*B3*B3*B3*B3)/(1920*Y3*Y3*K))-((E*B3
     1  *B3*B3)/(960*Y3*K)))
       N4=((5*E*(T3-T1))/4)-((3*k*(T03-T3))/(2*B3))

       H1=(M2*N1)-(M1*N2)
       H2=(M3*N1)-(M1*N3)
       H3=(M4*N1)-(M1*N4)
```

```
  F3=((G1*H3)-(G3*H2))/((G2*H2)-(G1*H1))
  F1=((G2*H3)-(G3*H1))/((G1*H1)-(G2*H2))
  F2=(-1)*(((A1*F1)+(A3*F3)+A4)/A2)
  F4=(-1)*(((M2*F3)+(M3*F1)+M4)/M1)

 RETURN
 END

 SUBROUTINE WALLC(M1,M2,M3,N1,N2,N3,Cp,RHO,VC,B4,Y3,J,k,T03,TH
1 ,F5,F6,T4)
 REAL M1,M2,M3,N1,N2,N3,Cp,RHO,VC,B4,T03,T4,Y3,J,K,TH,F5,F6
  M1=(6*Cp*RHO*VC)*((3*T03*B4/(10*Y3))-(T03*B4*B4/(5*Y3*Y3))-
1  (3*T4*B4/(10*Y3))+(T4*B4*B4/(5*Y3*Y3))-(J*T4*B4*B4/(10*Y3*K))+
1  (J*T4*B4*B4*B4/(15*Y3*Y3*K))+(J*TH*B4*B4/(10*Y3*K))-(J*TH*B4*
1  B4*B4/(15*Y3*Y3*K)))
  M2=(6*Cp*RHO*VC)*((B4*B4*B4/(15*Y3*Y3))-(3*B4*B4/(20*Y3))-
1  (J*B4*B4*B4/(30*Y3*K))+(J*B4*B4*B4*B4/(60*Y3*Y3*K)))
  M3=J*(TH-T4)

  N1=(6*Cp*RHO*VC)*((9*T03*B4/(160*Y3))-(9*T4*B4/(160*Y3))-(7
1  *T03*B4*B4/(320*Y3*Y3))+(7*T4*B4*B4/(320*Y3*Y3))-(J*T4*B4*B4/
1  (320*Y3*K))+(J*TH*B4*B4/(320*Y3*K))+(J*T4*B4*B4*B4/(480*Y3*Y3*
1  K))-(J*TH*B4*B4*B4/(480*Y3*Y3*K)))
  N2=(6*Cp*RHO*VC)*((7*B4*B4*B4/(960*Y3*Y3))-(9*B4*B4/(320*Y3
1  ))-(J*B4*B4*B4/(960*Y3*K))+(J*B4*B4*B4*B4/(1920*Y3*Y3*K)))
   N3=((5*J*(TH-T4))/4)+((3*k*(T03-T4))/(2*B4))

   F5=((M1*N3)-(M3*N1))/((M2*N1)-(M1*N2))
   F6=((M2*N3)-(M3*N2))/((M1*N2)-(M2*N1))

  RETURN
  END
```

c hot-no, cold-yes

```
  SUBROUTINE HNCY(A1,A2,A3,A4,C1,C2,C3,C4,M1,M2,M3,M4,N1,N2,N3,N4,
 1 G1,G2,G3,F3,F4,T1,B1,B30,F1,F2,k,T3,T4,E,T01,RHO,Cp,VH,VC,Y1,Y3,
 1 J,TH)
  REAL A1,A2,A3,A4,C1,C2,C3,C4,M1,M2,M3,M4,N1,N2,N3,N4,F3,F4,T1,B1,
 1F1,F2,G1,G2,G3,k,T3,E,T01,RHO,Cp,VH,VC,B30,Y1,Y3,T4,J,TH
   A1=((Cp*RHO*6*VH))*((3*T1*B1/(10*Y1))-(3*T01*B1/(10*Y1))-(T1*
 1  B1*B1/(5*Y1*Y1))+(T01*B1*B1/(5*Y1*Y1))+(E*T1*B1*B1/(10*Y1*K))-
 1  (E*T3*B1*B1/(10*Y1*K))-(E*T1*B1*B1*B1/(15*Y1*Y1*K))+(E*T3*B1*
 1  B1*B1/(15*Y1*Y1*K)))
   A2=((Cp*RHO*6*VH))*((3*B1*B1/(20*Y1))-(B1*B1*B1/(15*Y1*Y1))+
 1  (E*B1*B1*B1/(30*Y1*K))-(E*B1*B1*B1*B1/(60*Y1*Y1*K)))
   A3=((Cp*RHO*6*VH))*((((-1)*E*B1*B1*B1)/(30*Y1*K))+((E*B1*B1*B1*
```

```
1  B1)/(60*Y1*Y1*K)))
  A4=E*(T1-T3)

  C1=((Cp*RHO*6*VH))*((9*T1*B1/(160*Y1))-(9*T01*B1/(160*Y1))-(7
1  *T1*B1*B1/(320*Y1*Y1))+(7*T01*B1*B1/(320*Y1*Y1))+(E*T1*B1*B1/
1  (320*Y1*K))-(E*T3*B1*B1/(320*Y1*K))-(E*T1*B1*B1*B1/(480*Y1*Y1*
1  K))+(E*T3*B1*B1*B1/(480*Y1*Y1*K)))
  C2=((Cp*RHO*6*VH))*((9*B1*B1/(320*Y1))-(7*B1*B1*B1/(960*Y1*Y1
1  ))+(E*B1*B1*B1/(960*Y1*K))-(E*B1*B1*B1*B1/(1920*Y1*Y1*K)))
  C3=((Cp*RHO*6*VH))*((E*B1*B1*B1*B1/(1920*Y1*Y1*K))-(E*B1*B1*
1  B1/(960*Y1*K)))
  C4=((5*E*(T1-T3))/4)-((3*k*(T01-T1))/(2*B1))

  G1=(A2*C1)-(A1*C2)
  G2=(A3*C1)-(A1*C3)
  G3=(A4*C1)-(A1*C4)

M1=((Cp*RHO*6*VC))*((B30/12)+((E*B30*B30)/(60*k)))
M2=((Cp*RHO*6*VC))*((B30/12)+((J*B30*B30)/(60*k)))
M3=((Cp*RHO*6*VC))*((-1)*(E*B30*B30)/(60*k))
M4=E*(T3-T1)-(J*(TH-T4))

N1=((Cp*RHO*6*VC))*((B30/16)+((21*E*B30*B30)/(1920*k)))
N2=((Cp*RHO*6*VC))*((B30/48)+((11*J*B30*B30)/(1920*k)))
N3=((Cp*RHO*6*VC))*((-1)*(21*E*B30*B30)/(1920*k))
N4=((3*k*(T3-T4))/(2*B30))+((5*E*(T3-T1))/4)+((J*(TH-T4))/4)

  H1=(M1*N2)-(M2*N2)
  H2=(M3*N2)-(M2*N3)
  H3=(M4*N2)-(M2*N4)

  F3=((G1*H3)-(G3*H2))/((G2*H2)-(G1*H1))
  F1=((G2*H3)-(G3*H1))/((G1*H1)-(G2*H2))
  F2=(-1)*(((A2*F1)+(A3*F3)+A4)/A1)
  F4=(-1)*(((M1*F3)+(M3*F1)+M4)/M2)

RETURN
END

 SUBROUTINE WALLH(A1,A2,A3,C1,C2,C3,Cp,RHO,VH,B2,Y1,G,k,T01,TC
1 ,F5,F6,T2)
 REAL A1,A2,A3,C1,C2,C3,Cp,RHO,VH,B2,T01,T2,Y1,G,K,TC,F5,F6

   A1=(6*Cp*RHO*VH)*((3*T01*B2/(10*Y1))-(T01*B2*B2/(5*Y1*Y1))-
1   (3*T2*B2/(10*Y1))+(T2*B2*B2/(5*Y1*Y1))-(G*T2*B2*B2/(10*Y1*K))+
1   (G*T2*B2*B2*B2/(15*Y1*Y1*K))+(G*TC*B2*B2/(10*Y1*K))-(G*TC*B2*
1   B2*B2/(15*Y1*Y1*K)))
   A2=(6*Cp*RHO*VH)*((B2*B2*B2/(15*Y1*Y1))-(3*B2*B2/(20*Y1))-
1   (G*B2*B2*B2/(30*Y1*K))+(G*B2*B2*B2*B2/(60*Y1*Y1*K)))
```

```
      A3=G*(TC-T2)

      C1=(6*Cp*RHO*VH)*((9*T01*B2/(160*Y1))-(9*T2*B2/(160*Y1))-(7
     1  *T01*B2*B2/(320*Y1*Y1))+(7*T2*B2*B2/(320*Y1*Y1))-(G*T2*B2*B2/
     1  (320*Y1*K))+(G*TC*B2*B2/(320*Y1*K))+(G*T2*B2*B2*B2/(480*Y1*Y1*
     1  K))-(G*TC*B2*B2*B2/(480*Y1*Y1*K)))
      C2=(6*Cp*RHO*VH)*((7*B2*B2*B2/(960*Y1*Y1))-(9*B2*B2/(320*Y1
     1  ))-(G*B2*B2*B2/(960*Y1*K))+(G*B2*B2*B2*B2/(1920*Y1*Y1*K)))
      C3=((5*G*(TC-T2))/4)+((3*k*(T01-T2))/(2*B2))

      F5=((A1*C3)-(A3*C1))/((A2*C1)-(A1*C2))
       F6=((A2*C3)-(A3*C2))/((A1*C2)-(A2*C1))

      RETURN
      END
```

c hot-yes, cold-yes

```
      SUBROUTINE HYCY(A1,A2,A3,C1,C2,C3,M1,M2,M3,N1,N2,N3,T1,T2,T3,T4,
     1F1,F2,F3,F4,B10,B30,E,RHO,Cp,VH,VC,G,J,TH,TC,k,H1,H2,H3
     1,G1,G2,G3,A4,C4,M4,N4)
      REAL A1,A2,A3,C1,C2,C3,M1,M2,M3,N1,N2,N3,T1,T2,T3,T4,F1,F2,F3,F4
     1,B10,B30,E,RHO,Cp,VH,VC,G,J,TH,TC,k,H1,H2,H3,G1,G2,G3,A4,C4,M4,N4

      A1=(Cp*RHO*6*VH)*((B10/12)+(E*B10*B10/(60*k)))
      A2=(Cp*RHO*6*VH)*((B10/12)+(G*B10*B10/(60*k)))
      A3=(Cp*RHO*6*VH)*((-1)*(E*B10*B10/(60*k)))
      A4=(E*(T1-T3))-(G*(TC-T2))

      C1=(Cp*RHO*6*VH)*((B10/16)+(21*E*B10*B10/(1920*k)))
      C2=(Cp*RHO*6*VH)*((B10/48)+(11*G*B10*B10/(1920*K)))
      C3=(Cp*RHO*6*VH)*((-1)*(21*E*B10*B10/(1920*k)))
      C4=((5*E*(T1-T3))/4)+((3*k*(T1-T2))/(2*B10))+((G*(TC-T2))/4)

      G1=(A1*C2)-(A2*C1)
      G2=(A3*C2)-(A2*C3)
      G3=(A4*C2)-(A2*C4)

      M1=(Cp*RHO*6*VC)*((B30/12)+(E*B30*B30/(60*k)))
      M2=(Cp*RHO*6*VC)*((B30/12)+(J*B30*B30/(60*k)))
      M3=(Cp*RHO*6*VC)*((-1)*(E*B30*B30/(60*k)))
      M4=(E*(T3-T1))-(J*(TH-T4))

      N1=(Cp*RHO*6*VC)*((B30/16)+(21*E*B30*B30/(1920*k)))
      N2=(Cp*RHO*6*VC)*((B30/48)+(11*J*B30*B30/(1920*k)))
      N3=(Cp*RHO*6*VC)*((-1)*(21*E*B30*B30/(1920*k)))
      N4=((5*E*(T3-T1))/4)+((3*k*(T3-T4))/(2*B30))+((J*(TH-T4))/4)

      H1=(M1*N2)-(M2*N1)
```

```
H2=(M3*N2)-(M2*N3)
H3=(M4*N2)-(M2*N4)

F1=((G2*H3)-(G3*H1))/((G1*H1)-(G2*H2))
F3=((G1*H3)-(G3*H2))/((G2*H2)-(G1*H1))
F2=(-1)*(((A1*F1)+(A3*F3)+A4)/A2)
F4=(-1)*(((M1*F3)+(M3*F1)+M4)/M2)

RETURN
END
```